

0262
TM93-2089

NUWC-NPT TM 932089

Copy 1

NAVAL UNDERSEA WARFARE CENTER DIVISION
NEWPORT, RHODE ISLAND

LIBRARY USE ONLY

Technical Memorandum

PROCEEDINGS OF THE NUWC DIVISION NEWPORT SEMINAR SERIES ON
MICROFABRICATION AND TURBULENCE

19 July 1993

Compiled by: Promode Bandyopadhyay
Promode R. Bandyopadhyay
Weapons Technology and
Undersea Systems Department

UNCLASSIFIED
NAVAL UNDERSEA WARFARE CENTER
DIVISION NEWPORT
NEWPORT, RHODE ISLAND 02841-1708
RETURN TO: TECHNICAL LIBRARY

Approved for public release; distribution is unlimited.

LIBRARY USE ONLY

Report Documentation Page				Form Approved OMB No. 0704-0188	
Public reporting burden for the collection of information is estimated to average 1 hour per response, including the time for reviewing instructions, searching existing data sources, gathering and maintaining the data needed, and completing and reviewing the collection of information. Send comments regarding this burden estimate or any other aspect of this collection of information, including suggestions for reducing this burden, to Washington Headquarters Services, Directorate for Information Operations and Reports, 1215 Jefferson Davis Highway, Suite 1204, Arlington VA 22202-4302. Respondents should be aware that notwithstanding any other provision of law, no person shall be subject to a penalty for failing to comply with a collection of information if it does not display a currently valid OMB control number.					
1. REPORT DATE 19 JUL 1993		2. REPORT TYPE Technical Memorandum		3. DATES COVERED 01-02-1993 to 19-07-1993	
4. TITLE AND SUBTITLE Proceedings of the NUWC Division Newport Seminar on Microfabrication and Turbulence				5a. CONTRACT NUMBER	
				5b. GRANT NUMBER	
				5c. PROGRAM ELEMENT NUMBER	
6. AUTHOR(S) Promode Bandyopadhyay; Kenneth Breuer; Mohamed Gad-el-Hak; Chih-Ming Ho; Yu-Chong Tai				5d. PROJECT NUMBER	
				5e. TASK NUMBER	
				5f. WORK UNIT NUMBER	
7. PERFORMING ORGANIZATION NAME(S) AND ADDRESS(ES) Naval Undersea Warfare Center Division, Newport, RI, 02841				8. PERFORMING ORGANIZATION REPORT NUMBER TM 93-2089	
9. SPONSORING/MONITORING AGENCY NAME(S) AND ADDRESS(ES)				10. SPONSOR/MONITOR'S ACRONYM(S)	
				11. SPONSOR/MONITOR'S REPORT NUMBER(S)	
12. DISTRIBUTION/AVAILABILITY STATEMENT Approved for public release; distribution unlimited					
13. SUPPLEMENTARY NOTES NUWC2015 Additional authors: Smith, Charles R.; Telionus, Demetri P.; Leonard, Anthony					
14. ABSTRACT This memorandum records the proceedings of a two-part seminar series sponsored by the Naval Undersea Warfare Center Division, Newport, RI, during 1993. The first part of the seminar series dealt with the application of microfabrication to turbulence control; the second part dealt with vortex interactions.					
15. SUBJECT TERMS Microfabrication; Vortex interactions					
16. SECURITY CLASSIFICATION OF:			17. LIMITATION OF ABSTRACT Same as Report (SAR)	18. NUMBER OF PAGES 426	19a. NAME OF RESPONSIBLE PERSON
a. REPORT unclassified	b. ABSTRACT unclassified	c. THIS PAGE unclassified			



ABSTRACT

This memorandum records the proceedings of a two-part seminar series sponsored by the Naval Undersea Warfare Center Division, Newport, RI, during 1993. The first part of the seminar series dealt with the application of microfabrication to turbulence control; the second part dealt with vortex interactions.

ADMINISTRATIVE INFORMATION

This document was prepared by Code 8234 under internal funding.

The materials included in this document were provided by the seminar speakers and are reproduced with their permission. The technical views presented are those of the seminar speakers and not necessarily those of the U.S. Navy.

The compiler of this memorandum is located at the Naval Undersea Warfare Center Division, Newport, RI 02841-1708.

TABLE OF CONTENTS

Section	Page
Part I: Application of Microfabrication to Turbulence Control	
I-1 <i>Micromachined Sensors and Actuators for the Measurement and Control of Turbulent Boundary Layers</i> Kenneth S. Breuer	I-1
I-2 <i>Interactive Control of Turbulent Boundary Layers: A Futuristic View</i> Mohamed Gad-el-Hak	I-35
I-3 <i>Flows in Micro Systems</i> Chih-Ming Ho	I-109
I-4 <i>Silicon Micromachining and Its Applications</i> Yu-Chong Tai	I-163
Part II: Vortex Interactions	
II-1 <i>The Dynamics of Wall Turbulence: The Importance of Vortex Interactions</i> Charles R. Smith	II-1
II-2 <i>The Interaction of Coherent Vortices with Solid Surfaces</i> Demetri P. Telionis	II-53
II-3 <i>High Resolution Vortex Simulations of Bluff Body Flows</i> Anthony Leonard	II-113
<i>Appendix: Biographical Information on Seminar Speakers</i>	A-1

FOREWORD

The Naval Undersea Warfare Center Division, Newport, RI, sponsored a two-part seminar series in 1993 titled *Microfabrication and Turbulence*. The first part of the series comprised four seminars devoted to the application of microfabrication to turbulence control; the second part comprised three seminars that dealt with vortex interactions. The seminars—held in February, April, May, June, and July—were an activity of NUWC Newport's *Hydrodynamics Sphere of Excellence*, which is one of NUWC's leadership areas. The presentation materials used during the seminars, consisting mainly of viewgraphs, are reproduced in this report in their original form.

In the first seminar, Professor Kenneth Breuer of MIT used scaling arguments to show that only microfabrication offers the technology to implement active control strategies in a turbulent boundary layer.

In the second seminar, Professor Gad-el-Hak of the University of Notre Dame reviewed various turbulence control methodologies and gave order-of-magnitude arguments to compare the penalties and benefits inherent in each.

While many electrical engineers are developing the technology of microfabrication, Professor Chih-Ming Ho of UCLA is examining the science of the subject. In the third seminar, he compared the theory and experiments of the fluid mechanics of the process of etching micron-sized channels.

Professor Yu-Chong Tai of CalTech presented the fourth seminar, in which he reviewed microfabrication technology and then demonstrated a spectrum of applications ranging from neuron farms and micron-sized wind tunnels to the development of a host of fluid dynamics sensors of unprecedented resolution.

In the second part of the seminar series, vortex interaction in turbulence was examined. The turbulence production process in a high-Reynolds-number practical turbulent boundary layer is poorly understood, and it involves a diverse range of scales. To complicate matters, even at a very low Reynolds number, a typical coherent structure dimension can vary by a factor of as much as 10. To understand the regeneration process of the constituent hairpin vortices, Professor C. R. Smith of Lehigh University has conducted very-low-Reynolds-number experiments on what can be termed *turbulence with lesser variability*. In the fifth seminar, Professor Smith showed that his approach has elucidated several features of the production process, particularly the emergence of a thin, vertical-shear layer near the wall. He also presented the theoretical works of Professor J. D. A. Walker, which complement his experiments.

In the sixth seminar, Professor Demetri Telionis of Virginia PolyTech discussed the strategies of "chopping" discrete coherent vorticities and reducing the pressure spikes caused by the vorticities impacting the leading edge of a hydrofoil.

The final seminar of the series was given by Professor A. Leonard of CalTech. In the absence of a wall, in two-dimensional and axisymmetric flows, his vortex methods closely simulate several complex flow experiments. However, Professor Leonard pointed out that, because of three-dimensional viscous effects calculating drag due to the flow past a seemingly two-dimensional flat plate in the presence of a grazing wall remains a challenge.

Part I:

Application of Microfabrication to Turbulence Control

**I-1. Micromachined Sensors and Actuators
for the Measurement and Control
of Turbulent Boundary Layers**

**Kenneth S. Breuer
Massachusetts Institute of Technology**

SEMINAR NOTICE

**Micromachined sensors and actuators for the
measurement and control of turbulent boundary
layers**

by

KENNETH S. BREUER

Department of Aeronautics and Astronautics
Massachusetts Institute of Technology

The emerging field of micromachining has opened a new door to a wide variety of sensors and actuators that can be designed to implement boundary layer control. Using manufacturing techniques borrowed from the microelectronics industry, one can construct micro-electro-mechanical systems (MEMS) for the measurement of pressure, shear stress, etc. as well as actuators to provide closed loop flow control. These devices are small (50-100 microns), robust, high-bandwidth and very cheap and seem ideal for deployment in massive arrays for distributed flow sensing and control. Examples of the state-of-the-art in MEMS for flow control are presented along with some of the problems that must still be addressed.

Dynamical issues associated with active flow control are also discussed. The structure and dynamics of the "most dangerous" elements in a turbulent boundary layer are presented along with possible techniques for their control using massively distributed sensor-actuator arrays. Some comments on the application of this technology to the control of transition to turbulence are also offered.

Thursday, the 25th February 1993

Conference Room B, Bldg. 102

Time: 10:30 AM

POC: Dr. Promode R. Bandyopadhyay (Code 8234; x2588)

Micromachined sensors and actuators for boundary layer control

Kenneth S. Breuer

Department of Aeronautics & Astronautics
Massachusetts Institute of Technology

Seminar at NUWC, Newport, RI

March 2, 1993

(With assistance from Marty Schmidt & Errol Arkilic)

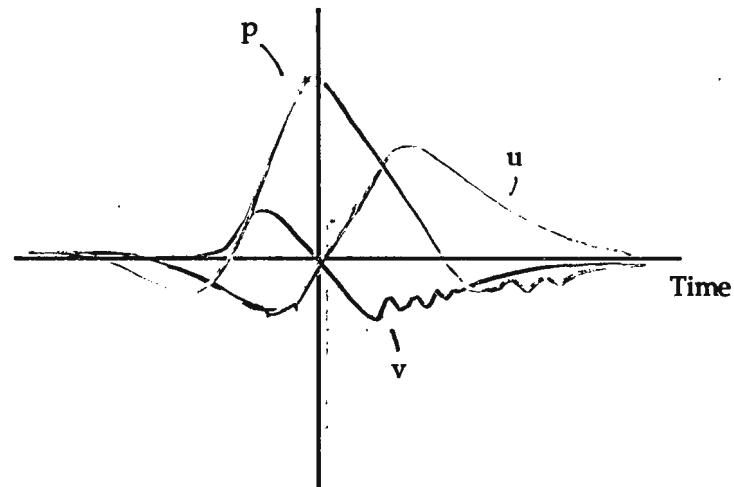
Outline

- Review of near-wall turbulent boundary layer structure
- Dynamical model for coherent structure evolution and control
- Limitations on practical control
- Review of Micromachined sensors and actuators
- Application of micromachining for boundary layer control
- Problems with micromachined devices

Near-wall turbulent boundary layer structure

Coherent Structures

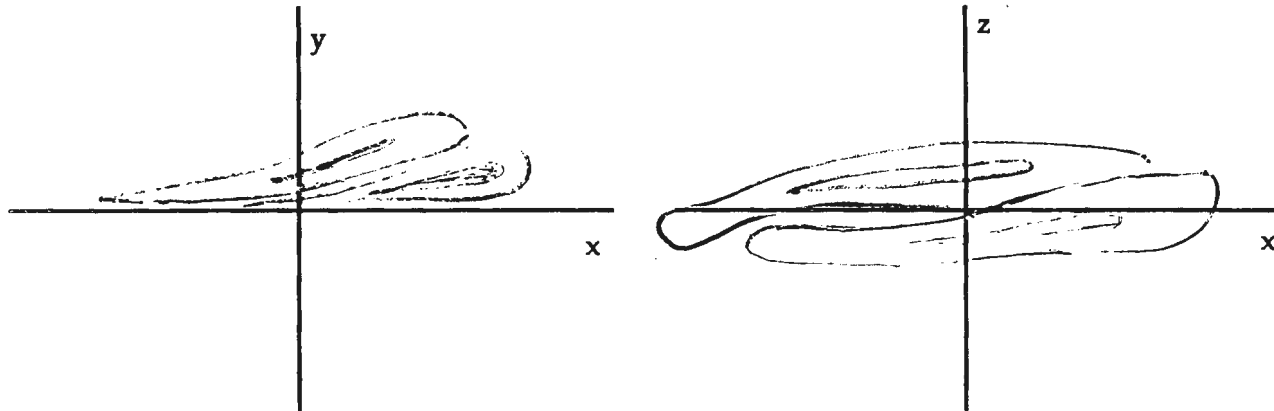
VITA



- Large fraction of rms wall-pressure fluctuations associated with large-amplitude pressure peaks
- “Waves” observed (?) in pressure and vertical velocity
 - instability/breakdown of coherent structure (?)

Near-wall turbulent structure

Inclined shear layers



- Reynolds stress and pressure peaks associated with elongated, inclined, shear layer structures
- Non-symmetric structures predominate ($\alpha = 0$ is present)

Dynamical model for near wall turbulent structures

$$\begin{aligned}\frac{Du}{Dt} + u'v &= -\frac{\partial p}{\partial x} \\ \frac{Dv}{Dt} &= -\frac{\partial p}{\partial y} + \frac{\partial u}{\partial x} + \frac{\partial v}{\partial y} + \frac{\partial w}{\partial z} = 0 \\ \frac{Dw}{Dt} &= -\frac{\partial p}{\partial z}\end{aligned}$$

LEADS TO: $\left\{ \left(\frac{\partial}{\partial t} + i\alpha U \right) \nabla^2 - i\alpha U'' \right\} \tilde{v} = 0$

$$\left(\frac{\partial}{\partial t} + i\alpha U \right) \hat{\eta} = -i\beta U' \tilde{v}$$

$$\hat{\eta} = i\beta \hat{u} - i\alpha \hat{w}$$

- Main evolution dominated by turbulent mean shear flow
- Viscous and nonlinear effects take place on a much longer (unimportant) timescale

Dynamical model for near wall flows

$\alpha = 0$ component

RAYLEIGH EQN: $\frac{\partial \tilde{v}_0}{\partial t} = 0$

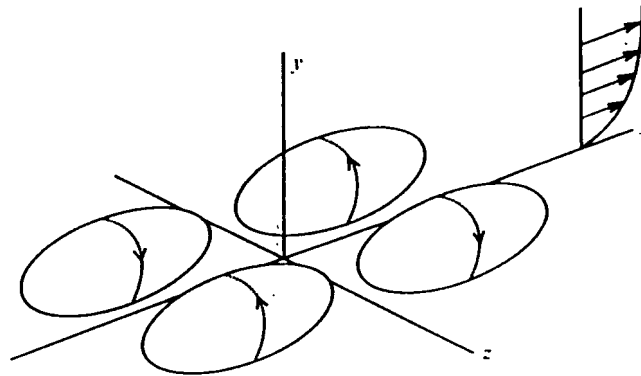
SQUIRE EQN: $\eta = \eta_0 - i\beta U' v_0 t$

$u =$

- Vertical component can (and does) decay
- Streamwise component grows algebraically due to three-dimensional "liftup" effect

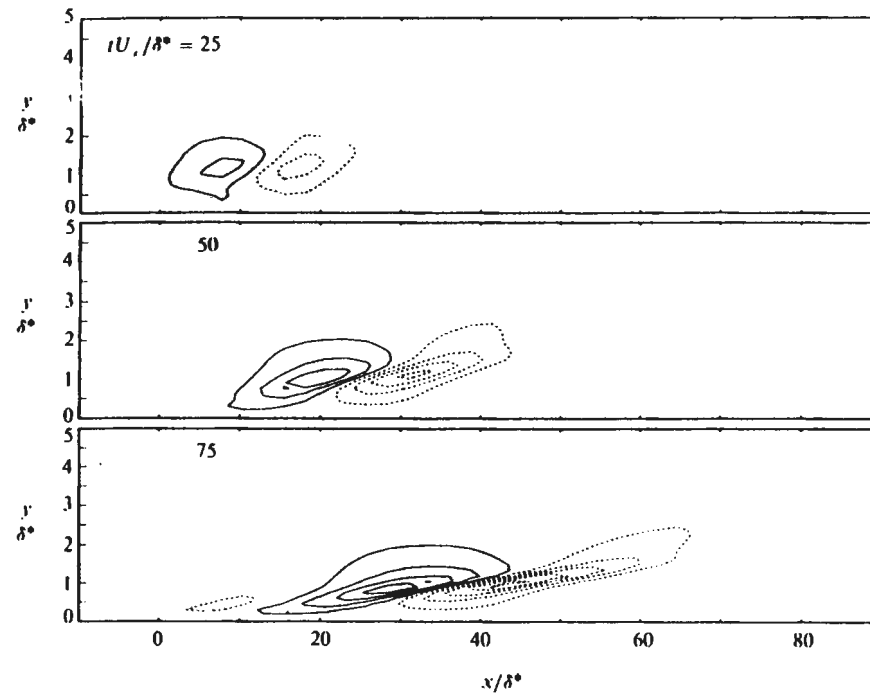
Numerical simulation of coherent structures

Initial conditions



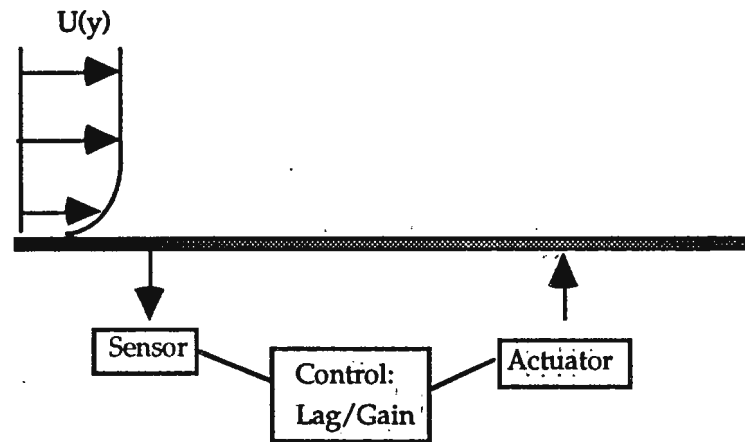
- Two pairs of counter-rotating vortices
- Result of a localized burst of Reynolds stress

Numerical simulation of coherent structure evolution (linear inviscid model)



- Development of inclined shear layer
- Intensification as time advances
- (No saturation or breakdown due to model simplicity - not important for control)

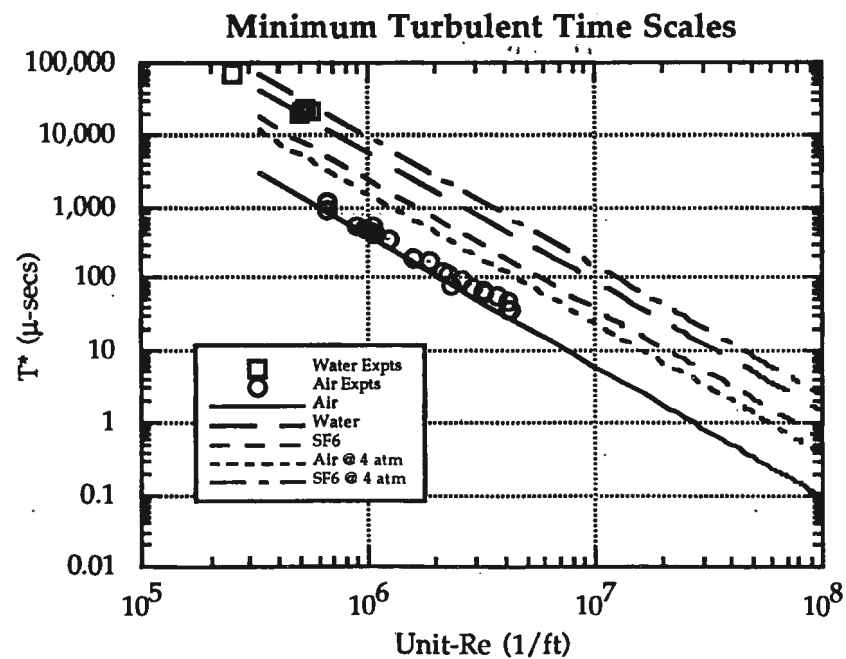
Methods for turbulent flow control



- Model active wall as localized wall motion (all wavenumbers excited)
- Dominant effects are:
 - $\alpha = 0$; dominant algebraic growth term
 - Lag due to non-collocation of sensor and actuator
 - Assume spanwise motion decoupled with $z^+ \approx 100$

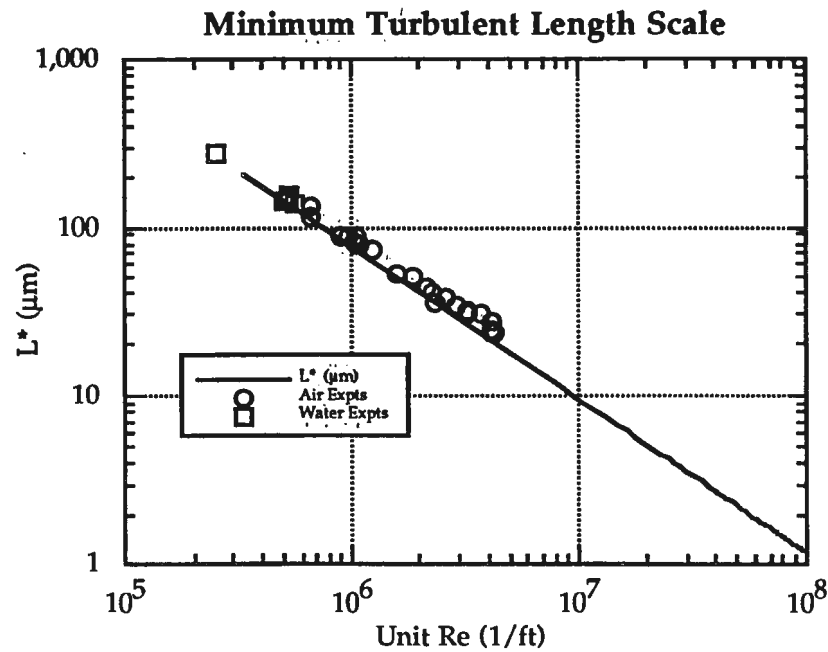
Problems with the implimentation of turbulent boundary layer control

(Time scales)



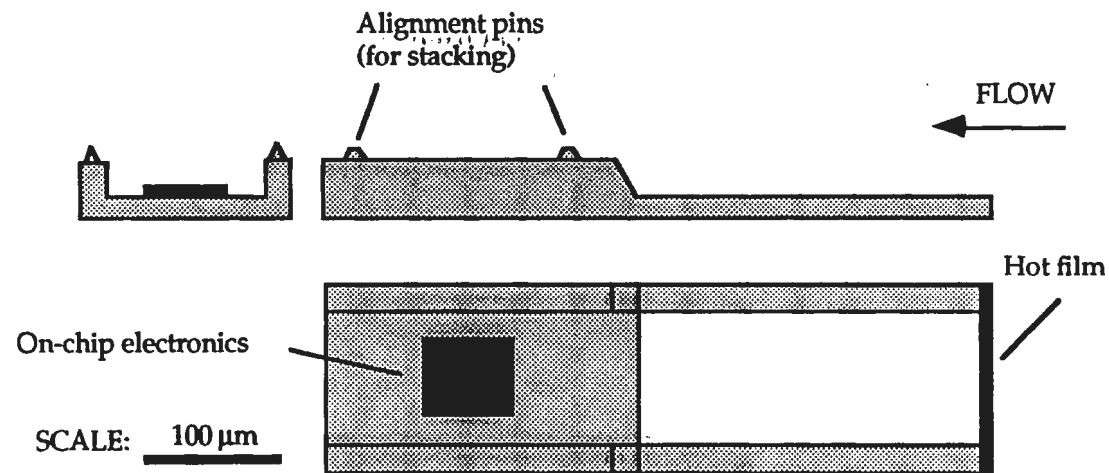
Problems with the implimentation of turbulent boundary layer control

(Length scales)



Development of micro-sensors and actuators

Example: Micro Hot-wire



- Sensing element size $0.5 \times 100 \mu\text{m}$
 - Thin film polysilicon bridge (good mechanical strength, selectable resistance)
- Stackable design - form multi-probe "rakes" for boundary layer measurements
 - 10 probes in a 0.5 mm span
 - Necessary for pressing need for high-Reynolds number instrumentation

What is Micromachining

What are its advantages

- Use of VLSI circuit manufacturing techniques for fabrication of Micro-electromechanical (MEM) devices:
 - Mechanical devices: gears, levers, micro-honeycombs, etc
 - Sensors: pressure, shear stress, temperature, chemical, etc
 - Actuators: pressure, force, strain, motors, etc
- Small dimension: $\mathcal{O}(1\mu m)$ in horizontal direction, $\mathcal{O}(100\text{\AA})$ in vertical direction.
- Ability to integrate on-chip electronics - reduce noise, lab complexity.
- High Frequency response: DC - 500 kHz, limited by sensitivity and electronics.
- Cheap: once commercialized, can be manufactured by the thousand at cost of “pennies” per device (e.g. DELCO pressure sensor).

Fabrication Techniques

A brief overview

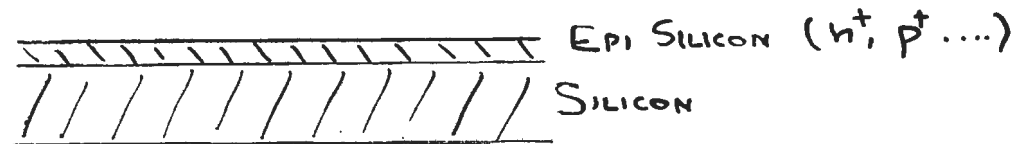
- Start with single crystal silicon wafer
- Build devices by cutting into wafer (“Bulk micromachining), putting materials on the surface (“Surface micromachining) and gluing wafers together (Wafer bonding)
- Use “Masks” to selectively protect and expose various layers to each operation
- Replicate the pattern across the wafer (10,000 elements on a single 4-inch wafer)
- Cut up the wafer
- Package (not a trivial step)
- Use/Sell.

Fabrication Techniques

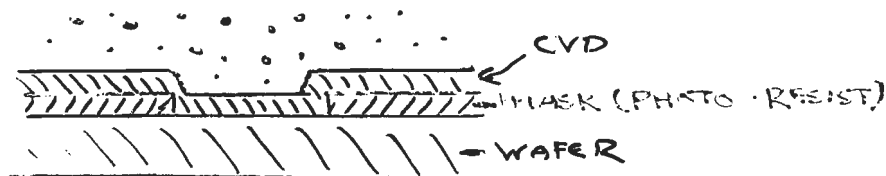
(continued)

- Additive techniques

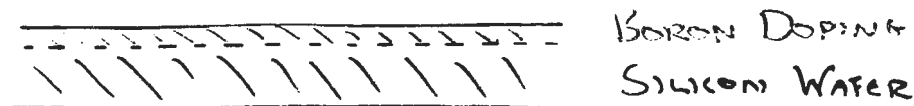
- Epitaxy - crystal growth



- Chemical Vapor Deposition (CVD) - addition of thin layers of almost any material (SiO_2 , Si_3N_4 , Poly-Si, metals, etc).



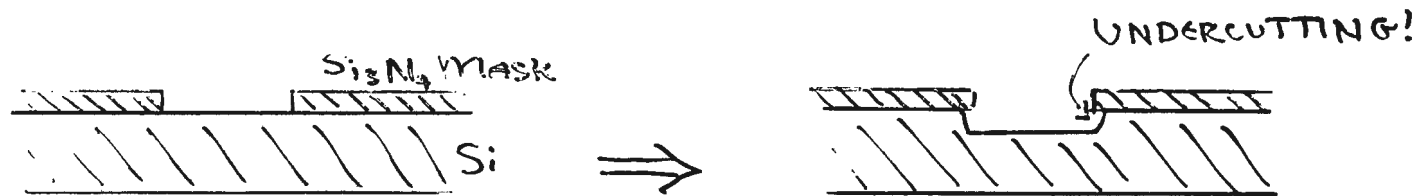
- Doping - Implantation of p^+ , n^+ silicon, Boron, Phosphorus, etc for:
(i) Electronic circuits, (ii) Etch-stop control



Fabrication Techniques

(continued)

- Subtractive techniques
 - Isotropic etching of Silicon



No spatial dependence, typically a HNO_3 , HF bath, masked by Si_3N_4 (or SiO_2).

Fabrication Techniques

(continued)

- Subtractive techniques (continued)
 - Anisotropic etching of Silicon.



Follows Crystal boundaries. Very precise control of shape and geometry.

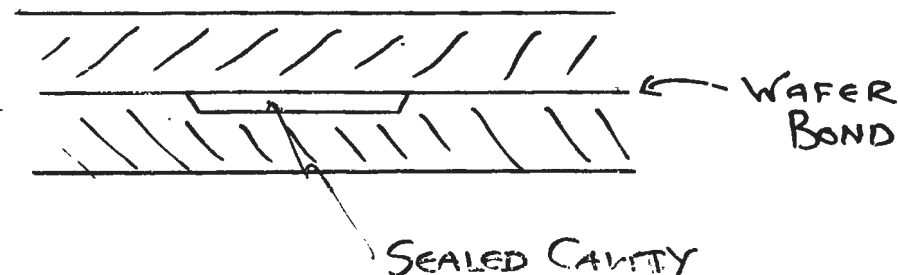
KOH bath, can be masked by SiO_2

Can be used to machine bridges and cantilevers.

Fabrication Techniques

(continued)

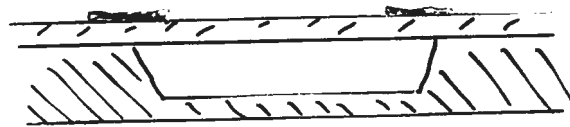
- Subtractive techniques (continued)
 - Isotropic etching of other materials (SiO_2 , Si_3N_4 , Poly- Si , metals, etc) - All kinds of etches and resists available.
- Wafer Bonding
 - Silicon equivalent of welding - Extremely strong joint formed.
 - in conjunction with doping techniques, can produce very accurate dimensional control in the vertical direction.



Examples - Pressure Sensor

Readout options

- Resistive readout:

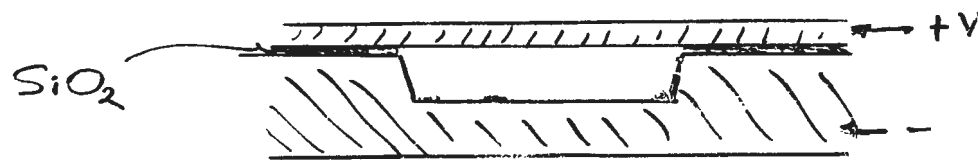


THIN FILM RESISTORS



Simple and accurate but has temperature dependence

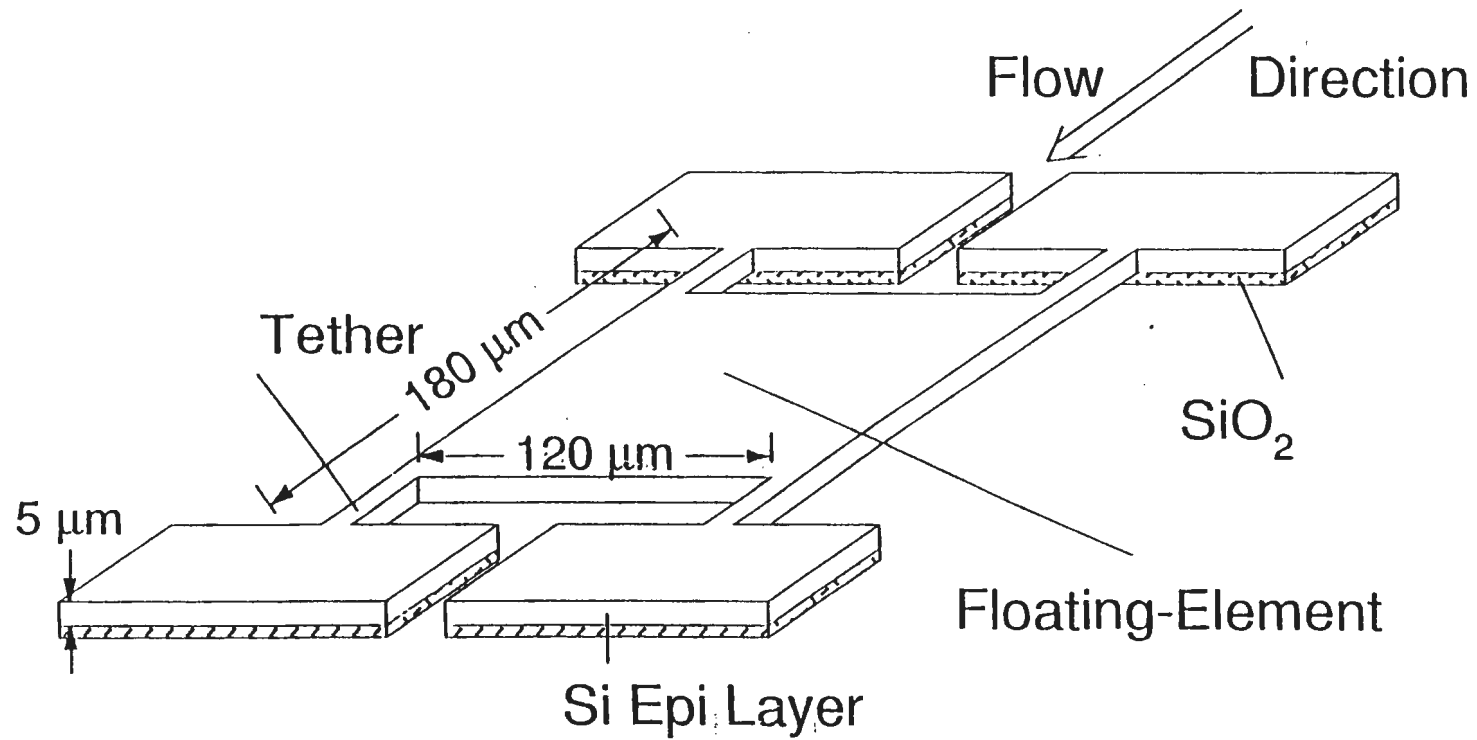
- Capacitive readout:



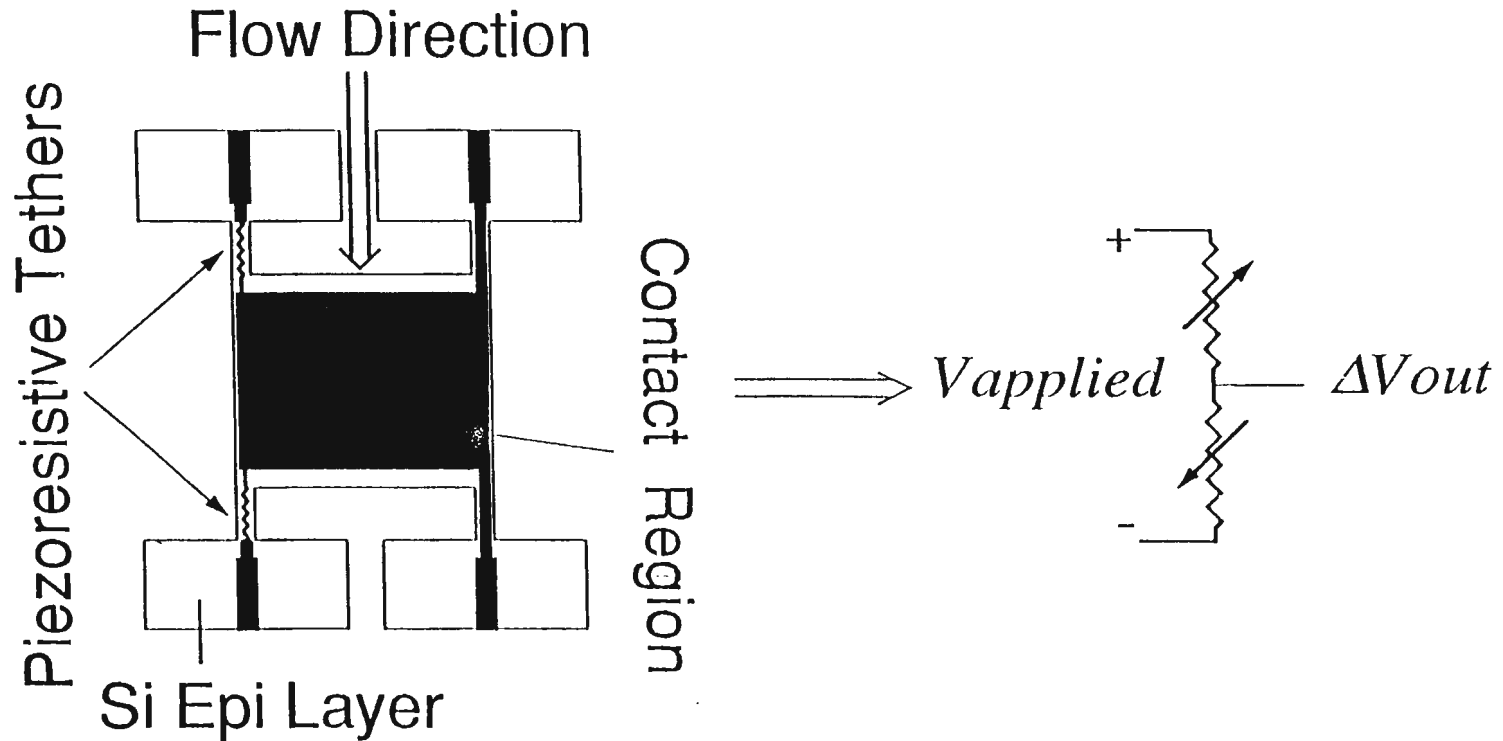
More complex, requires on-chip electronics, but *very* sensitive.

I-24

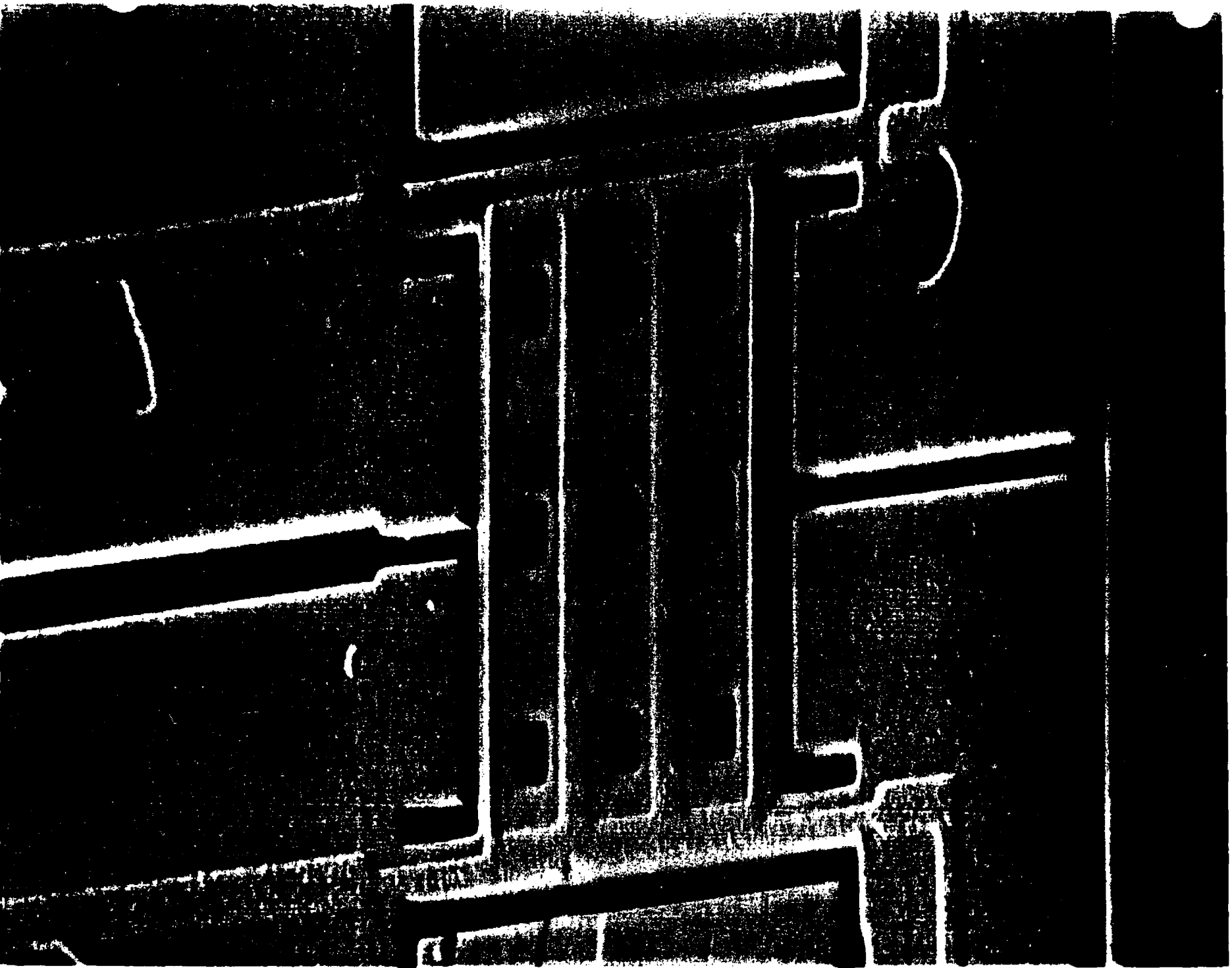
Microfabricated Floating-Element Schematic



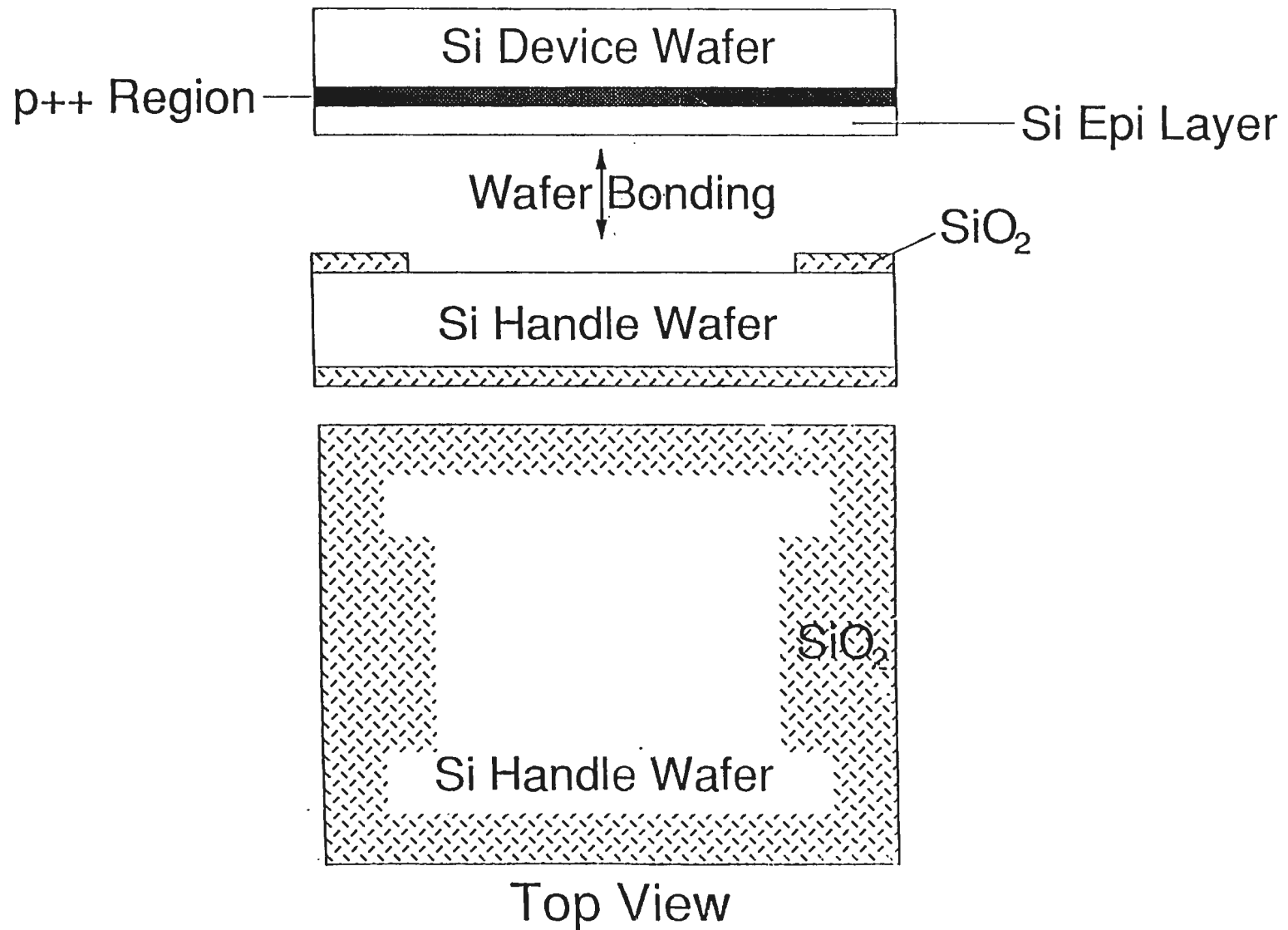
Piezoresistive Readout Scheme



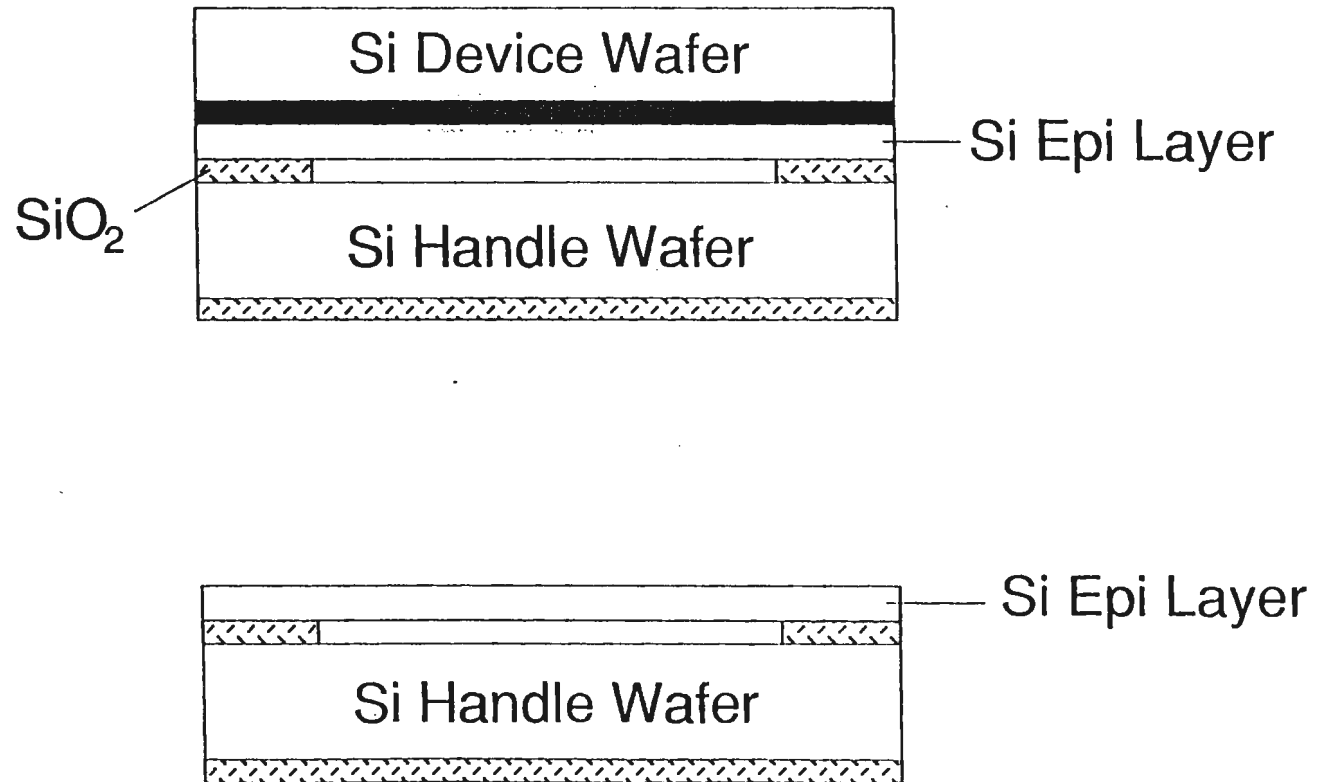
- Linear Response
 - Dielectric Isolation
- ⇒ High Temperature Operation



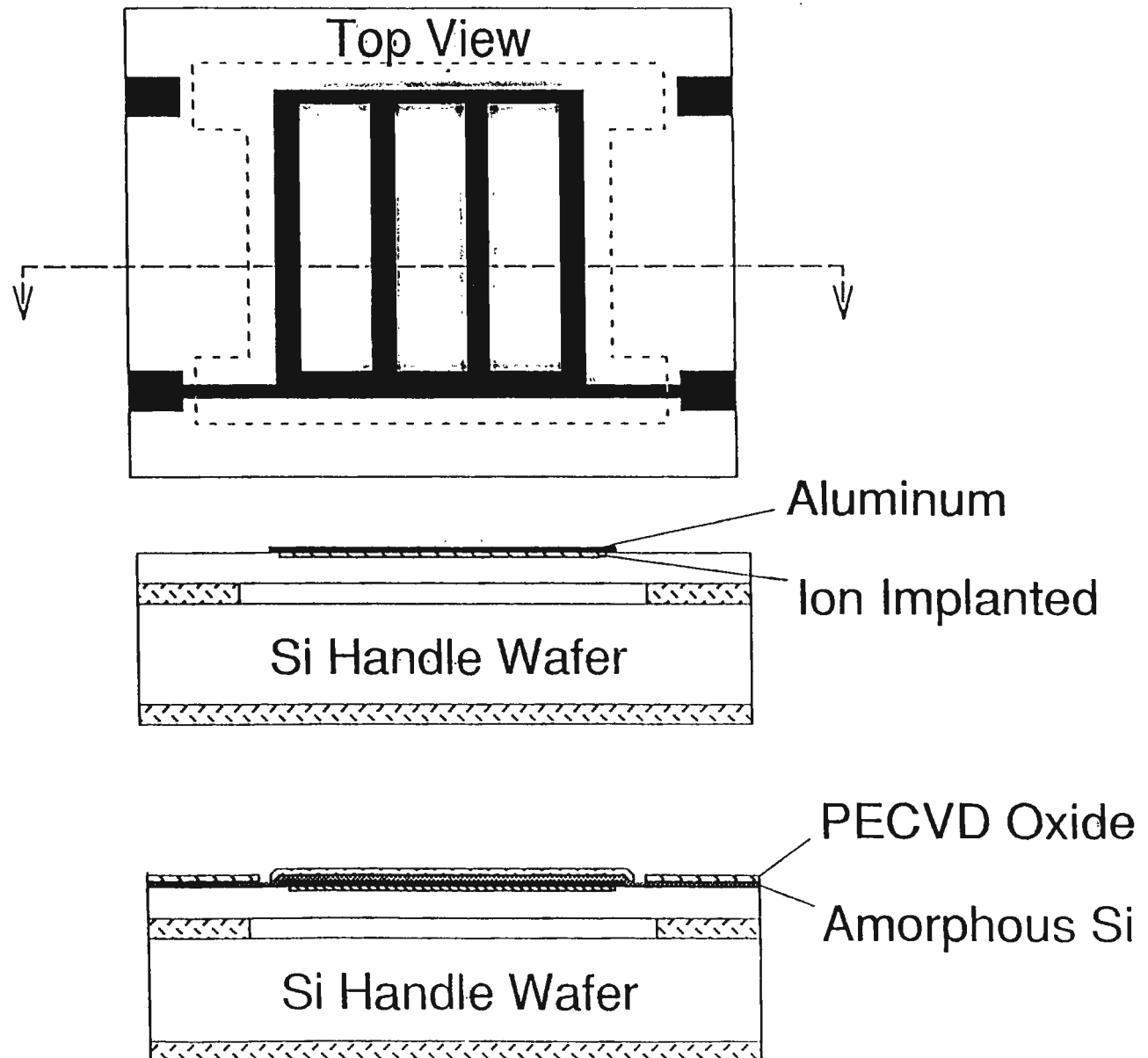
Fabrication Summary of the Shear-Stress Sensor



Fabrication Summary (cont.)

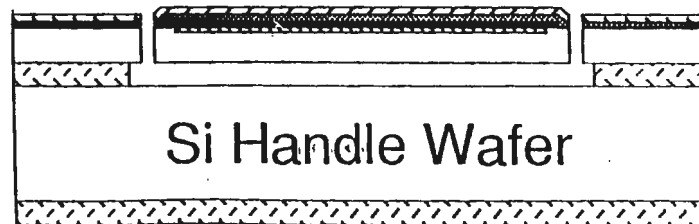
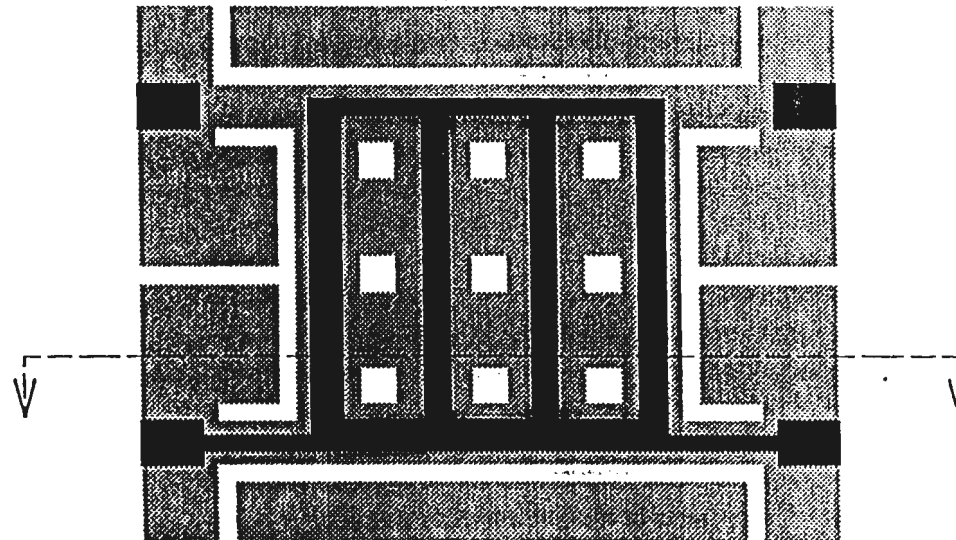


Fabrication Summary (cont.)



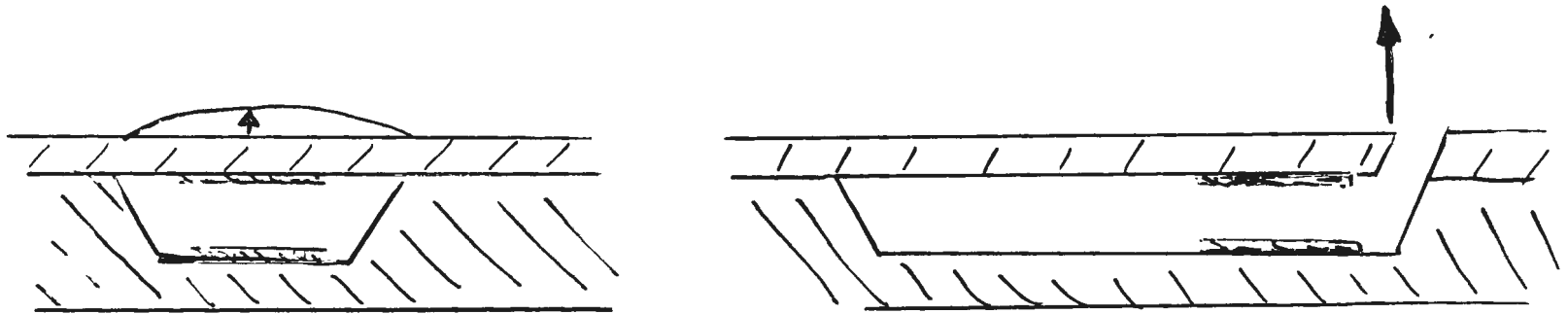
Fabrication Summary (cont.)

Top View



Micromachined Actuators

Preliminary designs



- Membranes (high forces, low displacements)
- Resonant cantilevers (low forces, high displacements)

Problems with microsensors and actuators

Micro-fluid mechanics

- Fluid mechanics at micron scale is not completely straightforward
- Gases: Mean-free-path effects become significant (High Knudsen number, low Reynolds number)
 - Viscous, transonic flow!
 - anomalously low viscosities
- Liquids: double layers and dielectric effects (especially with polar liquids)
 - more anomalous viscosities, charges, etc

Conclusions

- Wall pressure fluctuations dominated by passage of near-wall turbulent structures
- Near-wall coherent structures characterized by inclined shear layers.
 - dominated by long-wave structures ($\alpha = 0$)
- Dynamics dominated by “algebraic instability” (linear, inviscid, three-dimensional)
- Simple theory leads to dynamical equations for evolution and control
- Scales of normal turbulent flows require micro-fabricated sensors and actuators
- Micromachining leads to promise of “smart skins” for boundary layer (and transition) control
- Questions still remaining:
 - Micro-fluid mechanics (gaseous and liquid behaviour at micron scale)
 - Signal processing for sensor/actuator arrays
 - Control algorithms for massively distributed systems

**I-2. Interactive Control of Turbulent Boundary Layers:
A Futuristic View**

**Mohamed Gad-el-Hak
University of Notre Dame**

NUWC Division Newport, R. I.

SEMINAR NOTICE

**INTERACTIVE CONTROL OF TURBULENT BOUNDARY LAYERS:
A FUTURISTIC VIEW**

Mohamed Gad-el-Hak
Department of Aerospace & Mechanical Engineering
University of Notre Dame
Notre Dame, IN 46556

ABSTRACT

The ability to actively or passively manipulate a flow field to effect a desired change is of immense technological importance. In its broadest sense, the art of flow control probably has its roots in prehistoric times when streamlined spears, sickle-shaped boomerangs, and fin-stabilized arrows evolved empirically by archaic Homo sapiens. In this presentation, methods of control to achieve transition delay, separation postponement, lift enhancement, drag reduction, turbulence augmentation, or noise suppression are considered. An attempt is made to present a unified view of the means by which different methods of control achieve a variety of end results. It is argued that future systems for control of turbulent flows in general and turbulent boundary layers in particular would greatly benefit from the merging of a new science and a novel technology. Control of chaotic, nonlinear dynamical systems has been demonstrated theoretically as well as experimentally, at least for simple, one-degree-of-freedom systems. Microfabrication is an emerging technology which has the potential for producing inexpensive, programmable sensor/actuator chips that have dimensions of the order of a few microns. Together, these two disciplines could provide efficient interactive control systems to achieve a desired beneficial goal for practical flow fields.

Thursday, the 8th April 1993

Conference Room B, Bldg. 102

Time: 10:30 AM

POC: Dr. Promode R. Bandyopadhyay (Code 8234; x2588)

**INTERACTIVE CONTROL OF
TURBULENT BOUNDARY LAYERS:
*A FUTURISTIC VIEW***

MOHAMED GAD-EL-HAK
University of Notre Dame

8 April 1993

- * **Presented as part of the Turbulence Seminar Series: Applications of Microfabrication, held at the *Naval Undersea Warfare Center*; Newport, Rhode Island, 8 April 1993.**

INTERACTIVE CONTROL OF TURBULENT BOUNDARY LAYERS: A FUTURISTIC VIEW

Mohamed Gad-el-Hak
Department of Aerospace & Mechanical Engineering
University of Notre Dame
Notre Dame, IN 46556

ABSTRACT

The ability to actively or passively manipulate a flow field to effect a desired change is of immense technological importance. In its broadest sense, the art of flow control probably has its roots in prehistoric times when streamlined spears, sickle-shaped boomerangs, and fin-stabilized arrows evolved empirically by archaic Homo sapiens. In this presentation, methods of control to achieve transition delay, separation postponement, lift enhancement, drag reduction, turbulence augmentation, or noise suppression are considered. An attempt is made to present a unified view of the means by which different methods of control achieve a variety of end results. It is argued that future systems for control of turbulent flows in general and turbulent boundary layers in particular would greatly benefit from the merging of a new science and a novel technology. Control of chaotic, nonlinear dynamical systems has been demonstrated theoretically as well as experimentally, at least for simple, one-degree-of-freedom systems. Microfabrication is an emerging technology which has the potential for producing inexpensive, programmable sensor/actuator chips that have dimensions of the order of a few microns. Together, these two disciplines could provide efficient interactive control systems to achieve a desired beneficial goal for practical flow fields.

Aim

☛ Flow control:

The ability to actively or passively manipulate a flow field in order to effect a beneficial change.

)

☛ Provide a broad overview of the arts and sciences of flow control.

☛ Focus on control of wall-bounded flows:

Immense technological importance.

Aim

☞ **Control of a TBL to achieve a variety of beneficial changes.**

*** Unifying principles?**

*** Coherent structures.**

*** Selective control.**

*** Outlook for the future.**



Past:

Archaic Homo sapiens:

*Streamlined spears; sickle-shaped boomerangs;
fin-stabilized arrows.*



Present:

Prandtl (1904) pioneered the science of flow control.

Boundary layer theory has its roots in a question that boggled Prandtl for few years:

*Failure of conical diffusers in a large air duct
to achieve the expected pressure recovery.*



Future:

* Empirical Art \Rightarrow Predictive Science

* CFD

* Nonlinear Dynamical
Systems Theory

+

* Microfabrication

\Rightarrow

Interactive control

**15 x 10⁹
years ago**

Big Bang

4.6 x 10⁹

Solar System formed

1.5 x 10⁹

Life began on Earth

0.25 x 10⁹

Dragonfly

4 x 10⁶

Ancestral hominid

2 x 10⁶

***Homo habilis* (handy)**

1.5 x 10⁶

Homo erectus

500,000

***Archaic Homo sapiens* (wise)**

200,000

Homo sapiens

**10,000
years ago**

Agriculture

Present

**10,000
years ago**

Agriculture

5,500

Plough

5,000

Irrigation Systems/Writing

3,500

Metals

300

Modern Science/Newton's Laws

150

Navier-Stokes Equations

**< 100
years ago**

**Powered Flight/
Boundary Layer Theory/
Science of Flow Control**

Present



Future

????????





Flow Control Goals

- ☛ Transition delay/advancement.
 - ☛ Turbulence enhancement/suppression/relaminarization.
 - ☛ Separation prevention/provocation.
-



- ☛ Skin-friction/pressure drag reduction.
- ☛ Lift enhancement.
- ☛ Heat transfer/mixing/chemical reaction augmentation.
- ☛ Noise suppression.

Desired Traits for a Flow Control Device

-  **Simple.**
-  **Inexpensive to build.**
-)  **Inexpensive to operate.**
-  **Has no trade-offs.**

 **Does not exist!**

Drag Reduction



Pressure Drag:

- * Separation
- * Displacement
- * Wave
- * Induced



Skin Friction:

- * LBL
- * Transition
- * TBL

Drag Reduction

Internal Flows: Close to 100% is skin friction.

* Throughput; pumping power; duct size/cost.

External Flows: Land, air, and sea vehicles.

* Range; fuel cost/volume; payload; speed.

Submarines: 90% skin friction.

Aircraft: 50% skin friction; 25% induced drag.

Annual fuel costs for U.S. commercial fleet exceed \$10B.

It costs \$2B to develop a new wing.

Tools for Controlling



Surface:

- * Roughness; Riblets; Fences
- * Curvature
- * Shape
- * Compliant
- * Mass transfer
- * Heat transfer



Freestream:

- * LEBU
- * Acoustics
- * Turbulence levels; Gust



Additives

- * Polymers; surfactants
- * Micro-bubbles
- * Particles; dust; fibers

Types of Control Devices



Passive:

- No energy expenditure
 - e.g., riblets
-



Active:

- Requires energy
- e.g., suction
- Is *saving* larger than *penalty*?

* Interactive:

- ⊗ Control input based on measurement
- ⊗ Open or feedback control loop
- ⊗ Sensor(s) + actuator(s) needed

)

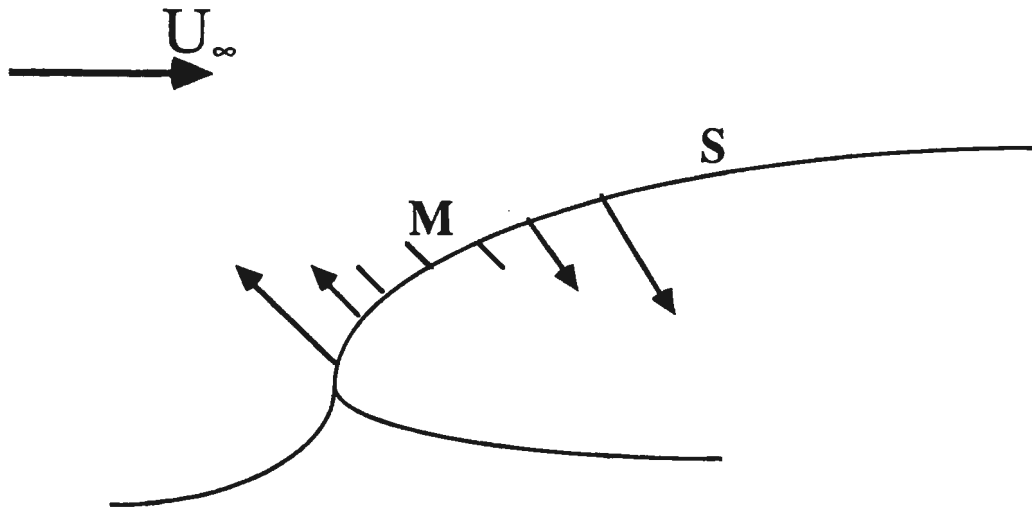
Is there a unifying principle that ties together a majority of flow control devices?

- ☛ **Help to understand the physics.**
 - ☛ **Help in contemplating new artifacts.**
 - ☛ **Help in minimizing adverse tradeoffs.**
-)

Vorticity Framework

Wall as a source/sink of spanwise/streamwise vorticity.

Magnitude and direction of vorticity flux.



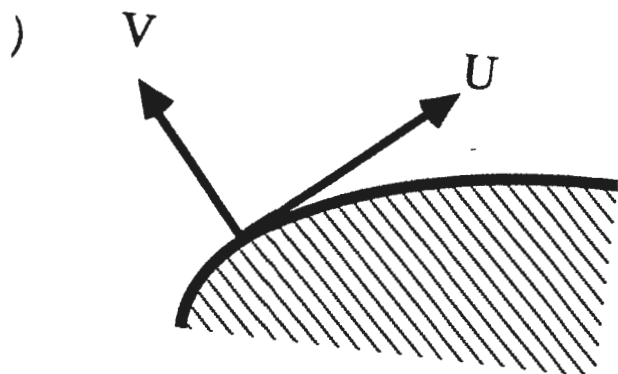
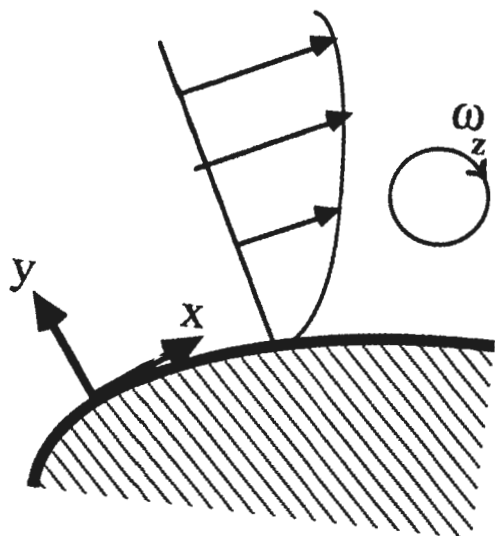
- * **Lighthill (1963):** Place boundary layer correctly in the flow whole.
- * **Willmarth (1975):** Nature and structure of TBL.
- * **Reshotko (1976):** Transition control.
- * **Reynolds&Carr (1985):** Separation control.

x-Momentum at Wall:

$$\begin{aligned}
 & \left. \begin{aligned} & v_w \left[\frac{\partial U}{\partial y} \right]_o \\ & + \frac{1}{\rho} \left[\frac{\partial P}{\partial x} \right]_o \\ & - \left[\frac{\partial v}{\partial y} \right]_o \left[\frac{\partial U}{\partial y} \right]_o \end{aligned} \right\} \\
 & = \left[v \frac{\partial^2 U}{\partial y^2} \right]_o
 \end{aligned}$$

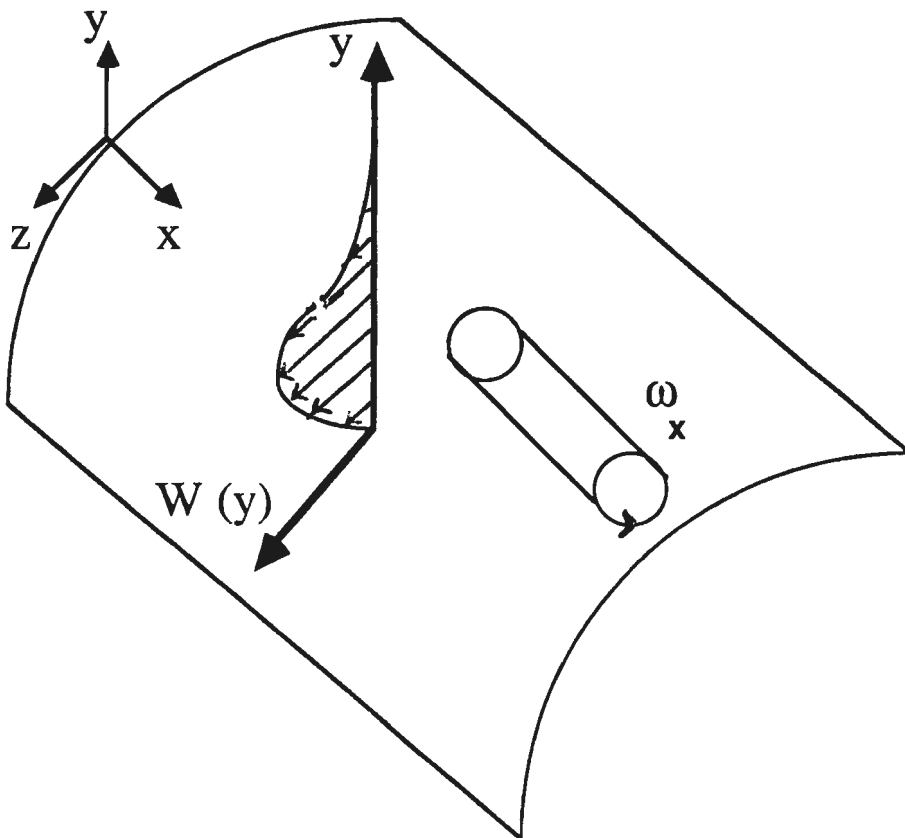
y-Momentum at Wall:

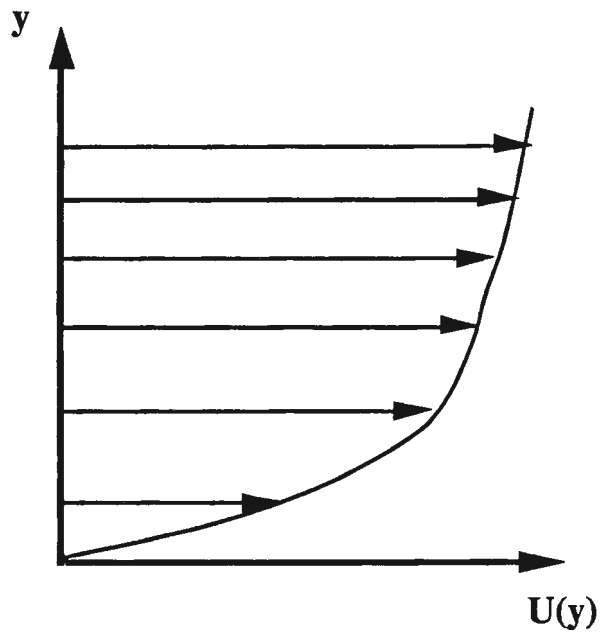
$$\begin{aligned}
 & \left. \begin{aligned} & 0 \\ & + \frac{1}{\rho} \left[\frac{\partial P}{\partial y} \right]_o \\ & - 0 \end{aligned} \right\} \\
 & = \left[v \frac{\partial^2 v}{\partial y^2} \right]_o
 \end{aligned}$$



z-Momentum at Wall:

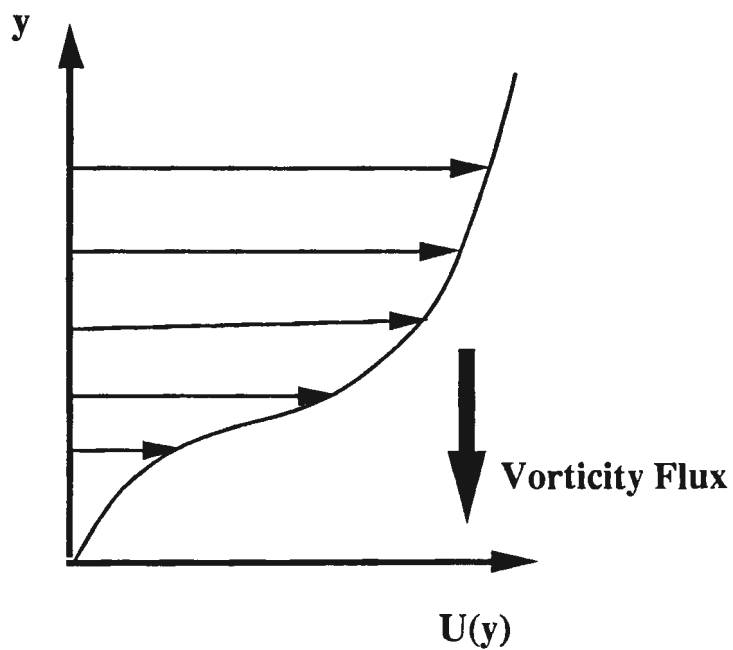
$$\begin{aligned}
 & \left. \begin{aligned}
 & v_w \left[\frac{\partial W}{\partial y} \right]_0 \\
 & + \frac{1}{\rho} \left[\frac{\partial P}{\partial z} \right]_0 \\
 & - \left[\frac{\partial v}{\partial y} \right]_0 \left[\frac{\partial W}{\partial y} \right]_0
 \end{aligned} \right\} \\
 & = \left[v \frac{\partial^2 W}{\partial y^2} \right]_0
 \end{aligned}$$





FULL PROFILE

- Suction
- Favorable P-grad.
- Heating (water)



INFLECTIONAL PROFILE

- Injection
- Adverse P-grad.
- Cooling

Velocity Profile Modifiers

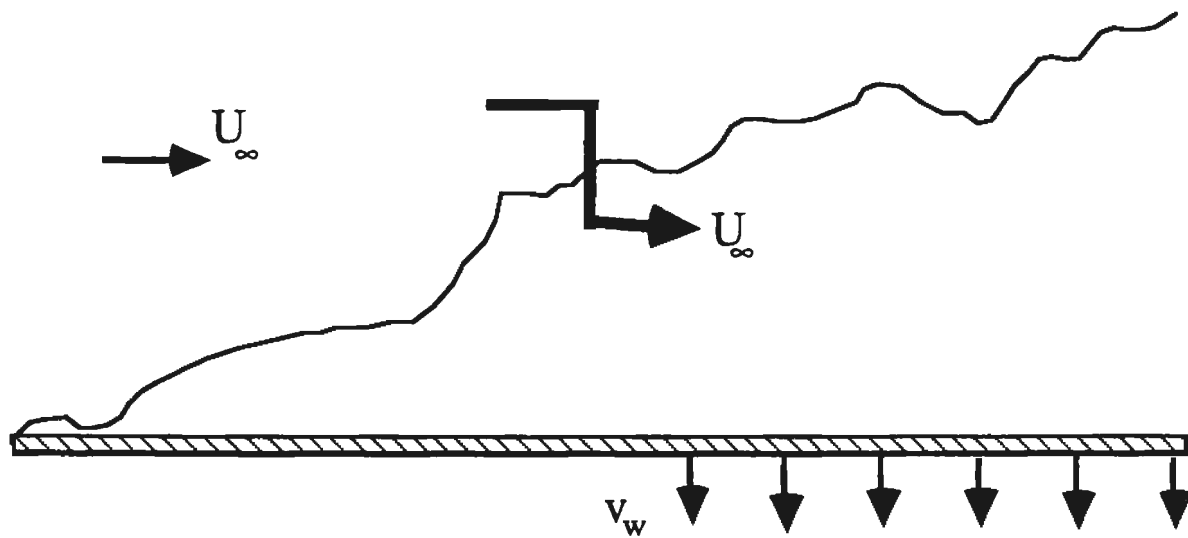
A fuller velocity profile (negative curvature or vorticity source at wall) will lead to:

*separation/transition resistance;
turbulence suppression;
higher skin friction.*

- * Wall suction; $v_w < 0$.**
- * Favorable pressure gradient; $dP_0/dx < 0$.**
- * Lower viscosity at wall; $\partial\mu/\partial y > 0$.**

Suction

$$C_q \equiv v_w / U_\infty$$



$$\text{LBL: } C_q \sim Re^{-0.5}$$

To prevent
separation

$$\text{TBL: } C_q = 0.002 - 0.004$$

$$(C_f = 2 \frac{d\delta_\theta}{dx} + 2 C_q + \text{Pressure gradient terms}).$$

At $Re = 10^7$: $C_f|_T = 0.003$
 $C_f|_L = 0.0004$

----- $C_f = 0.0030$

Suction

$$C_f = 2 \frac{d\delta_\theta}{dx} + 2 C_q .$$

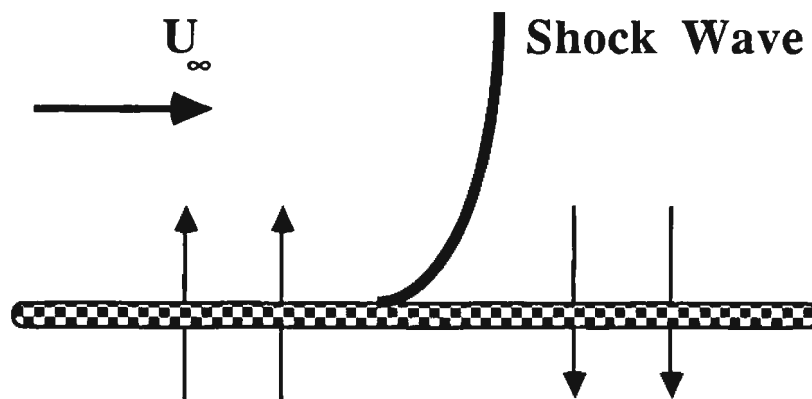
----- $C_f = 0.0004$

----- $C_f = 0.0000$

- ☛ To delay transition: $C_q = 0.0001$
- ☛ Laminar separation: $C_q = 0.0003$
- ☛ Turbulent separation: $C_q = 0.003$
- ☛ Asymptotic profile (TBL): $C_q = 0.003$
- ☛ Relaminarization: $C_q = 0.01$

Passive Suction

- In high-speed flows.
- Porous surface underneath shock wave.
- Mass self-bleed from downstream of shock to upstream to mitigate the local pressure gradient.



⇒ A series of weaker shock waves;
prevent separation;
reduce wave drag.

Shaping

LBL: If fluid decelerates faster than

$U_0 \sim x^{-0.09}$
boundary layer separates.

TBL: If fluid decelerates faster than

$U_0 \sim x^{-0.23}$
boundary layer separates.

Efficient momentum transport provides the mechanism for mixing slower fluid near wall with faster fluid particles further out.

✿ **Transition advance.
Turbulators.**

Stratford (1959) Closure

- * Flow with continuously zero skin-friction throughout its region of pressure rise.
- * Achieve a specified pressure rise in the shortest possible distance and with the least possible dissipation of energy.
- * Apply Stratford closure immediately after transition to maximize L/D .



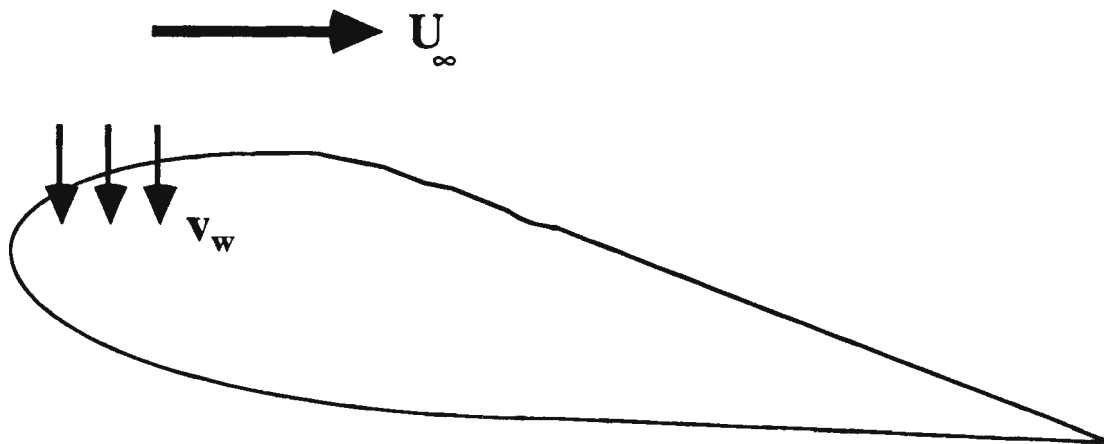
Liebeck (1978)

- ☛ **Assume incipient separation**
- ☛ **Calculate pressure field required**
- ☛ **Use inverse calculation procedure to derive shape**

✿ **Major Concern:
Off-design conditions**

Hybrid Laminar Flow Control

- ☛ Suction at leading edge region
+ careful contouring of airfoil shape elsewhere.
- ☛ Very promising to delay separation as well as to prevent transition.
-)
- ☛ High lift during takeoff and landing.
Lower skin friction during cruise.



Lower viscosity at wall

- ☞ **Cooling wall in gases.**
(also increases density and, thus, near-wall momentum)
- ☞ **Heating wall in liquids.** * *
- ☞ **Film boiling.** * *
- ☞ **Cavitation.** * *
- ☞ **Sublimation.**
- ☞ **Chemical reaction.**
- ☞ **Wall injection of a lower-viscosity fluid.**
- ☞ **Shear-thinning additives.** * *

Wall Heating/Cooling

- ☛ Lower wall viscosity leads to:
 - separation/transition resistance;*
 - turbulence suppression;*
 - higher skin friction.*

- ☛ Demonstrated for high-speed flows in gases
 - * Requires a heat sink
(e.g. Cryogenically-fueled aircraft)

- ☛ In liquids, wall heating lowers near-wall viscosity but density remains essentially unchanged.
 - * Very little research
 - * How about marine propellers?

New Way of Looking at Turbulent Flows

☞ *Coherent structures* seem to be ubiquitous in all turbulent shear flows.

☞ Enormous technological interest in that they offer the possibility for controlling:

Jets; wakes; mixing layers;
wall-bounded flows.

☞ In a TBL, hierarchy of quasi-periodic structures:

Large eddies; Falco's eddies;
low-speed streaks; bursts.

Little use of structural information in searching for innovative control methods.

Possible reason:

Flow control is as old as man, while organized structures were shown to exist in a TBL only 30 years ago.

At best, we are presently trying to use structural information to *explain* why a specific control device works.

✿ How about trying to create control artifacts to suppress/enhance a particular structure?

COHERENT STRUCTURES



Large Outer Structures.



Intermediate Falco Eddies.



Near-Wall Events.

* **Low-speed streaks.**

* **Ejection.**

* **Sweep.**

Bursting

Polymers; Particles; Riblets

✿ Increased losses in near-wall region.

⇒ To stay in equilibrium:
Energy gain goes up.

⇒ Scales go up:
$$\begin{array}{lcl} \text{gain} & \sim & (\text{size})^2 \\ \text{loss} & \sim & \text{size} \end{array}$$

⇒ Buffer layer thickens.

- ⇒ **Position for maximum $\overline{u^2}$ and \overline{uv} farther away from wall.**
- ⇒ **Production of Reynolds stress inhibited.**
- ⇒ **Momentum transport lowered.**
- ⇒ **Skin friction lowered.**

Is skin-friction reduction associated with turbulence suppression?

✿ ✿ **Yes:**

**Polymers; Particles; LEBUs;
Riblets.**

[Act *selectively* on a particular structure]

✿ ✿ **No:**

**Suction; Wall Cooling/Heating;
Favorable Pressure Gradient.**

[Act *globally* on all eddies]

SUCCESSFUL TECHNIQUES



Polymers, etc., act indirectly through local interaction with discrete turbulent structures.

*** Particularly, small-scale eddies.**

LESS EFFICIENT METHODS



Suction, etc., acts directly on mean flow.

*** Mean velocity modifiers.**

SUCTION

■ Flat Plate:

☞ $C_f = 2 (d\delta_\theta / dx) + 2 C_q$

\Downarrow
 \Downarrow

\Downarrow
 \Downarrow

\Downarrow
 \Downarrow

✿ No suction:

0.003
 2×0.015
0.0

✿ Suction (asymptotic velocity profile):

0.006
0.0
 2×0.003

Control of a TBL



Global.



Selective:

* By the flow.

* By design.



Near-wall events:

Very intermittent and random
in space & time.



**Temporal phasing and
spatial selectivity are
needed for
*selective control.***

WHAT TO TARGET?



Low-speed streaks

are the most

**|| visible
|| reliable
|| detectable**

indicators

**of the preburst
turbulence production
process.**

EXAMPLE



Submarine

Aircraft
(10 km)

* $U_o = 10 \text{ m/s}$

300 m/s

* $Re = 10^7 / m$

$10^7 / m$

* $\nu / u^* = 2.6 \mu$

2.6μ

SENSORS/ACTUATORS

✱ 100 wall units spanwise.
(260 μ)

✱ 1000 wall units streamwise.
(2.6 mm)

■ Number of elements = $1.5 \times 10^6/\text{m}^2$.

■ Frequency = 600 Hz (submarine).
= 18 kHz (aircraft).

Actuator's Response:

⊗ Wall displacement = 26 μ .

⊗ $C_q = 0.0006$ ($C_f = 0 + 2 \times 0.0006$)

⊗ $\Delta T = 2^\circ\text{C}$ (heating; water)
= 40°C (cooling; air)

Vision for a Control System



Checkerboard of wall sensors + actuators.

*** Sensors:**

Pressure; velocity; wall shear; etc.

*** Actuators:**

**Heating/cooling; suction/injection;
wall movement; etc.**



For example:

☉ Piezoelectric devices under flexible skin.

☉ Terfenol-d materials.

John Lumley (1991).

Can it be done?

*) Breakthrough # 1:

Microfabrication.

*) Breakthrough # 2:

Control of Chaos.

Microfabrication

Micro-Machinery:

Manufacturing processes that can create microscopic machinery.



Combine electronic and mechanical components on a single chip:



Sensor/Actuator.



Sensors:



Pressure; temperature; velocity; mass flow; sound; smell.



Actuators:



Motors; pumps; moving rods; valves; gears; tweezers.



Micro-robot on a single chip:



Sensing; guidance; and control systems.

Microfabrication



**Combine electronic and
mechanical components on a
single chip:**

Sensor/Actuator.



- **Small size.**
- **Smart machine.**
- **Inexpensive.**

SENSORS



Sensors detect instantaneous wall pressure or wall shear-stress.

- * **Location.**
- * **Amplitude.**
- * **Phase.**



Example:



Laser-powered *picophones* machined in silicon using integrated circuit fabrication technology.



MIT.



**Diameter: 0.2 mm (200 μ).
(77 wall units)**

ACTUATORS



Suction slots



Wall displacement



Heating (electric-resistance heating)



Cooling (thermoelectric devices
based upon the Peltier effect)

ACTUATORS

- ☞ **Smart materials that might allow a wing to react and adjust to fluctuating wind conditions.**

(Grumman Corporation.)

- ☞ **Terfenol-d:**

- * Metal composite that changes its length when exposed to a magnetic field.**

- * Nonlinear material.**

- ⊗ (classical control impractical.)**

- ⊗ (potential candidate for chaotic control.)**

- * Able to exert large forces.**


- ☞ **Example: Apply magnetic field to change the length of Terfenol-d inside a wing.
 (Change the wing's shape.)**

ADVANCES IN MATERIALS


Photochromic glass:

-  Darkens in strong light.

Electrochromic films:

-  Change color when subjected to electric current.

Encapsulated enzymes inside glass:




-  Change color in the presence of certain chemicals.

Electro-rheological fluids:


-  Change from liquid to near-solid when subjected to current.

ADVANCES IN MATERIALS


Nitinol (1962):

-  A titanium and nickel alloy with memory.
-  Changes shape when heated/cooled.
-  Used in satellite antennas.

Magnetoelastic ribbons:

-  Nonlinear materials that change their stiffness in the presence of varying magnetic fields.

Terfenol-d:

-  Metal composite that changes its length when exposed to a magnetic field.

Fiber-optic skin to measure deformation field with a resolution of 0.03μ .

Possible Pitfalls

☞ Checkerboard of || wall sensors
+
|| actuators.

)
* Information sensed incomplete.



⊗ Might be misinterpreted.

)
* Checkerboard actuators might be less effective.

Nonlinear Dynamical Systems Theory

Butterfly Effect:

- Sensitive dependence of nonlinear differential equations on initial conditions.
- Small disturbances can radically alter a deterministic system to yield rich, unpredictable behavior.

Chaos

☞ Douglas Hofstadter:

"It turns out that an eerie type of chaos can lurk just behind a façade of order--

and yet, deep inside the chaos lurks an even eerier type of order."

☞ Chaotic system continually shifts from one periodic pattern to another, creating the appearance of randomness.

* Apparent randomness of a chaotic system is only *skin deep*.

☞ Beneath the apparent unpredictability lies an intricate but highly ordered structure.

) * A complicated web of interwoven patterns of regular (periodic) motion.

Control of Chaos

☞ A chaotic system,
though apparently random,
actually consists of a number of
different periodic motions (orbits).

☞ System will shift from one motion to
the other, abruptly and arbitrarily,
ad infinitum.

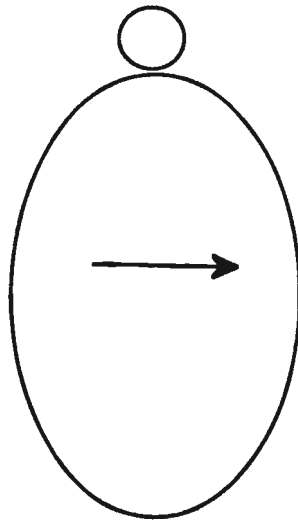
⊗ *Reverse Chaos:*

* Pick one of these orbits and lock
onto it.

* Apply a tiny *push* at just the right
moment.

Control of Chaos

☞ Like balancing a ball on a saddle.



* Saddle stays still



Ball rolls off.

* Continuously adjusted slightly



Ball stays in place.

Control of Chaos

☛ **Theory for continuous systems:**

Ott, Grebogi and York (1990).
(University of Maryland.)

☛ **Control the chaotic behavior of a
parametrically driven, gravitationally
buckled, amorphous magnetoelastic
ribbon.**

Ditto, Rauseo and Spano (1990).
(Naval Surface Warfare Center, Silver Spring, MD.)

☛ **Laminarize a chaotic thermal
convection loop (thermosyphon).**

Singer, Wang and Bau (1991).
(University of Pennsylvania.)

Control of Chaos

☞ Chaotic attractor typically has embedded within it an infinite number of unstable periodic orbits.

)

☞ Apply small time-dependent parameter perturbations so as to stabilize anyone of the existing orbits (which reside on strange attractors).

* Lock system into one particular type of repeating motion.

Advantages

☞ Chaotic motion



Periodic motion.

☞ A priori analytical knowledge of the system dynamics is not needed.

☞ Could apply to any chaotic system for which a faithful Poincaré section can be constructed.

☞ Effective even in the presence of small-amplitude noise or small modelling errors.

Direct Trajectories to Targets

- ☞ Exploit the exponential sensitivity of a chaotic system to minute perturbations.**
- ☞ Direct the system to a desired accessible state in a short time.**
- ☞ Effective even in the presence of small-amplitude noise or small modelling errors.**
- ☞ Substantially alter the future state by a minute perturbation.**

Procedure

Direct Trajectories to Targets:

- * Sense present state.
- * Apply a judiciously chosen perturbation.
- * System is rapidly directed towards the desired state.

Turbulent Boundary Layers

- ☞ Recent advances in dynamical systems theory provide opportunities for achieving efficient control of TBL.**

- ☞ Control bursting events to:**
 - * Prevent/provoke separation.**
 - * Delay/advance transition.**
 - * Reduce drag.**
 - * Relaminarize a TBL.**

- ☞ By making small time-dependent adjustments to one of the parameters governing the system's behavior.**

Turbulent Boundary Layers

- ☞ Need to establish a conceptual framework for adapting York's theory to control (intermittent) bursting events in TBL.**
- ☞ Quasi-periodic events modelled as a dynamical system.**
- ☞ Control about anyone of its many unstable fixed points (periodic orbits) embedded in the chaotic attractor.**
- ☞ Aim is to control the bursting events superposed on the fixed point solution of the 6-mode (or higher) dynamical system that describes the near-wall activities.**

Bursting Phenomenon

- ☞ Use proper orthogonal decomposition to extract a low-dimensional dynamical system from experimental data for the near-wall region of TBL.

Aubry, Holmes and Lumley (1988; 1991).
(Cornell University.)

- ☞ Expand instantaneous velocity field using experimentally determined eigenfunctions which are in the form of streamwise rolls.

- ☞ Apply Galerkin projection.

- ☞ Truncate to obtain a low-dimensional set of (six) ODE.

- ☞ Examine fixed points and topology of their stable as well as unstable manifolds.

- ☞ Chaos as well as regular intermittency are exhibited.

Control of Bursting

- ☞ **Proper orthogonal decomposition.**
(an optimally convergent representation.)
- ☞ **Dynamical system leaves one fixed point and jumps to another along a hetroclinic cycle.**
- ☞ **Holding system near first fixed point**
 - **Delaying jump**
 - **Drag reduction.**

Procedure

- ☞ Construct a Poincaré map to classify the type of intermittency

$$\mathbf{x}_{i+1} = \mathbf{f}(\mathbf{x}_i, \mathbf{p})$$

- * \mathbf{x}_i discrete time signal
- * \mathbf{p} parameter to be controlled

- ☞ Apply a small time-dependent perturbation to the parameter controlling the stability of the fixed point.

- ☞ Force the eigenvalue to remain within the circle of stability that surrounds the (unstable) fixed point.

Possible Pitfalls

- ☞ System with infinite number of degrees of freedom are not readily susceptible to an easy dynamical systems approximation.

- ☞ Noise in the system tends to kick the orbit out of the circle of stability (surrounds the unstable fixed point).
 - * Forces the operator to increase the control amplitude in order to keep the orbit close to the fixed point.

- ☞ Manifold along which the system leaves fixed point might not be one-dimensional.

- ☞ A burst is assumed to leave a fixed point along the *average path*.
Actuator pushes back along same path.
 - * In reality, most bursts would leave to one side or the other of the average path.

Microfabrication

+

**Nonlinear Dynamical
System Theory**



Interactive control

Outlook

- ☛ Tremendous energy saving potential for vehicles which have notoriously high drag: Automobiles; helicopters; tractor-trailer trucks.
- ☛ *Stand-by* techniques for *off-design* situations??
- ☛ Combination of approaches??
- ☛ Microfabrication
+
Nonlinear Dynamical Systems Theory
⇓
Interactive control

Additional Reading

1. Gad-el-Hak, M. (1989) "Flow Control," *Applied Mechanics Reviews* 42, pp. 261-293.
2. Gad-el-Hak, M. (1990) "Control of Low-Speed Airfoil Aerodynamics," *AIAA Journal* 28, pp. 1537-1552.
3. Gad-el-Hak, M., and Bushnell, D.M. (1991) "Separation Control: Review," *Journal of Fluids Engineering* 113, pp. 5-30.

I-3. Flows in Micro Systems

Chih-Ming Ho
University of California at Los Angeles

NUWC Division Newport, R. I.

SEMINAR NOTICE

FLOWS IN MICRO-SYSTEMS

Professor Chih-Ming Ho

University of California, Los Angeles

The pressure distribution of an integrated pressure-sensor/microchannel system will be presented. We will first discuss the scientific aspects of the etching technique that is used to manufacture the microsystem. Based upon the findings of the diffusion and the chemical reaction processes, a universal etching model has been established. This model can accurately predict the etching length vs. time over a wide range of HF concentrations (3-49 wt%). We then examine the pressure distributions in the channels measured by the integrated micro pressure transducers. The micro channels are one micron thick and the width ranges from five microns to forty microns. The characteristics of the transducers and the physical aspects of the pressure distributions will be discussed.

Thursday, 1 July 1993

Conference Room, Bldg. 679

Time: 10:30 AM

POC: Dr. Promode R. Bandyopadhyay (Code 8234; x2588)

FLOWS IN MICRO SYSTEMS

Ho, Chih-Ming

CMS

Center for Micro Systems

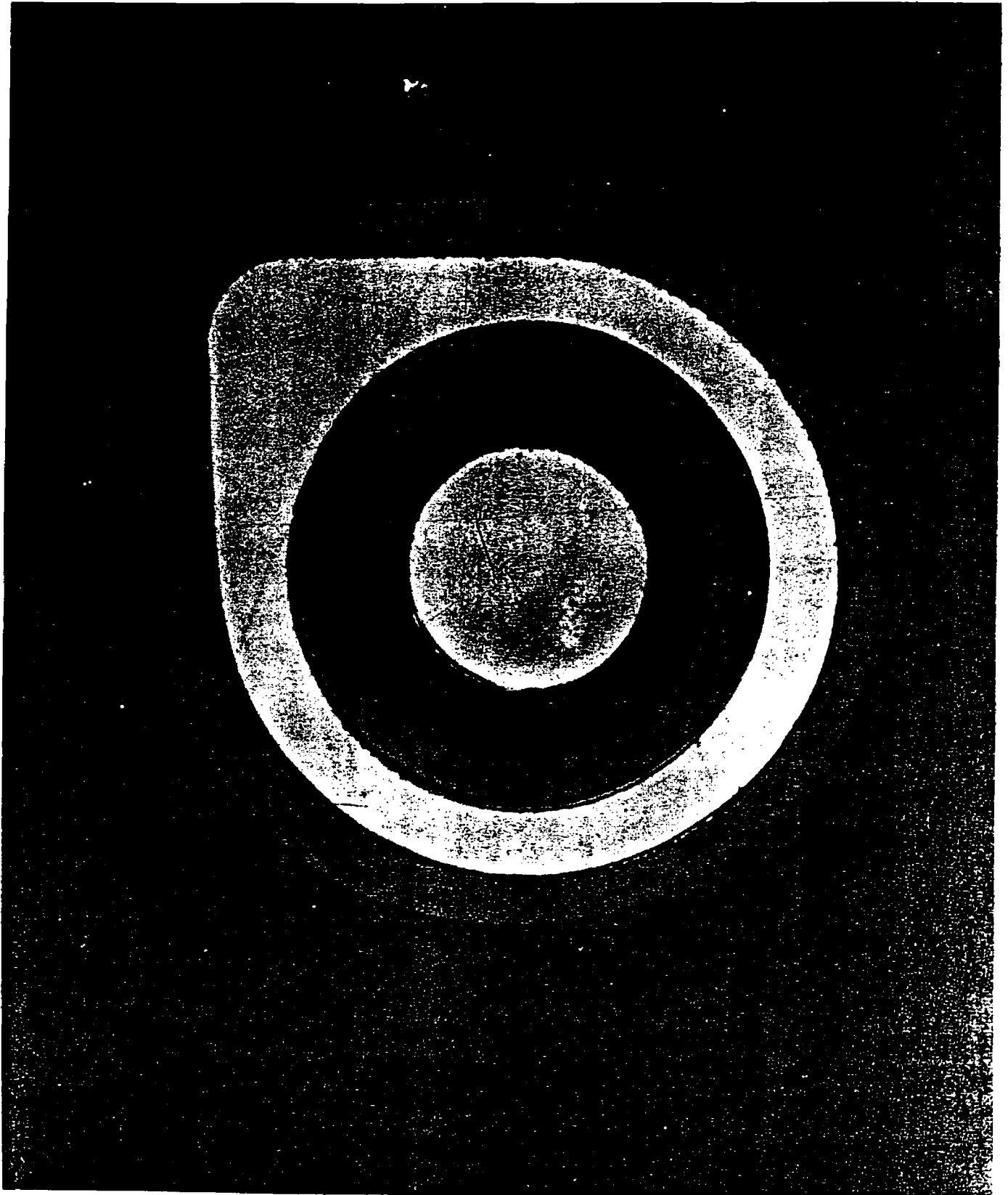
***University of California, Los Angeles
Los Angeles, California 90024***

OUTLINE

- **Motivation**
- **Manufacturing Process**
- **Experimental Method**
- **Diffusion and Chemistry**
- **General Etching Model**
- **Pressure Drop in Micro Channel**

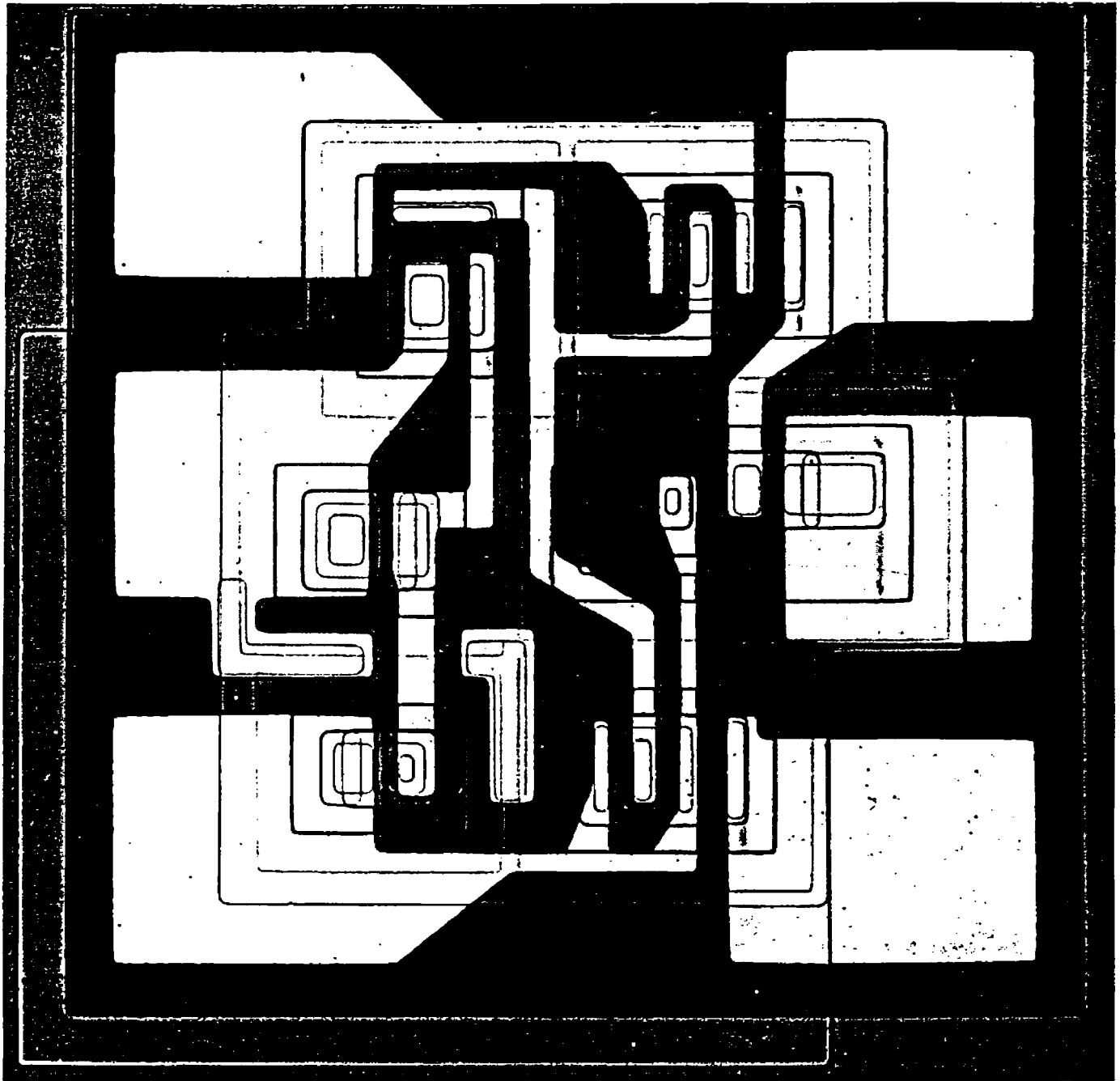
1959

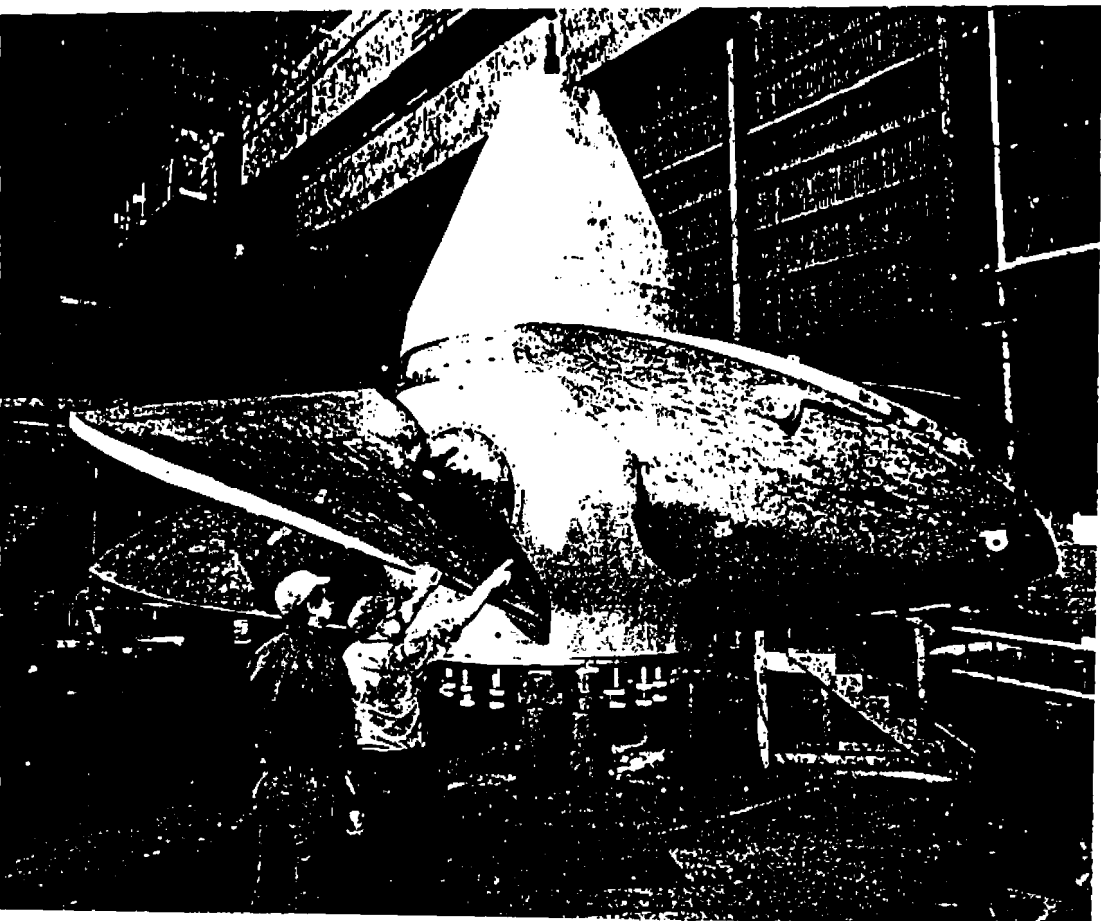
THE FIRST PLANAR TRANSISTOR—A
TEARDROP DEVICE WHICH MARKED THE BEGINNING OF
AN INDUSTRY REVOLUTION.



1964

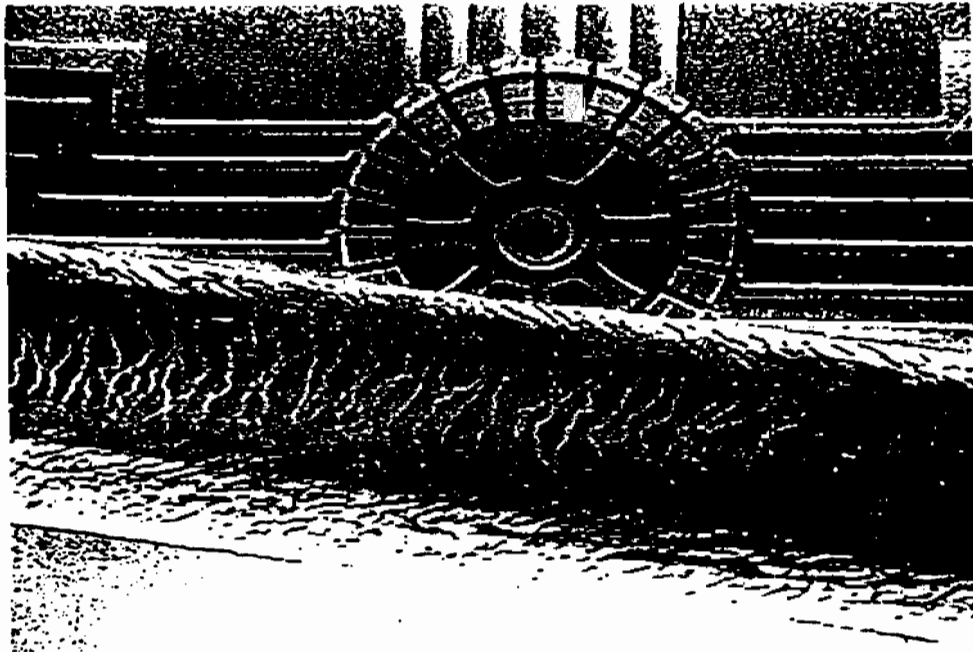
THE FIRST CONSUMER-ORIENTED LINEAR INTEGRATED
CIRCUIT IN THE WORLD.





1988

MICRO MOTOR



We are witnessing another industrial revolution.

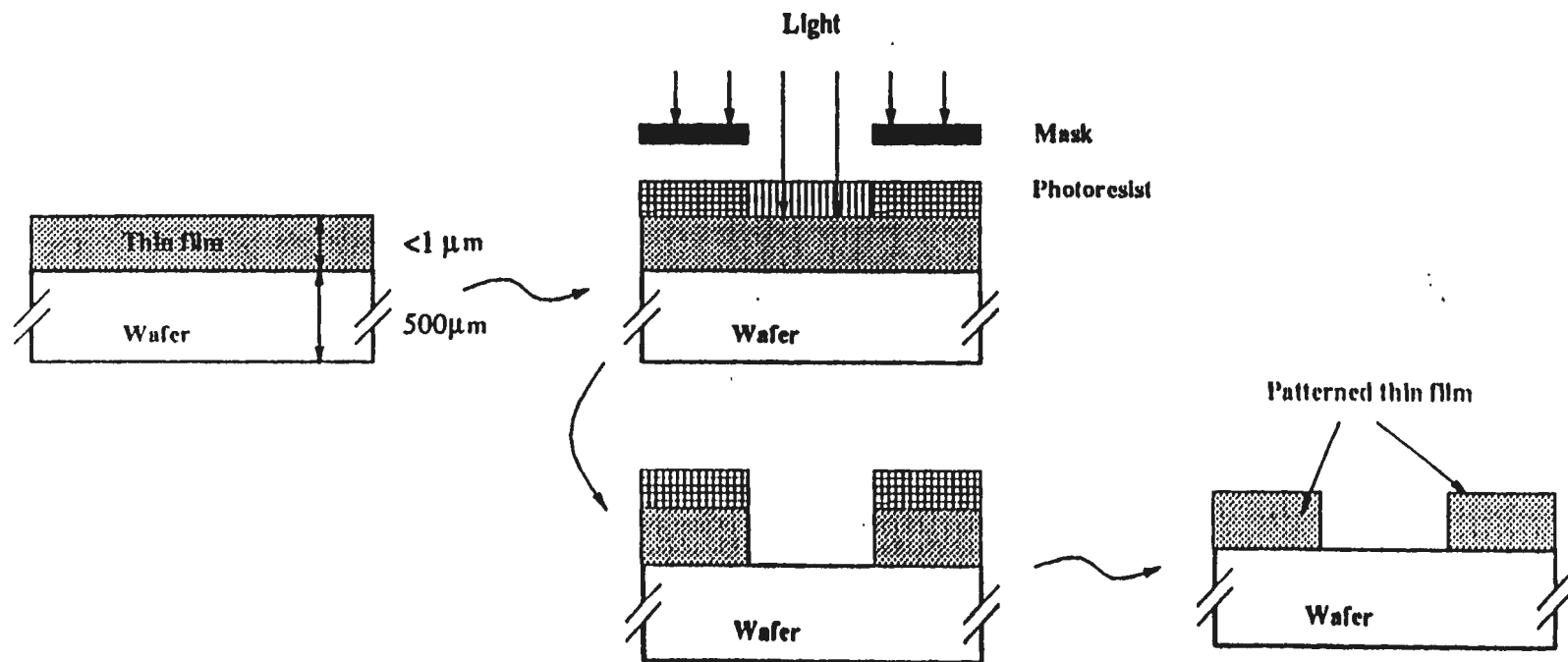
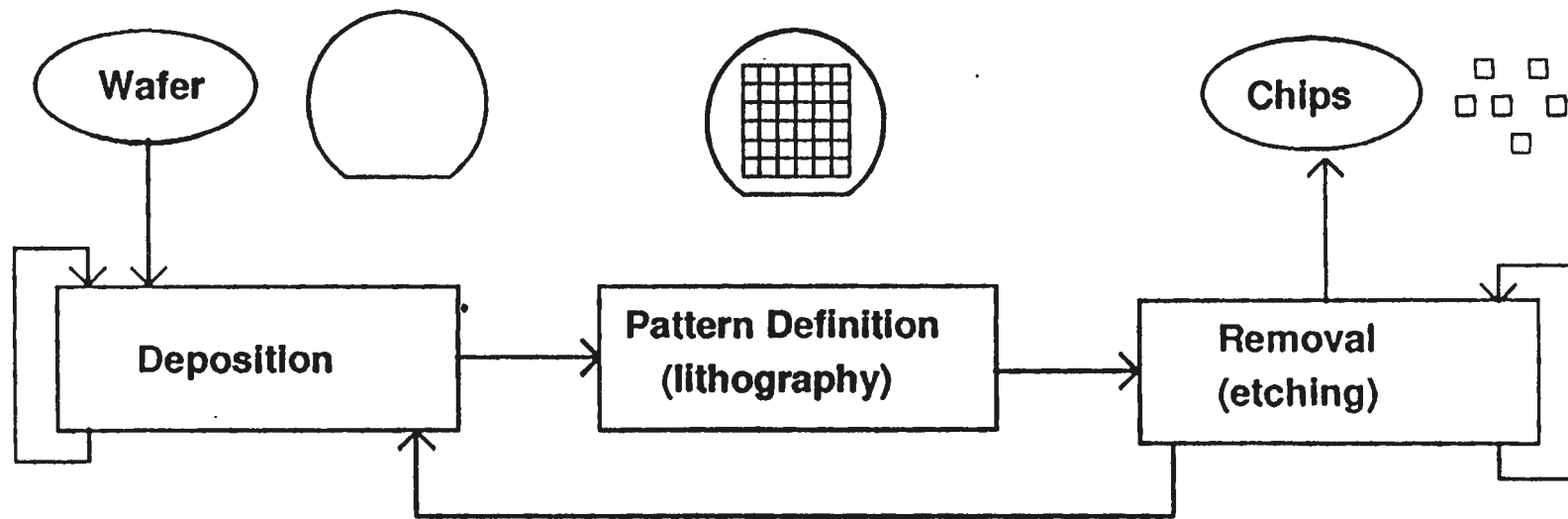
APPLICATIONS

SENSOR AND ACTUATOR

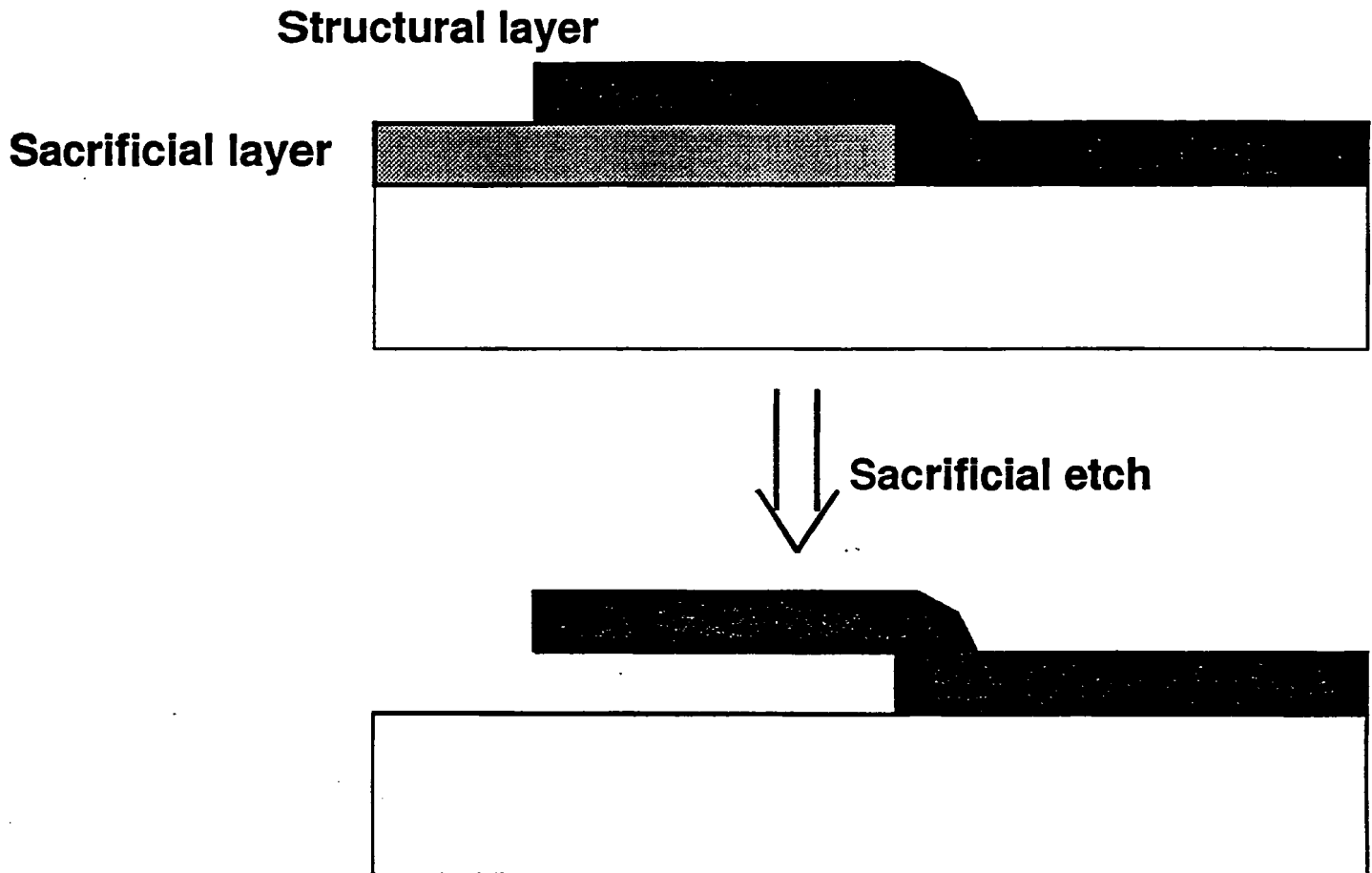
- | | |
|--------------------------------|------------------------------------|
| # Micro Prosthetic Devices | # Microvalves and Pumps |
| # Biomedical "Smart Pills" | # Optical Fiber Connectors |
| # Biological Tissue Connectors | # Microfilters |
| # Biological Micromanipulators | # Micro Spacecraft |
| # Catheter-Based Tools | # Micro Electrode Arrays |
| # Microsurgical Tools | # Electric Switches and Relays |
| # Clean Room Instrument | # Microelectromechanical Muscle |
| # Micro Optical Benches | # Electromechanical Memories |
| # Micro Light Modulators | # Miniature Printer Mechanisms |
| # Force-Balanced Transducers | # Ultra-Precise Positioning Device |

SCIENCE ISSUES

- **Length Scale**
- **Time Scale**
- **Surface Force *vs* Body Force**
- **Material Properties**
- **.....**



"Sacrificial" Etching



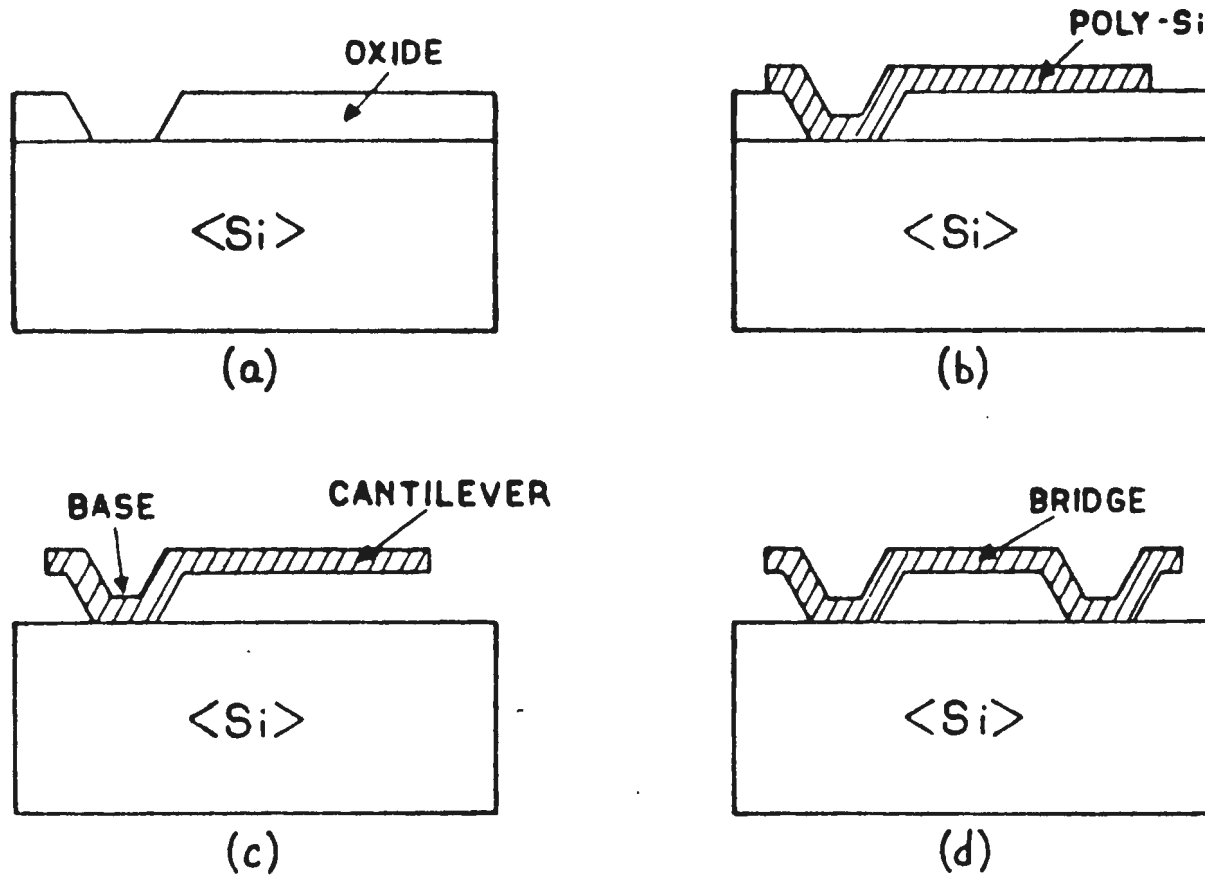
Sacrificial layer: Silicon Dioxide

Structural layer: Polycrystalline Silicon

Etchant: Hydrofluoric Acid

Selectivity: > 1000:1

POLYSILICON MICROBEAM TECHNOLOGY



(R.T. Howe and R.S. Muller, *J. Electrochem. Soc.*, 1983)

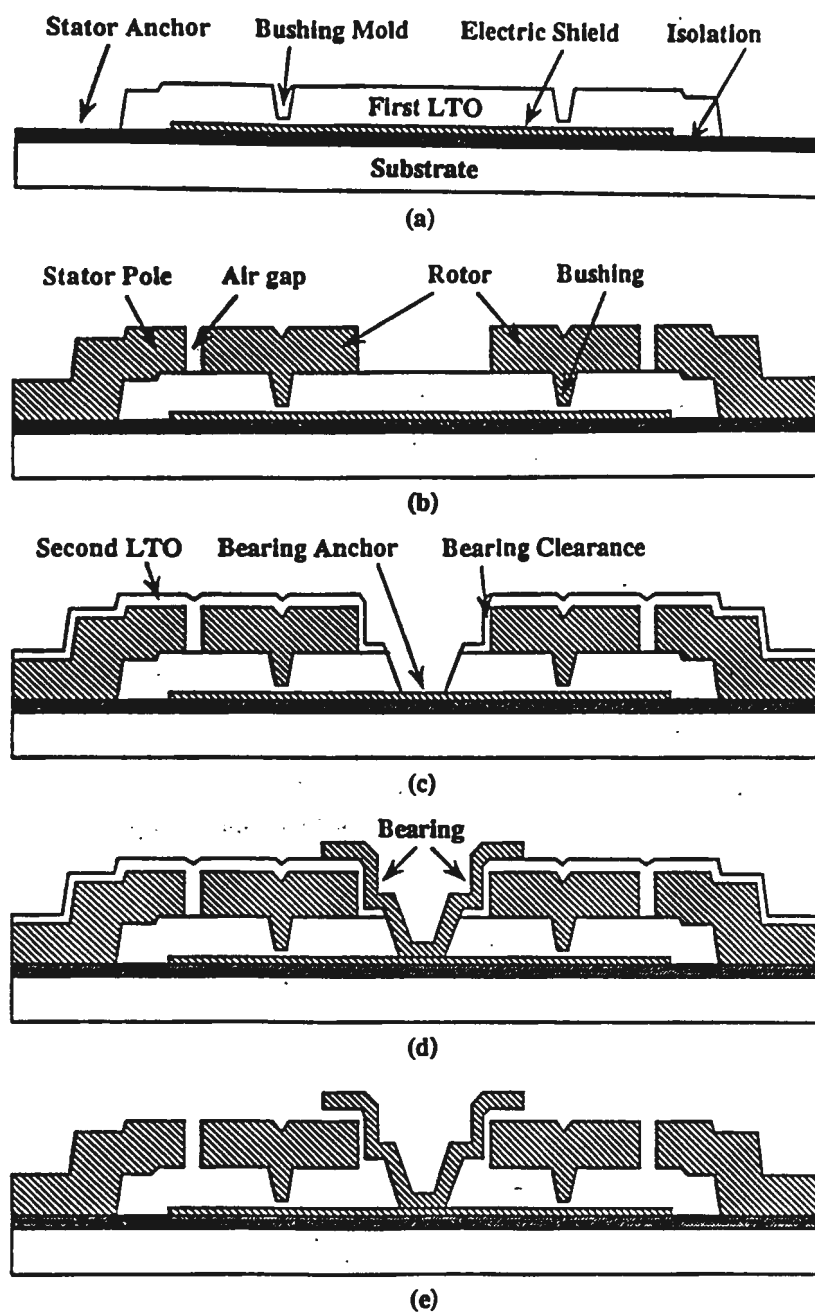
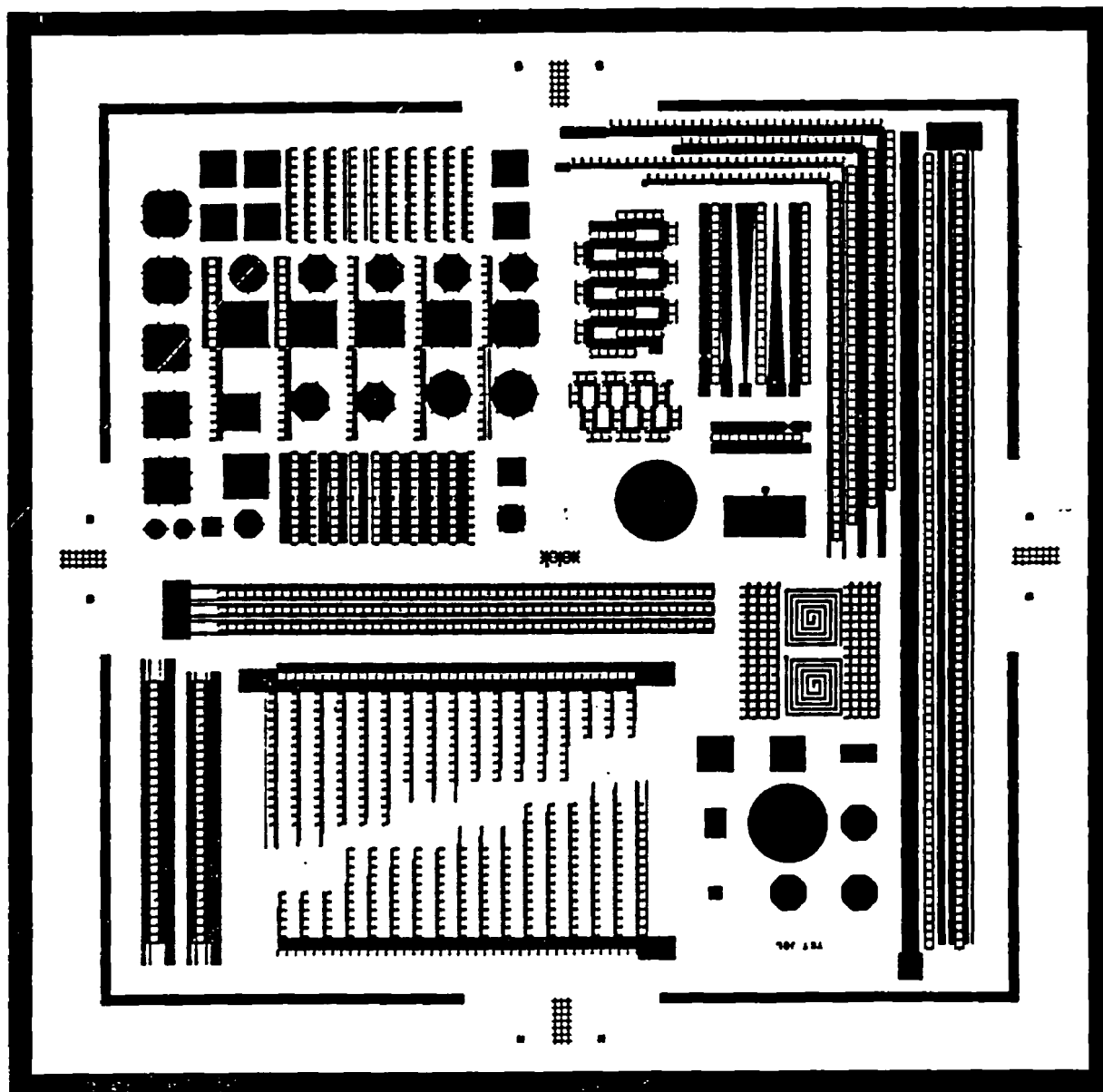


Fig. 6. Micromotor fabrication process: (a) After the first LTO; (b) after the rotor-stator polysilicon; (c) after the second LTO; (d) after the bearing polysilicon; and (e) released motor.



Channels

Width: $2\mu \sim 200 \mu$

Length: 3000μ

Thickness: $0.2 \mu \sim 1.2 \mu$

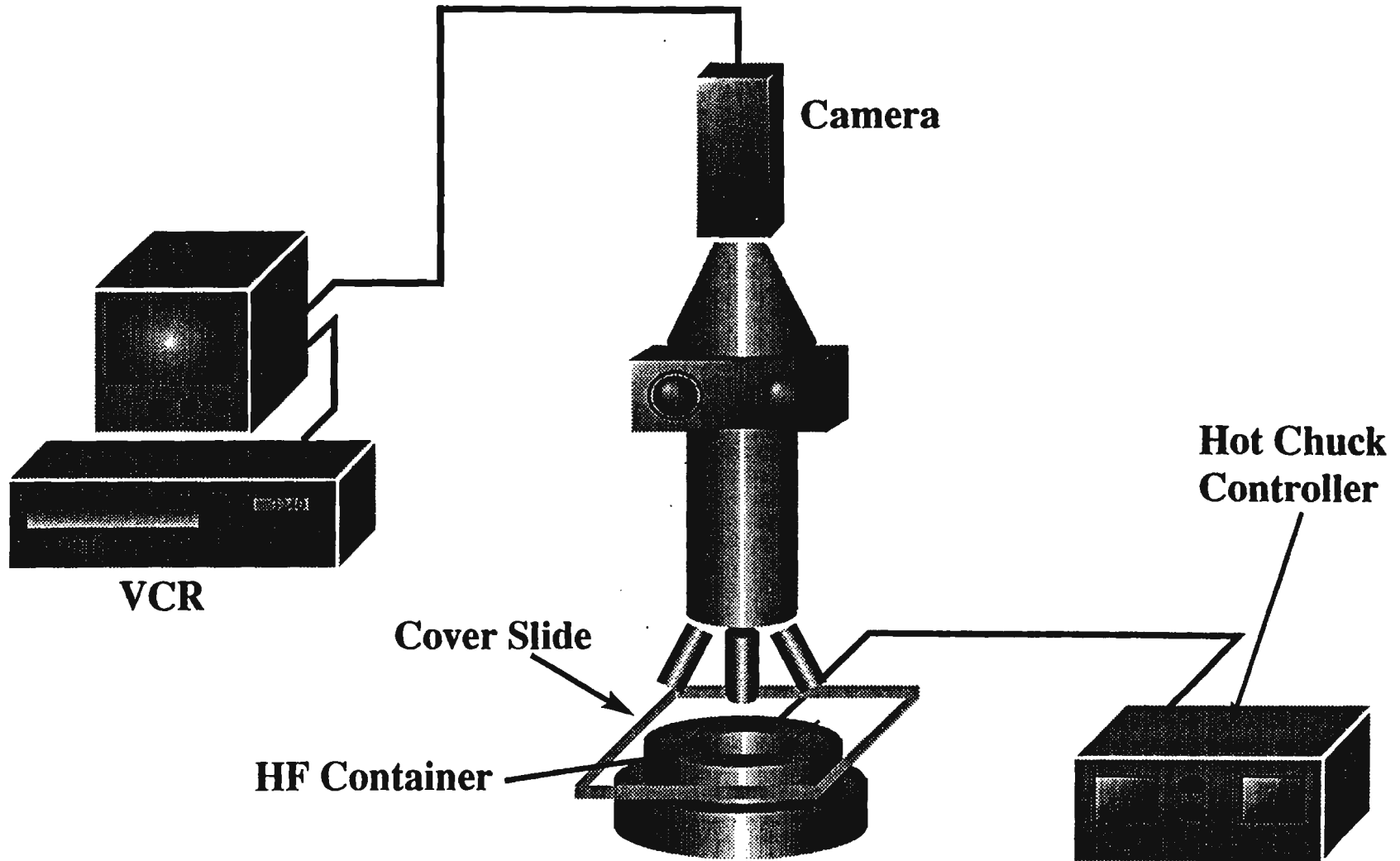
Acid

HF: $1.8\% \sim 49\%$
14 concentrations

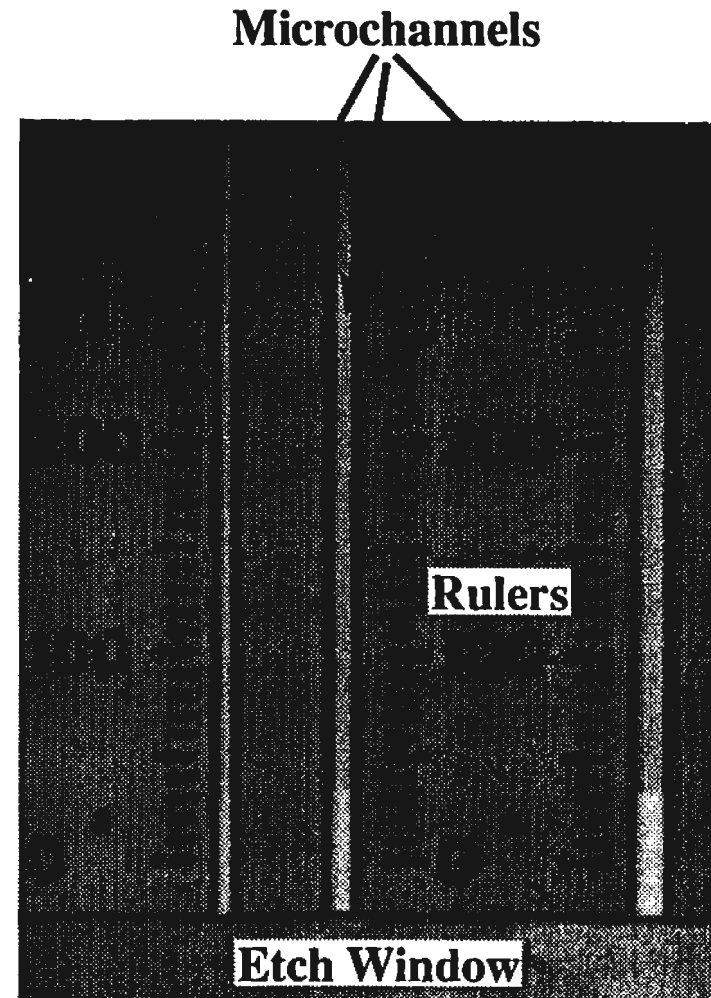
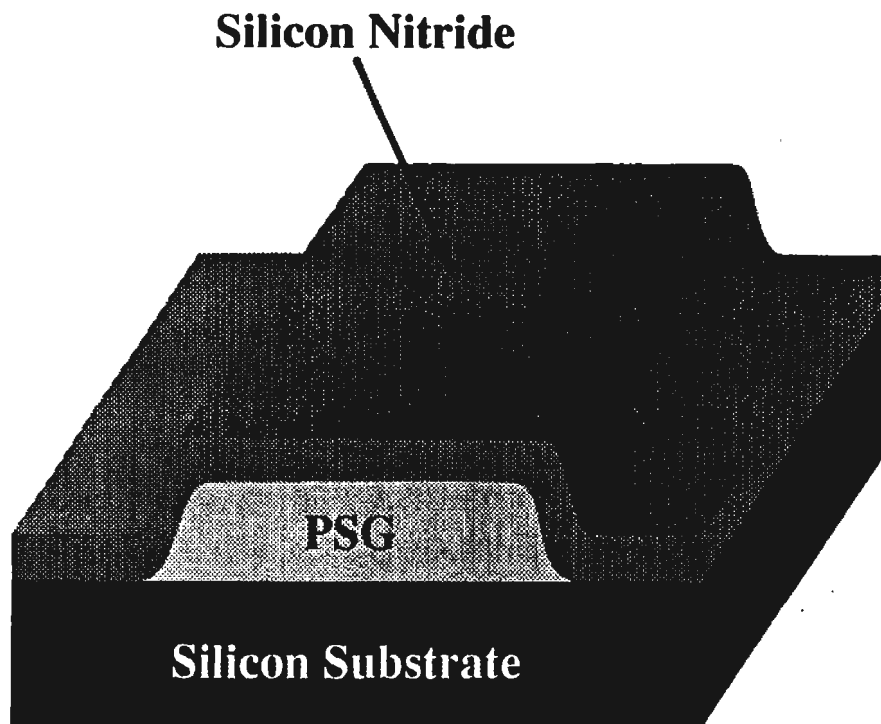
Sacrificial Material

PSG

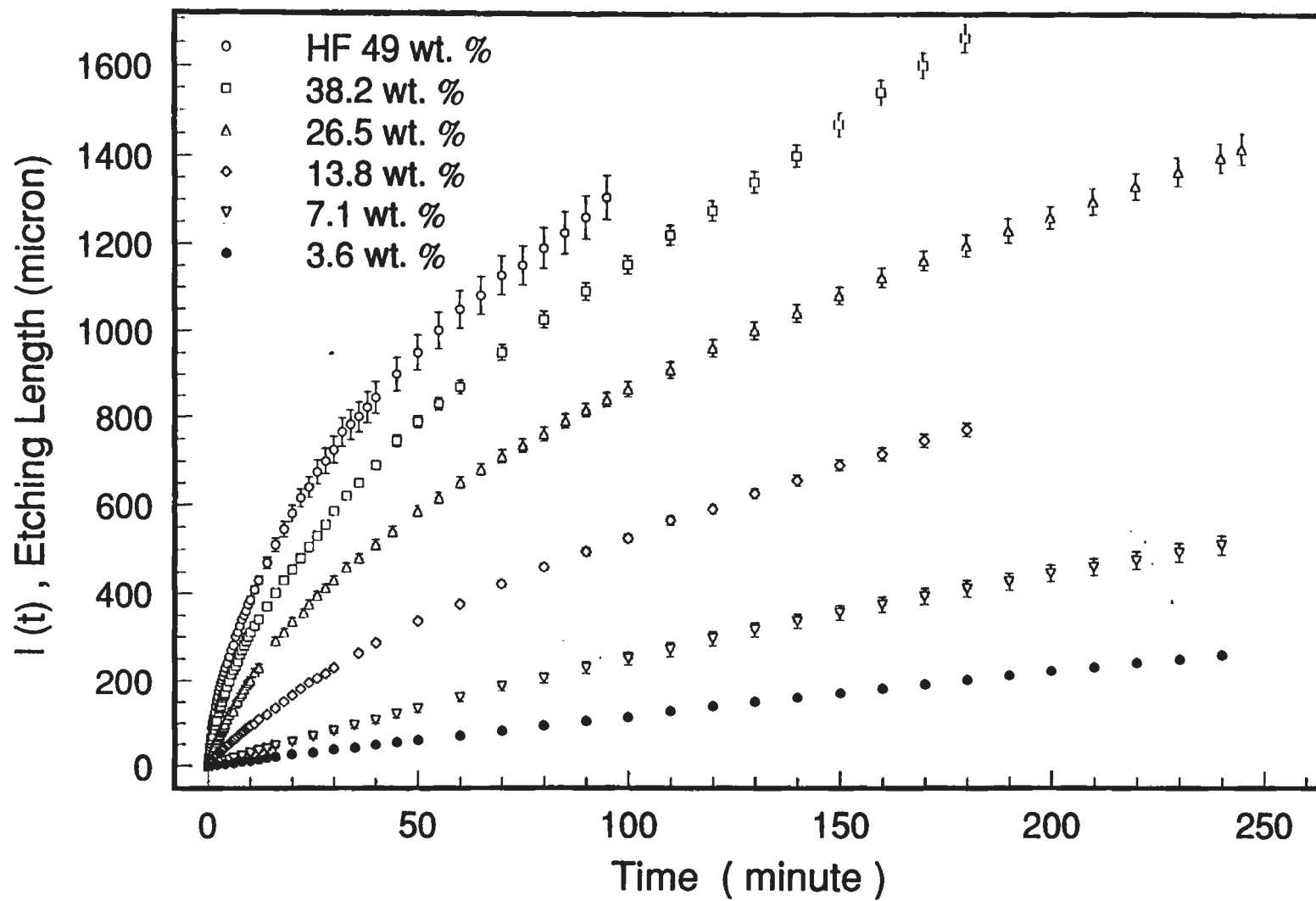
Experimental Setup



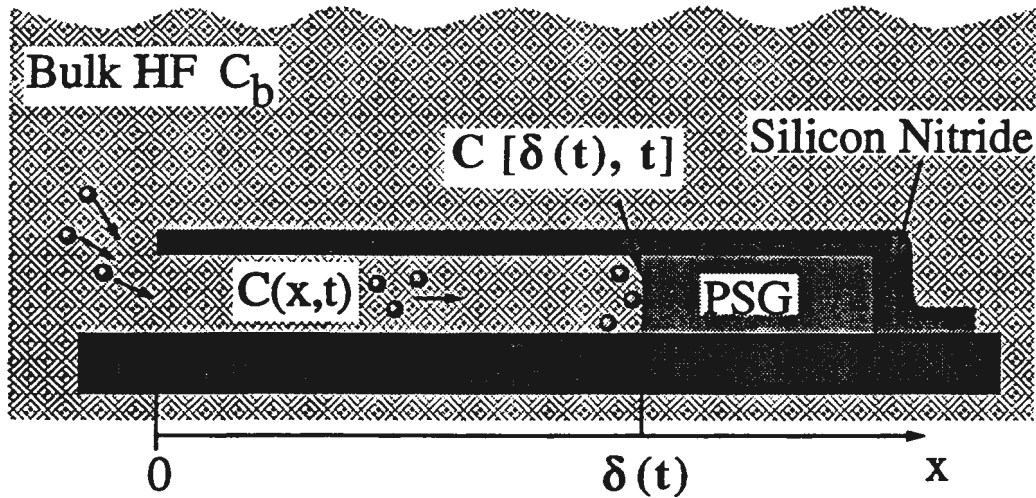
Microchannels



Data



Governing Equations



One-Dimensional Eq. of Concentration

$$\frac{\partial C(x, t)}{\partial t} + u \frac{\partial C(x, t)}{\partial x} = D \frac{\partial^2 C(x, t)}{\partial x^2}$$

B.C.

$$C[0, t] = C_b$$

$$C[\delta(t), t] = C_s \quad ???$$

Chemistry



Reaction Flux

$$J_r(\delta) = f[k, C_s(\delta)] \quad ???$$

Convective Term

$$\frac{\partial C}{\partial t} + u \frac{\partial C}{\partial x} = D \frac{\partial^2 C}{\partial x^2}$$

$$u \frac{\partial C}{\partial x} \sim U \frac{C}{\delta}$$

$$D \frac{\partial^2 C}{\partial x^2} \sim D \frac{C}{\delta^2}$$

$$\frac{u \partial C / \partial x}{D \partial^2 C / \partial x^2} \sim \frac{U \delta}{D}$$

$$U \text{ ???}$$



- Assume HF & H₂SiF₆ dissolve in H₂O
- Change of the volume of the solution = depletion of SiO₂ + production of H₂O
- Molecular Weight [MW]

H ₂ O	18 gm/mole
SiO ₂	60gm/mole
- Density

H ₂ O	1 gm/cm ³
SiO ₂	2.1gm/cm ³
- Depletion of 1 mole of SiO₂ 29cm³
 Gain 2 mole of H₂O 36cm³
- Net Volume Gain - 26%

- From δ - t diagram

$$\rightarrow d\delta/dt$$

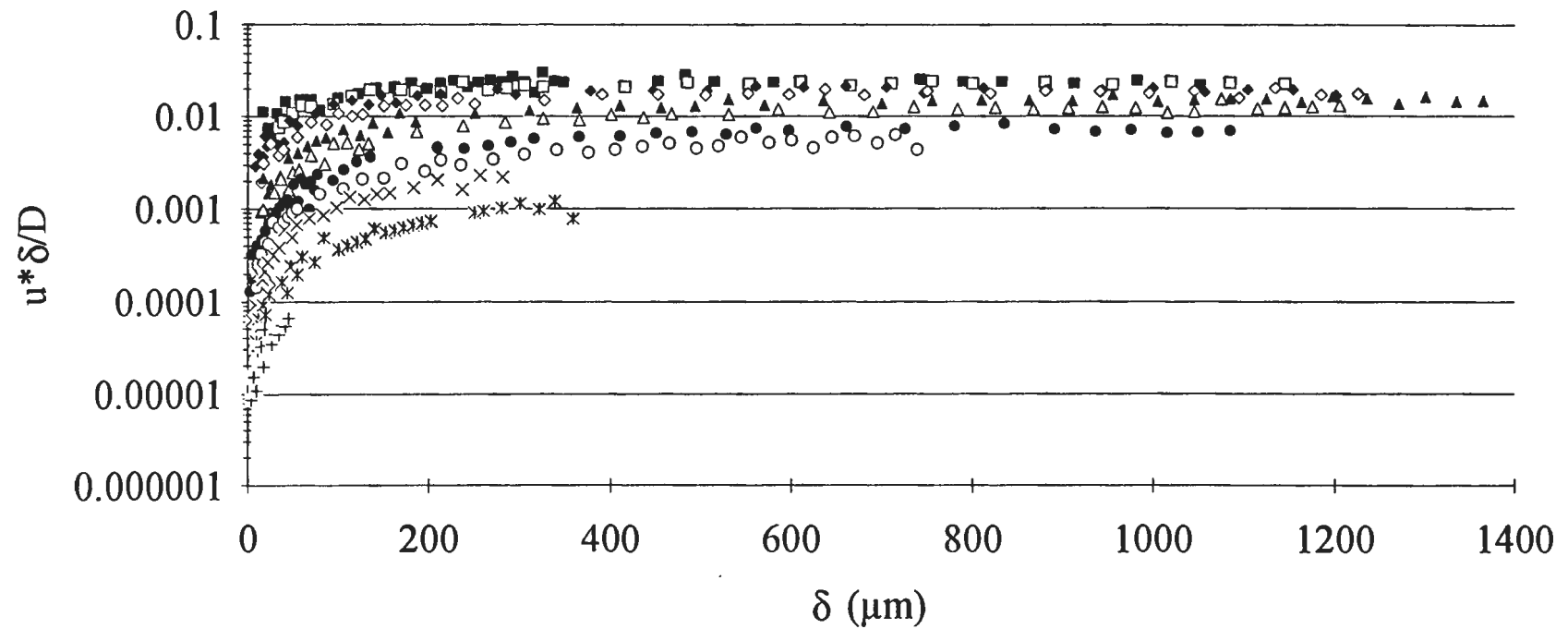
Vel. of solid/liquid interface

- $U = 0.26 d\delta / dt$

- $$\frac{u}{D} \frac{\partial C / \partial x}{\partial^2 C / \partial x^2} \sim \frac{U \delta}{D}$$

$$\sim [0.26 \delta d\delta/dt] / D$$

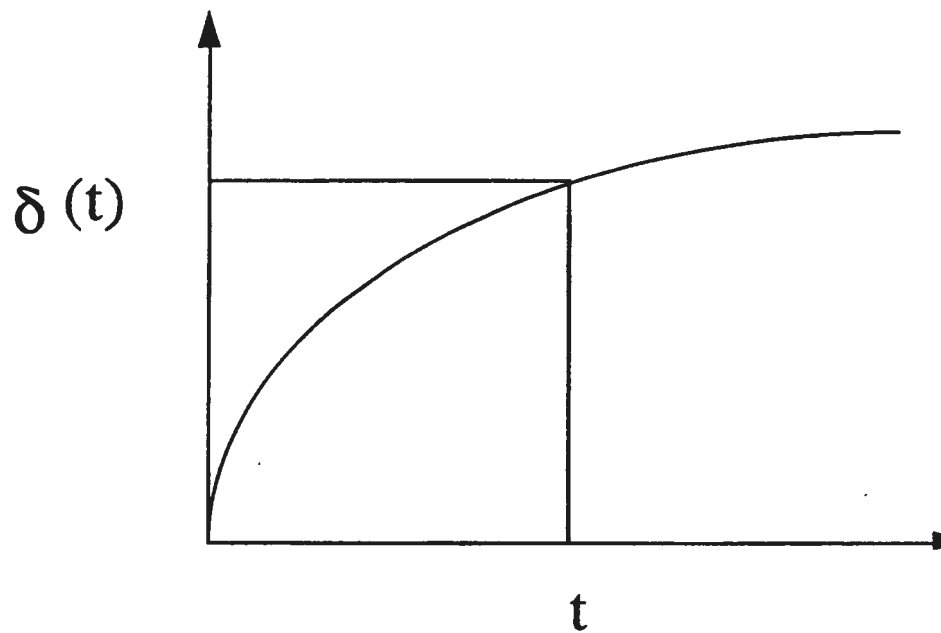
Comparison the Convection and Diffusion Terms for Different Concentration of HF



■ 49%	□ 43.5%	◆ 38.2%	◇ 32%	▲ 26.5%	△ 20%	● 13.8%	○ 10%	× 7.1%	* 3.6%	+ 1.8%
-------	---------	---------	-------	---------	-------	---------	-------	--------	--------	--------

Diffusion Eq.: $\frac{\partial C}{\partial t} = D \frac{\partial^2 C}{\partial x^2}$

Diffusion Time: $t_d = \delta^2(t) / D$

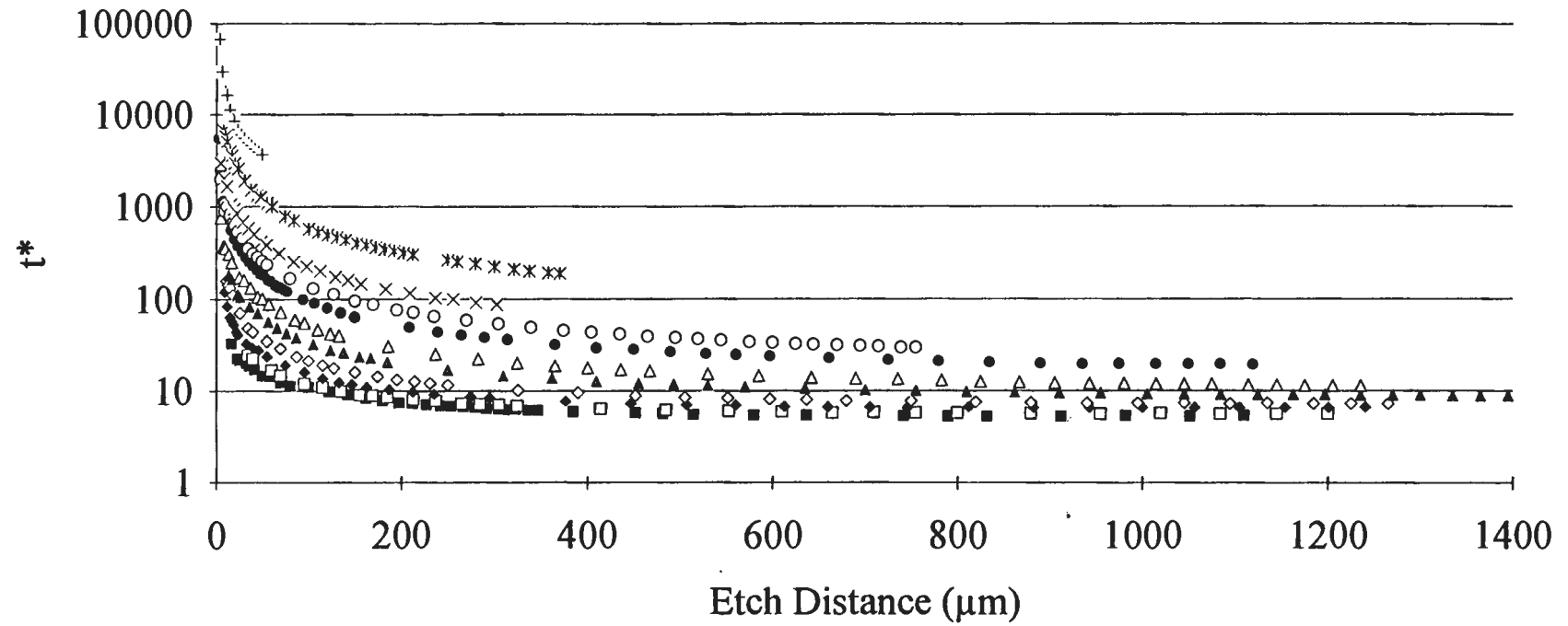


Etching Time : t

Ratio between etching time and
diffusion time:

$$t^* = t / t_d$$

Nondimensional Time Scale VS Etch Distance for Different Concentration of HF



■ 49.0% □ 43.5% ◆ 38.2% ◇ 32.0% ▲ 26.5% △ 20.0% ● 13.8% ○ 10.0% × 7.1% * 3.6% + 1.8%

Summary

- **Small convective term**

$$\frac{\partial C}{\partial t} = D \frac{\partial^2 C}{\partial x^2}$$

- **$t / t_d \gg 1$**

Concentration

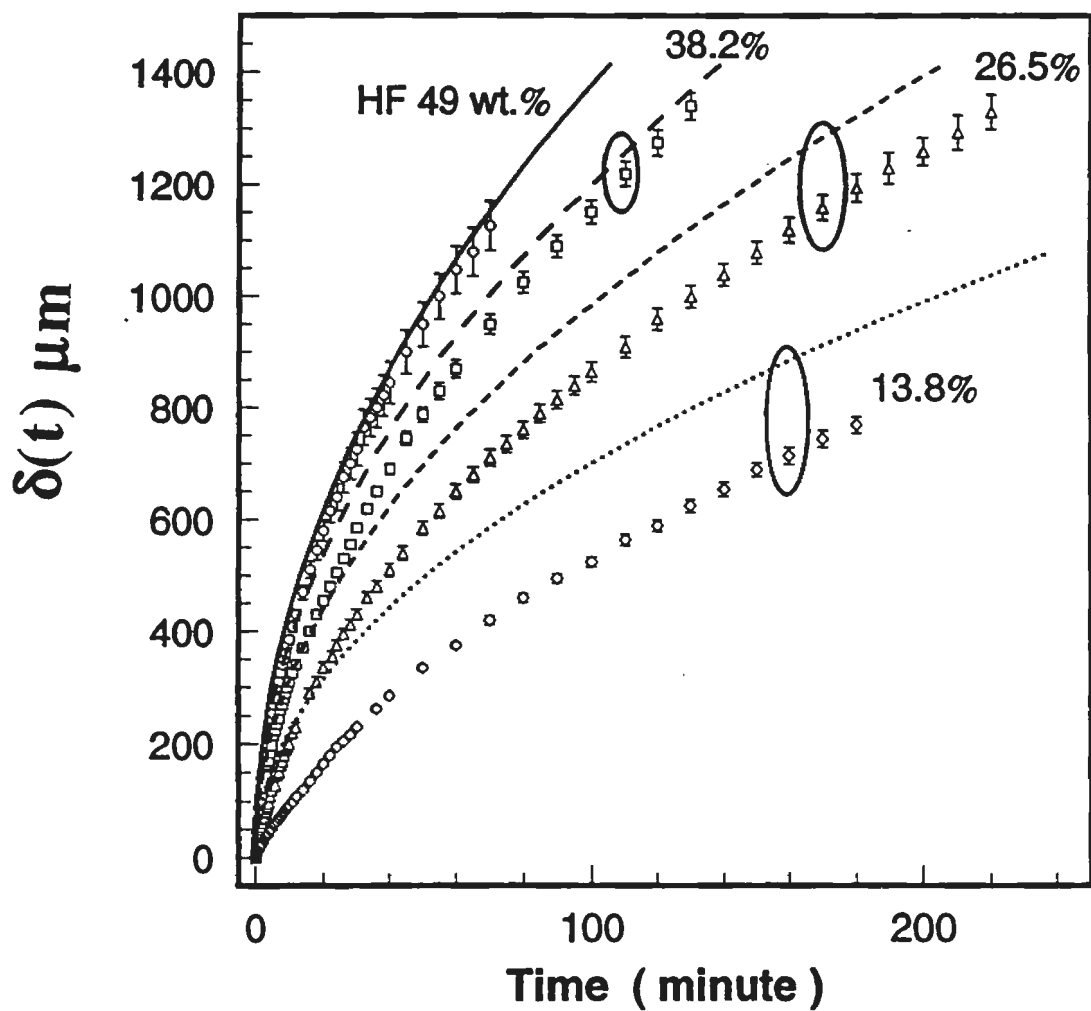
\Rightarrow linear distribution in x

Chemistry

Fast Reaction - Infinite Reaction Rate

$$C_S = 0$$

Diffusion Limited



Chemical Reaction

Reaction Flux

$$J_r(\delta) = f[k, C_s(\delta)]$$

Etching Rate

$$d\delta / dt \sim J_{SiO_2}$$

$$\begin{aligned} \frac{d\delta}{dt} &= \frac{[MW]_{SiO_2}}{\rho_{SiO_2}} J_{SiO_2} \\ &= \frac{3[MW]_{HF}}{\rho_{SiO_2}} \frac{J_{HF}}{6} \end{aligned}$$

$$\sim f[k, C_s(\delta)] \quad C_s(\delta) ???$$

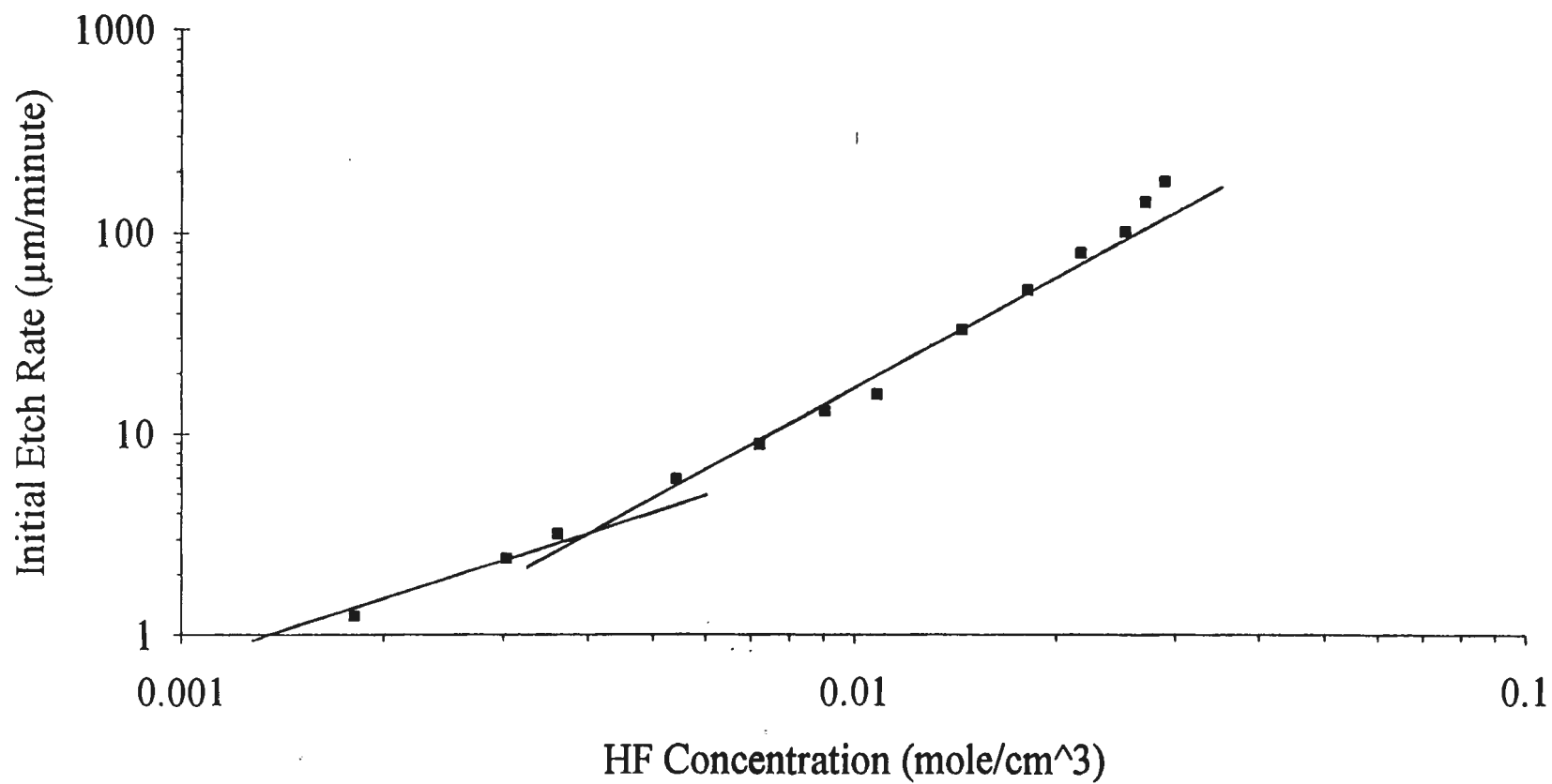
Initial Etching Rate

$$t \rightarrow 0 \quad \delta \rightarrow 0$$

$$C_s(\delta) \rightarrow C_b$$

$$d\delta / dt]_{init.} \sim f[k, C_b]$$

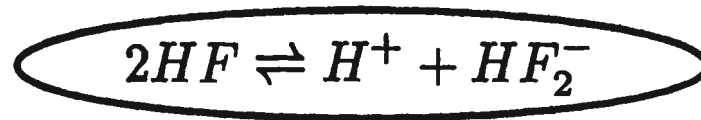
Initial Etch Rate VS Concentration



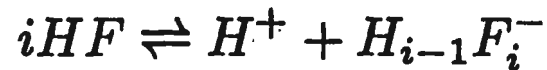
$$d\delta / dt]_{init.} \sim k_1 C_b + k_2 C_b^2$$

Chemical Reactions

HF Equilibria :



... ..



Rate Law : (Judge, 1971)

$$-r = A[HF] + \frac{B[HF_2^-]}{C}$$

$$\approx k_1[HF] + \frac{k_2[HF]^2}{C}$$

Reaction Flux at δ

$$J_r(\delta) = f[k, C_s(\delta)] = k_1 C_s(\delta) + k_2 C_s(\delta)^2$$

Diffusion Flux at δ

$$\begin{aligned} J_d(\delta) &= -D \, dC(x) / dx \\ &= D[C_b - C_s(\delta)] / \delta \quad - \quad \text{linear distribution} \end{aligned}$$

$$J_r(\delta) = J_d(\delta) = J_{HF}(\delta) \text{ at } \delta \quad \& \quad \text{Eliminating } C_s$$

$$J_{HF}(\delta) = \frac{1}{2k_2} \left(\frac{D}{\delta} \right)^2 \left(1 + b \left(\frac{\delta}{D} \right) - \varphi \right)$$

$$\text{where } b = k_1 + 2C_b k_2 \qquad \varphi = \sqrt{1 + 2b \left(\frac{\delta}{D} \right) + k_1^2 \left(\frac{\delta}{D} \right)^2}$$

$$\frac{d\delta}{dt} = \frac{3[\text{MW}]_{\text{HF}}}{\rho_{\text{SiO}_2}} \frac{J_{\text{HF}}}{6}$$

$$= a \left(\frac{D}{\delta} \right)^2 \left(1 + b \left(\frac{\delta}{D} \right) - \phi \right)$$

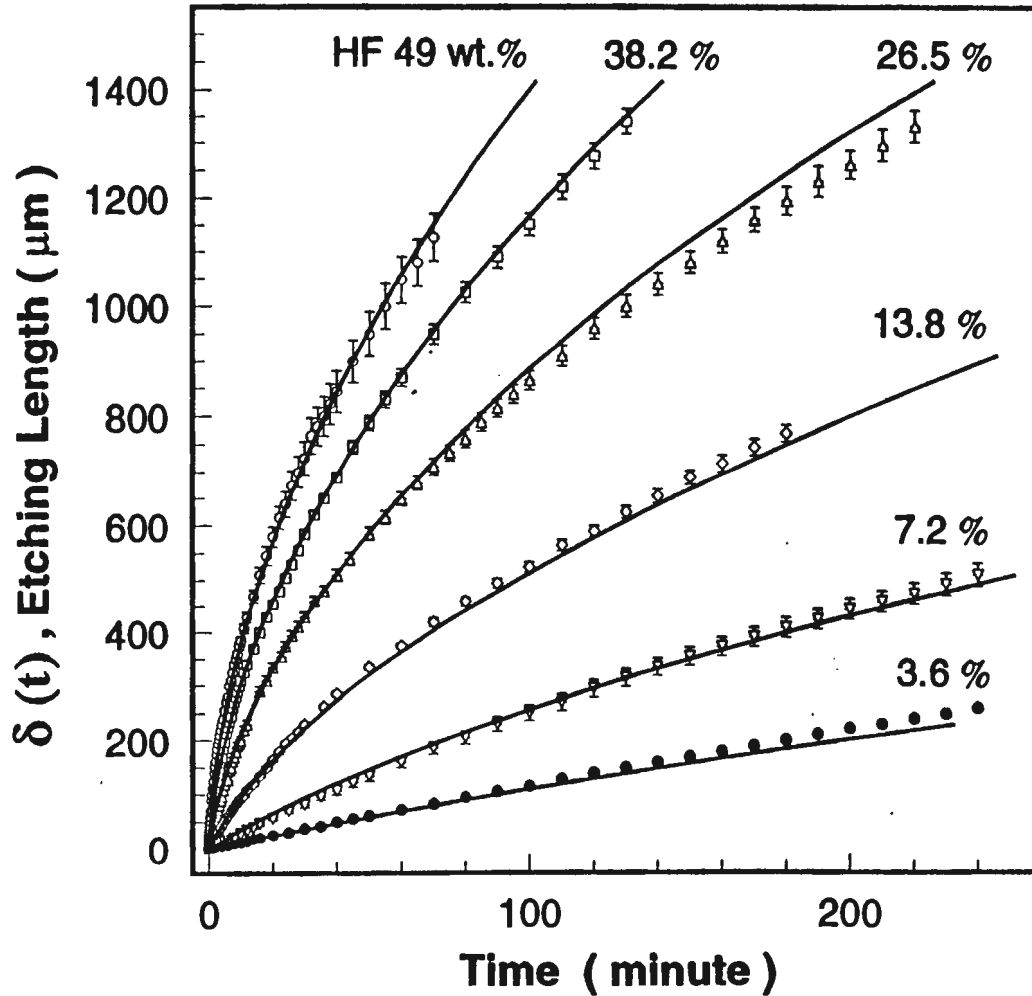
Solving t in terms of δ

$$t = \frac{D \{ \phi \phi + 2k_1^2 \left(\frac{\delta}{d} \right) + [k_1^2 \left(\frac{\delta}{d} \right)^2 - 1] \}}{8aC_b k_1^2 k_2 (k_1 + C_b k_2)} - \frac{D}{2ak_1^3} \log \left[\frac{\phi + k_1 \phi}{2(k_1 + C_b k_2)} \right]$$

where $\phi = k_1 + 2C_b k_2 + k_1^2 \left(\frac{\delta}{D} \right)$

$$a = \{ \text{MW} \}_{\text{HF}} / 4\rho_{\text{SiO}_2} k_2$$

First-and-Second Order Model



Assumptions :

- $J_{[\text{HF}]} = k_1 C_s + k_2 C_s^2$
- $dC(x) / dx = [C_b - C_s(\delta)] / \delta(t)$

Results :

$$D = 1.6 \times 10^{-5} \text{ cm}^2 / \text{s}$$

$$k_1 = 1.2 \times 10^{-4} \text{ cm} / \text{s}$$

$$k_2 = 6.5 \times 10^{-2} \text{ cm}^4 / \text{mole s}$$

Reaction Flux at δ

$$J_r(\delta) = f[k, C_s(\delta)] = k_1 C_s(\delta) + k_2 C_s(\delta)^2$$

Diffusion Flux at δ

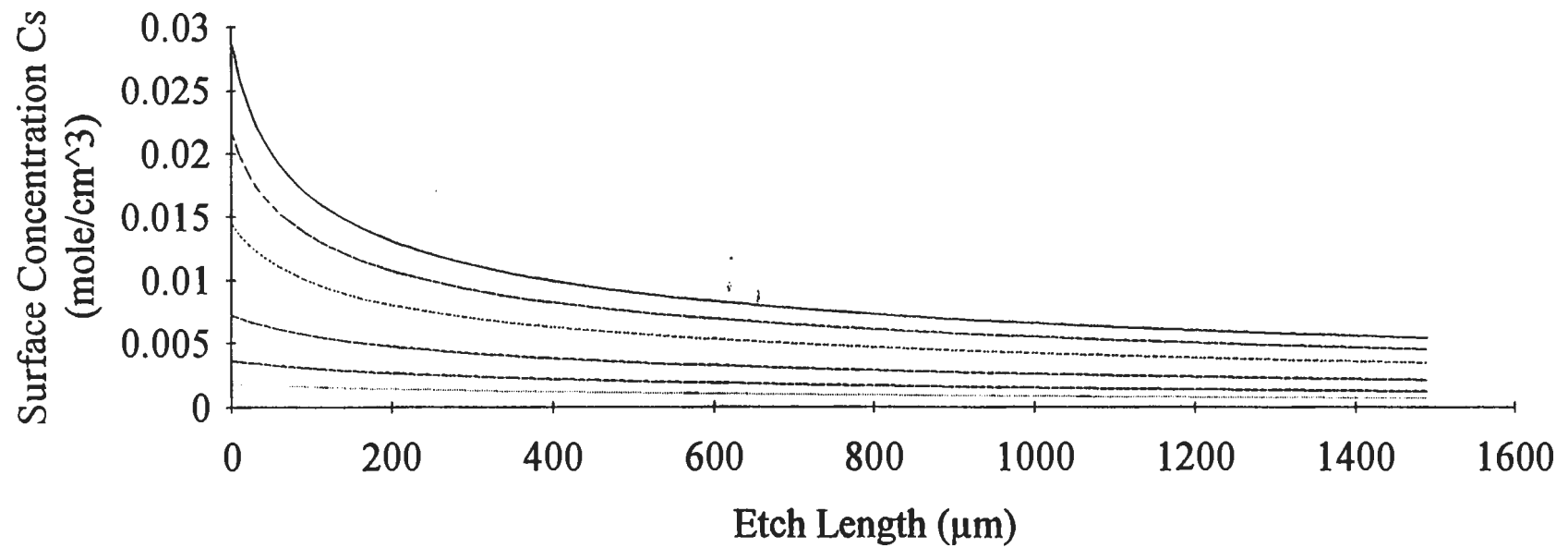
$$J_d(\delta) = D[C_b - C_s(\delta)] / \delta \quad - \quad \text{linear distribution}$$

$$J_r(\delta) = J_d(\delta) \text{ at } \delta \quad \& \quad \text{Solving } C_s(\delta)$$

Surface Concentration

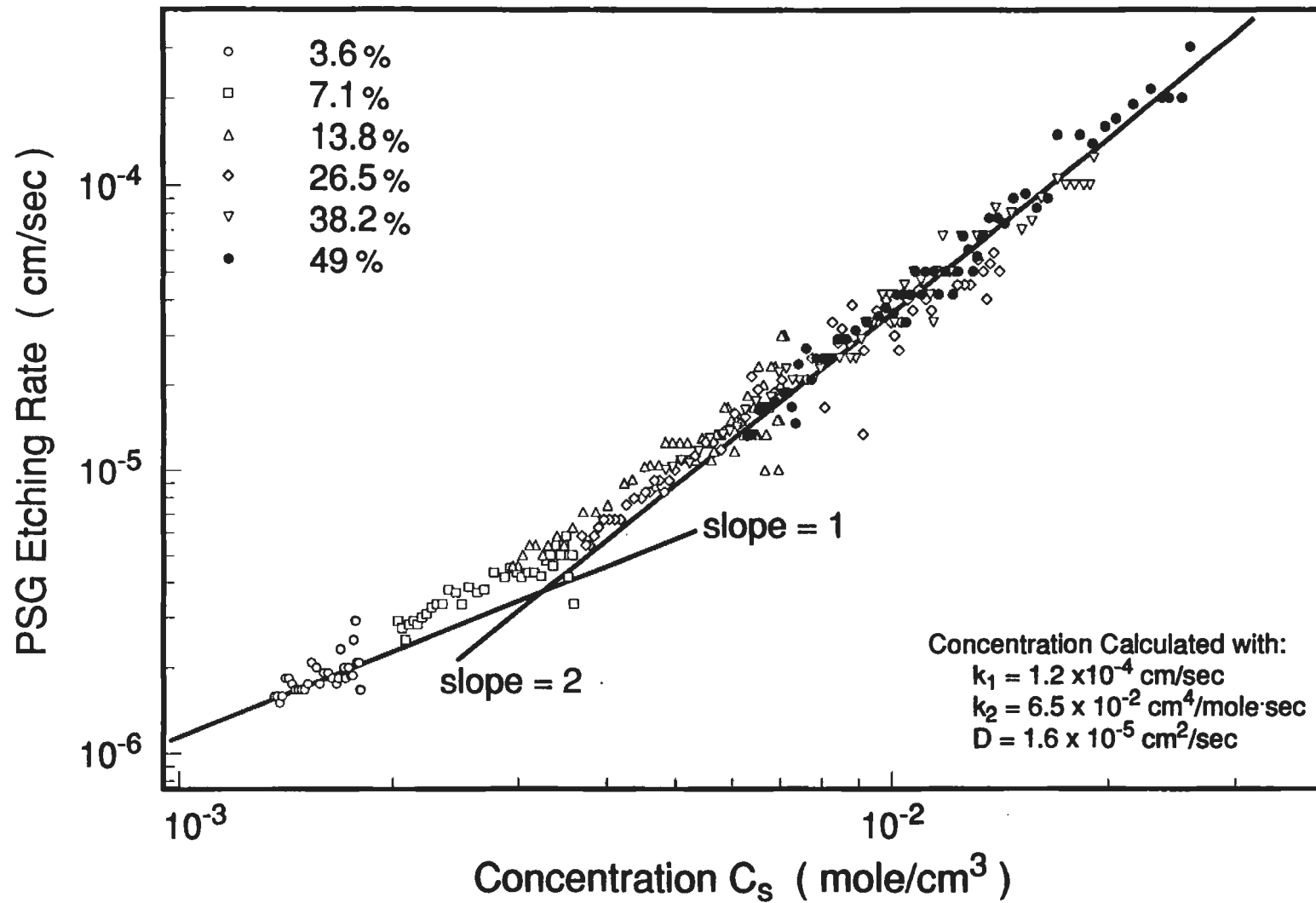
$$C_s^2(\delta) + \left(\frac{k_1}{k_2} + \frac{D}{k_2 \delta} \right) C_s(\delta) - \frac{D C_b}{k_2 \delta} = 0$$

Surface Concentration VS Etch Length



HF 3.6% HF 7.1% HF 13.8% HF 26.5% HF 38.2% HF 49%

$$d\delta /dt \sim k_1 C_s(\delta) + k_2 C_s(\delta)^2$$

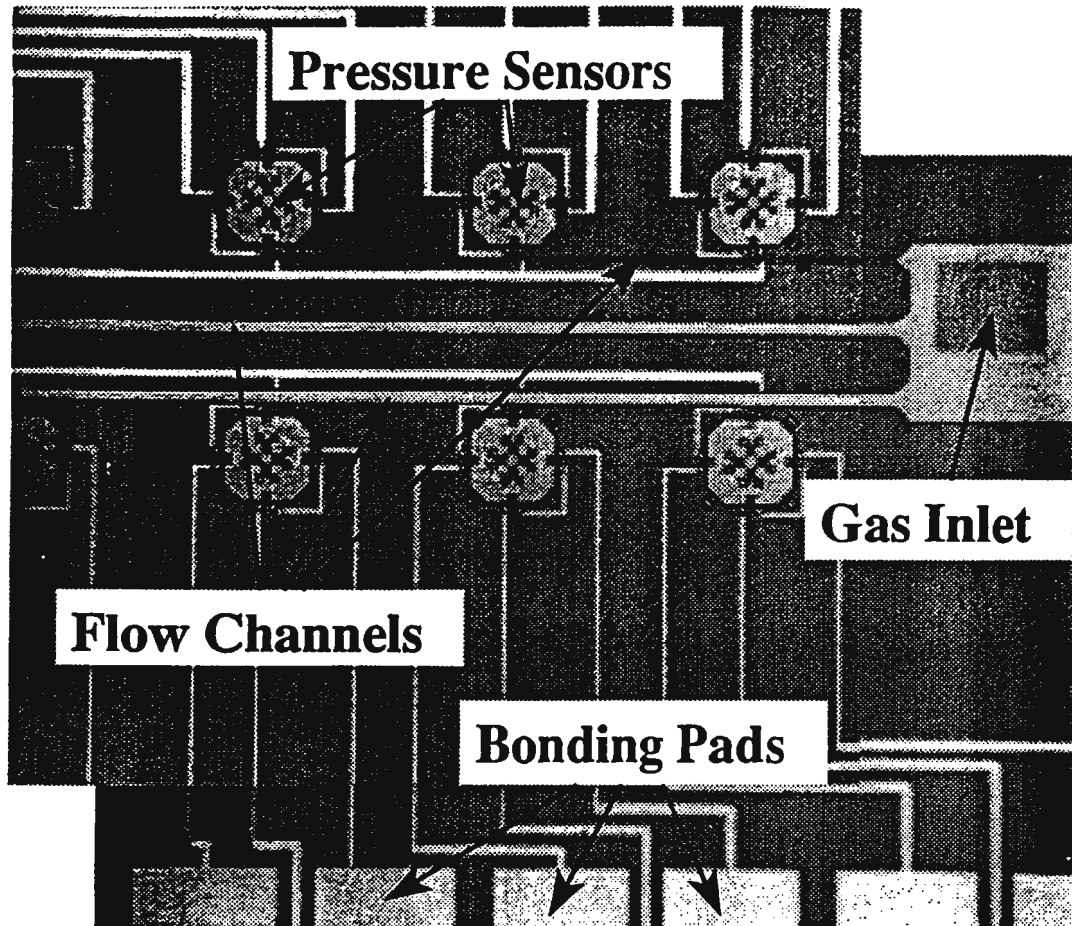


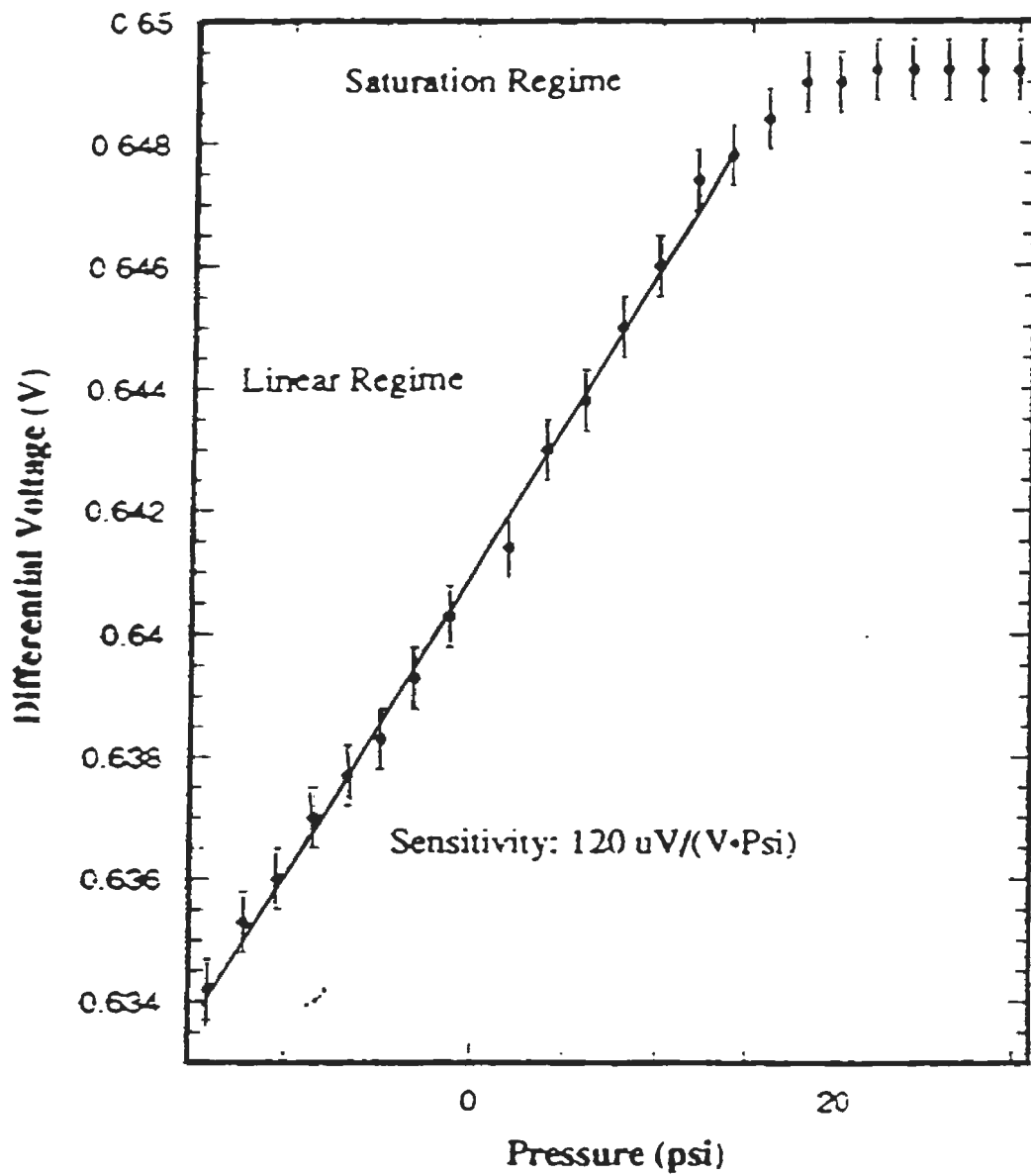
SUMMARY

- **Diffusion**
 - * **Convection Effect $\rightarrow 0$**
 - * **Concentration $|_{HF} \sim x$**
 - * **Asymptotic $d\delta/dt$**
 - **Diffusion limited**
- **Chemistry**
 - * **$k_1 C_s(\delta) + k_2 C_s(\delta)^2$**
 - * **Initial $d\delta/dt$**
 - **Reaction rate limited**
- **Collapse all $d\delta/dt$ with $C_s(\delta)$**

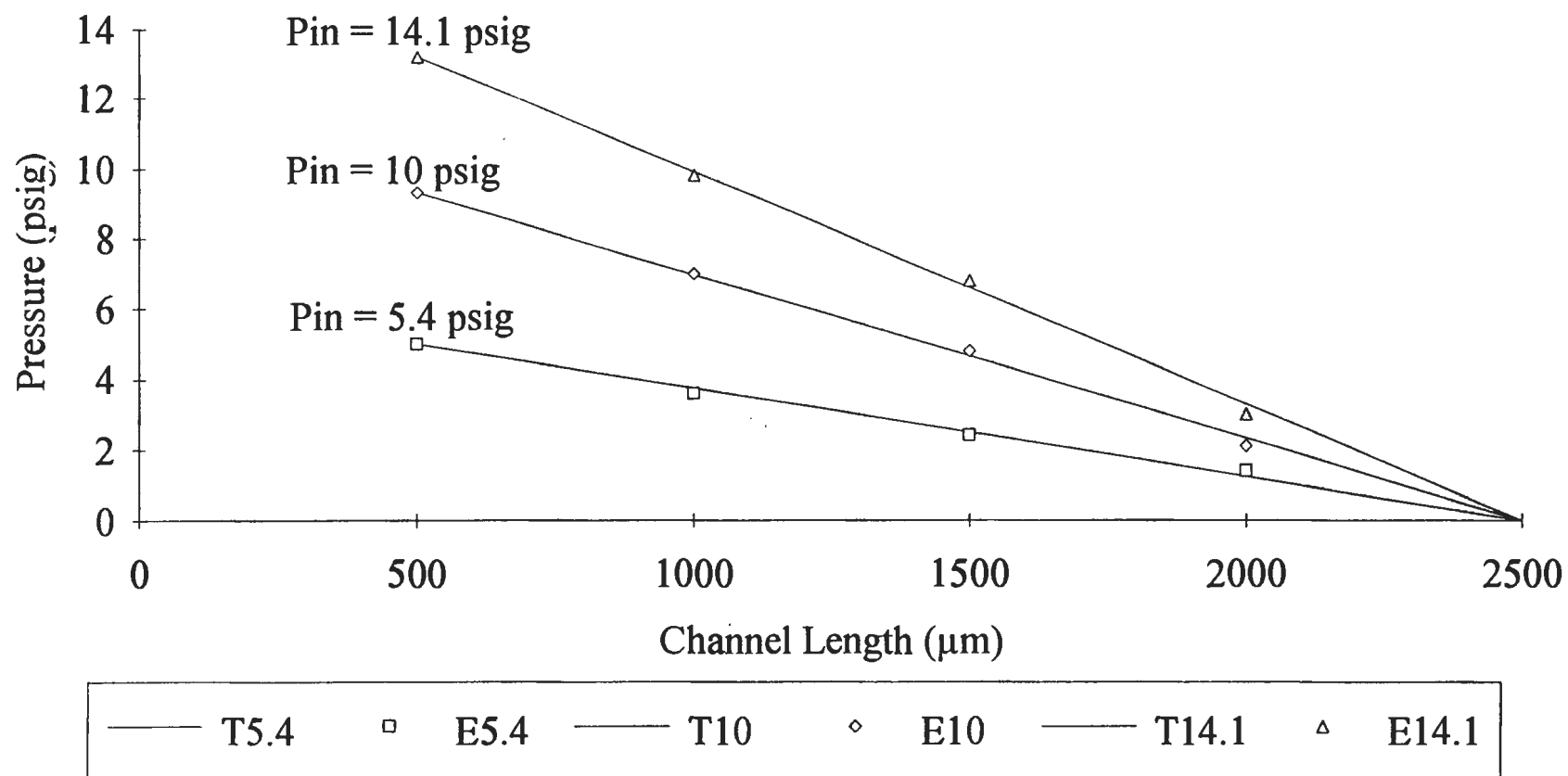
PRESSURE DROP IN RECTANGULAR CHANNELS

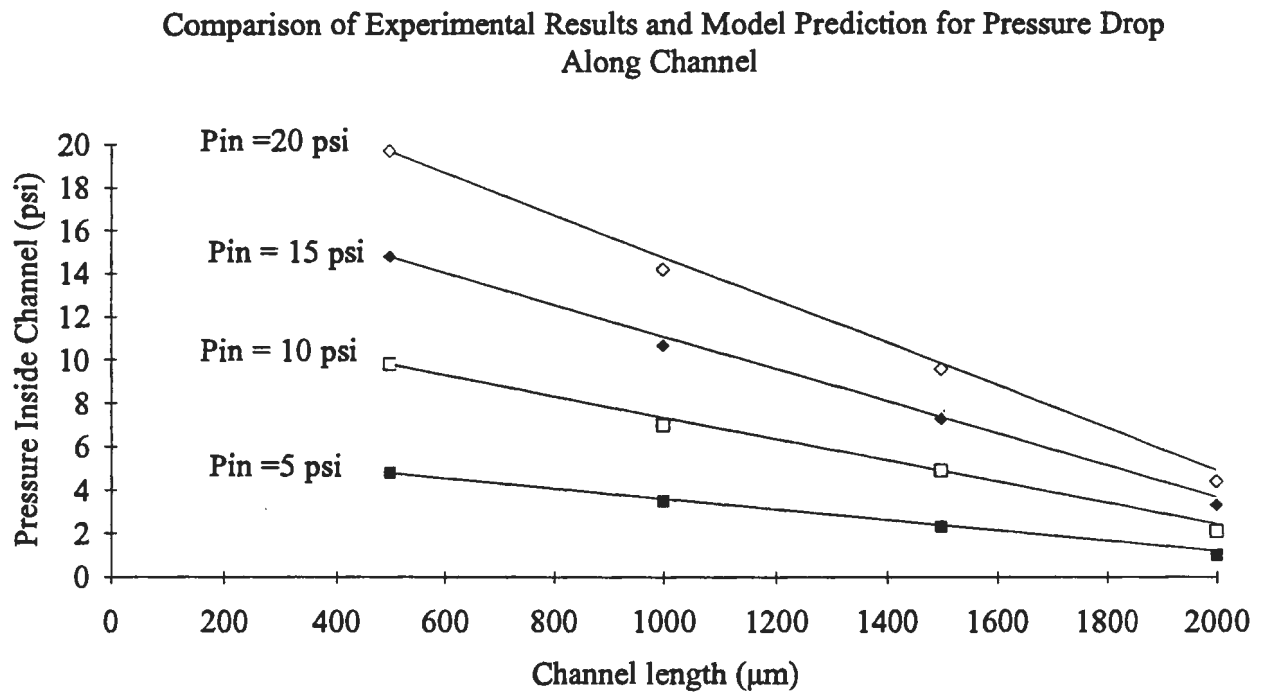
- **Height: $h = 1.2 \mu\text{m}$**
- **Width: $w = 40 \mu\text{m}$**
- **Length = 2000 mm**
- **Distance between Pressure Transducers: $500 \mu\text{m}$**
- **Piezoresistive Transducer : $250 \mu\text{m} \times 250 \mu\text{m}$**
- **Transducer Sensitivity : $120 \mu\text{V}/(\text{V} \cdot \text{Psi})$**





Pressure Distribution Along Microchannel





- $Kn = \lambda / 2h$
- $\lambda = \frac{16\mu}{5\rho\sqrt{2\pi RT}}$
- $Re = 2h U / \nu$
- $M = U / a$
- $Kn \sim M / Re$

For $dp/dx = 9 \text{ psi}/\mu\text{m}$

$$V = 28.9 \text{ cm/sec}$$

$$Re = 4.3 \times 10^{-2} \quad M = 7.7 \times 10^{-4}$$

$$\lambda = 0.068 \mu\text{m} \quad Kn = 0.028$$

- $k_n = \frac{8}{5\sqrt{2\pi}} \frac{\nu}{h\sqrt{RT}}$

$$\nu_{He} = 10 \nu_{air}$$

- **Multi-disciplinary**

MANE, EE, Material Science

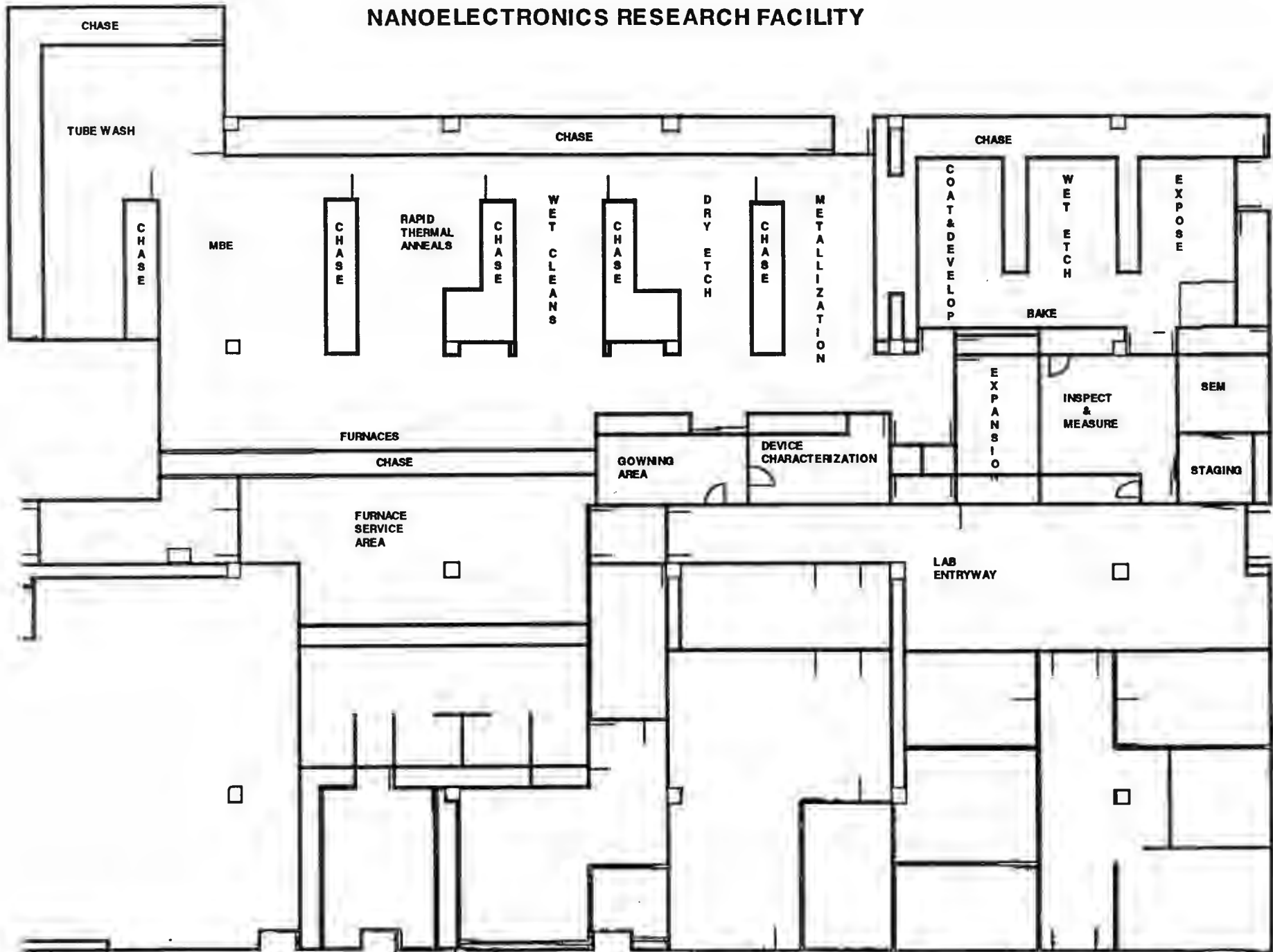
- **UCLA & Caltech**

- **8000 ft² clean room**

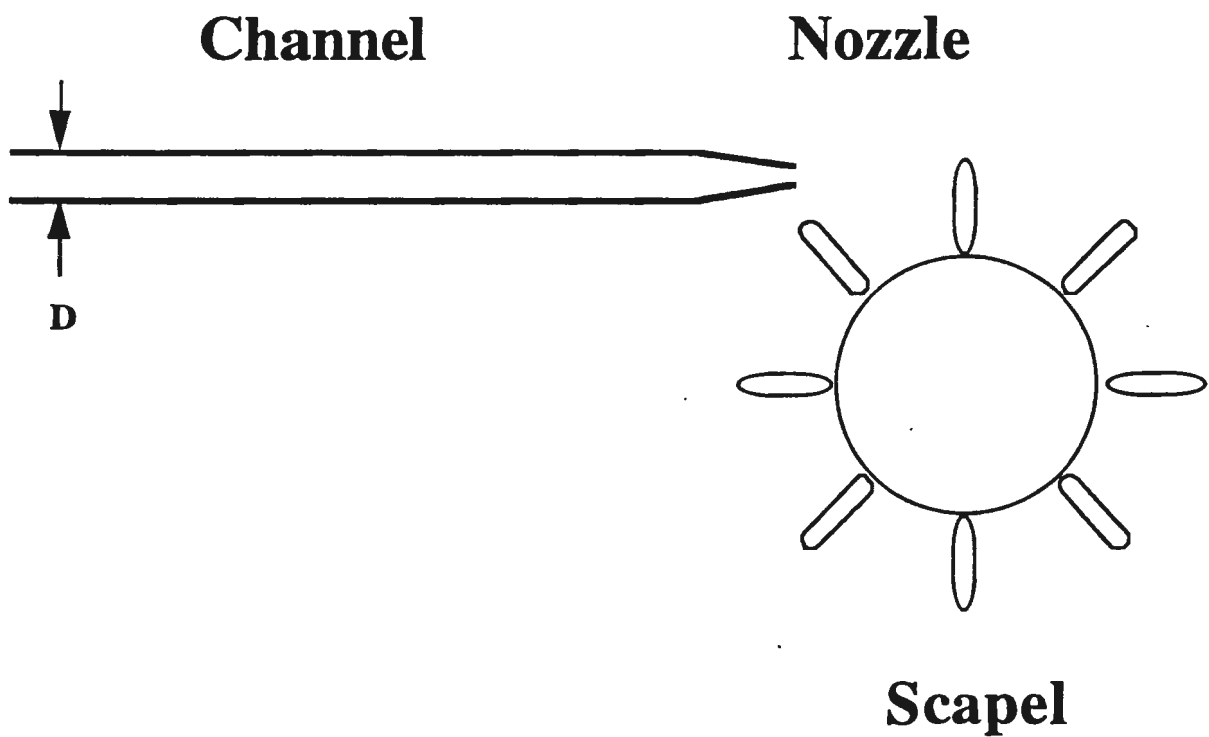
) **# largest one in U.S. University**

**# compatible for micromachining
& microelectronics**

I-156



MICRO SCALPEL



- **Micro flow meter**
- **Micro pressure transducer**
- **Microwave wave guide**

Center for Micro Systems

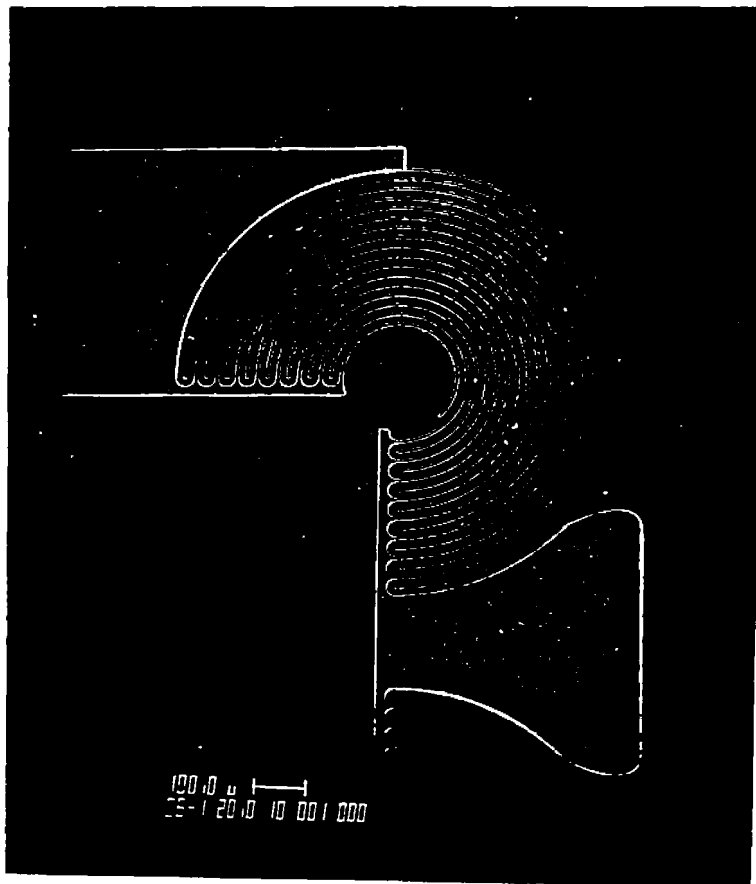
CMS

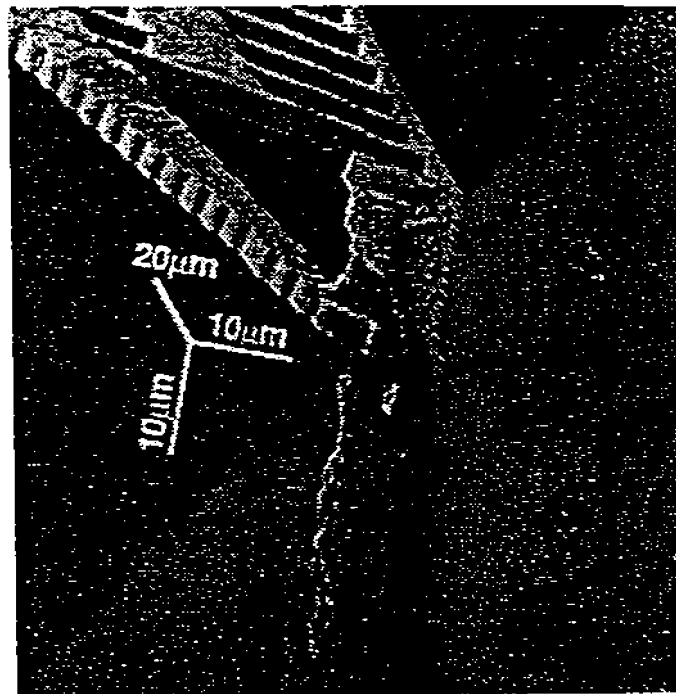
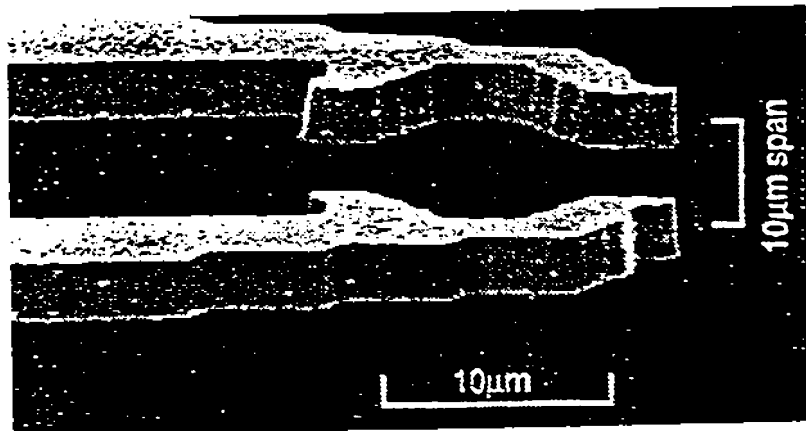
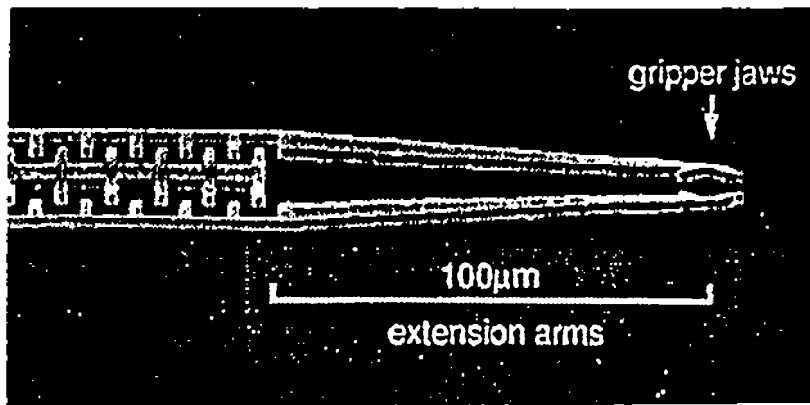
CMS is organized for the purpose of advancing scientific frontiers and manufacturing technologies of micro systems. This center will pursue academic excellence in fundamental research and will actively collaborate with industries and government for technological developments.

Center for Micro Systems

CMS

- **Science \Rightarrow Technology \Rightarrow Application**
- **15 Internationally Renowned Members**
- **Awarded Research Fund - US\$ 5.5 million**
- **Industrial Participation**





A one-celled protozoa, a euglena, being hold by the microgripper. The euglena is 40 μm long and 7 μm in diameter

There's Plenty of Room at the Bottom

Richard P. Feynman

Imagine experimental physicists must often look with envy at men like Kamerlingh Onnes, who discovered a field like low temperature, which seems to be bottomless and in which one can go down and down. Such a man is then a leader and has some temporary monopoly in a scientific adventure. Percy Bridgman, in designing a way to obtain higher pressures, opened up another new field and was able to move into it and to lead us all along. The development of ever higher vacuum was a continuing development of the same kind.

I would like to describe a field, in which little has been done, but in which an enormous amount can be done in principle. This field is not quite the same as the others in that it will not tell us much of fundamental physics (in the sense of, "What are the strange particles?") but it is more like solid-state physics in the sense that it might tell us much of great interest about the strange phenomena that occur in complex situations. Furthermore, a point that is most important is that it would have an enormous number of technical applications.

What I want to talk about is the problem of manipulating and controlling things on a small scale.

As soon as I mention this, people tell me about miniaturization, and how far it has progressed today. They tell me about electric motors that are the size of the nail on your small finger. And there is a device on the market, they tell me, by which you can write the Lord's Prayer on the head of a pin. But that's nothing; that's the most primitive, halting step in the direction I intend to discuss. It is a staggeringly small world that is below. In the year 2000, when they look back at this age, they will wonder why it was not until the year 1960 that anybody began seriously to move in this direction.

Why cannot we write the entire 24 volumes of the Encyclopaedia Britannica on the head of a pin?

Let's see what would be involved. The head of a pin is a sixteenth of an inch across. If you magnify it by 25 000 diameters, the area of the head of the pin is then equal to the area of all the pages of the Encyclopaedia Britannica. Therefore, all it is necessary to do is to reduce in size all the writing in the Encyclopaedia by 25 000 times. Is that possible? The resolving power of the eye is about $1/120$ of an inch—that is roughly the diameter of one of the little

dots on the fine half-tone reproductions in the Encyclopaedia. This, when you demagnify it by 25 000 times, is still 80 angstroms in diameter—32 atoms across, in an ordinary metal. In other words, one of those dots still would contain in its area 1000 atoms. So, each dot can easily be adjusted in size as required by the photoengraving, and there is no question that there is enough room on the head of a pin to put all of the Encyclopaedia Britannica.

Furthermore, it can be read if it is so written. Let's imagine that it is written in raised letters of metal; that is, where the black is in the Encyclopaedia, we have raised letters of metal that are actually $1/25\,000$ of their ordinary size. How would we read it?

If we had something written in such a way, we could read it using techniques in common use today. (They will undoubtedly find a better way when we do actually have it written, but to make my point conservatively I shall just take techniques we know today.) We would press the metal into a plastic material and make a mold of it, then peel the plastic off very carefully, evaporate silica into the plastic to get a very thin film, then shadow it by evaporating gold at an angle against the silica so that all the little letters will appear clearly, dissolve the plastic away from the silica film, and then look through it with an electron microscope!

There is no question that if the thing were reduced by 25 000 times in the form of raised letters on the pin, it would be easy for us to read it today. Furthermore, there is no question that we would find it easy to make copies of the master; we would just need to press the same metal plate again into plastic and we would have another copy.

HOW DO WE WRITE SMALL?

The next question is: How do we write it? We have no standard technique to do this now. But let me argue that it is not as difficult as it first appears to be. We can reverse the lenses of the electron microscope in order to demagnify as well as magnify. A source of ions, sent through the microscope lenses in reverse, could be focused to a very small spot. We could write with that spot like we write in a TV cathode ray oscilloscope, by going across in lines, and having an adjustment which determines the amount of material which is going to be deposited as we scan in lines.

This method might be very slow because of space charge limitations. There will be more rapid methods. We could first make, perhaps by some photo process, a screen which has holes in it in the form of the letters. Then we would strike an arc behind the holes and draw metallic ions through the holes; then we could again use our sys-

MEMS Editor's Note: This manuscript addresses many current research issues. It is the transcript of a talk given by Richard P. Feynman on December 26, 1959, at the annual meeting of the American Physical Society at the California Institute of Technology, and was published as a chapter in the Reinhold Publishing Corporation book, *Miniaturization*, Horace D. Gilbert, Ed. It is reprinted with the consent of Van Nostrand Reinhold, New York, NY 10003.

The author, deceased, was with the California Institute of Technology, Pasadena, CA.

IEEE Log Number 9105621.

I-4. Silicon Micromachining and Its Applications

Yu-Chong Tai
California Institute of Technology

NUWC Division Newport, R. I.

SEMINAR NOTICE

SILICON MICROMACHINING AND ITS APPLICATIONS

Yu-Chong Tai, Ph. D.

Assistant Professor of Electrical Engineering

California Institute of Technology

Recent development of silicon micromachining technology has made possible the fabrication of micromechanical parts such as beams, springs, pin joints, gears, cranks, sliders, and many other novel structures measured in microns. This micromachining technology is derived and modified from silicon integrated-circuit technology. Therefore, it also has many important advantages, such as precision and mass production, which conventional machining techniques can not offer. Potential applications of the micromachining technology are many and wide. In fact, this new field of micromachining has attracted attention from so many disciplines including physics, chemistry, engineering, biology, medicine, etc. The presentation will review the concept and technology of this new technology. Examples recently developed at Caltech will be used to demonstrate applications of micromachining including miniature pressure sensors, Tera Hz wave guides, atomic force microscope (AFM) tips, and neuron prosthetic devices. Finally, because a large surface to volume ratio is a distinctive feature of these microstructures, many microscience issues have become extremely important in the fabrication, characterization, and operation of micromechanical devices. Among the issues, micro fluid mechanics and material strength will specially be covered.

Thursday, 15th July 1993

Conference Room, Bldg. 679

Time: 10:30 AM

POC: Dr. Promode R. Bandyopadhyay (Code 8234; x2588)

SILICON MICROMACHINING AND ITS APPLICATIONS

Yu-Chong Tai, Ph.D.

Assistant Professor of Electrical Engineering

Division of Engineering and Applied Science

California Institute of Technology, Pasadena 91125

There's Plenty of Room at the Bottom

Richard P. Feynman

Imagine experimental physicists must often look with envy at men like Kamerlingh Onnes, who discovered a field like low temperature, which seems to be bottomless and in which one can go down and down. Such a man is then a leader and has some temporary monopoly in a scientific adventure. Percy Bridgman, in designing a way to obtain higher pressures, opened up another new field and was able to move into it and to lead us all along. The development of ever higher vacuum was a continuing development of the same kind.

I would like to describe a field, in which little has been done, but in which an enormous amount can be done in principle. This field is not quite the same as the others in that it will not tell us much of fundamental physics (in the sense of, "What are the strange particles?") but it is more like solid-state physics in the sense that it might tell us much of great interest about the strange phenomena that occur in complex situations. Furthermore, a point that is most important is that it would have an enormous number of technical applications.

What I want to talk about is the problem of manipulating and controlling things on a small scale.

As soon as I mention this, people tell me about miniaturization, and how far it has progressed today. They tell me about electric motors that are the size of the nail on your small finger. And there is a device on the market, they tell me, by which you can write the Lord's Prayer on the head of a pin. But that's nothing; that's the most primitive, halting step in the direction I intend to discuss. It is a staggeringly small world that is below. In the year 2000, when they look back at this age, they will wonder why it was not until the year 1960 that anybody began seriously to move in this direction.

Why cannot we write the entire 24 volumes of the Encyclopaedia Britannica on the head of a pin?

Let's see what would be involved. The head of a pin is a sixteenth of an inch across. If you magnify it by 25 000 diameters, the area of the head of the pin is then equal to the area of all the pages of the Encyclopaedia Britannica. Therefore, all it is necessary to do is to reduce in size all the writing in the Encyclopaedia by 25 000 times. Is that possible? The resolving power of the eye is about 1/120 of an inch—that is roughly the diameter of one of the little

dots on the fine half-tone reproductions in the Encyclopaedia. This, when you demagnify it by 25 000 times, is still 80 angstroms in diameter—32 atoms across, in an ordinary metal. In other words, one of those dots still would contain in its area 1000 atoms. So, each dot can easily be adjusted in size as required by the photoengraving, and there is no question that there is enough room on the head of a pin to put all of the Encyclopaedia Britannica.

Furthermore, it can be read if it is so written. Let's imagine that it is written in raised letters of metal; that is, where the black is in the Encyclopaedia, we have raised letters of metal that are actually 1/25 000 of their ordinary size. How would we read it?

If we had something written in such a way, we could read it using techniques in common use today. (They will undoubtedly find a better way when we do actually have it written, but to make my point conservatively I shall just take techniques we know today.) We would press the metal into a plastic material and make a mold of it, then peel the plastic off very carefully, evaporate silica into the plastic to get a very thin film, then shadow it by evaporating gold at an angle against the silica so that all the little letters will appear clearly, dissolve the plastic away from the silica film, and then look through it with an electron microscope!

There is no question that if the thing were reduced by 25 000 times in the form of raised letters on the pin, it would be easy for us to read it today. Furthermore, there is no question that we would find it easy to make copies of the master; we would just need to press the same metal plate again into plastic and we would have another copy.

HOW DO WE WRITE SMALL?

The next question is: How do we *write* it? We have no standard technique to do this now. But let me argue that it is not as difficult as it first appears to be. We can reverse the lenses of the electron microscope in order to demagnify as well as magnify. A source of ions, sent through the microscope lenses in reverse, could be focused to a very small spot. We could write with that spot like we write in a TV cathode ray oscilloscope, by going across in lines, and having an adjustment which determines the amount of material which is going to be deposited as we scan in lines.

This method might be very slow because of space charge limitations. There will be more rapid methods. We could first make, perhaps by some photo process, a screen which has holes in it in the form of the letters. Then we would strike an arc behind the holes and draw metallic ions through the holes; then we could again use our sys-

MEMS Editor's Note: This manuscript addresses many current research issues. It is the transcript of a talk given by Richard P. Feynman on December 26, 1959, at the annual meeting of the American Physical Society at the California Institute of Technology, and was published as a chapter in the Reinhold Publishing Corporation book, *Miniaturization*, Horace D. Gilbert, Ed. It is reprinted with the consent of Van Nostrand Reinhold, New York, NY 10003.

The author, deceased, was with the California Institute of Technology, Pasadena, CA.

IEEE Log Number 9105621.

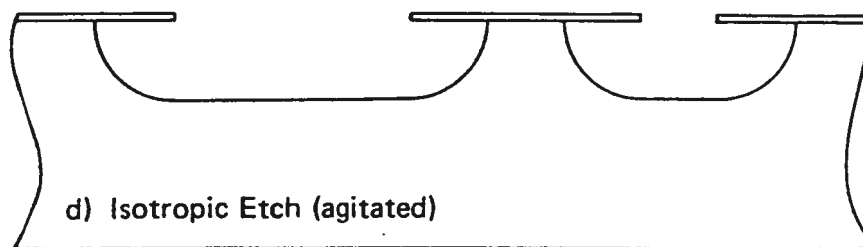
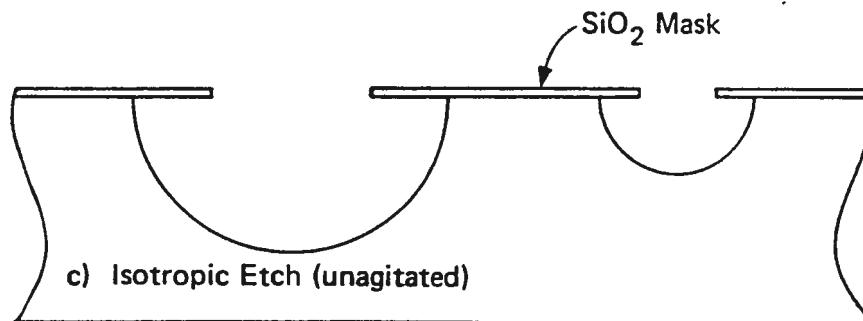
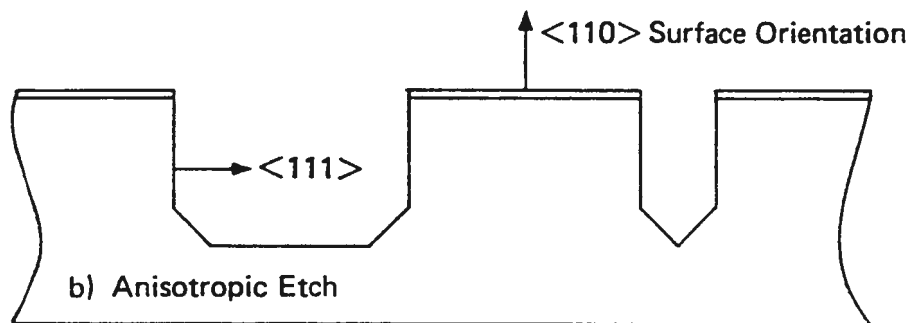
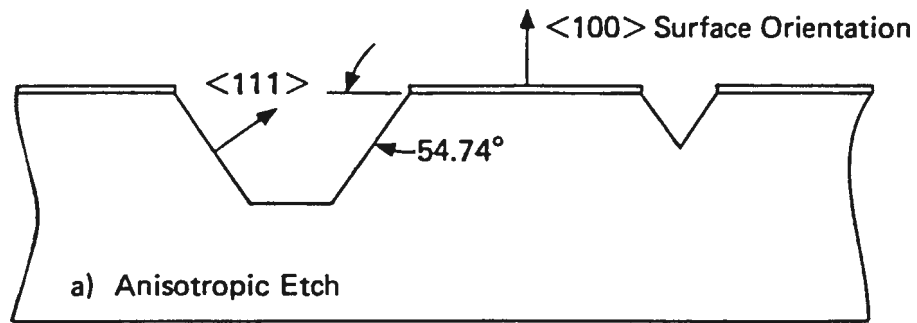
SILICON MICROMACHINING

- **BULK MICROMACHINING -- SUBSTRATE**

- Isotropic and anisotropic etchants (KOH, NaOH, EDP)
- Etching stop (p+ boron)

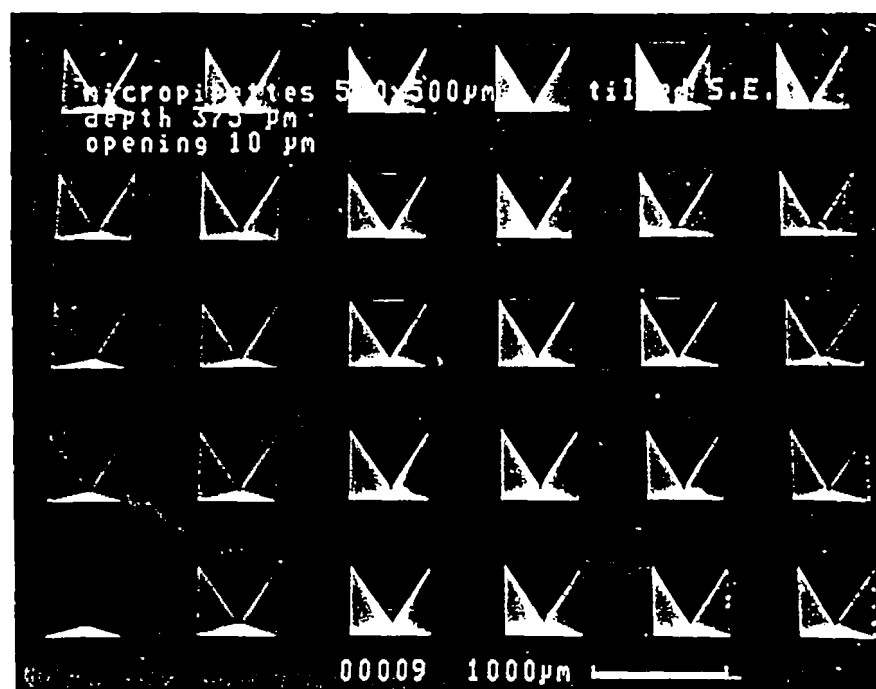
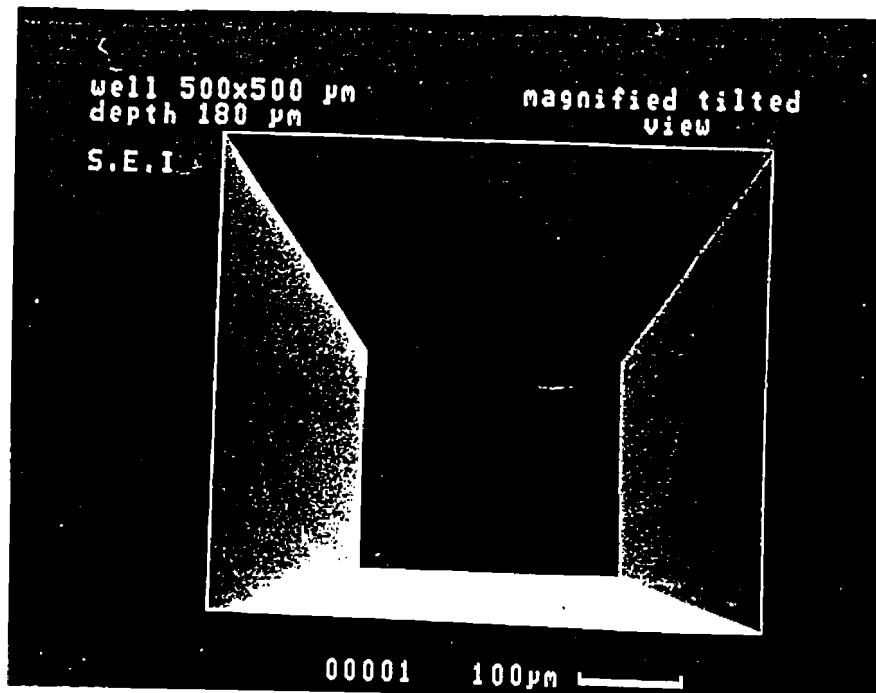
- **SURFACE MICROMACHINING -- THIN FILMS**

- Structural materials (Si, Si₃N₄, metals)
- Sacrificial layers (SiO₂, Photoresist)
- Selective etchants



COMPARISON OF ANISOTROPIC ETCHANTS FOR SILICON [5.8,5.9,5.10]

ETCHANT (Diluent)	TYPICAL COMP.	TEMP. °C	(100) ETCH RATE $\mu\text{m}/\text{min}$	(100)/(111) ETCH RATE RATIO	MASK (ETCH RATE)
KOH (Water)	44 gr 100 ml	85	1.4	400:1	Si_3N_4 SiO_2 (14 Å/min)
NaOH (Water)	10 gr 100 ml	65	0.25-1.0	>300:1	Si_3N_4 SiO_2 (7 Å/min)
Ethylene diamine	750 ml				SiO_2 (2 Å/min)
Pyrocatechol (Water)	120 gr 240 ml	115	1.25	35:1	Si_3N_4 (1 Å/min) Ta,Au,Cr,Ag,Cu
H_2N_4 (Water)	100 ml 100 ml	100	2.0	10:1	SiO_2 (<2 Å/min)



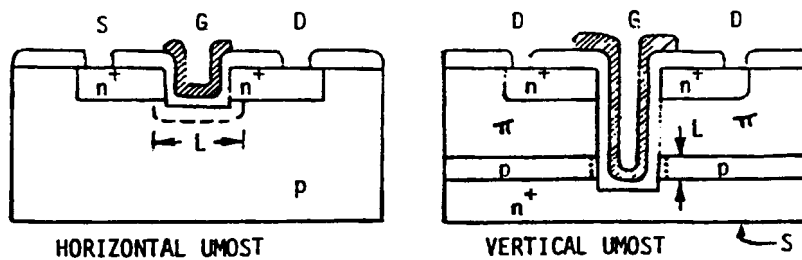


Figure 5. Two MOS type devices on the (110). The dotted lines show the inversion layers.

D.L. Kendall & G.R. de Guel, Workshop on M. M. T., Cleveland, 1984.

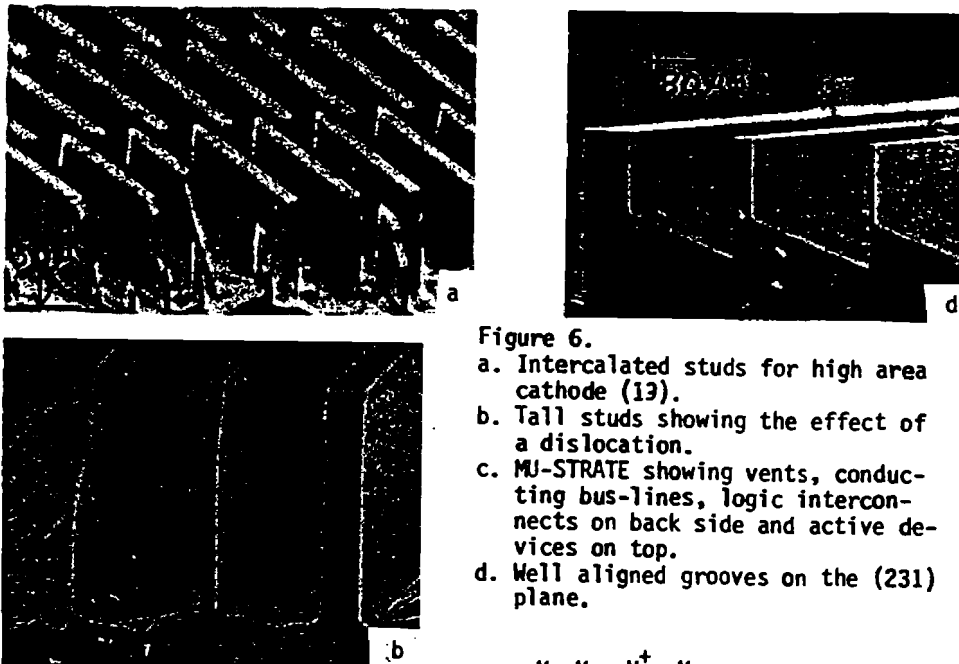
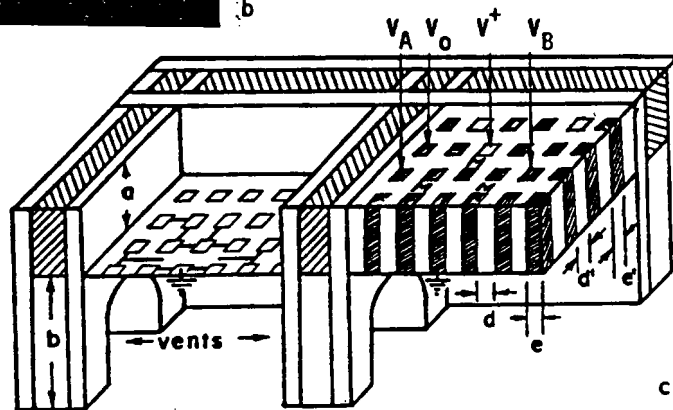
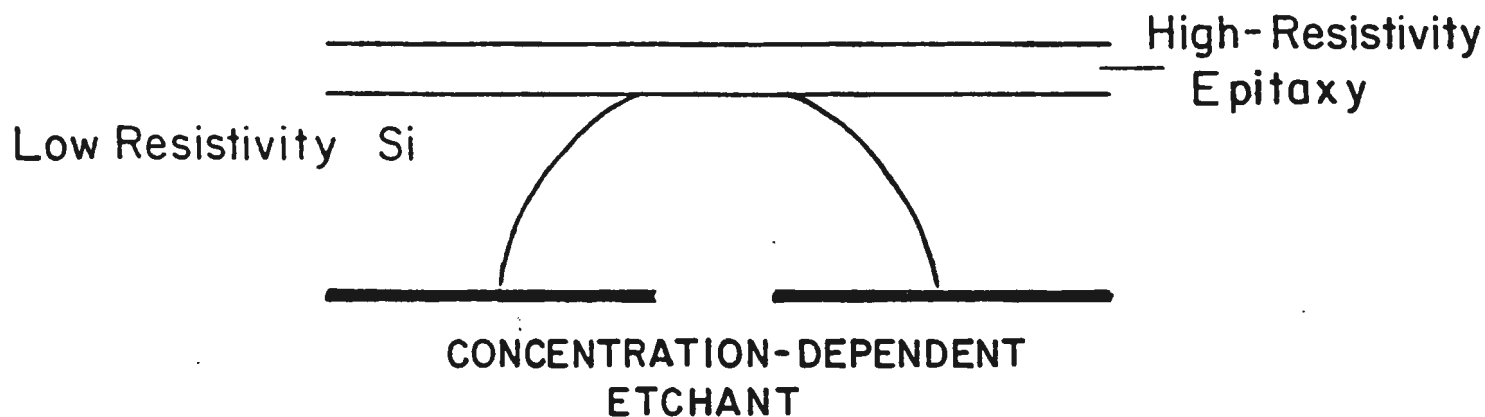


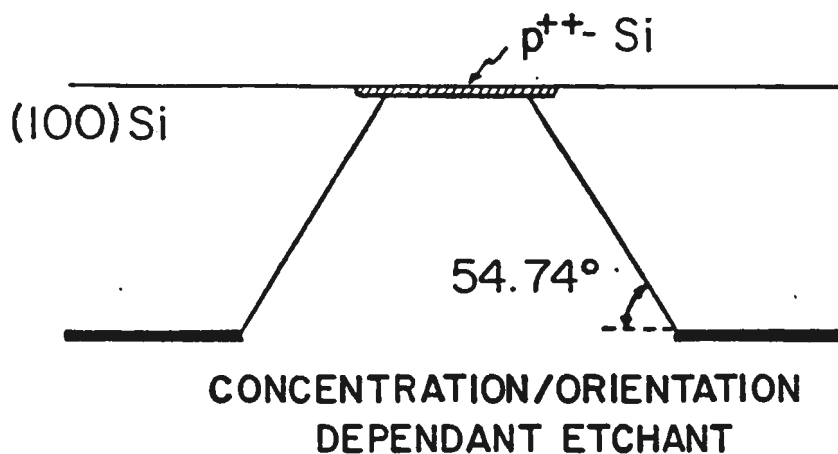
Figure 6.

- a. Intercalated studs for high area cathode (13).
- b. Tall studs showing the effect of a dislocation.
- c. MU-STRATE showing vents, conducting bus-lines, logic interconnects on back side and active devices on top.
- d. Well aligned grooves on the (231) plane.





Example: HF, HNO_3 , CH_3COOH stops
if $\rho > 0.07 \Omega\text{cm}$.



Example: KOH, Isopropyl, H_2O - $R_{(100)} > 60R_{(111)}$
EDP - $R_{(100)} > 50R_{(111)}$; Etch stops if
 $N_a > \sim 10^{19} \text{cm}^{-3}$

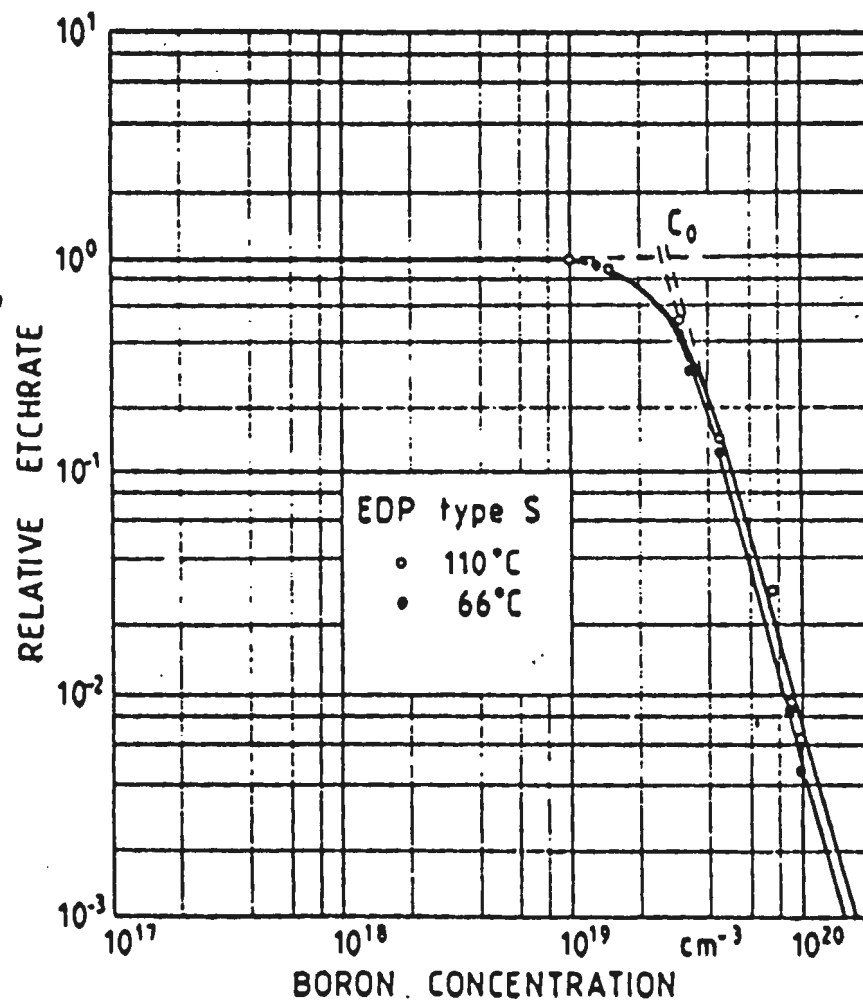
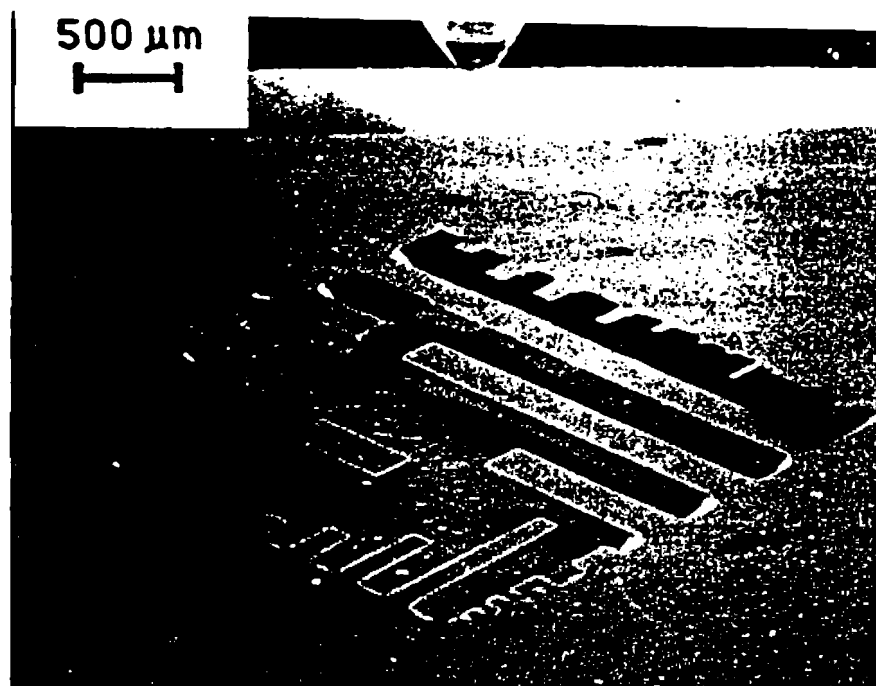
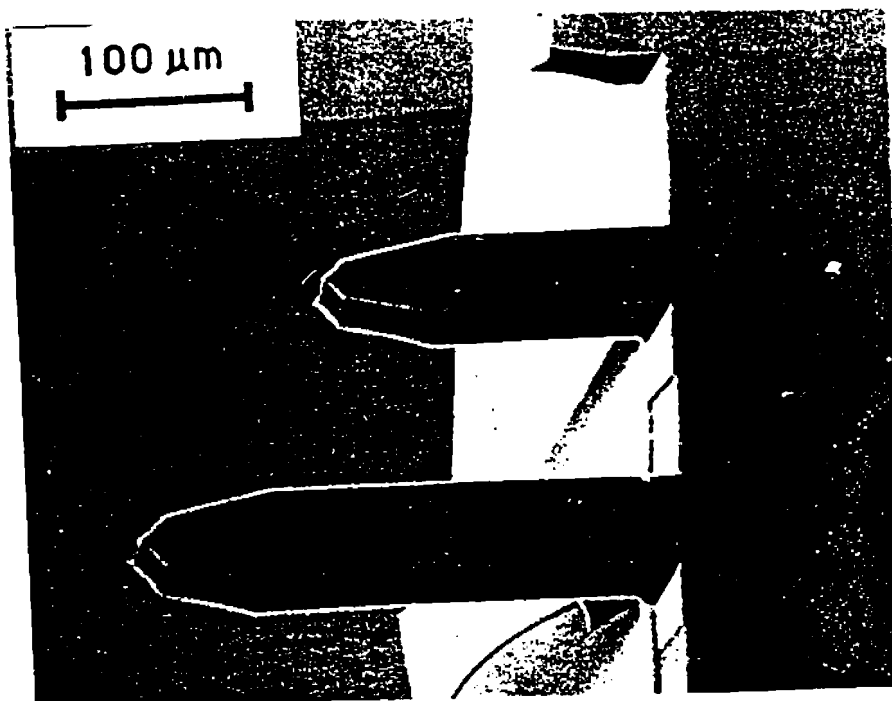
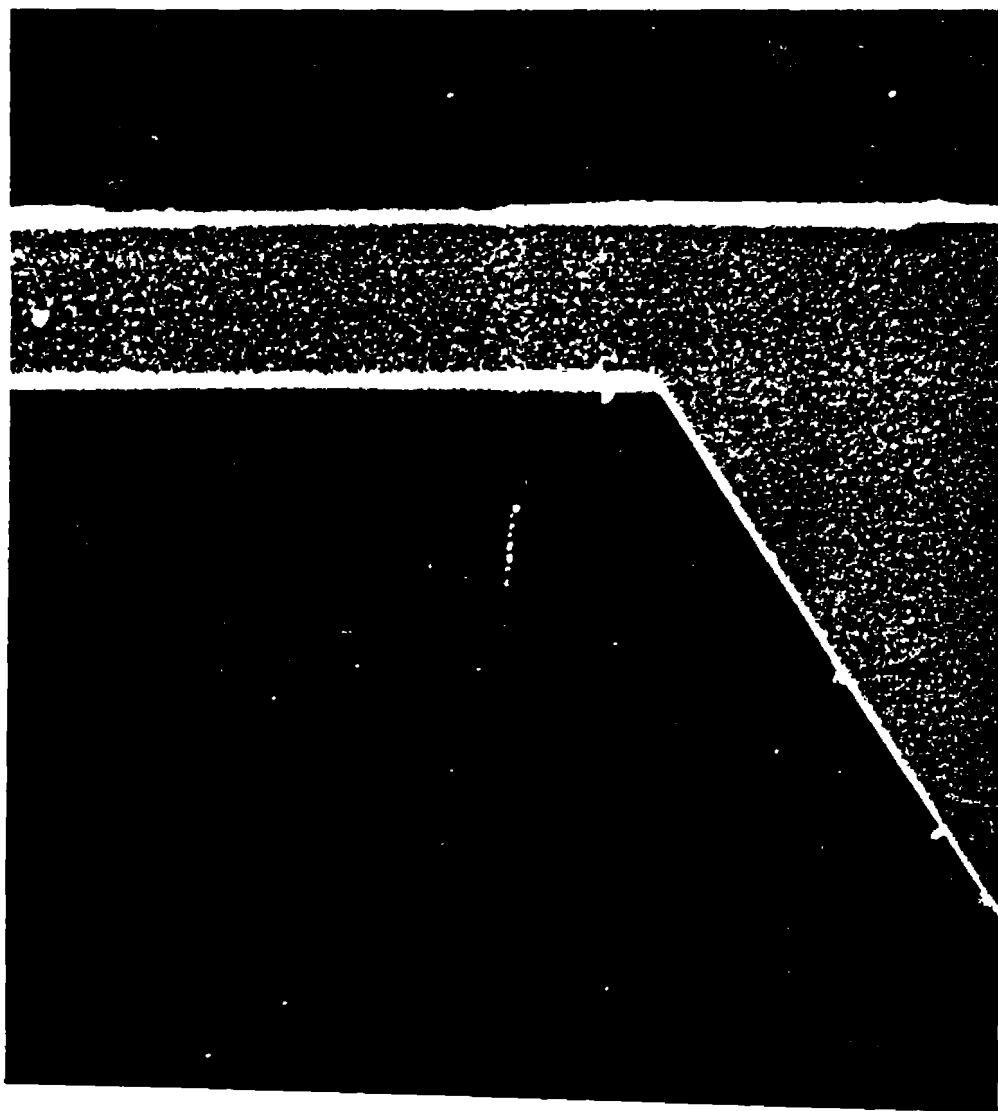


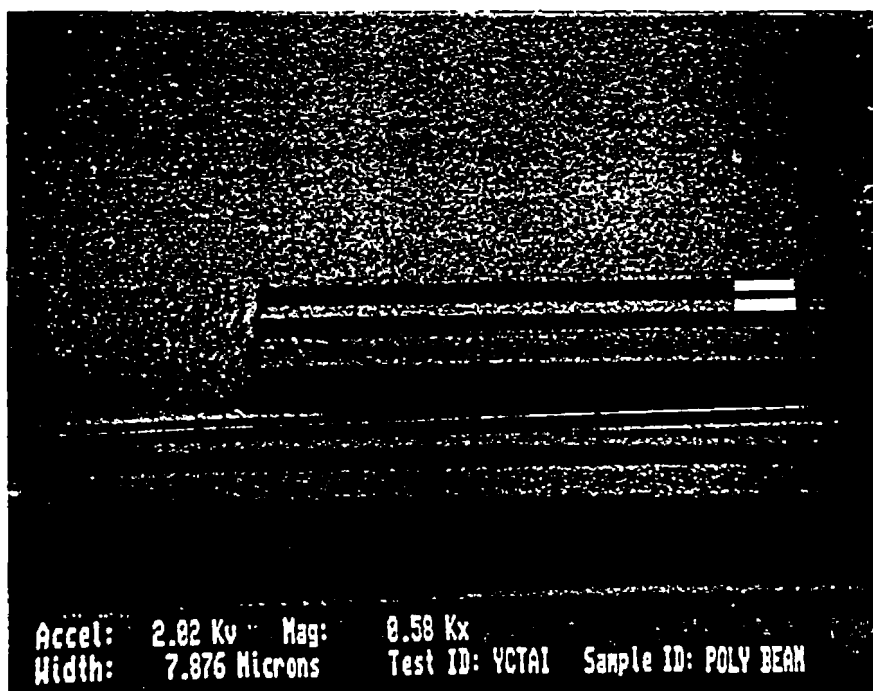
Fig. 6: Relative silicon etch rate as a function of boron dopant concentration for EDP type S.





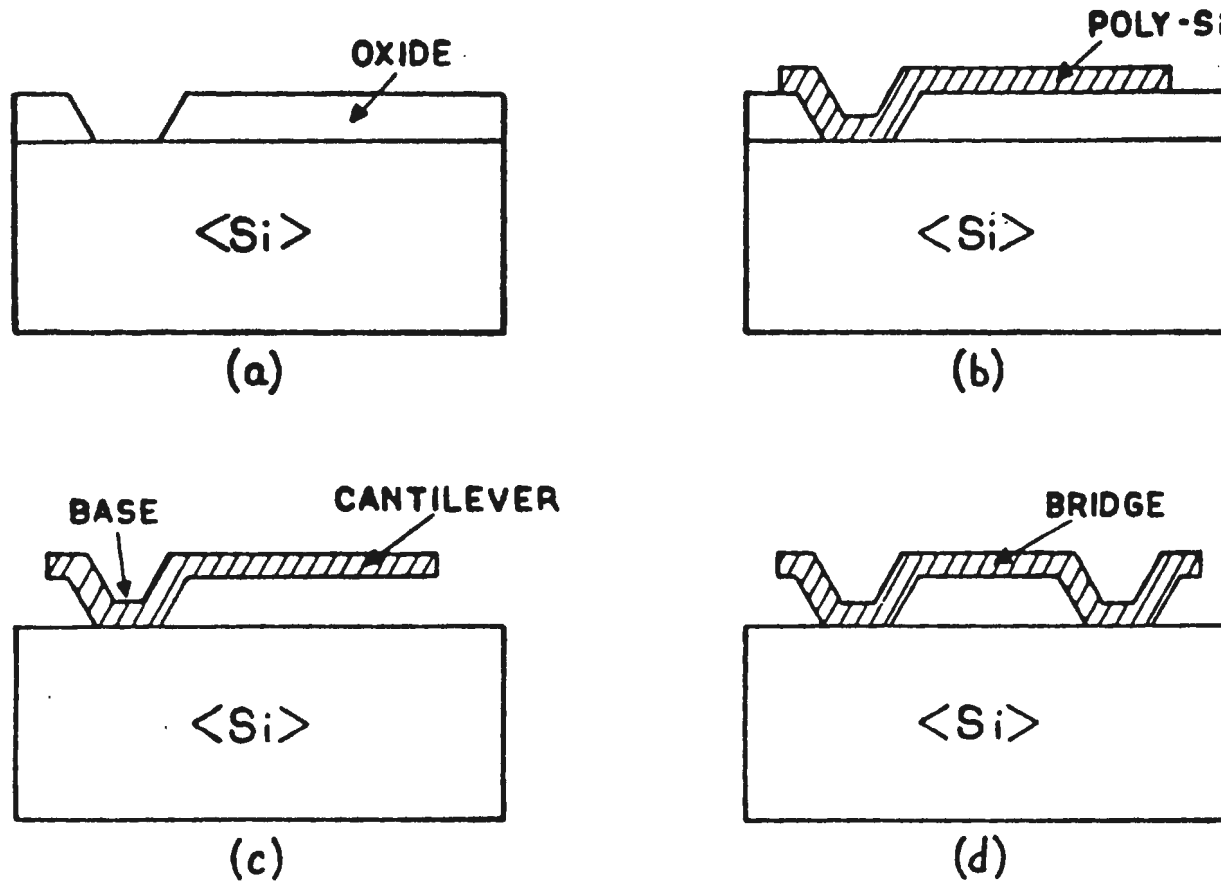


Accel: 1.61 Kv Mag: 8.83 Kx
Width: 6.883 Microns Test ID: YCTAI Sample ID: POLY BRIDGE



Accel: 2.82 Kv Mag: 8.58 Kx
Width: 7.876 Microns Test ID: YCTAI Sample ID: POLY BEAM

POLYSILICON MICROBEAM TECHNOLOGY

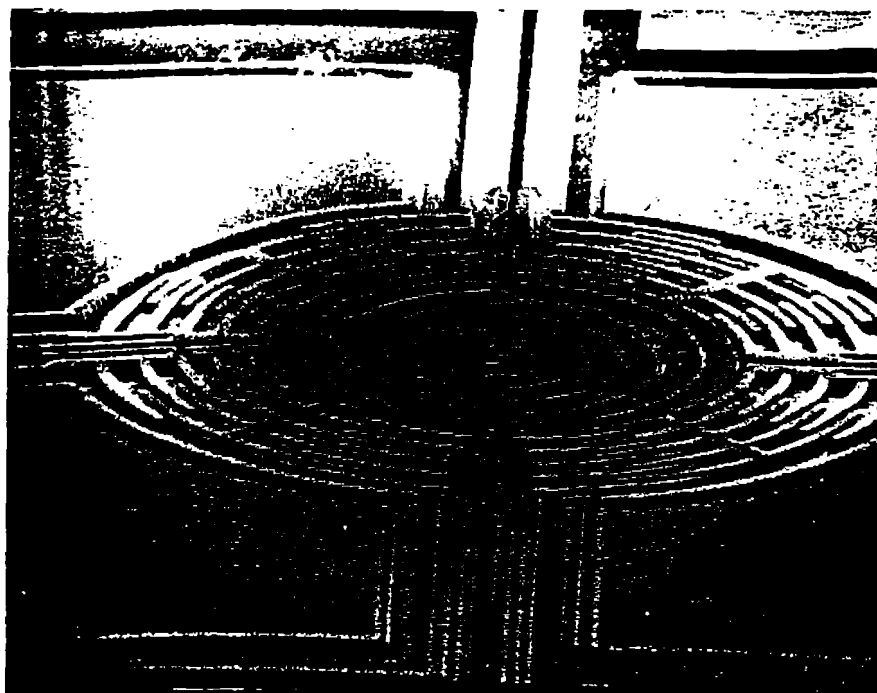
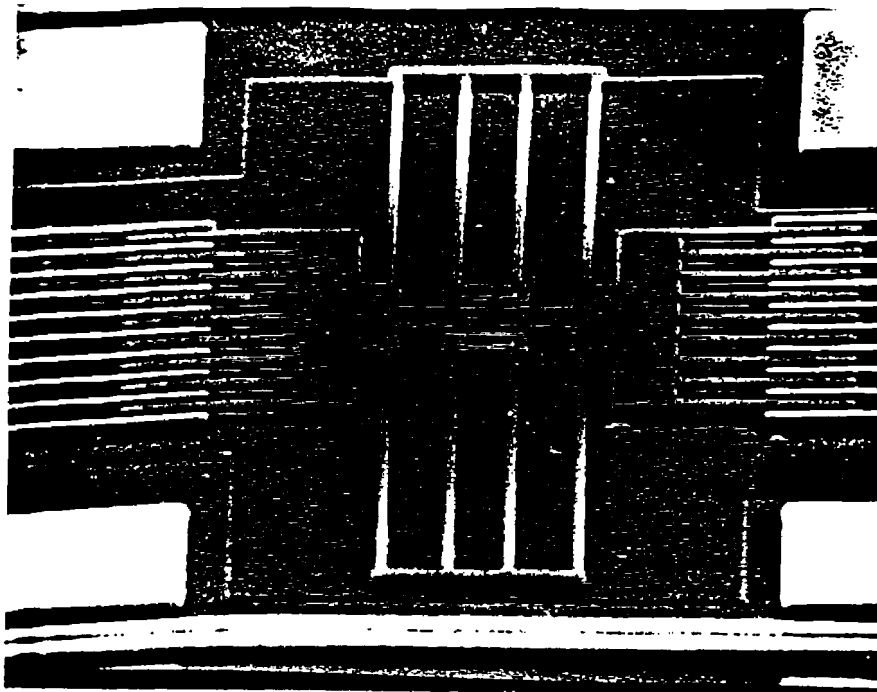


I-179

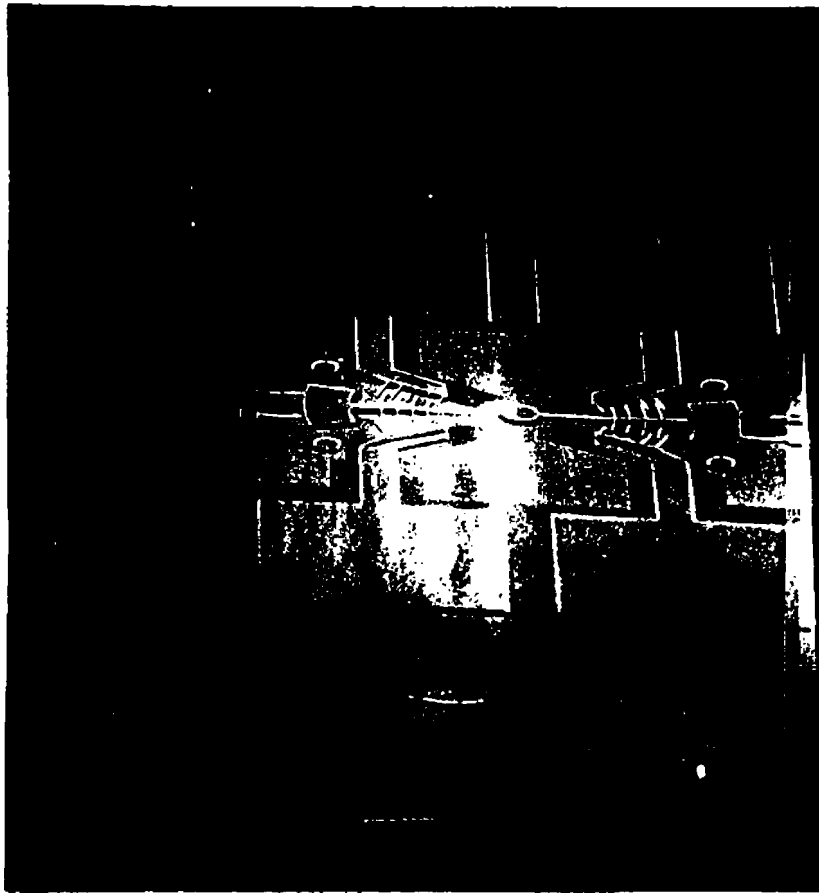
(R.T. Howe and R.S. Muller, *J. Electrochem. Soc.*, 1983)

SURFACE MICROMACHINING

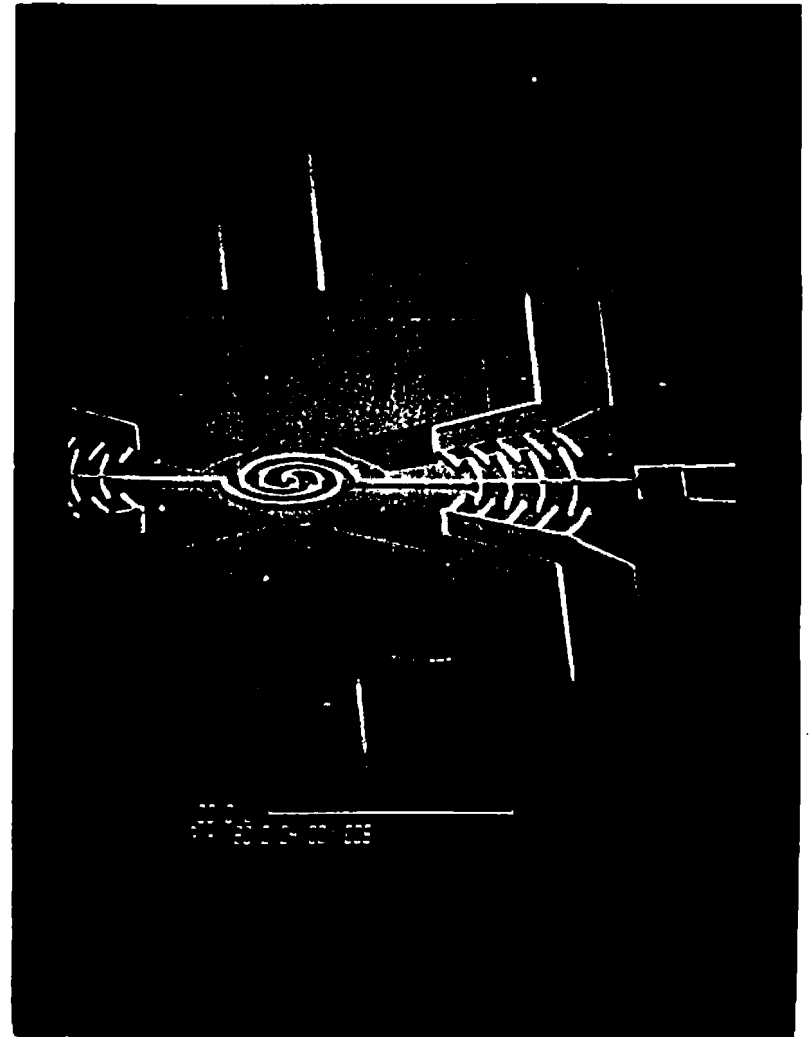
- # Structural Materials
- # Sacrificial Materials
- # Selective Etchants



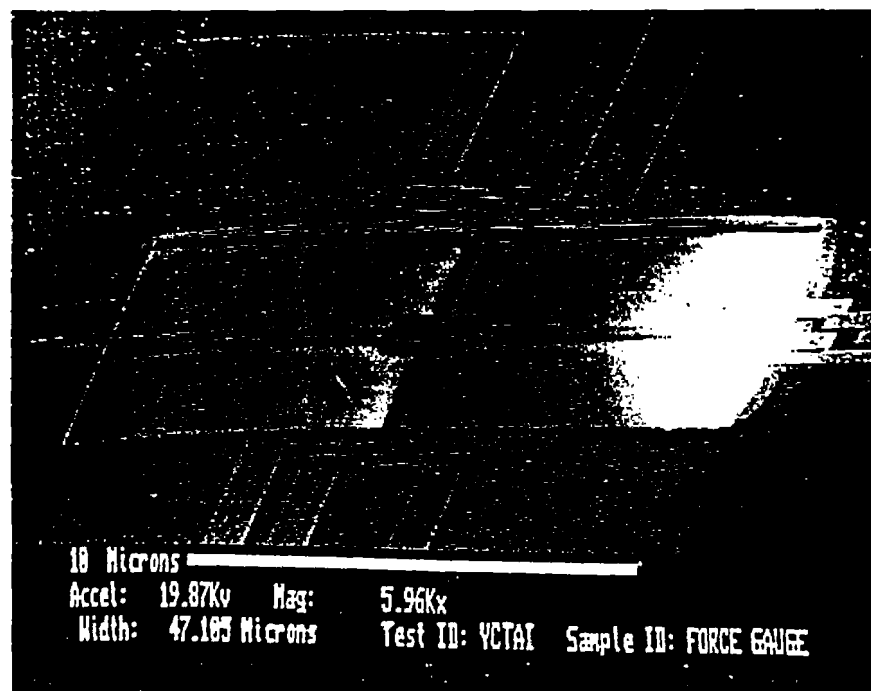
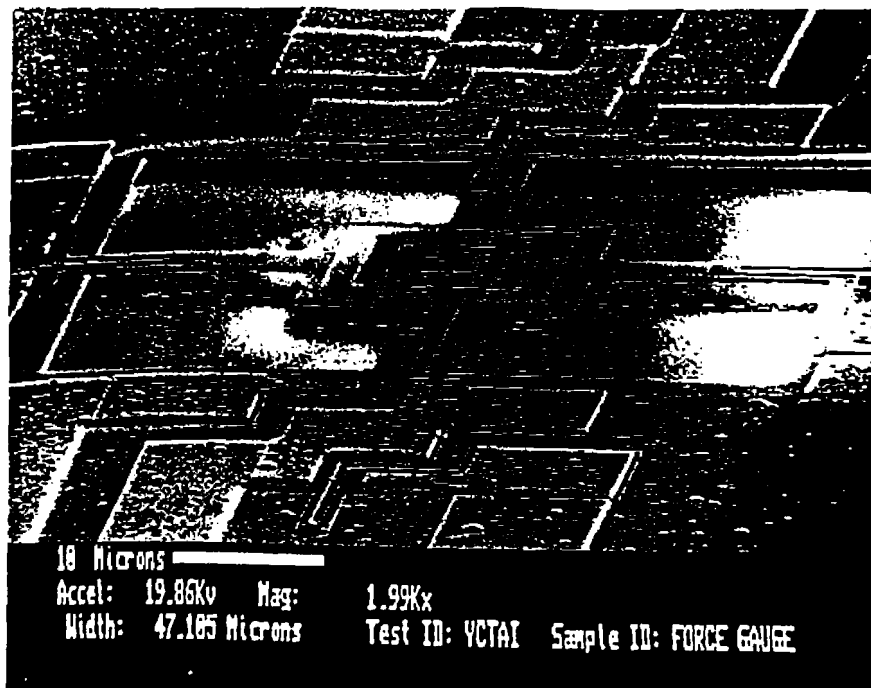
SEM photographs of the cantilever and spring joint shutters

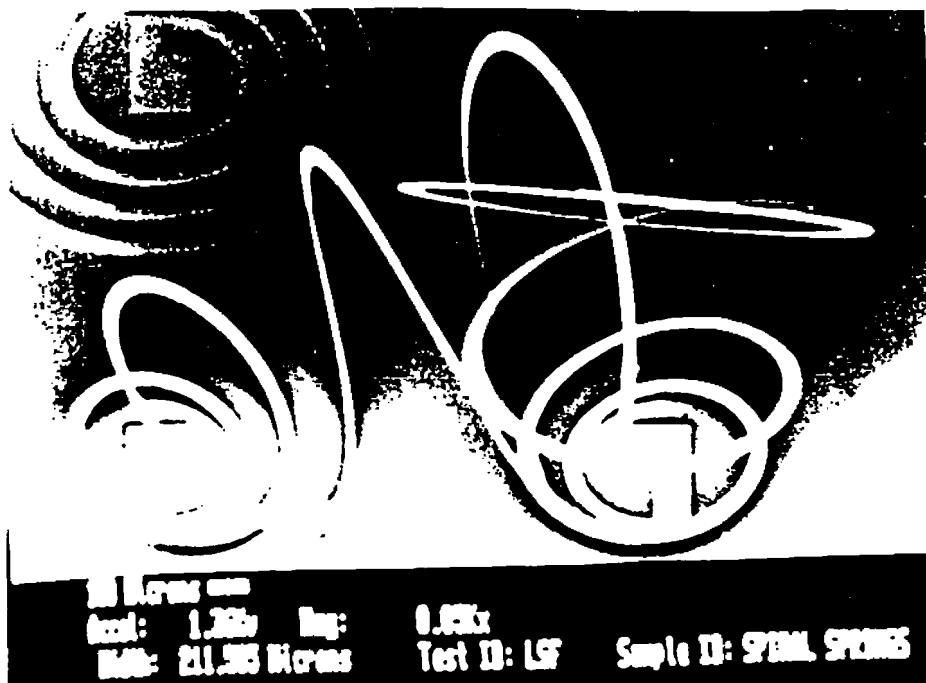


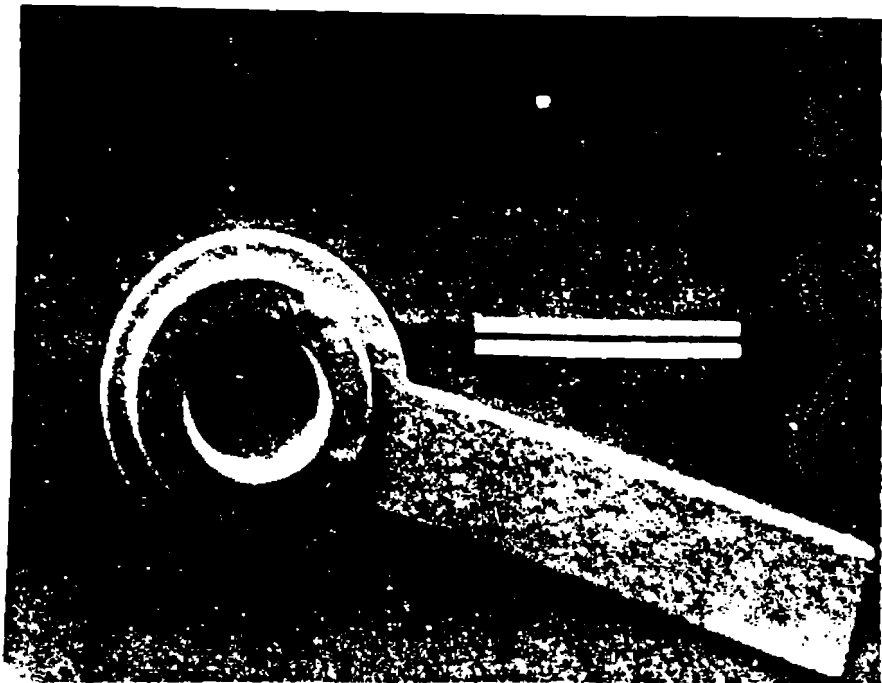
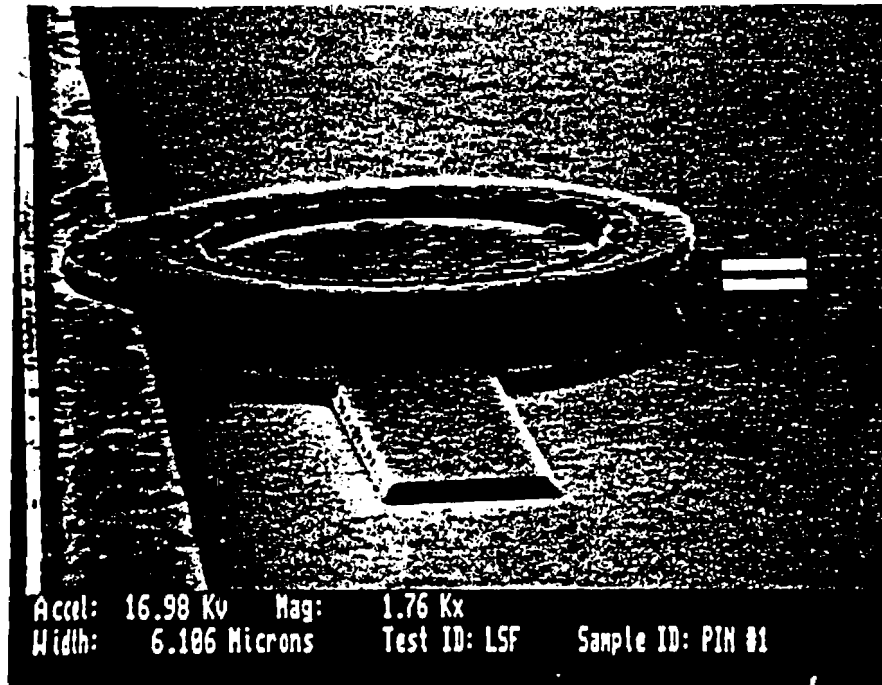
Fixed Joint

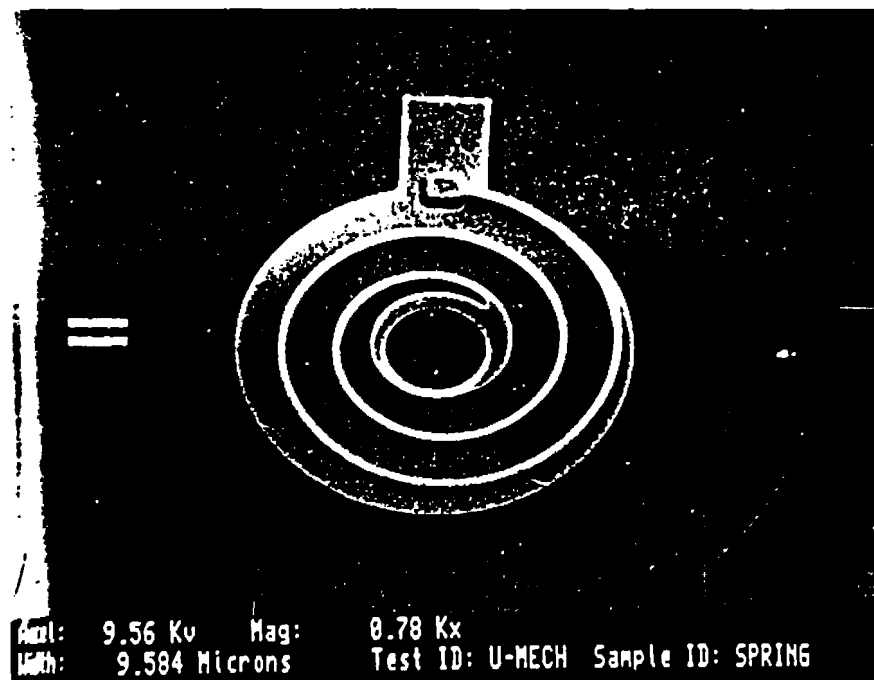


Spring Joint

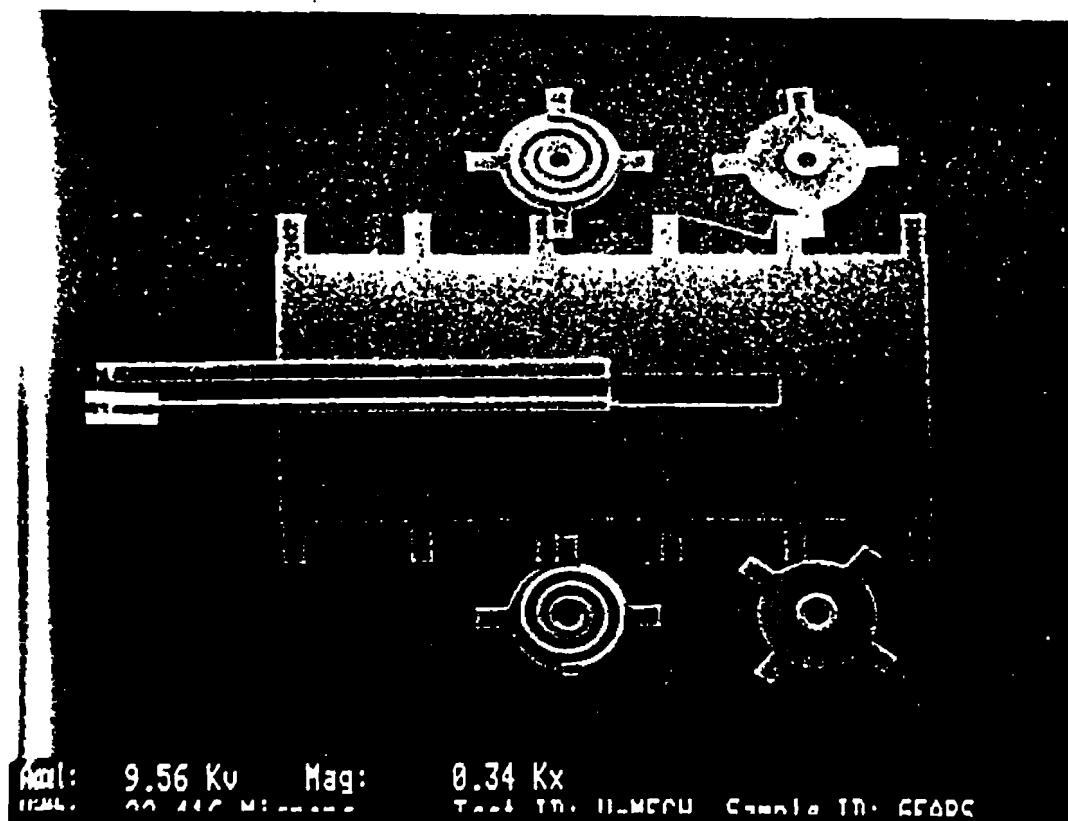


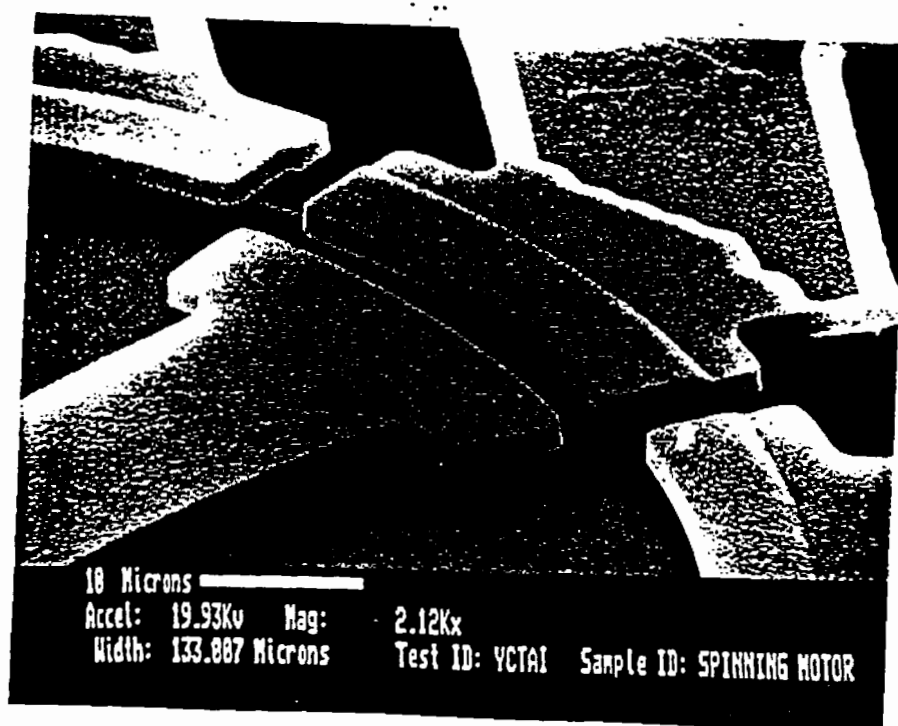
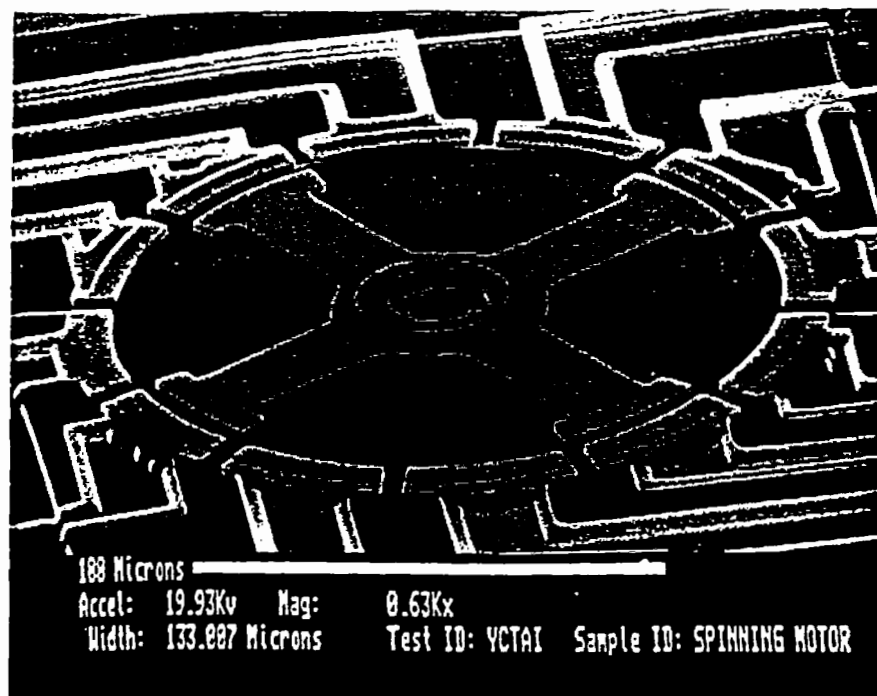












Caltech Micromachining Lab

Space

- # Surface micromachining area (class 100, 800 sq. ft.)
- # Bulk micromachining area (class 10,000, 700 sq. ft.)
- # CAD and measurement area (500 sq. ft.)

Equipment

- # GCA stepper and contact aligner
- # LPCVD polysilicon reactor
- # LPCVD Si₃N₄ (SiN) reactor
- # LPCVD SiO₂ (PSG) reactor
- # Diffusion furnaces
- # PECVD reactor
- # Plasma etcher
- # RIE etcher
- # Evaporators

Planned Equipment

- # LPCVD Tungsten
- # Electroforming Tank
- # Sputtering machine

CURRENT CALTECH PROJECTS

- # Culture Neuron Probes
- # Si STM and AFM Probes
- # Integrated Tera Hz Waveguide Circuits
- # Miniature Disc Head (Micromagnetics)
- # Hot-point Anemometer
- # Surface-Micromachined Pressure Sensors
- # Microchannel Flow
- # Accelerometer
- # Micro Gyros
- # Micromechanical Properties

Cultured Neurons



? →

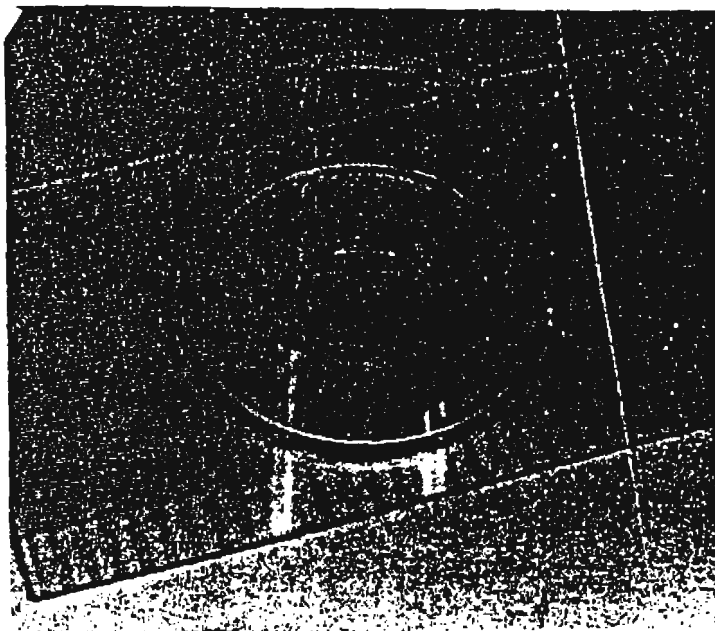


Figure 1 A culture dish mounted on a glass substrate.

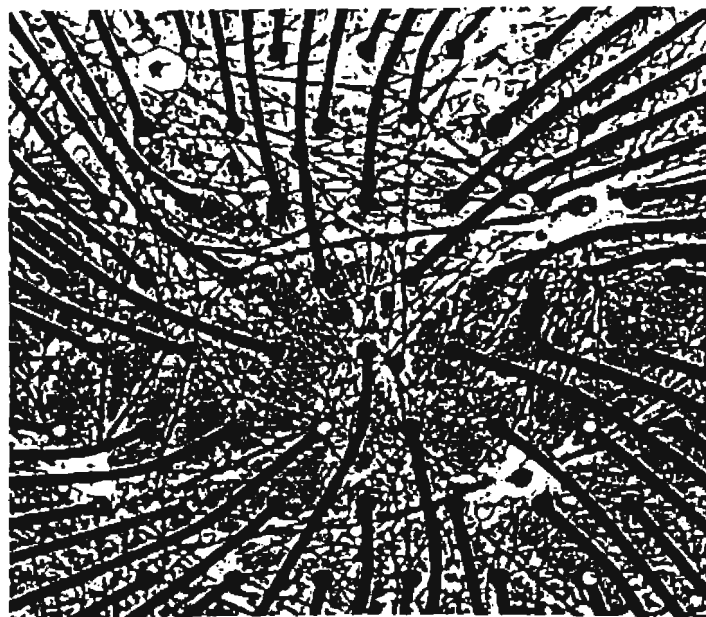
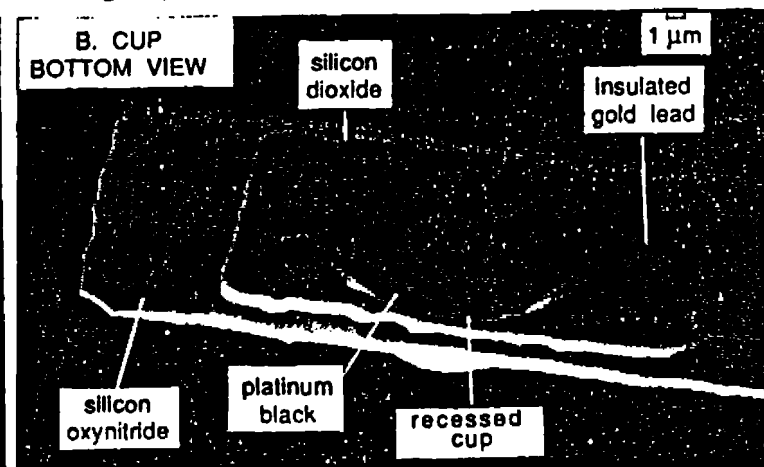
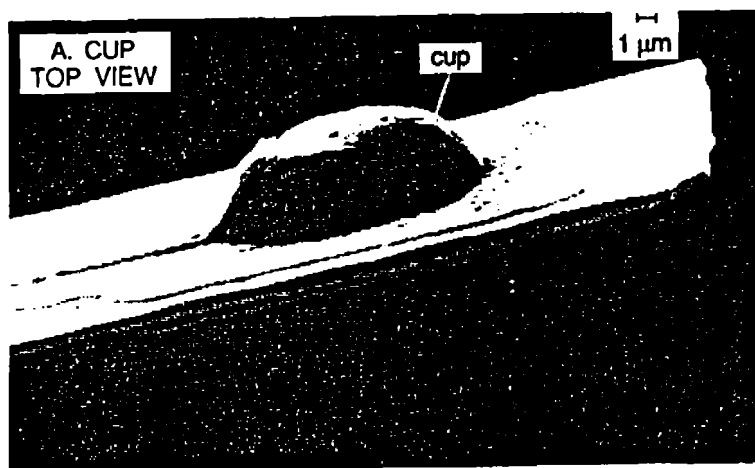
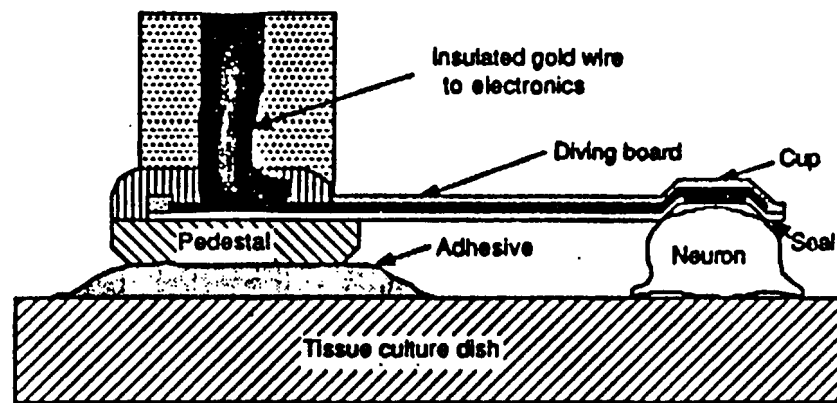
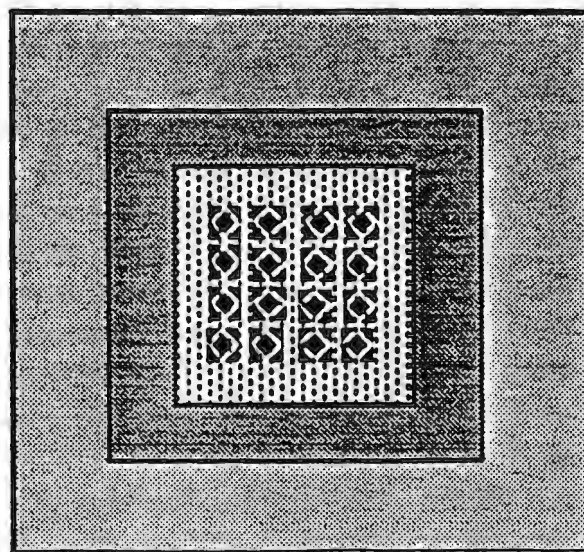
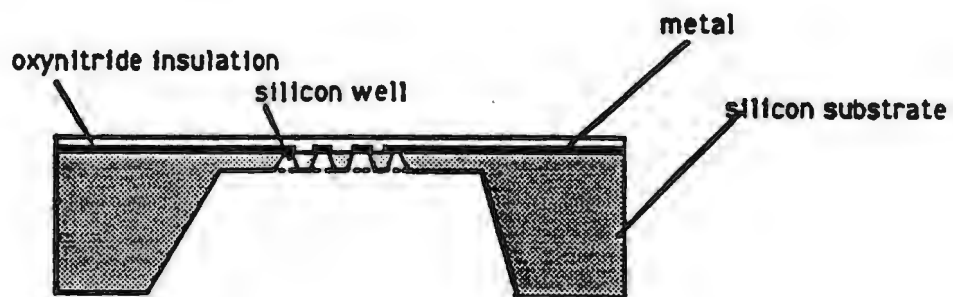
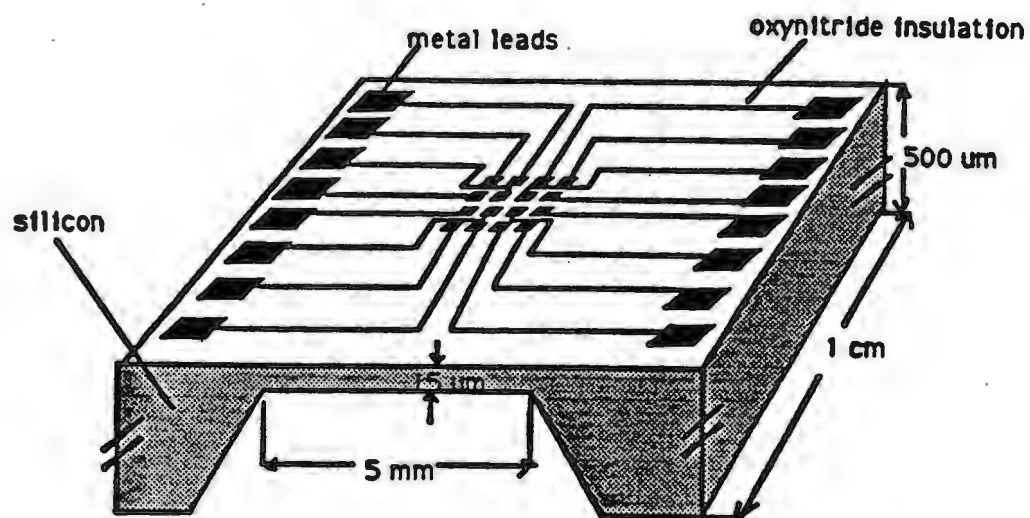
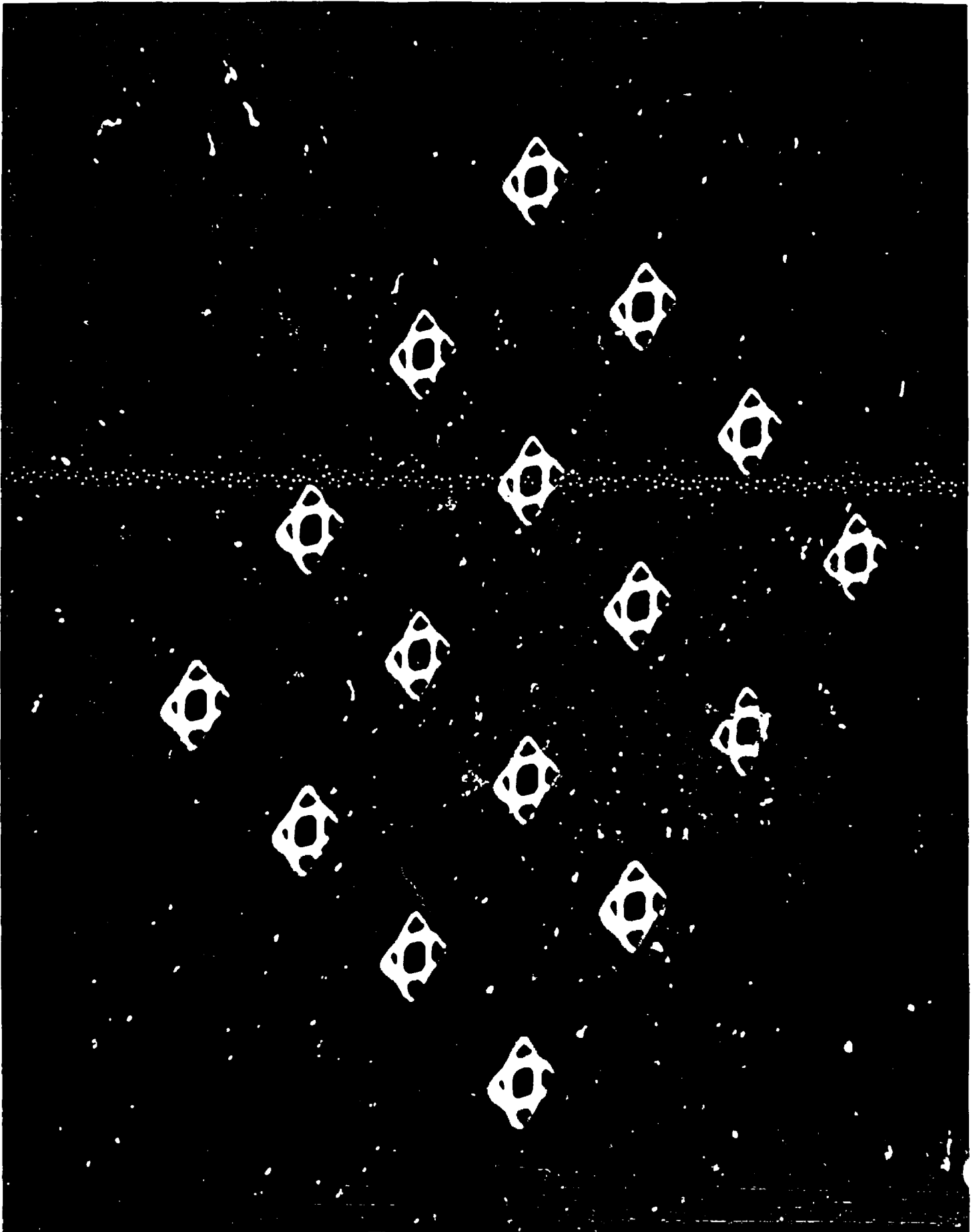


Figure 2 The central electrode pattern of the dish in Fig. 1.



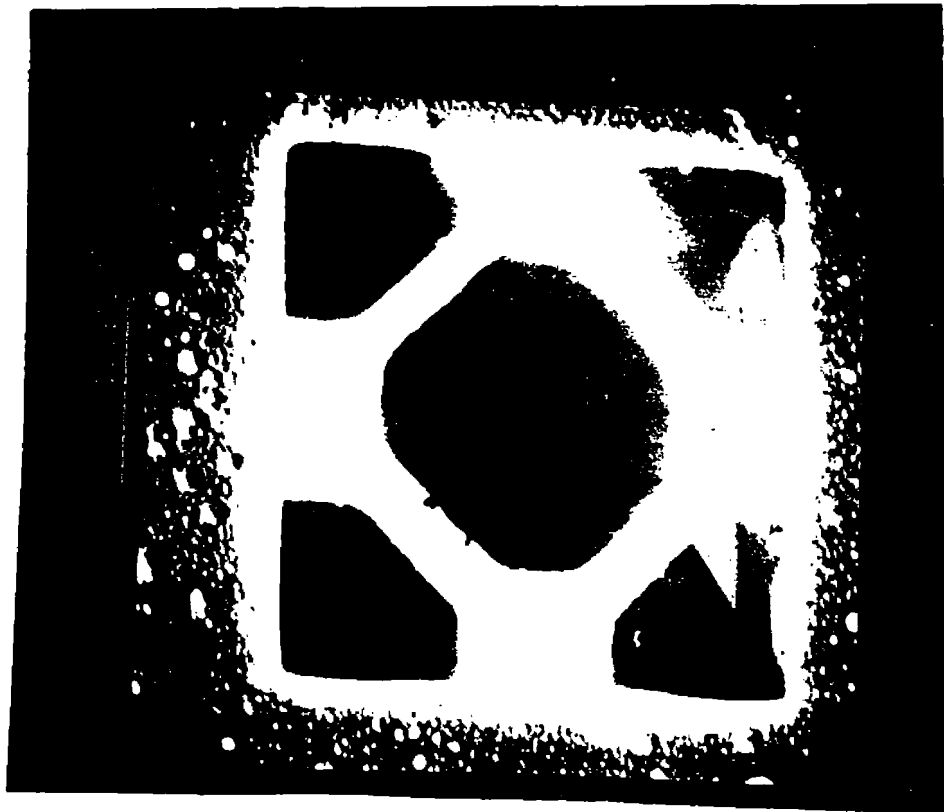
NEUROCHIP



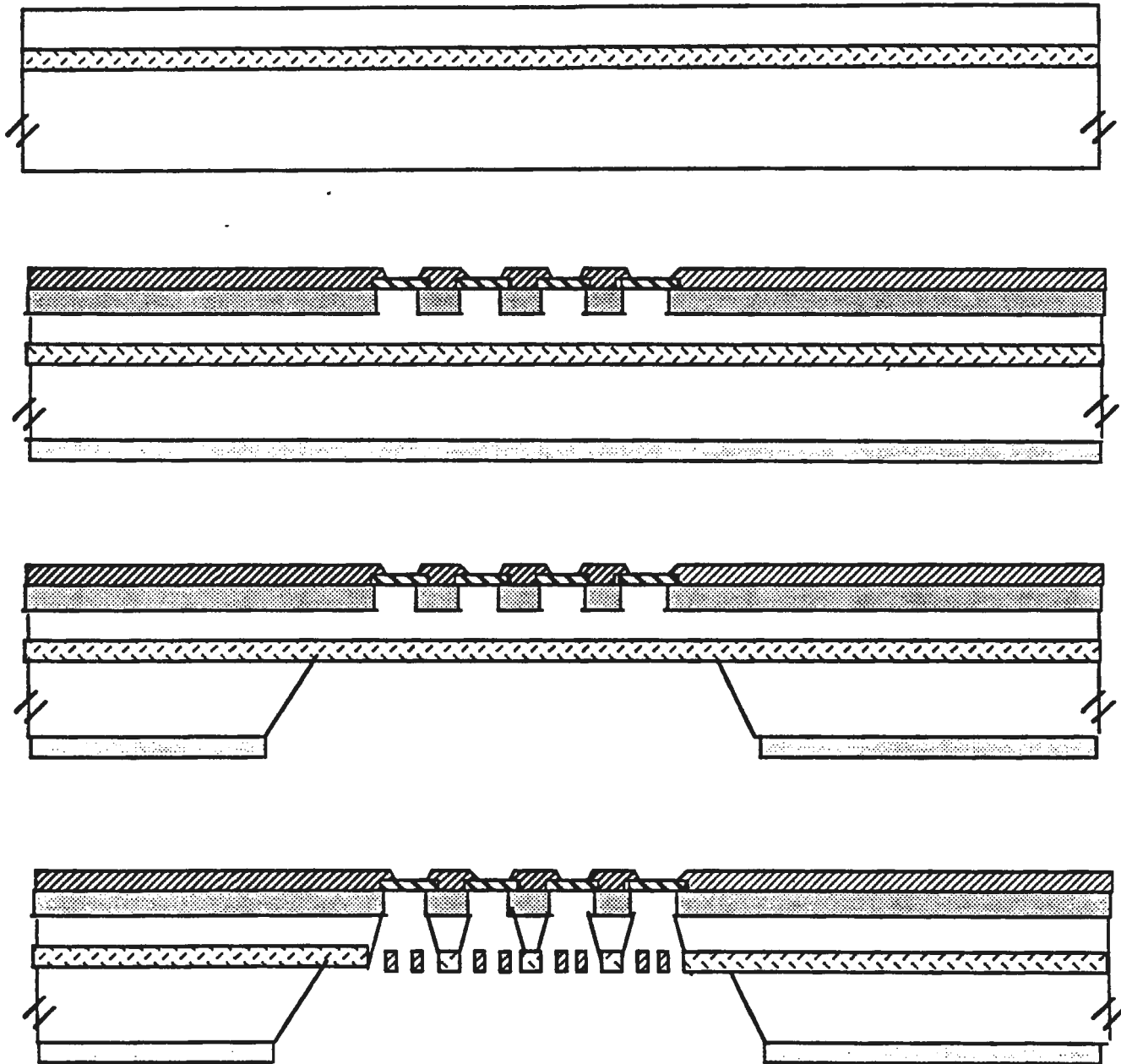




)



NEUROCHIP FABRICATION PROCESS



□ - Si

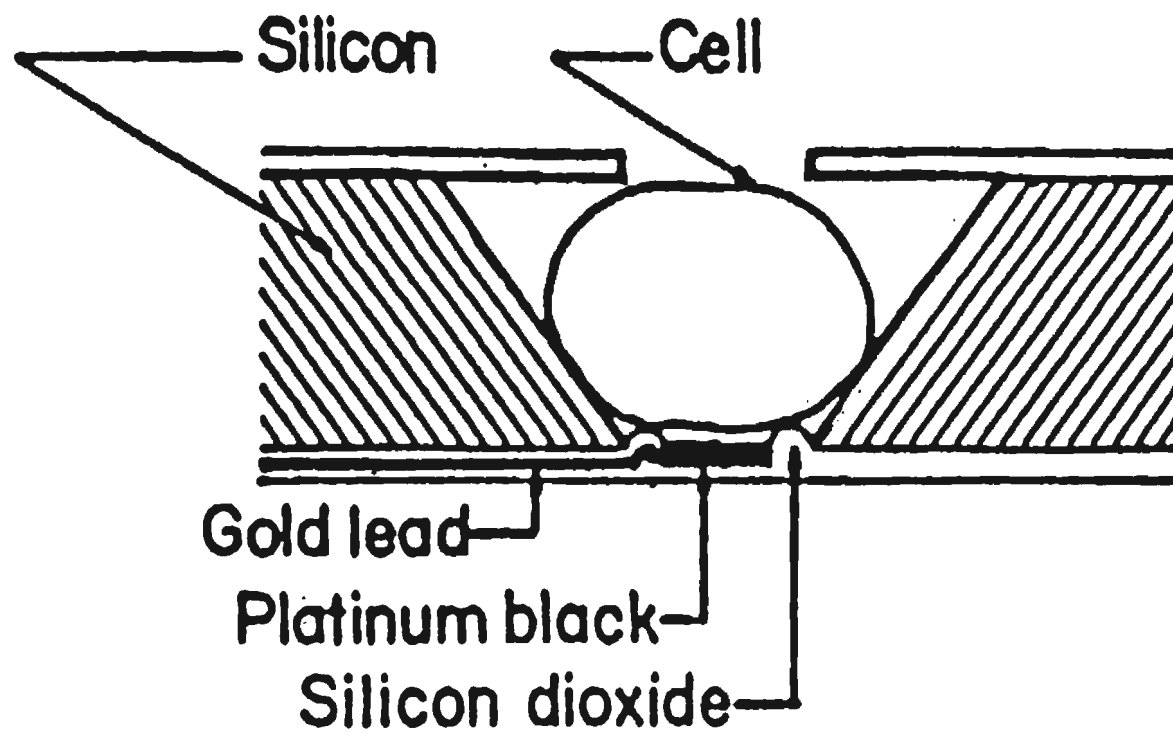
▨ - metal

▩ - insulation

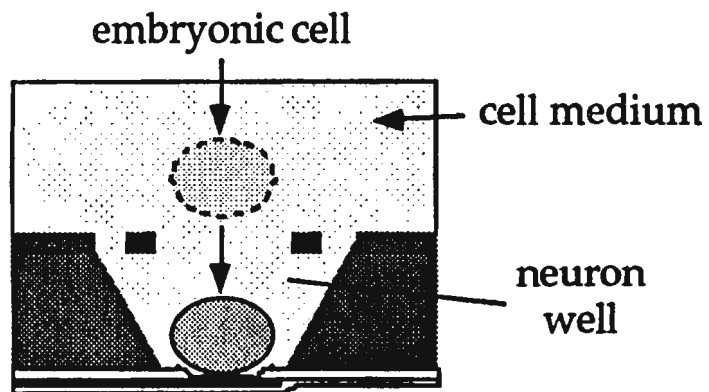
□ - SiO₂

▧ - B doped Si

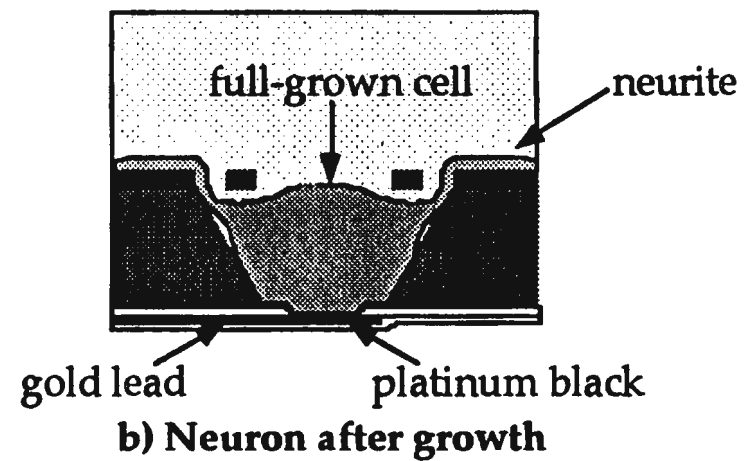
▦ - Si₃N₄



In Vitro Use of Neurochips



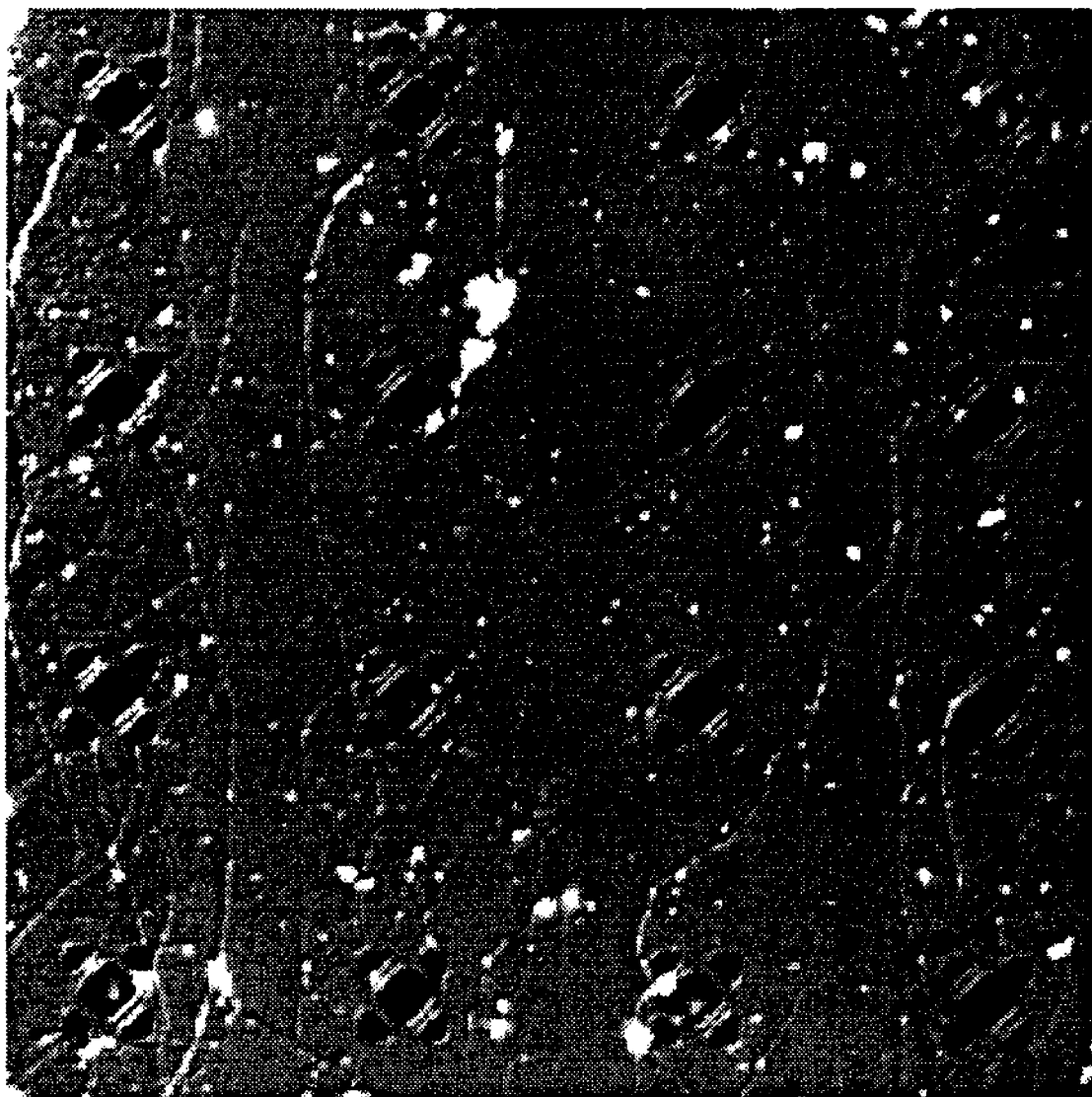
a) Neuron after implantation



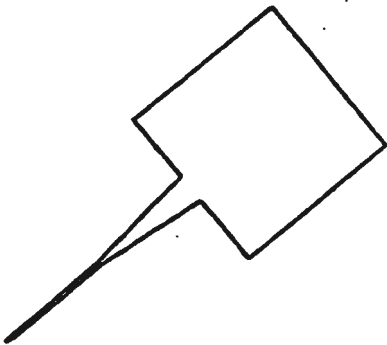
b) Neuron after growth



A Live Neural Network



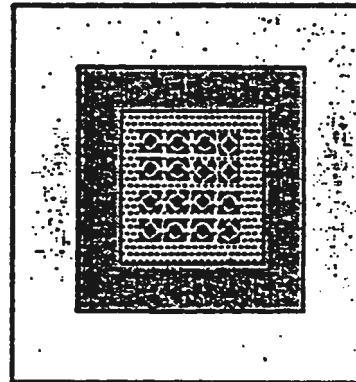
NEUROPROBE



SILICON NEUROPROBE

NEURON WELLS, NO ELECTRODES

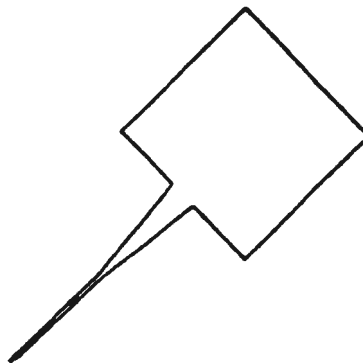
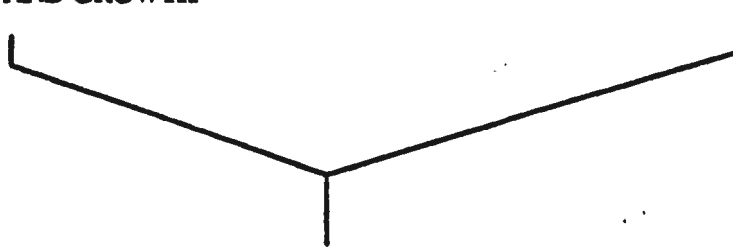
FOR IN VIVO STUDIES, CENTRAL
NERVOUS SYSTEM; NEURON
SURVIVABILITY AND GROWTH



SILICON NEUROCHIP

NEURON WELLS WITH ELECTRODES

FOR IN VITRO STUDIES; NEURON
SURVIVABILITY AND EXCITABILITY

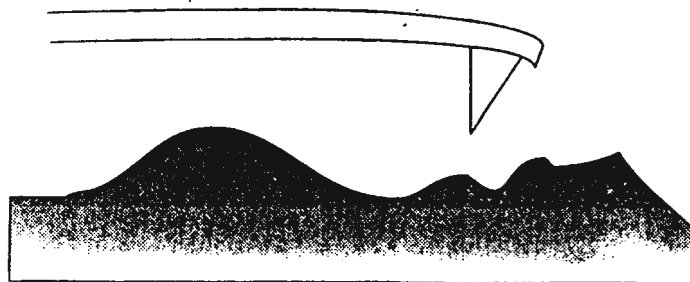
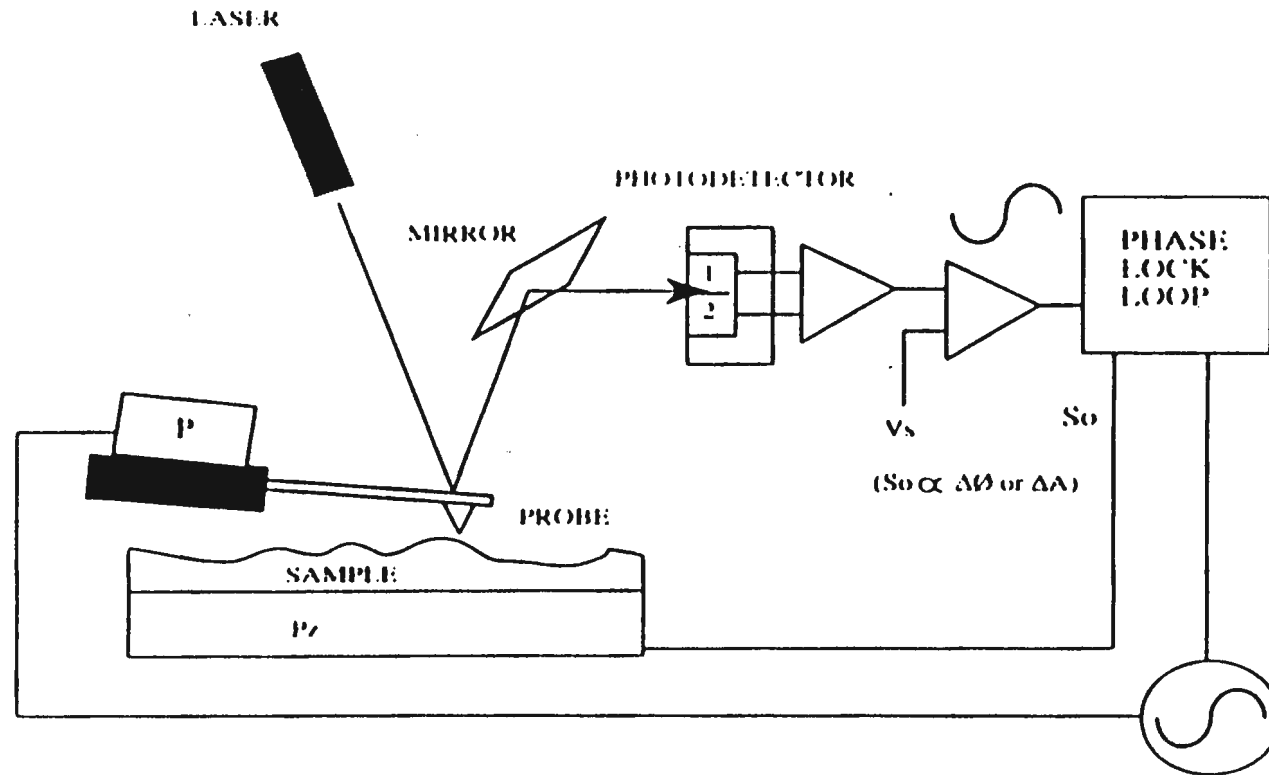


SILICON NEUROPROBE

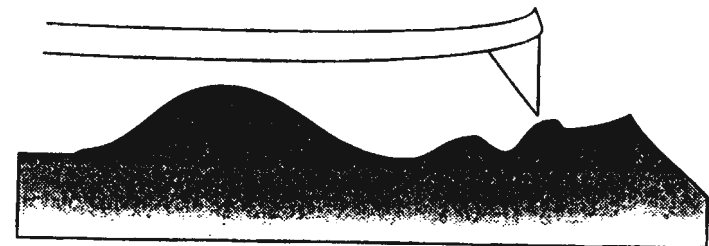
NEURON WELLS WITH ELECTRODES

FOR IN VIVO STUDIES;
STIMULATION AND RECORDING

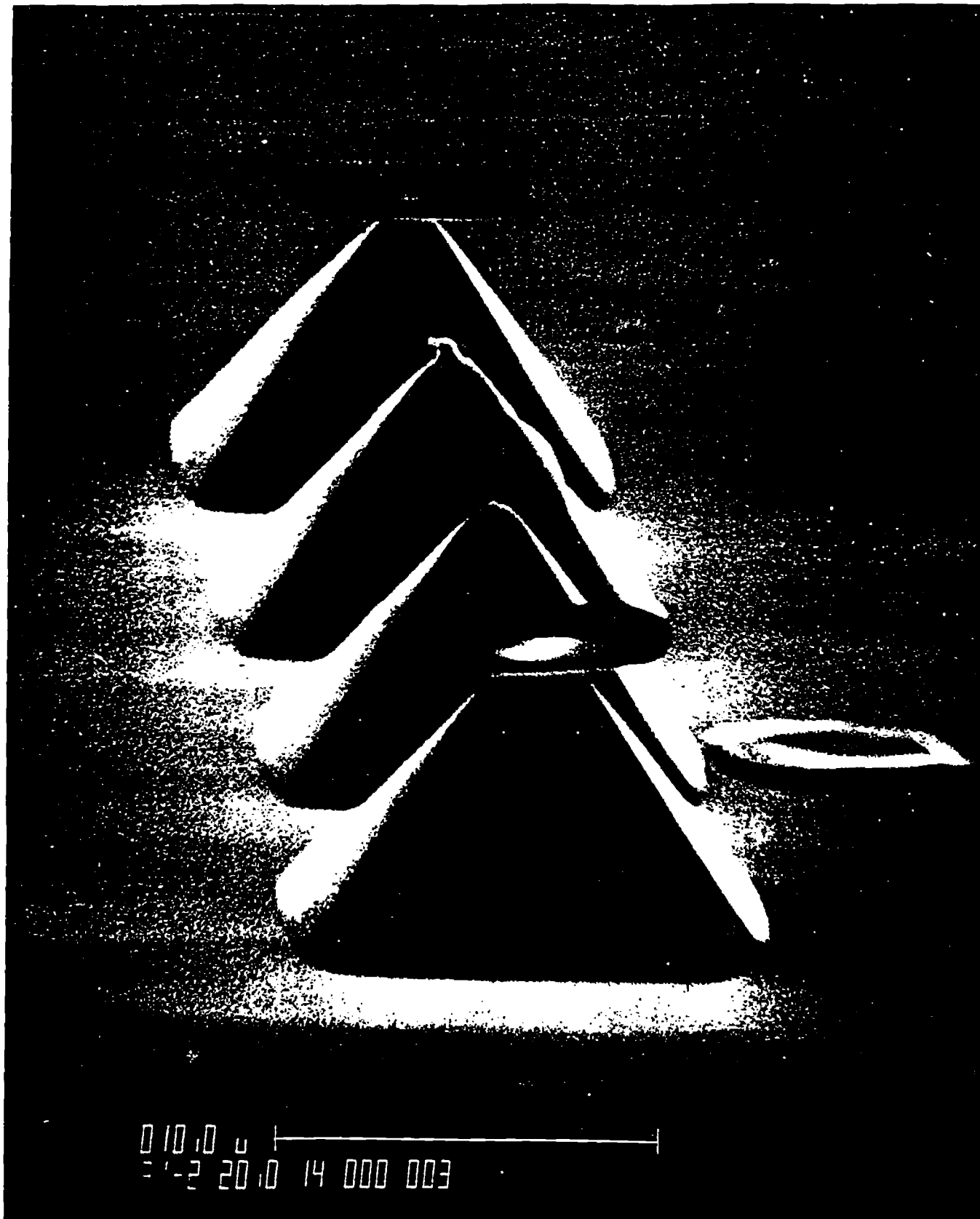
AFM Imaging



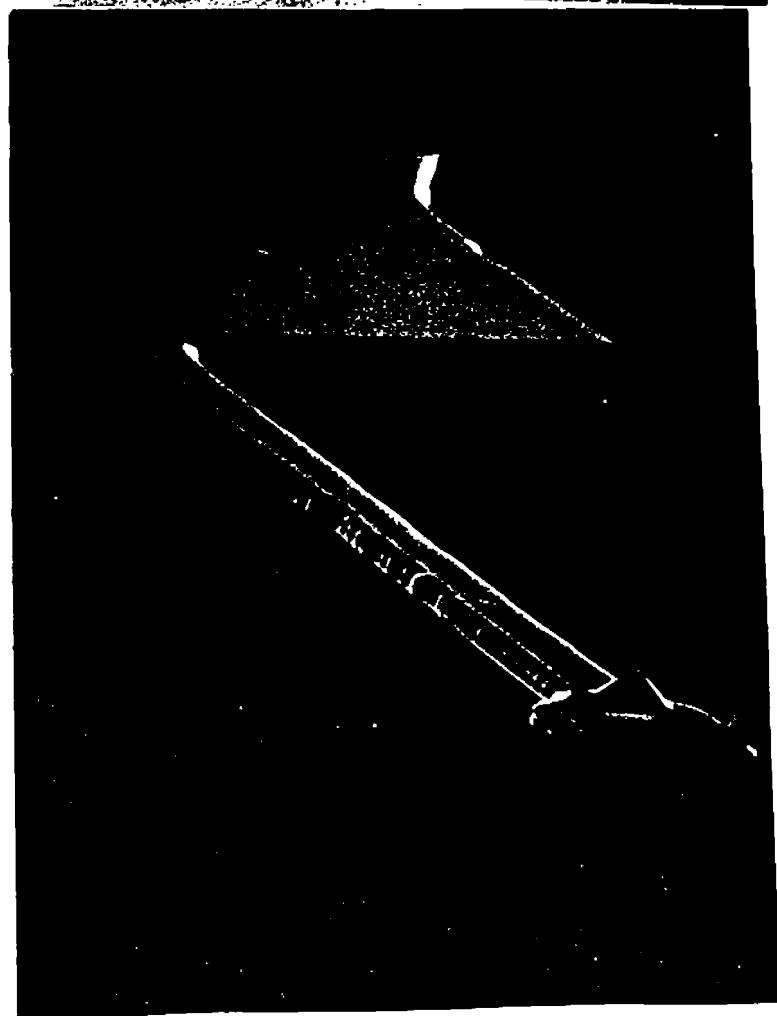
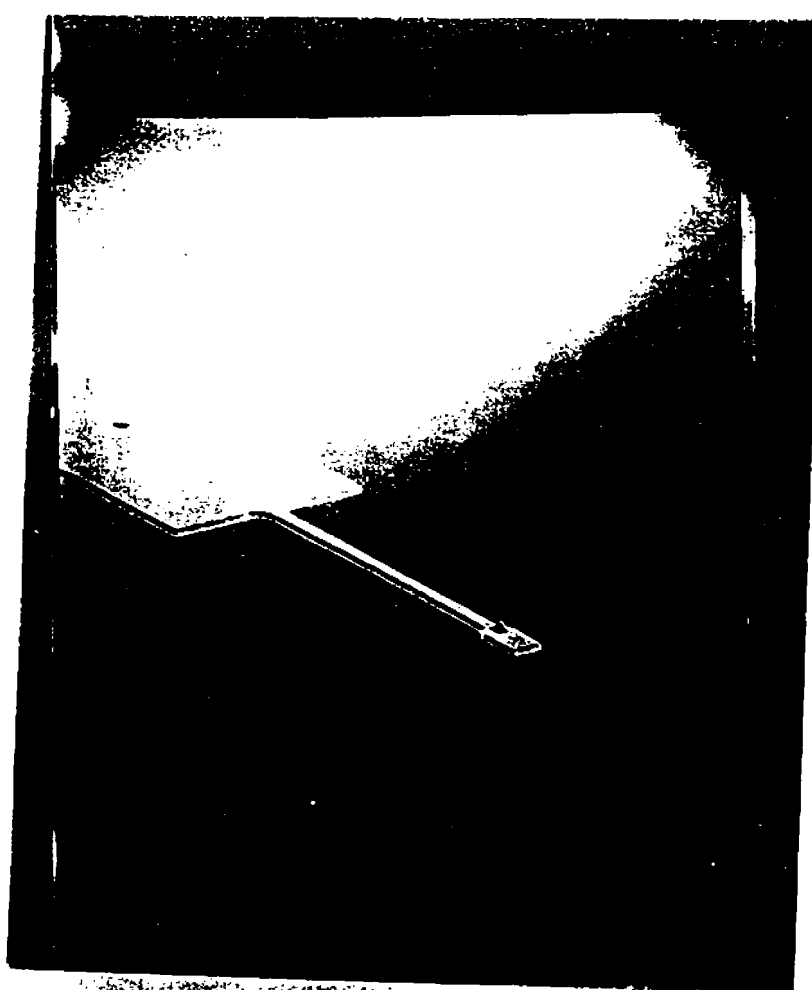
Non-Contact Modes



Contact Modes



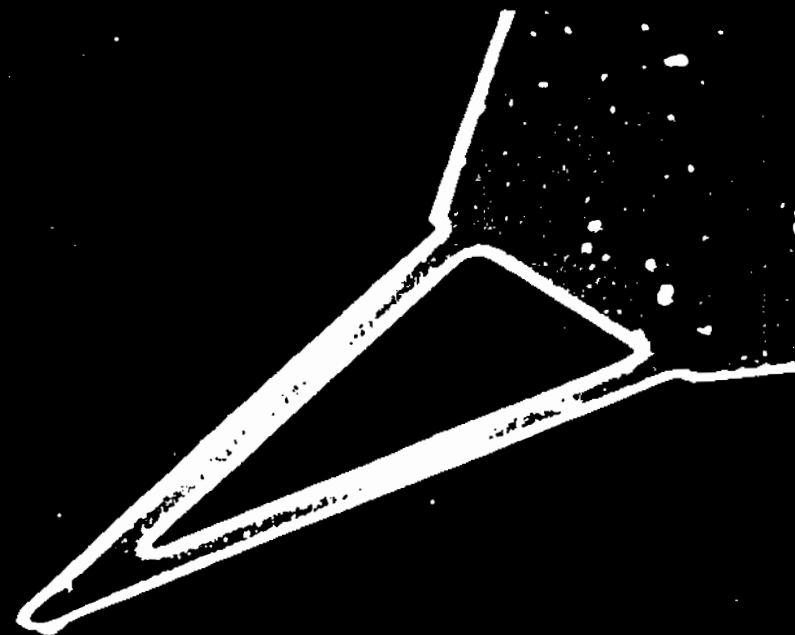
0 10 10 0 1
1-2 20 10 14 000 003



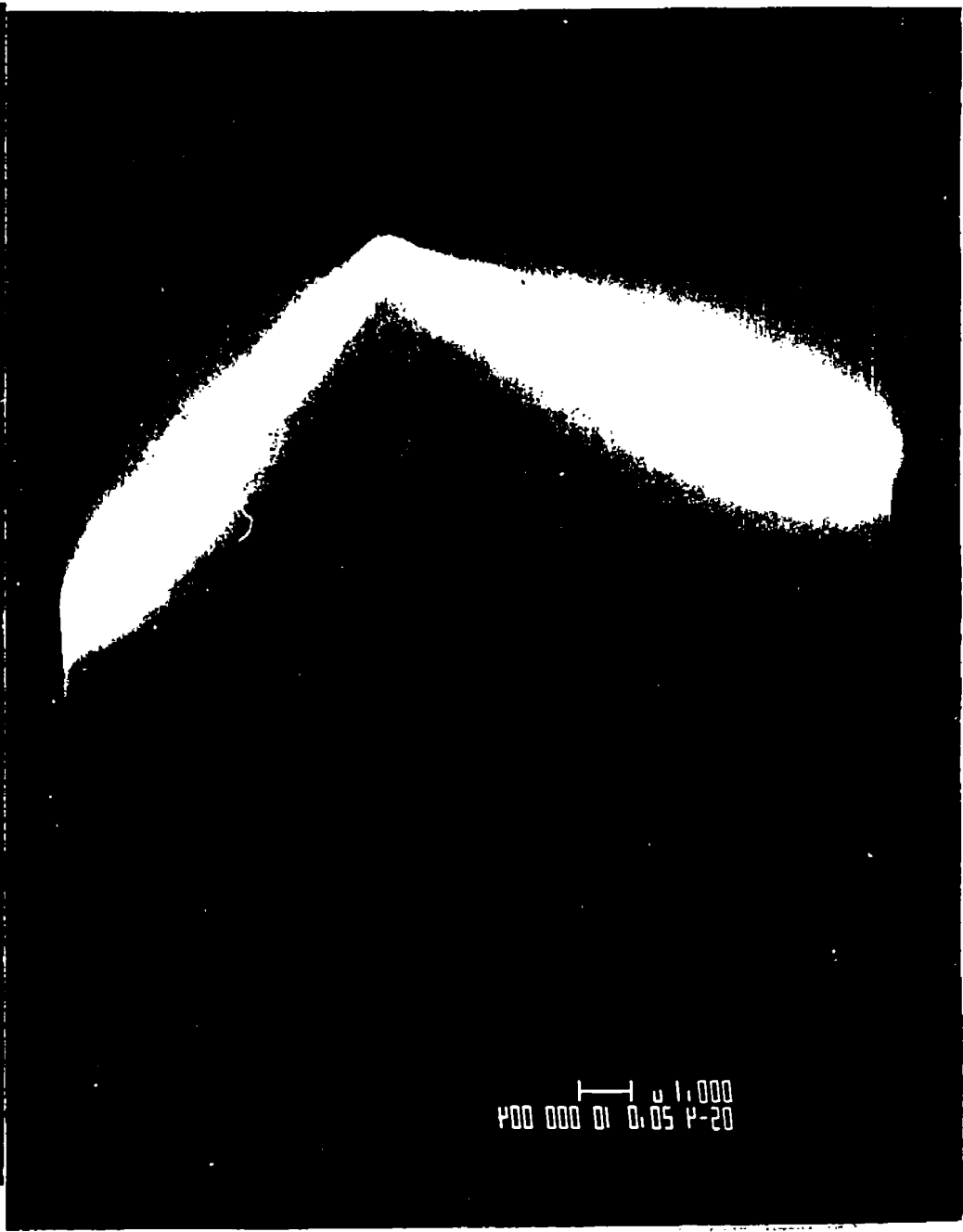
I-207

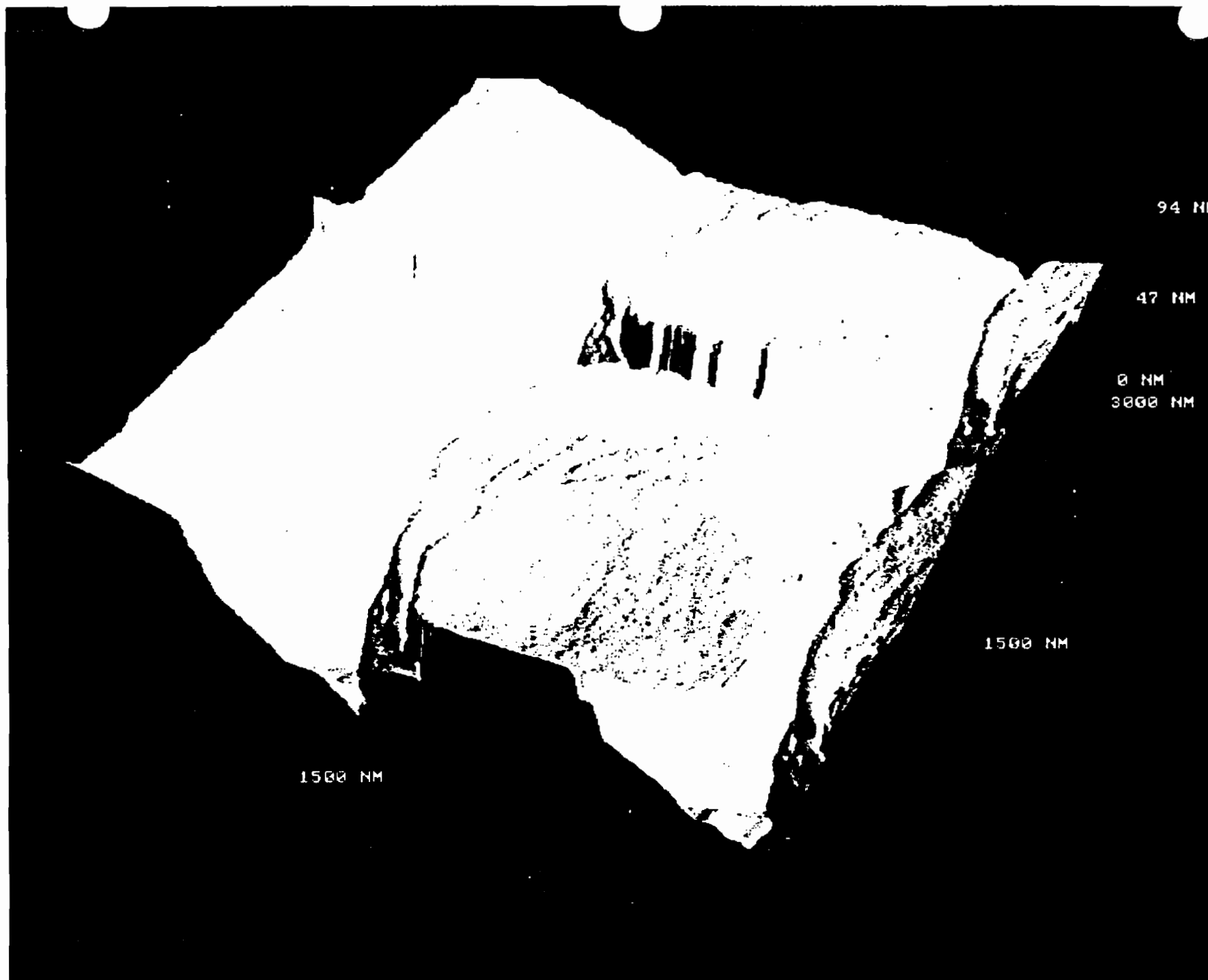


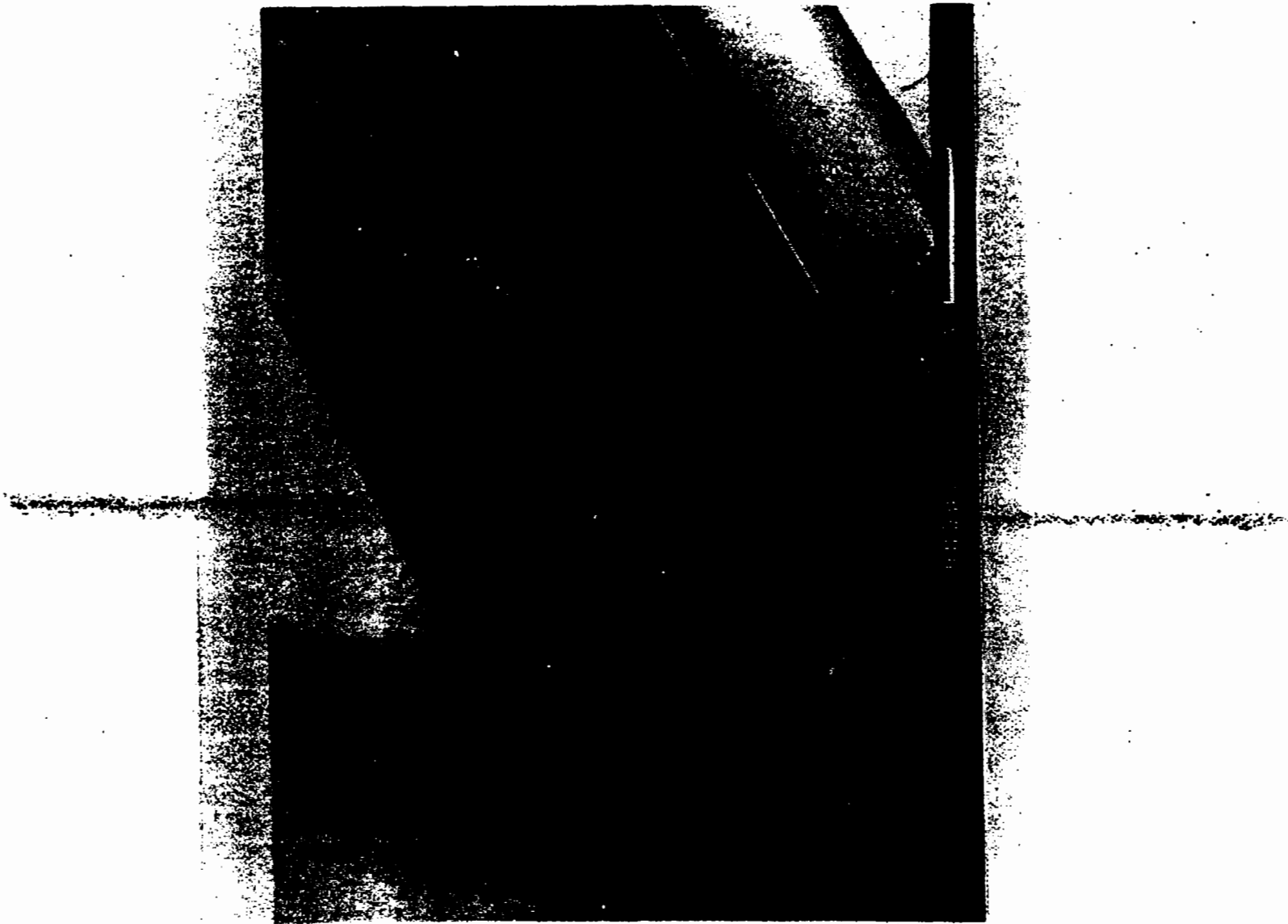
100.0 0 1
05-1 20.0 08 005 0 10



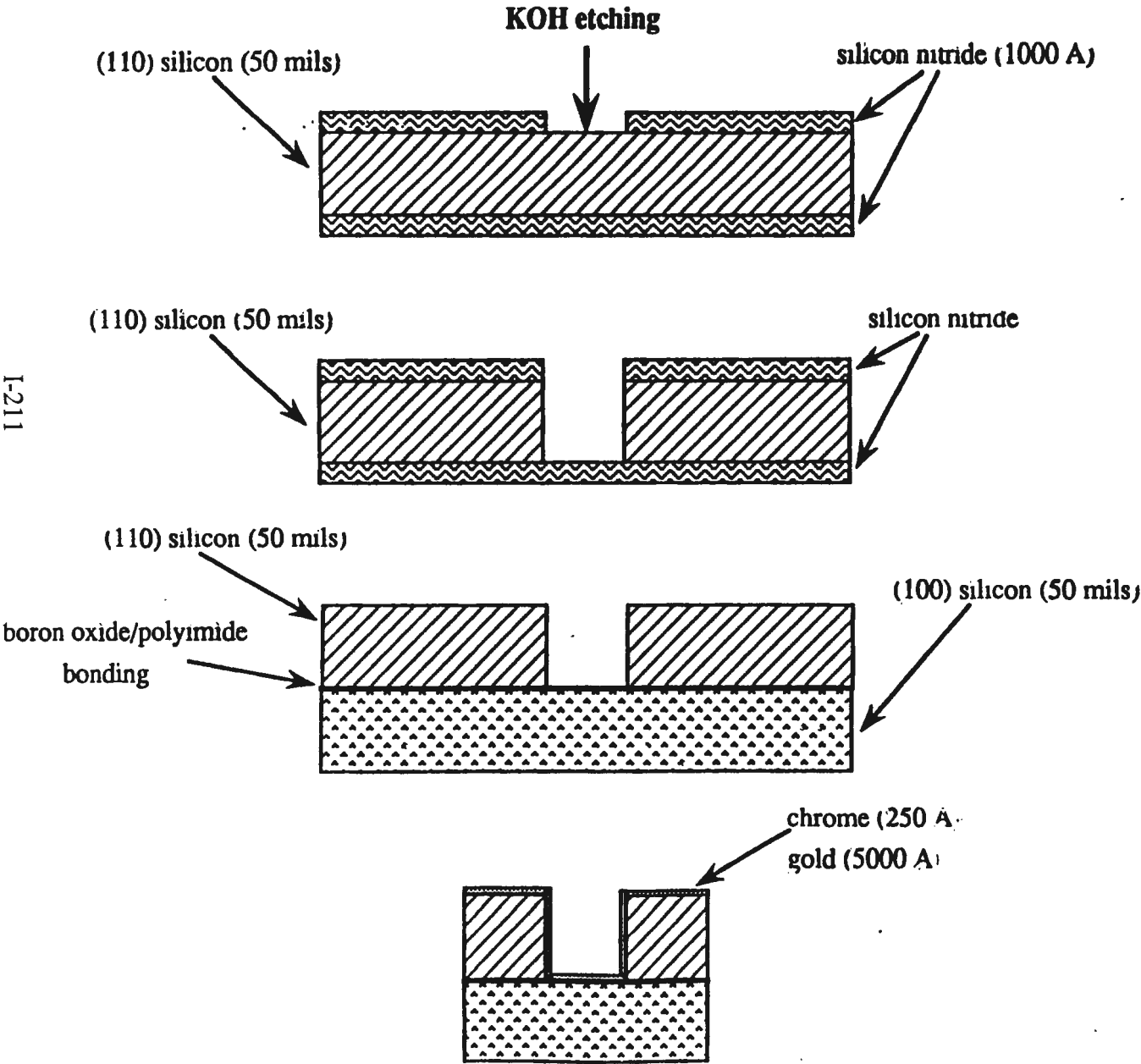
100.0 0 1
35-1 20.0 08 005 0 11







WR-10 WAVEGUIDE FABRICATION PROCESS

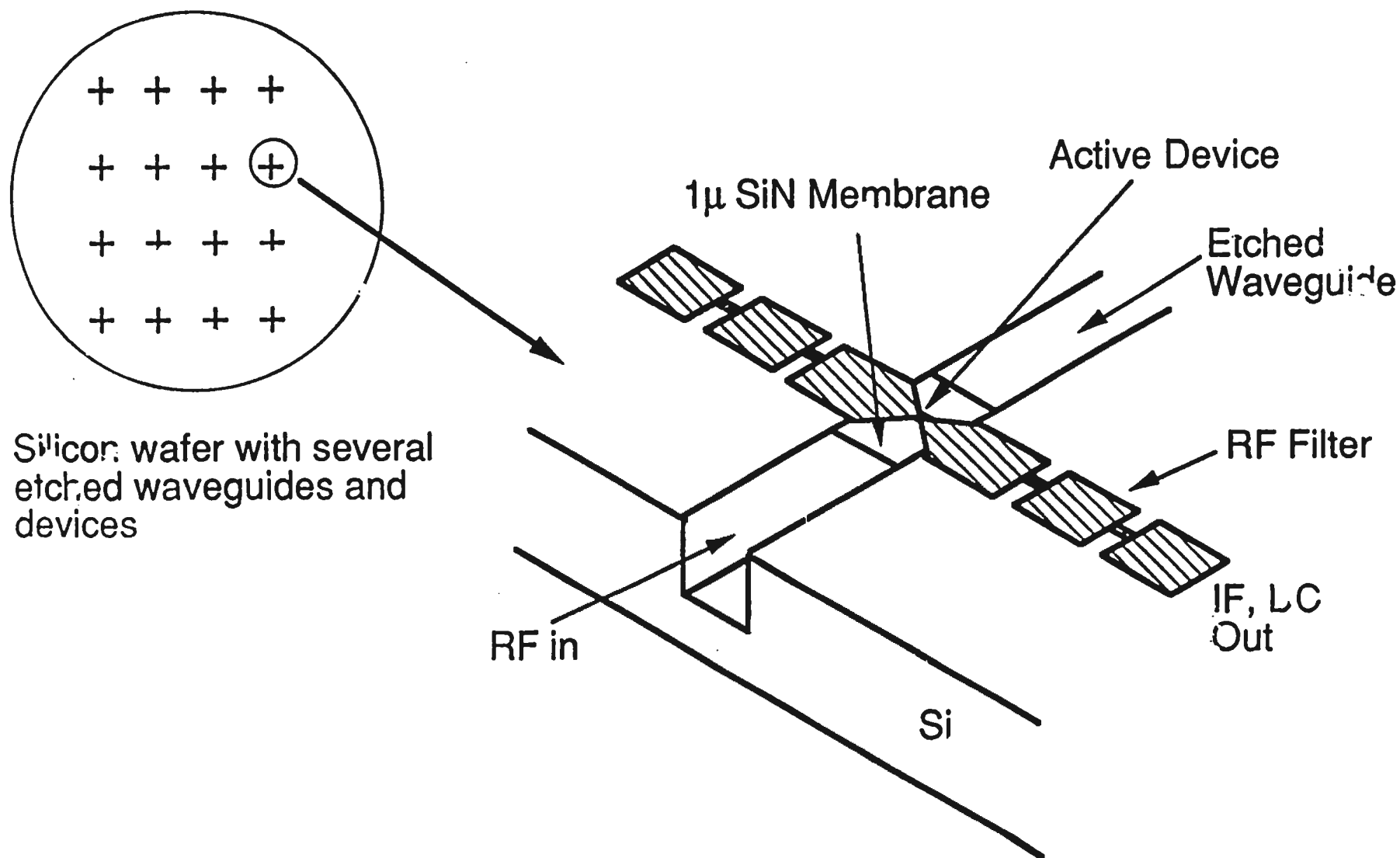


I-211

IMPORTANT MILLIMETER WAVE AND SUBMILLIMETER WAVE APPLICATIONS

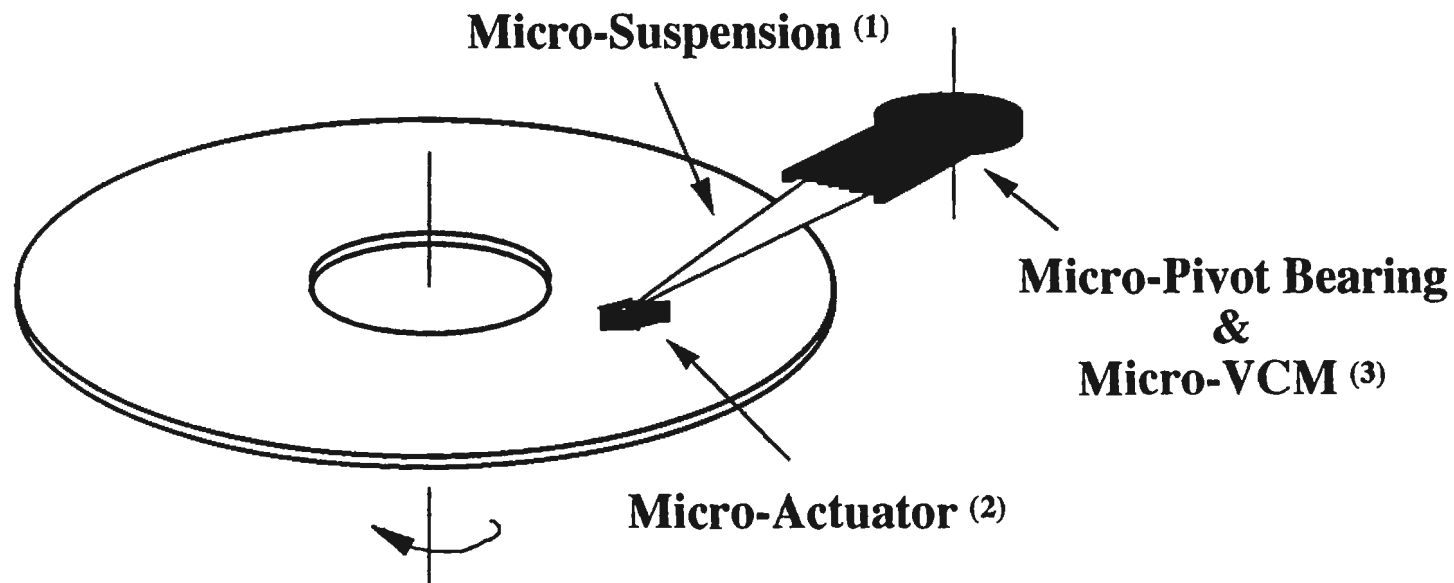
- Mixer and Frequency Multiplier Embedding Circuits
- Directional Couplers
- Waveguide Transformers
- Waveguide - to - Planar Circuit Transitions
- Low Loss Filters
- Rectangular and Conical Feedhorns
- Dichroic Filter Plates

Si Micromachined Waveguide Circuit



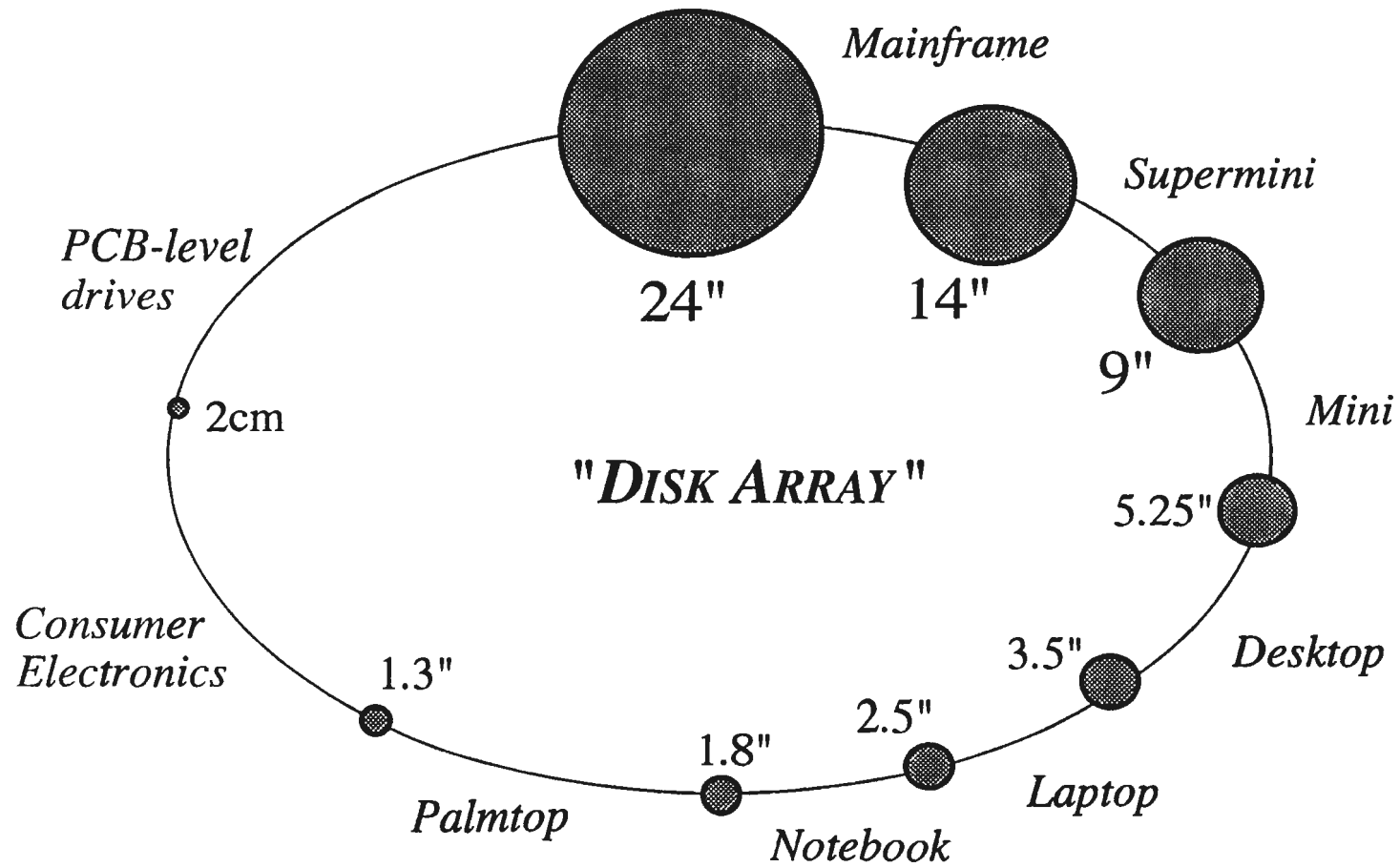
Silicon wafer with several etched waveguides and devices

Current Research Activities at UCLA/CalTech

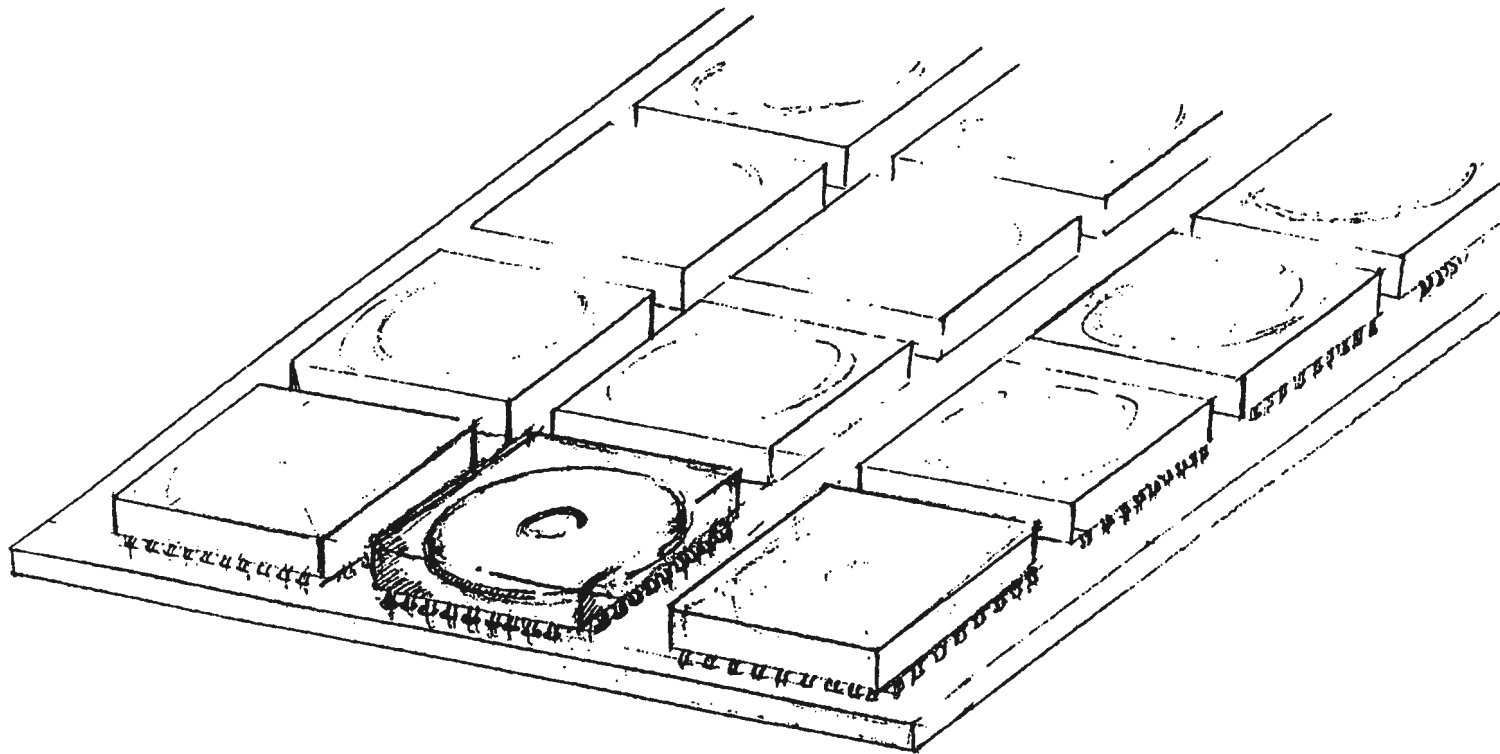


- (1) supported by AMC, HP, IBM, Maxtor, Quantum, Read-Rite and Seagate Technology Corporations with matching funds from the State of California MICRO program.
- (2) supported by the National Storage Industry Consortium (NSIC).
- (3) proposal submitted to the Defense Advanced Research Program Agency (DARPA).

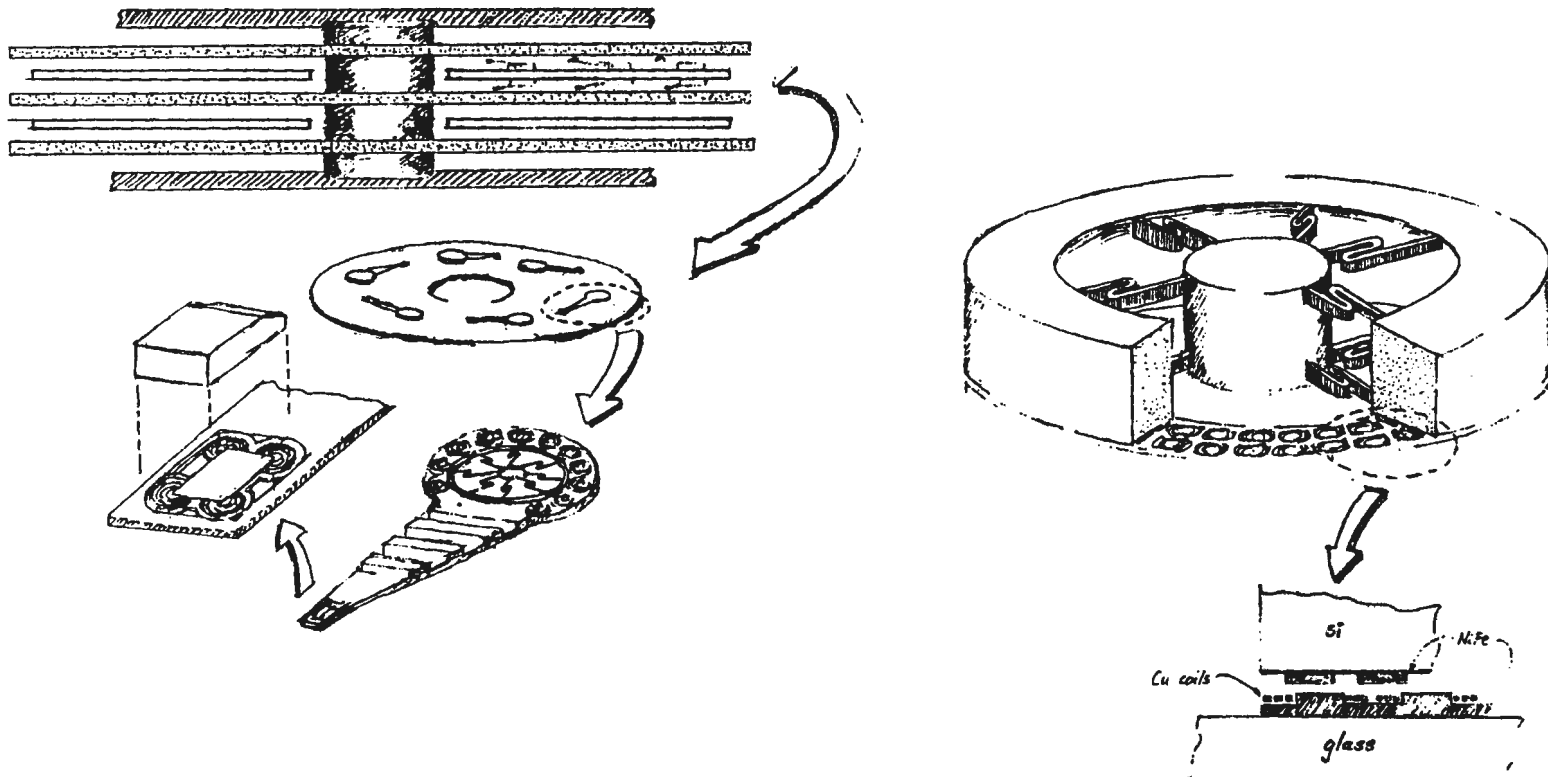
Form Factor Food-Chain



SCALED Technology - Super Compact Array of Low-cost Enormous-capacity Disk-drives

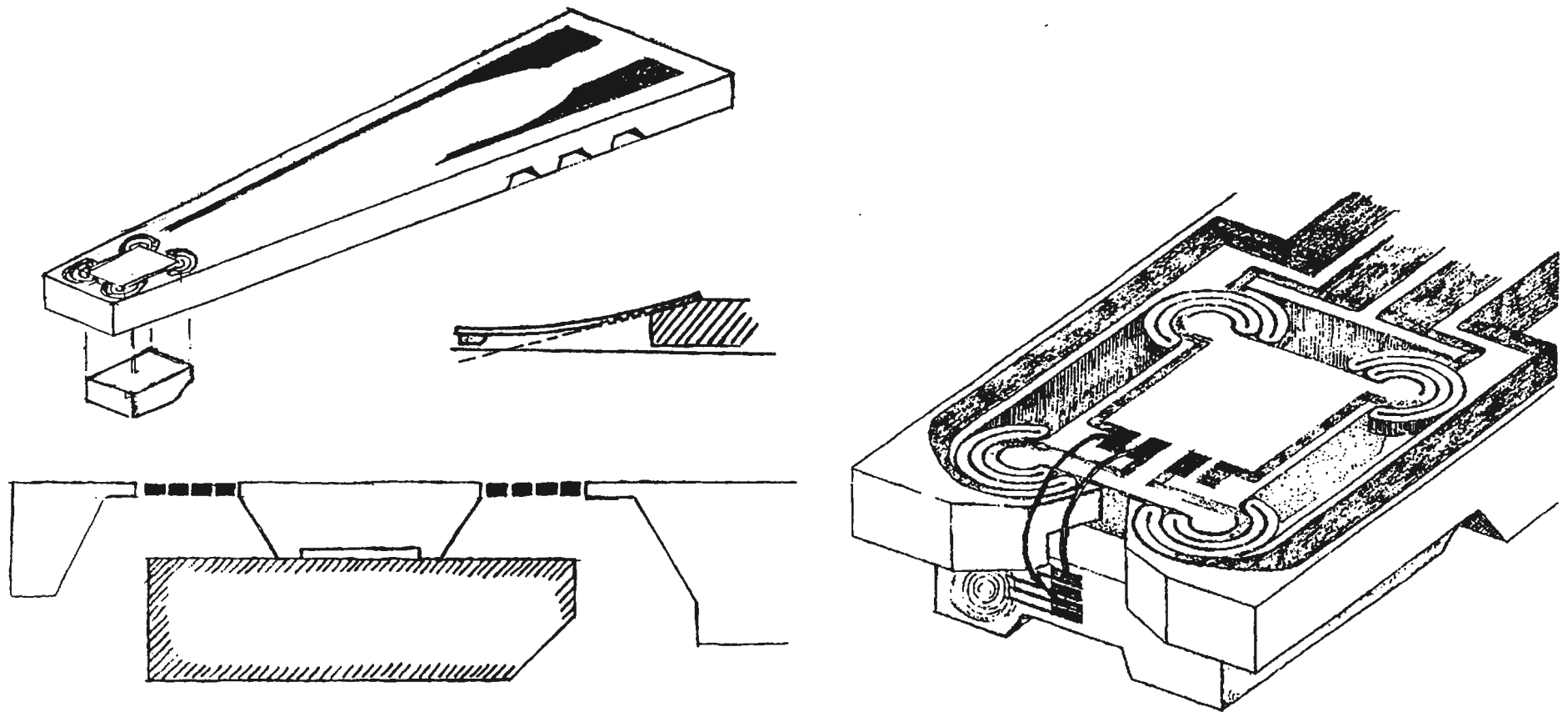


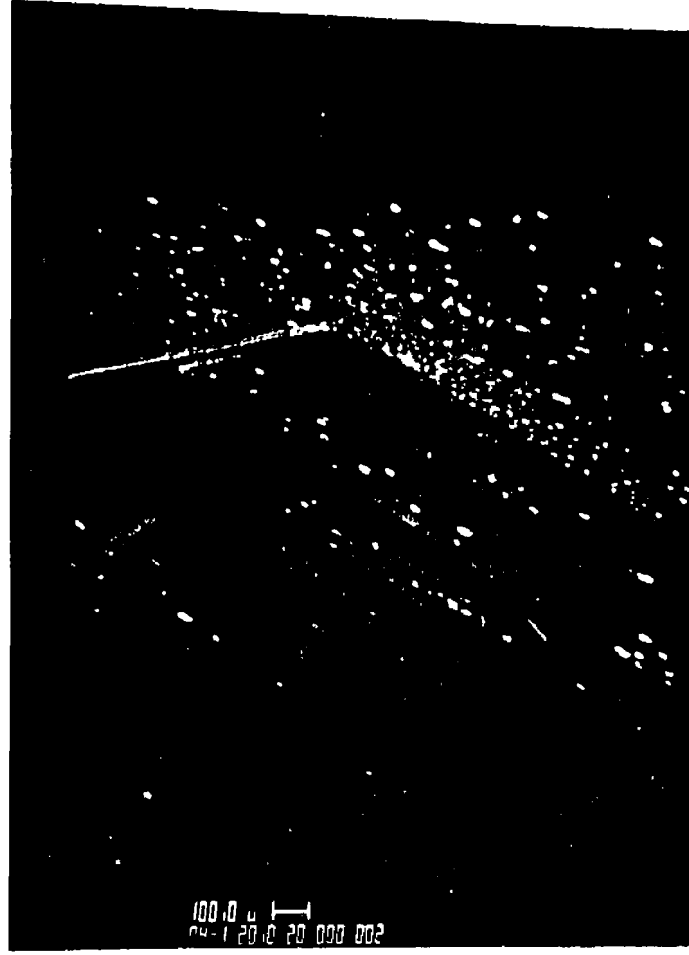
Integrated Read-Write-Head/Suspension/ Torsional-Bearings/Voice-Coil-Motor (Long-Term Goal)



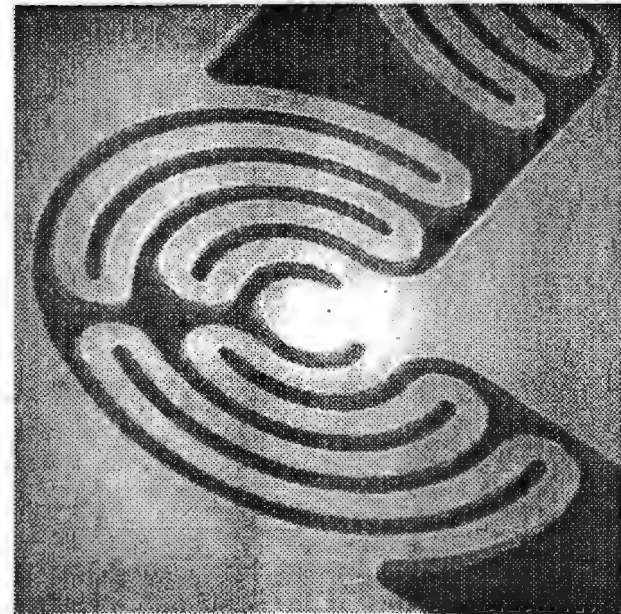
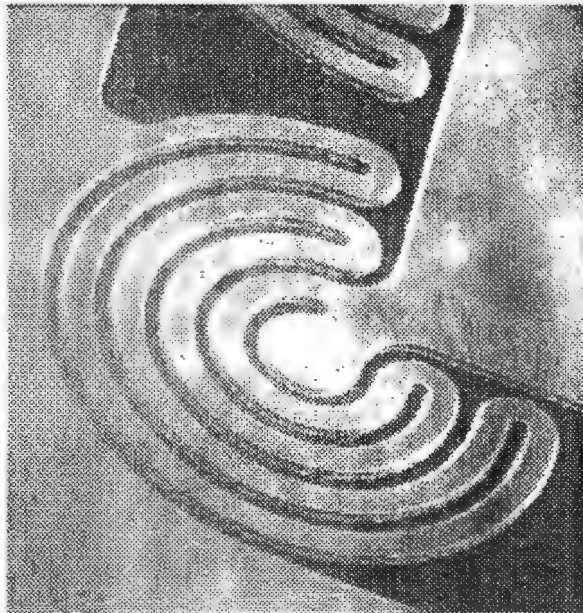
Silicon Micromachined Gimbal/Suspension with integrated Electrodes

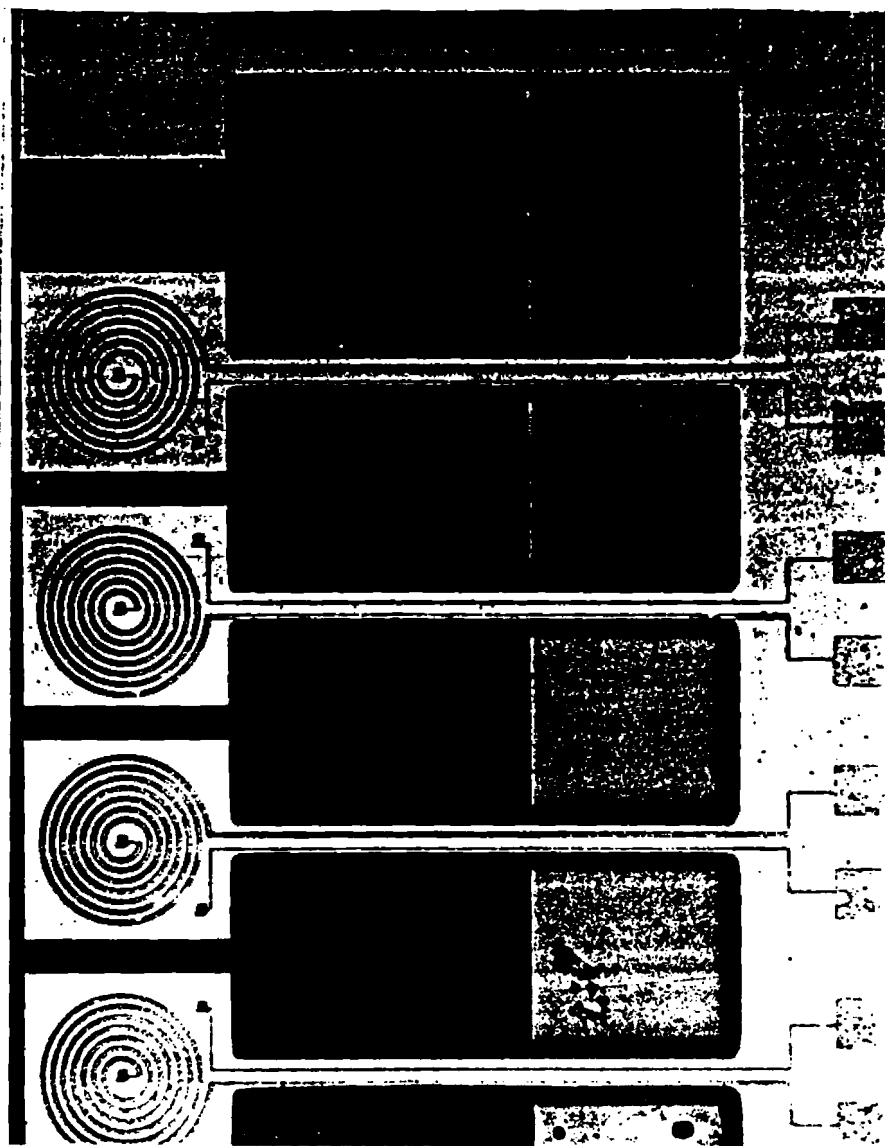
I-218

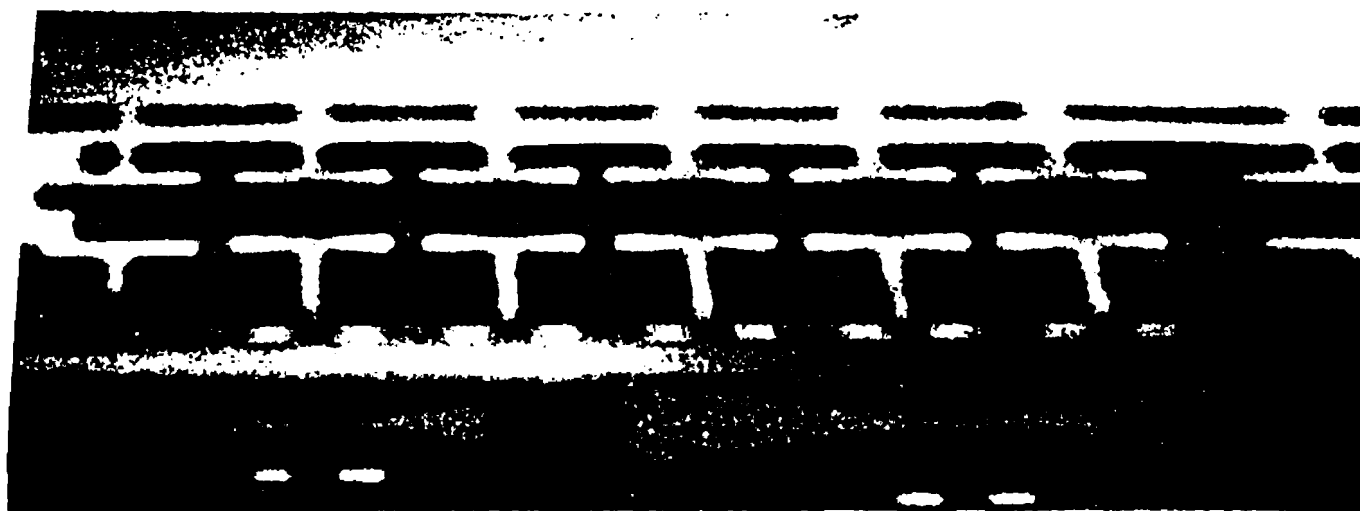


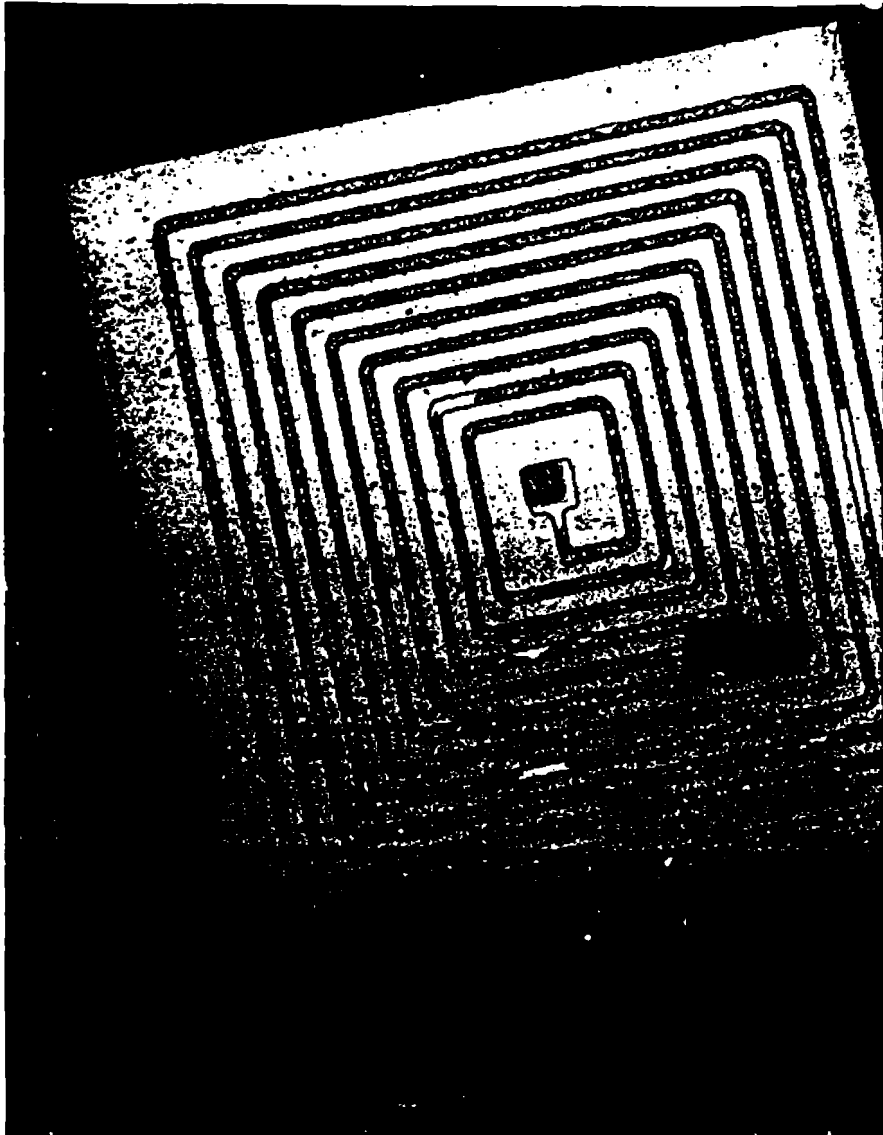


Some Recently Fabricated Silicon Microgimbals (beam width ~ 80 microns)

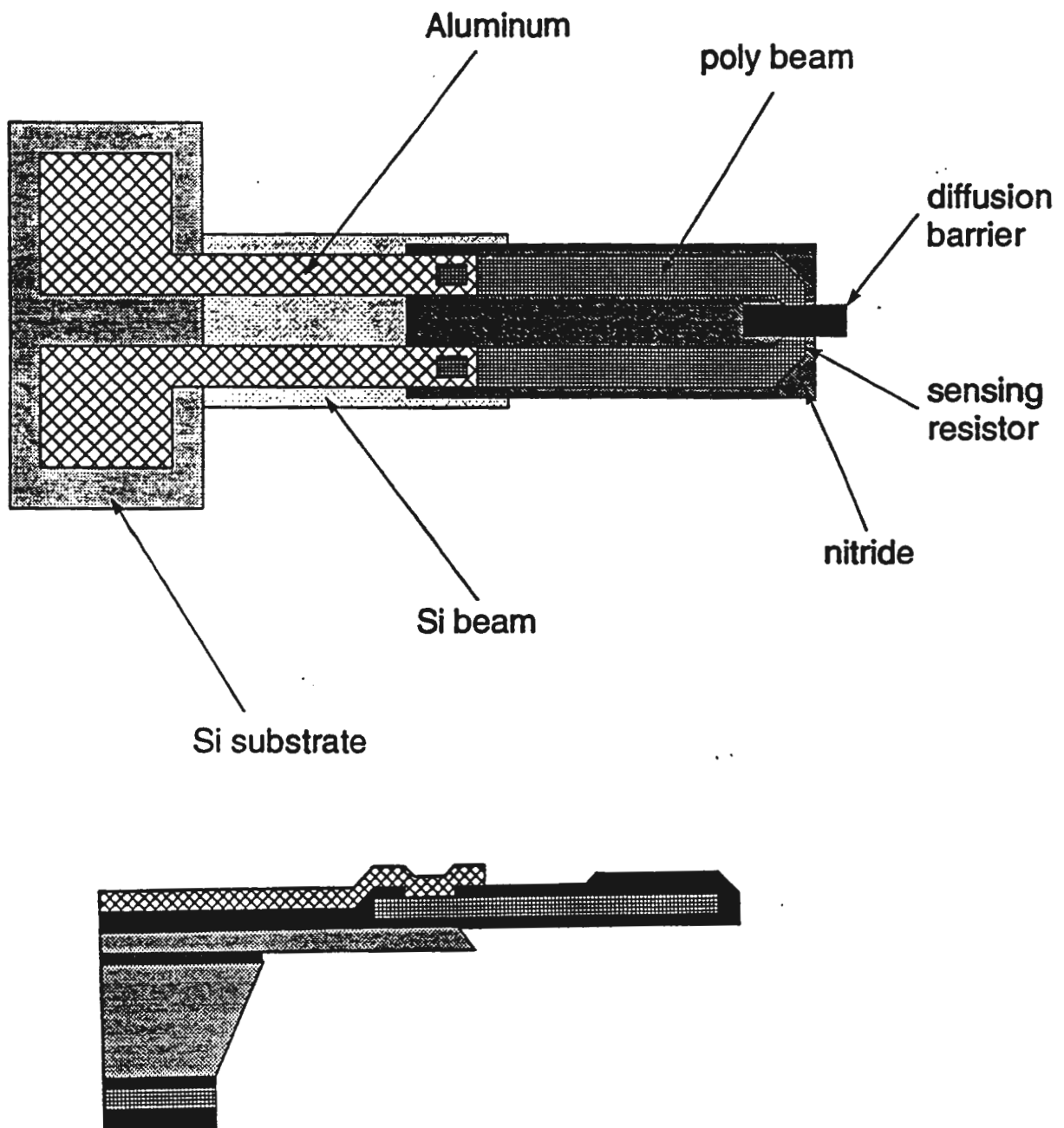


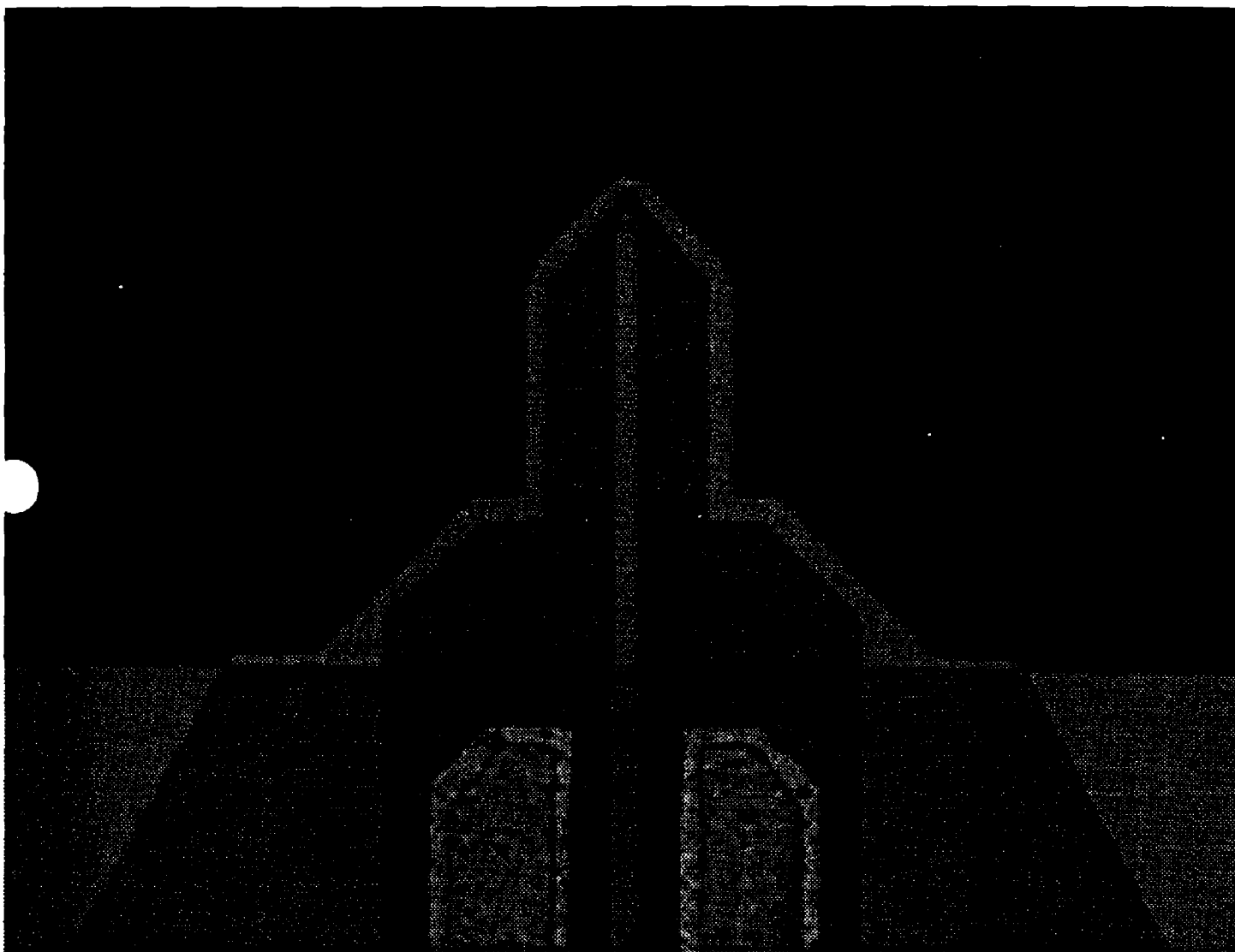


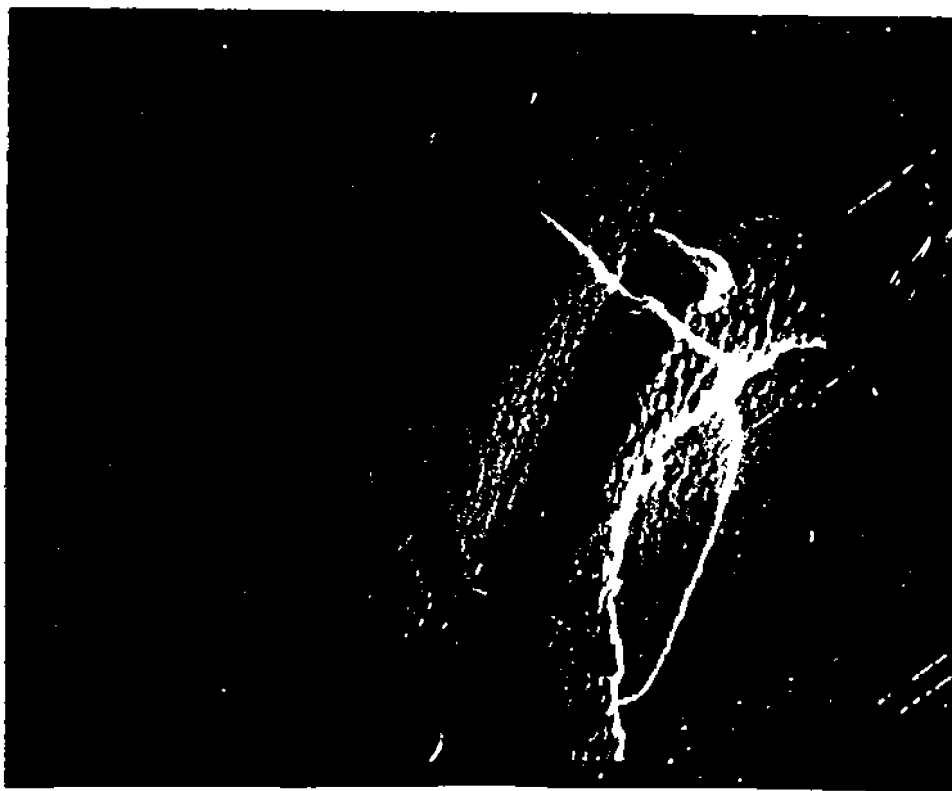
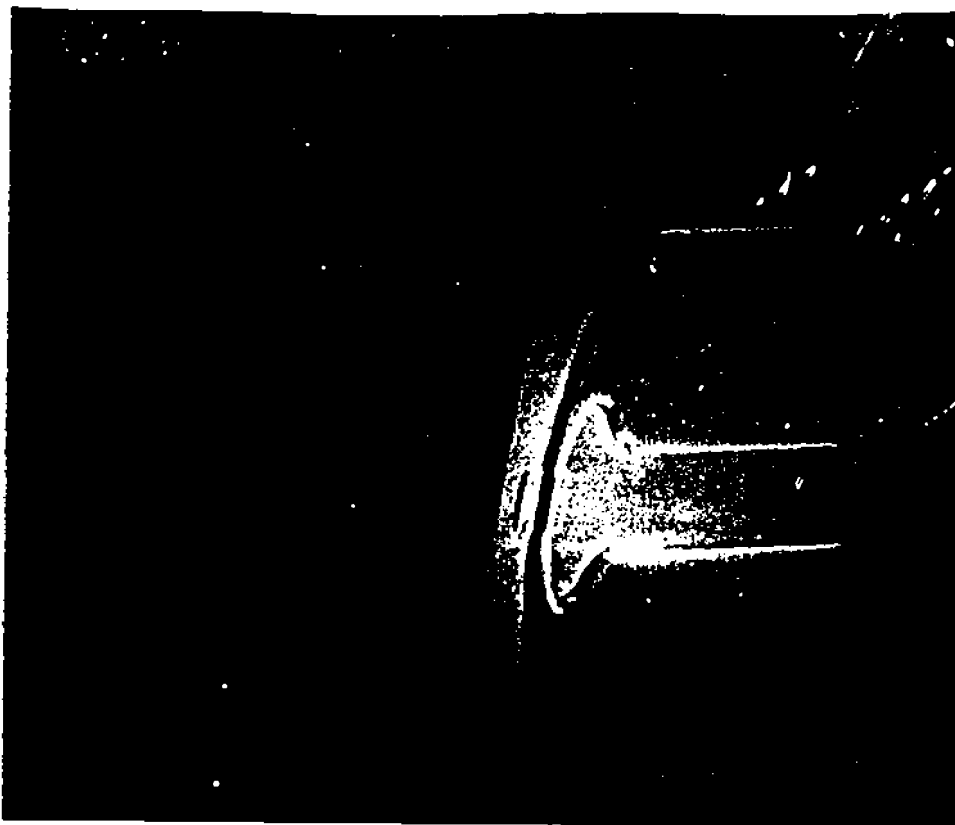


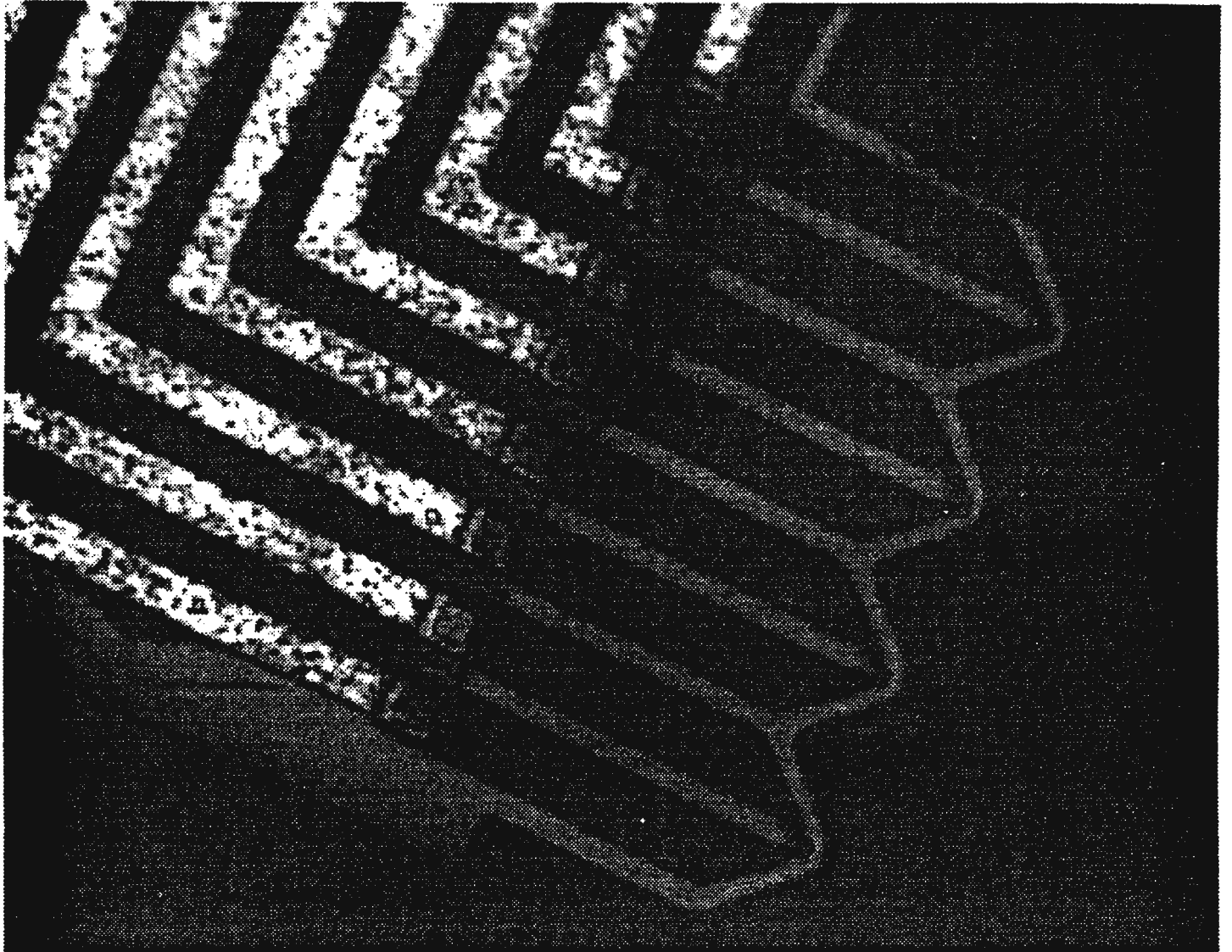


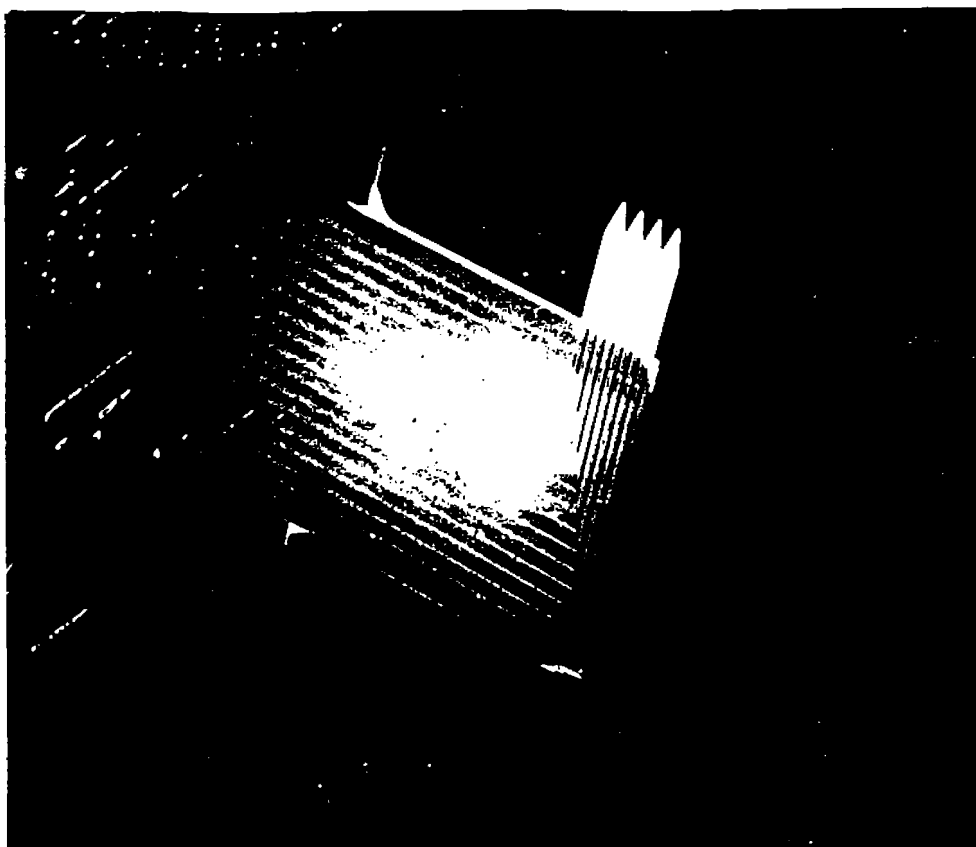
HOT-POINT ANEMOMETER



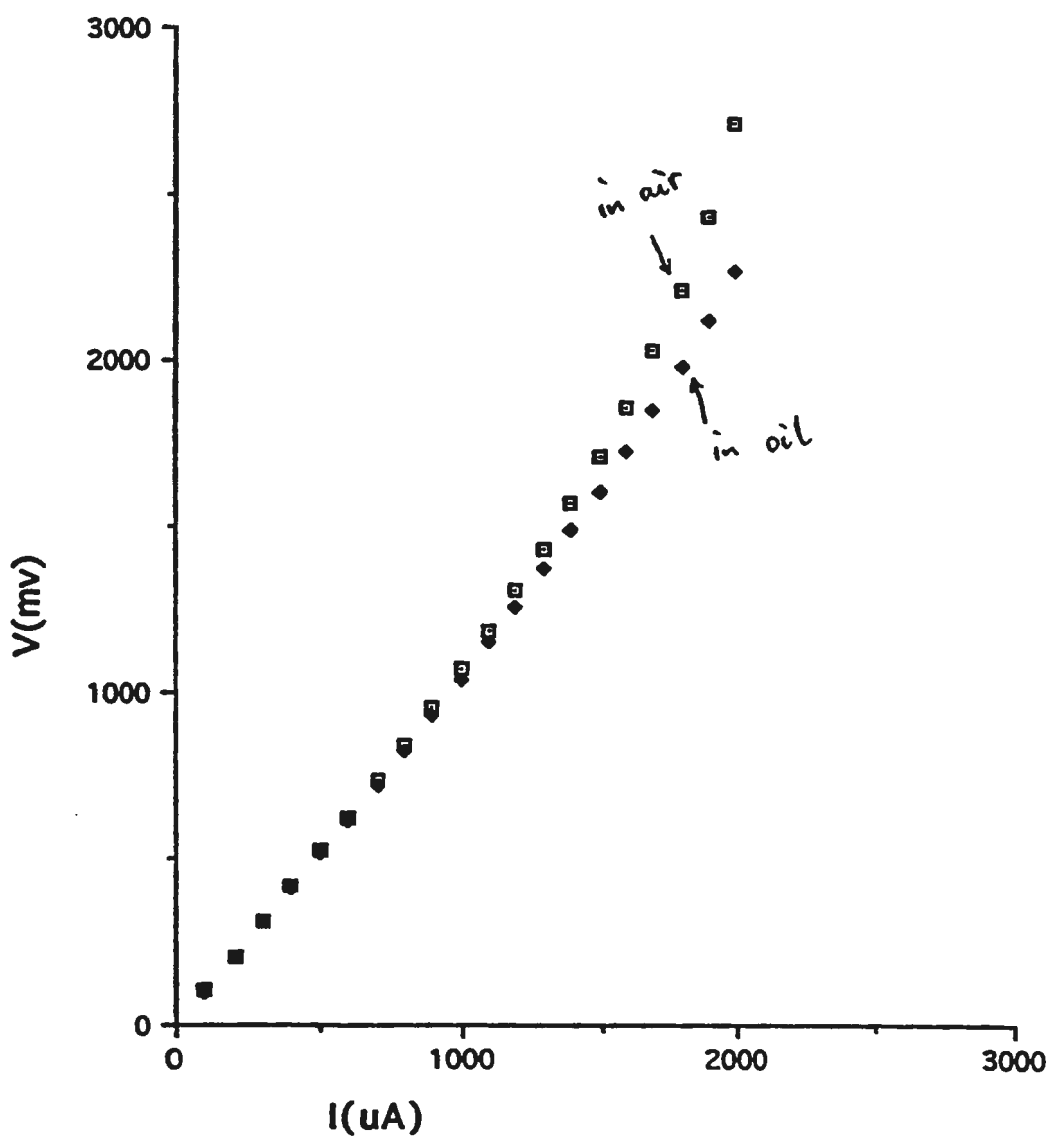






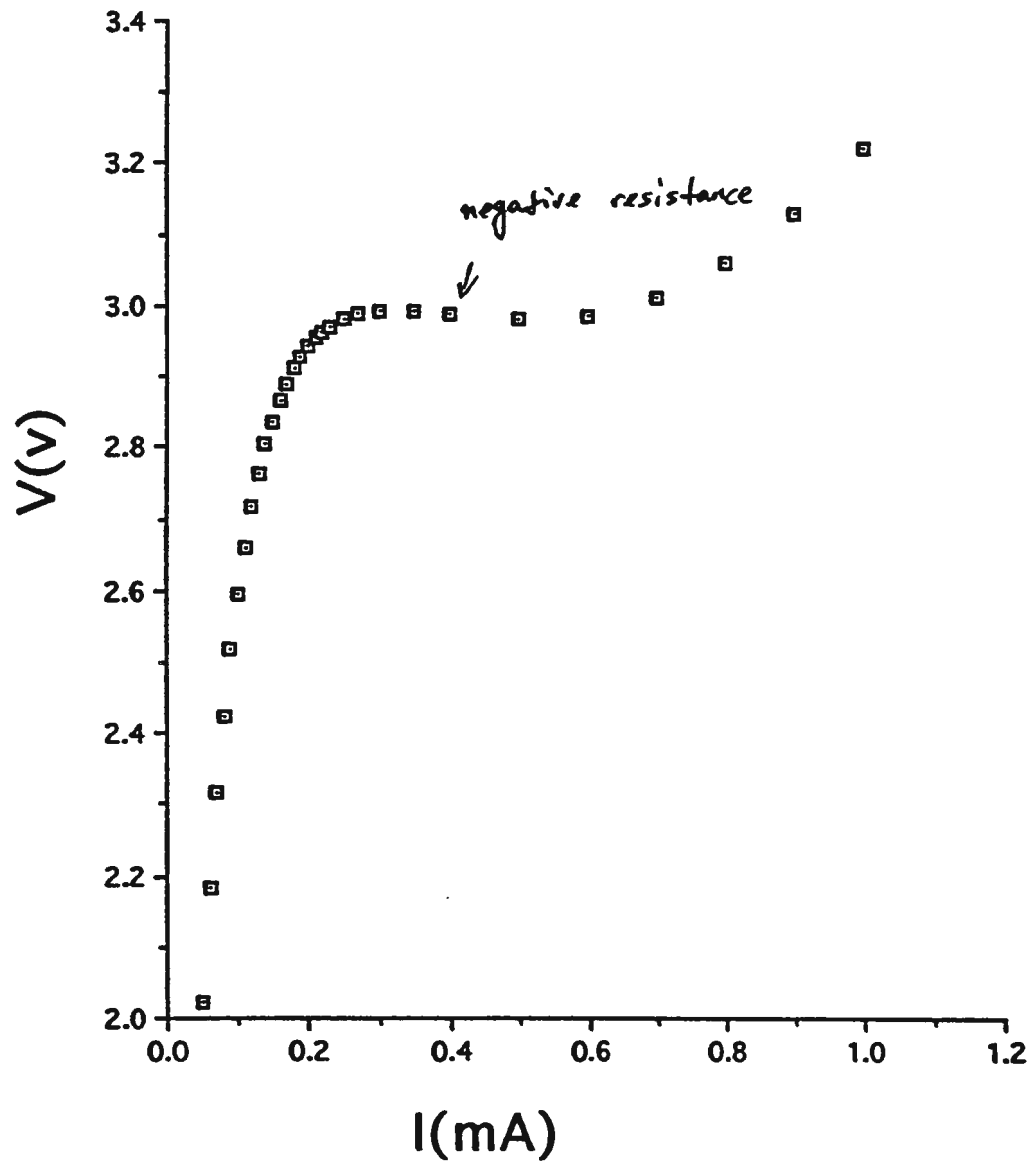


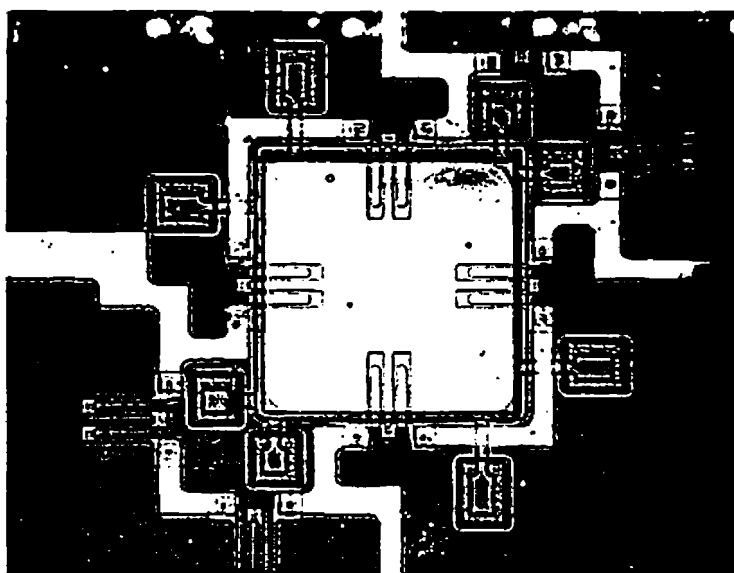
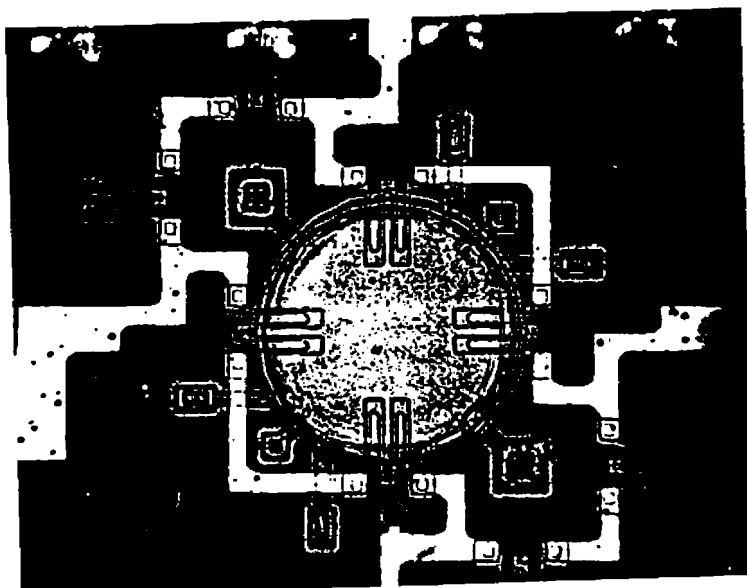
I-V Curve of a 1K Probe in Air and Oil



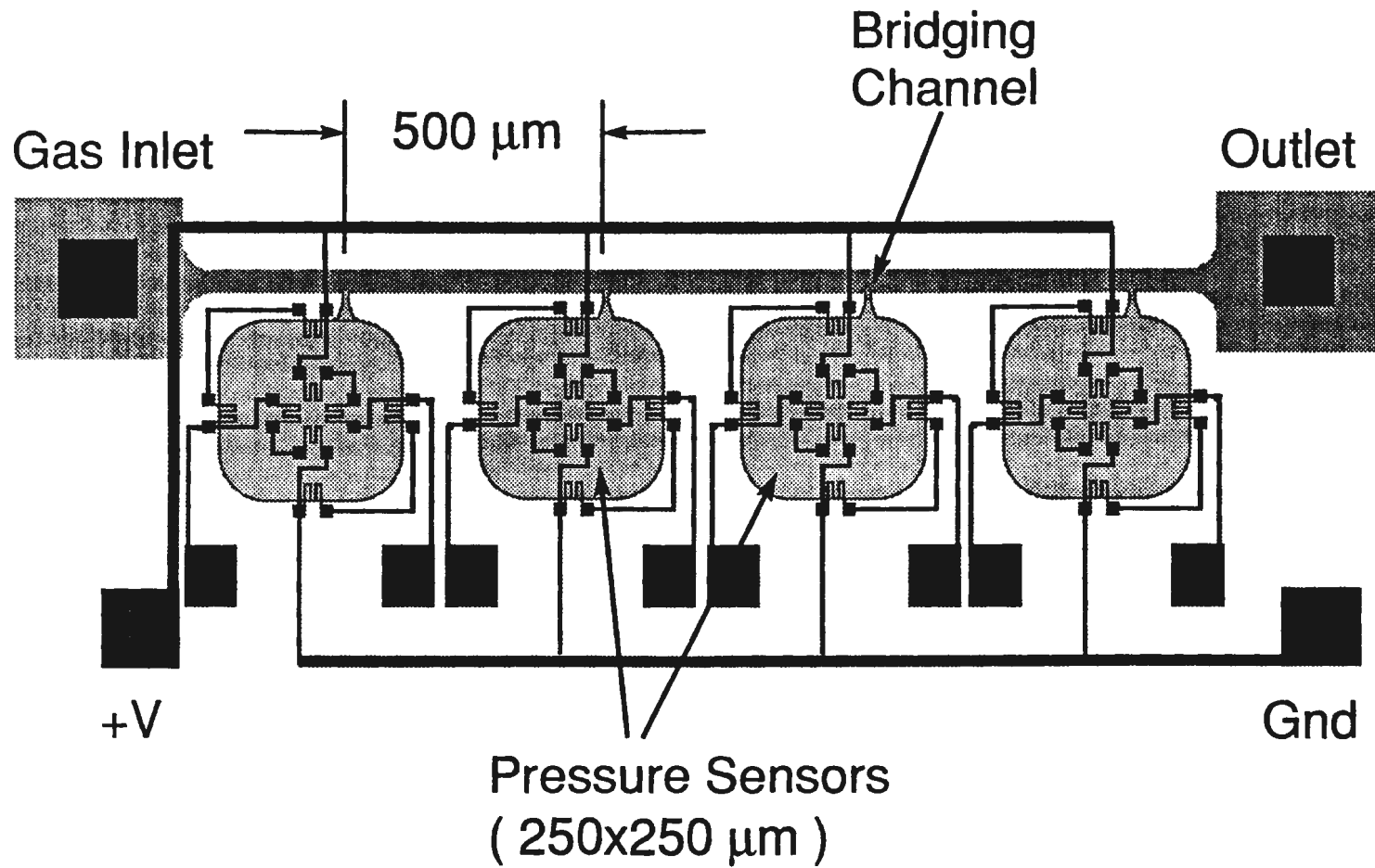
V-I Characteristic

** resistance in linear region : $9k\Omega$



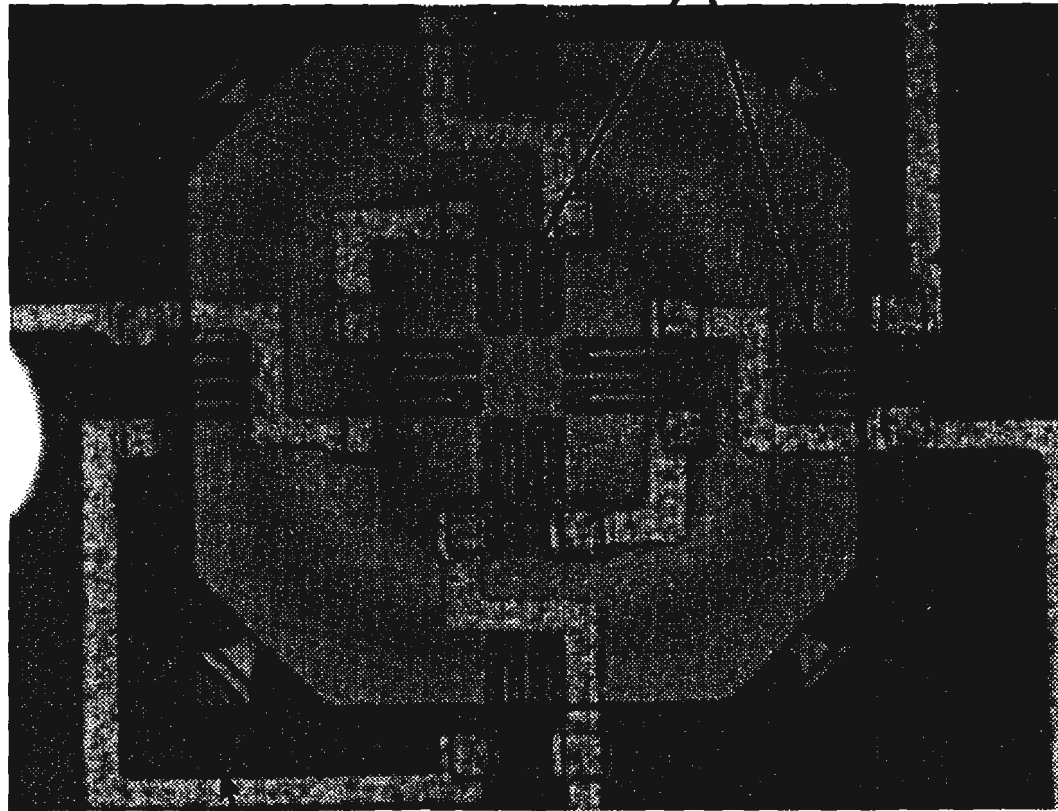


Flow Channel & Pressure Sensors Design



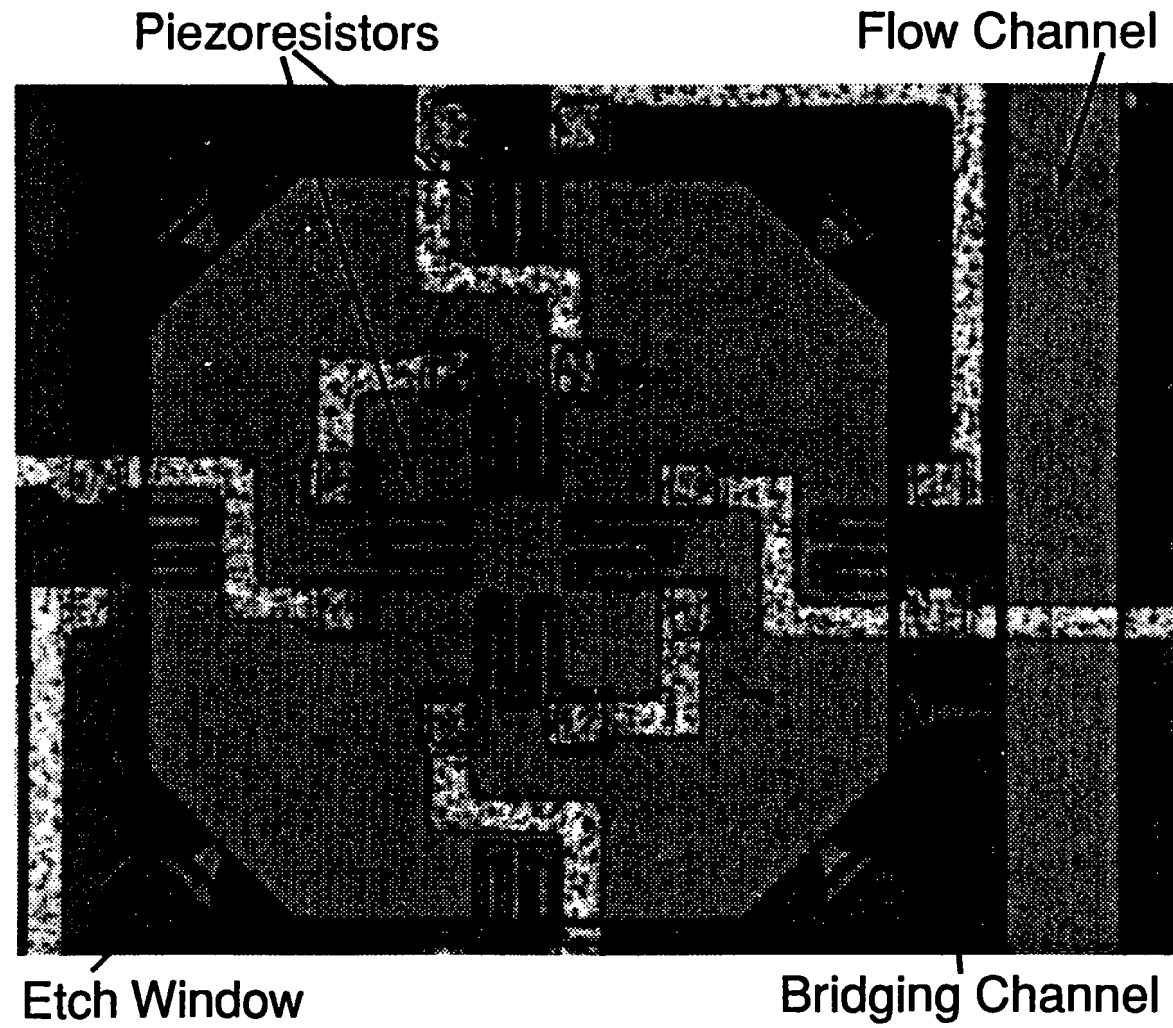
Pressure Sensor

Piezoresistors

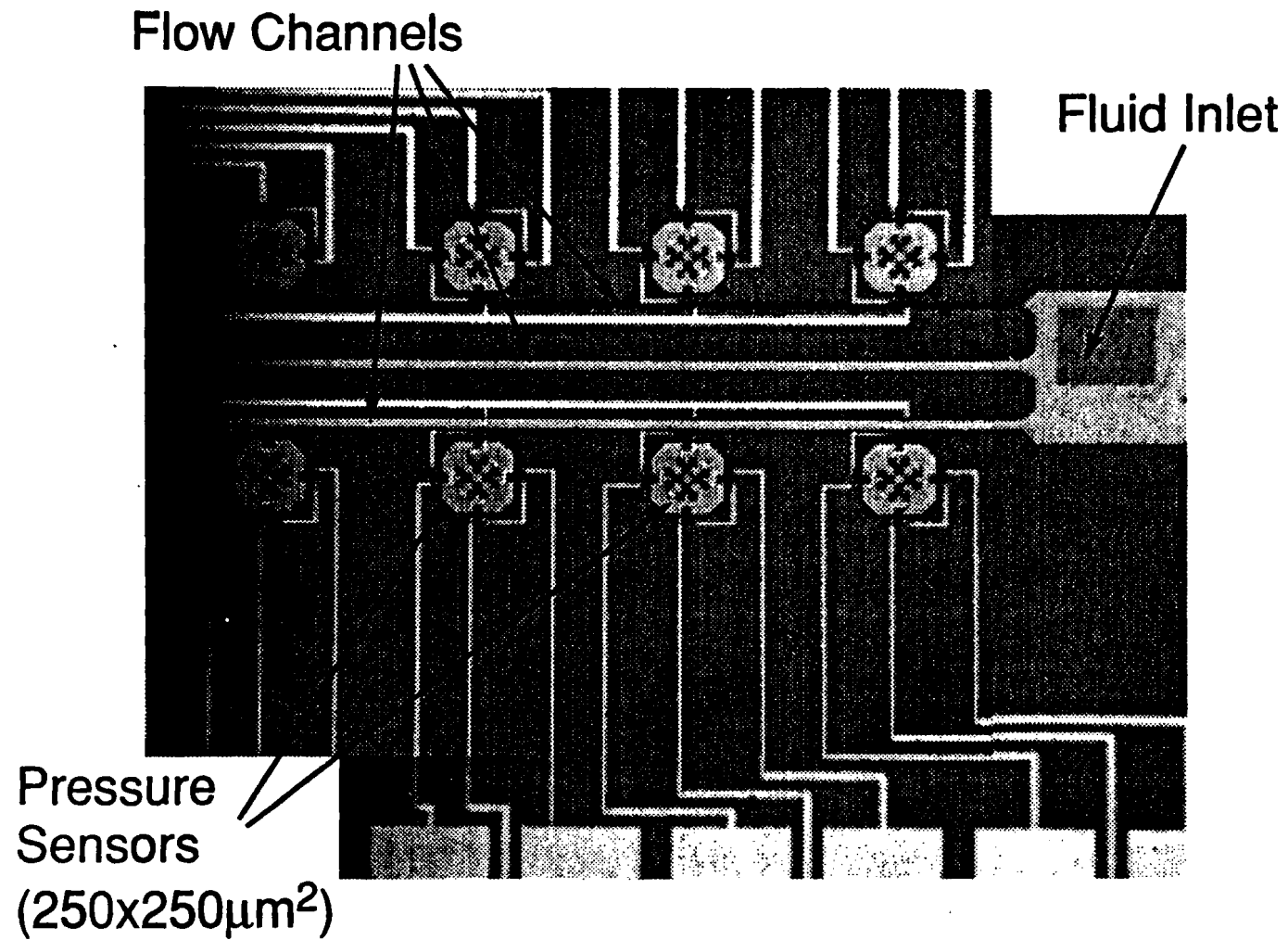


Etch Window

Pressure Sensor



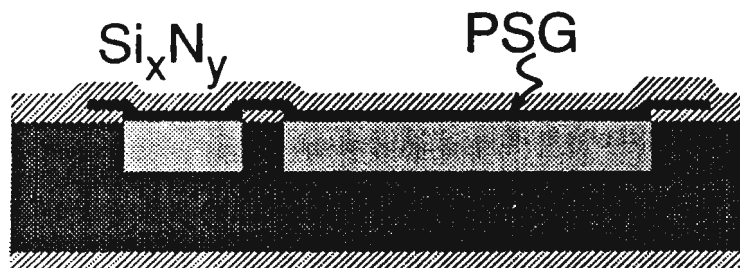
Micro Flow System Chip



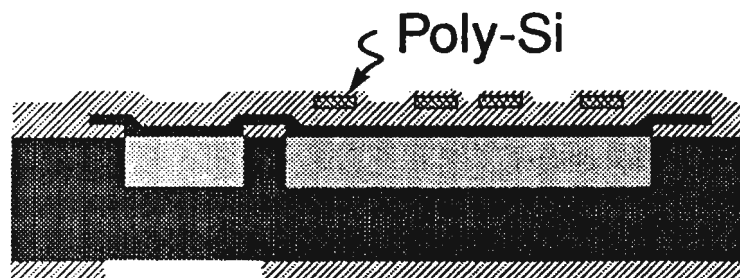
Fabrication Process



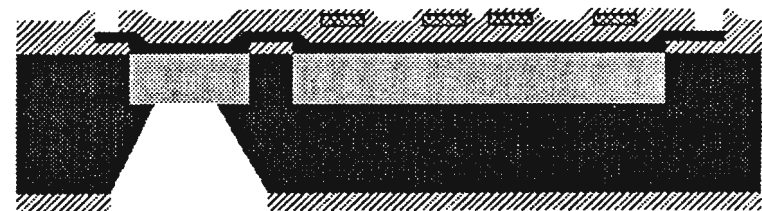
(1)



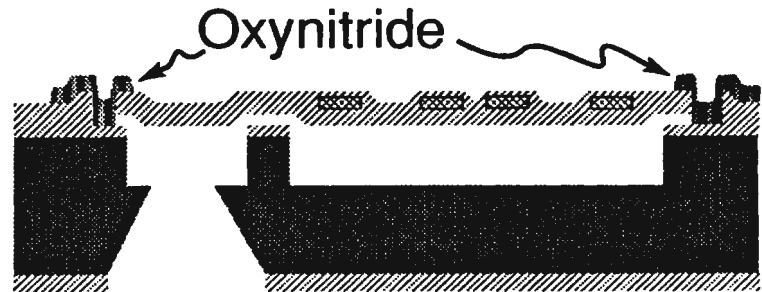
(2)



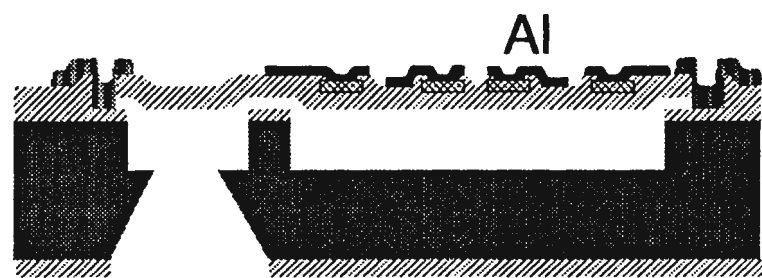
(3)



(4)

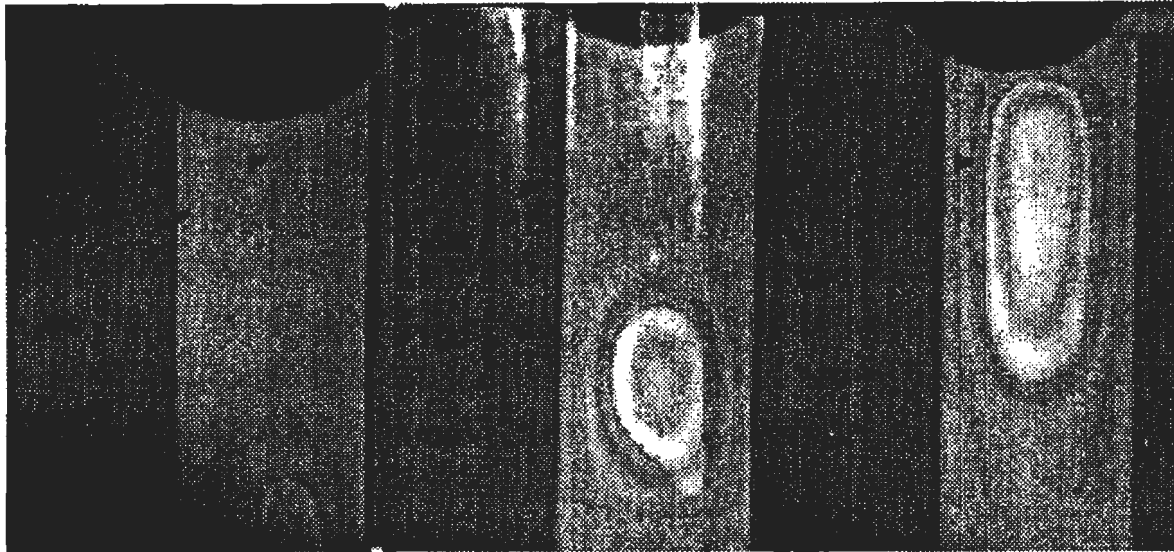


(5)



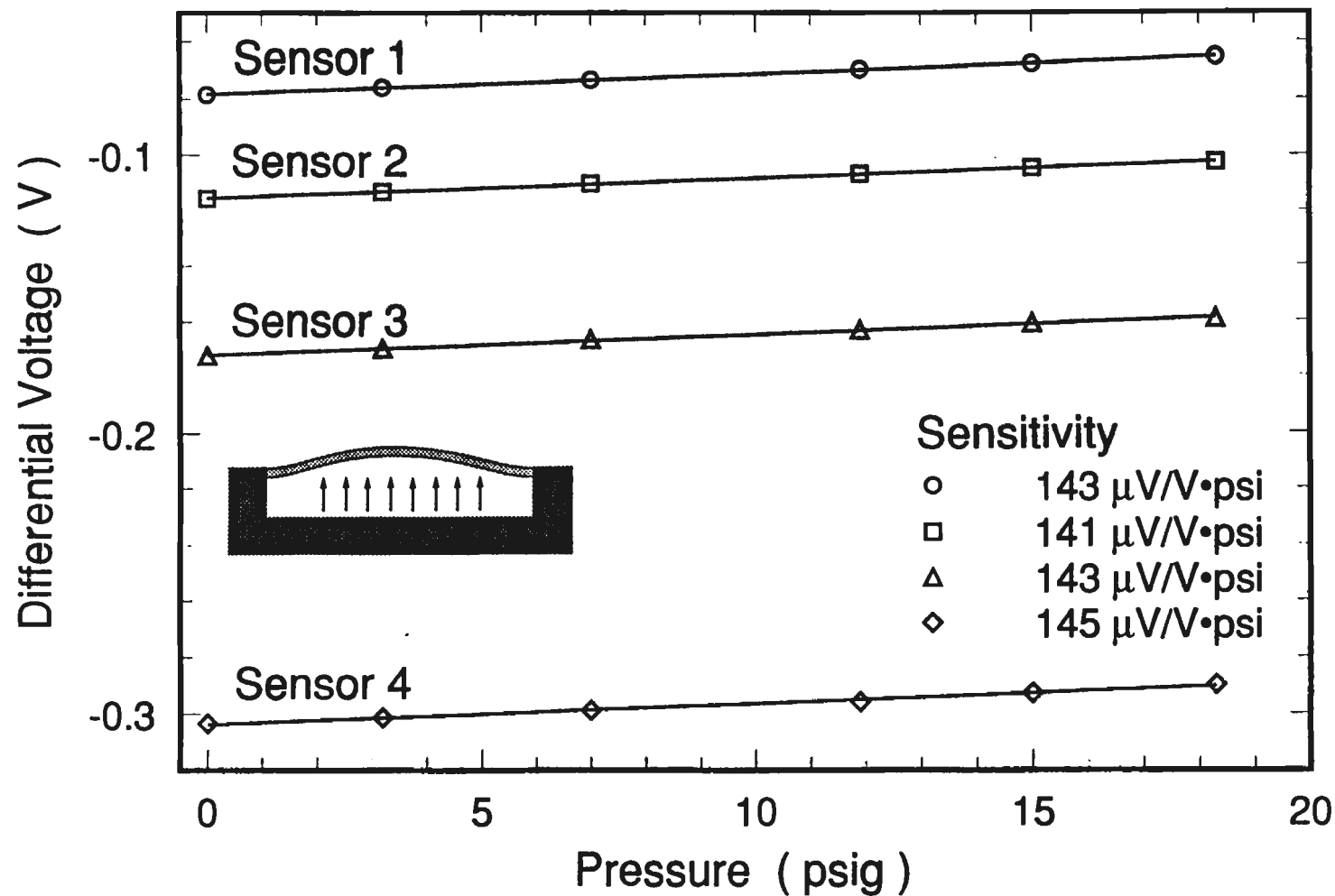
(6)

Bubbles Inside Microchannels

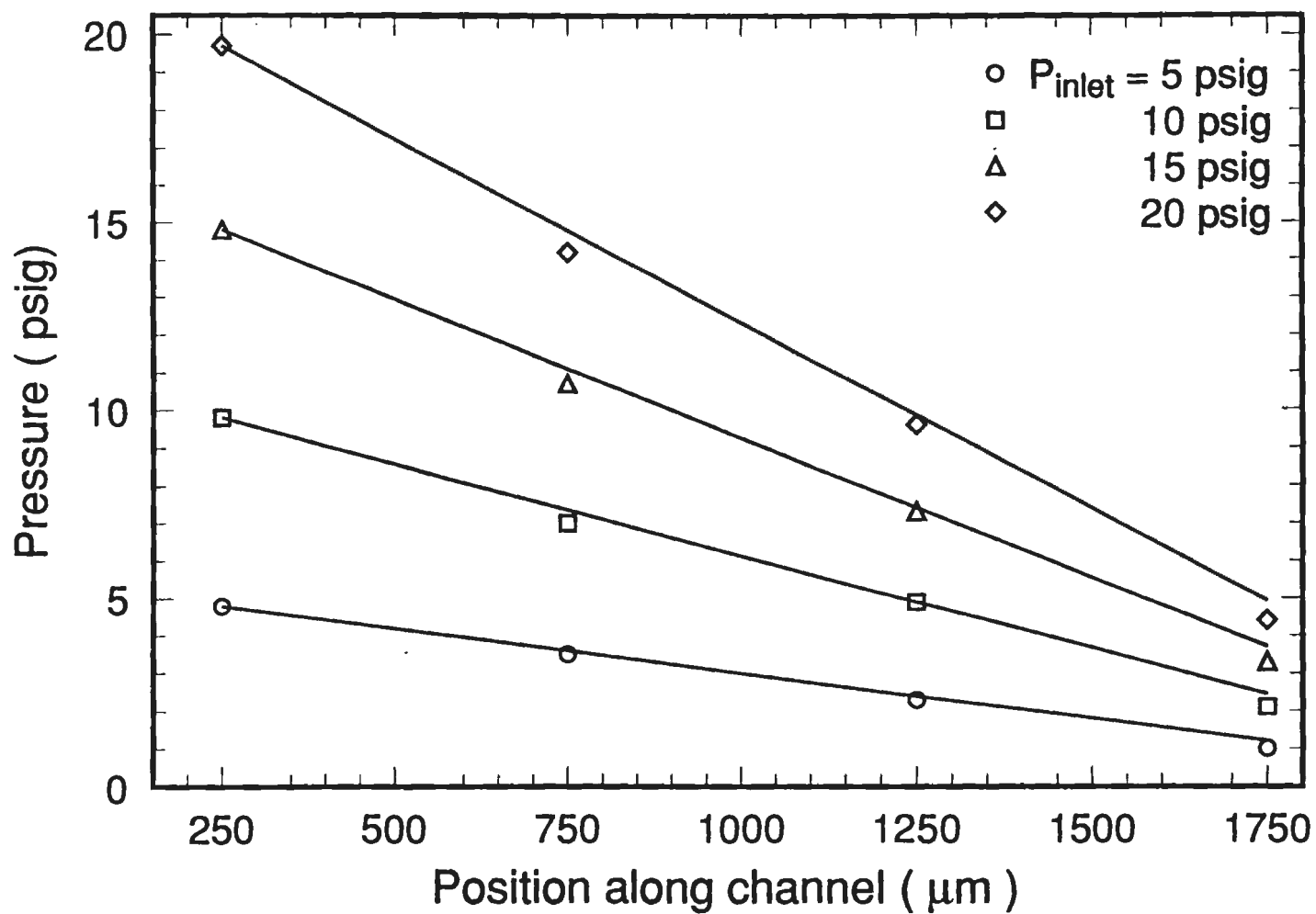


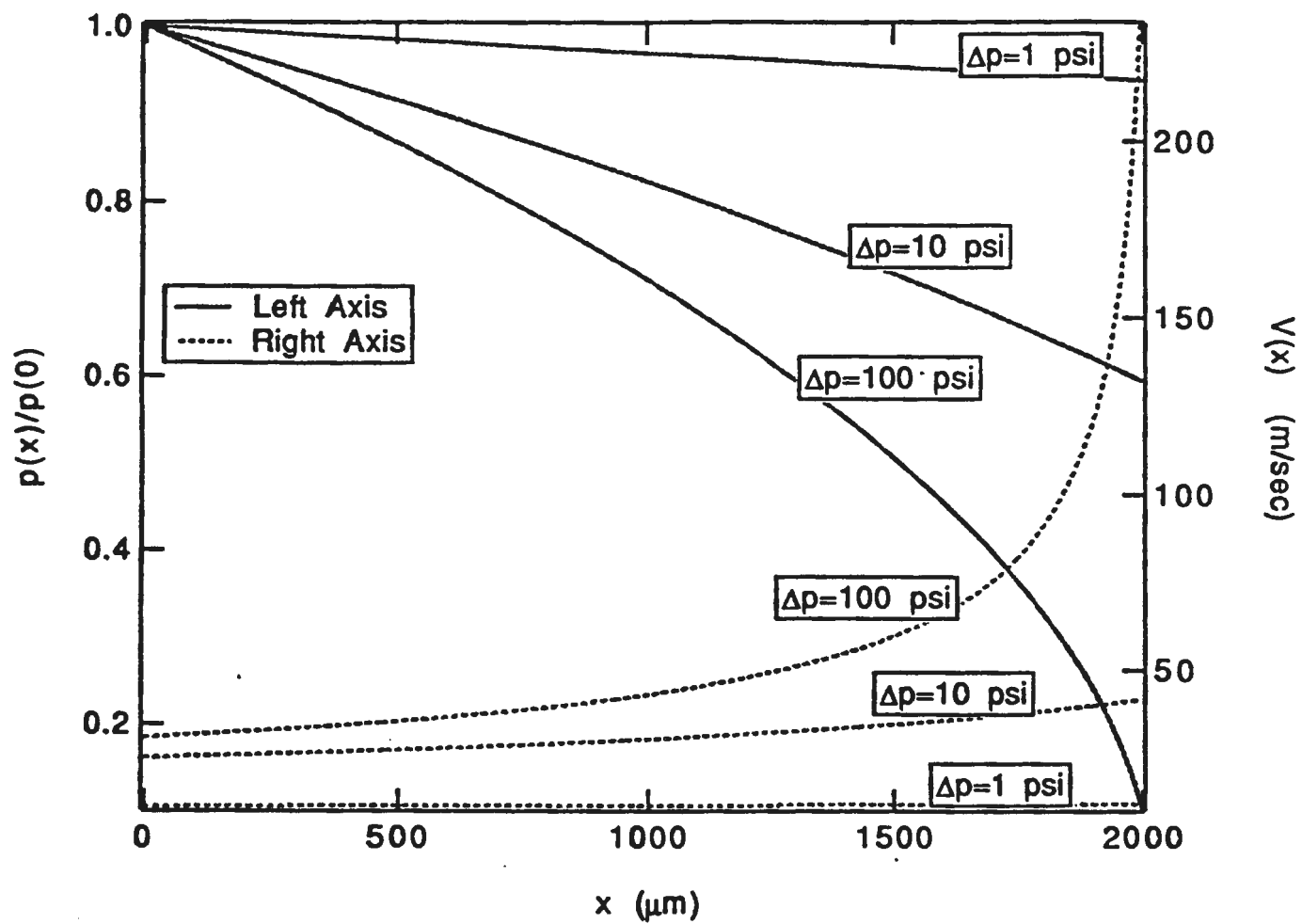
Pressure Sensor for Integrated Microchannel/Pressure Sensor System

Experimental Results (Pressure Sensor)



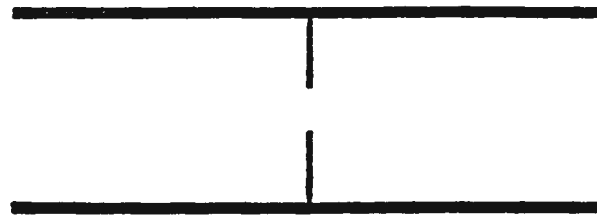
Experimental Results (Micro Channel)



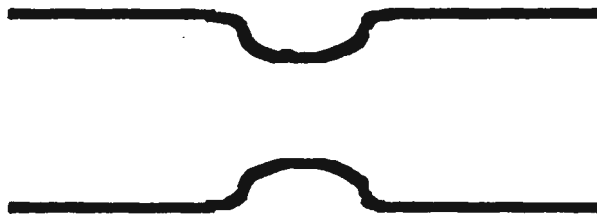


Pressure distribution of air flow in a microchannel under various pressure, $D = 1 \text{ } \mu\text{m}$, $L = 2000 \text{ } \mu\text{m}$.

Figure 5



ORIFICE TUBE



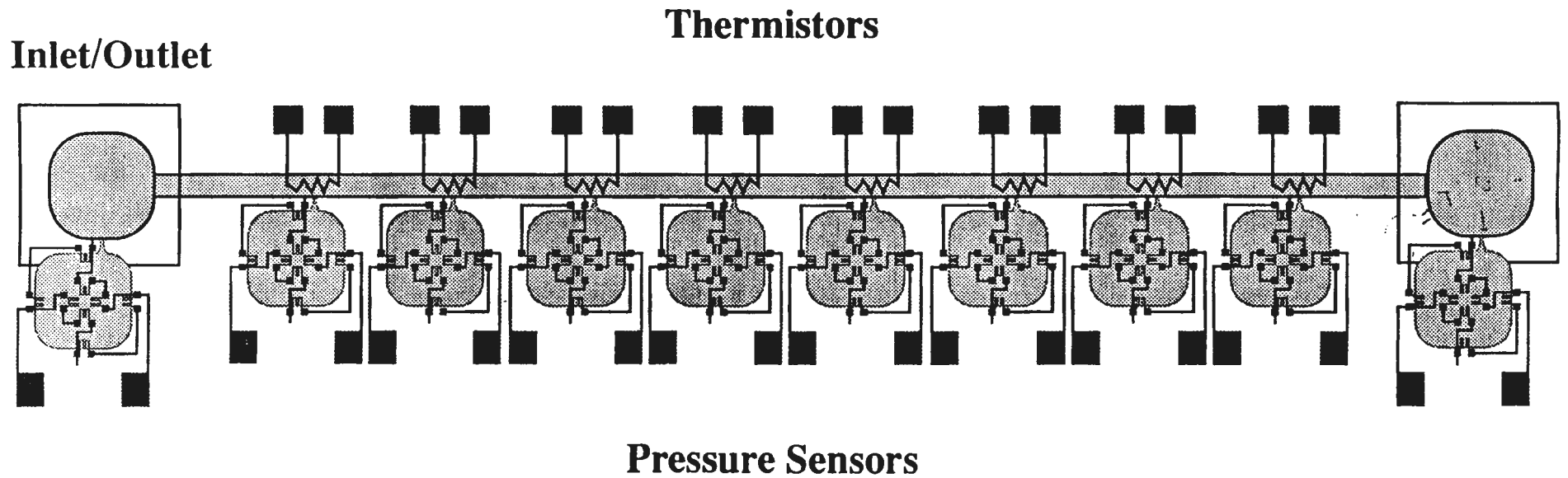
VENTURI TUBE



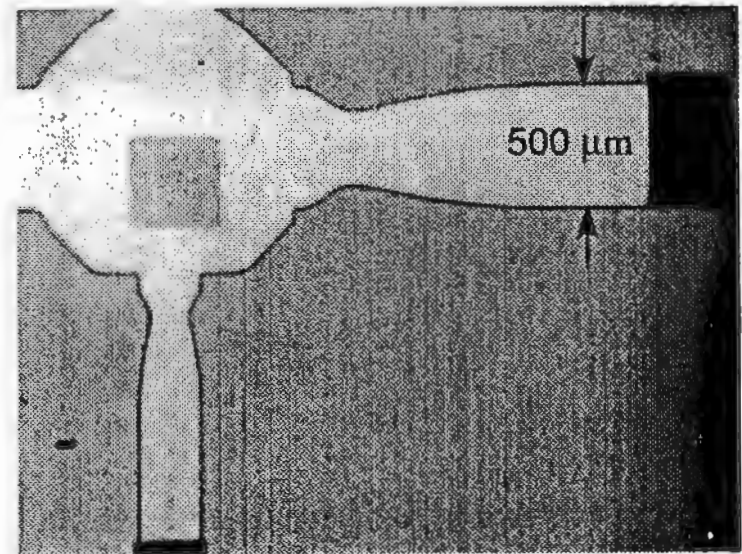
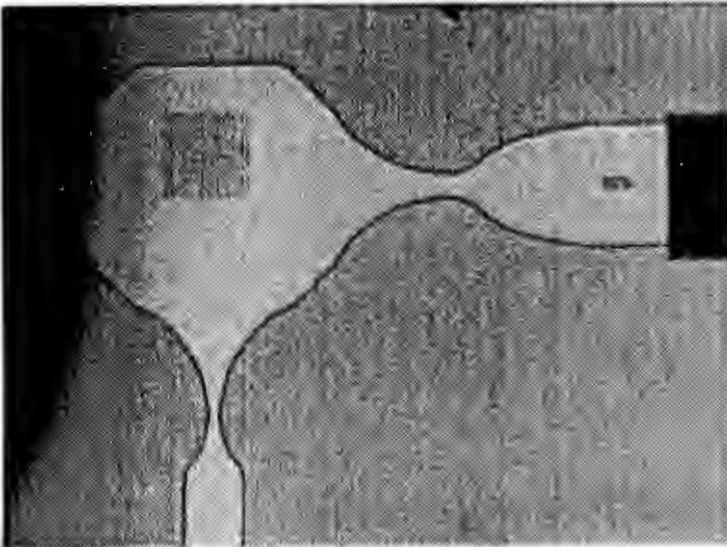
VISCOUS DRAG TUBE

Fig. 4: Mean Flow Rate Sensors

Flow/Sensor Chip (Next Generation)



2D Micro Jets



POTENTIAL MICROFLOW APPLICATIONS

1. Microsurgical tools
2. Micromanipulators
3. Air bearing
4. Microfluidics
5. Chemical sensors
6. Flow sensors
7. Chromatograph
8. Biomedical devices

Typical Applications for Micromechanical Structures in Silicon

Cryogenic Microconnectors	Microprobes
Fiber Optic Couplers	Micropumps
Film Stress Measurement	Microswitches
Fluidic Components	Microvacuum Tubes
IC Coolers	Microvalves
Ink Jet Nozzles	Nerve Regenerators
Laser Beam Deflectors	Photolithography Masks
Laser Resonators	Pressure Switches
Light Modulators	Pressure Regulators
Membranes	Programmable
Microaligners	RMS Converters
Microbalances	Thermal Print Heads
Microfuses	Thermopile
Microgears	Torsional Mirrors
Micromolds	Vibrating Microstructures
Micromotors	Wind Tunnel Skin Friction Gages
Micropositioners	

SENSOR APPLICATIONS

1. Flow Sensors
2. Humidity Sensors
3. Chemical Sensors
4. Infrared Sensors
5. Force Sensor
6. Pressure Sensors
7. Acceleration Sensors
8. Tactile Sensors

LONG TERM INTERESTS

- *** 1. Microelectronics +
Microsensors +
Micromachines (~~\$~~M's).
- 2. Implantable "Insulin Pill."
- 3. Micro-gyroscope.
- 4. Micro-robots and Micro-spacecraft.

Small Machines, Large Opportunities:

A Report on the Emerging
Field of Microdynamics

Report of the NSF Workshop
on Microelectromechanical
Systems Research



POSSIBLE APPLICATIONS

- | | |
|--------------------------------|------------------------------------|
| # Micro Prosthetic Devices | # Microvalves and Pumps |
| # Biomedical "Smart Pills" | # Optical Fiber Connectors |
| # Biological Tissue Connectors | # Microfilters |
| # Biological Micromanipulators | # Micro Spacecraft |
| # Catheter-Based Tools | # Micro Electrode Arrays |
| # Microsurgical Tools | # Electric Switches and Relays |
| # Clean Room Instrument | # Microelectromechanical Muscle |
| # Micro Optical Benches | # Electromechanical Memories |
| # Micro Light Modulators | # Miniature Printer Mechanisms |
| # Force-Balanced Transducers | # Ultra-Precise Positioning Device |



There's still plenty of room at the bottom!

In-Situ Monitoring and Universal Modelling of sacrificial SiO₂ Etching by Hydrofluoric Acid

Jianqiang Liu, Yu-Chong Tai

MS 116-81, Caltech, Pasadena, CA 91125

Kin-Cheok Pong, Jiajing Lee, Yitshak Zohar, Chin-Ming Hu

MANE, UCLA, Los Angeles, CA 90024

Summary

A video system is designed to do in-situ and accurate monitoring of sacrificial phosphosilicate glass (PSG) etching in microchannels by hydrofluoric acid. New phenomena including bubble formation and liquid condensation have been found to either enhance or hinder etching process depending on the size and geometry of the channels. For the first time, an universal model for microchannel etching is identified to cover a wide range (10-49 wt%) of HF concentration. This model includes chemical diffusion and second-order chemical reaction.

Abstract

Surface micromachining requires chemical etching of sacrificial layers. Silicon dioxide or PSG etching in HF-based solution is one of the most frequently used techniques [1, 2]. In most of the surface micromachining, the length of the sacrificial layer is short ($< 100 \mu\text{m}$) so that there are no serious problems such as unbearable long etching time and structural damage. However, several Caltech projects involve large silicon-nitride diaphragms and long microchannels, and prolonged exposure of these structures to HF ($> 40 \text{ wt}\%$) greatly reduces yield. To solve the problems, one needs a model that covers a wide range of HF concentration, hence called a universal model. This is because the starting HF concentration could be different, and, once etching starts, chemical concentration inside the sacrificial gap during etching varies as a function of time and position. Many works have been done on modelling silicon-dioxide etching, e.g. Monk et. al.[3] and Helms et. al. [4]; However, no universal model has been identified so far. In the following, we describe our effort in search of such a model.

First, a video system is designed to do in-situ and accurate monitoring of sacrificial phosphosilicate glass (PSG) etching (Fig. 1). This system basically consists of a microscope, a video camera and a tape recorder. A polypropylene container covered by a transparent plastic slide is used to take sample dies and HF. For etching at different temperatures, a hot chuck is used underneath the container with calibrated temperature control. The container can take a 1 by 1 cm² silicon die, which has various straight PSG ($\sim 6 \text{ wt}\%$) channels covered by LPCVD low-stress silicon nitride (Fig. 2). Each channel has a ruler nearby with 10 micron divisions for convenient reading of the etching length. Many experiments have been done, and a large amount of repeatable data ($\pm 5 \%$) have been collected at different HF concentrations and temperatures as in Figs. 3 and 4.

New phenomena have been found during the etching observation. For example, bubbles inside the channels may

form during the HF etching. Interestingly, when channel width is larger than a threshold value ($\sim 4 \mu\text{m}$), bubbles are movable. They always move from the nucleation site to the etching window. In this case, bubbles tend to enhance etching by probably introducing micro-flows in the channel. On the other hand, when width is below the threshold value bubbles, if formed, become stationary but grow big enough to block the channel. These bubbles then significantly hinder the etching of the channels. In general, the formation of bubble doesn't always happen, and it depends on the temperature and the quality of PSG. It is also found that after the bubble formation liquid condensation can happen on the silicon nitride surface containing the bubbles.

Our data are collected from video tape with an accurate enough time resolution of 33 ms to examine many possible models. The result is summarized in Table 1. Pure diffusion model doesn't fit the data well enough. Deal-Grove model (diffusion and first order chemical reaction) can only fit data with a fixed HF concentration. In other words, it doesn't cover a wide range of HF concentration. Langmuir-Hinshelwood model (special chemical kinetics coupled with diffusion) is similar to Deal-Grove model. It turns out that only a model using diffusion and second-order chemical reaction ($r = -kC_{\text{HF}}^2$) universally fit all data covering a wide HF concentration range from 10-49 wt % with a $k = 0.1 \text{ cm}^2/\text{mole sec.}$ and diffusion constant $D = 1.5 \times 10^{-5} \text{ cm}^2/\text{sec}$ (Fig. 3). The accuracy of this model is about 10%.

Finally, temperature effects on sacrificial layer etching have been also studied (Fig. 4). It is found that chemical reaction constant is affected more than that in diffusion constant. Including the temperature effects in the model has also been done. A lot more of the details will be presented if this abstract is accepted.

References

- [1] R.T. Howe, *J. Vac. Sci. Technol.*, 1988, B 6, pp 1809-1813.
- [2] L. S. Fan, Y. C. Tai & R.S. Muller, *Technical Digest, IEEE Int. Electron Devices meeting* (San Francisco, CA, Dec. 1988), pp.666.
- [3] David J. Monk et al., *IEEE Solid-State Sensor and Actuator Workshop* (Hilton Head Island, South Carolina), 1992, pp 46-49.
- [4] C. R. Helms & B.E. Deal, *J. Vac. Sci. Technol. A* 10(4), pp. 806-811.

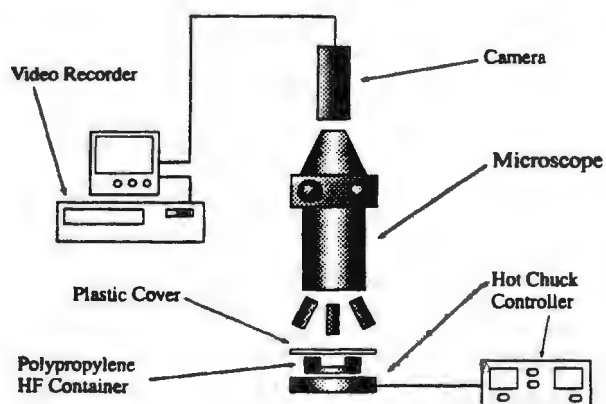


Figure 1. Schematic of experimental setup. Vapor condensation is avoided by using a plastic cover on the HF container.

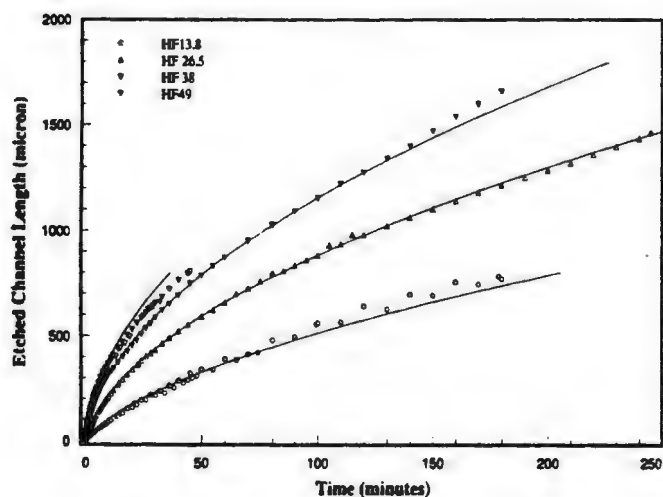


Figure 3. Typical PSG channel etching data. Solid lines are modelled using diffusion and a second order chemical reaction and diffusion model fit.

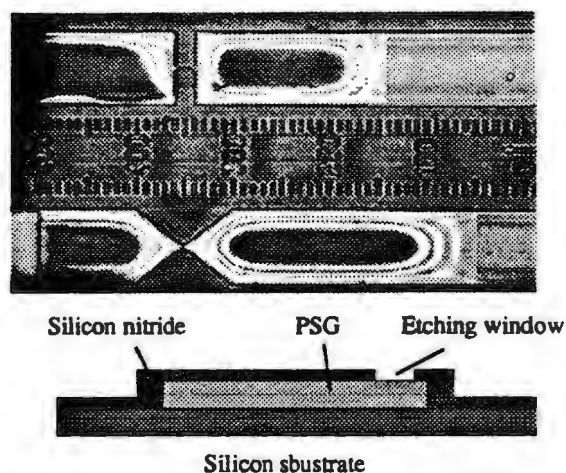


Figure 2. (a) An etched microchannel with a ruler. The silicon nitride diaphragm was flat during etching. (b) Schematic of its cross-section.

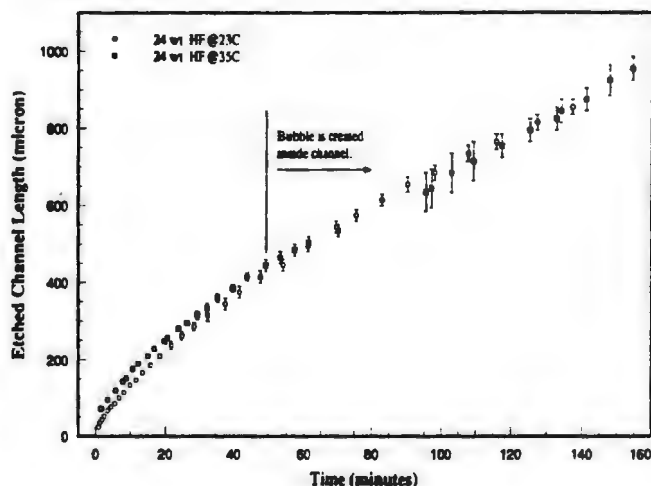


Figure 4. Temperature and bubble effects on channel etching.

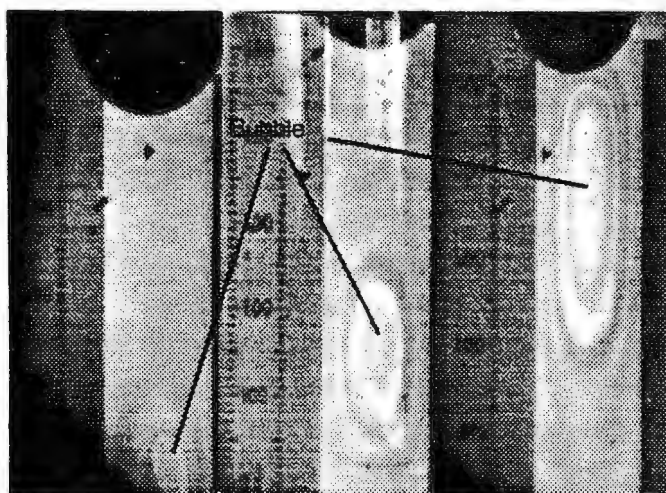


Figure 5. Bubble formation and its sequential movement. (a) A bubble forms at the interface between HF and PSG. (b) The bubble expands and moves toward etching window. (c) The bubble saturates at etching window. Black circular spots are accumulated gas around windows.

Table 1. Model List

Model	Chemical Rate Law	Parameters	Fitting
Diffusion	infinite reaction rate	D	Inadequate
Deal-Grove	$r = -k[HF]$	D, k	Inadequate
Langmuir-Hinshelwood	$r = -k_1[HF]/(1+k_2[HF])$	D, k ₁ , k ₂	Inadequate
Second-order	$r = -k[HF]^n$	D, k, n	Good, n=2

12. Systems and Applications

A MICROMACHINED SILICON STRUCTURE FOR IN VITRO STUDIES OF NEURAL NETWORKS

Svetlana Tatić-Lučić*, Yu-Chong Tai, John Wright

Department of Electrical Engineering, California Institute of Technology, Pasadena, CA 91125, U.S.A

Jerome Pine, Timothy Denison

Department of Biology, California Institute of Technology, Pasadena, CA 91125, U.S.A

Summary—This paper describes a novel structure for an extracellular recording. A 4x4 array of neuron wells has been fabricated on a 20 μm thick silicon membrane using double side photolithography. The neuron well is 25 μm square, with a circular gold electrode 3 μm diameter at the bottom and the heavily doped silicon grillwork at the top. The experiments confirmed that this structure is biocompatible. In this way simultaneous recording with one-to-one correspondence between the electrode and the cell can be performed from the sixteen neurons.

Abstract—The understanding of the functioning of the nervous system became an imperative in the scientific world. One way to achieve that difficult task is to do studies on so-called cultured neurons. They are the individual neurons, isolated from the brain and grown in the solution which has all necessary components essential for their growth (sugars, proteins, etc.) The goal is to measure the electric signals originating from the cultured neurons. Different techniques were developed, both intracellular and extracellular. The extracellular techniques are not invasive or harmful for the cell, although the signal-to-noise ratio is not as good as with intracellular recording. Easy fabrication of the silicon microdevices has a potential for the significant improvement of the existing methods.

The ancestors of our structure (in further text, we'll refer to it as a "neurochip") are the diving board electrode (Fig1(a)) and the polyimide wells (Fig1(b)), both previously fabricated at CALTECH. They enabled the long term recording and stimulation of the neurons, but the diving board electrodes were difficult to mount and unable to detect postsynaptic potentials, and the polyimide wells were not suitable for the mass production.

The neurochip represents the combination of the well structure with an electrode structure like that of the diving board. It has a 4x4 array of the silicon wells situated at the center of a 9x3 mm silicon membrane, 20 μm thick. The structure of the individual neuron well as well as the dimensions and the design of the neurochip are shown in Fig 2.

The fabrication process begins with formation of 6 μm diameter nitride dots, which determine the position of the neuron wells electrodes. The LOCOS process is used to create a 1 μm oxide step in the bottom of the neuron well. Then a Cr/Au/Cr metalization is deposited using a lift-off process. The insulation layer is deposited after the metalization. The holes in dielectric are opened to expose the bonding pads. The windows are etched in the insulation layer at the back and succeeding anisotropic EDP etch removes silicon all the way to the heavily boron-doped layer. Then the grillwork for the neuron wells is patterned at the bottom of the cavity, using the projection stepper. RIE etching selectively removes the heavily doped boron layer and the neuron wells are then formed with an EDP etch.

Fig.3 shows the SEM of the single neuron well. The small circle at the bottom of the well is a gold electrode. The network of the successfully growing rat superior cervical ganglion (SCG) neurons is shown at Fig.4. The picture shows the neurites growing out of the wells from the invisible neurons implanted in them and connecting among themselves.

* The author to whom correspondence should be addressed.

Phone: (818)356-3884

Fax: (818)356-2944

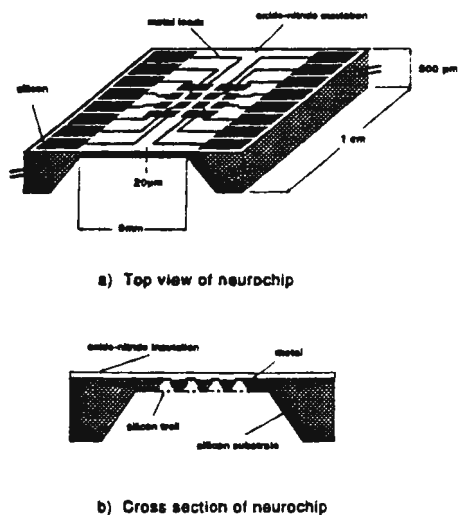


Figure 1: Design and dimensions of a neurochip.

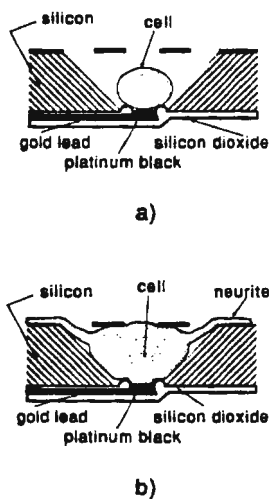


Figure 2: a) Neuron just implanted in a well, b) Neuron increases in size and grows processes out of the well.

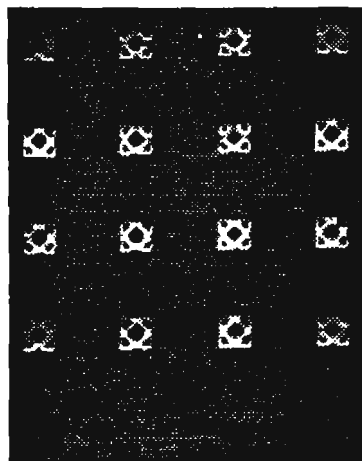


Figure 3: SEM of a 4x4 array of neuron wells at the bottom of a neurochip.

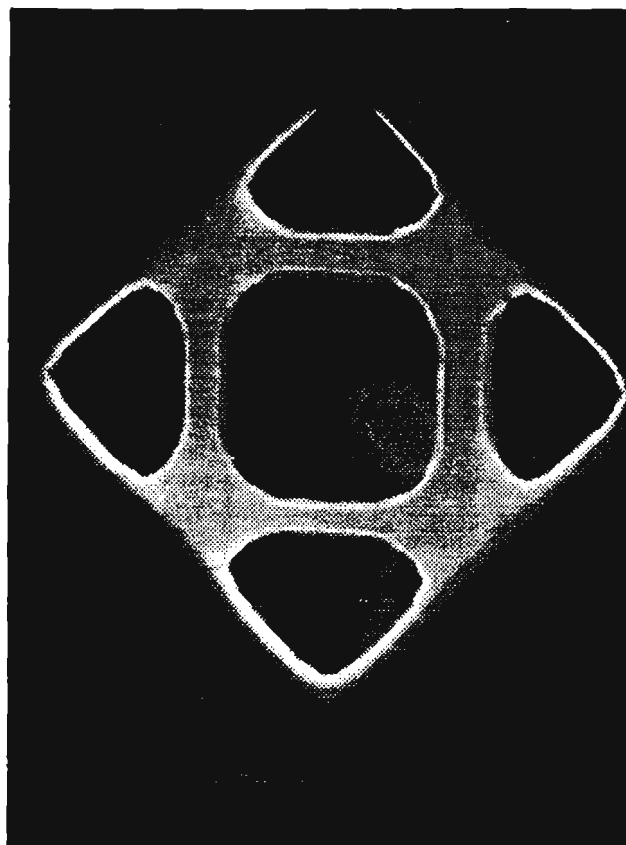


Figure 4: SEM of a single neuron well $25 \times 25 \mu\text{m}^2$ at the top with $3 \mu\text{m}$ circular gold electrode at the bottom.

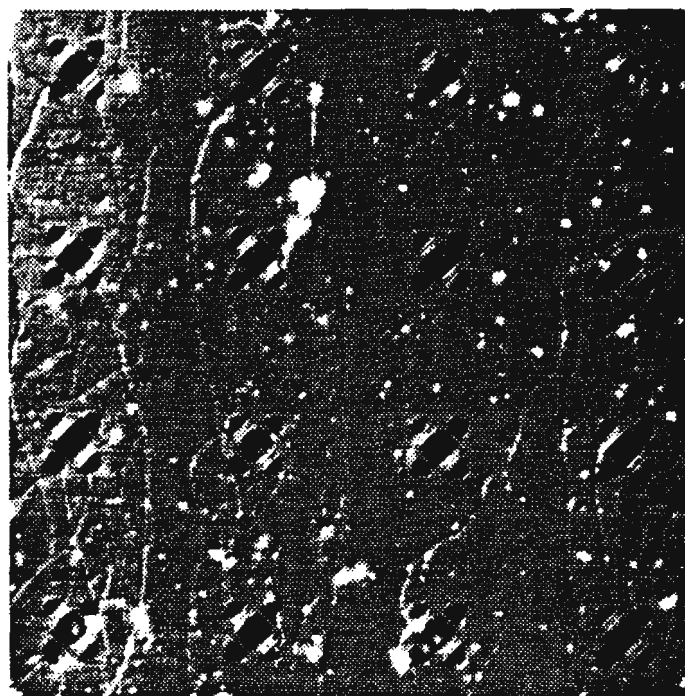


Figure 5: A live neural network formed by rat superior cervical ganglion neurons. Clearly seen are the processes growing out of the wells.

Micromachined Channel/Pressure Sensor Systems for Micro Flow Studies

Jianqiang Liu & Yu-Chong Tai

Electrical Engineering, 116-81, Caltech, Pasadena, CA 91125

Kim-Cheok Pong & Chih-Ming Ho

MANE, UCLA, Los Angeles, CA 90024

Summary

For the first time, integrated microchannel/pressure sensor systems have been designed and fabricated for direct measurement of pressure distribution along a microchannel. Both bulk and surface micromachining techniques are used in the fabrication process. Burst pressures as high as 75 psi have been achieved for the integrated system which are limited by the $500 \times 500 \mu\text{m}^2$ gas inlet/outlet diaphragms.

Abstract

Fluid-driven mechanisms for micromechanical systems are attractive alternatives for microactuators. Unfortunately, micro flows with low Reynold's numbers are not well understood. Several works have been done to study microchannel flows[1, 2, 3], but so far there is no experimental data on pressure distribution along a microchannel. This missing information is very important because it can be used to develop flow models (since conventional fluid dynamics theory can not predict the microflow behavior[3]). To provide this information, an integrated microchannel/sensor system for direct pressure measurement is presented here.

Fig. 1 shows a schematic of the designed microchannel/pressure sensor system. The size of the sensor diaphragm, $250 \times 250 \mu\text{m}^2$, is selected to provide sufficient pressure sensitivity to detect a pressure drop between any two neighboring sensors which are $500 \mu\text{m}$ apart along a microchannel. A small bridging channel between the pressure sensor and the microchannel is also designed to minimize the sensor's interference with the flow. Piezoresistors on the pressure sensor are connected to form a Wheatstone bridge for temperature compensation (Fig. 3). In addition to the structures shown in Fig. 1, venturi channels with pressure sensors (not shown) are also fabricated for velocity-pressure calibration.

Fig. 2 shows the major fabrication steps. First, 1000 \AA LPCVD nitride is deposited and patterned to define diaphragms and microchannels. Exposed silicon substrate is etched down 6000 \AA and a $1.0 \mu\text{m}$ thick oxide layer is then grown by wet oxidation. Next, a 3000 \AA LPCVD PSG sacrificial layer is patterned (Fig. 2a). A $1.2 \mu\text{m}$ thick LPCVD low-stress nitride (Si_3N_4) layer is deposited as the pressure sensor diaphragm. A boron-doped polysilicon layer 2500 \AA is then deposited and patterned to form piezoresistors for pressure sensors (Fig. 2b). After a 2000 \AA nitride layer deposition, gas inlet/outlet holes are patterned on the back of the wafer and etched to the front inlet/outlet diaphragms in EDP (8 hours). Front holes for sacrificial layer etching are then opened by an

SF_6 plasma. High concentrated HF is then used to etch PSG/ SiO_2 sacrificial layer to form microchannels and pressure sensors (Fig. 2c). An accurate time-controlled etch is crucial in this process[4]. To seal the front etching holes, $1.0 \mu\text{m}$ thick PECVD nitride is deposited. A metallization step follows to finish the process.

Fig. 5 shows the integrated microchannel/pressure sensor system. This system has two channels (the top one is $5 \mu\text{m}$ wide, the bottom one is $40 \mu\text{m}$ wide) with four sensors distributed along each of them. The experimental setup of the system is shown in Fig. 6. The mechanical strength of the low-stress nitride diaphragm determines the maximum pressure that can be loaded to the system. Our test shows that the gas inlet/outlet diaphragms, $500 \times 500 \mu\text{m}^2$, are the weakest parts of the system, but they survive static pressures as high as 75 psi. We notice no plastic deformation of the whole system after many pressure cycles (65 psi). A photograph of the pressure sensor is shown in Fig. 3. The resistance of each wheatstone bridge arm is $18 \text{ k}\Omega$. In Fig. 4a, an SEM photograph shows a pressure sensor, the bridging channel, and the flow channel. This sensor displays a linear range from -15 psi to 15 psi. It saturates at 20 psi, where the diaphragm touches the bottom of the sensor chamber with the pressure applied from outside. Fig. 4b gives a sensitivity of $120 \mu\text{V/V/psi}$ which agrees well with our design and is enough to detect a pressure drop between any two neighboring sensors $500 \mu\text{m}$ apart. Extensive measurements of the pressure drop along microchannels are under way.

Acknowledgement

This work is supported by AFOSR. We specially thank Chang Liu for suggestions about pressure sensors. We thank Trevor Roper for his help in fabrication.

References

- [1] K. J. Gabriel et. al., *Sensors and Actuators*, A 21-23 (1990)184-188
- [2] Leslie Ann Field, Ph.D thesis, EECS, UC Berkeley, 1991.
- [3] J. Pfahler, et.al., *Micromechanical Sensors, Actuators, and Systems*, ASME 1991, DSC-Vol. 32.
- [4] J. Q. Liu, et. al., *IEEE Micro Electro Mechanical Systems Workshop*, 1993, to be published.

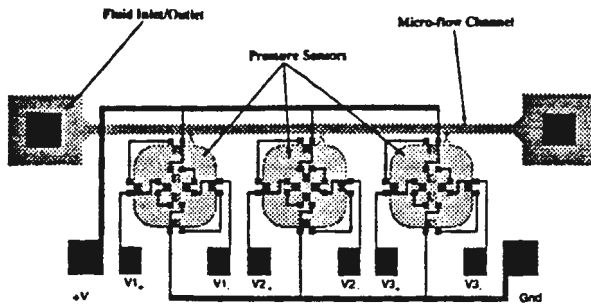


Fig. 1. Schematic of a microchannel/pressure sensors system.

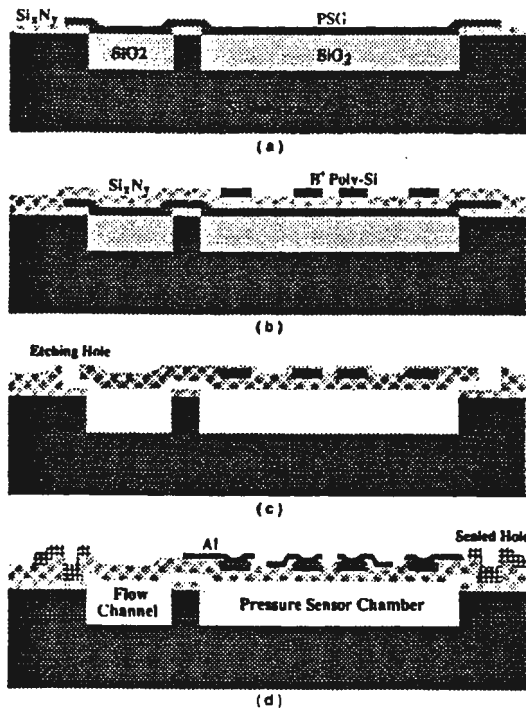


Fig. 2. Major fabrication steps of the integrated microchannel/pressure sensor system. Not shown are the gas inlet/outlet holes etched from the back of the silicon wafer for fluid connections (Fig. 5).

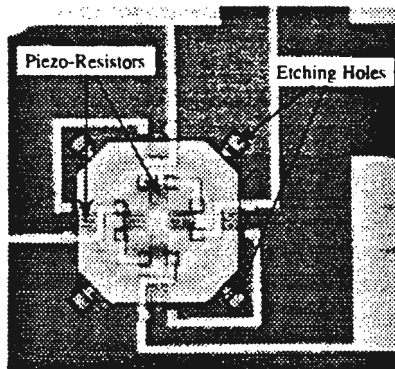


Fig. 3. Photograph of a fabricated pressure sensor. Piezo-resistors are made of boron doped polysilicon. Each arm resistance of the wheatstone bridge is 18 k Ω .

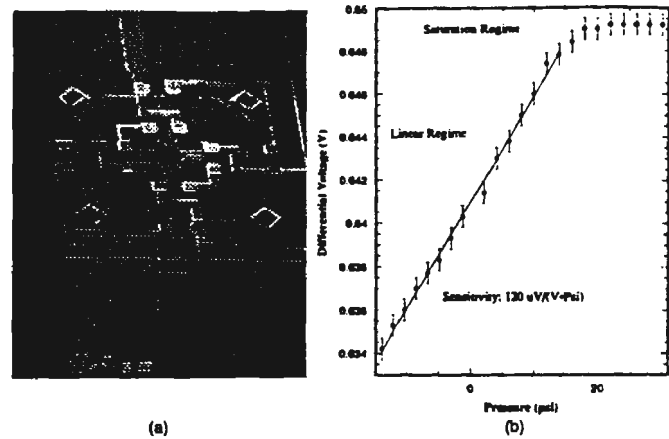


Fig. 4. (a) SEM photograph of a pressure sensor. (b) Voltage output vs. pressure characteristics. The bias voltage of the wheatstone bridge is 4 V. The signal saturates when the diaphragm touches the chamber bottom at about 20 psi. The linear part gives a sensitivity of 120 $\mu\text{V/V/psi}$.

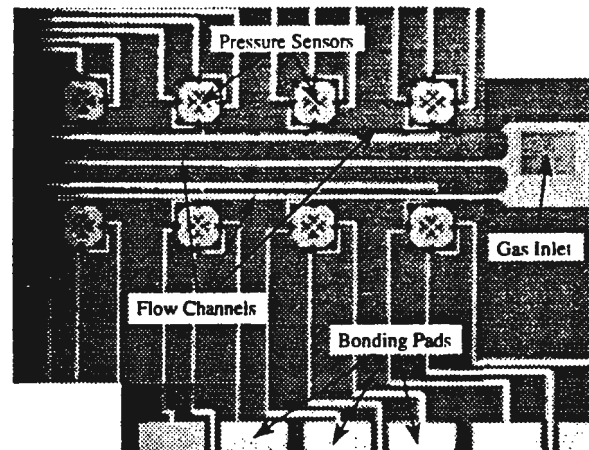


Fig. 5. Photograph of a finished microchannel/pressure sensor chip, ready for connections to external gas sources. The chip has two flow channels; the bottom is 40 μm wide and the top one is 5 μm wide; Four pressure sensors (250 \times 250 μm^2) are connected to each microchannel through a small (5 \times 0.3 μm^2) bridging channel to monitor the pressure distribution along the channel.

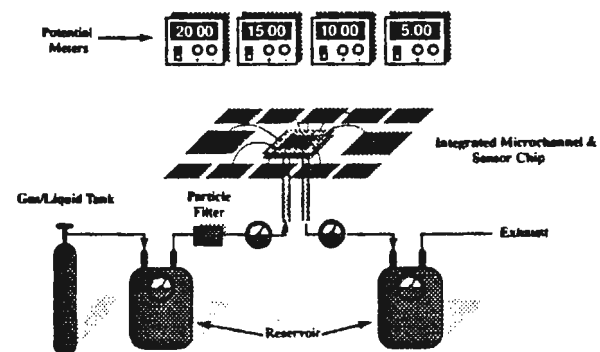


Fig. 6. Schematic experimental setup of the system. The channel/sensor chip is packaged in a DIP. The fluid connections are through machined holes on the bottom of the DIP. Electrical connections are through bonding wires.

(7. Mechanical Sensors)

Surface Micromachining Issues of a Silicon Pressure Sensor

Chang Liu and Yu-Chong Tai

Electrical Engineering 116-81, Caltech, Pasadena, CA 91125, USA

Bert Wolfkamp and Weijie Yun

Pressure Sensor Division, BEI Electronics Inc., CA 91342, USA

Summary — A surface micromachined pressure sensor using a silicon nitride diaphragm and an oxide/PSG composite sacrificial layer is presented (Figs. 1 and 2). Special emphases are important micromachining issues that produce a high diaphragm yield. These issues include minimizing free-etching time, avoiding bubble formation, and designing proper etching geometry. Accordingly, a diaphragm yield of almost 100% is obtained with membrane sizes smaller than $200 \times 200 \mu\text{m}^2$.

Abstract — Surface-micromachined pressure sensors are attractive for many reasons[1]. Guckel reported a polysilicon diaphragm pressure sensor using thermal oxide as a sacrificial layer[2]. However, no information on yield issues was reported. Silicon-nitride pressure sensors have also been reported[1,3] using silicon and polysilicon as the sacrificial layers, respectively. It is pointed out that hydrogen bubbles produced from silicon etching using KOH can cause membrane fracture, hence reduce the yield. Here, we describe a surface-micromachined silicon-nitride pressure sensor with a new design that leads to a high diaphragm yield of almost 100%.

In our design, both square and circular pressure sensors are available. Their sizes are 150, 200, 250 and $500 \mu\text{m}$ on the side or in diameter. Figure 3 shows major steps of our process. First, cavity windows are opened on silicon nitride to expose silicon substrate. An isotropic silicon etchant then creates 660 nm step into the substrate. A recessed LOCOS process follows to planarize the surface and form a $1.3 \mu\text{m}$ thick thermal oxide island. Next, a 200 nm thick PSG layer is deposited and patterned to complete the composite oxide/PSG sacrificial layer. This step is followed by a 800 nm LPCVD nitride deposition to provide membrane material. Polysilicon is then deposited, doped, patterned, and passivated to form piezoresistors. Next, an SF_6 plasma etches through the nitride layers to open etching holes. The composite sacrificial layer is subsequently removed using concentrated HF (48%). This etching process is specially video recorded for yield study. PECVD nitride deposition then seals the cavity at a pressure of 200 mTorr . Finally, metalization follows and the whole devices except the diaphragm bonding pads is passivated using PECVD nitride.

In our process, silicon nitride is chosen for the diaphragm material because of its good mechanical properties. However, nitride membranes may still be damaged during fabrication process. It is found that there are three major causes of damage. First, prolonged HF etching attacks silicon nitride, although at a slow rate. Secondly, the geometry of the etching holes creates special free-standing patterns of the diaphragm during etching process, which may cause stress concentration and diaphragm fracture (Fig. 4). Thirdly, the 48% HF etchant is found to generate bubbles after the sacrificial layer is completely consumed, which may break or lift off the diaphragm. In conclusion, our studies show that the solutions to these problems are to minimize the free-etching time, to design proper etching patterns, and to avoid over etch. In order to minimize the etching time, an oxide/PSG composite sacrificial layer is used for two major advantages. First, thermal oxide allows a recessed LOCOS process to planarize the surface. Secondly, the etching time of the composite layer is minimized because of the fast etching rate of PSG in HF. For example, a $200 \times 200 \mu\text{m}^2$ diaphragm cavity (totally $2 \mu\text{m}$ deep) can be freed in 35 minutes. Geometry of the etching patterns is also an important issue. Sizes, locations and number of the etching channels determine the diaphragm free-etching time and stress distribution. Different etching channel patterns are included in our design. It is found from *in situ* video monitoring that diaphragm fracture happens at high stress areas such as the edges of etching channels and the etching patterns during the freeing process (Figure 4). Finally, the bubble formation during sacrificial layer etching is detrimental but avoidable using a precisely timed etching. This suggests that uniform diaphragm sizes over the whole wafer is desirable because bubble formation happens mostly after the diaphragm is completely freed. The diaphragm size effects on the yield has also been studied. It is found that a yield of 100% is obtainable for diaphragm sizes smaller than $250 \times 250 \mu\text{m}^2$. Larger diaphragms have a smaller yield. For example, the yield for $500 \times 500 \mu\text{m}^2$ diaphragms is only 60%. However, the size effects on the yield depend heavily on the process and nitride quality.

Finally, finished pressure sensors are also tested. Typically, the output response is linear within a range from 14 to 30 psi, with a pressure sensitivity of 0.27 mV/V/psi (Fig. 5) and a temperature sensitivity of $6 \mu\text{V/V/}^\circ\text{C}$. The polysilicon piezoresistors are heavily doped ($> 10^{20} \text{ cm}^{-3}$) to have a small temperature coefficient of resistance, $0.02\% / ^\circ\text{C}$ from -50 to $100 ^\circ\text{C}$ (Fig. 6) and a gauge factor of 8.

References—

1. S. Sugiyama *et al.*, "Micro-Diaphragm Pressure Sensor," *Proceedings of the 6th Sensor Symposium*, pp. 23-27, 1986.
2. H. Guckel, "Surface Micromachined Pressure Sensor," *Sensors and Actuators A*, Vol. 28, pp. 133-146, 1991.
3. K. Shimaoka *et al.*, "Micro Pressure Sensor," *Proceedings of the 9th Sensor Symposium*, pp. 47-50, 1990.

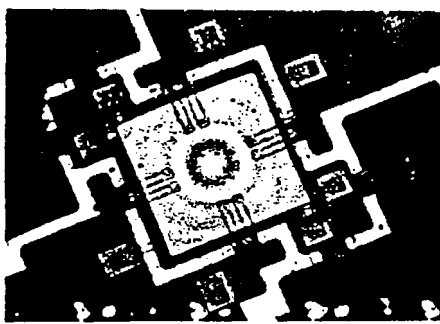


Figure 1: A square pressure sensor. The interference pattern is caused by sealing of the diaphragm at 200 mTorr.

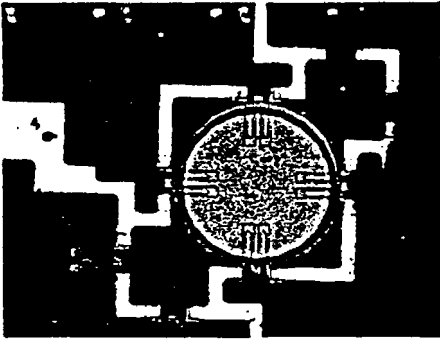


Figure 2: A circular pressure sensor with etching holes left open on purpose for temperature sensitivity study. Interference pattern therefore disappears.

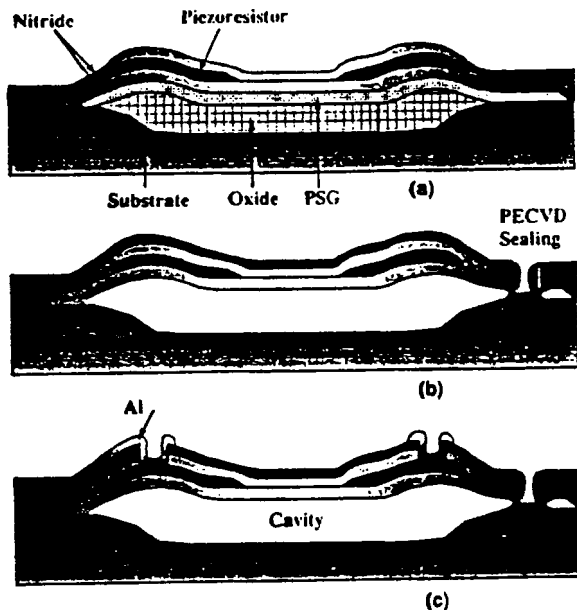


Figure 3: Major fabrication steps for the pressure sensor. (a) a composite oxide/PSG sacrificial layer covered by diaphragm nitride. (b) after diaphragm freeing etching and sealing. (c) the complete structure after metalization.

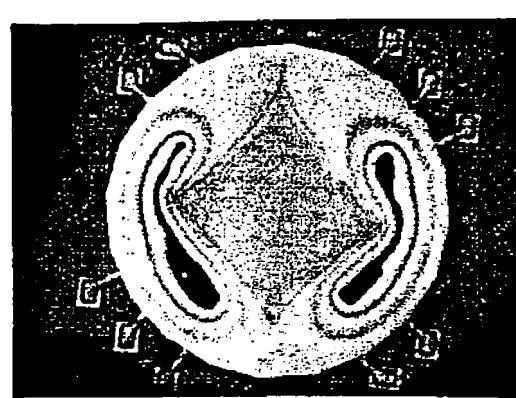


Figure 4: A circular diaphragm with specially designed etching holes for etching pattern study. The etching process was stopped half-way through. The diamond-shaped area at the center of the diaphragm is the remaining oxide/PSG layer. Sharp corners developed during the etching process to cause stress concentration and, sometimes, diaphragm fracture. The two hot-dog shaped areas are due to diaphragm warpage.

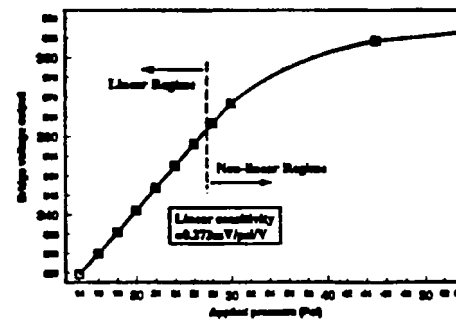


Figure 5: Pressure sensor response. A linear region from 14 to 30 psi is obtained. The pressure sensitivity is found to be 0.127 mV/V/psi. The saturation over 30 psi is because the diaphragm touches the bottom of the cavity.

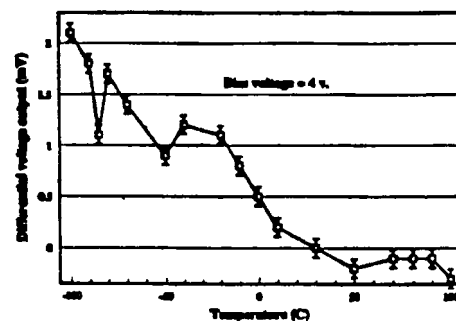


Figure 6: Temperature sensitivity characteristic of the output voltage for an un-sealed pressure sensor. The piezoresistor Wheatstone bridge is biased at 4V, and the reference voltage is 0.221 V at 30°C due to mismatch of the piezoresistors. An averaged output temperature sensitivity of 6 μ V/V/°C is obtained.

Silicon Micromachined Microstructures for Super-Compact Magnetic Recording Rigid Disk Drives

D.K. Miu,* P.C. Chan,[†] S. Tatic-Lucic,[‡] and Y.C. Tai[§]

Summary

This paper focuses on the design and fabrication of millimeter-scale silicon microstructures for super-compact magnetic recording rigid disk drives (Figures 2 to 4). The fabrication processes consist of a combination of RIE and EDP etching on epitaxial wafers with heavily boron-doped buried layers. Both experimental data (Figure 5) and finite-element computations (Figure 6) are presented.

Abstract

A new generation of super-compact (≤ 1.3 -inch form factor) magnetic recording rigid disk drives is being introduced to accommodate the storage and processing requirements of real-time, high-resolution digitized graphical images in extremely challenging computing environments such as those in multimedia portable computers, interactive televisions, digital cameras, and handheld consumer-oriented information and communication systems.

The activities described here are part of a larger industry-supported, jointed UCLA/CalTech research program to design and fabricate a variety of silicon microstructures and microactuators for super-compact data storage devices. Specifically, our focus here is a micro-gimbal/suspension using silicon as the substrate material.

The gimbal/suspension assembly (Figure 1) is a very critical component for high-performance magnetic disk drives and is designed to serve some very important functions. Typically, one thinks of silicon as a brittle material and would not normally use it to construct flexible structures. However, it

is well known that the ultimate strength of silicon microstructures is orders of magnitude higher than that in bulk form. Therefore, when properly micro-machined, the silicon suspension can be made very flexible but with a very high load-carrying capacity.

Fabrications of our micro-gimbals/suspensions are performed on 4-inch epi-wafers. The composite epitaxial layers on these wafers consist of a 16 μm lightly-doped layer on top of a 4 μm heavily boron-doped buried layer. This buried boron layer is used as an etch-stop for subsequent anisotropic etching.

A 500 Å chromium is first evaporated on the epi-wafers, which is then patterned using photolithography, outlining the contours of the microstructures. RIE then follows, etching through both epitaxial layers. After removal of any residual chromium, wafers are either wet-oxidized to a 1 μm thermal oxide or deposited with a 4 μm PECVD oxynitride to form protective layer on all surfaces. Second photolithography step is performed on the backside of the epi-wafers enabling the opening of windows in the oxide (or oxynitride) layer. EDP etching is then performed to form cavities under the microstructures. Finally, oxide/nitride is removed to release the desired free-standing microstructures.

Figures 2 to 4 present the SEM pictures of a number of prototype micro-gimbals, measuring typically 2.5 by 2.5 mm. Specifically, Figure 2 shows a scaled-down gimbal design resembling that of the industry-standard type-16 suspension. Figure 3 is a simpler design consisting of only straight cantilever beams and has a form factor consistent with the so-called 35% sliders. Finally, Figure 4 shows some test structures for the purpose of determining the micromechanical properties of silicon.

Component-level performance characteristics of these microstructures are investigated, using both an ultra-sensitive load-cell for static deflection and fracture measurements as well as a nonintrusive laser Doppler vibrometer for dynamic analysis (Figure 5). In addition, finite-element calculations are performed (Figure 6), allowing comparison and design.

*Assistant Professor, Mechanical Engineering, University of California, Los Angeles, California 90024-1597. (818) 356-3885, 584-9104 FAX, miu@seas.ucla.edu

[†]Research Assistant

[‡]Research Assistant

[§]Assistant Professor, Electrical Engineering, California Institute of Technology, Pasadena, California 91125

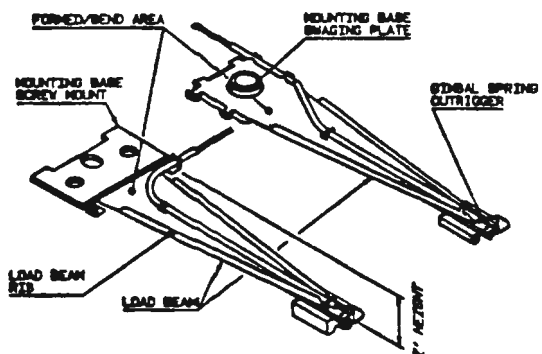


Figure 1: Detailed drawings of the conventional 3370-type read/write suspensions with a screw and a swage mount.

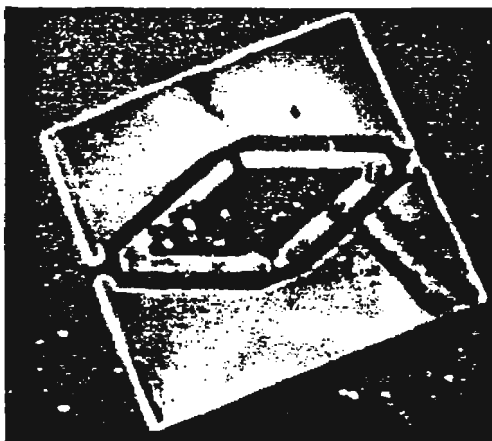


Figure 2: SEM micrograph of a type-16-like silicon micromachined gimbal (top view).

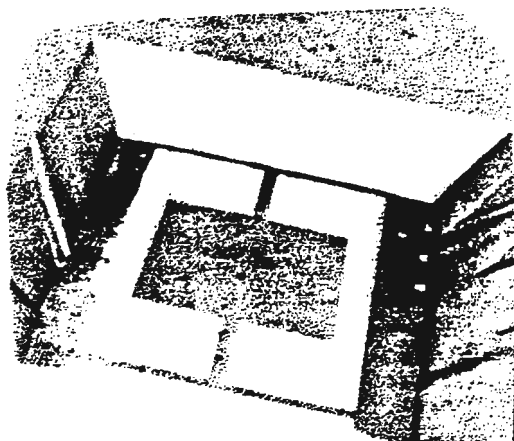


Figure 3: SEM micrograph of a simple-frame silicon micromachined gimbal (bottom view).

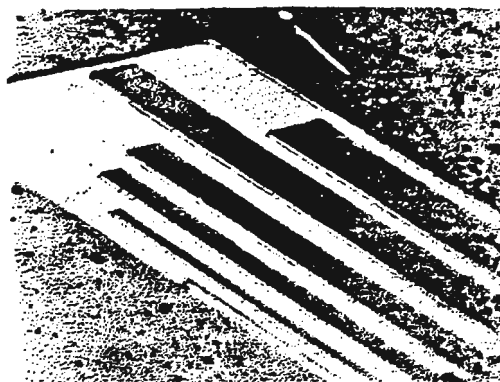


Figure 4: SEM micrograph of some simple test microstructures (top view).

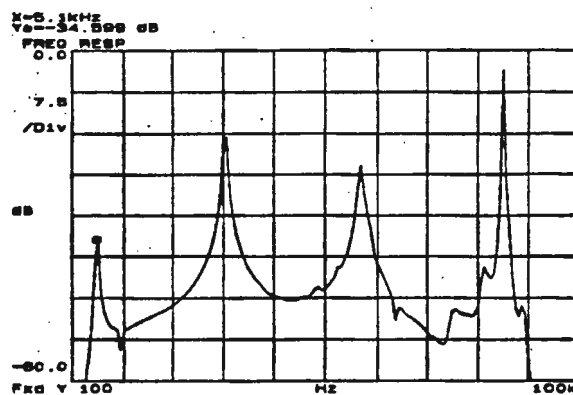


Figure 5: Frequency response of the simple test structure using a nonintrusive laser Doppler Vibrometer.

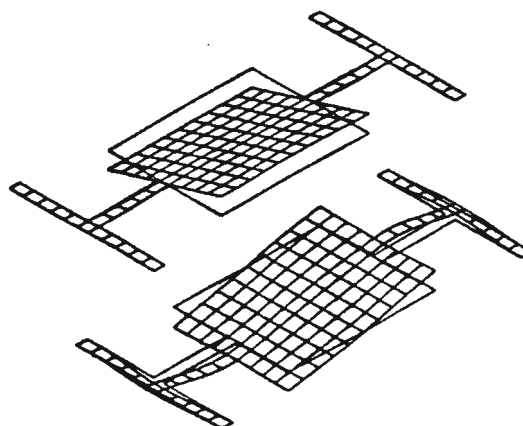


Figure 6: Finite element analysis of the simple-frame silicon gimbal.

(3. Fabrication Technologies)

Mass-Producible All-Silicon Atomic Force Microscope Probes

Chang Liu and Yu-Chong Tai

Electrical Engineering 116-81, Caltech, Pasadena, CA91125, USA

Ronald Gamble

Topometrics Corp., Santa Clara, CA95054-1524, USA

Summary — Mass-producible all-silicon Atomic Force Microscope (AFM) probes (Figures 1 and 2) are presented. A new approach of using heavily boron-doped buried layer as the beam material to provide robust fabrication process is adopted. Mechanical characteristics of the probes have been measured by a Doppler laser vibrometer. Good AFM images (Fig. 4) are obtained using these probes.

Abstract — Since its invention, the Atomic Force Microscope (AFM) has become a powerful tool for surface study with atomic resolution¹. However, in order to maintain its high performance, it is mandatory to have high quality probes with reliable mechanical characteristics and good tip sharpness. Here, we then present an all-silicon probe which meets these requirements. This probe has three parts: a tip, a beam and a handle. The probe is completely made of single crystalline silicon in order to have highly reliable mechanical properties². To make the probe, we design a process using (100) epitaxial wafers that have a 10 μm lightly doped layer on top of a 4 μm heavily boron-doped buried layer. The lightly doped layer is used to form the sharp tips, and the heavily doped buried layer is to form the beam. This approach of using a buried layer to make the beam allows good control of the beam thickness since EDP etching automatically stops at this layer. To our knowledge, this is the first time this approach has been reported.

Major steps of our process is described here. The fabrication starts with forming silicon pyramids in the lightly doped epitaxial layer by EDP etching (Figure 6a). A 1- μm -thick low-temperature-oxide (LTO) masking layer is then deposited on the wafer and patterned to define the cantilever beams. The beams are etched by SF_6 plasma. An LPCVD low-stress nitride layer (200 nm thick) is deposited, followed by beam-freeing EDP etch from the back of the wafer. Next, the LPCVD nitride is stripped in phosphoric acid to free the beam. Tip sharpening then finishes the process by growing wet oxide on the tip and removing it (Figure 6b). The finished tips typically have a radius of less than 100 nm and an aspect ratio of 1. Figures 1 and 2 show a probe with a sharp tip, a V-shaped beam and a handle. The beam is 200 μm long, 20 μm wide, and 2 μm thick.

Mechanical characteristics of the probes have been measured using a vibrometer, which consists of a Doppler laser interferometer. For example, the resonant frequency of the probe shown in Figure 1 is 42 KHz, which is in good agreement with finite element simulations. Quality factor, Q, of the probe is also found to be 80 in the air using both band-width and time-domain step response methods (Figure 3). Aging of the boron-doped beams has also been studied by exciting the beam at its resonant frequency for as long as 10 hours (about 1.5×10^9 cycles), and no measurable change of the resonant frequency and Q was found.

The probes have also been tested in AFM machines (Topometrics TMX-2000) under both contact and non-contact modes. Figure 4 shows an AFM image of a compact disc surface using our probes. As shown, the μm -sized pits are clearly seen. Finally, a "Superprobe" process can be added to our probes so that even better tip sharpness and aspect ratio can be obtained, if necessary. Figure 5 demonstrates such a superprobe. The radius of the superprobe is about 10 nm and the aspect ratio is more than 10.

References—

1. G.Binnig, C.F. Quate, "Atomic Force Microscope," *Physical Review Letters*, Vol. 56, No. 9, pp. 930-933, 1986.
2. K.E. Petersen, "Silicon as a Mechanical Material," *Proceedings of the IEEE*, Vol. 70, No. 5, pp. 420-457, 1982.
3. K.E. Bean, "Anisotropic Etching of Silicon," *IEEE Trans. on Electrical Devices*, Vol. ED-25, No. 11, 1978, pp. 1185-1193.



Figure 1: SEM picture of a V-shaped beam. At the end of the beam is an oxidation-sharpened tip.



Figure 2: SEM picture of a complete probe which consists of a tip, a beam and a handle. The handle is designed for easy mounting of the probe to AFMs.

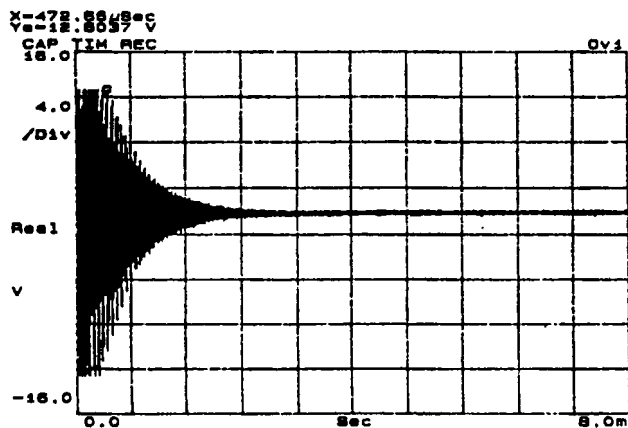


Figure 3: Time-domain step response of an AFM probe. A quality factor of 80 is extracted from the figure.

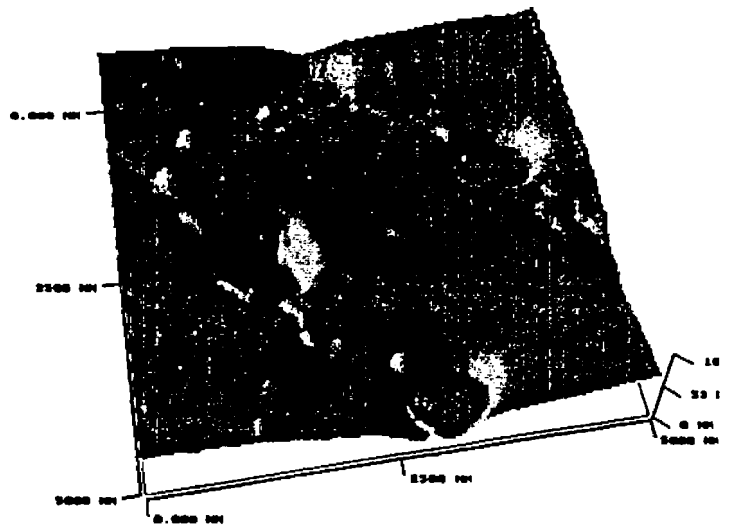


Figure 4: An AFM image of a compact disc surface obtained using the probe shown in Fig.2. The CD track pitch is about $2.5 \mu\text{m}$ and the pits are $1 \mu\text{m}$ in diameter.

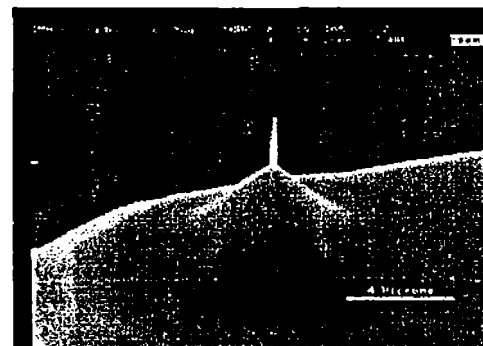


Figure 5: SEM picture of a superprobe grown on a silicon tip.

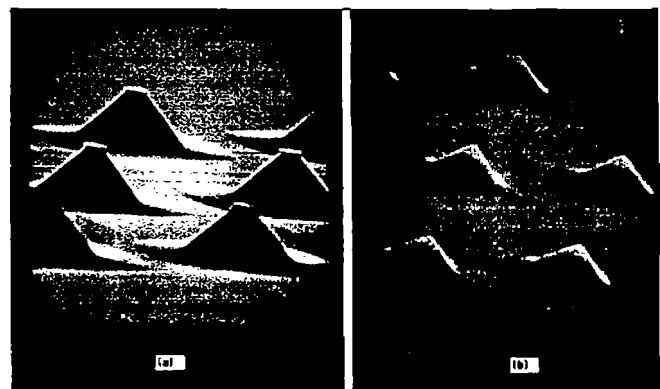


Figure 6: (a) Anisotropically etched silicon pyramids. (b) the same tips after oxidation sharpening.

Part II:

Vortex Interactions

II-1. The Dynamics of Wall Turbulence: The Importance of Vortex Interactions

**Charles R. Smith
Lehigh University**

SEMINAR NOTICE

**THE DYNAMICS OF WALL TURBULENCE:
THE IMPORTANCE OF VORTEX INTERACTIONS**

Professor C. R. Smith

Department of Mechanical Engineering and Mechanics

Lehigh University

A variety of flow structures have been suggested as important in the development and regeneration of turbulent boundary layers. The majority of these suggested flow structures are associated with some form of vortex structure, from streamwise and transverse vortices to multiple hairpin vortices. However, most of the flow structures and their hypothesized behavior are based on inferences from measurements or simulations of fully-turbulent flows, often revolving around a discussion of kinematics, but with little dynamic support. A particularly important process involved in the dynamics of turbulence is that of vortex interaction with surfaces, a process which provides a sustaining mechanism for turbulence through the regeneration of new vortices. The present talk will summarize the findings of a series of "kernel" experiments which have examined the basic kinematic and dynamic behavior of various vortex phenomena believed to be relevant to wall turbulence, focussing on how vortices interact with surfaces, and how these interactions lead to generation of "new" vorticity and vortices. Using both flow visualization and PIV results, several different vortex flow structures will be discussed, including ring vortices, streamwise vortices, hairpin vortices, and necklace/horseshoe vortices in junction regions. A conceptual model of near-wall turbulence, based upon the results of these vortex interaction studies and other relevant work will be discussed.

Thursday, the 15th April 1993

Conference Room B, Bldg. 102

Time: 10:30 AM

POC: Dr. Promode R. Bandyopadhyay (Code 8234; x2588)

The Dynamics of Wall Turbulence:
The Importance of Vortex Interactions

C.R. Smith
Department of Mechanical Engineering and Mechanics
Lehigh University

Supported by AFOSR

Intoduction

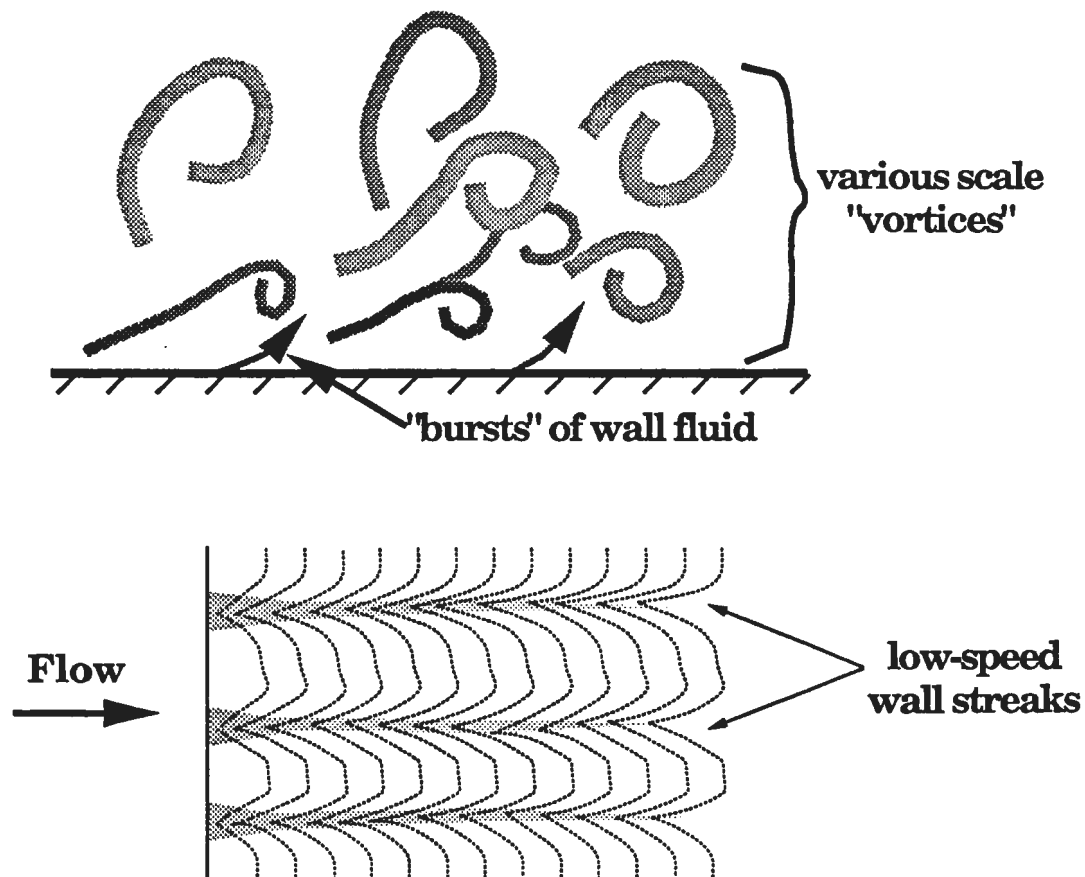
Turbulence — what is it?

- **Measurements reflect property fluctuations**
- **Originally: Statistical interpretation**
- **Recently: Coherent structure interpretation**

**Difficulty \Rightarrow Establishing and Modeling of
relevant flow structure**

Example: Flow visualization of TBL on flat plate

- **H₂ bubbles in water flow**
- **Side-view & Plan-view**



Suggestion of organization \Rightarrow Coherent Structure

- **Complicated, unclear interactions**

Kucheman \Rightarrow "Vortices are sinews and muscles of turbulence"

- **What part do vortices play?**
- **Where do they originate?**
- **How do they interact:**
 - **with each other?**
 - **with the surface?**

Vortex Kernel Studies

Kernel study:

- **Examination of a simpler flow structure in order to understand the dynamics and processes relevant to turbulence**

Examples:

- **Deformation of a line vortex in a shear flow**
- **Interaction of a controlled vortex with a surface**

Objective:

- **To understand the processes giving rise to observed/detected turbulent behavior**

To be considered in this seminar

- **Review of selected kernel studies**
 - √ **Inviscid 3-D vortex interactions in shear flow**
 - √ **Vortex-surface interactions**
 - √ **Hairpin vortex evolution/interactions**
- **Video of selected behavior**
- **Wall turbulence model suggested by kernel studies**

Inviscid Vortex Deformation/Interaction

(Courtesy of J.D.A. Walker et al.)

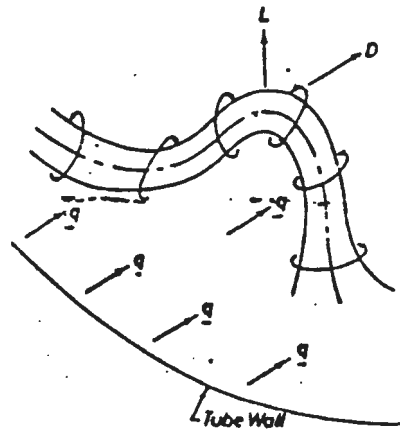


Fig. 3. Primary structure of wallbound turbulence (Presented at the Second Midwestern Conference on Fluid Mechanics, March 17, 1952)

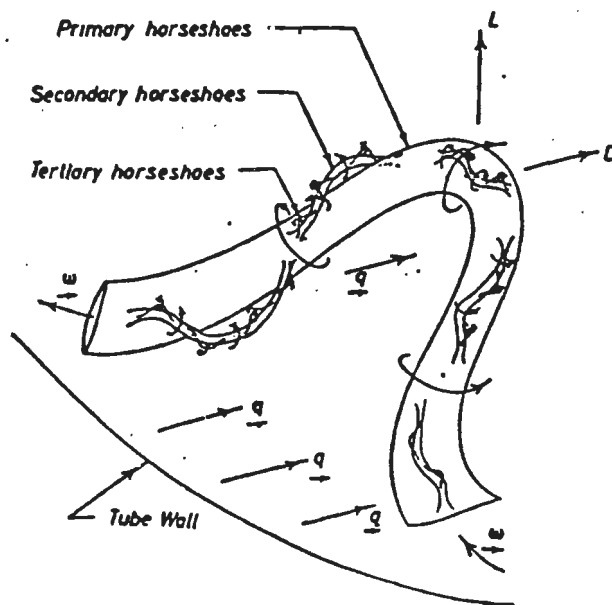
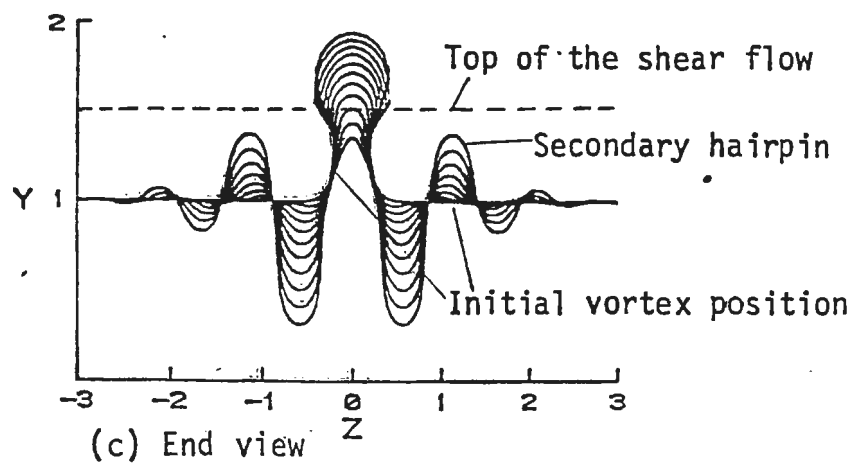
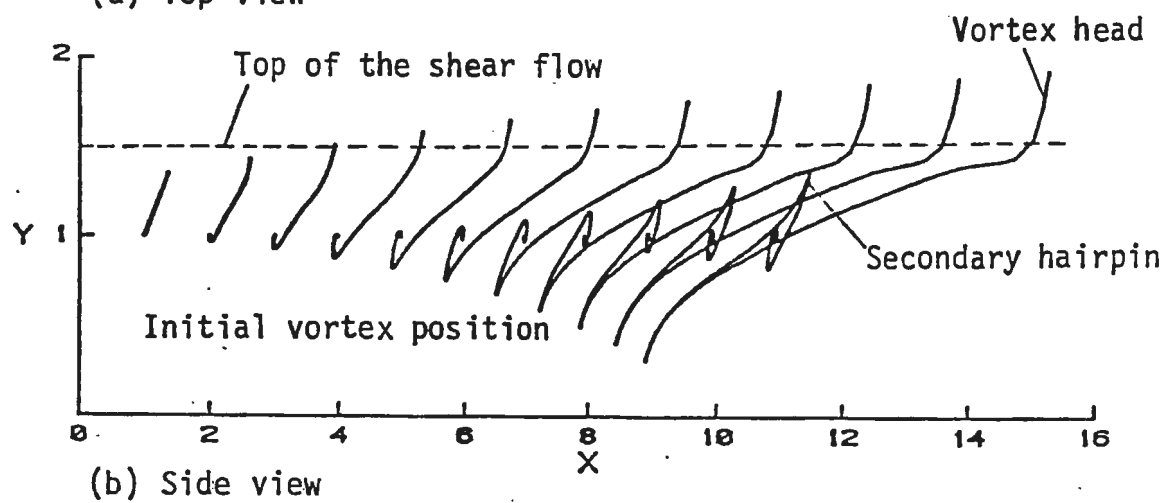
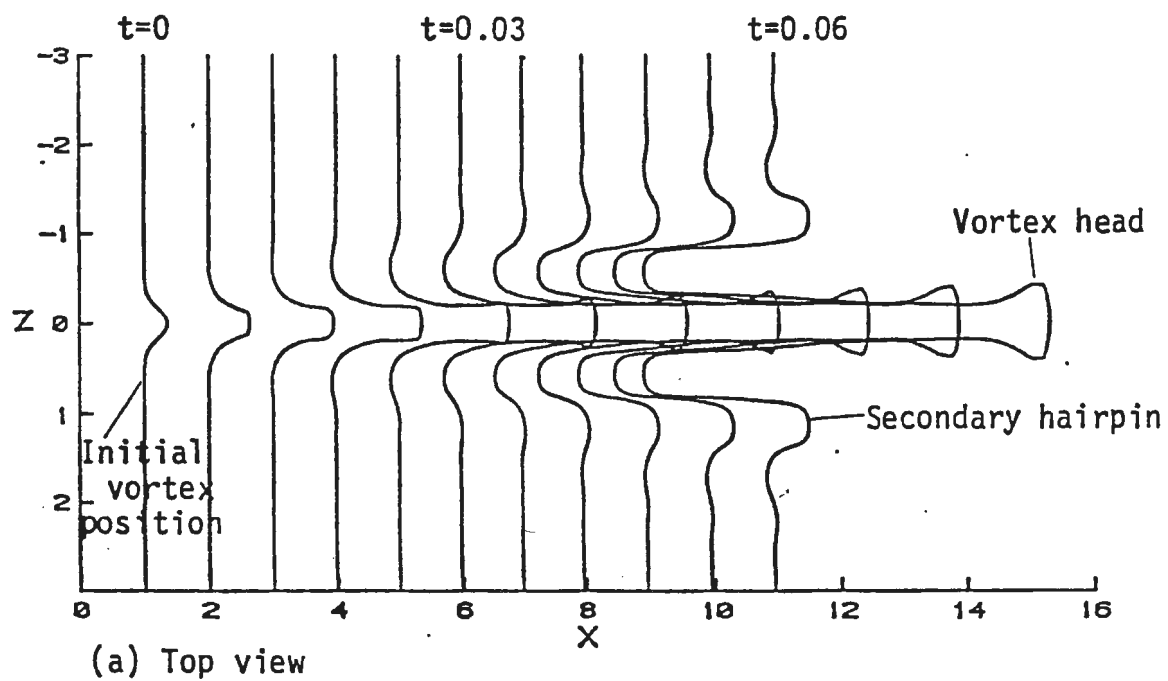


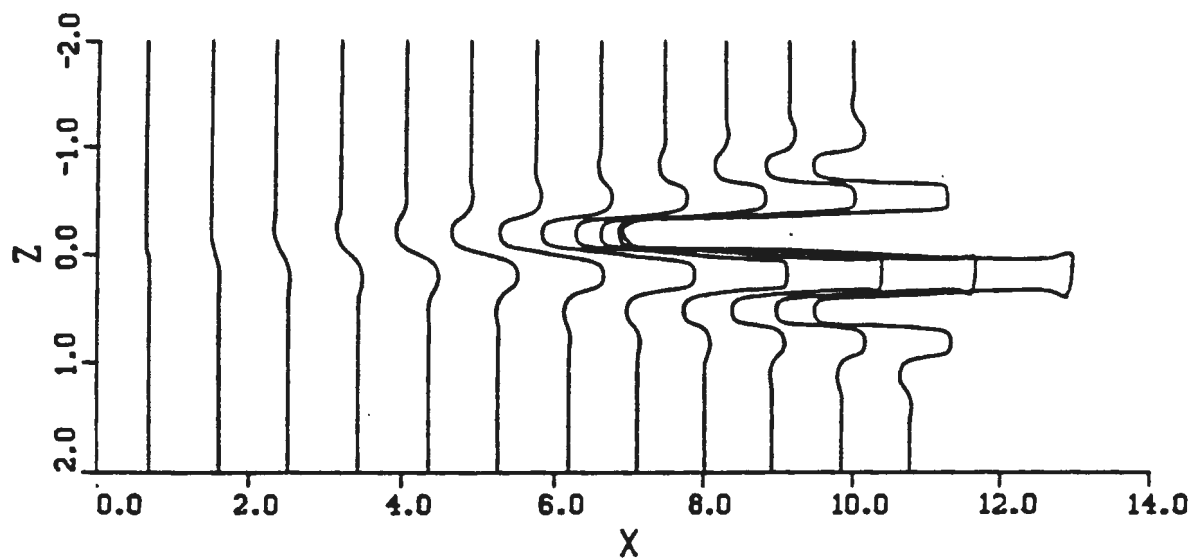
Fig. 4. Horseshoe of large Reynolds number

From T. Theodorsen (1952).

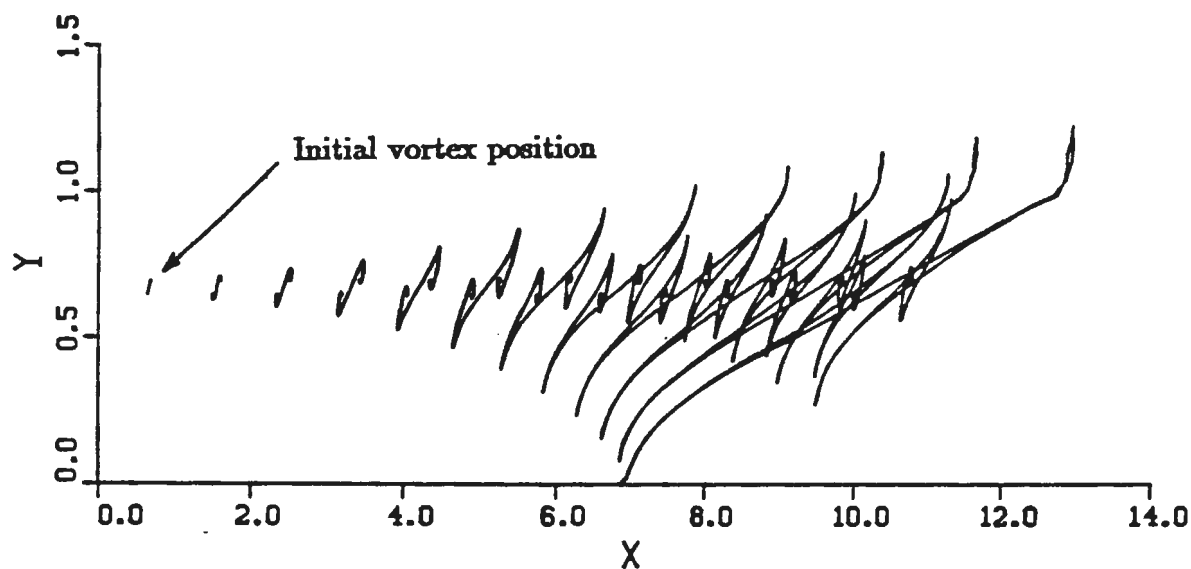


from Hon & Walker

(a)



(b)



(c)

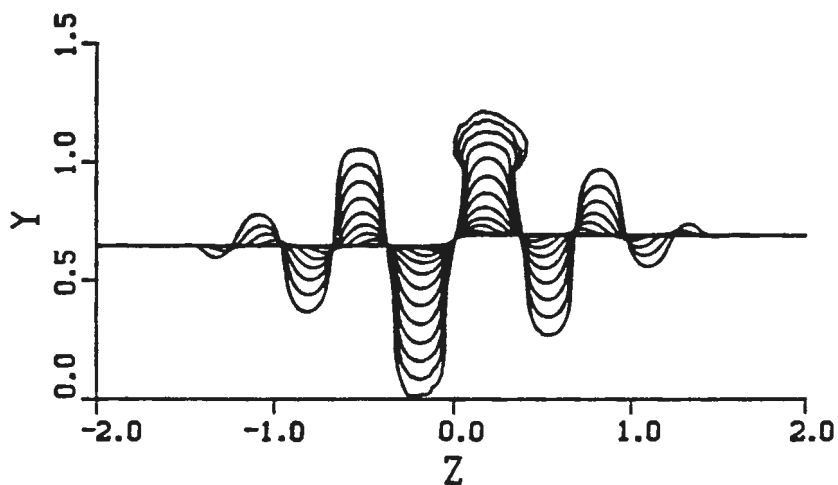


Figure 8. Evolution of a small "step" in a two-dimensional vortex convected in a uniform shear flow: (a) top view, (b) side view, (c) end view; $\epsilon = 0.00267$, 440 time steps with $\Delta t = 0.034$. The vortex position is plotted every 40 time steps.

from Sohnen & Walker

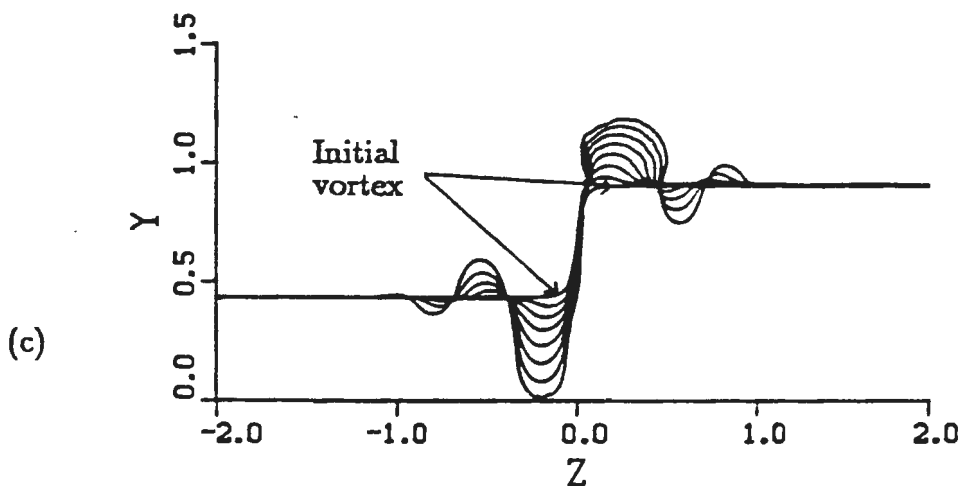
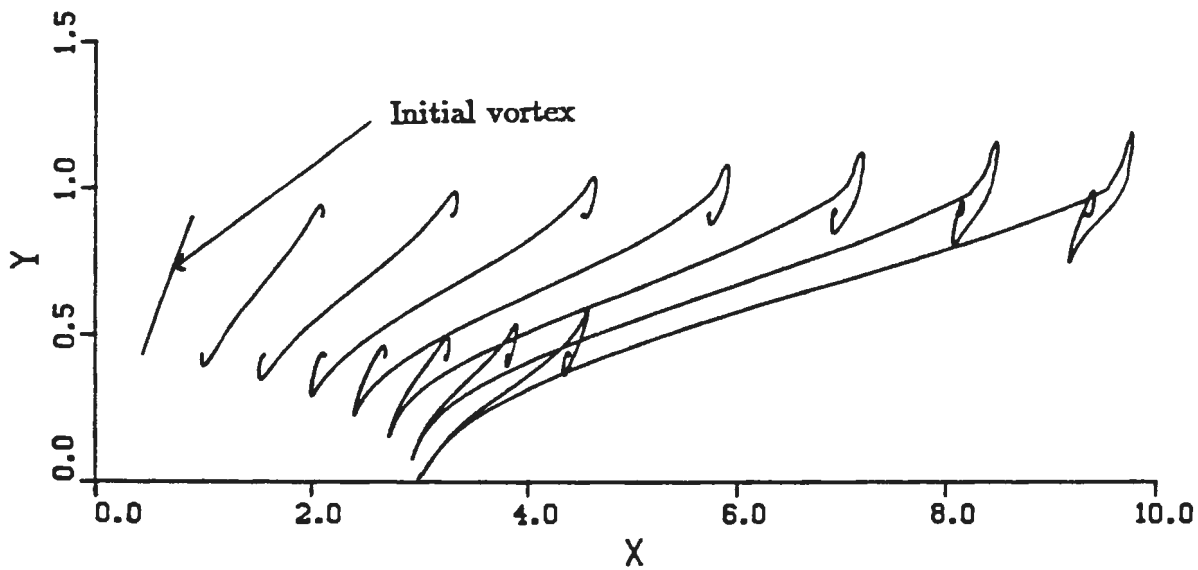
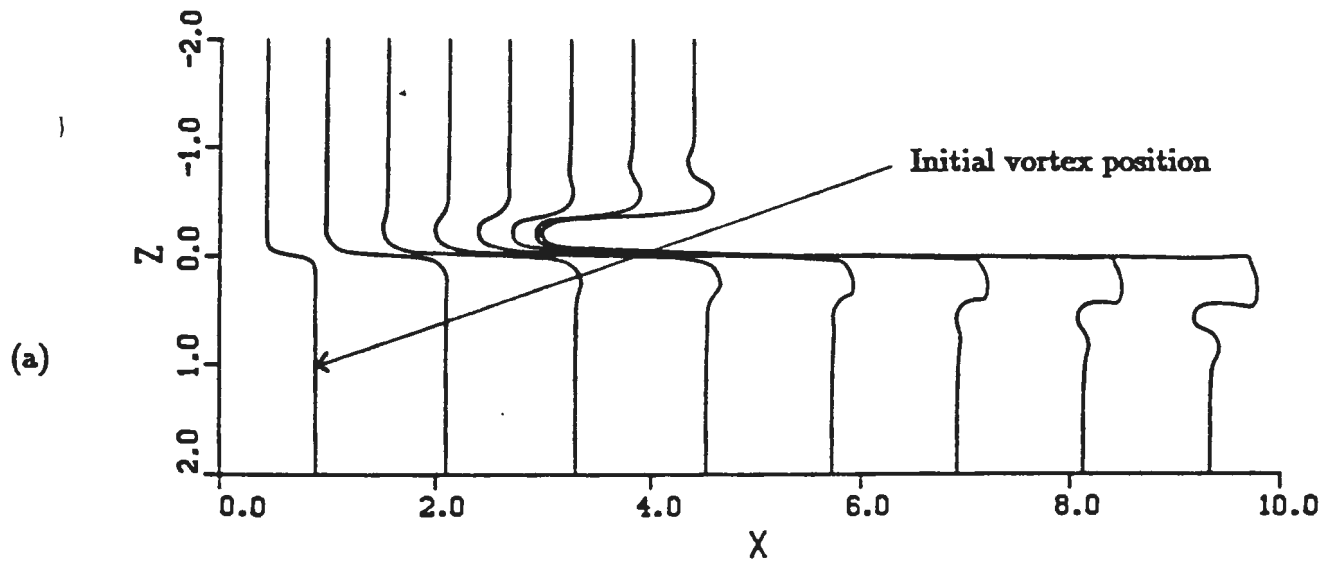


Figure 7. Evolution of a "step" in a two-dimensional vortex convected in a uniform shear flow; the vortex position is shown every 40 time steps in (a) top view, (b) side view, and (c) end view.

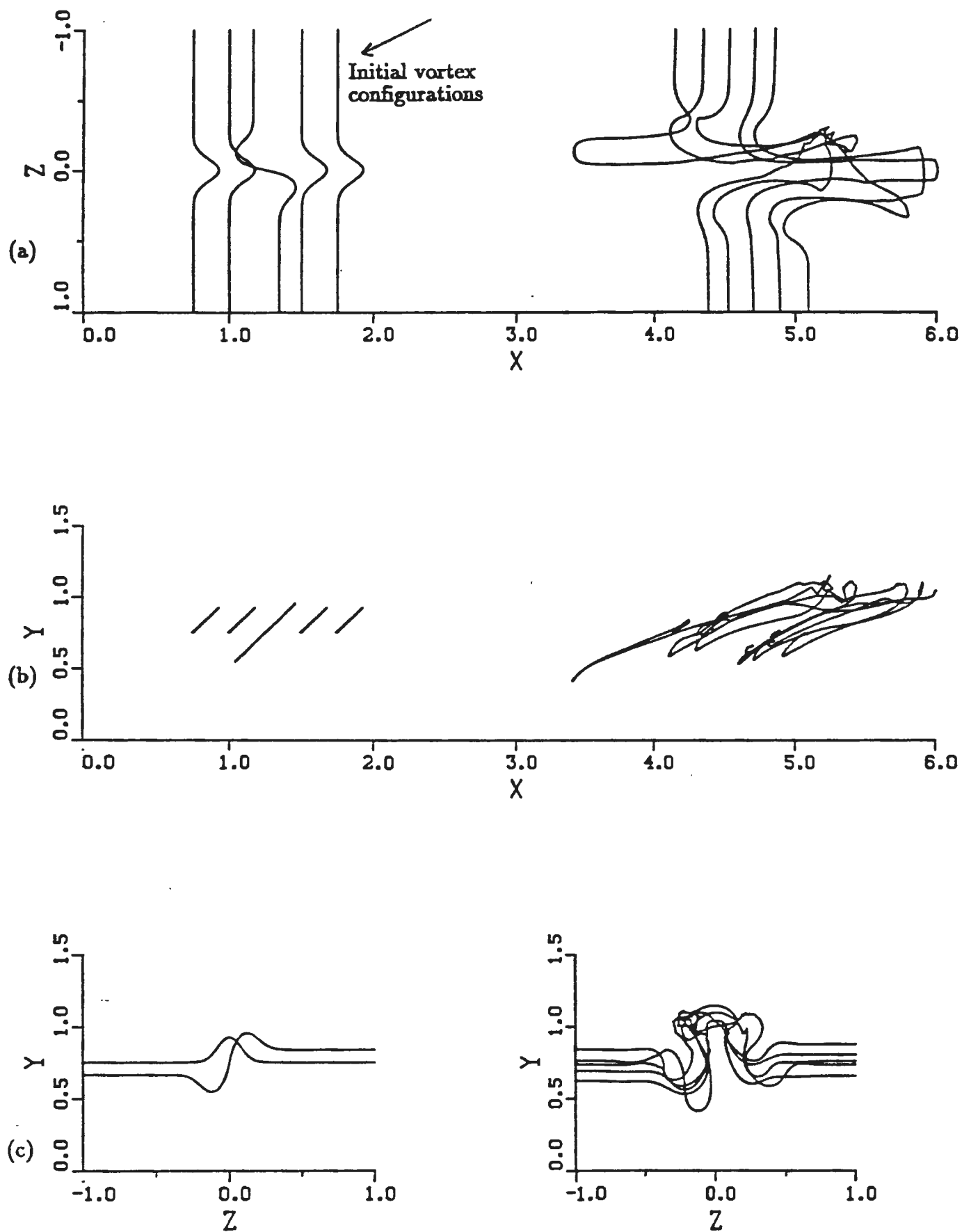


Figure 12. Evolution of multiple hairpin vortices in a uniform shear: (a) top view, (b) side view, (c) end view; all three coordinates are plotted on the same scale.

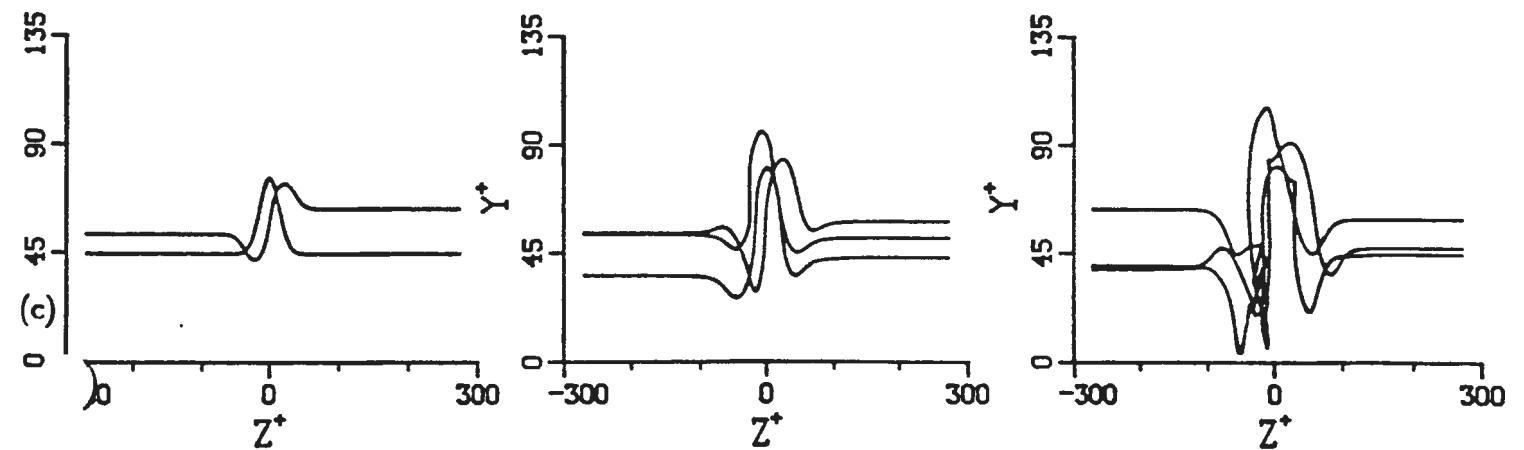
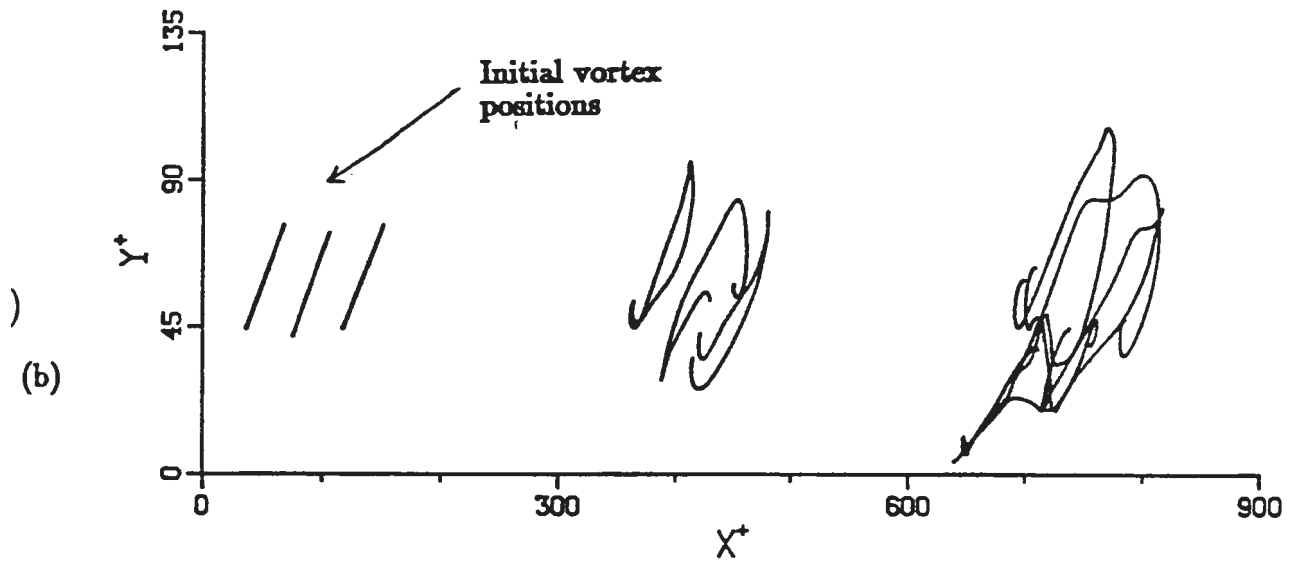
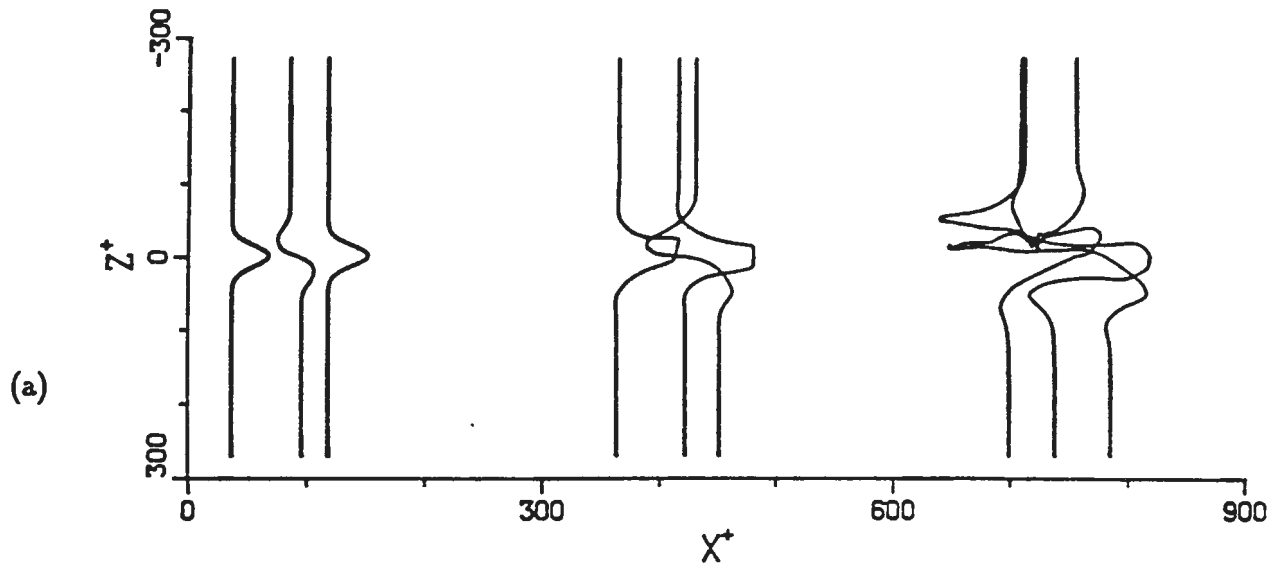
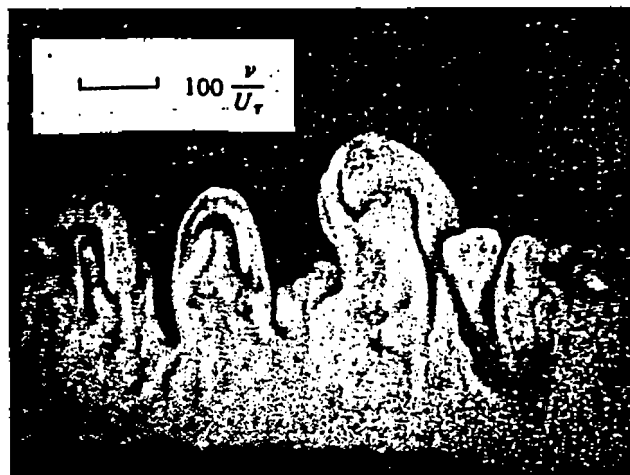
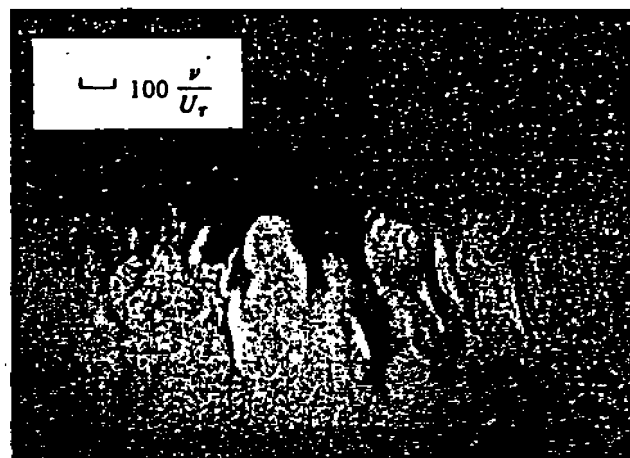


Figure 13. Evolution of three vortices in a turbulent mean profile: (a) top view, (b) side view, (c) end view; $\epsilon = 0.0013$, vortices shown after 120 and 240 time steps with $\Delta t = 0.016$.



Head
 &
 Bandyopadhyay
 (1981)



$Re_\theta = 1700$



Wallace & Balint

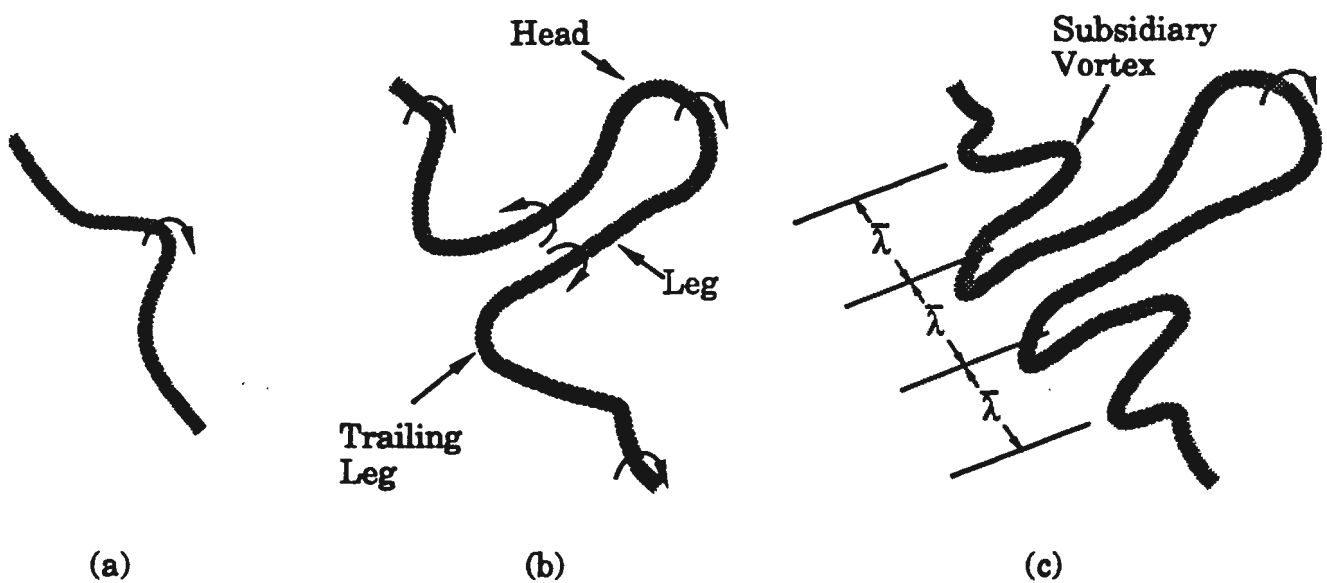
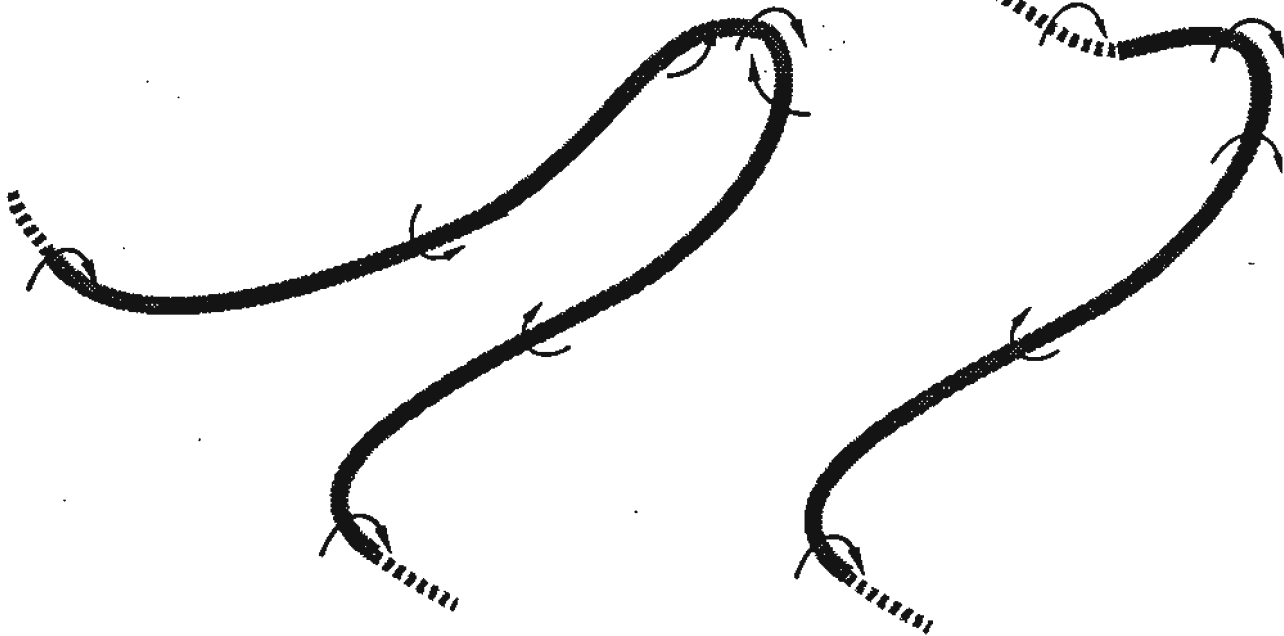


Figure 6. Evolution of a symmetric hairpin vortex in a shear flow.
 (a) initial distortion, (b) development of vortex legs and head,
 (c) evolution of subsidiary vortices and penetration toward the surface.



(a) Symmetric

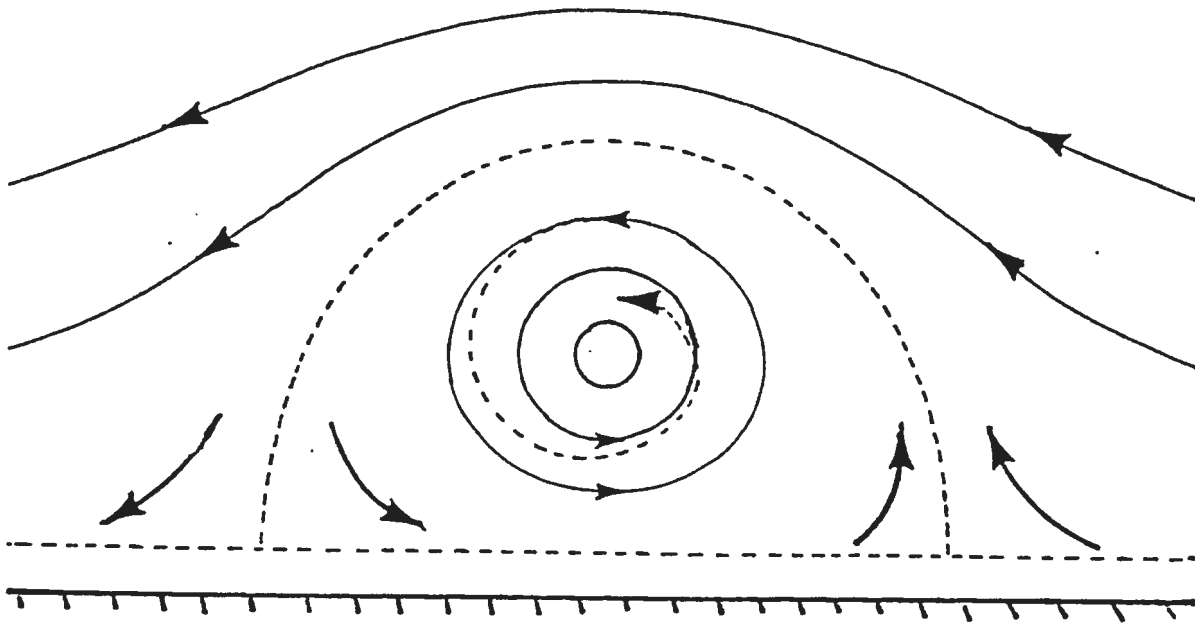
(b) Asymmetric

Typical Surface Vortices

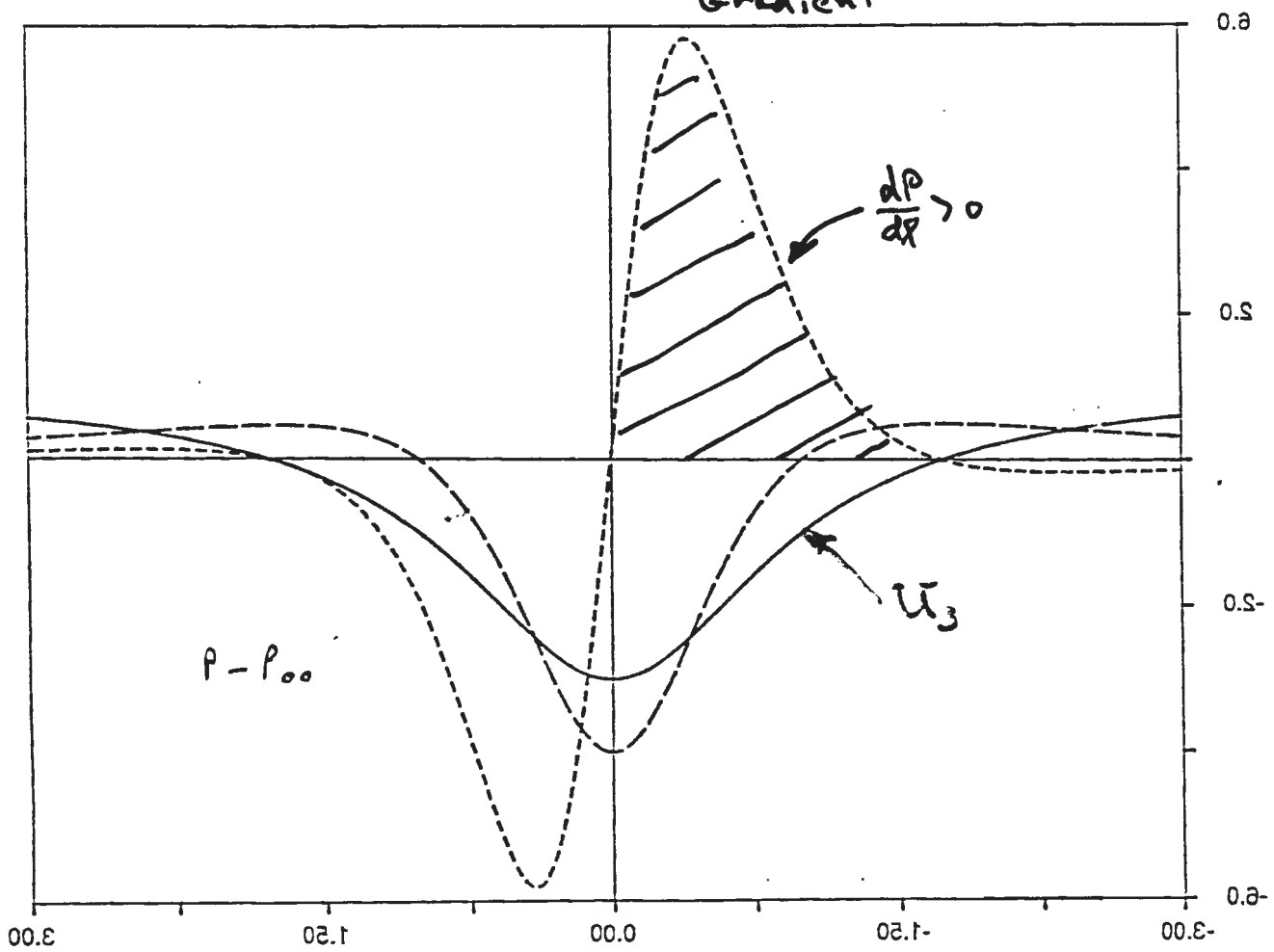
- **Collectively, expect irregularity**
- **Process of interaction similar**

Vortex-Surface Interaction

)



Adverse Pressure Gradient



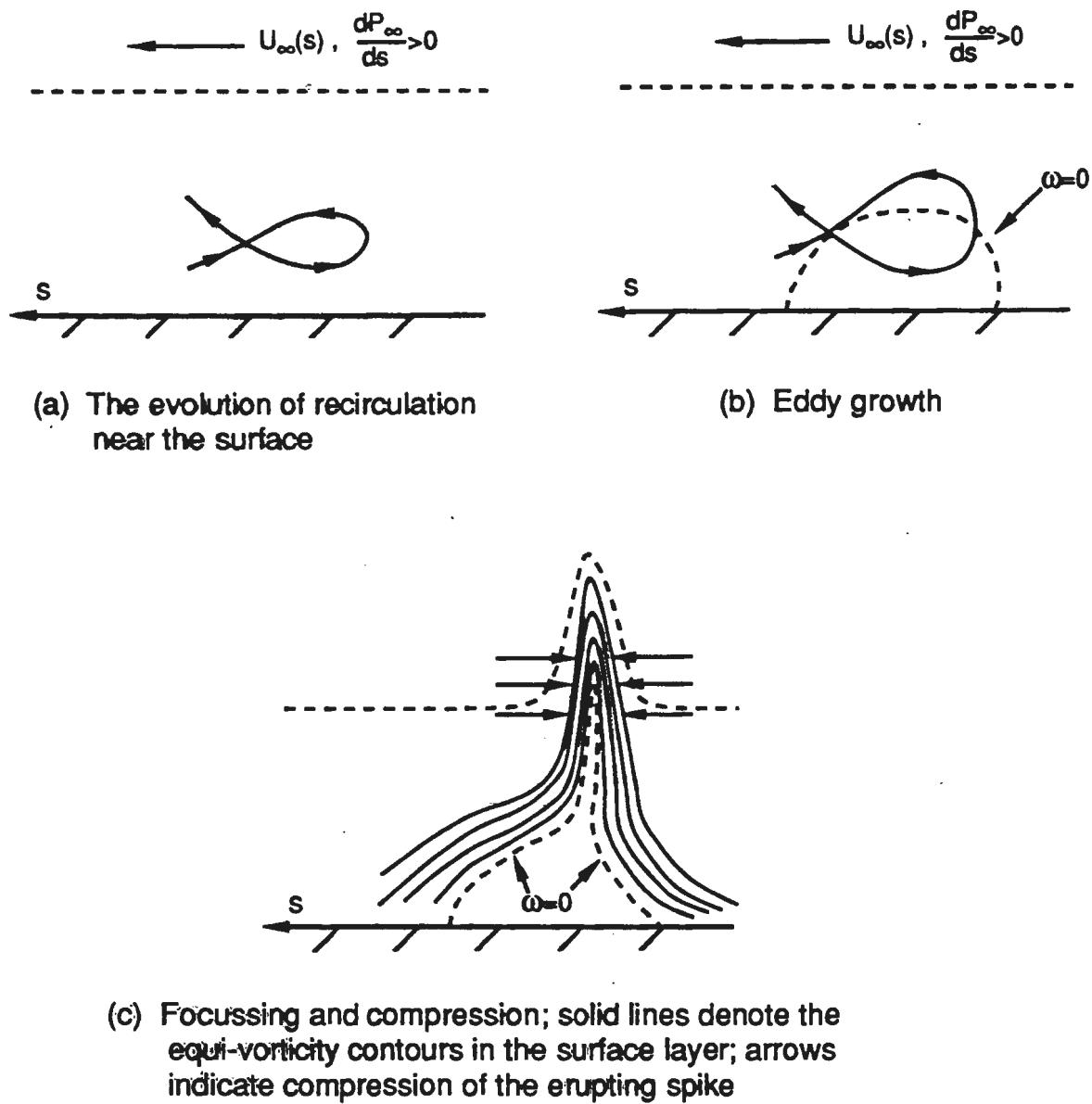
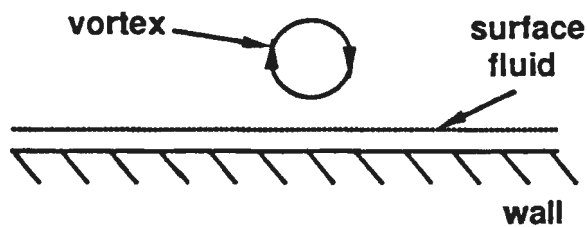
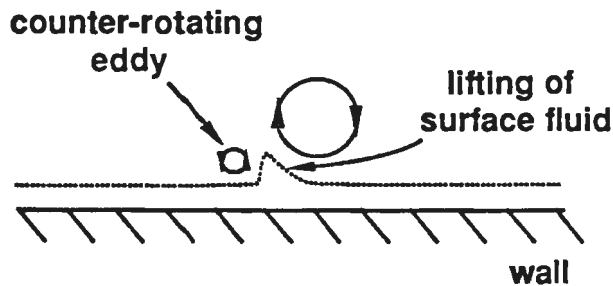


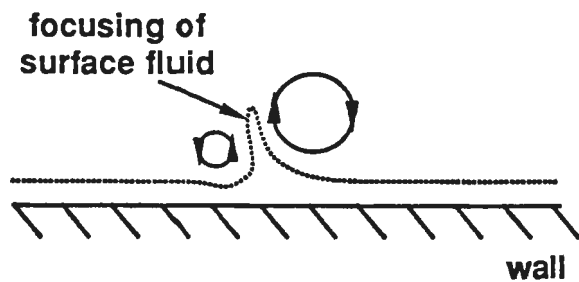
Figure 3. Schematic diagram of the stages in the separation of a two-dimensional surface layer (not to scale).



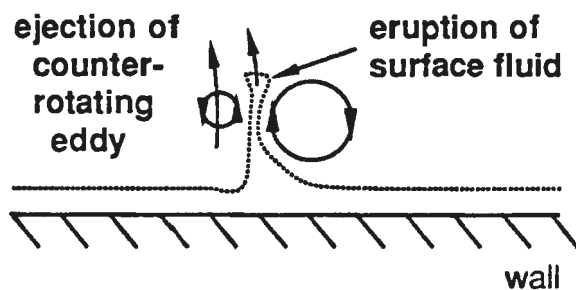
- 1) An isolated vortex is in the vicinity of a solid wall.



- 2) A counter-rotating eddy develops, and surface fluid lifts from the wall.



- 3) The combined influences of the parent vortex and the strengthening counter-rotating vortex have a focusing effect on the surface fluid lifting off the wall.



- 4) The narrow band of surface fluid violently erupts away from the wall, interacting with the outer flow. The counter-rotating eddy is ejected into the outer flow during the process.

Schematic Illustration of a Vortex-Surface (Inviscid-Viscous) Interaction.

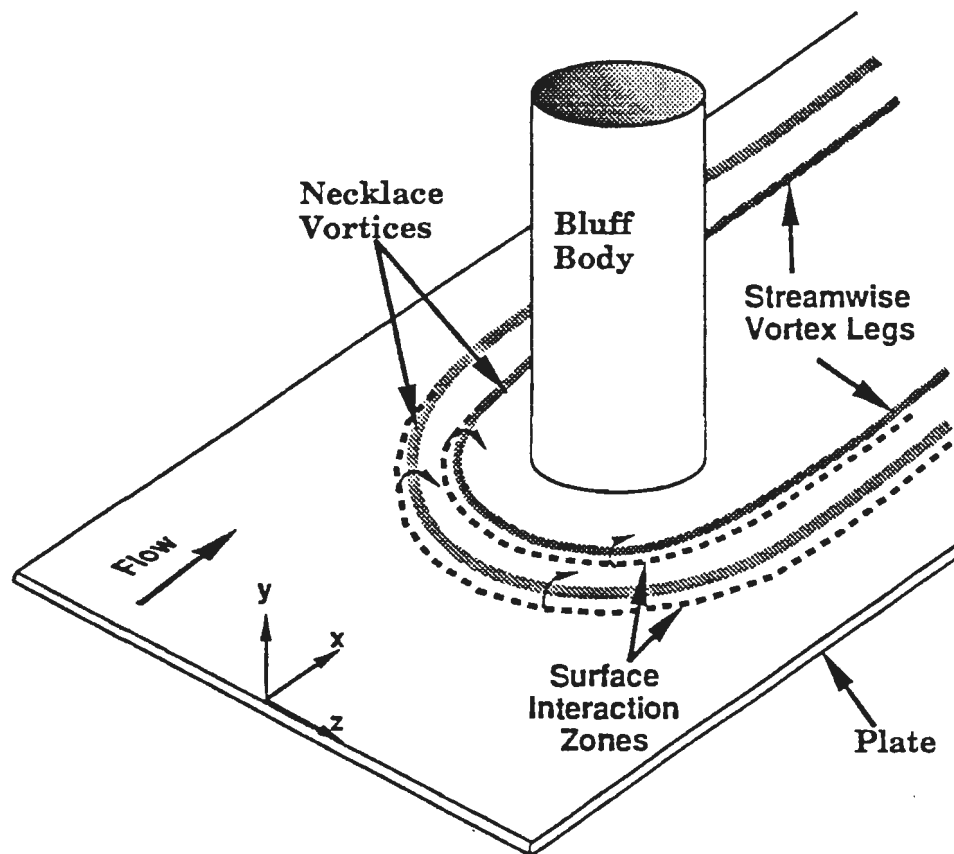
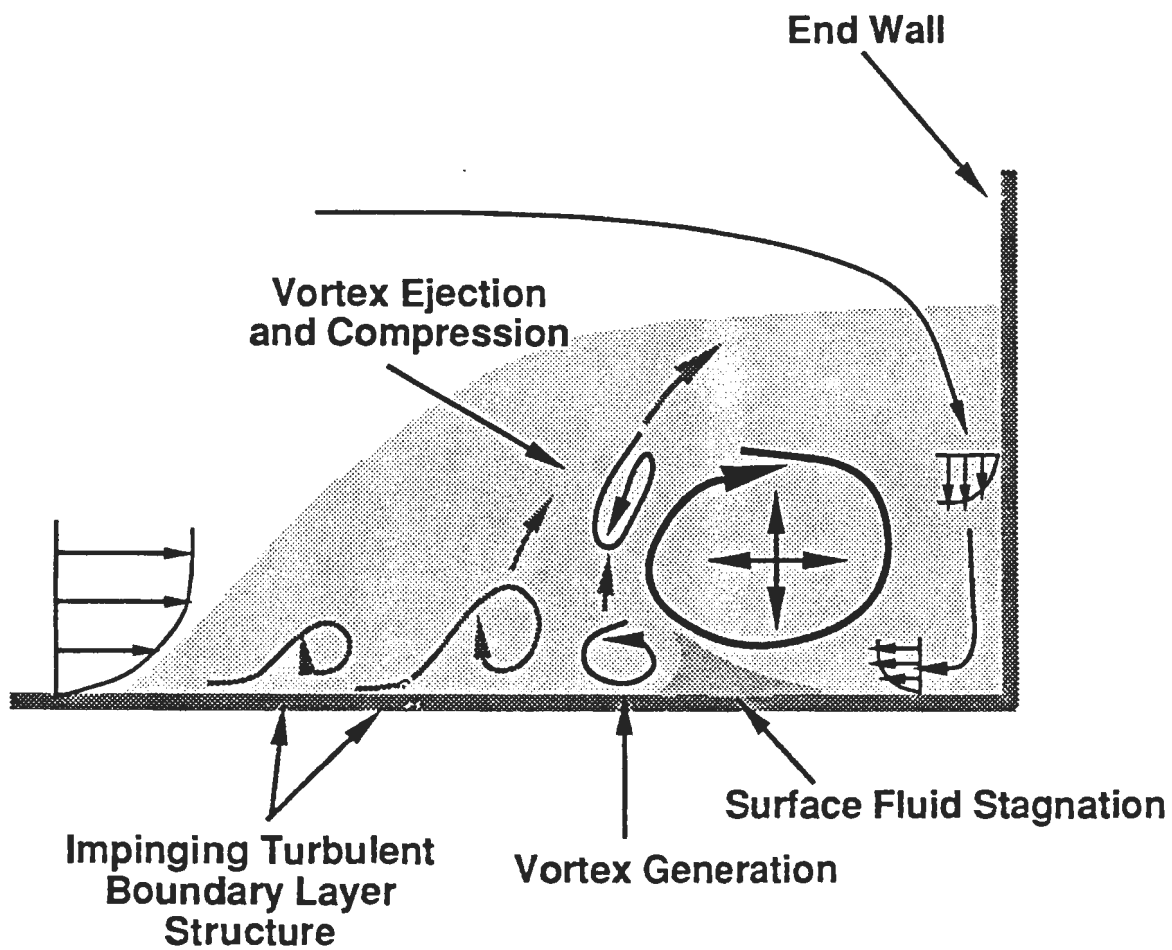
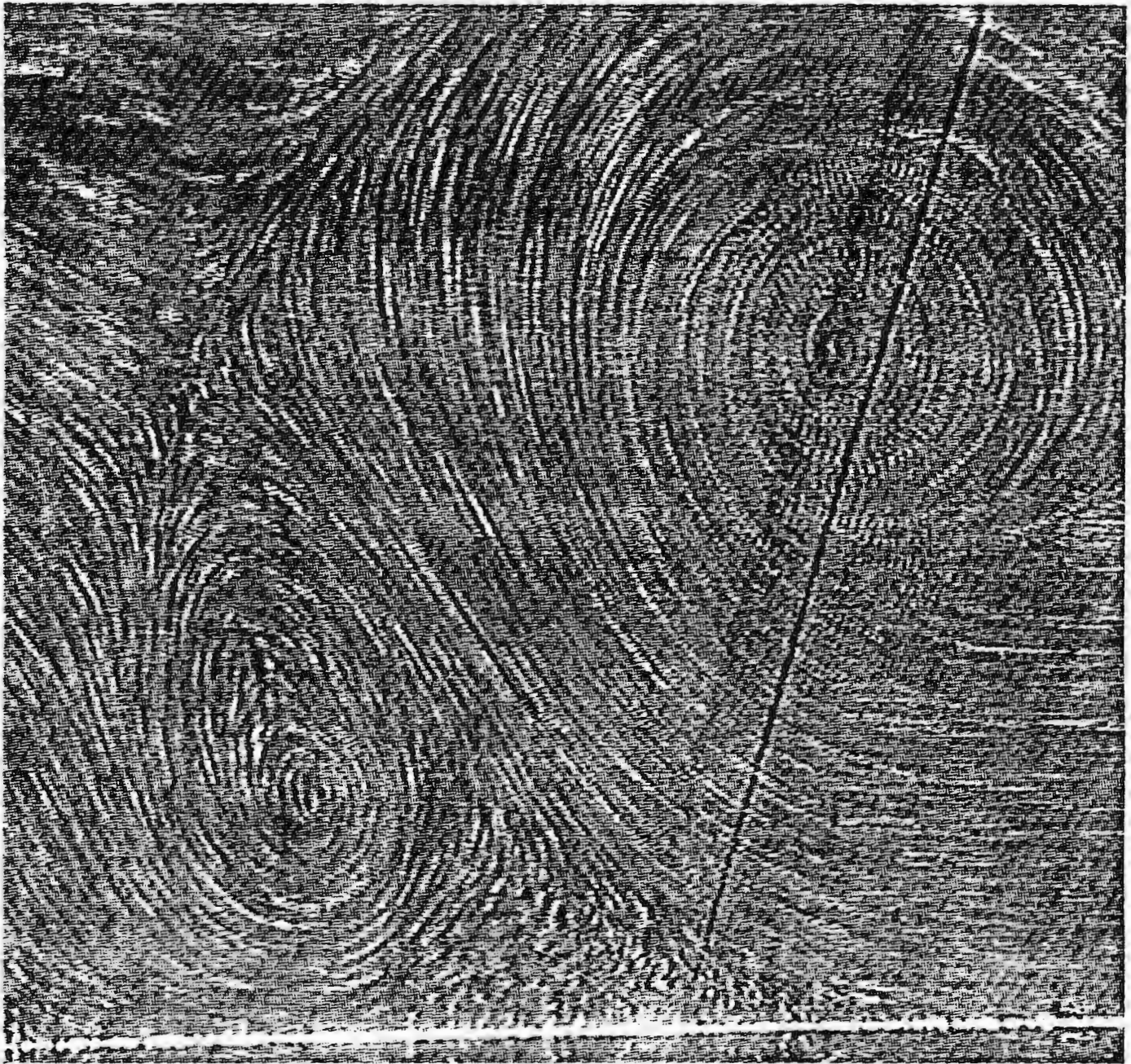


Figure 11. Schematic of flow structure near a juncture

Processes in Unsteady End-Wall Flow: Turbulent Approach Flow



turb1.tif



Particle Image Visualization on Symmetry Plane

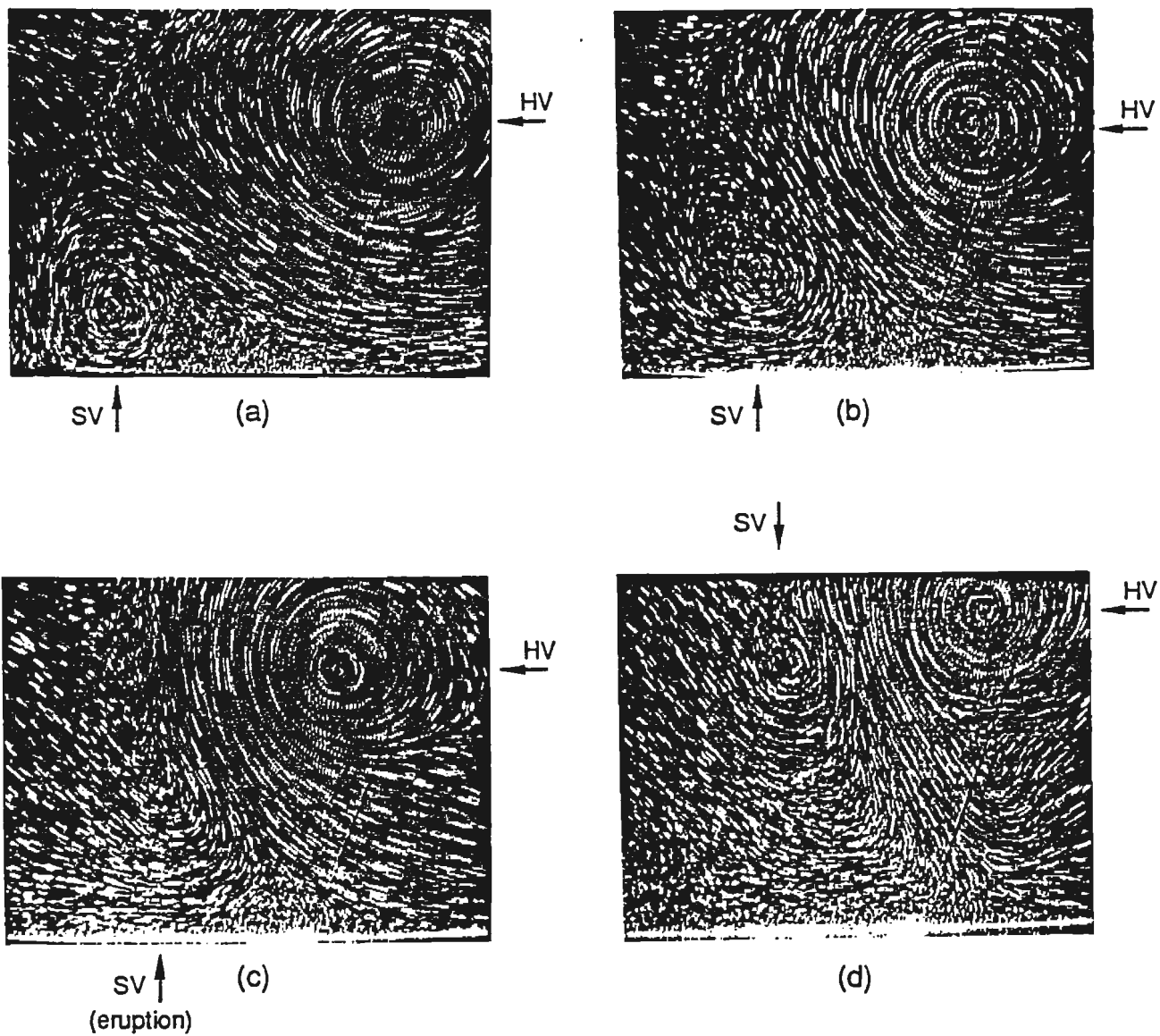
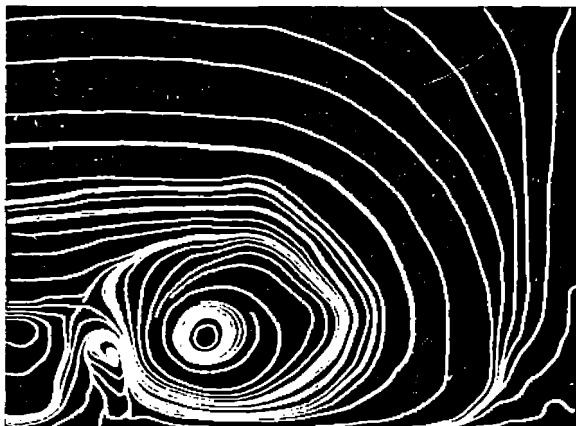
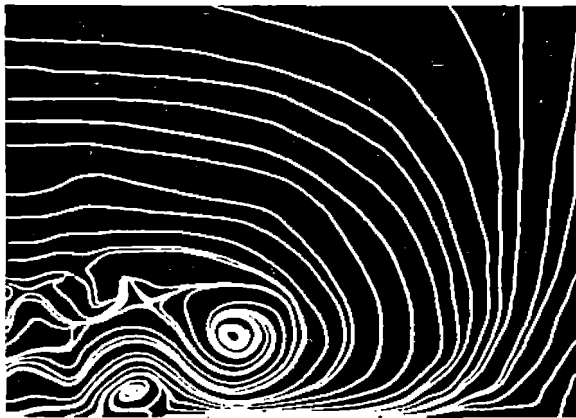


Figure 14. Four sequential particle image visualizations of surface interaction on symmetry plane of turbulent horseshoe vortex in junction region of rectangular body. $Re_0=700$; each picture taken 0.25 seconds apart.

HV⇒horseshoe vortex; SV⇒secondary vortex.

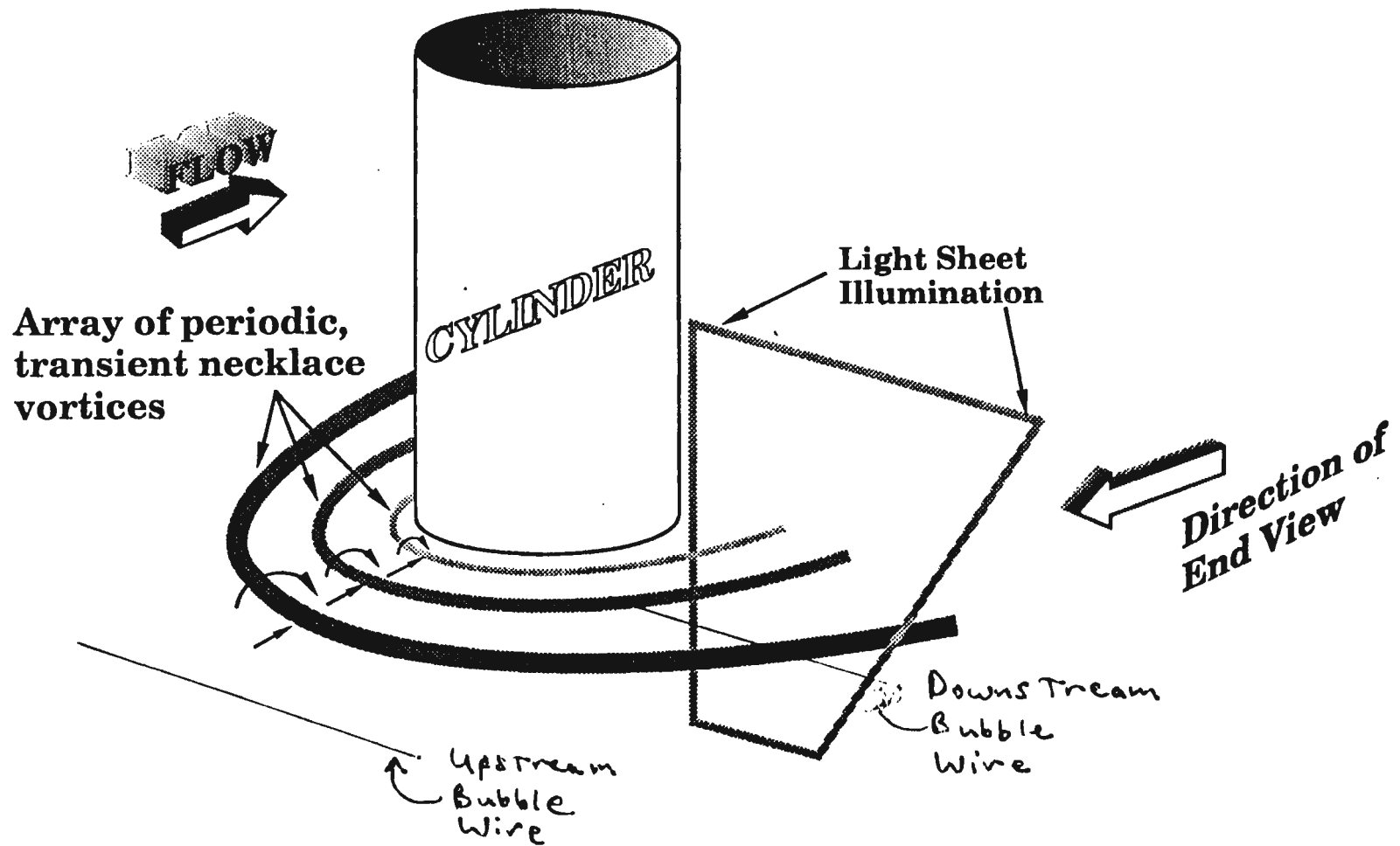
PIV REALIZATIONS OF A TURBULENT HORSESHOE VORTEX



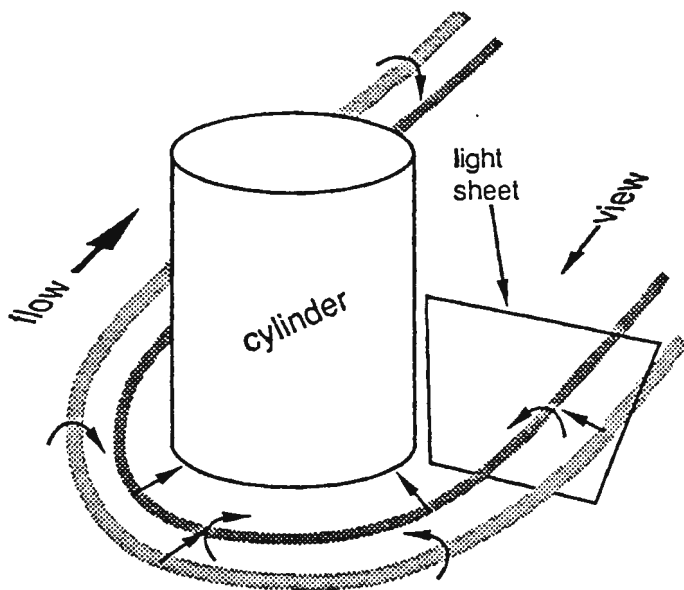
STREAMLINES

VORTICITY

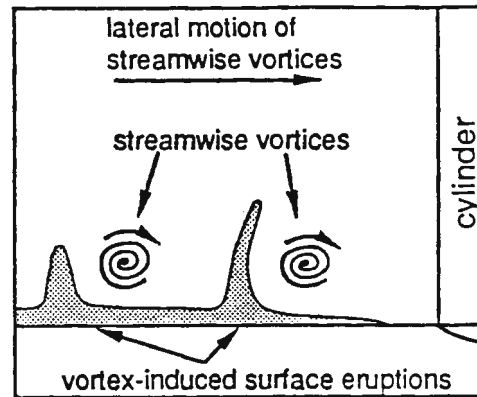
from C. Seal



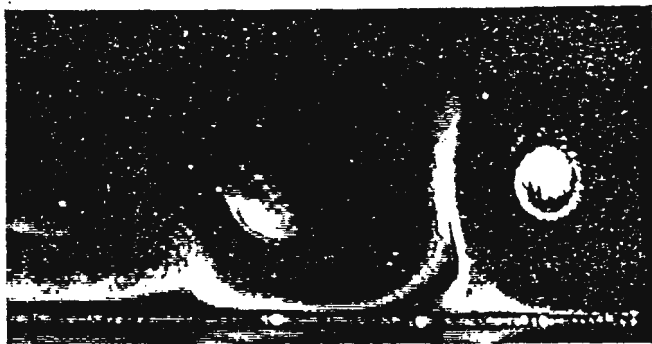
Oblique View: Symmetric Necklace Vortices



(a) Necklace vortex formation



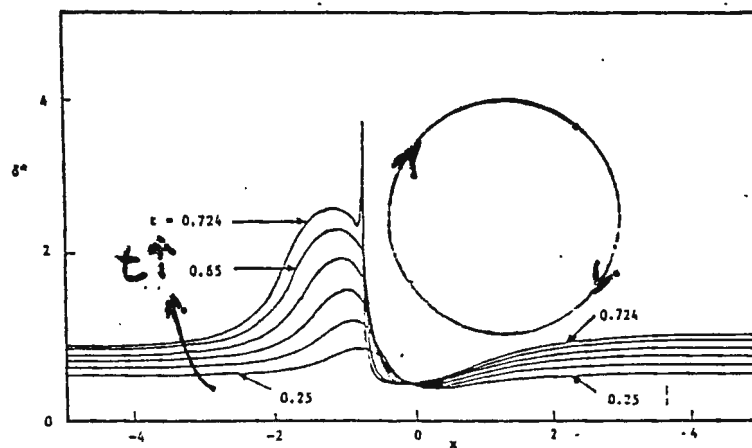
(b) Necklace vortex legs and induced surface eruptions in end view



(c) Induced surface eruptions

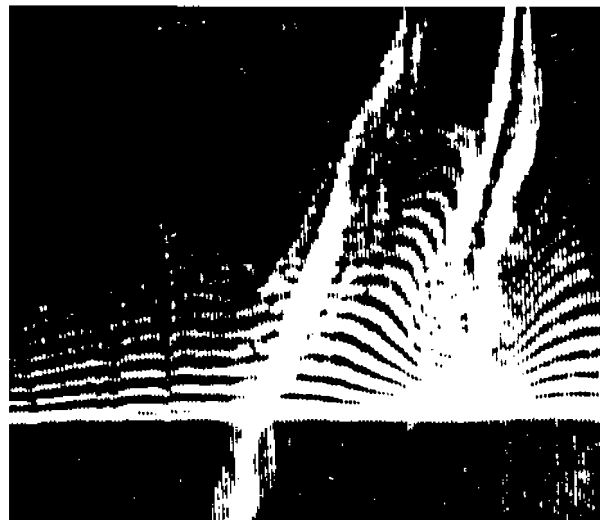
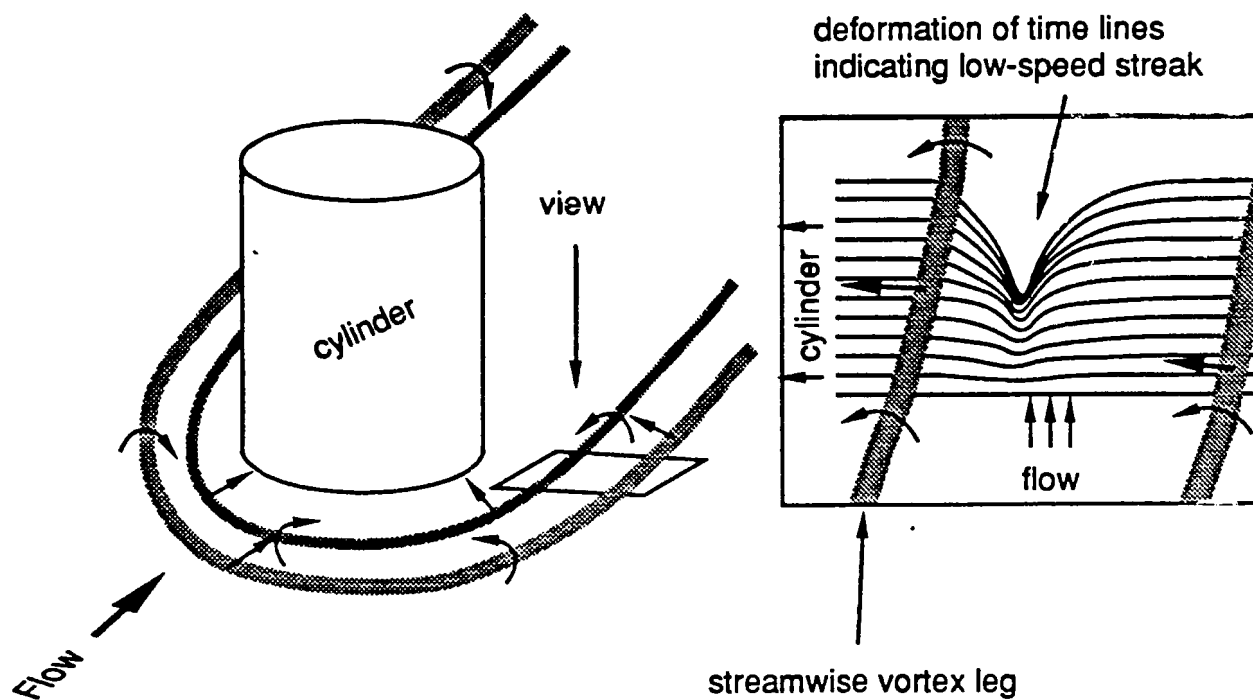


(d) Rollover into asymmetric hairpin



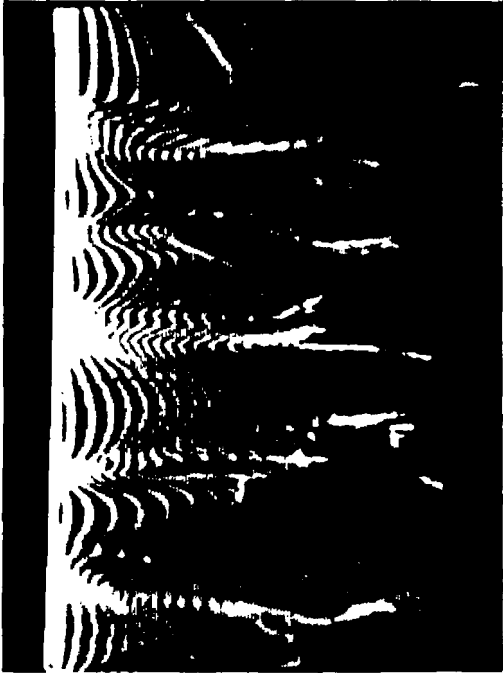
(e) Lagrangian computation of vortex-induced, temporal development of a material line illustrating development of eruptive spike

Figure 1. End-view of surface eruptions and hairpin generation induced by necklace vortex legs. Visualization using hydrogen bubbles and light-sheet illumination.

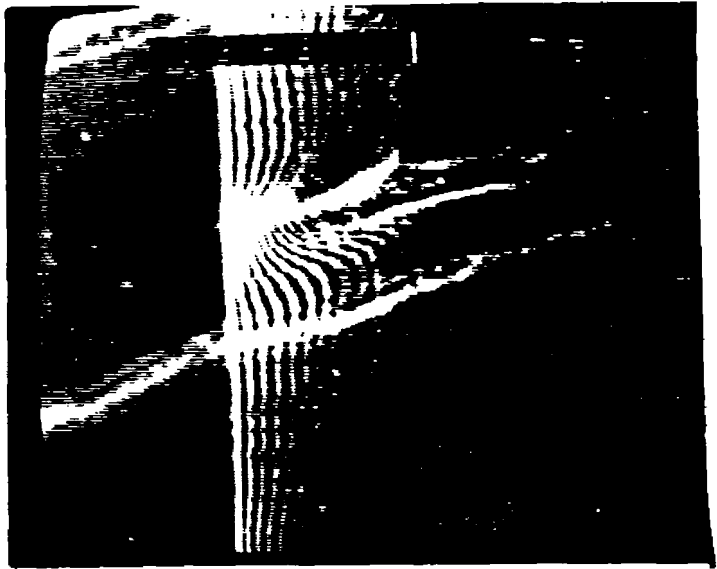


Plan-view photograph showing a streamwise necklace vortex leg (visualized by upstream hydrogen bubble wire) interacting with surface fluid (visualized by bubble wire near surface) to create low-speed streak at surface.

Figure 18 Plan-view of necklace vortex leg interaction to create low-speed streak

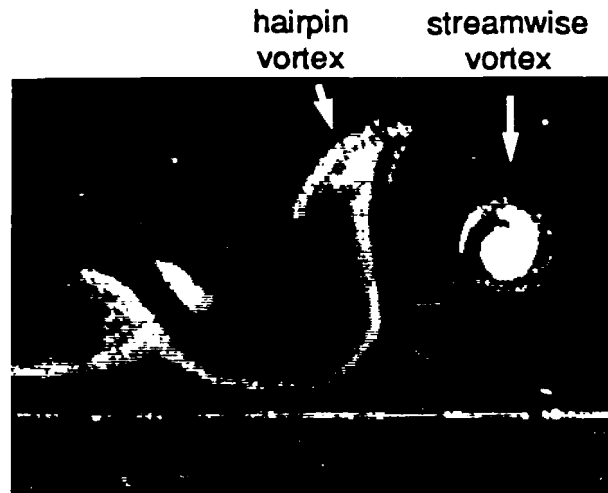


Low-Speed Streaks:
Turbulent Boundary
Layer, $Re_\delta = 1500$

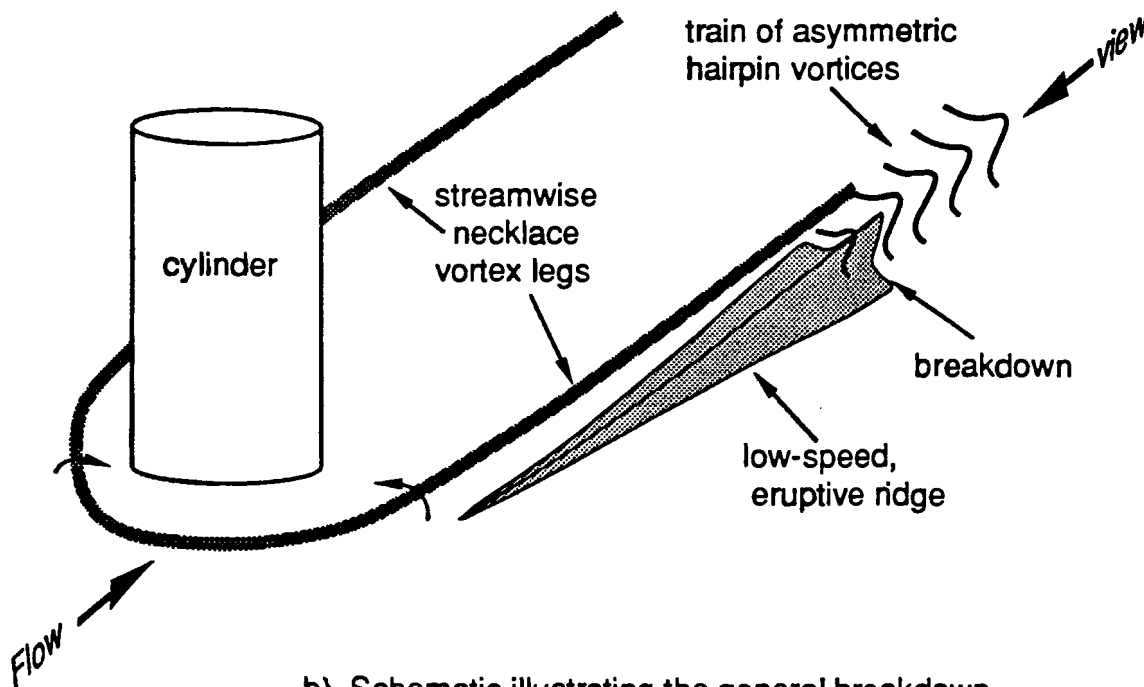


Surface Eruption Caused
by Streamwise Laminar,
Junction Vortex

Comparison of Plan-View Hydrogen Bubble
Visualization of Flow Near the Surface Beneath:
A) a Turbulent Boundary Layer, and
B) the Streamwise Portion of a Necklace Vortex



a) End-view, light-sheet photograph showing the breakdown of an eruptive spire (low-speed ridge) induced by a streamwise necklace vortex leg.



b) Schematic illustrating the general breakdown process for the low-speed, eruptive ridge.

Figure 20. Characteristics of the breakdown of the eruptive spires induced by streamwise necklace vortex legs.

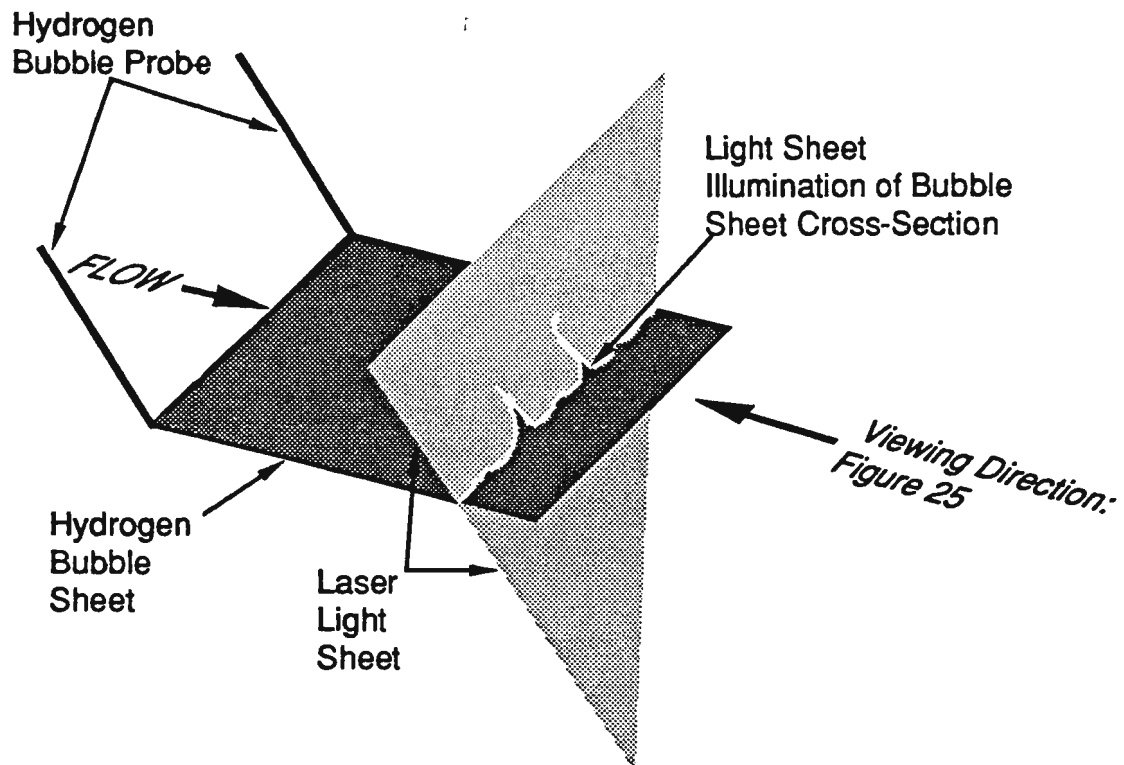


Figure 25. Schematic diagram of laser sheet visualization technique employed to visualize eruptive events in a turbulent boundary layer.



From
Fitzgerald
&
Smith

(a)



(b)

Figure 19. End-view visualizations of surface eruptions in both a transitional and turbulent boundary layer. (a) Thin, eruptive spire adjacent to surface in a tripped, transitional boundary layer (hydrogen bubble visualization). (b) Series of eruptive surface spires in a turbulent boundary layer (surface smoke visualization) from Wallace et al. (1990).

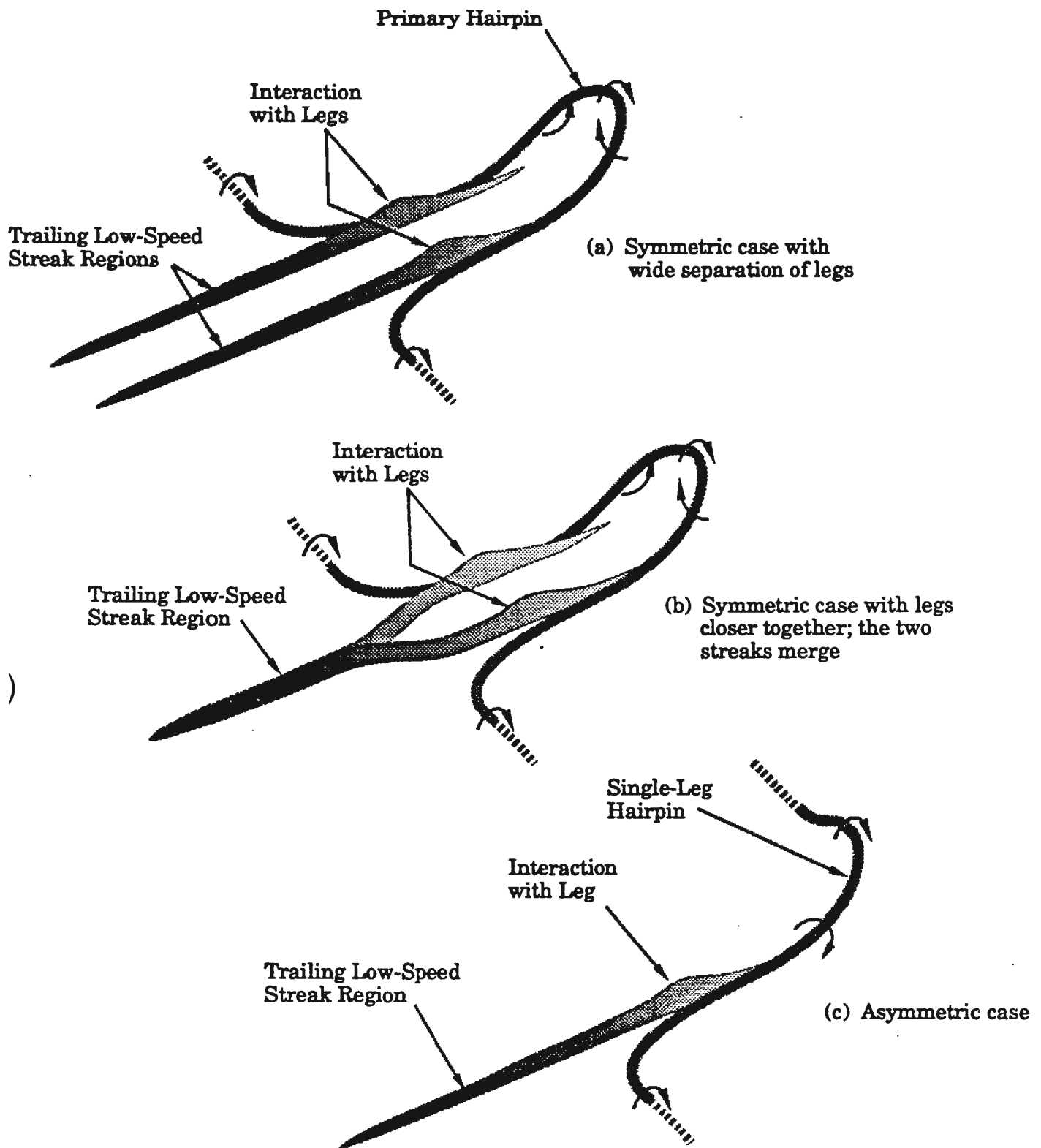
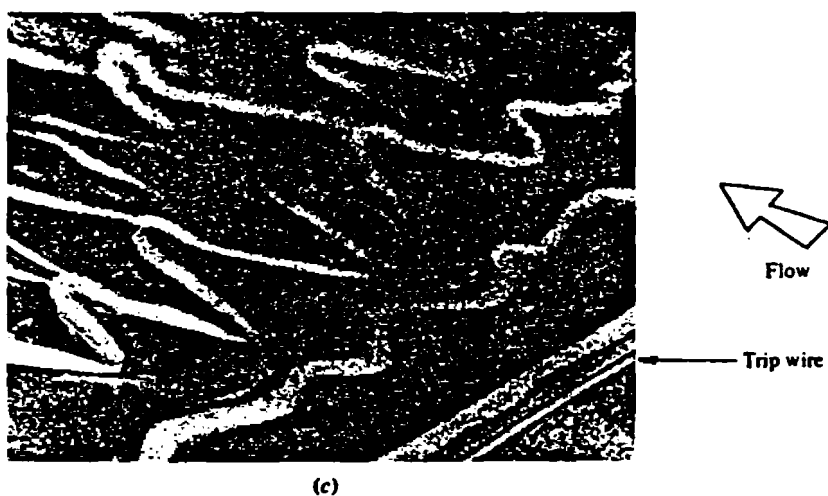


Figure 19. Schematic diagram of the processes whereby moving hairpin vortices induce low-speed streaks.

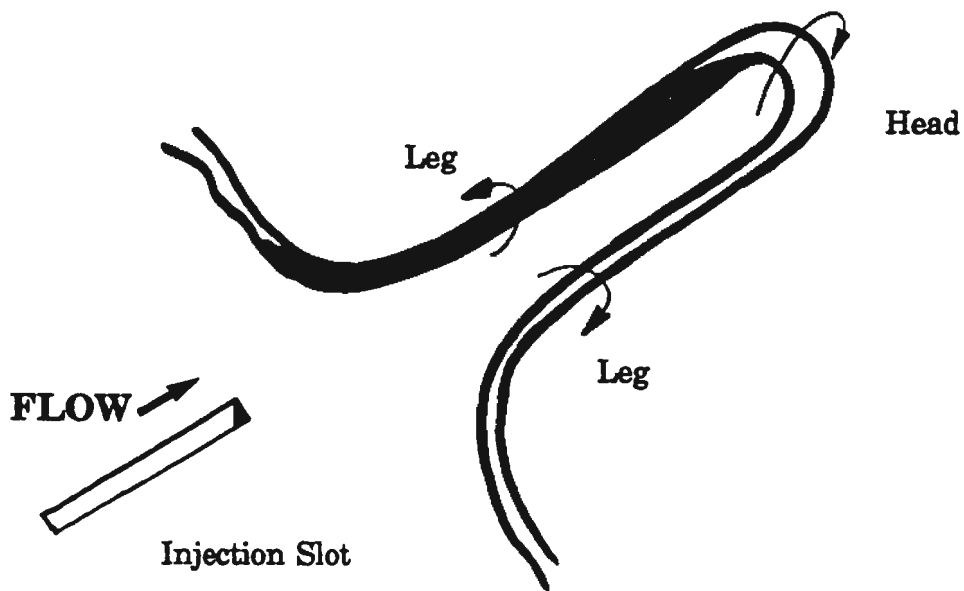
Hairpin Vortex Evolution/Interaction

- EARLY STAGES OF OBSERVATION
PERRY, LIM AND TEH (1981)





(a)



(b)

Figure 15. Illustration of experimental generation of a single hairpin vortex by surface injection using system shown in figure 14. (a) Dual-view picture of dye-marked single hairpin vortex. (b) Isometric schematic of single hairpin after generation. *from Haidavi & Smith*

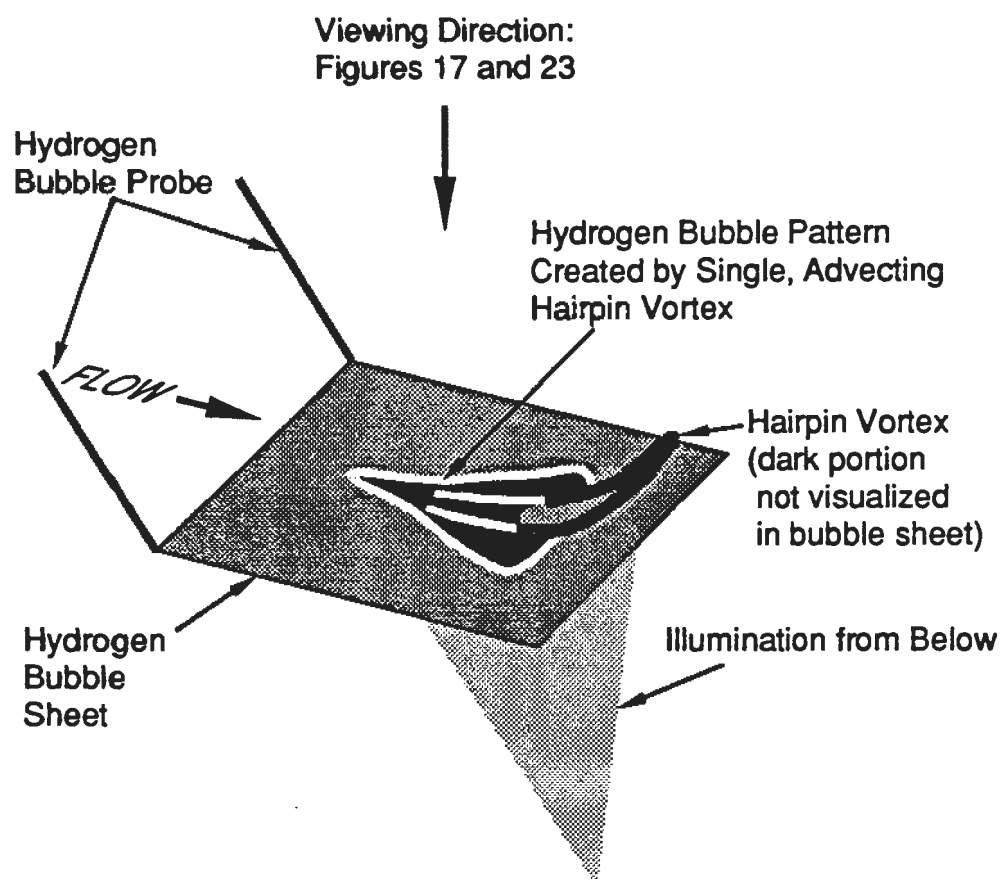


Figure 16. Schematic diagram of technique employed to visualize flow development associated with a single hairpin vortex

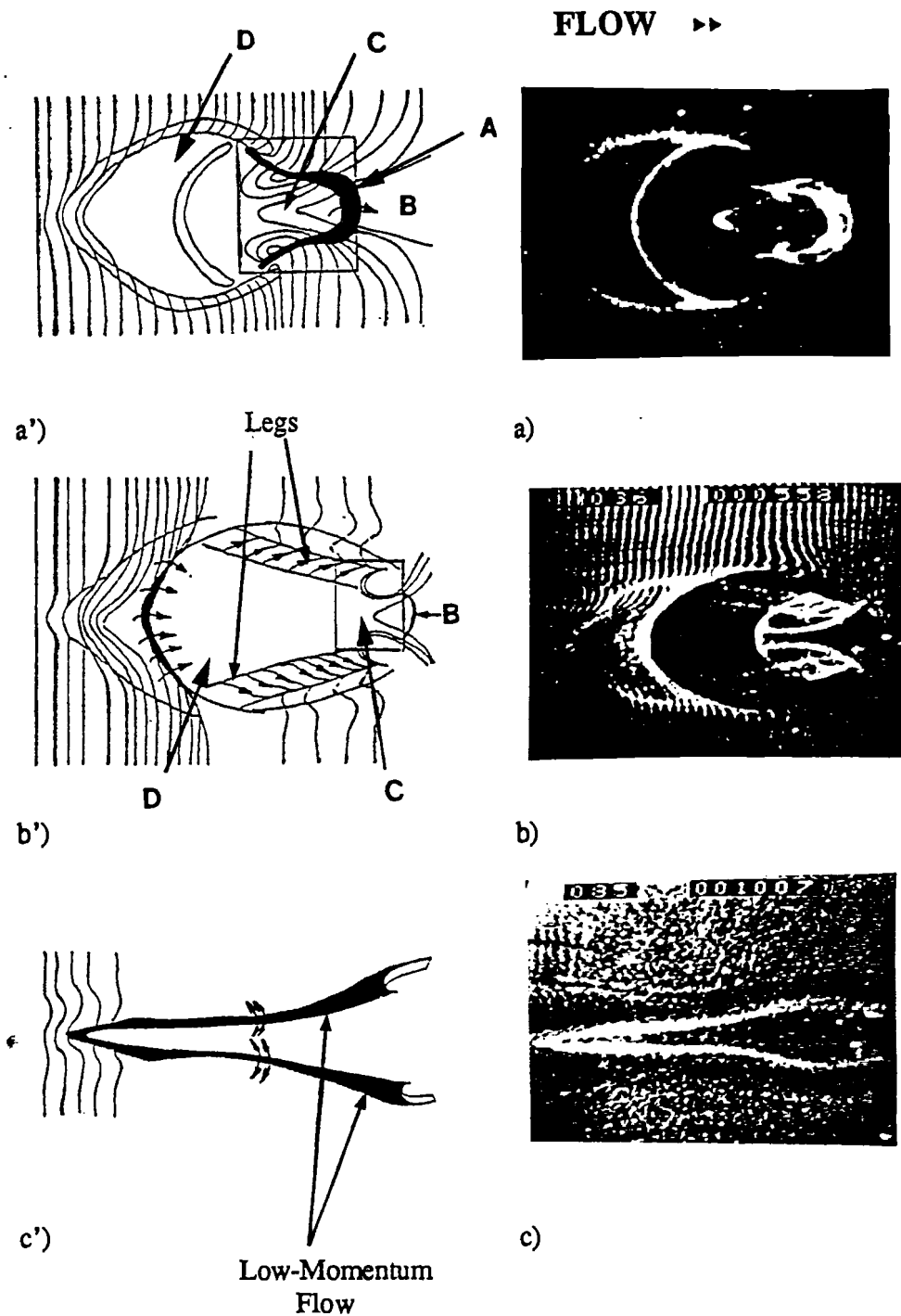
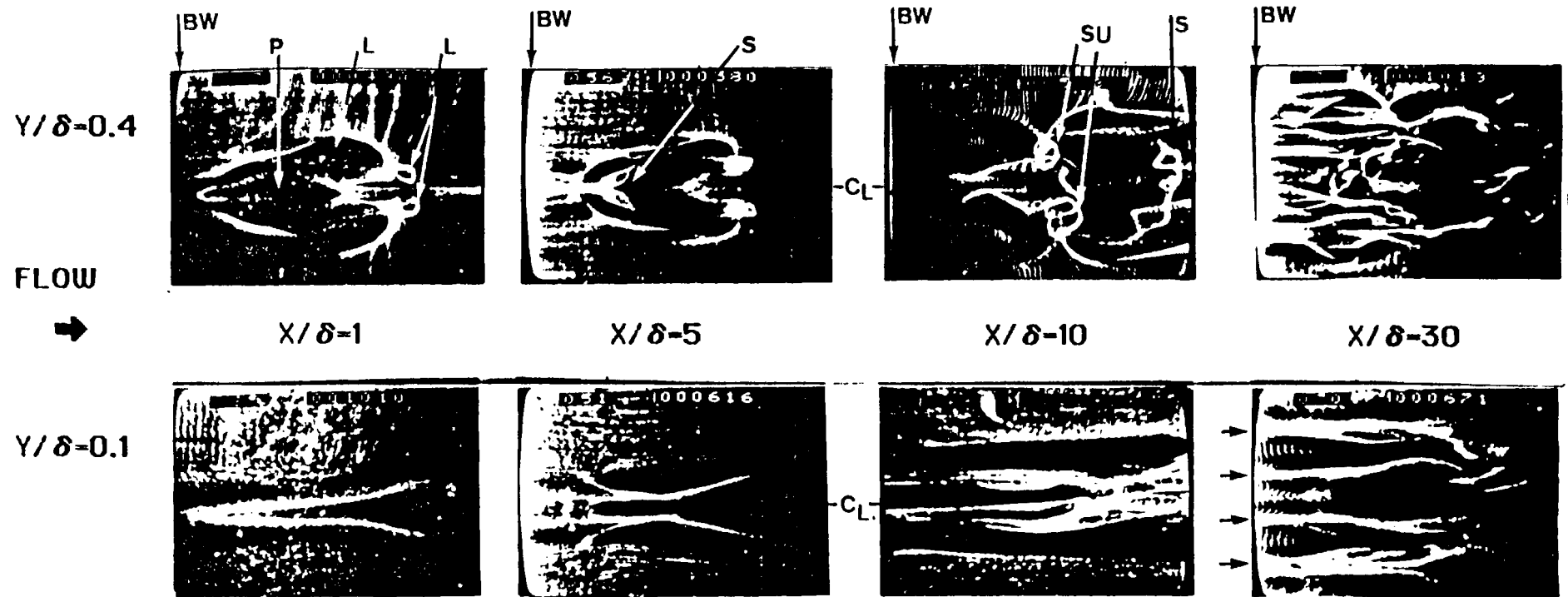


Figure 4.3 The dominant flow patterns associated with a single hairpin vortex immediately after formation. $Re_\delta^+ = 440$, $x_{wire} = 1.0$ cm., a) $y_{wire} = 0.63$ cm, b) $y_{wire} = 0.51$ cm, c) $y_{wire} = 0.127$ cm.



**Dual-Level, Plan-View Visualization of Hydrogen Bubble Patterns
Generated by Developing Hairpin Vortex**

FLOW >>

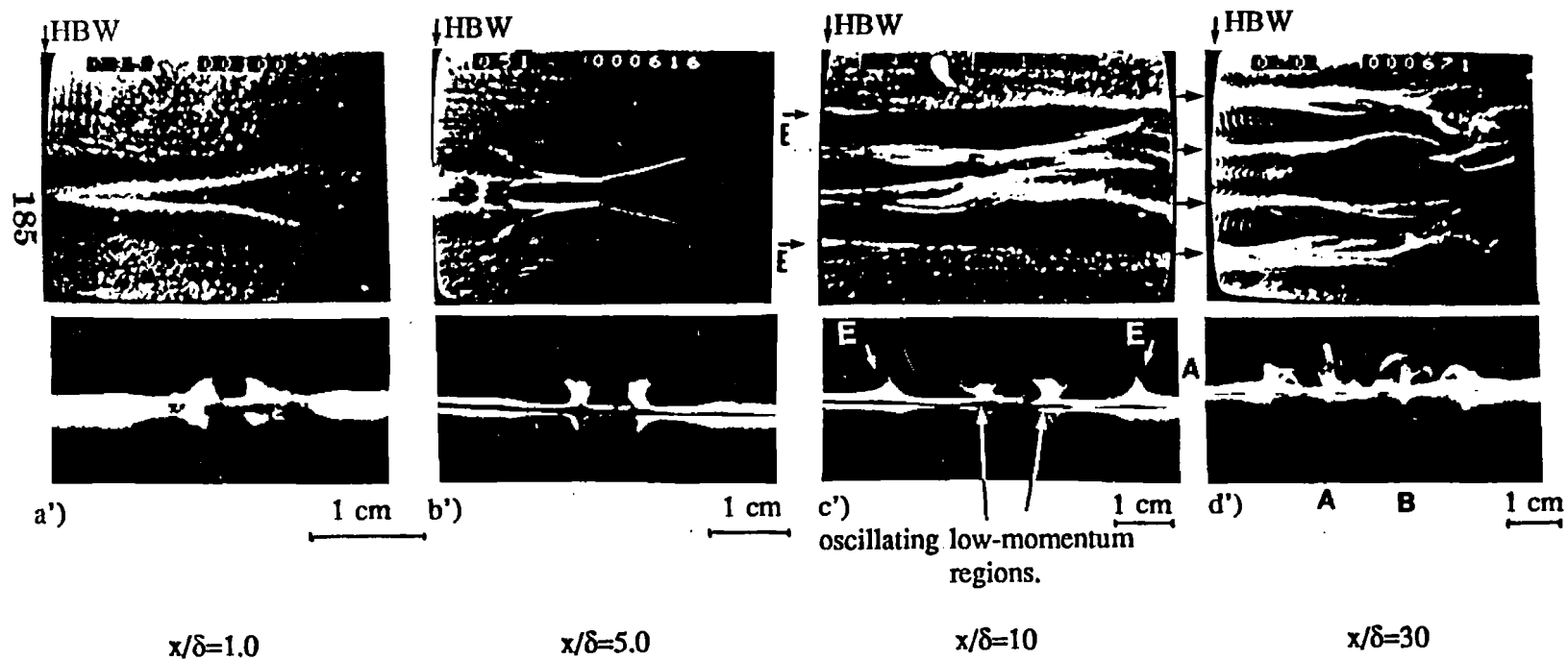


Figure 4.16 (Continued) for caption see figure 4.16.

FLOW \gg

Primary Hairpin Vortex

\gg INCREASING TIME

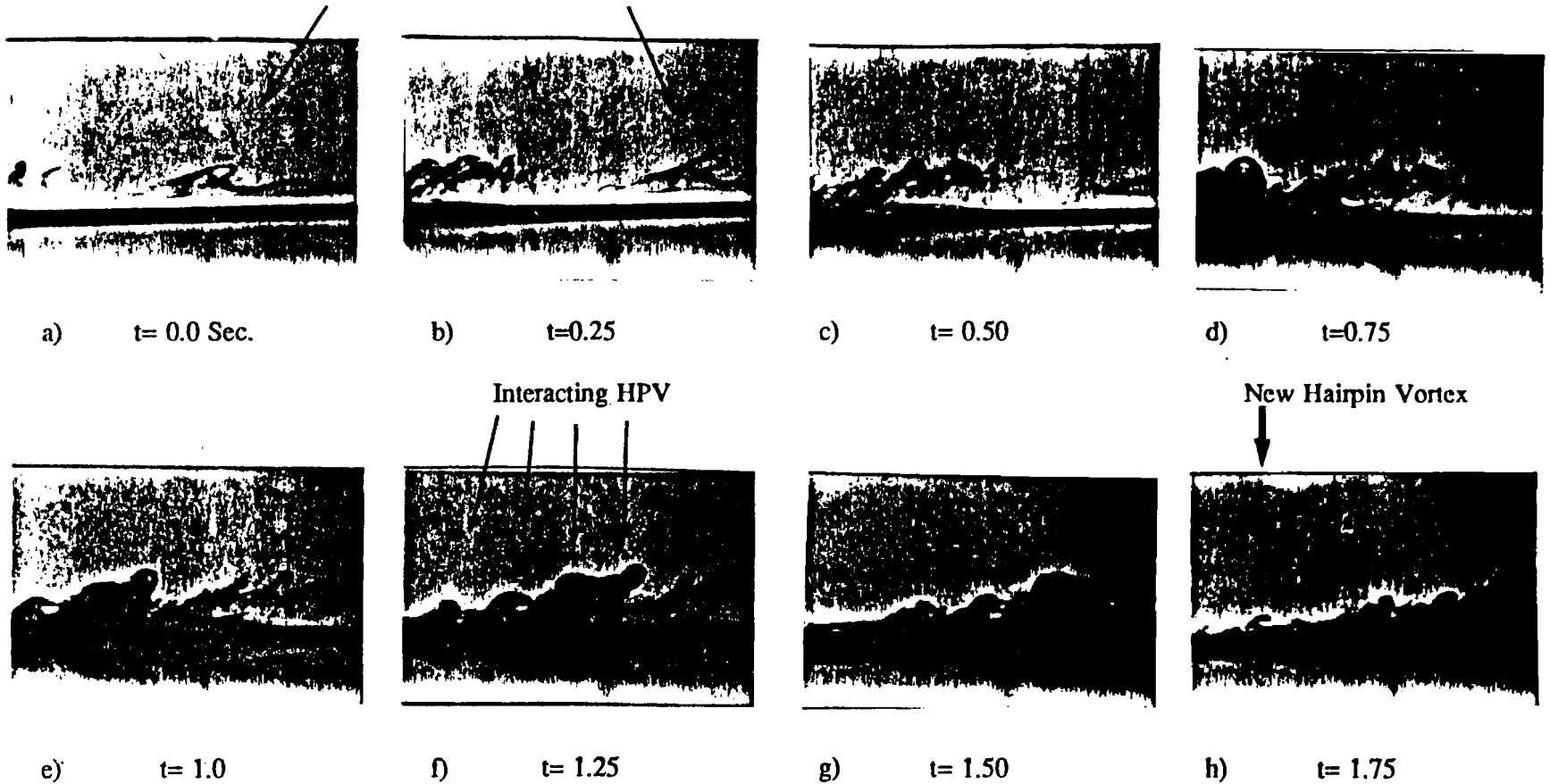


Figure 5.1 Side-view dye visualization of a turbulent spot generated from growth of a single hairpin vortex. Photographs are obtained with still photography at 4 frames per second. $Re_{\delta}^* = 440$, $Re_{VW} = 10.5$, $x = 60$ cm.

from Haidari & Smith



b') $x=7.0$ cm
 $y=0.25$ cm

Turb. Spot (T.E.)



b) $x=1.0$ cm
 $y=0.39$ cm

Single Hairpin Vortex

II-45

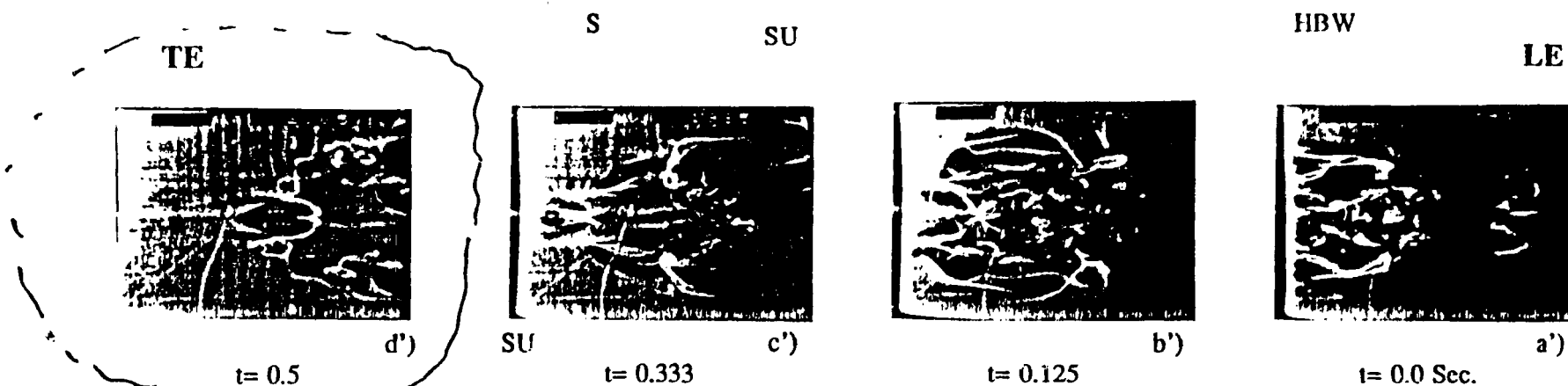


Figure 5.6 Effect of Reynolds number on the growth to a turbulent spot, as visualized by hydrogen bubbles. a) through d) $Re_{\delta 1}^* = 440$, a') through d') $Re_{\delta 2}^* = 530$.

FLOW >>

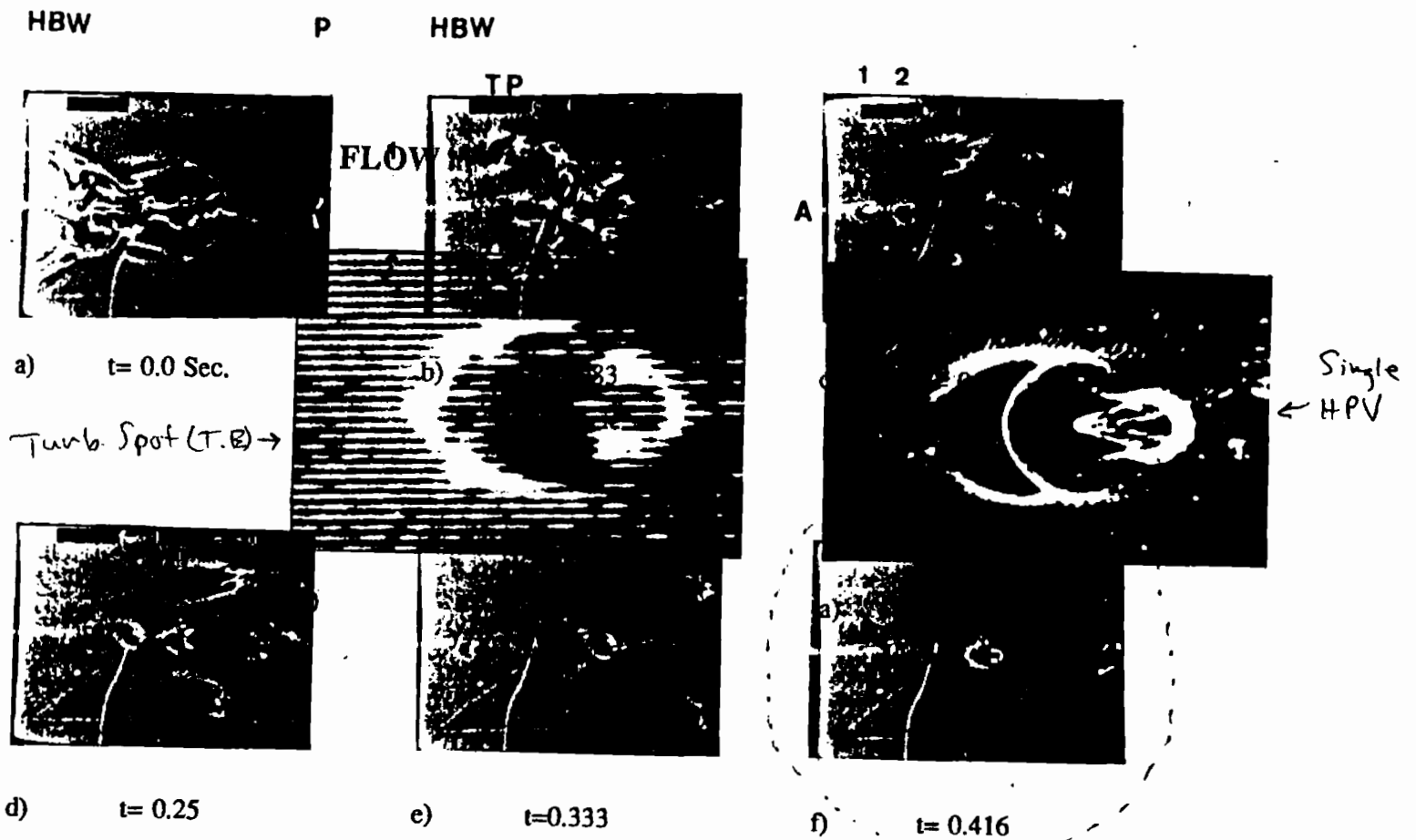
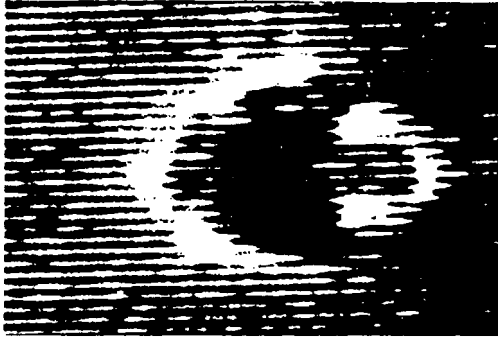
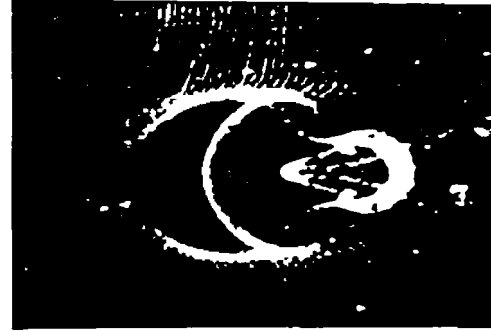


Figure 5.2 Plan-view visualization of a turbulent spot generated by a hairpin vortex. The sequence, illustrates formation of new vortices within the turbulent spot. $Re_{\delta^*} = 530$, $y_{wire} = 0.57 \text{ cm}$, $x_{wire} = 7 \text{ cm}$.

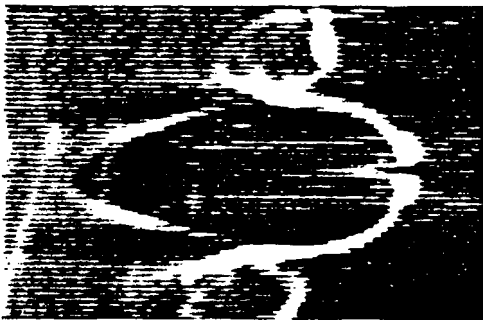
FLOW ►►



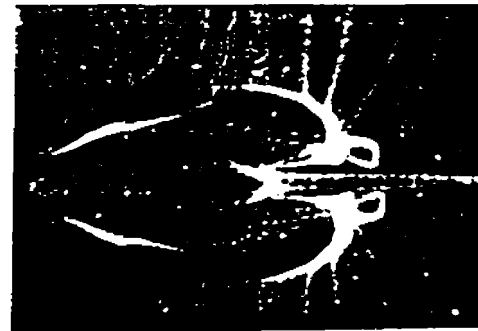
a') $x=7.0$ cm
 $y=0.57$ cm



a) $x=1.0$ cm
 $y=0.65$ cm

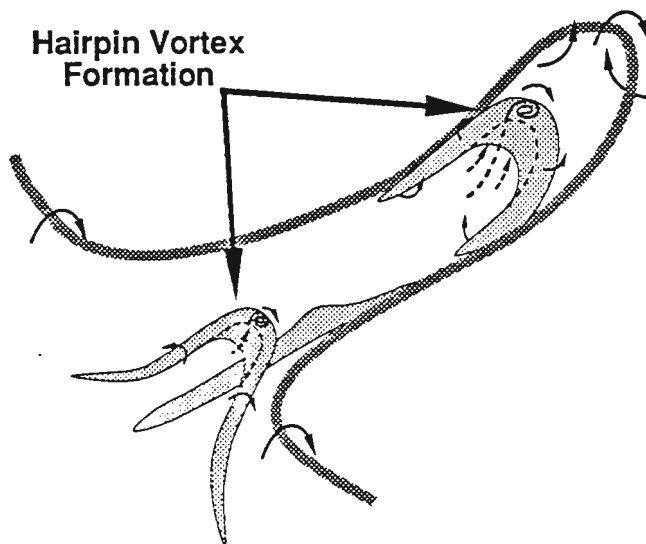
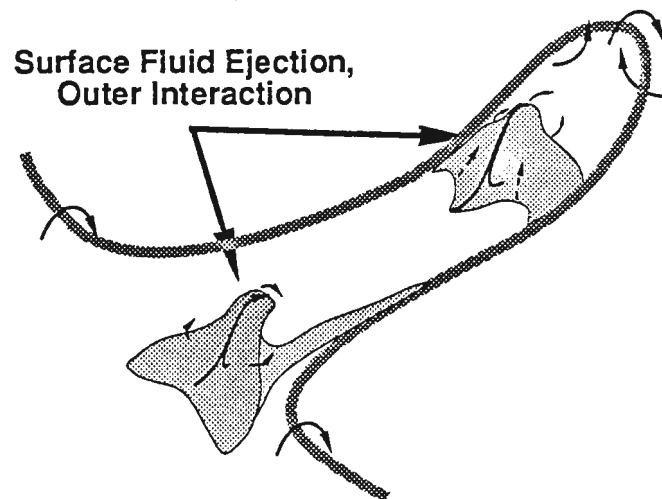
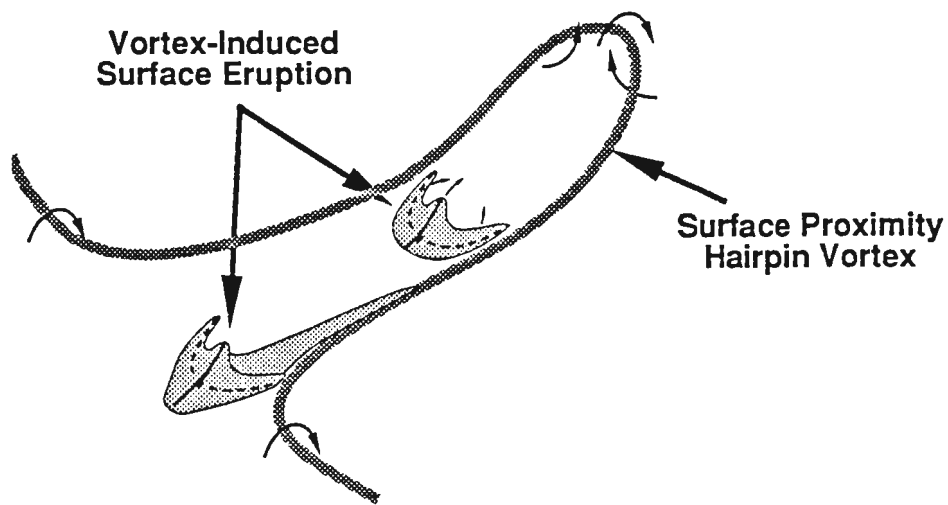


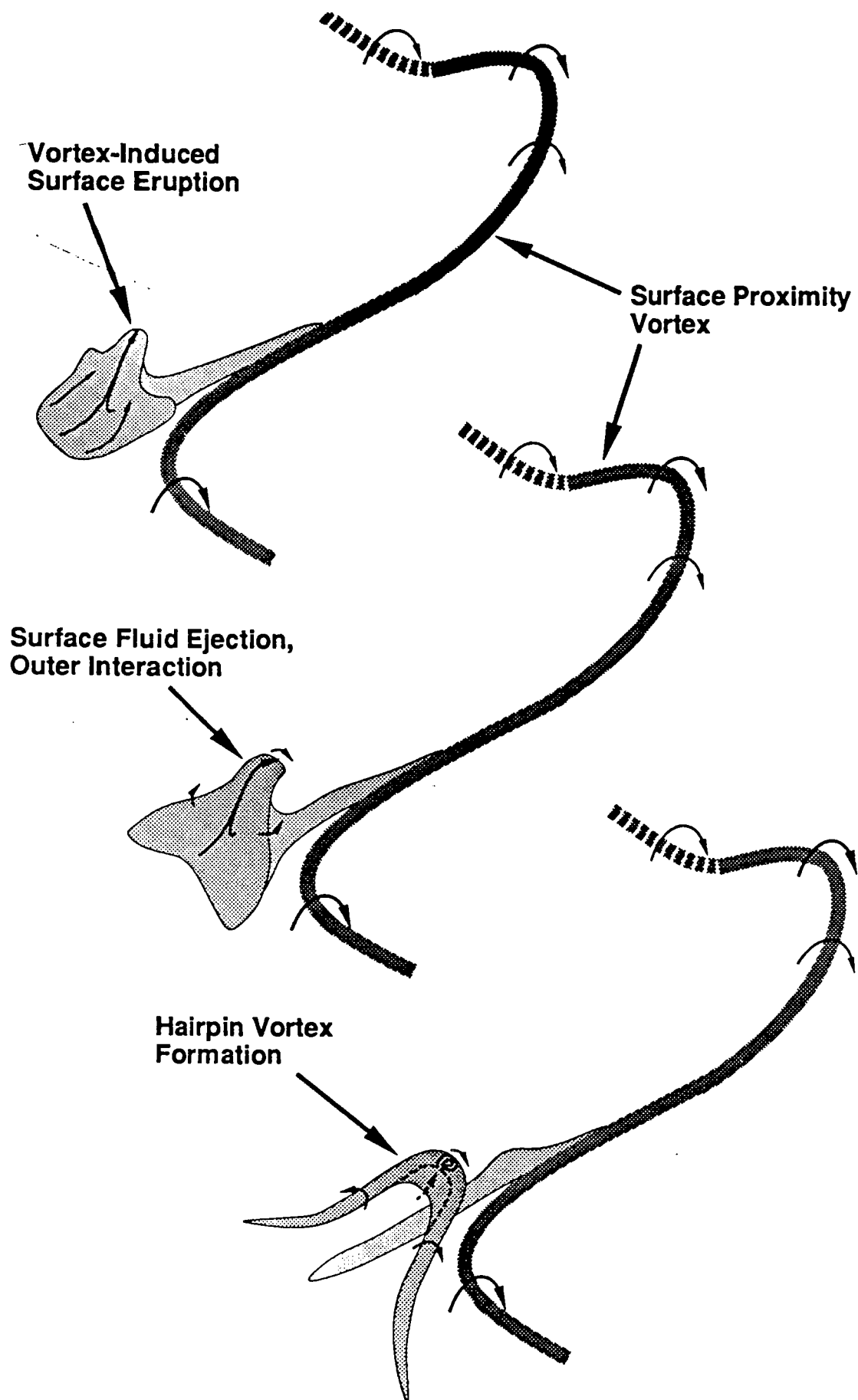
b') $x=7.0$ cm
 $y=0.25$ cm

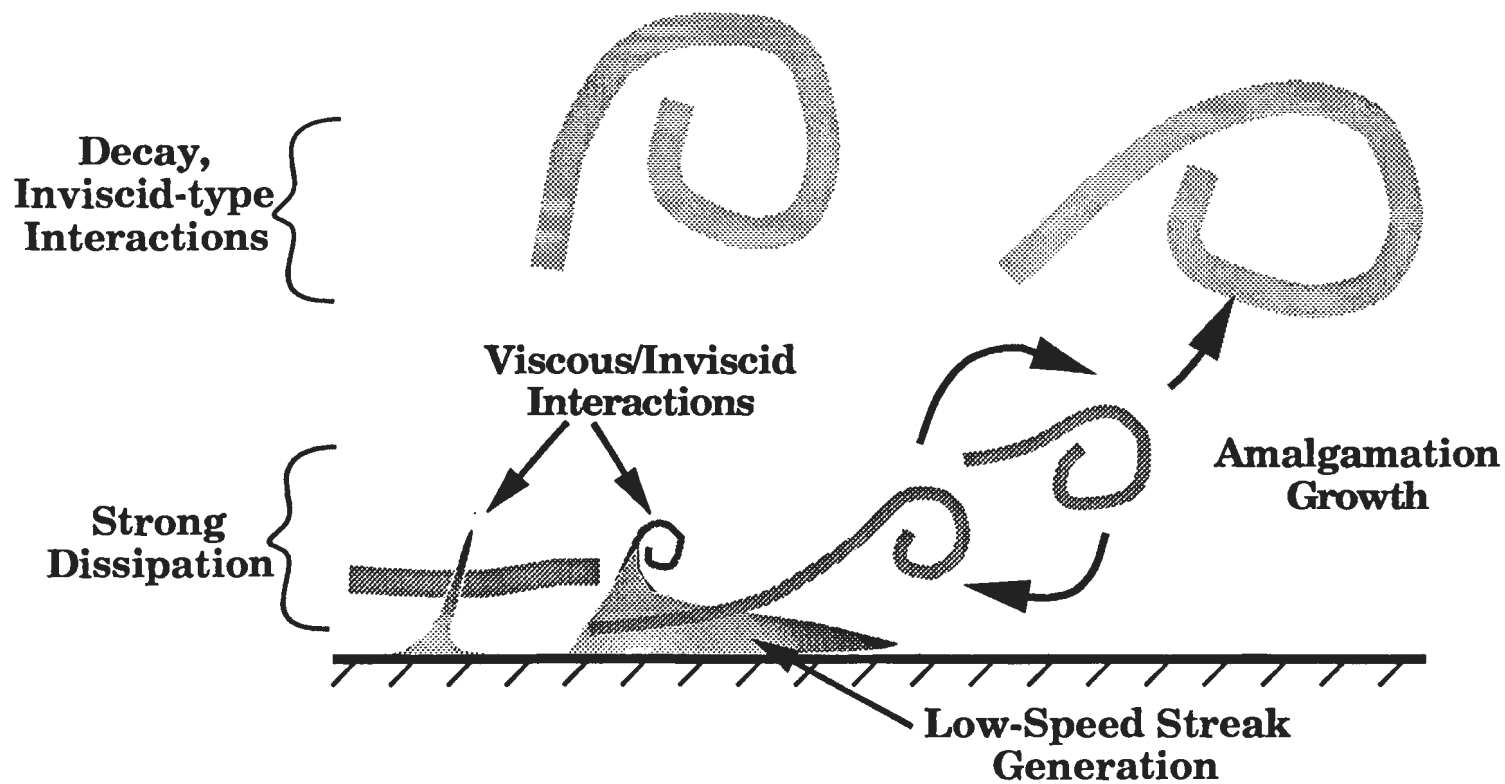


b) $x=1.0$ cm
 $y=0.39$ cm

Figure 5.3: Comparison between flow patterns for a single vortex and local flow patterns observed in a turbulent spot. a), and b) single HPV, $Re_\delta^*=440$, $Re_{vw}=10.5$, $x_{wire}=1$ cm. a') and b') trailing vortices in a turbulent spot $Re_\delta^*=530$, $Re_{vw}=7.8$, $x_{wire}=7$ cm.







Model of Generalized Turbulent Boundary Layer Processes

What Kernel Studies Indicate

Low-Speed Streaks

- **Caused by vortex-surface interaction**
- **Inviscid-viscous interaction \Rightarrow other 3-D vortices**

Propagation of Turbulence

- **Due to 3-D vortex deformation in velocity gradient, and**
- **Surface eruptions resulting in secondary vortex generation**

Growth

- **Amalgamation and coalescence of vortex scales**
- **Energy input \Rightarrow vortex stretching by velocity gradient**

II-2. The Interaction of Coherent Vortices with Solid Surfaces

Demetri P. Telionis
Virginia Polytechnic Institute and State University

NUWC Division Newport, R. I.

SEMINAR NOTICE

**THE INTERACTION OF COHERENT VORTICES
WITH SOLID SURFACES**

Professor Demetri P. Telionis

Virginia Polytechnic Institute and State University

) Experimental and numerical methods have been employed to study the formation of coherent vortices generated over sharp edges and their subsequent interaction with blades further downstream. Laser-Doppler velocimetry and flow visualization were employed in a water tunnel. Periodic flows were generated and two-dimensional fields were obtained by conditional averaging. The numerical methods were based on discrete vortex dynamics. The results indicate that the vortex cores are created by purely inviscid mechanisms and should therefore be termed 'inviscid cores' rather than 'viscous cores'. When coherent structures encounter solid surfaces, their distortion and further development conform with Kelvin-Helmholtz theorem. However, the large pressure gradients induce separation and the creation of separated bubbles which drift together with the disturbing vortices.

Thursday, 27th May 1993

Conference Room, Bldg. 679

Time: 10:30 AM

) **POC: Dr. Promode R. Bandyopadhyay (Code 8234; x2588)**

**THE INTERACTION OF COHERENT
VORTICES WITH SOLID SURFACES**

presented by

Demetri P. Telionis

Collaborators

**David R. Poling
Demetri S. Mathioulakis
Michael C. Wilder
Matthew M. Pesce
Jerzy Swirydzuk**

supported by

NASA, Boeing Helicopter

Related Publications

1. "Unsteady Vortical Wakes Over a Prolate Spheroid," AIAA Paper #84-0419, Jan. 1984, by Costis, C., and Telionis, D. P.; also AIAA Journal, Vol. 26, pp. 1189-1193, 1988.
2. "The Near Wake of a Pitching Airfoil," 18th AIAA Fluid Mechanics, Plasma Dynamics and Laser Conference, AIAA Paper #85-162, July 1985, by D. S. Mathioulakis, J. Kim, D. P. Telionis, and D. T. Mook.
3. "The Trailing Edge of a Pitching Airfoil at High Reduced Frequencies," in Forum on Unsteady Flow - 1985, ed. P. H. Rothe, ASME, FED, Vol. 27, pp. 36-38, by D. R. Poling and D. P. Telionis, also Journal of Fluids Engineering, Vol. 109, pp. 410-414, 1987.
4. "Blade-Vortex Interaction," presented at the AIAA 1987 Aerospace Sciences Meeting, AIAA Paper No. 87-0497, also AIAA Journal, Vol. 27, pp. 694-699. June 1989, by Poling, D. R., Dadone, L., and D. P. Telionis.
5. "Two-Dimensional Interaction of Vortices with a Blade," AIAA 26th Aerospace Sciences Meeting, AIAA Paper #88-0044, by D. R. Poling, M. C. Wilder and D. P. Telionis.
6. "Blade-Vortex Interaction Experiments - Velocity & Vorticity Fields," AIAA Paper No. 90-0030, by M. C. Wilder, M. M. Pesce, and D. P. Telionis.

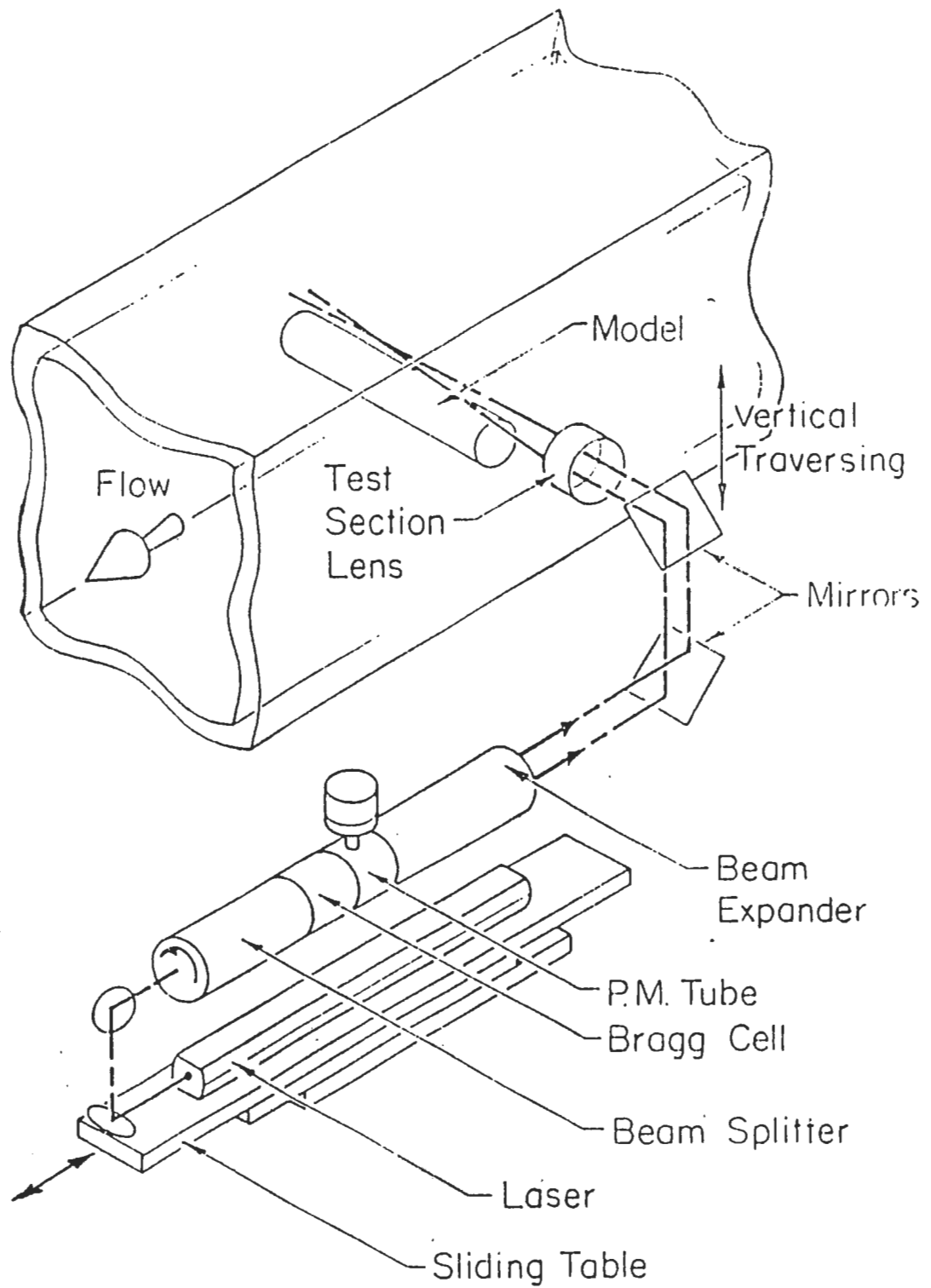


Figure 2.12 Traversing mechanism

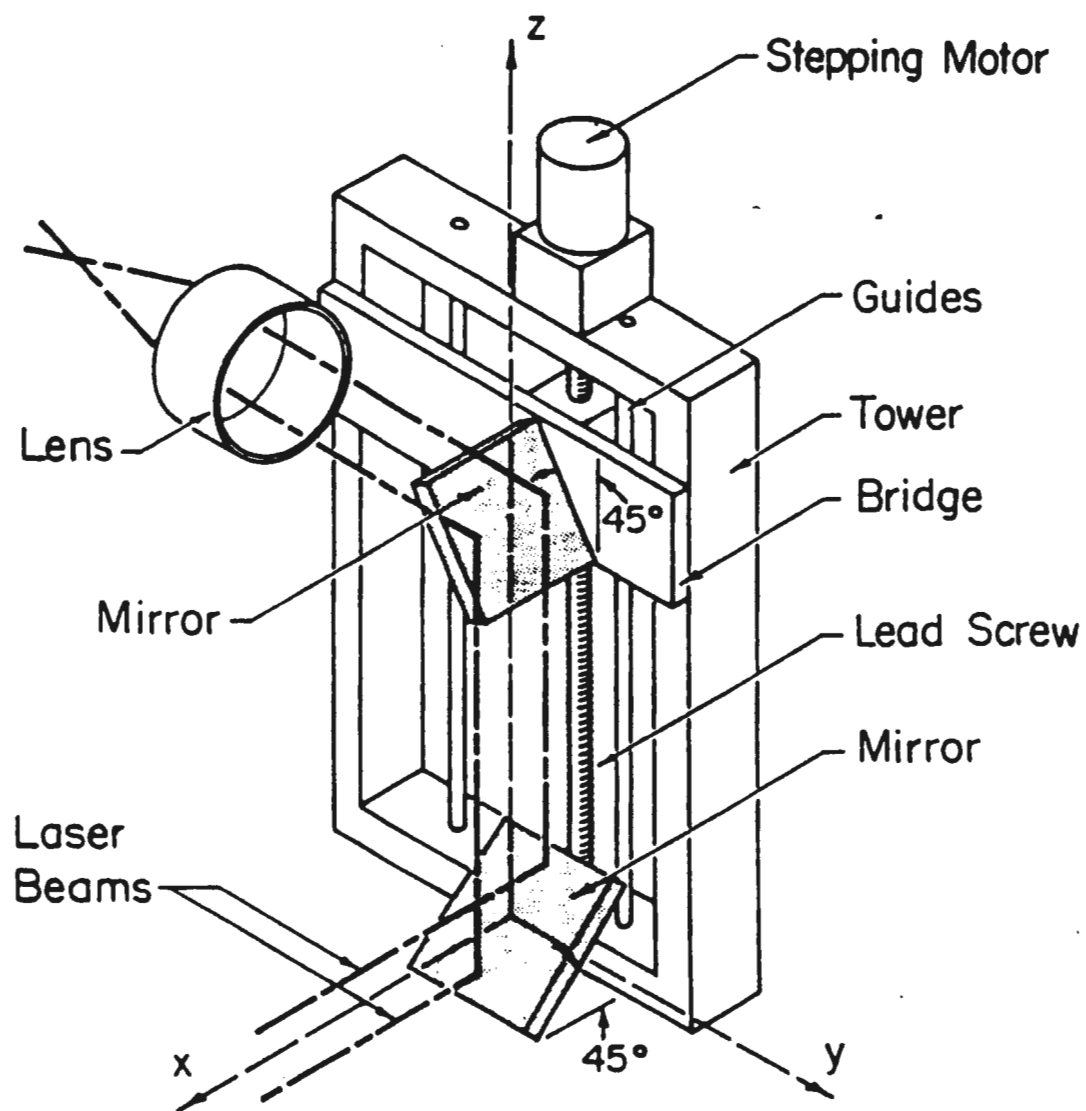


Figure 2.3.6 The mirror tower assembly

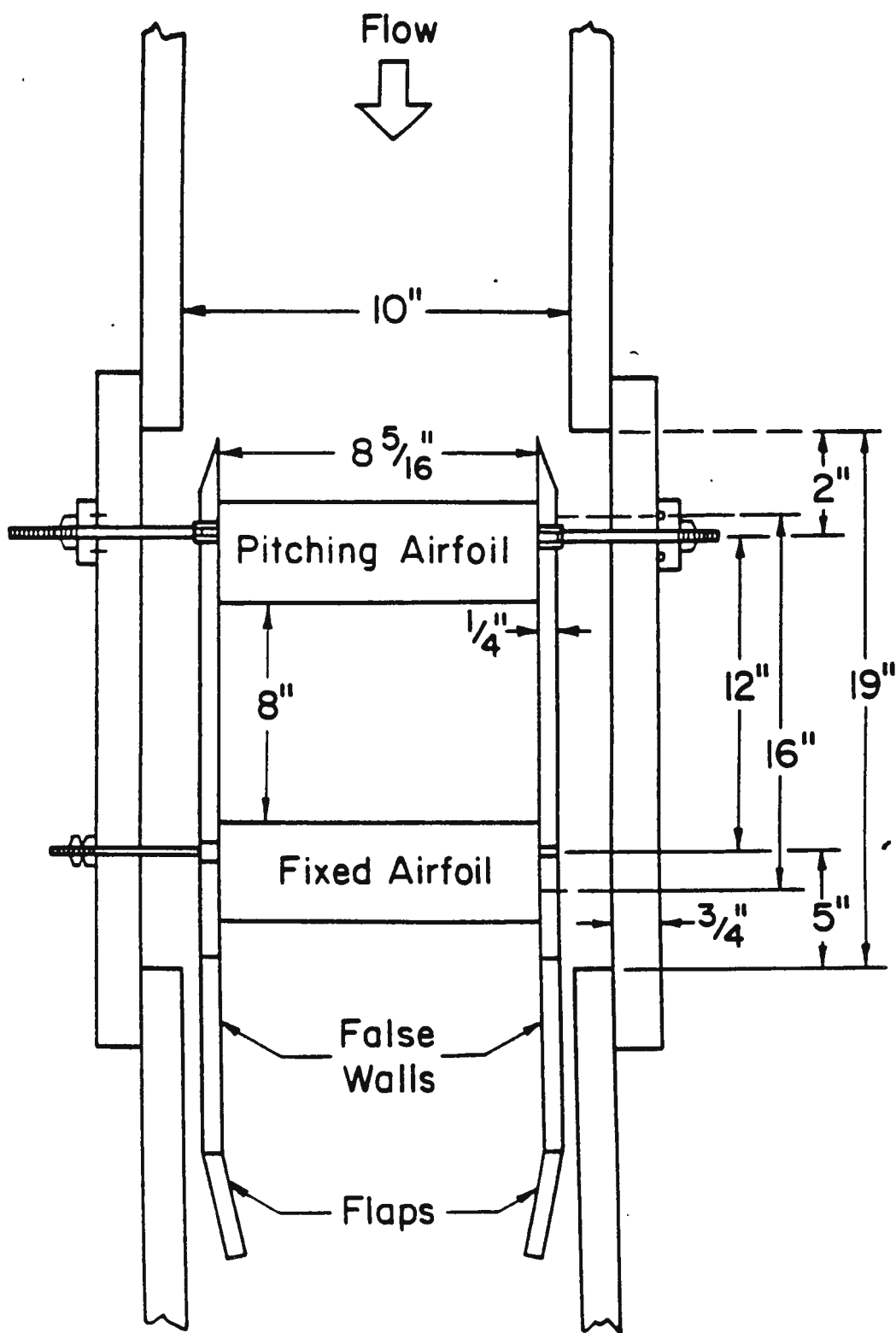


Figure 2.1.2 The test section and false walls

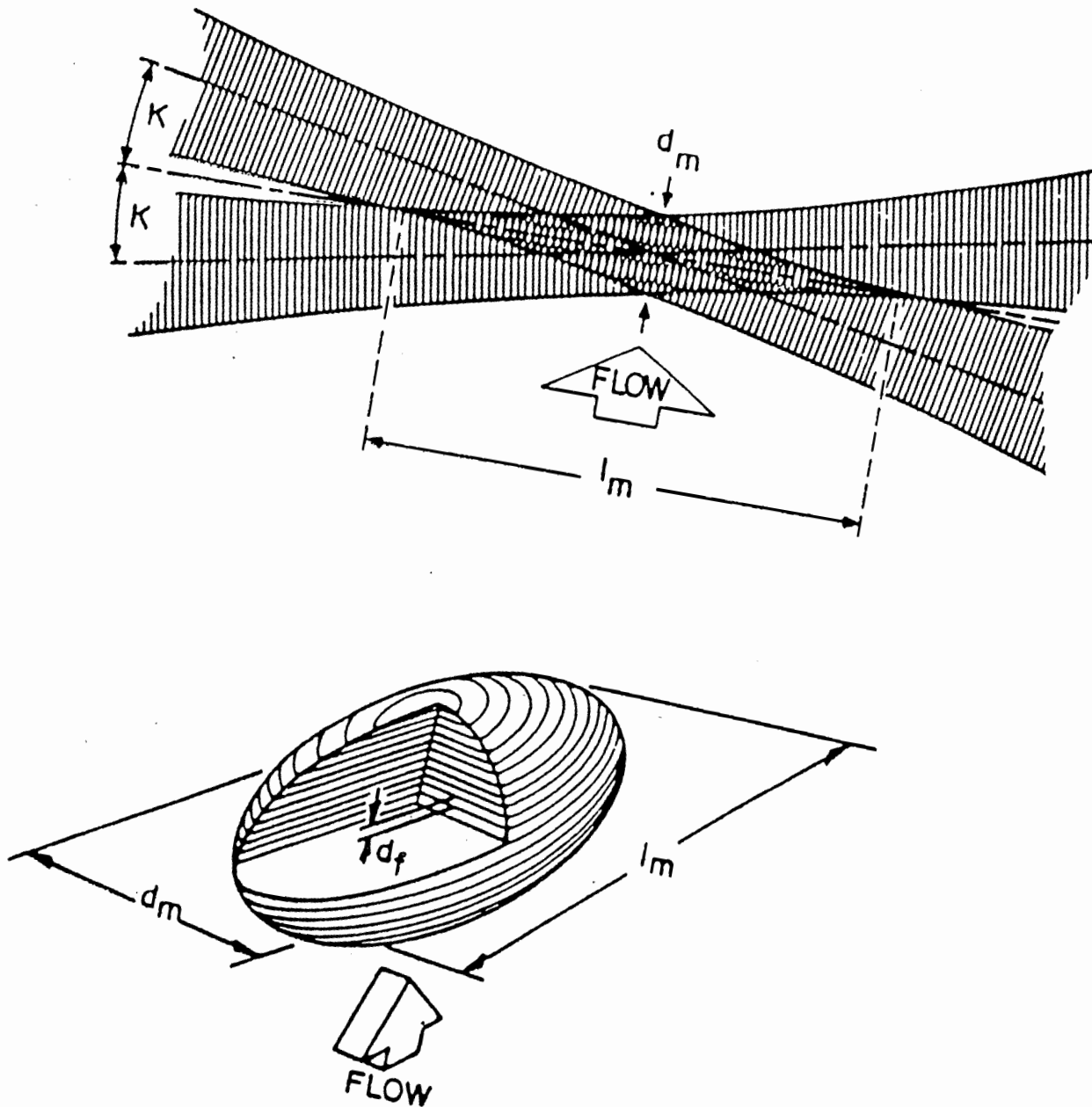


Figure 2.3. Dual-beam laser-Doppler velocimeter.

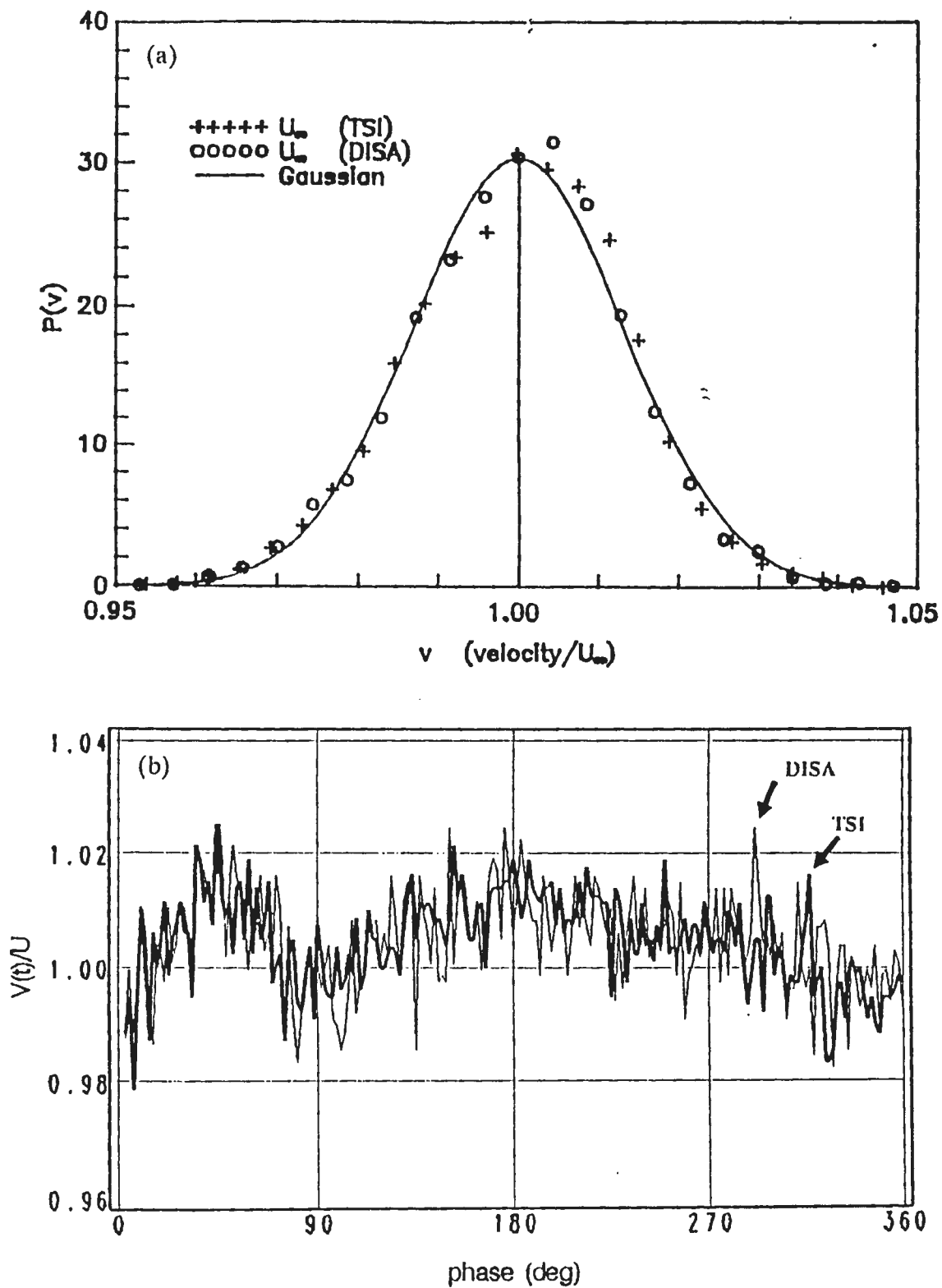
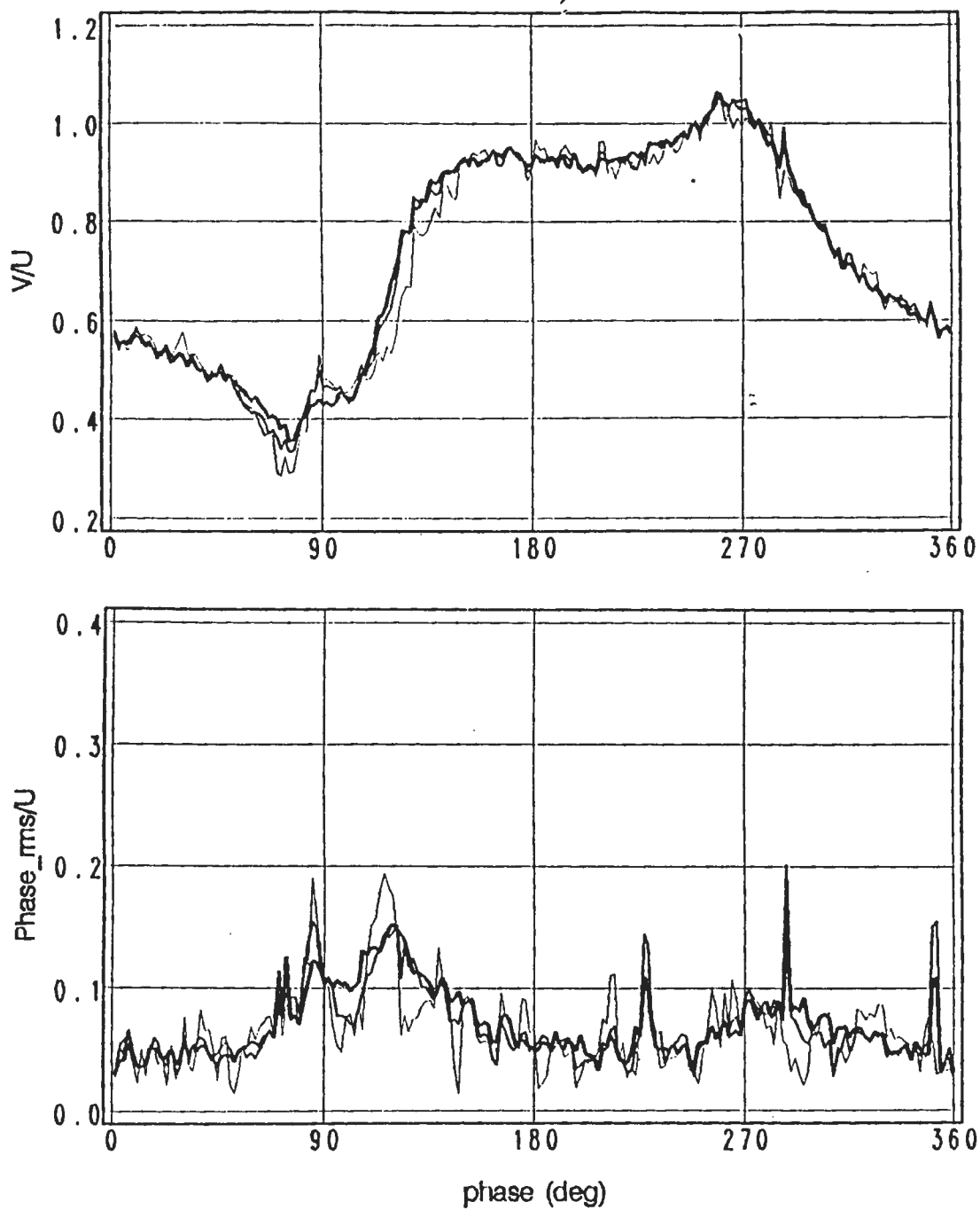


Figure 2.9. A comparison between the DISA and TSI signal processors for steady flow: (a) Normalized velocity probability histogram (b) Velocity time record.



— 45 deg — component

Figure 2.13. Ensemble averaged velocity and phase-rms for 5, 15 and 30 ensembles
: $U_{\infty} = 12.5 \text{ cm/s}$, $k = 2.05$, $x/c_s = 2.0$, $y/c_s = 0.1$

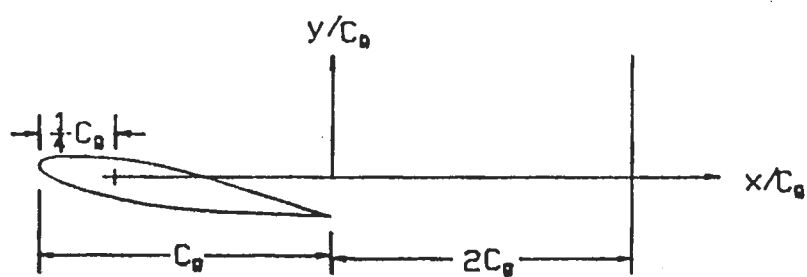
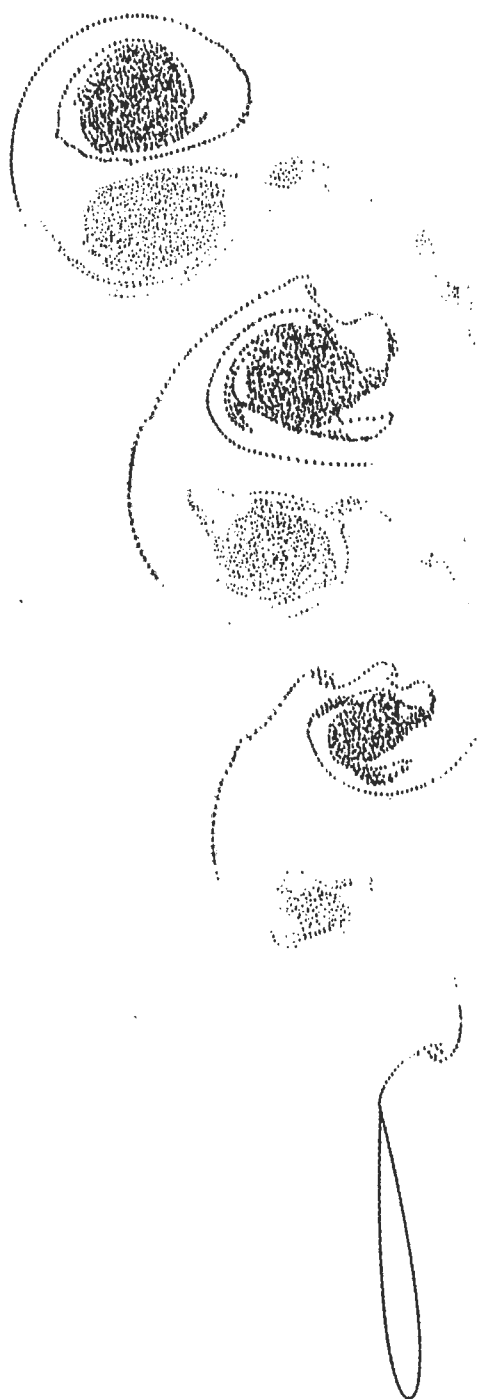


Figure 3.3. Coordinate system.



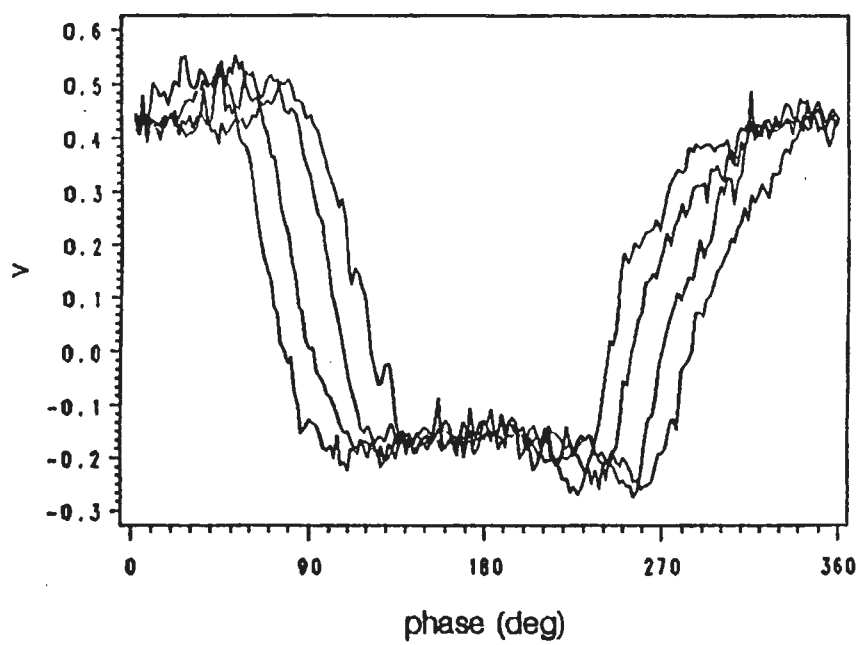


Figure 3.4. Velocity waveforms at four downstream locations in the wake: $x/c_1 = 1.85, 1.925, 2.0, 2.075$; $y/c_1 = 0.1$; $k = 2.0$

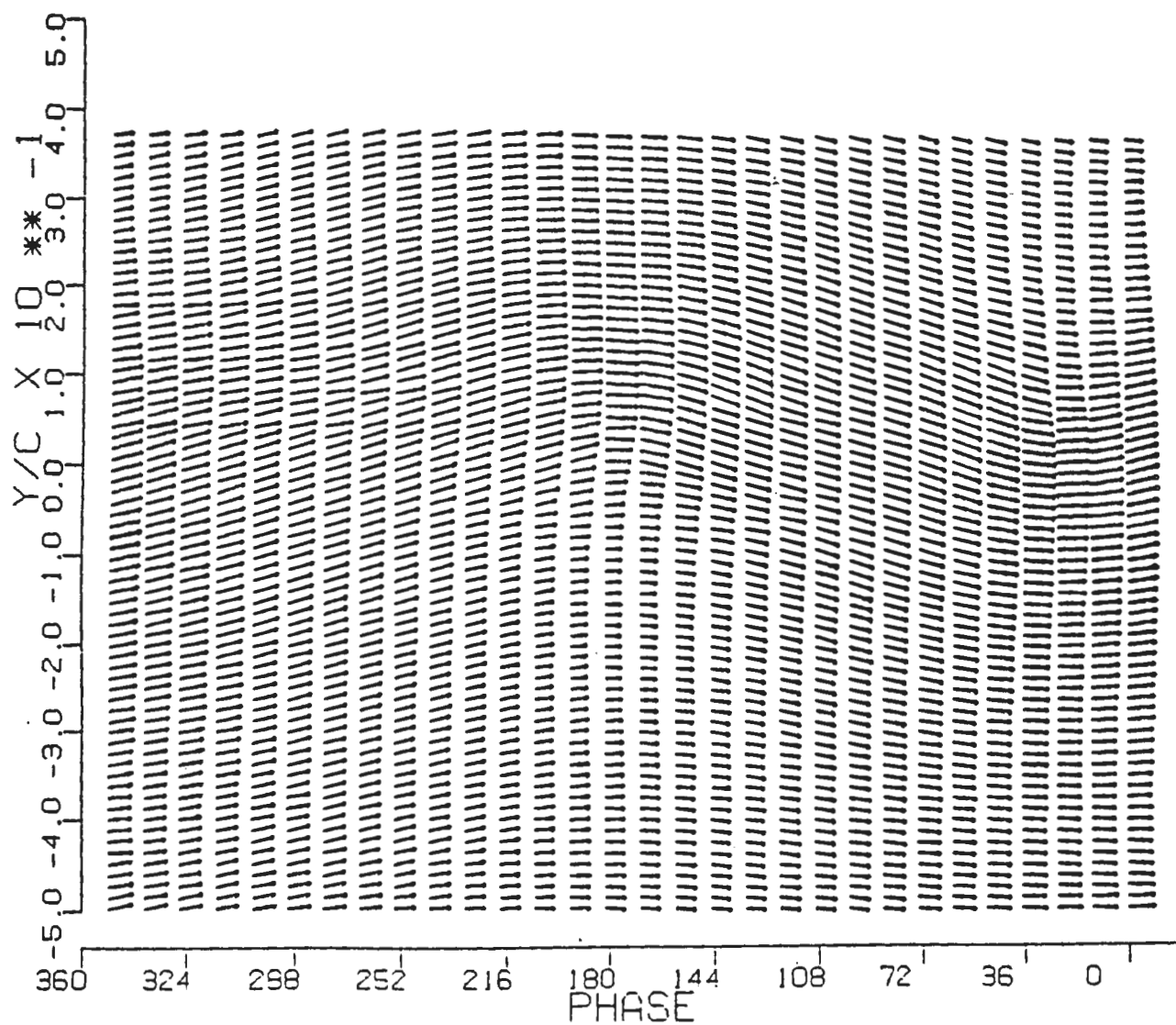


Figure 3.5. Velocity vector field constructed from a single column of measurements: $x/c_x = 2.0$, $k = 2.05$, $Re = 14000$

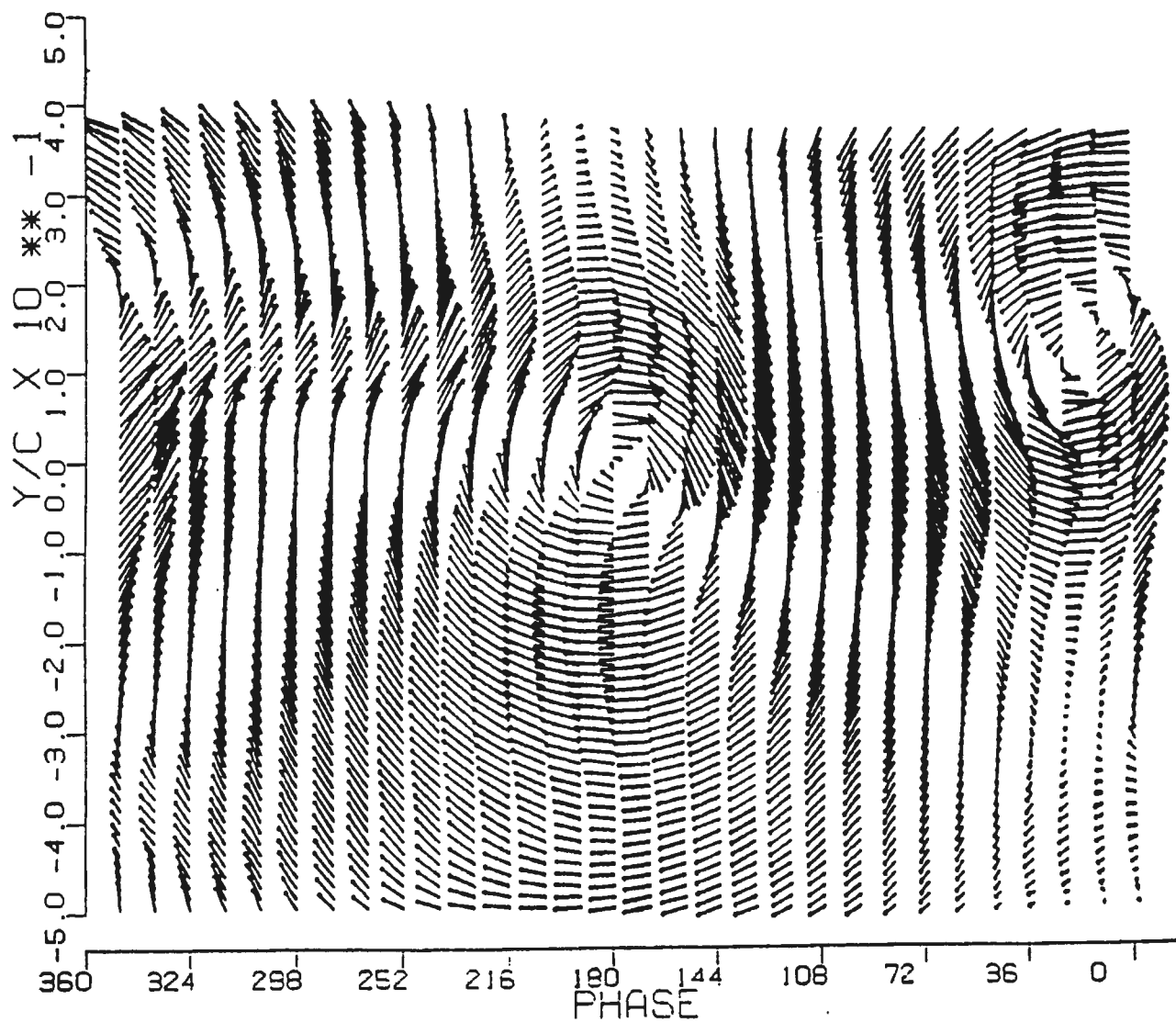
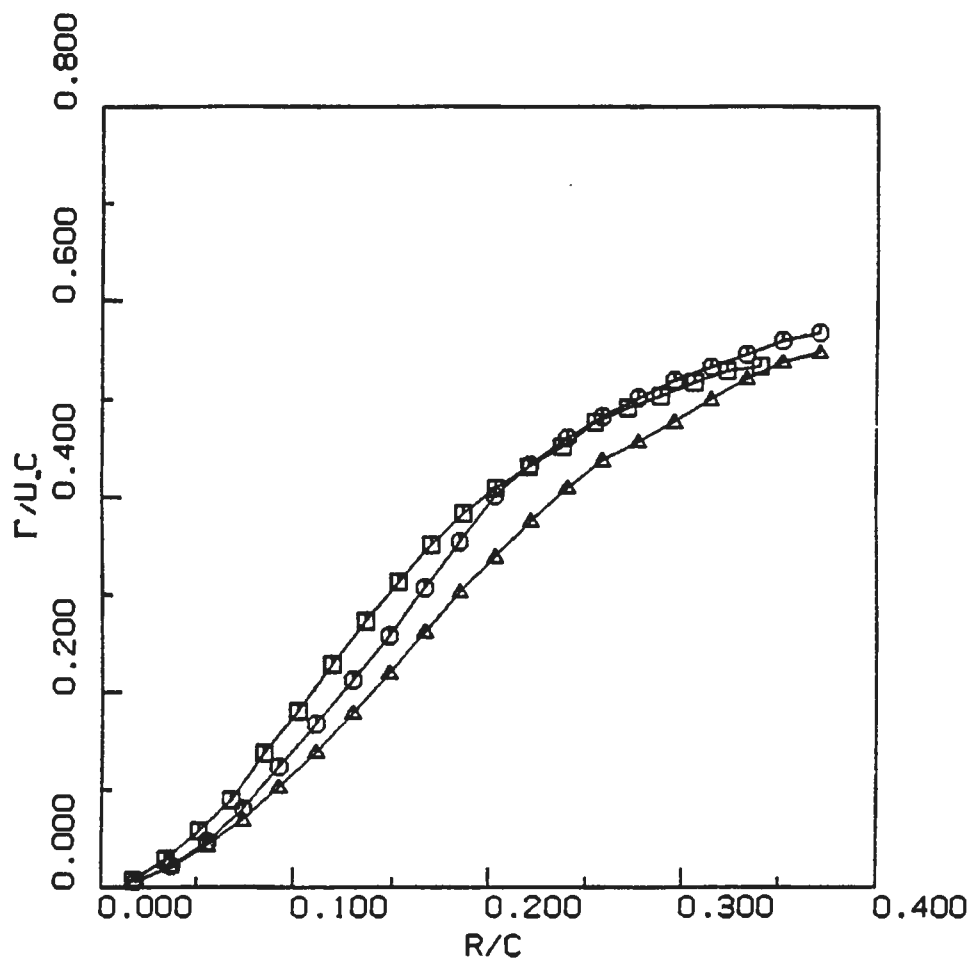


Figure 3.6. Velocity vector field in reference frame of vortex (from Fig. 3.6): $x/c_s = 2.0$, $k = 2.05$, $Re = 14000$



SINUSOIDAL PITCHING SCHEDULE
 $U_i = 1.300 U_\infty$

□ Re . 25119.72
 U_∞ . 0.249 m/s
 k . 2.07
X/C - 2.000
Y/C - 0.092

○ Re . 25211.15
 U_∞ . 0.250 m/s
 k . 2.06
X/C - 3.000
Y/C - 0.125

Δ Re . 25121.28
 U_∞ . 0.249 m/s
 k . 2.07
X/C - 4.000
Y/C - 0.122

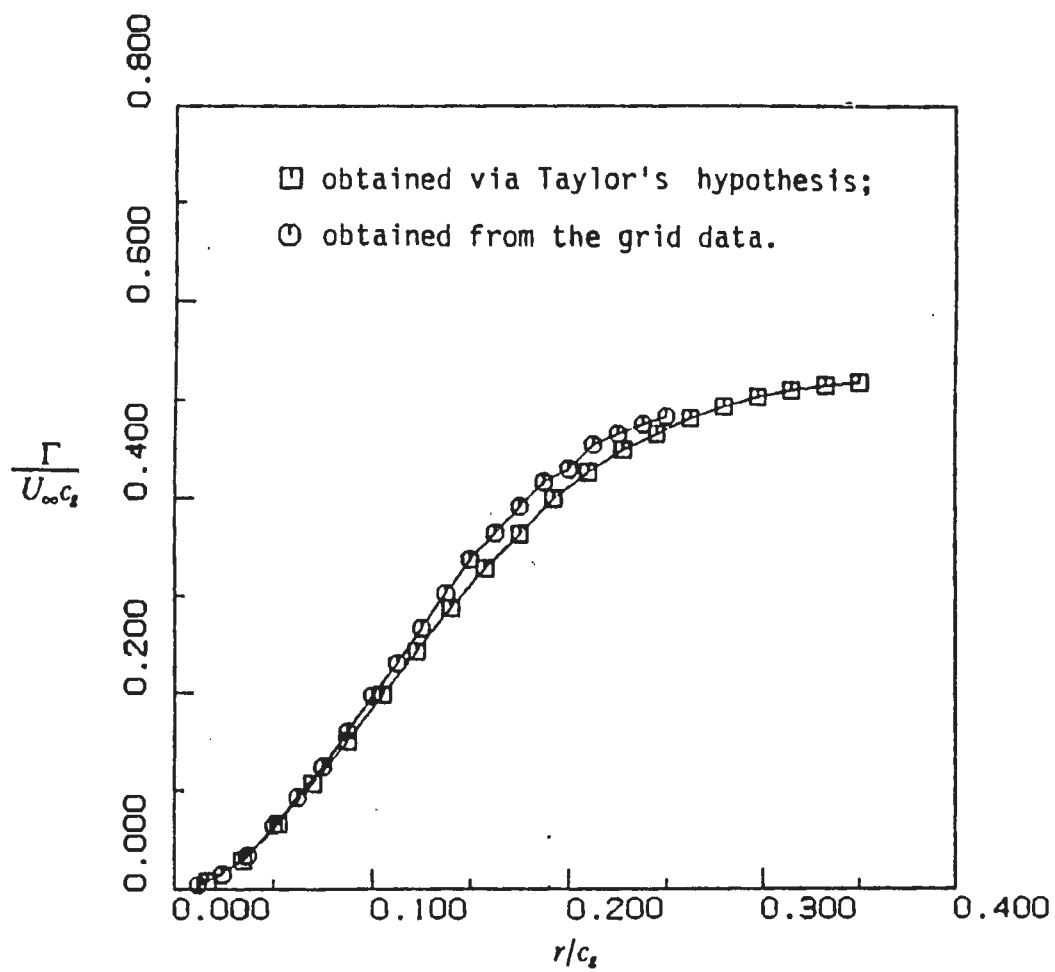
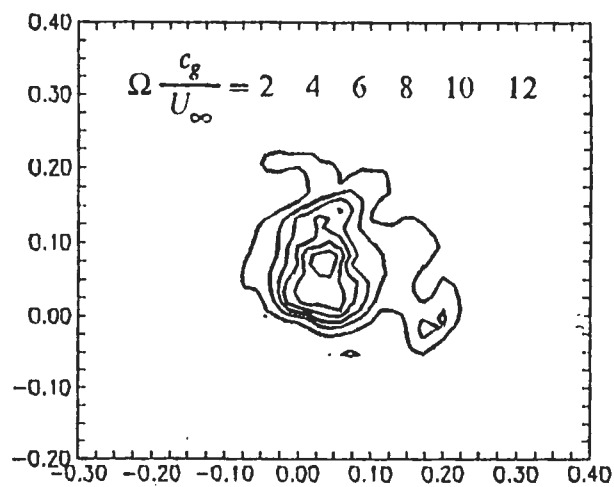
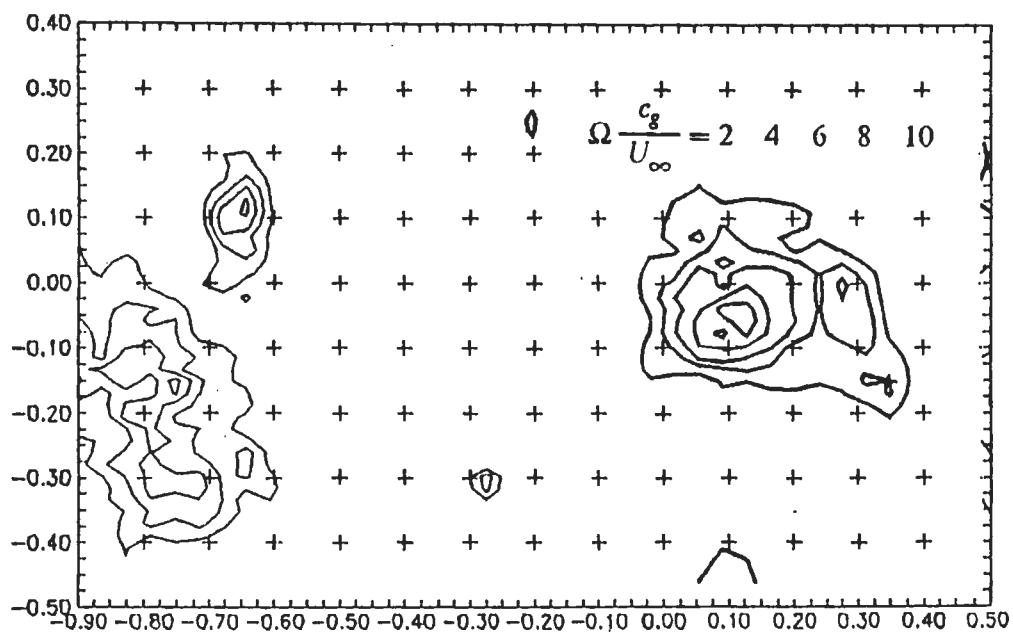


Figure 3.8. A comparison of grid and column data: Total circulation
: $x/c_g = 2.0$, $k = 2.05$, $Re = 14000$



(c)



(d)

Figure 3.9 continued: (c) single window (d) multiple windows, $x/c_d = 2.0$, $k = 2.05$, $H = 0.265$, $Re = 12600$.

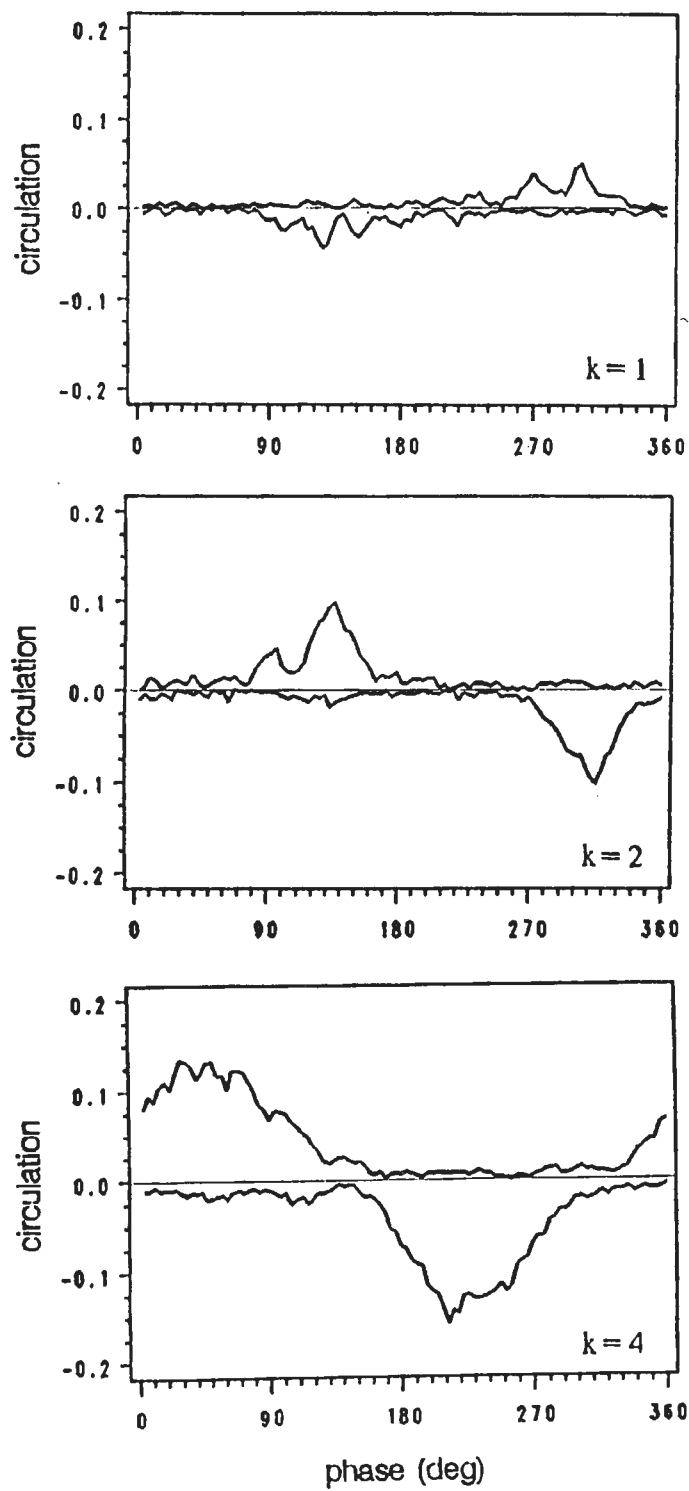


Figure 3.13. Circulation flux for $k=1, 2$, and 4 : $h=0.265$ ($\alpha=\pm 10^\circ$), $x/c_x=2.0$.

- Rolling up of vortex sheets is independent of turbulent character.
- There are no “viscous cores.” Cores are created by convection, hence: “inviscid cores.”
- Many problems involving coherent vortices - laminar or turbulent - could be solved with inviscid methods.
- New vorticity transport process: vortex stretching normal to vortex lines.

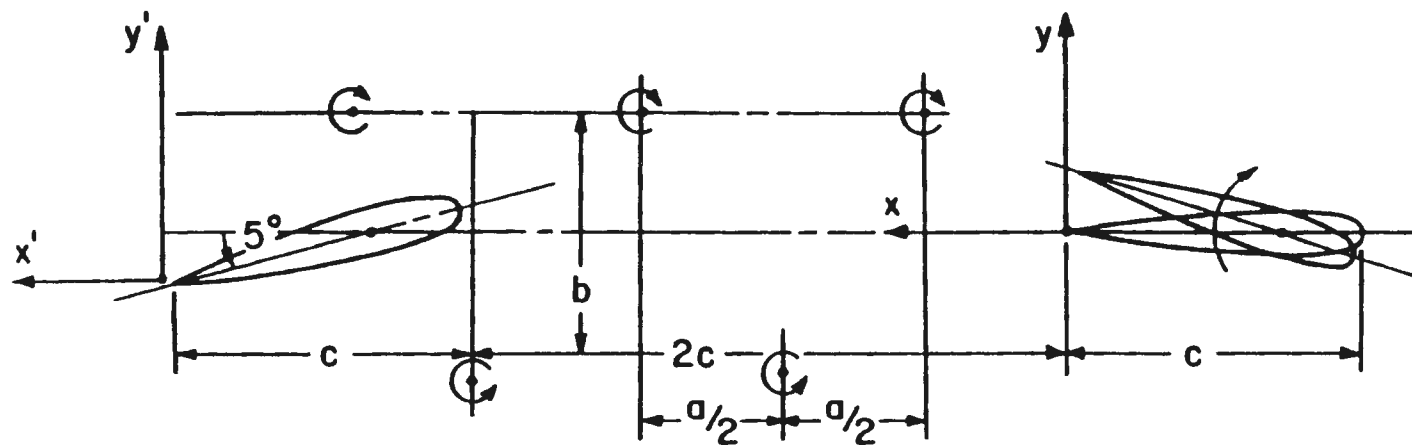


Figure 2.2.1 The pitching airfoil and target airfoil arrangement in the test section

BVI

VECTOR VELOCITY
REFERENCE FRAI

SINUSOIDAL PI

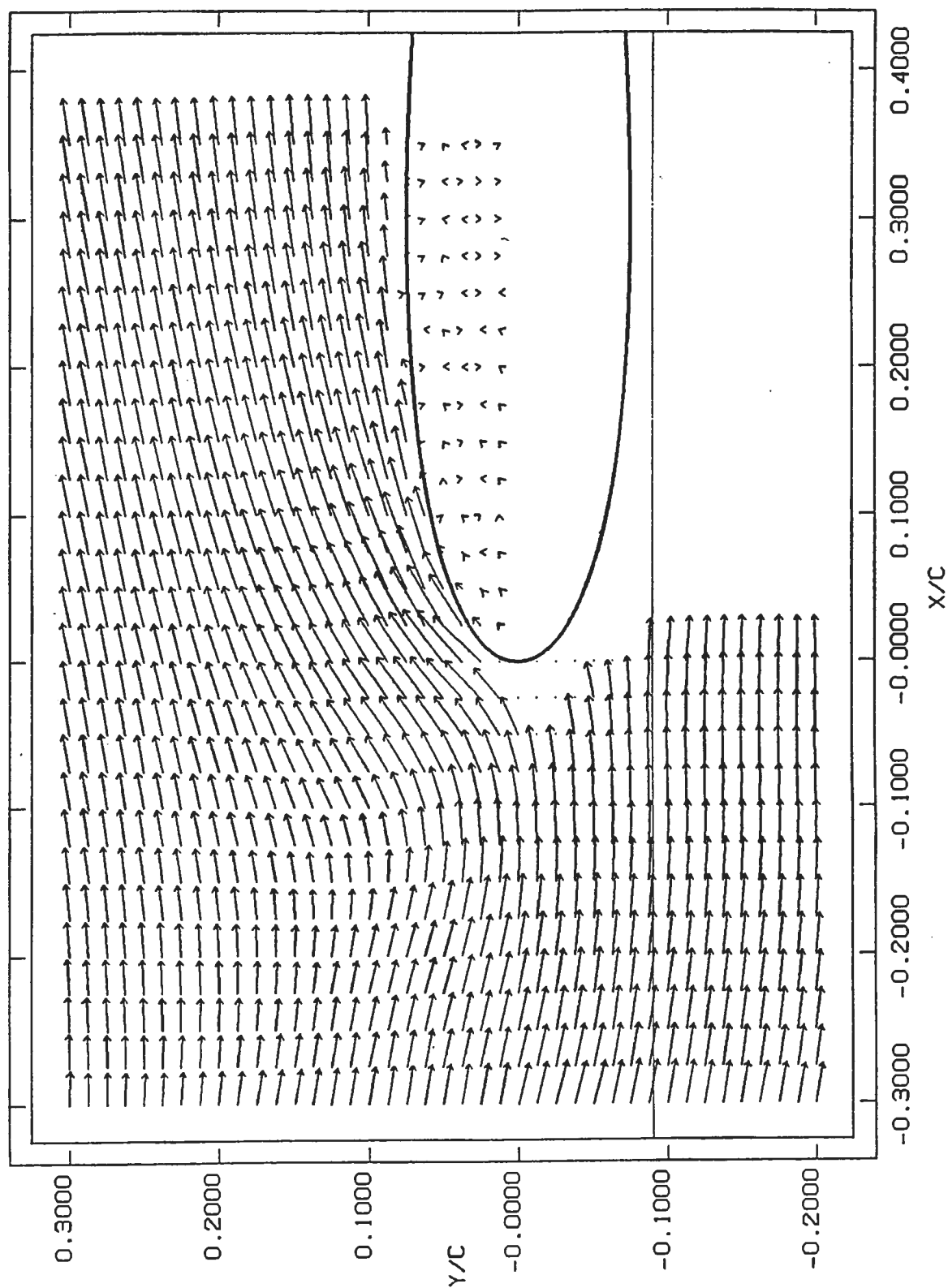
PHASE = 93.6

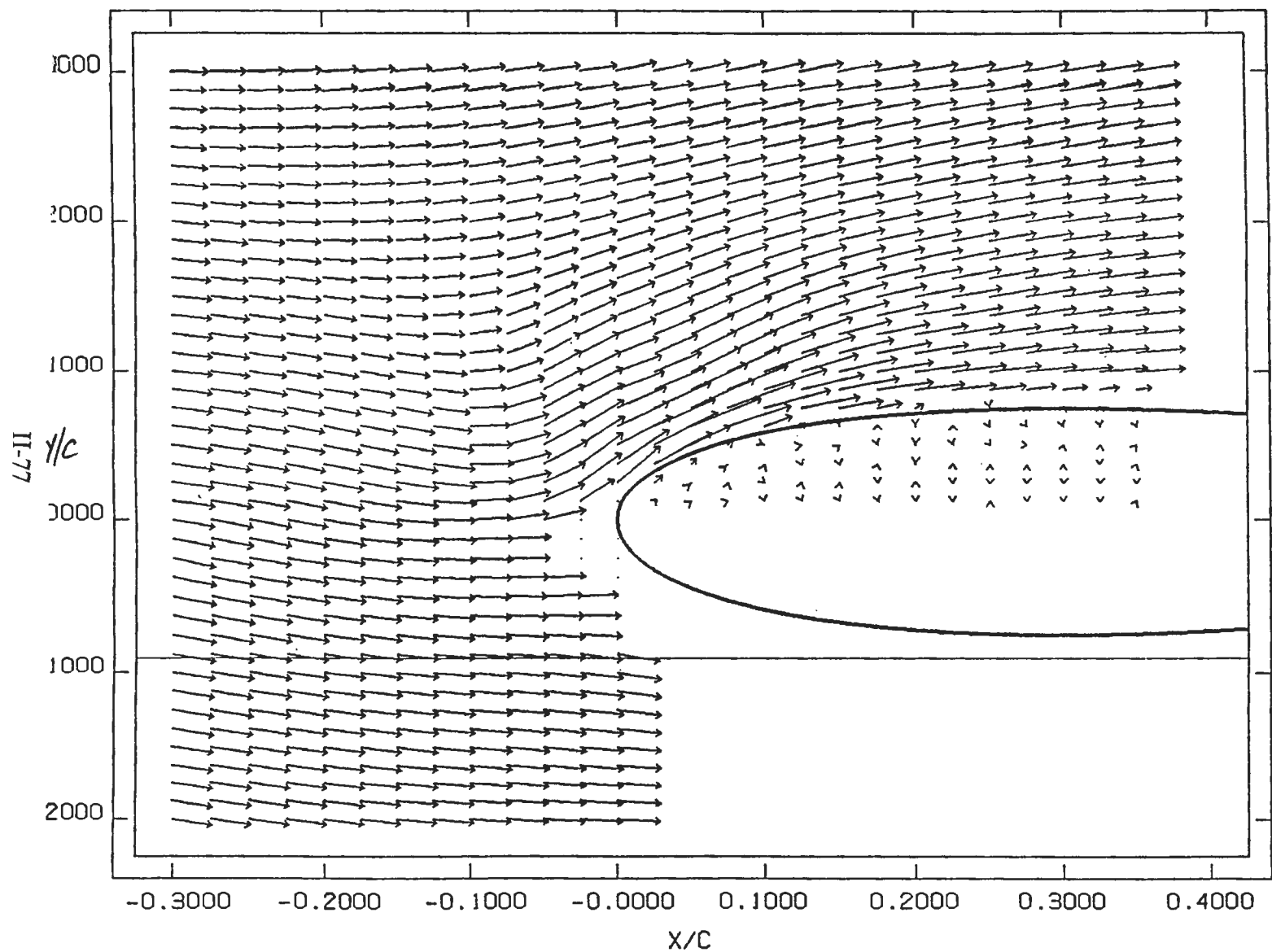
k = 2.02

Re = 12879.4

U_∞ = 0.128 m/s

α = 0.0 (DE





BVI

VECTOR VELOCITY FIELD
REFERENCE FRAME FIXED WRT 1

SINUSOIDAL PITCHING SCHEDULE
PHASE = 108.0 (DEG)
k = 2.02

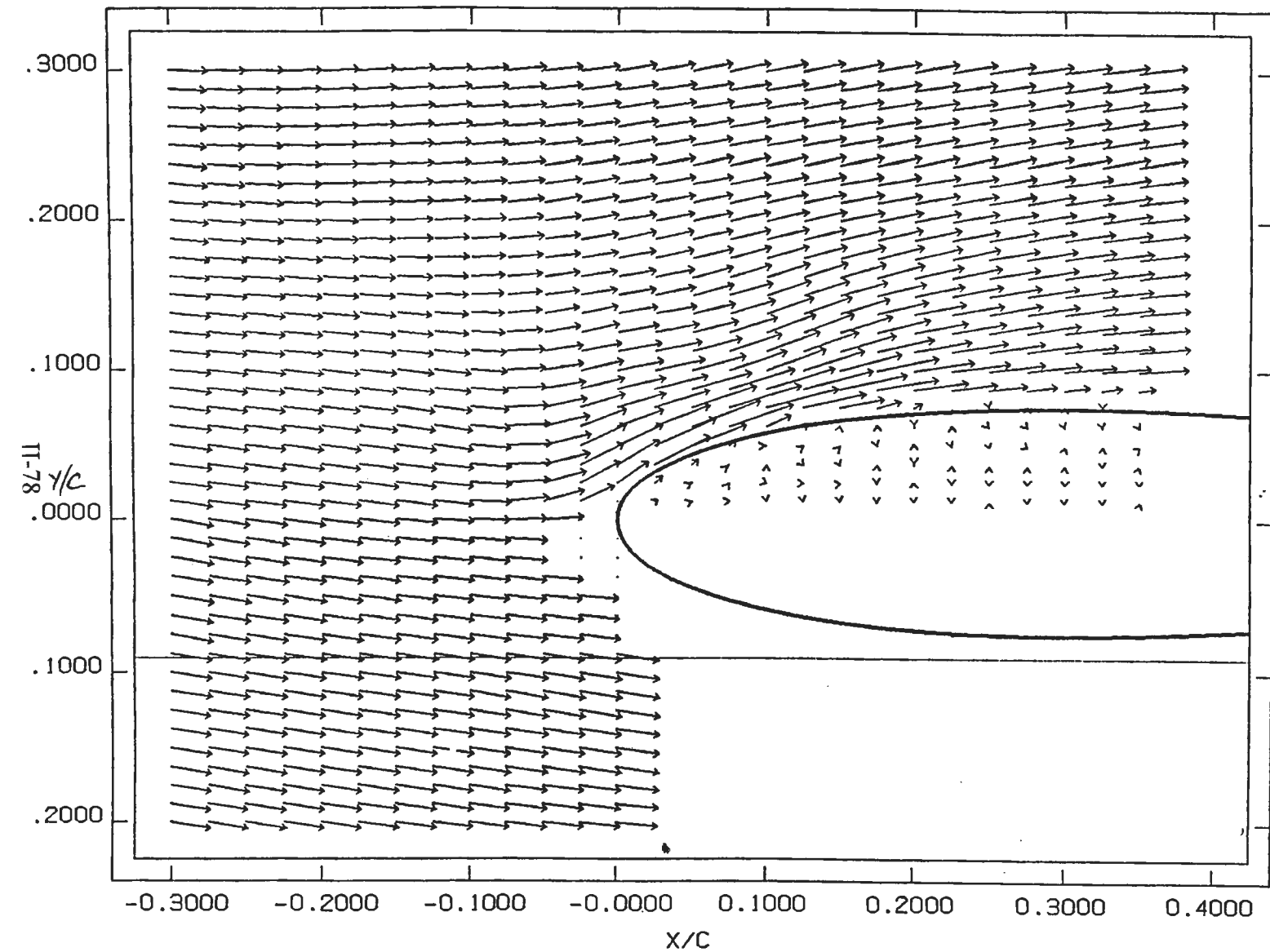
Re = 12879.4
U_∞ = 0.128 m/s
α = 0.0 (DEG.)

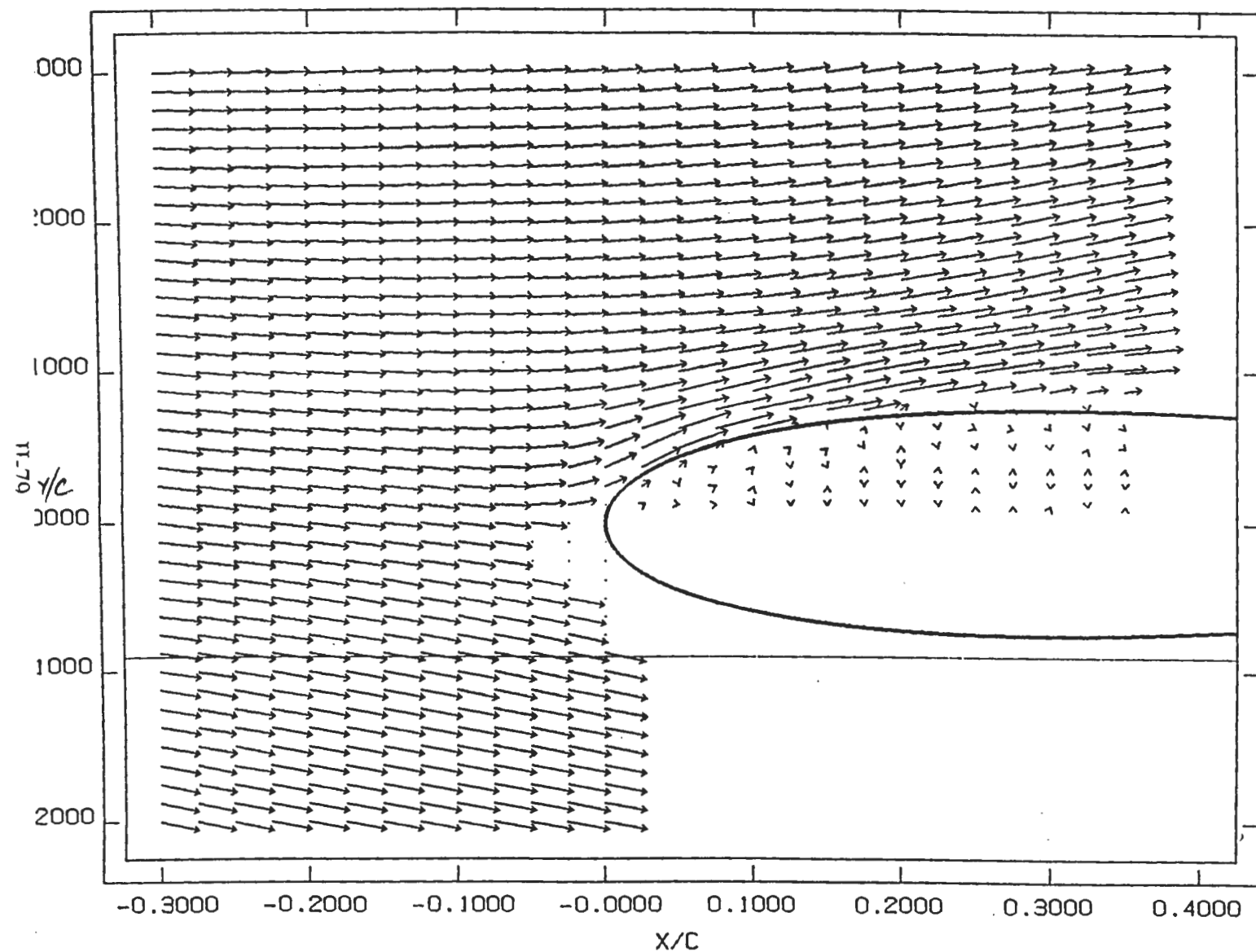
BVI

VECTOR VELOCITY FIELD
REFERENCE FRAME FIXED WRT 1

SINUSOIDAL PITCHING SCHEDULE
PHASE = 122.4 (DEG)
 $k = 2.02$

$Re = 12879.4$
 $U_{\infty} = 0.128 \text{ m/s}$
 $\alpha = 0.0 \text{ (DEG.)}$





BVI

VECTOR VELOCITY FIELD
REFERENCE FRAME FIXED WRT TH

SINUSOIDAL PITCHING SCHEDULE

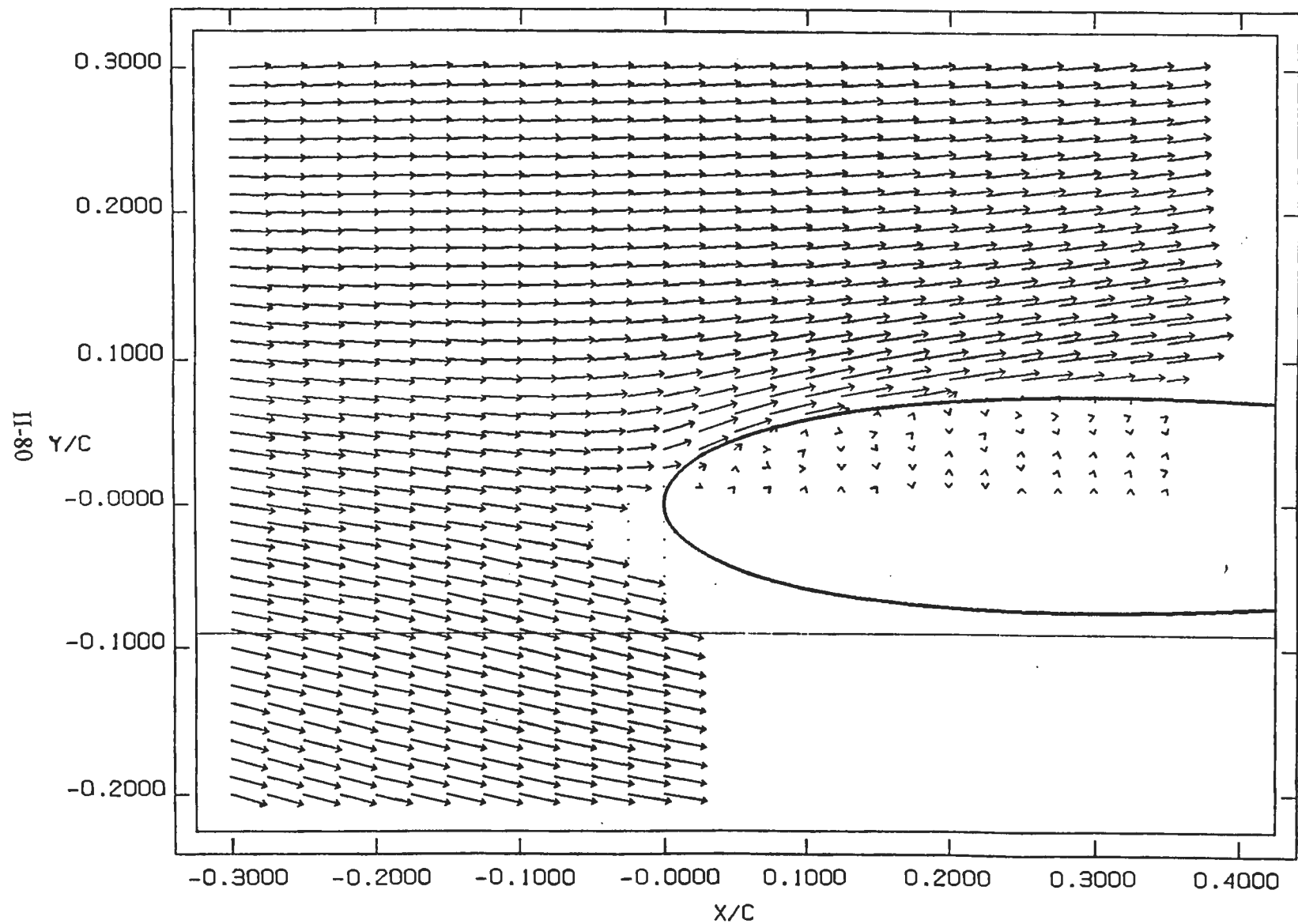
PHASE = 151.2 (DEG)

k = 2.02

Re = 12879.4

U_{∞} = 0.128 m/s

α = 0.0 (DEG.)

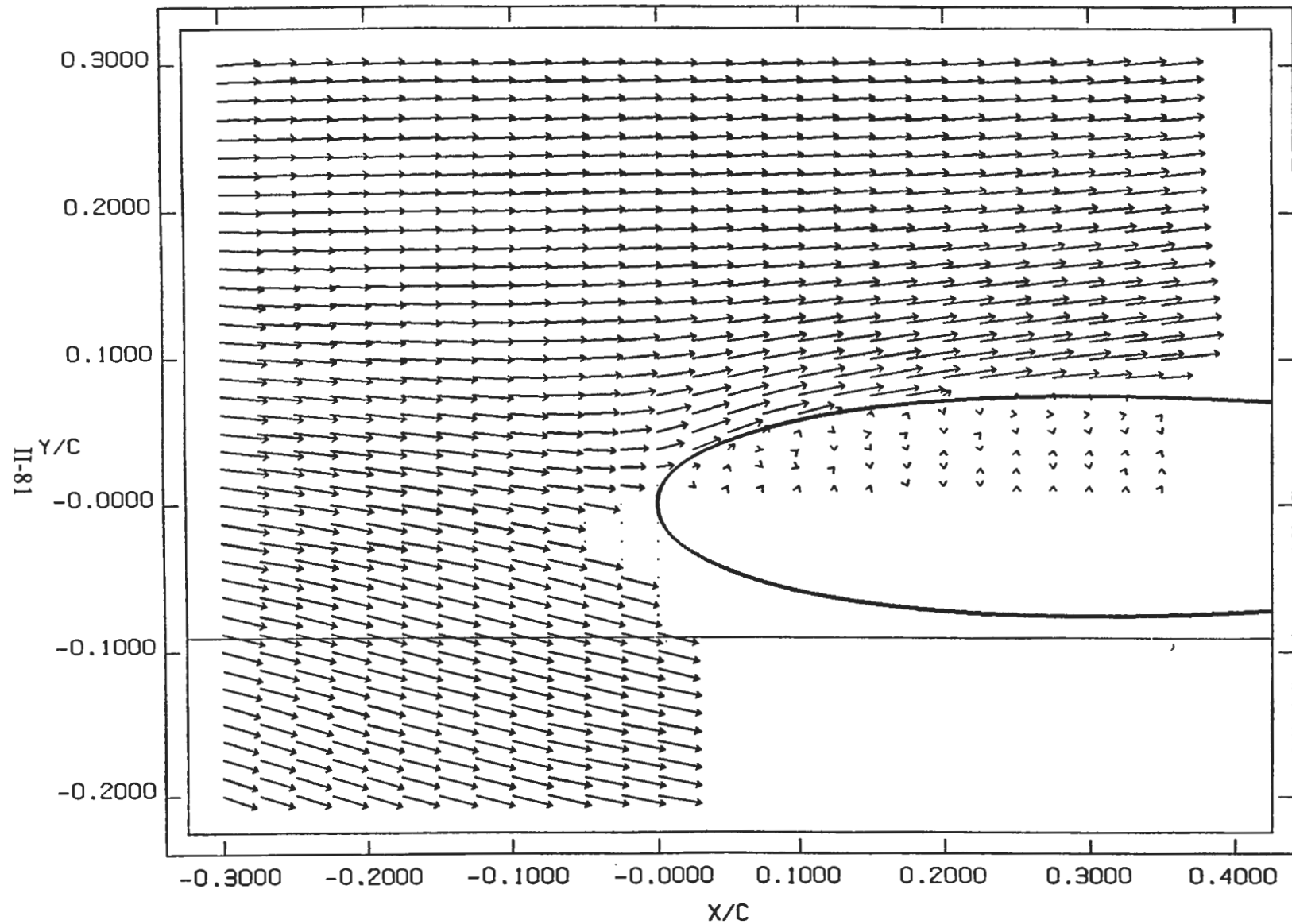


BVI

VECTOR VELOCITY FIELD
REFERENCE FRAME FIXED

SINUSOIDAL PITCHING δ
PHASE = 180.0 (DEG)
 k = 2.02

Re = 12879.4
 U_{∞} = 0.128 m/s
 α = 0.0 (DEG.)

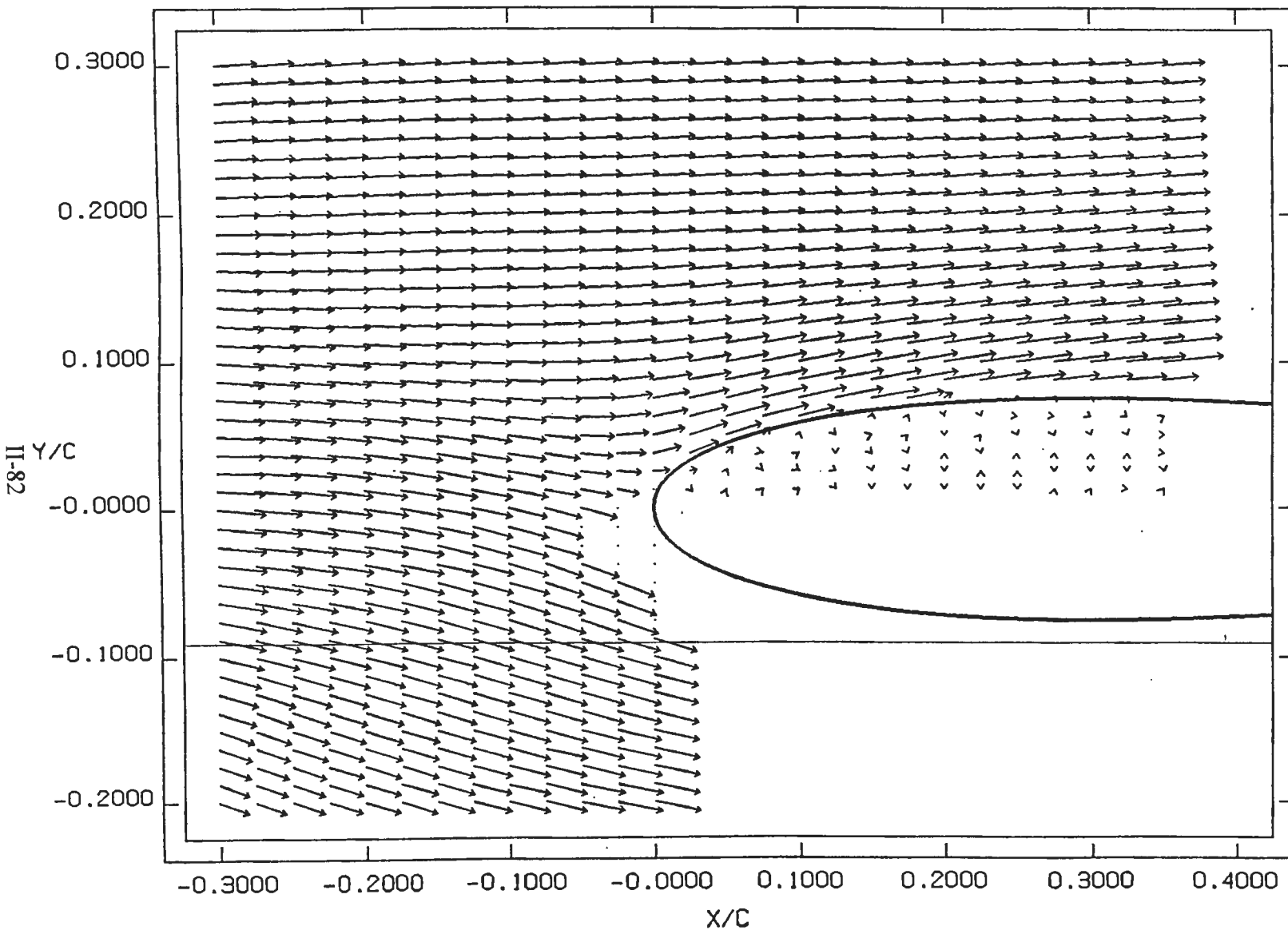


BVI

VECTOR VELOCITY FIELD
REFERENCE FRAME FIXED I

SINUSOIDAL PITCHING SCI
PHASE = 194.4 (DEG)
k = 2.02

Re = 12879.4
U_∞ = 0.128 m/s
α = 0.0 (DEG.)

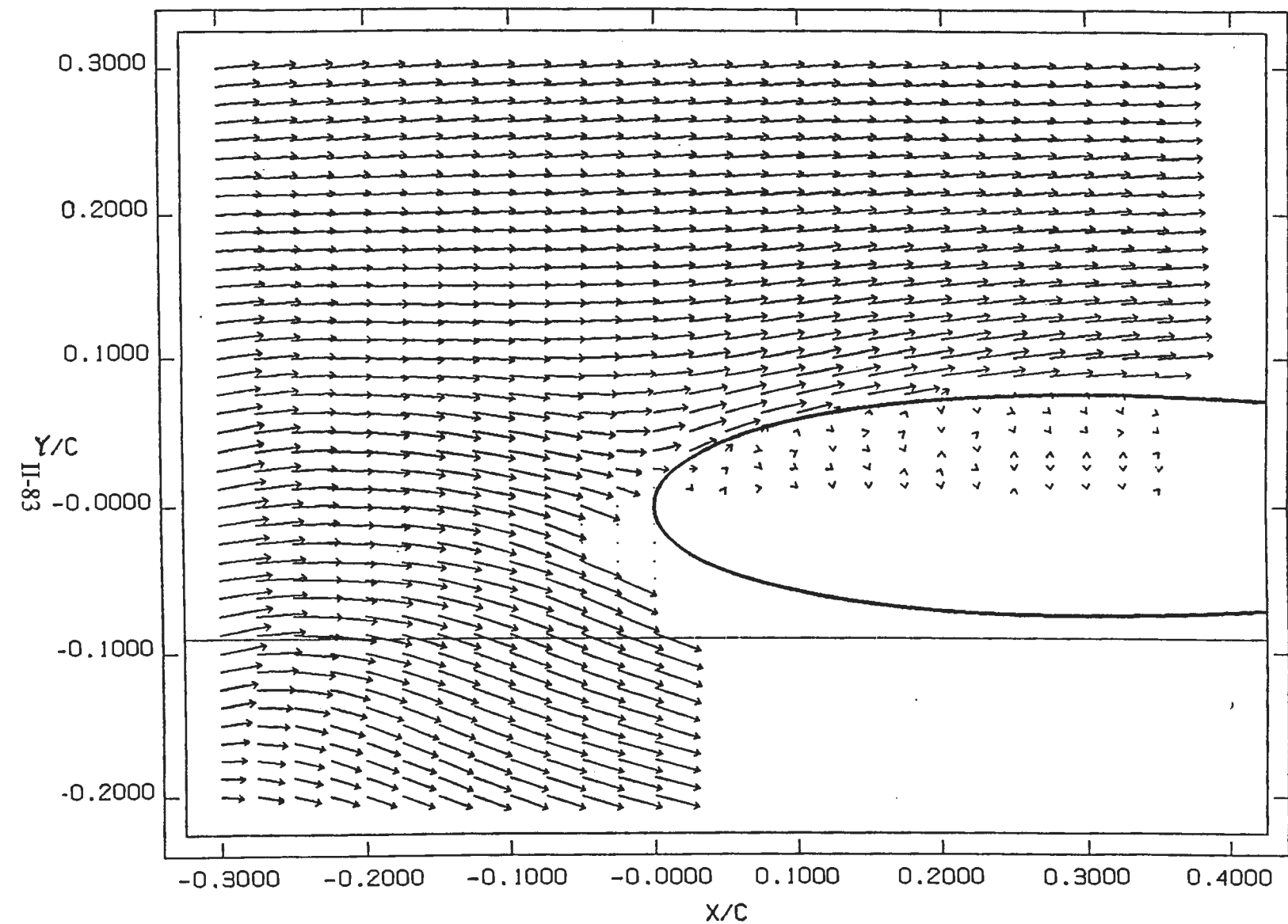


BVI

VECTOR VELOCITY FIELD
REFERENCE FRAME FIXED I

SINUSOIDAL PITCHING SC
PHASE = 208.8 (DEG)
 $k = 2.02$

$Re = 12879.4$
 $U_{\infty} = 0.128 \text{ m/s}$
 $\alpha = 0.0 \text{ (DEG.)}$

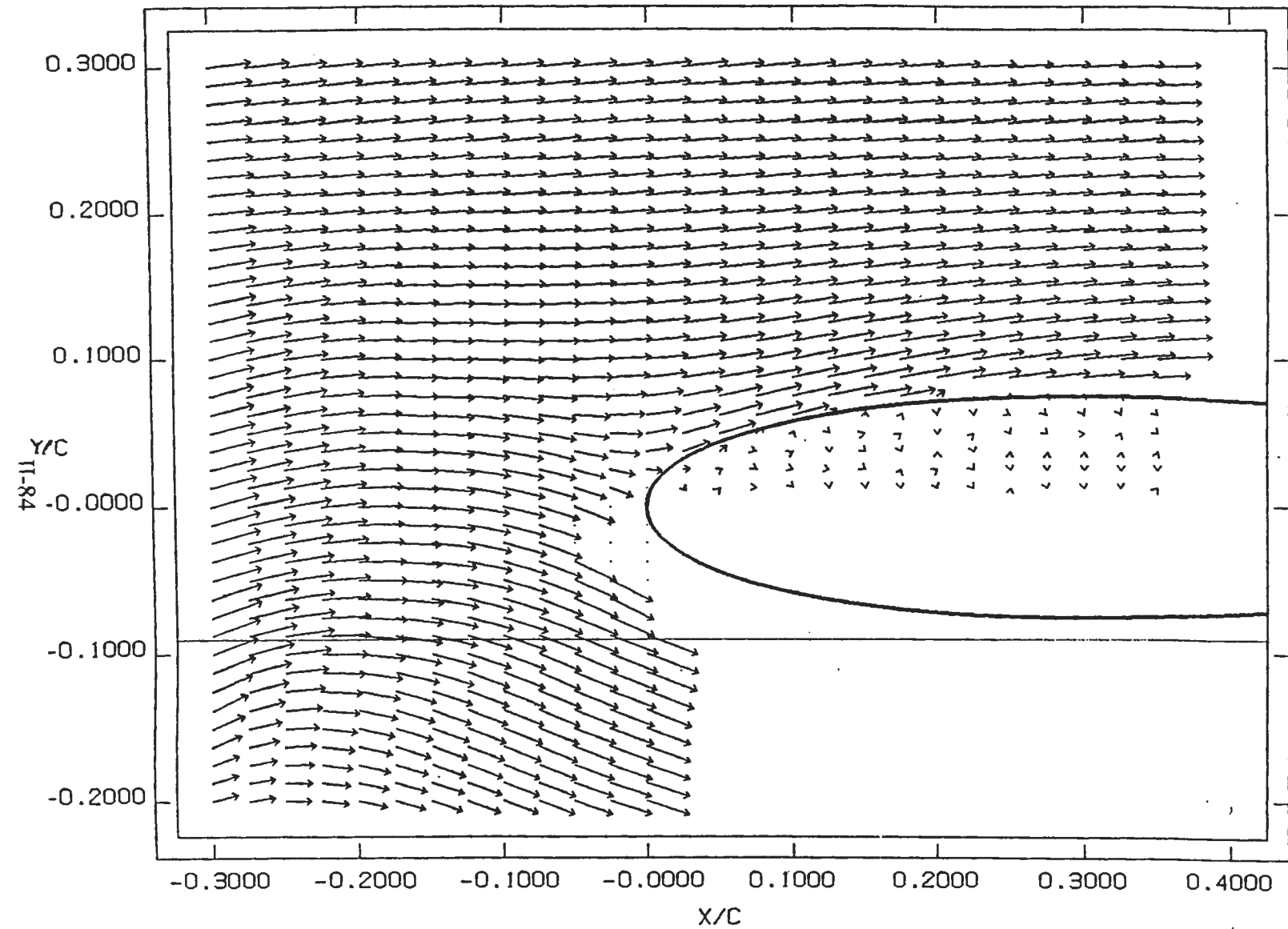


BVI

VECTOR VELOCITY FIELD
REFERENCE FRAME FIXED

SINUSOIDAL PITCHING SC
PHASE = 230.4 (DEG)
 $k = 2.02$

$Re = 12879.4$
 $U_{\infty} = 0.128 \text{ m/s}$
 $\alpha = 0.0 \text{ (DEG.)}$

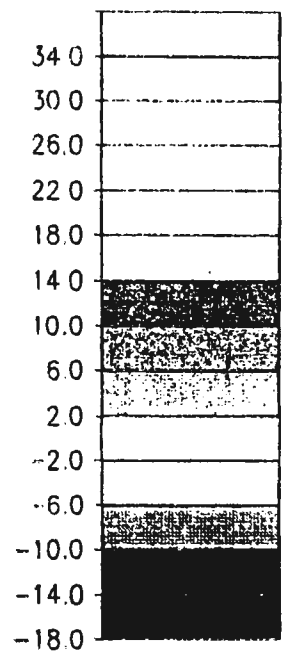
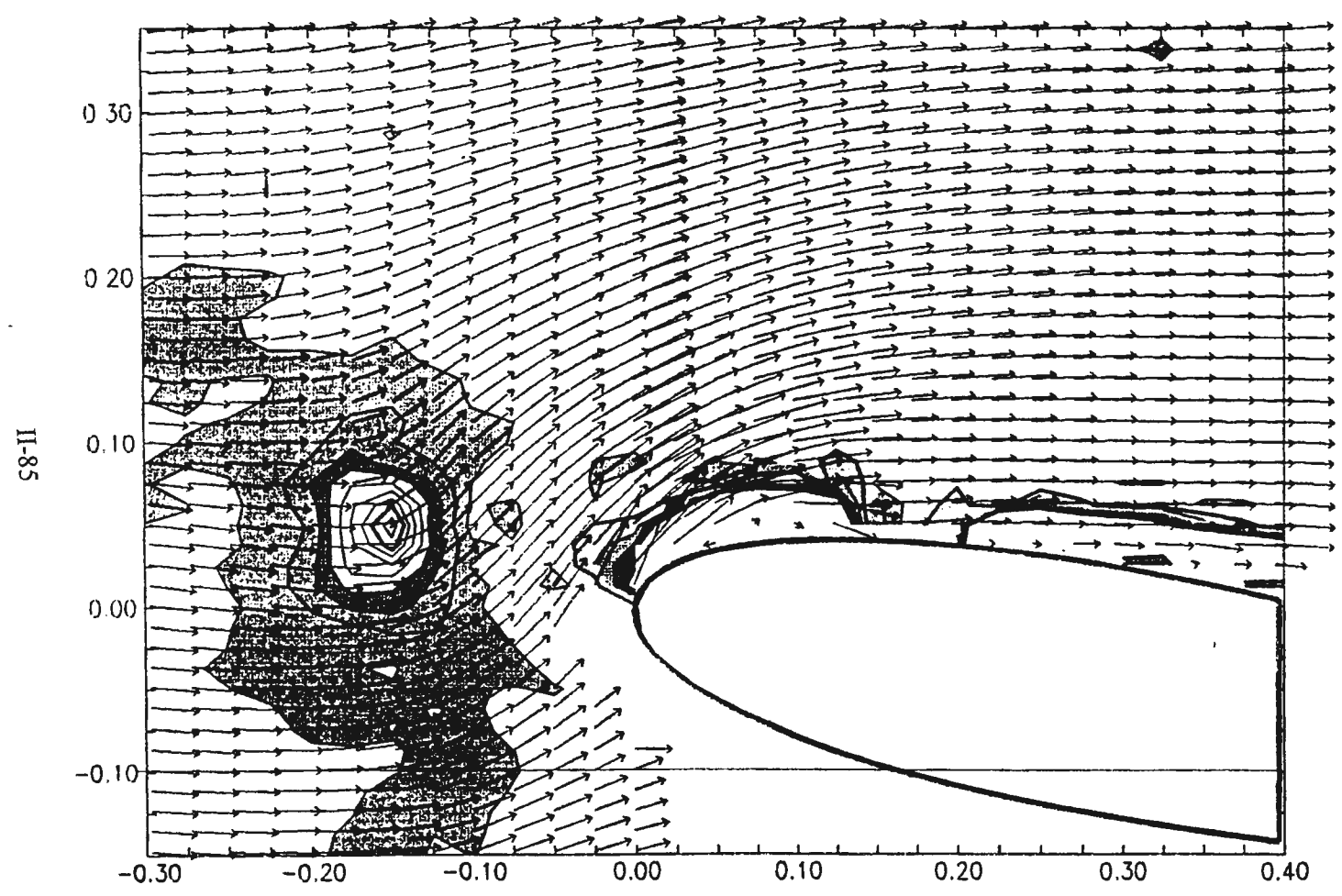


BVI

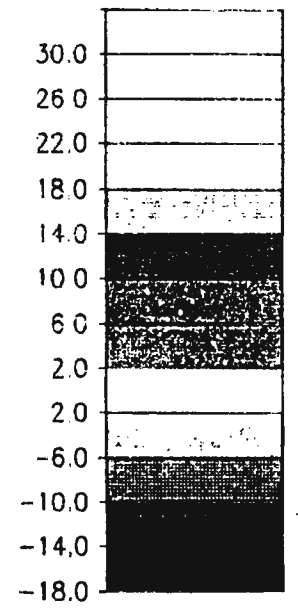
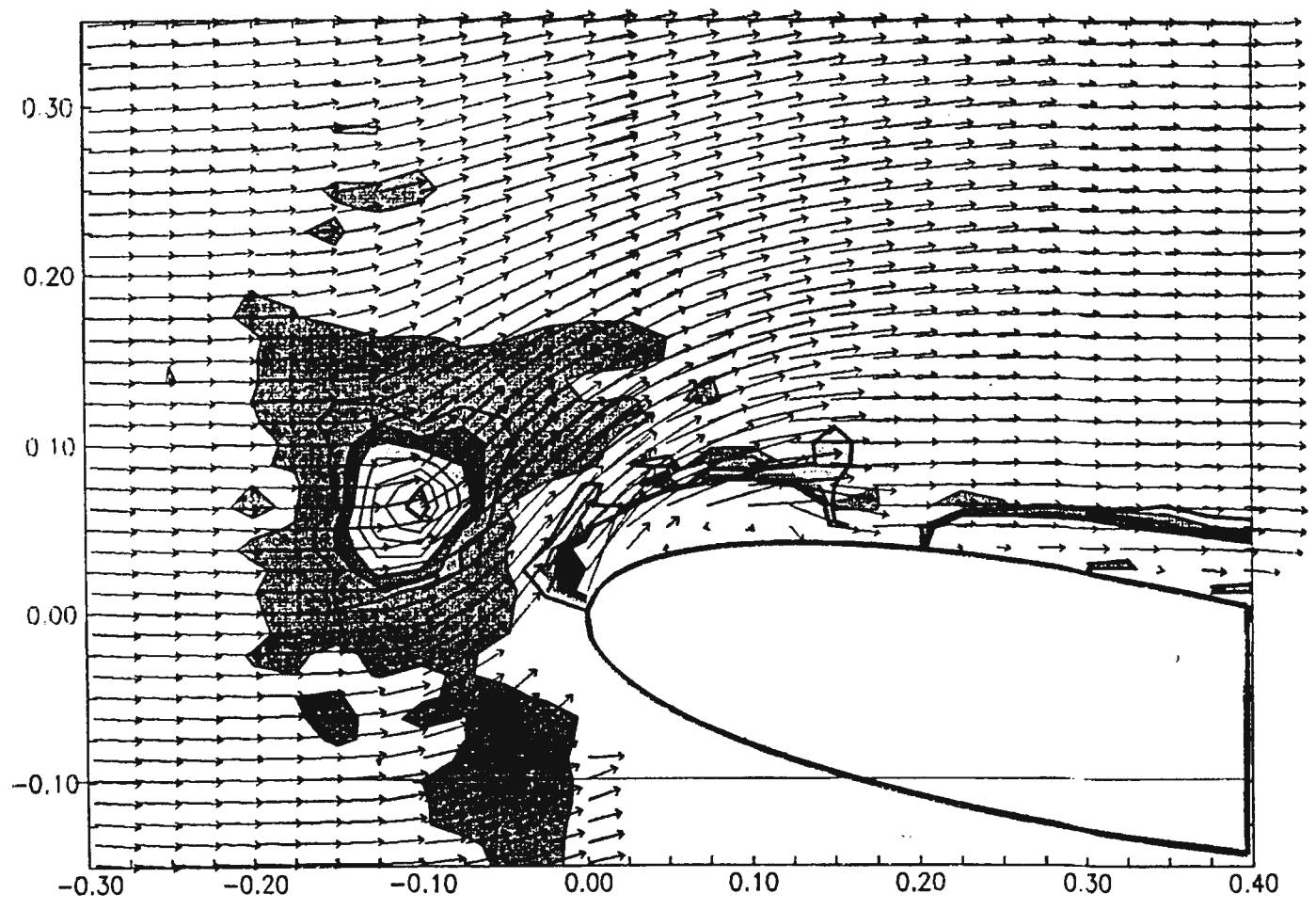
VECTOR VELOCITY FIELD
REFERENCE FRAME FIXED WF

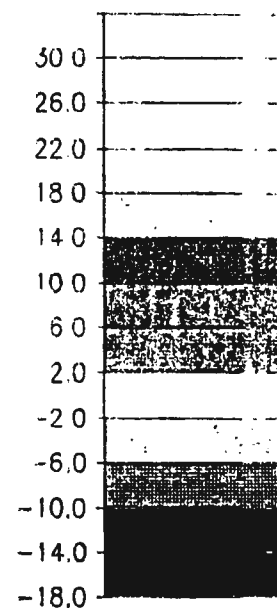
SINUSOIDAL PITCHING SCHE
PHASE = 244.8 (DEG)
 $k = 2.02$

$Re = 12879.4$
 $U_{\infty} = 0.128 \text{ m/s}$
 $\alpha = 0.0 \text{ (DEG.)}$

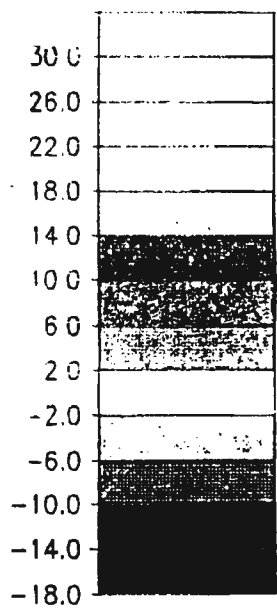
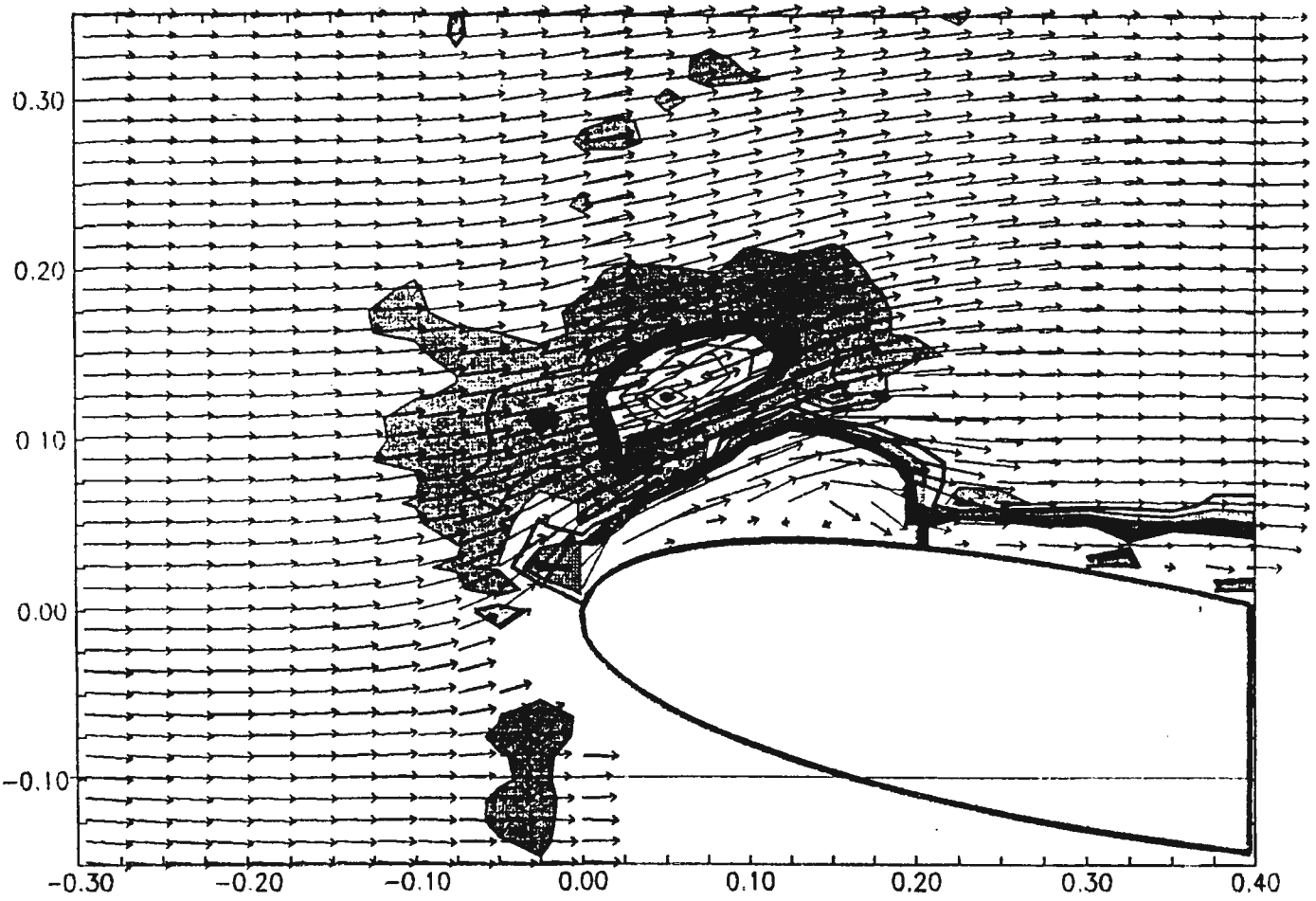


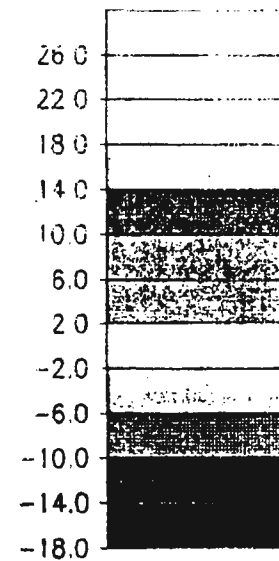
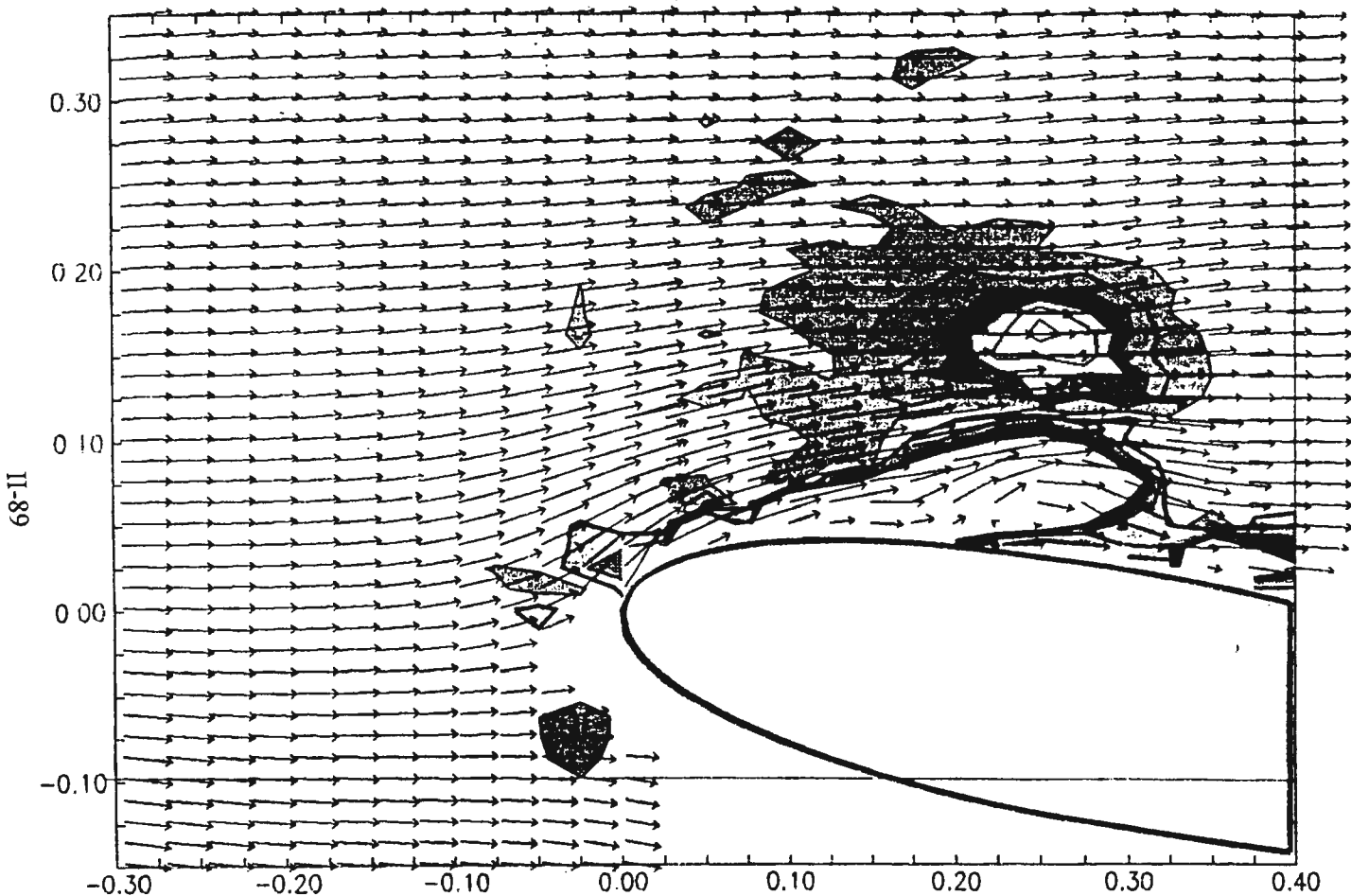
98-II

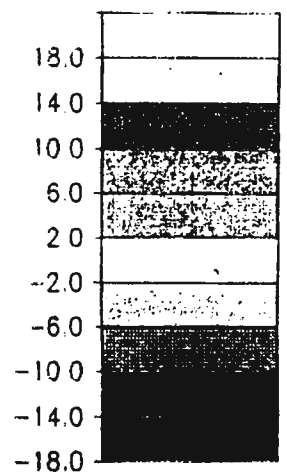
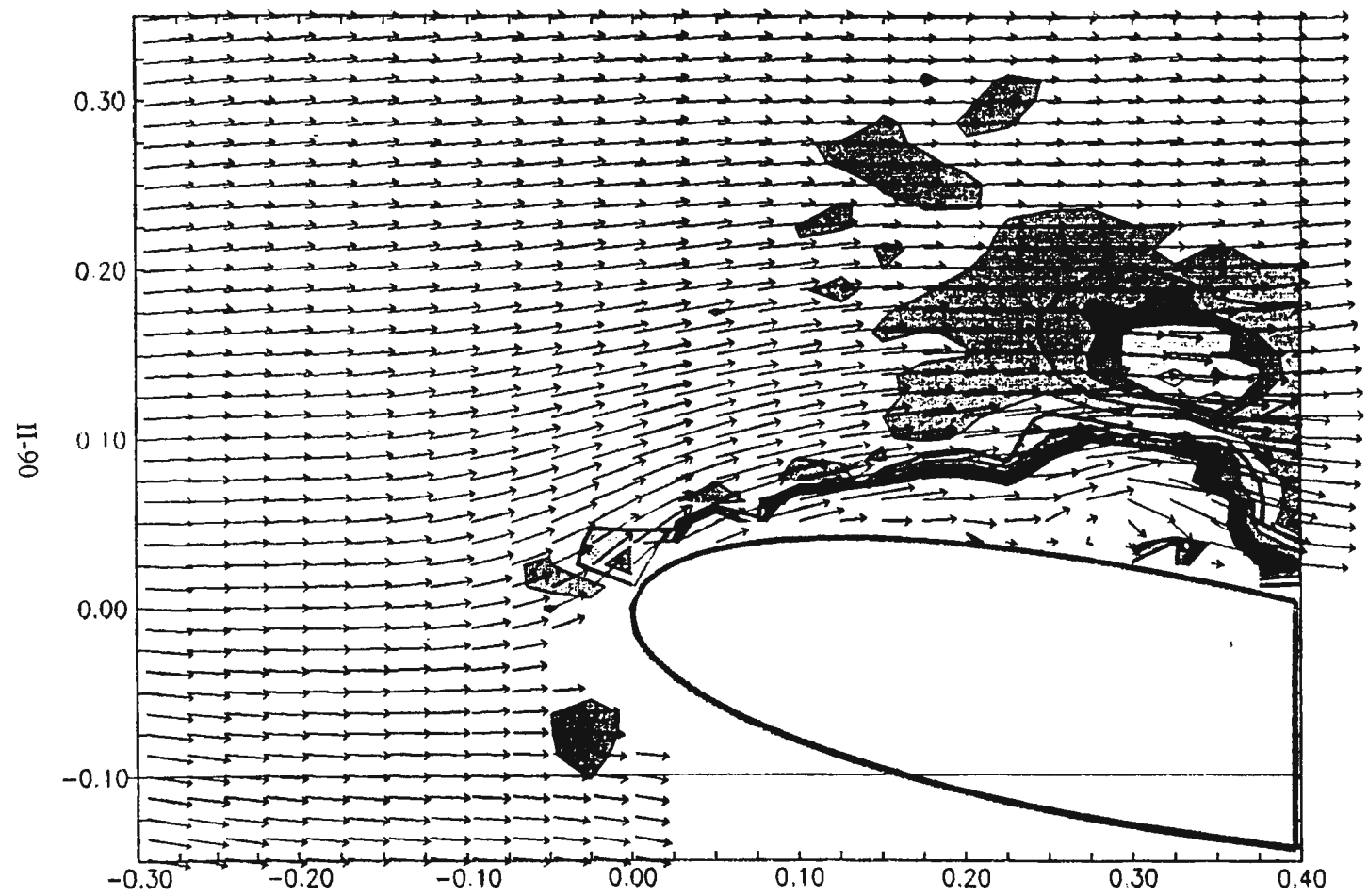




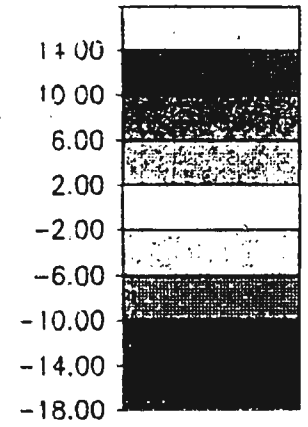
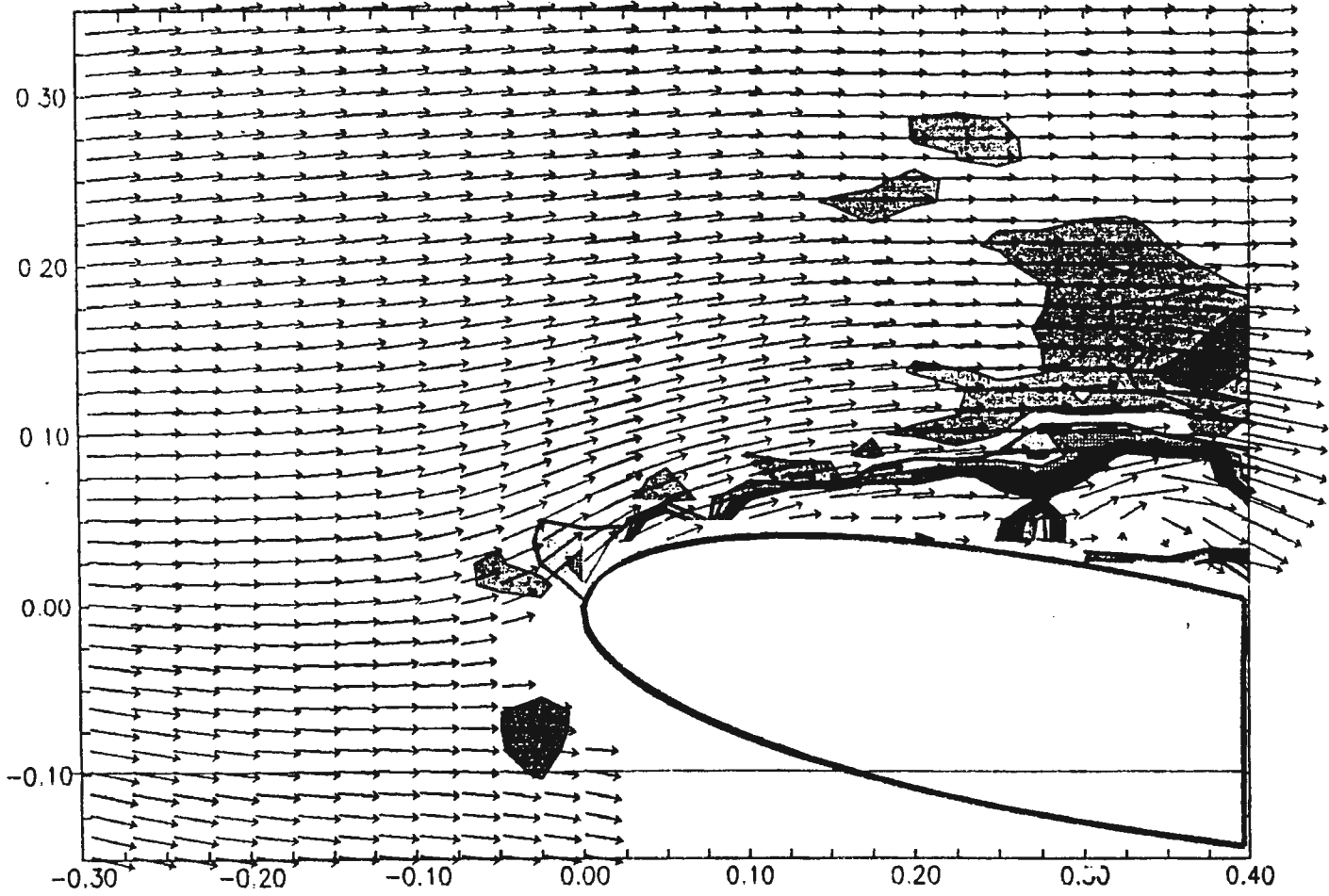
88-II







16-II



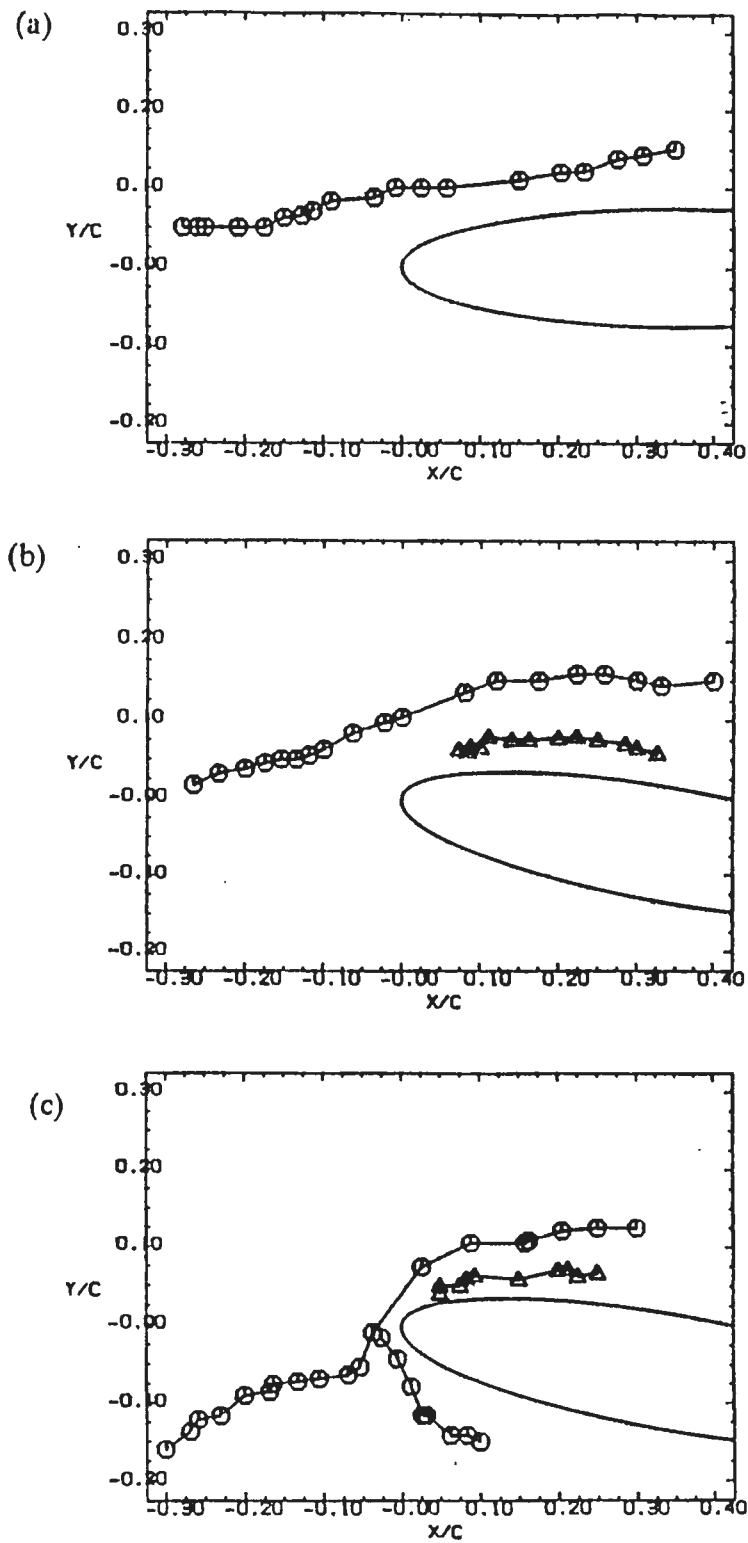


Figure 4.9. Trajectory of primary and secondary vortices for each case: (a) $\alpha = 0^\circ, \Delta h = 0.09c$ (b) $\alpha = 10^\circ, \Delta h = 0.1c$ (c) $\alpha = 10^\circ, \Delta h = 0.125c$

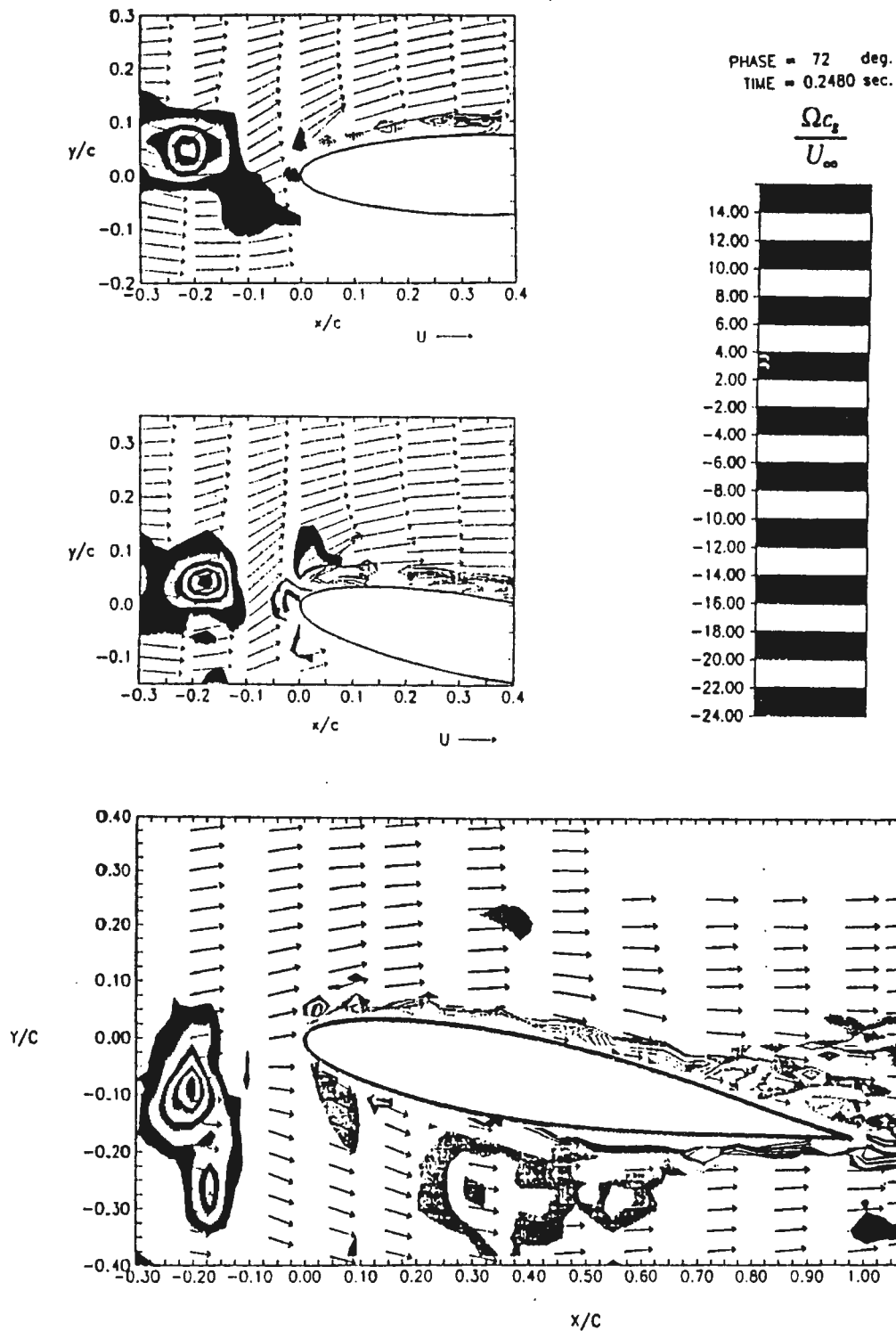
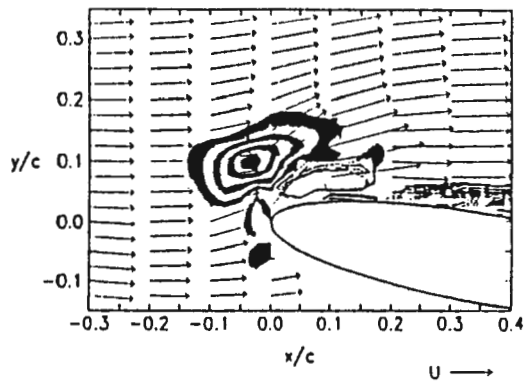
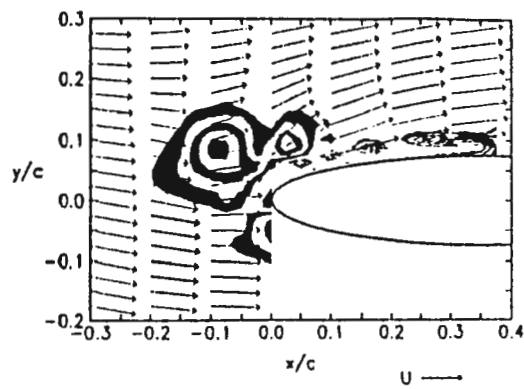


Figure 4.11. Vorticity contour maps: (a) $\alpha=0^\circ$, $\Delta h=0.09c$ (b) $\alpha=10^\circ$, $\Delta h=0.1c$ (c) $\alpha=10^\circ$, $\Delta h=0.125c$



PHASE = 135 deg.
TIME = 0.4650 sec.

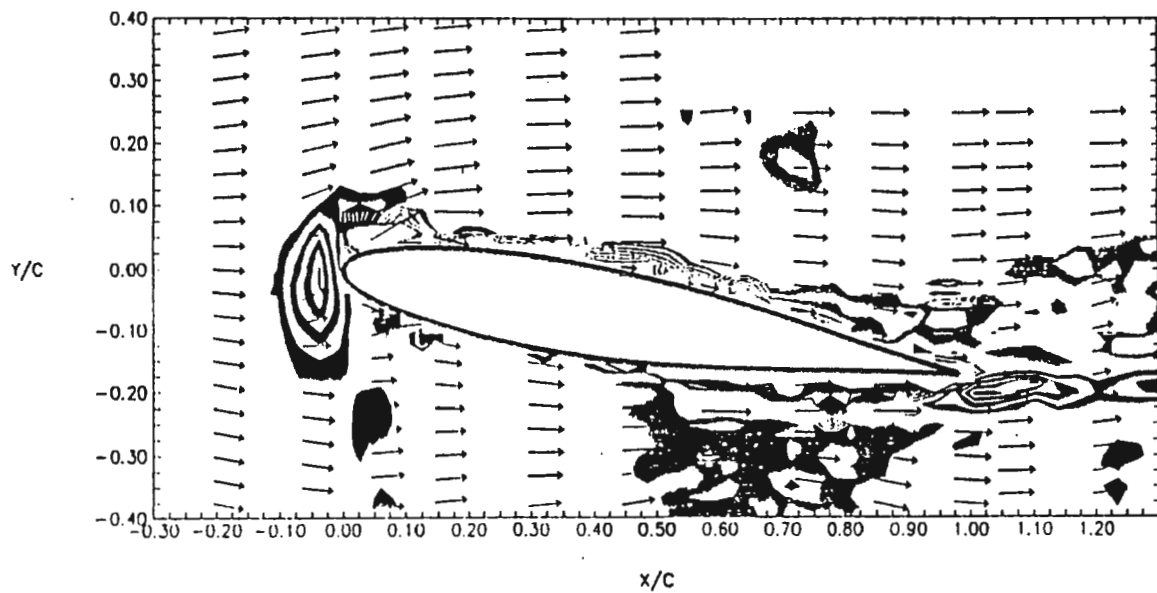
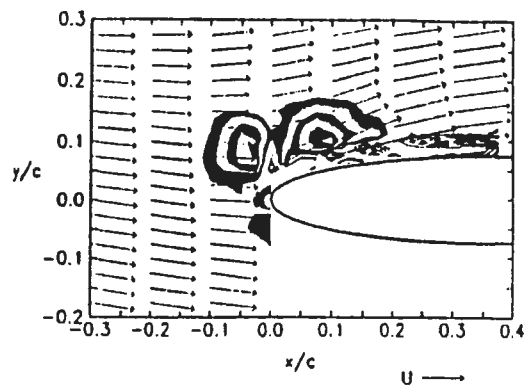
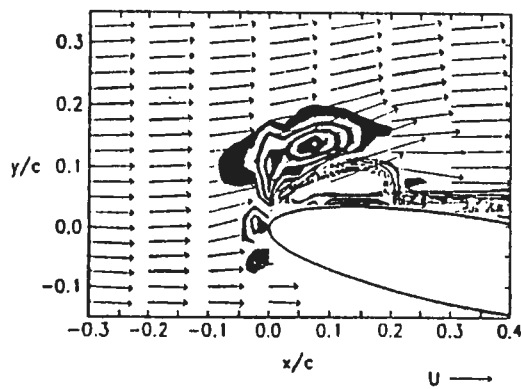


Figure 4.11. continued: (a) $\alpha = 0^\circ$, $\Delta h = 0.09c$ (b) $\alpha = 10^\circ$, $\Delta h = 0.1c$ (c) $\alpha = 10^\circ$, $\Delta h = 0.125c$



PHASE = 129.6 deg.
TIME = 0.4464 sec.



PHASE = 129.6 deg.
TIME = 0.4464 sec.

PHASE = 153 deg.
TIME = 0.5270 sec.

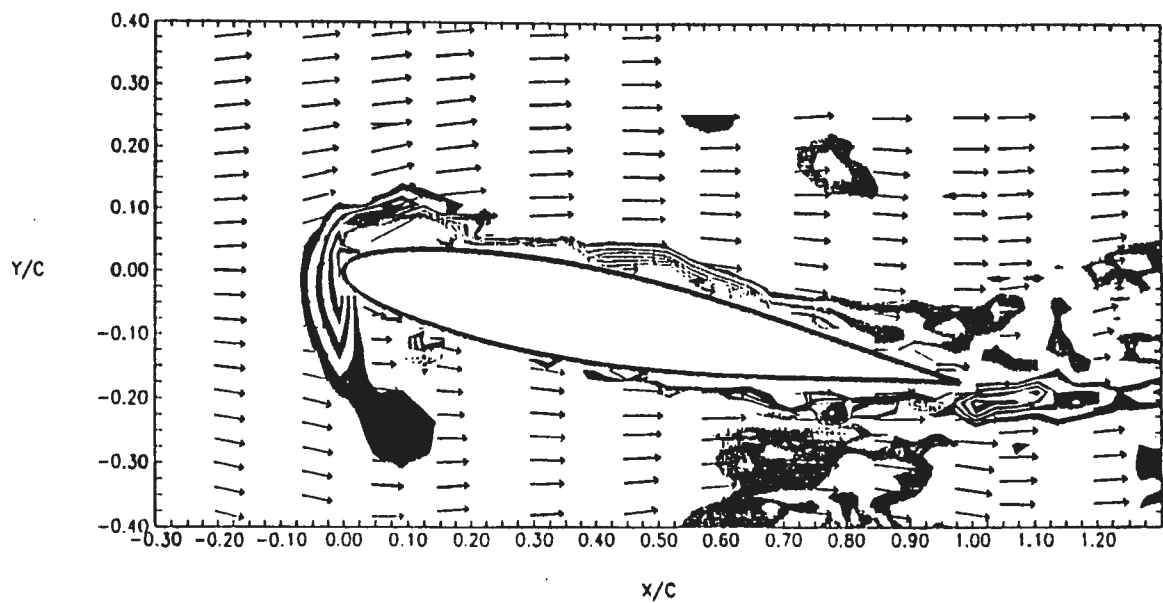
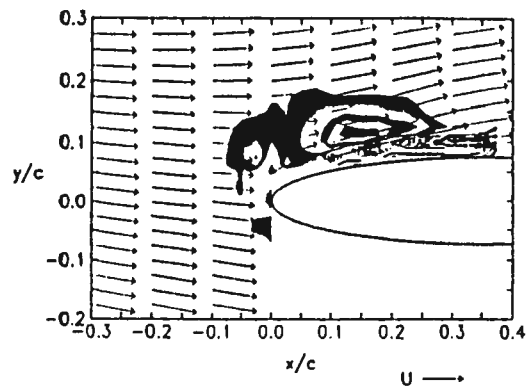
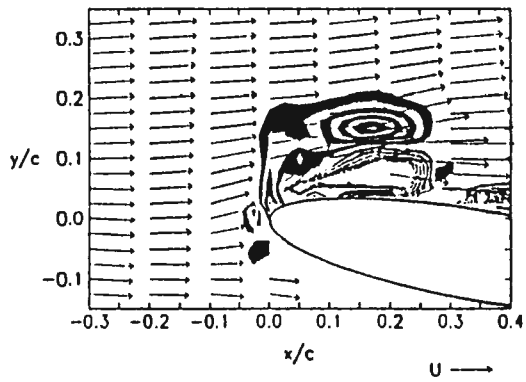


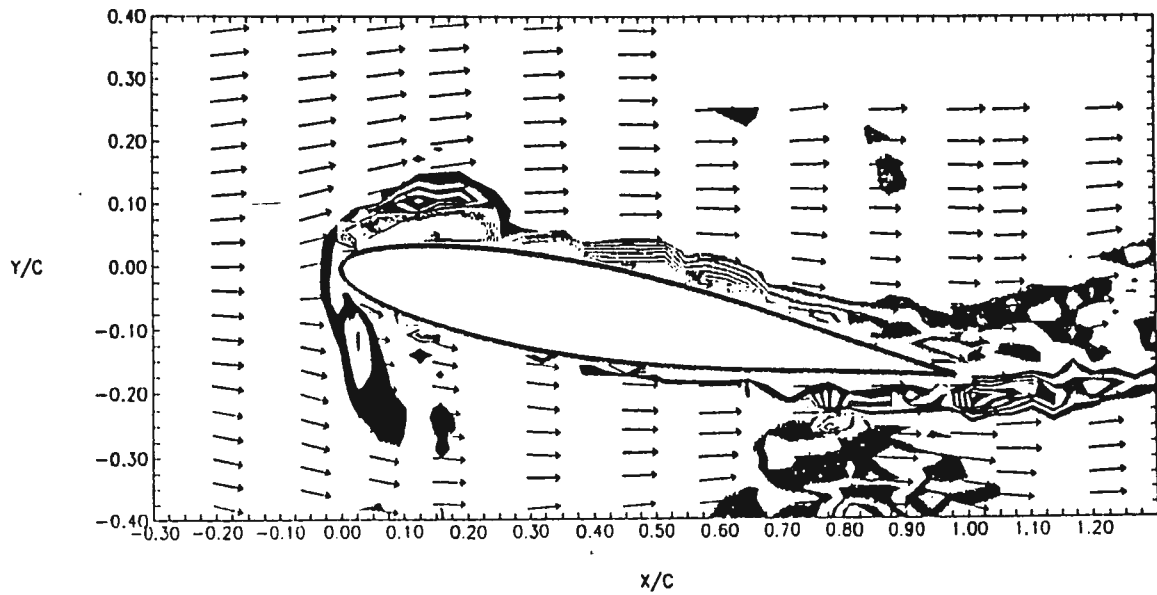
Figure 4.11. continued: (a) $\alpha = 0^\circ$, $\Delta h = 0.09c$ (b) $\alpha = 10^\circ$, $\Delta h = 0.1c$ (c) $\alpha = 10^\circ$, $\Delta h = 0.125c$



PHASE = 144.0 deg.
TIME = 0.4960 sec.

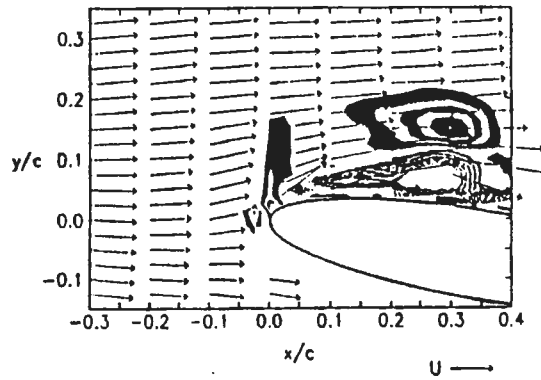
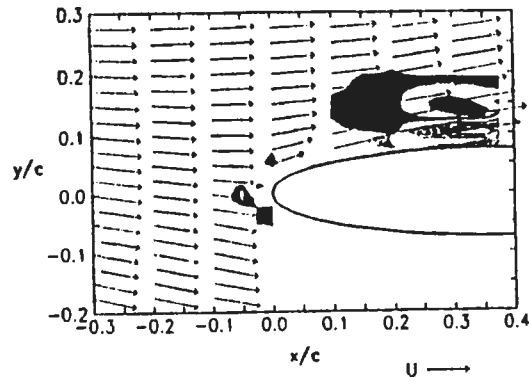


PHASE = 144.0 deg.
TIME = 0.4960 sec.



PHASE = 171 deg.
TIME = 0.5890 sec.

Figure 4.11. continued: (a) $\alpha = 0^\circ$, $\Delta h = 0.09c$ (b) $\alpha = 10^\circ$, $\Delta h = 0.1c$ (c) $\alpha = 10^\circ$, $\Delta h = 0.125c$



PHASE = 198 deg.
TIME = 0.6820 sec.

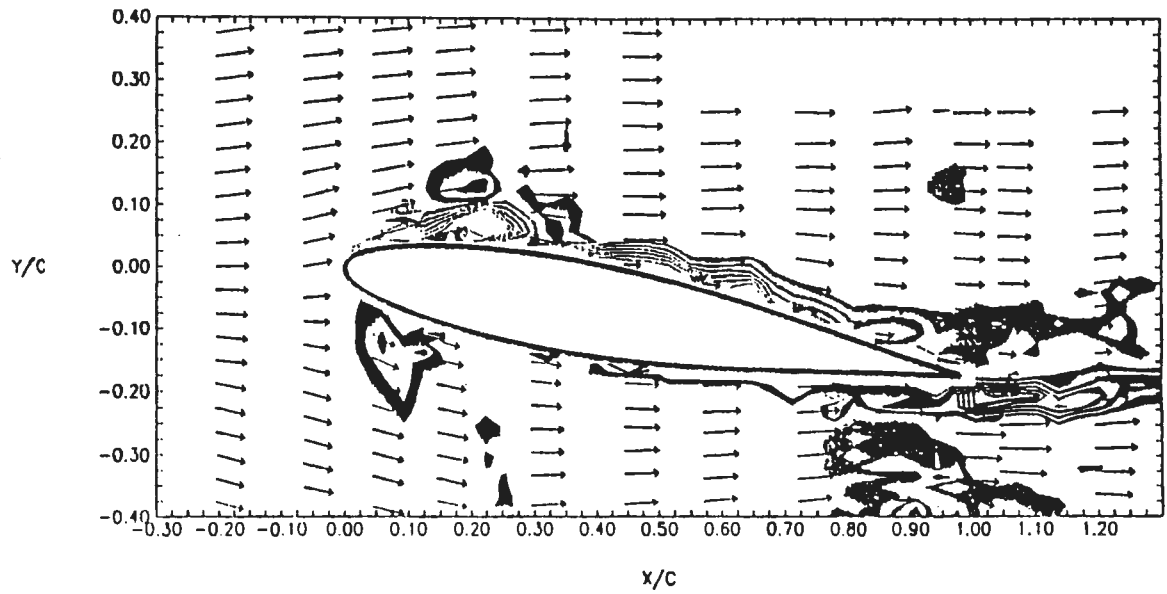


Figure 4.11. continued: (a) $\alpha = 0^\circ$, $\Delta h = 0.09c$ (b) $\alpha = 10^\circ$, $\Delta h = 0.1c$ (c) $\alpha = 10^\circ$, $\Delta h = 0.125c$

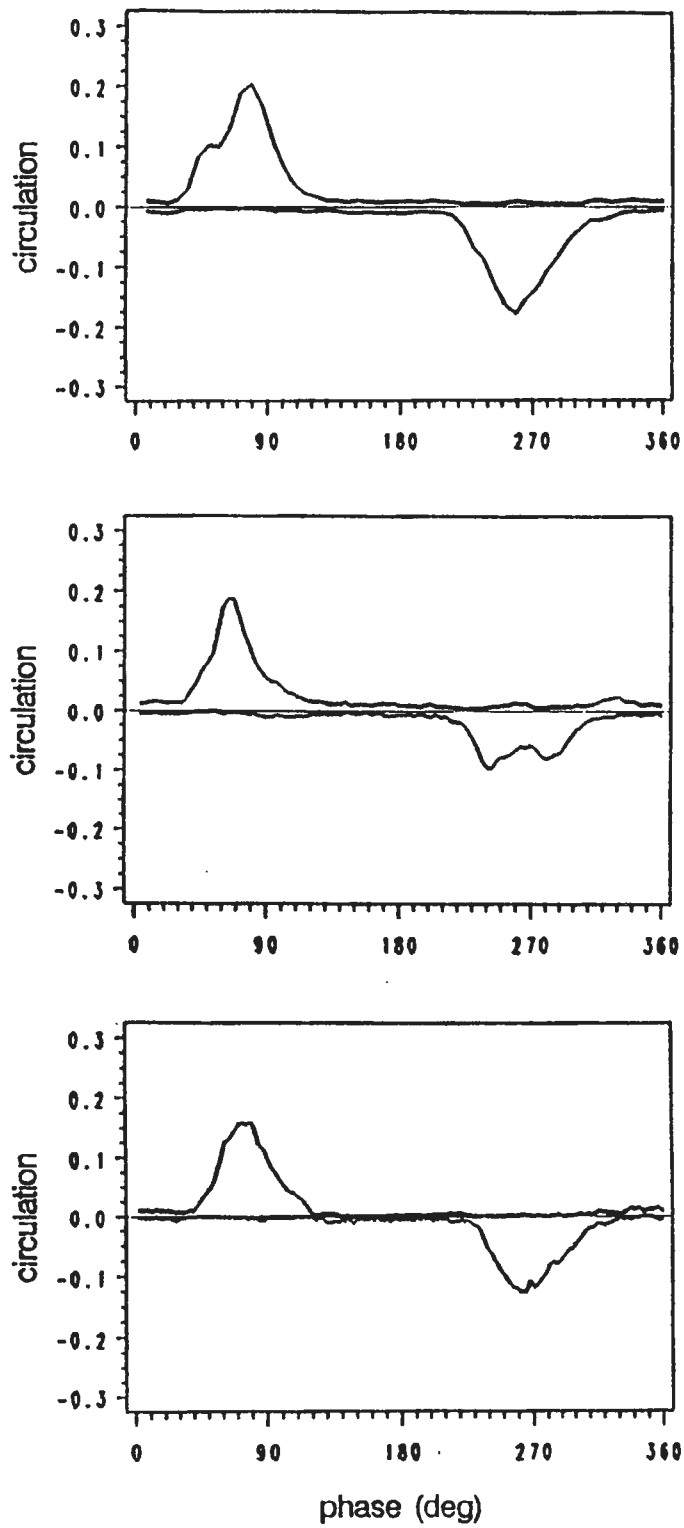


Figure 4.12. Cross-sectional circulation flux: $x/c = -0.2$: (a) $\alpha = 0^\circ$, $\Delta h = 0.09c$ (b) $\alpha = 10^\circ$, $\Delta h = 0.1c$ (c) $\alpha = 10^\circ$, $\Delta h = 0.125c$

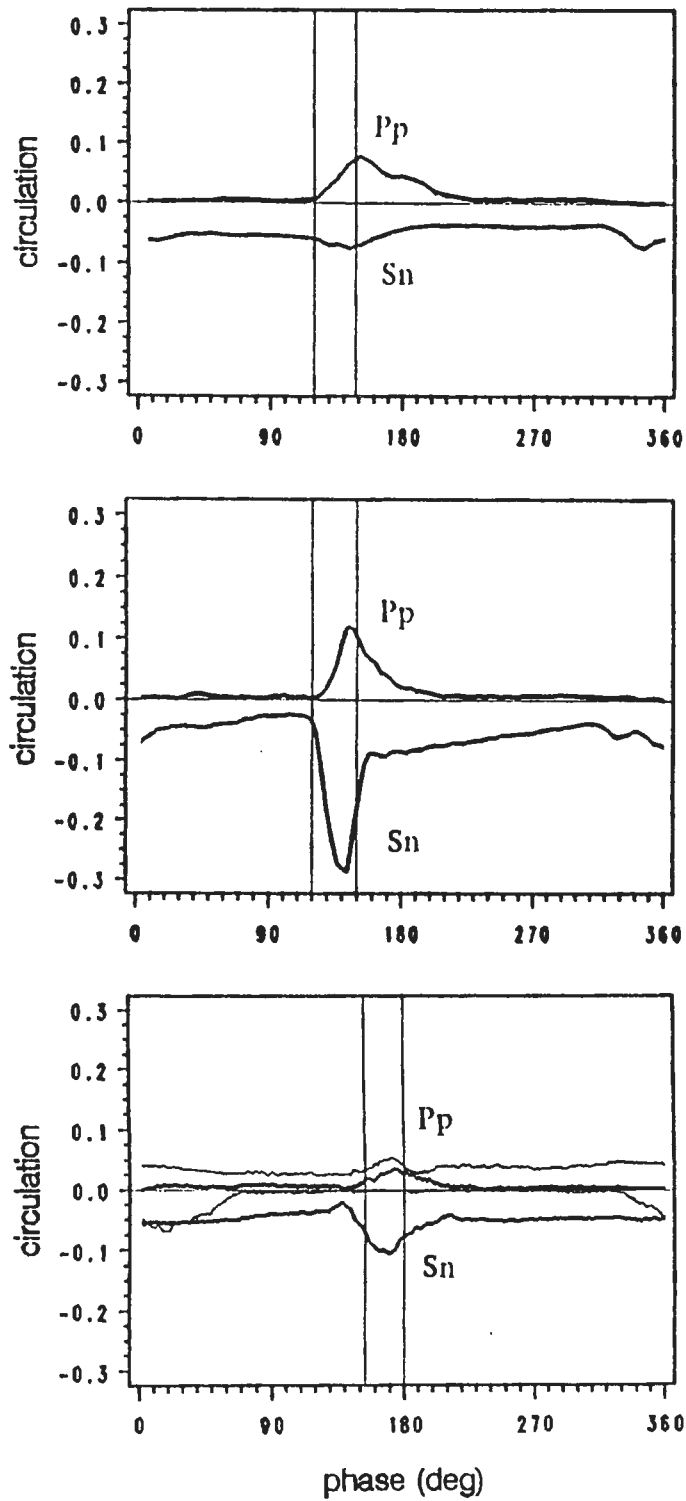


Figure 4.12. continued: $x/c = 0.15$: (a) $\alpha = 0^\circ$, $\Delta h = 0.09c$ (b) $\alpha = 10^\circ$, $\Delta h = 0.1c$ (c) $\alpha = 10^\circ$, $\Delta h = 0.125c$

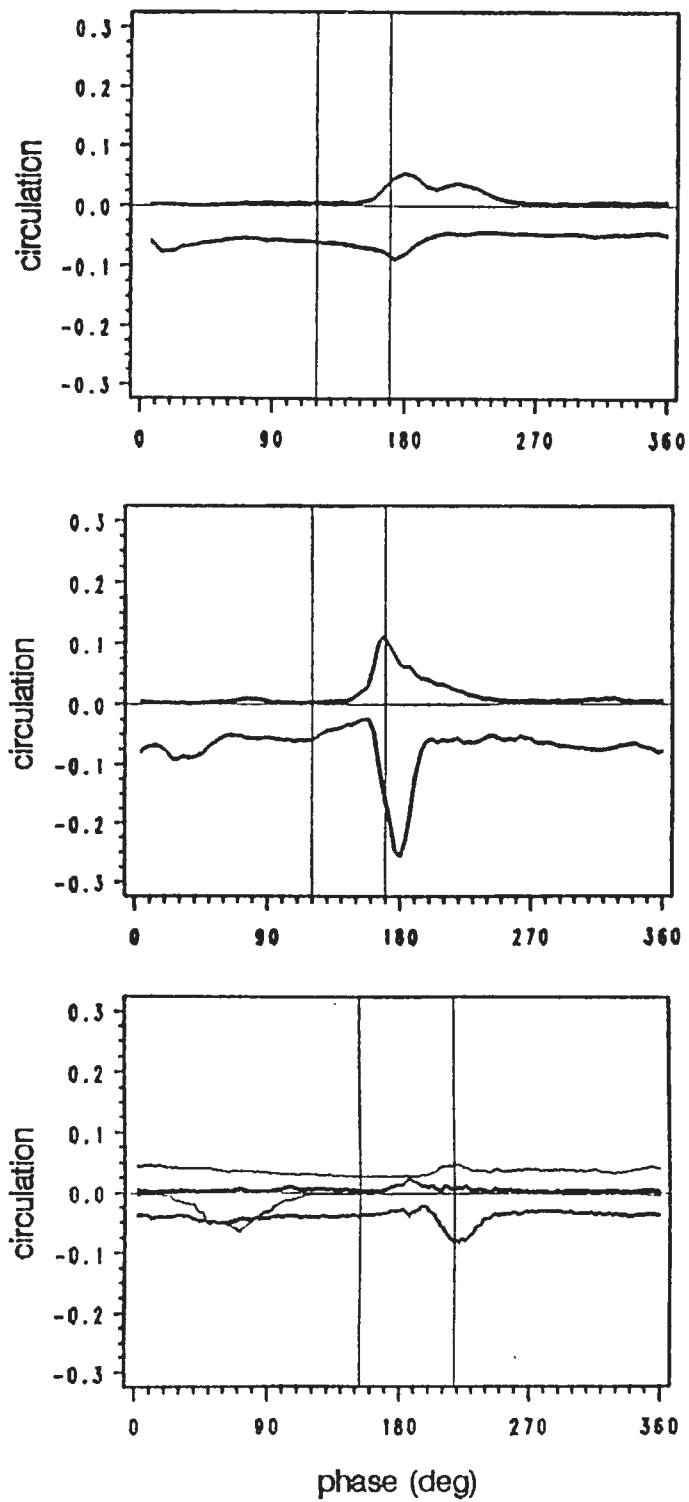


Figure 4.12. continued: $x/c = 0.3$: (a) $\alpha = 0^\circ$, $\Delta h = 0.09c$ (b) $\alpha = 10^\circ$, $\Delta h = 0.1c$ (c) $\alpha = 10^\circ$, $\Delta h = 0.125c$

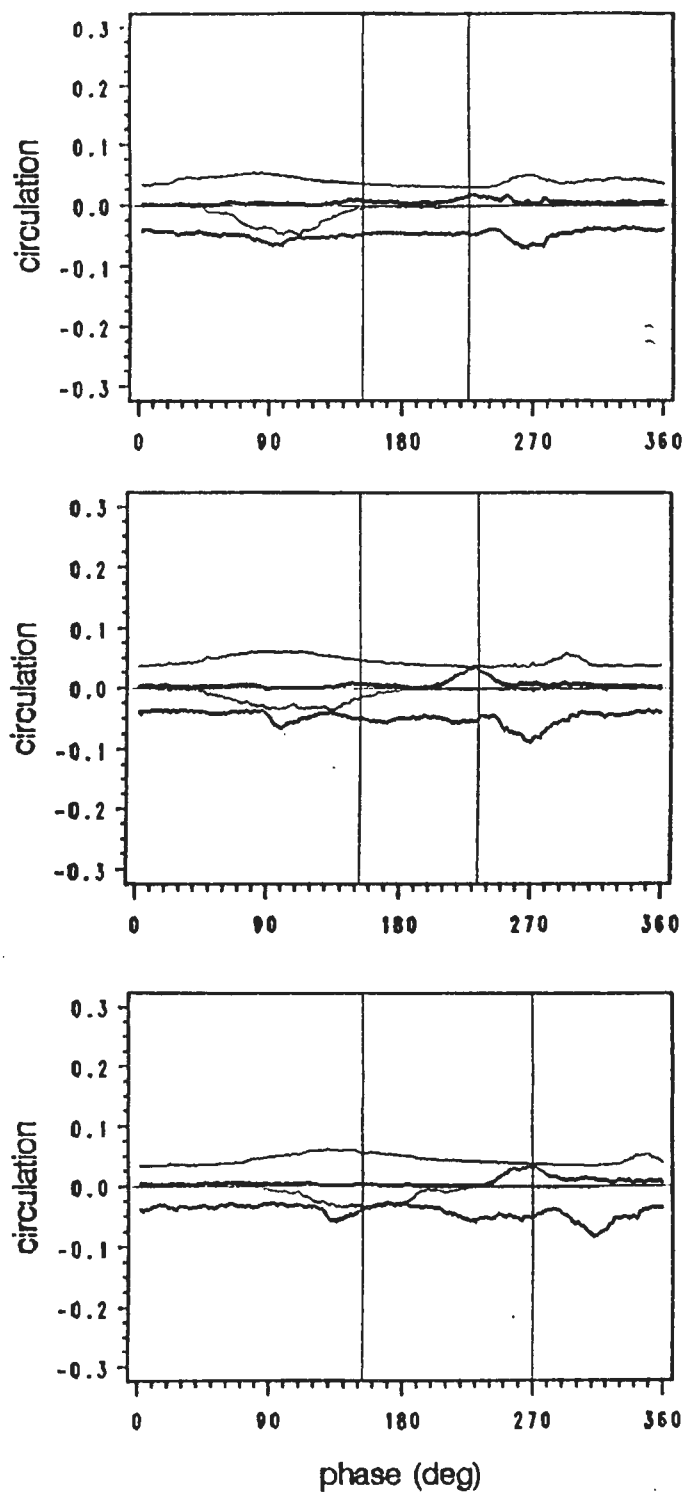


Figure 4.12. continued (case iii only): (a) $x/c = 0.45$ (b) $x/c = 0.575$ (c) $x/c = 0.725$

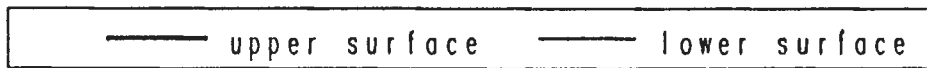
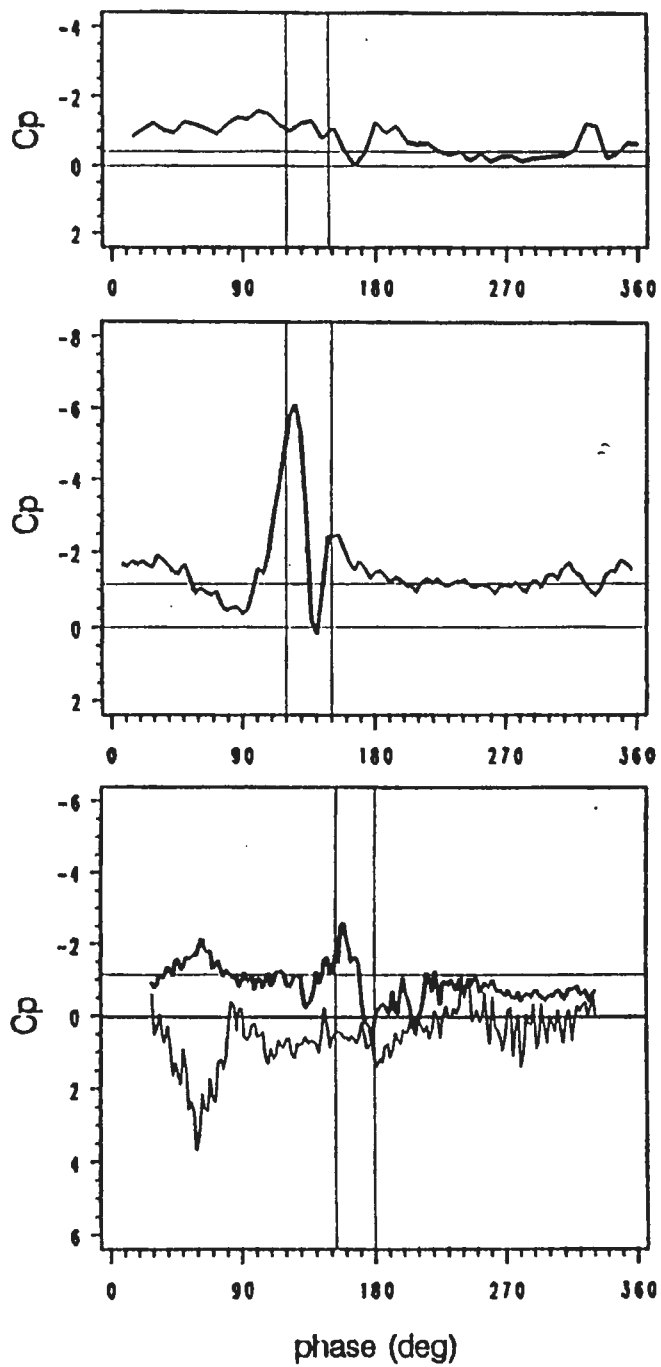
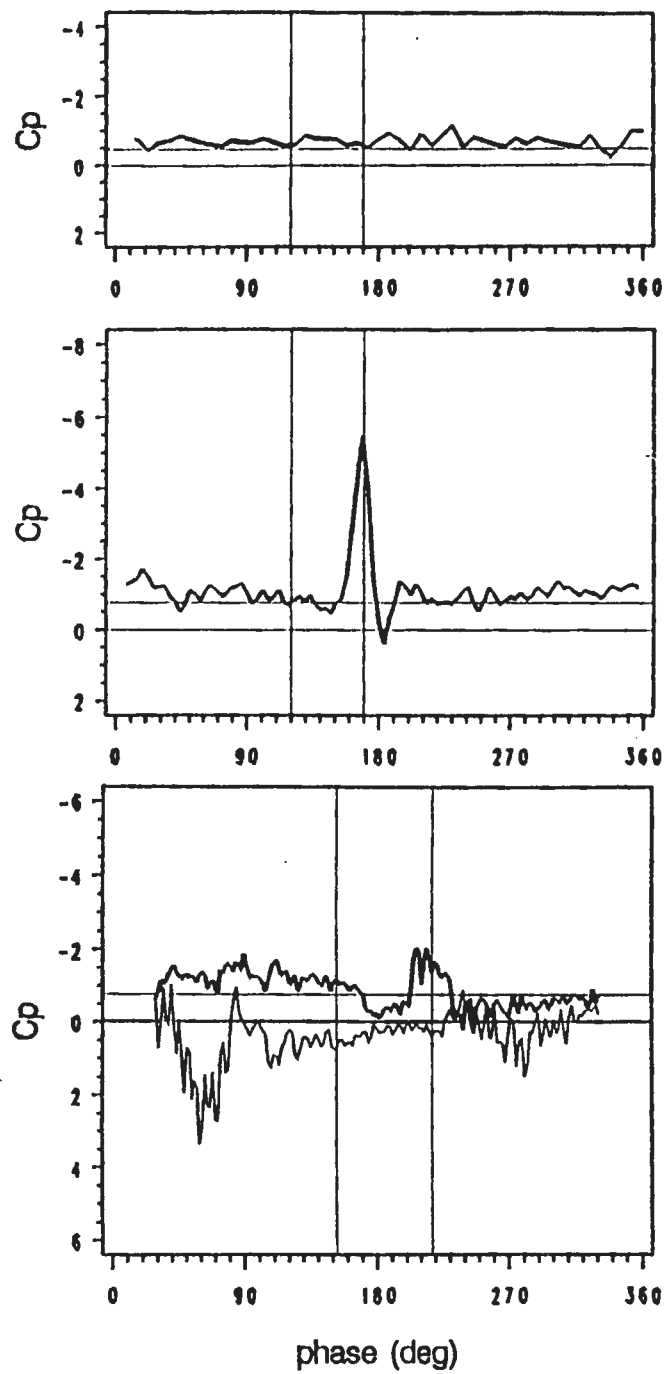


Figure 4.13. continued: $x/c = 0.15$



— upper surface — lower surface

Figure 4.13. continued: $x/c = 0.3$

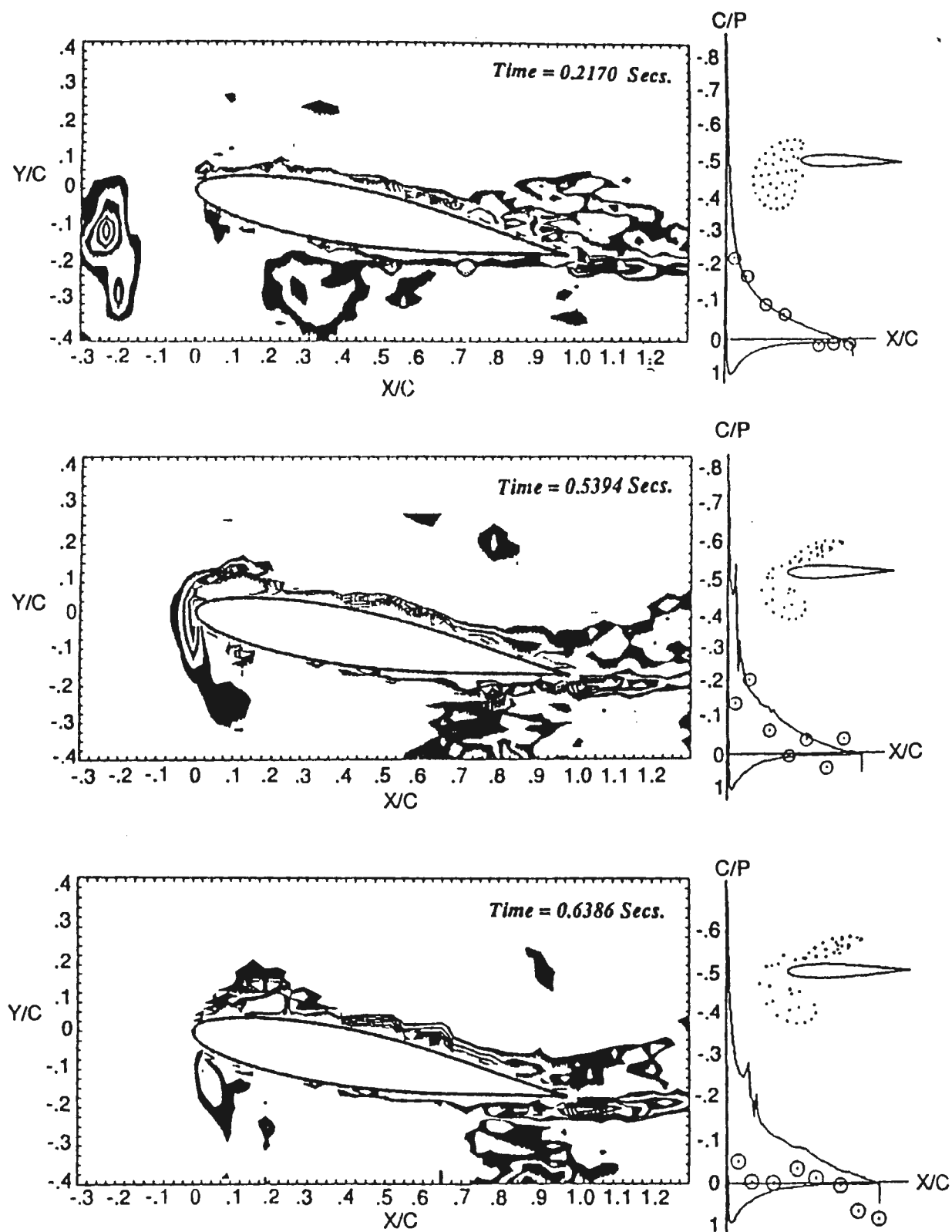
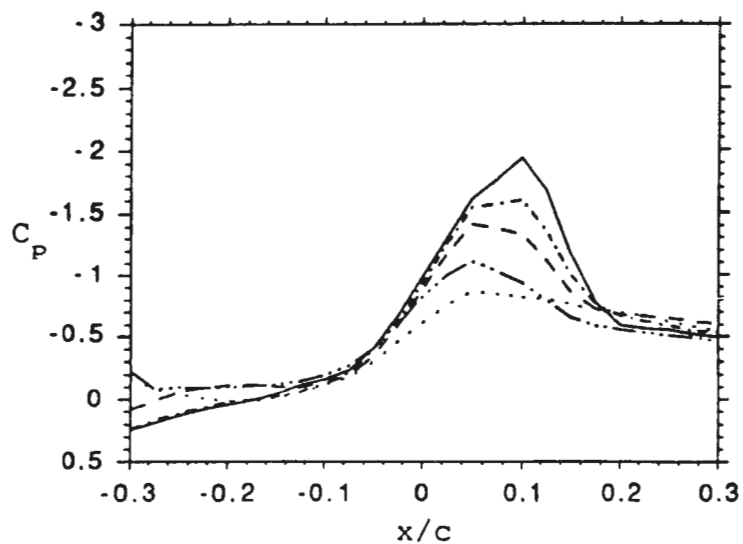
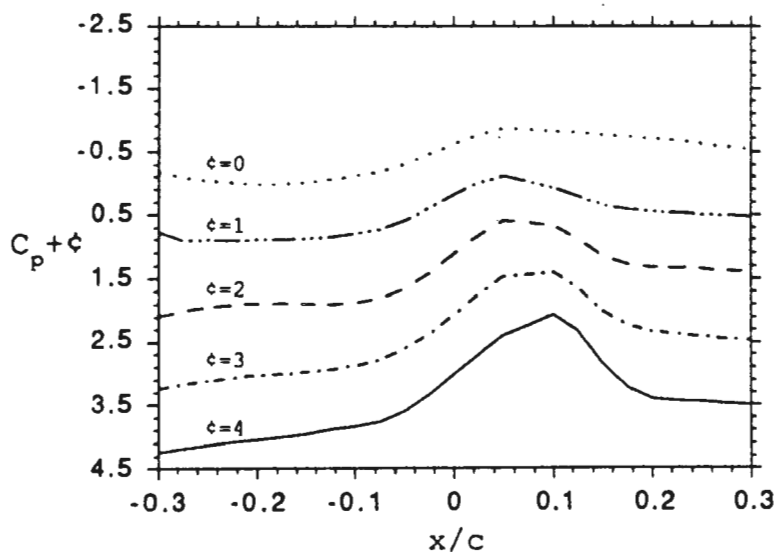
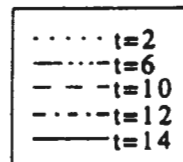


Figure 4.15. Comparison of chordwise pressure distributions with theory: $\alpha = 10^\circ$, source of theory: Poling et al., 1991.



Time Levels



Time Levels

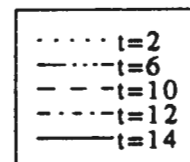


Figure 4.3.76 At $y/c = 0.0625$, pressure coefficients for time levels 2, 6, 10, 12, and 14 are combined. Also, the same curves are shifted by an integer constant.

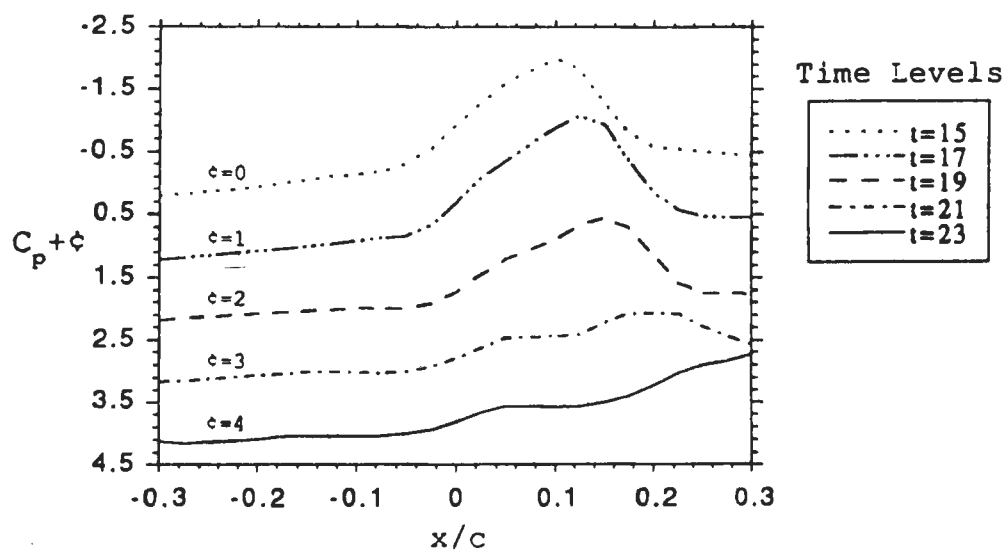
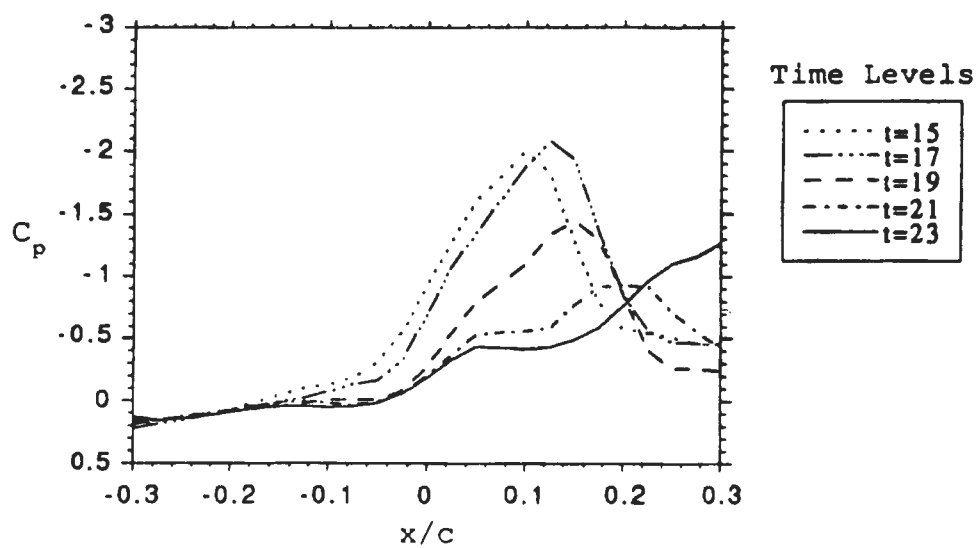


Figure 4.3.77 At $y/c = 0.0625$, pressure coefficients for time levels 15, 17, 19, 21, and 23 are combined. Also, the same curves are shifted by an integer constant.

- **Greatest effects observed for skimming vortex and loaded blade.**
- **Direct impact results in “disintegration” of the vortex.**
- **Coherence of vortex is preserved if secondary vortex is created.**
- **Pressure spikes weaken as vortices drift downstream over the blade.**

)

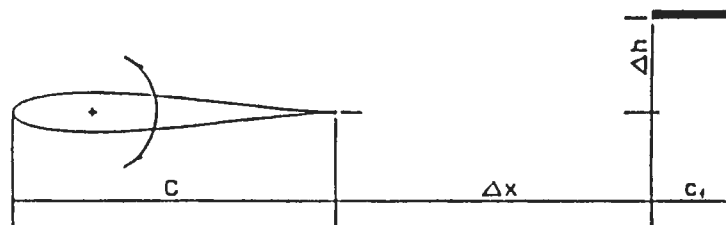


Fig. 1. Profile-plate arrangement.

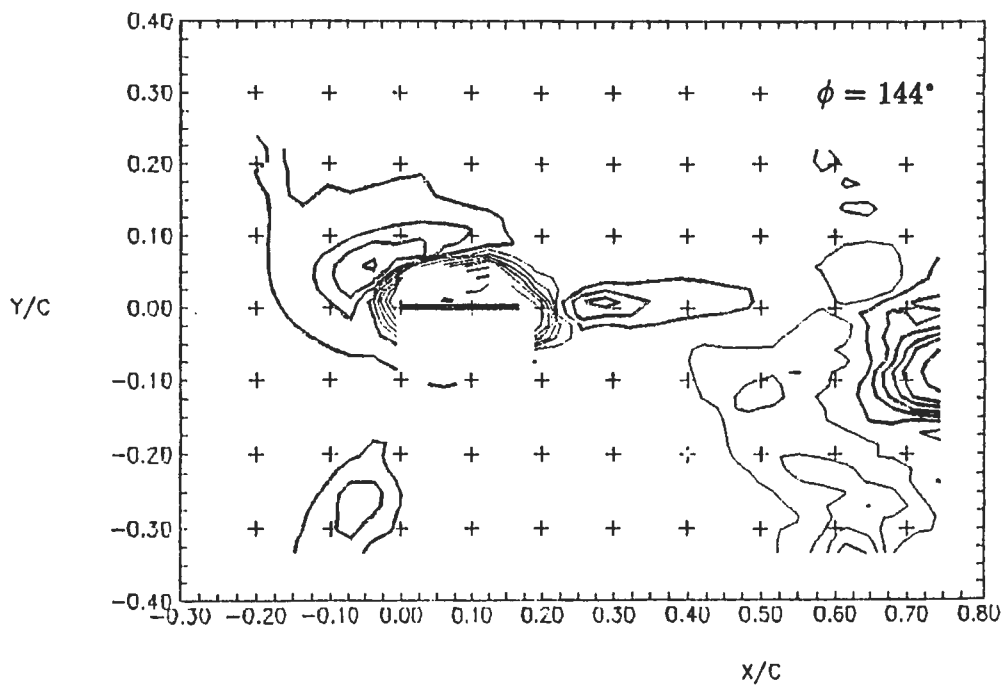
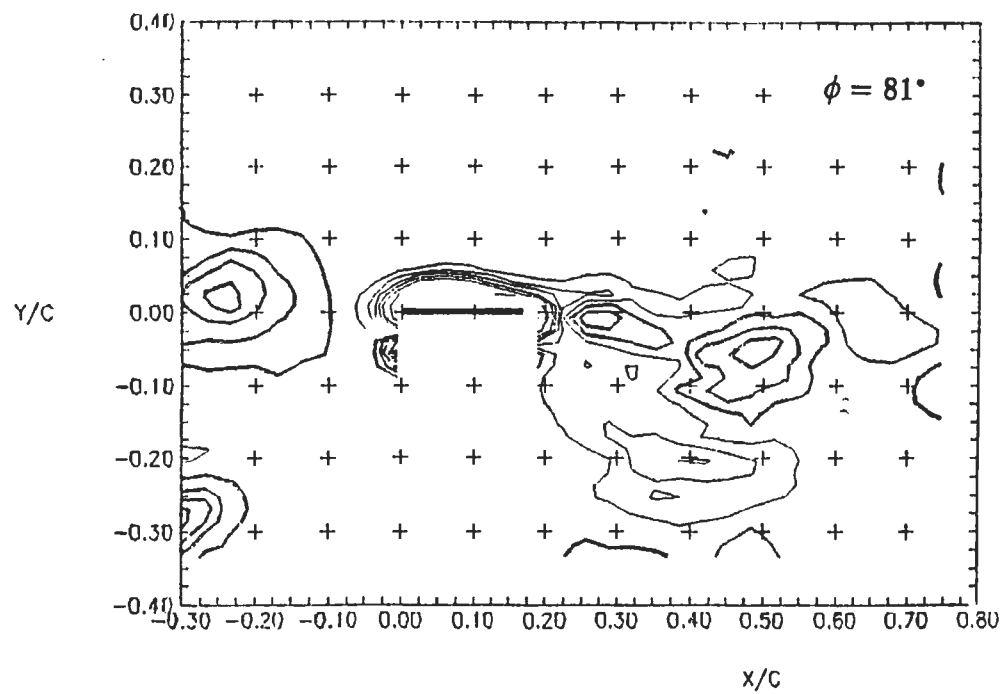


Fig. 5. Vorticity contours for the 25.4 mm plate, $\Delta h = 10$ mm: Phase, $\phi = \frac{t}{T} \cdot 360^\circ$. Thick and thin lines represent positive (counterclockwise) and negative vorticity respectively. The levels in positive and negative contour lines correspond to dimensionless values of 2,6,10,15,20,30 and 50 starting from the open domain. Spatial uncertainty estimate of contours: ± 0.01 C in both directions.

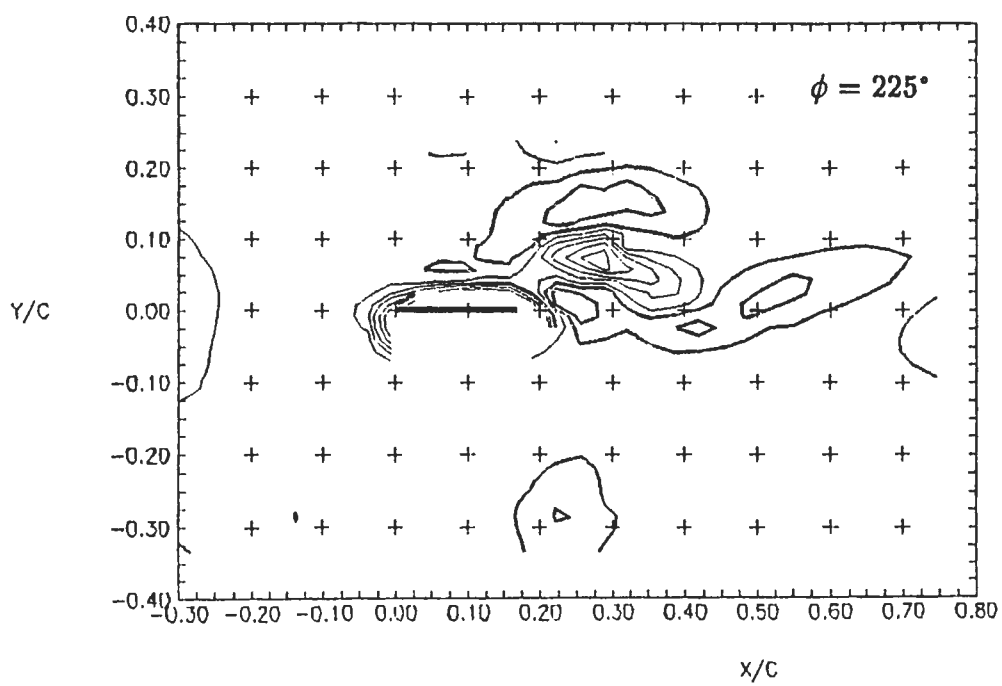
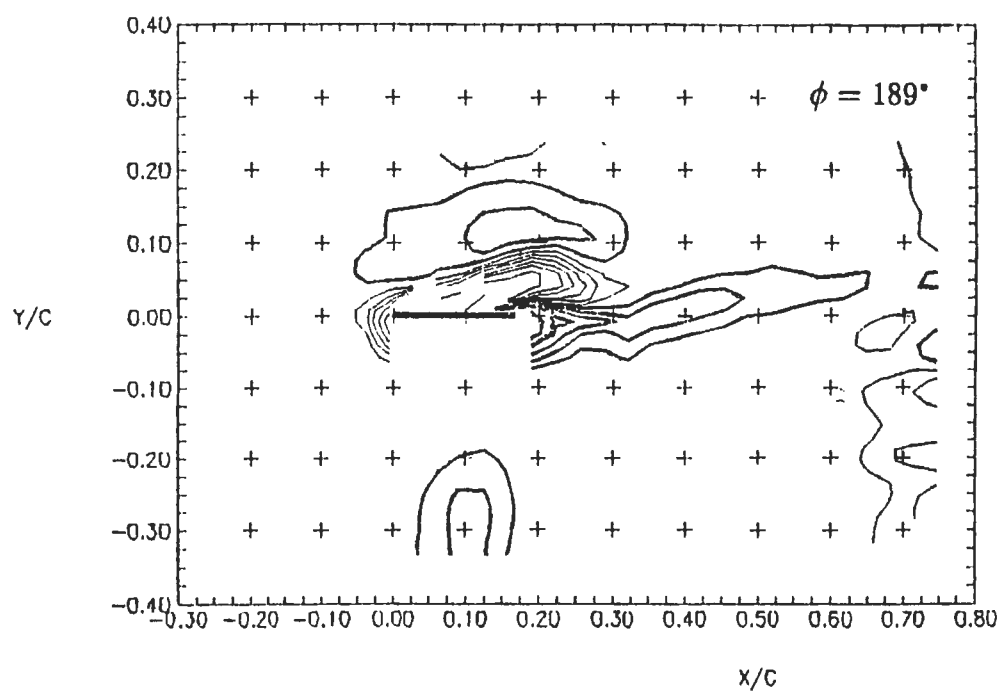


Fig. 5. Continued

- **Smaller plates are more effective vortex “choppers.”**
- **Secondary vortex could be more powerful than primary**
- **Plates with rounded rather than sharp edges are more effective.**

II-3. High Resolution Vortex Simulations of Bluff Body Flows

**Anthony Leonard
California Institute of Technology**

NUWC Division Newport, R. I.

SEMINAR NOTICE

HIGH RESOLUTION VORTEX SIMULATIONS OF
BLUFF BODIES

Professor A. Leonard

California Institute of Technology

The main theme of this ongoing research is to study the vortex dynamics of bluff body flows and the relation of these dynamics to the unsteady forces experienced by the body. In addition, means of controlling these forces and dynamics are being explored. Our computational approach is to use discrete representations of the vorticity transport equation, a form of the Navier-Stokes equations for incompressible flows. In particular, computational elements of vector-valued vorticity are convected with the local fluid velocity and the vorticity vector associated with an element is continually strained by the local velocity gradient. A mix of improvements to the usual vortex method were implemented for these studies, including a fast vortex algorithm and improved treatment of viscous effects. In two-dimensions, unsteady, separated flows past a flat plate, nominally at 90 degrees angle of attack, and past a cylinder are investigated, using a Cray-YMP. Comparison with tow-tank experiments is made. For the three-dimensional work we use the Intel Delta parallel computer. Extension of the the viscous technique to three-dimensional flows in the presence of arbitrarily-shaped solid bodies is complete and implementation of this extension with a fast three-dimensional vortex algorithm on the Delta to study, for example, the unsteady pitching and yawing of a three-dimensional bluff body is nearly complete.

Friday, 18th June 1993

Conference Room, Bldg. 679

Time: 10:30 AM

POC: Dr. Promode R. Bandyopadhyay (Code 8234; x2588)

18 June 1993

High Resolution Vortex Simulations of Bluff Body Flows

A. Leonard
Graduate Aeronautical Laboratories
California Institute of Technology, Pasadena, CA 91125

Physical Theory

Navier-Stokes Equations, Vorticity Transport Equation, Vortex Dynamics, Surface Generation of Vorticity, Viscous Transfer, Body Forces and Moments

Numerical Techniques

Vortex Particles, Remeshing, Panel Method, Particle-Particle Circulation Exchange, Panel-Particle Transfer

Parallel Implementation

Fast Algorithm, Error Control, Data Structure, Load Balancing

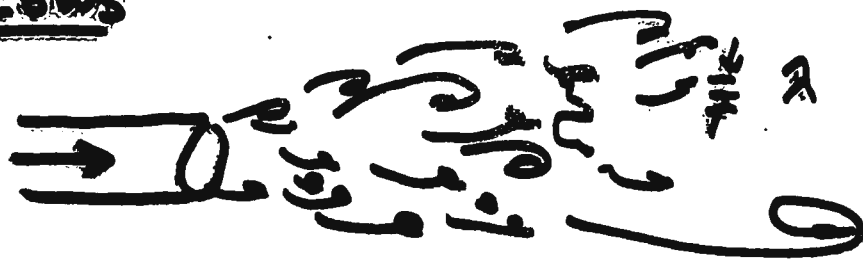
Turbulence

Subgrid-scale Modeling, Transition to Turbulence

Applications

Cylinder, Sphere, Prolate Spheroid,.....

Flows



Vorticity Eqn

$$\frac{\partial \underline{\omega}}{\partial t} + \underline{u} \cdot \nabla \underline{\omega} = \underline{\omega} \cdot \nabla \underline{u} + \nu \nabla^2 \underline{\omega}$$

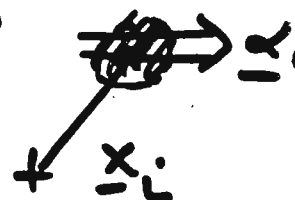
$$\nabla^2 \underline{u} = -\nabla \times \underline{\omega}$$

Computational Elements

$$\underline{\omega}(\underline{x}, t) = \sum_{i=1}^N \alpha_i(t) \gamma(\underline{x} - \underline{x}_i(t))$$

$$\frac{d\underline{x}_i}{dt} = \underline{u}(\underline{x}_i, t)$$

$$\frac{d\alpha_i}{dt} = (\alpha_i \cdot \nabla) \underline{u} \Big|_{\underline{x}=\underline{x}_i}$$



classical - $O(N^2)$

Fast - $O(N \log N)$

Vortical Flows



2D Vorticity Equation ($\omega \hat{e}_z = \nabla \times \underline{u}$)

$$\underbrace{\frac{\partial \omega}{\partial t} + \underline{u} \cdot \nabla \omega}_{\text{vorticity moves with fluid}} = \omega \nabla^2 \omega$$


vorticity moves with fluid

$$\underbrace{\nabla^2 \underline{u} = -\nabla \times (\omega \hat{e}_z)}_{\downarrow}$$

$$\underline{u} = -\frac{1}{2\pi} \int \frac{(\underline{x} - \underline{x}') \times \hat{e}_z \omega(\underline{x}') d\underline{x}'}{|\underline{x} - \underline{x}'|^2}$$

Vortex Method - N computational elements

$$\omega(\underline{x}, t) = \sum_i^N \Gamma_i \delta(\underline{x} - \underline{x}_i(t))$$

$\Gamma_i = \text{const} = \text{circulation}$ 

$$\frac{d\underline{x}_i}{dt} = \sum_j^N \frac{\Gamma_j (\underline{x}_i - \underline{x}_j) \times \hat{e}_z}{|\underline{x}_i - \underline{x}_j|^2} \delta(\underline{x}_i - \underline{x}_j)$$

Numerical Studies

VORTEX METHODS

I. Classical Vortex Method

N^2 algorithm

$10^3 - 10^4$ elements - CRAY

II Very Few Vortices

1 element per large structure

$O(10^1)$ elements

III High Resolution Viscous Method

$O(N)$ Fast Algorithm

Navier-Stokes / Accurate Viscous
Effects

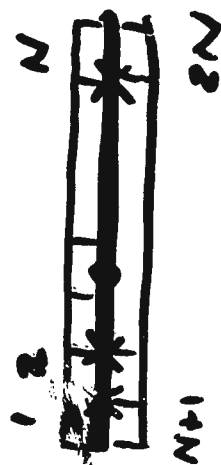
$10^5 - 10^6$ elements - CRAY

$10^6 - 10^7$ elements Intel Delta

2D & 3D

Separated flow past normal flat plate

U_∞ 



$$\times (u_n = 0) \quad n=1$$

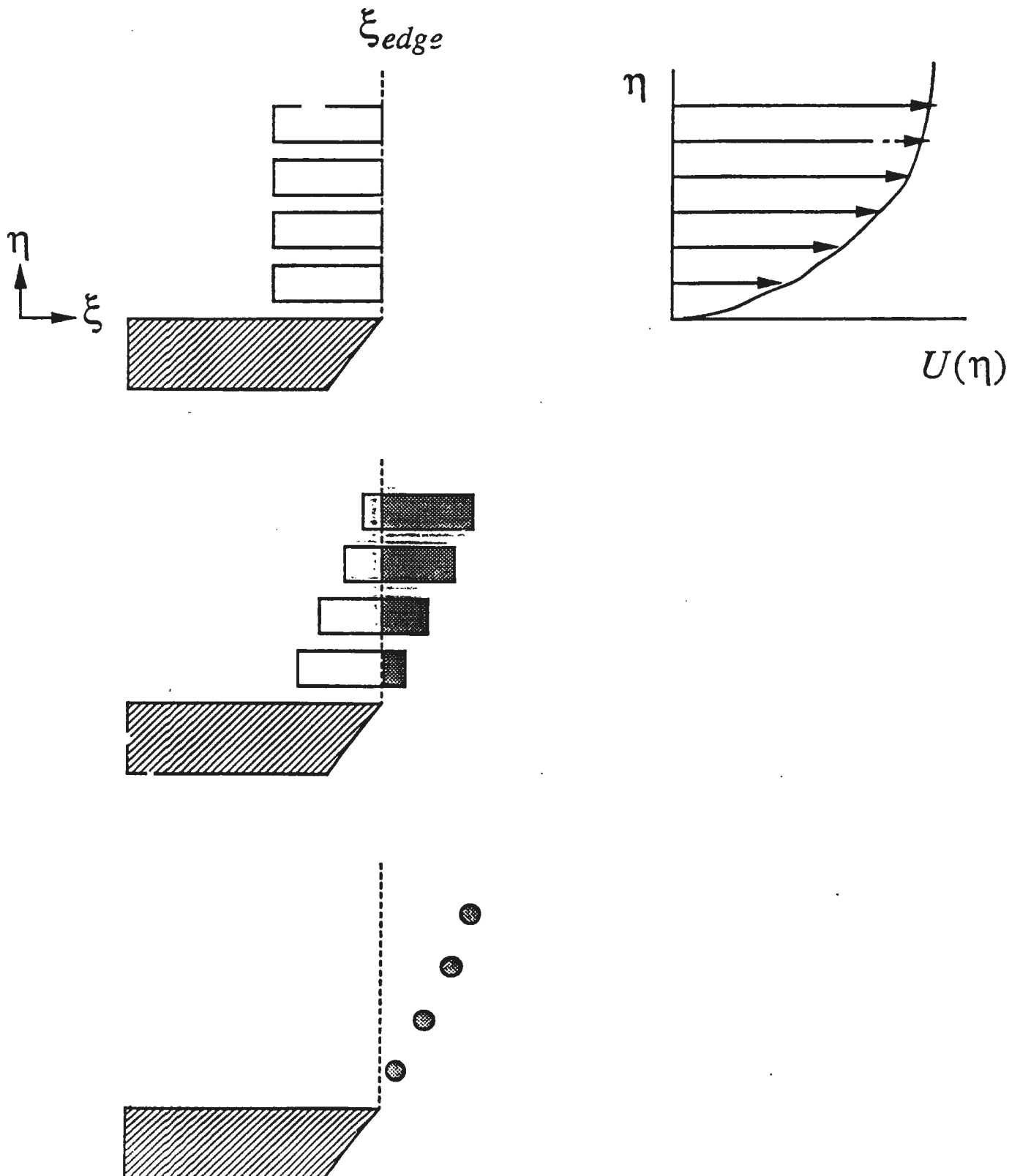
$$\bullet (u_t = 0) \quad N$$

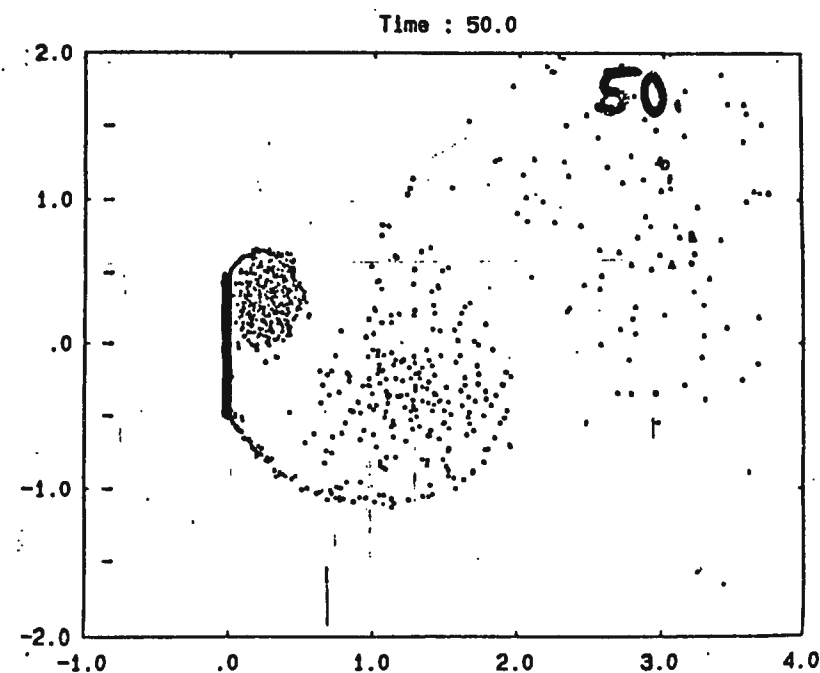
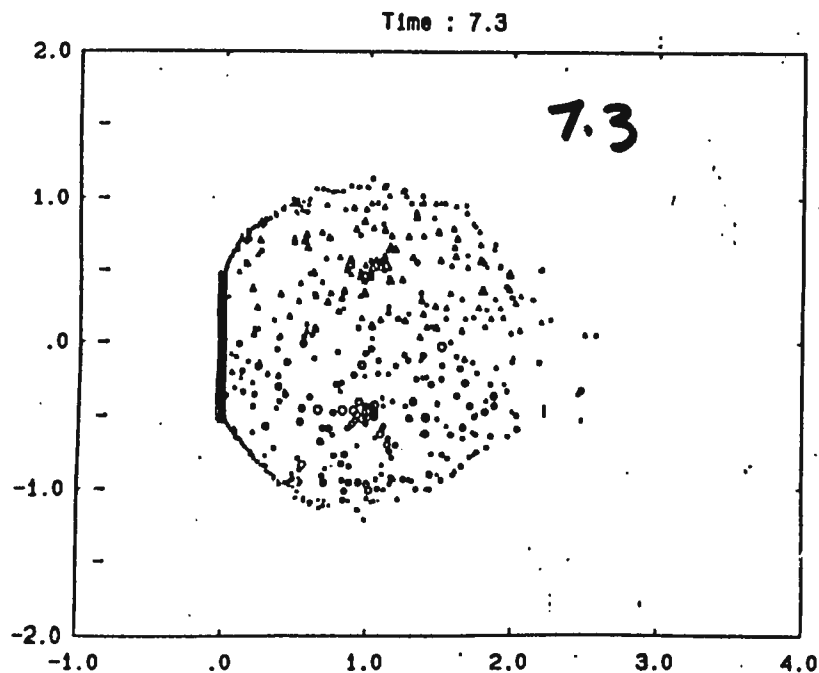
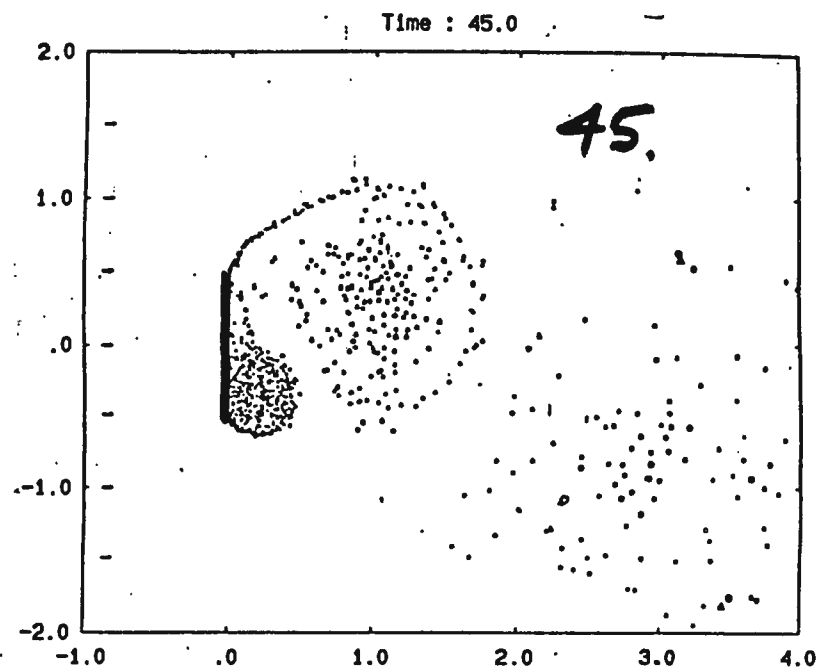
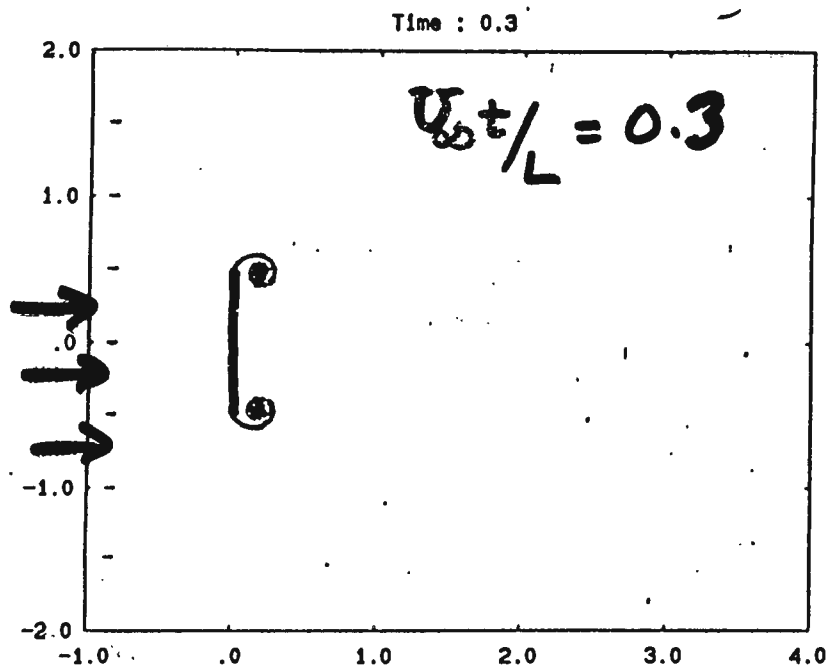
and

$$\sum \Gamma_i + \sum \Gamma_i = 0$$

panels wake

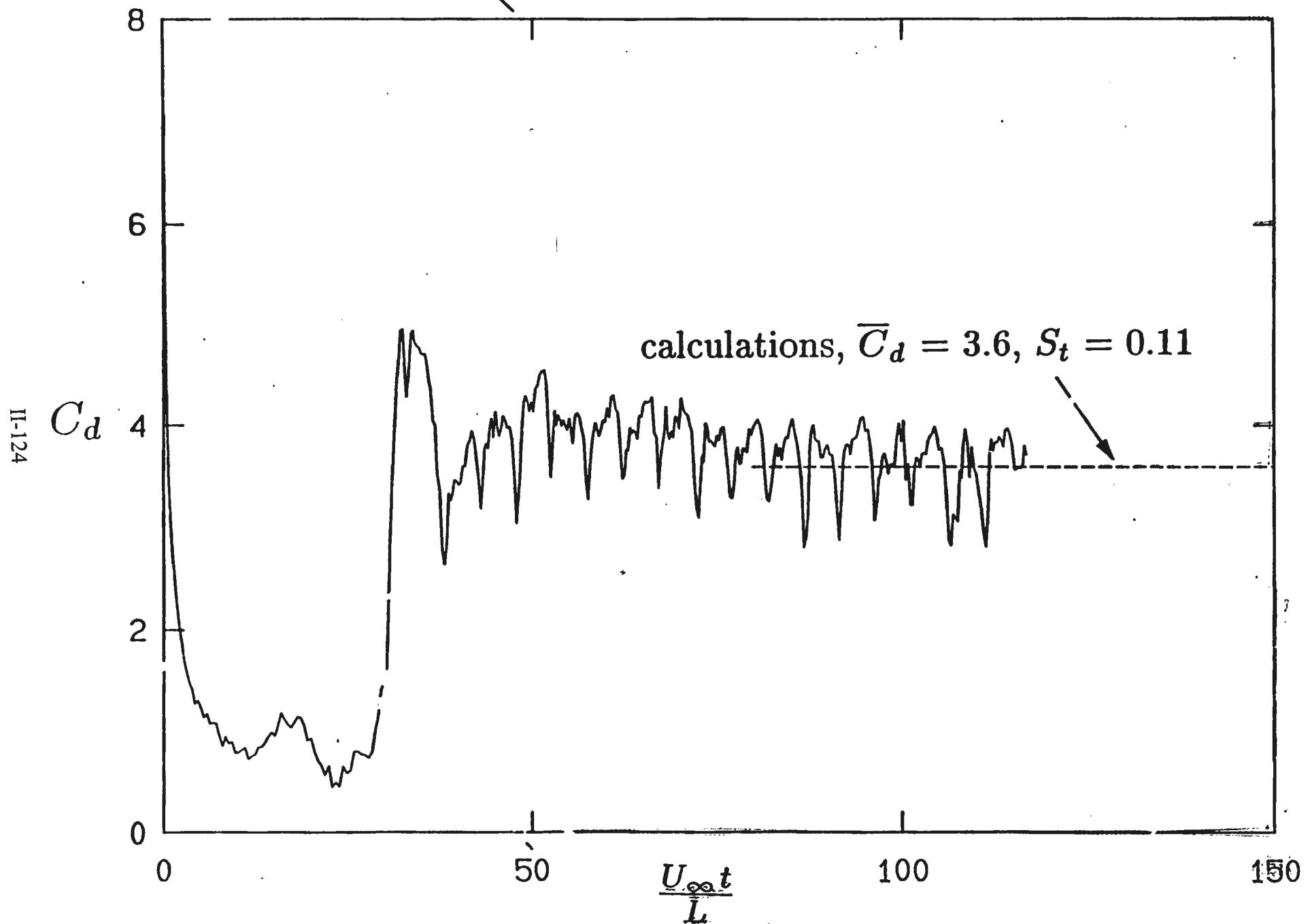
Vorticity shedding model



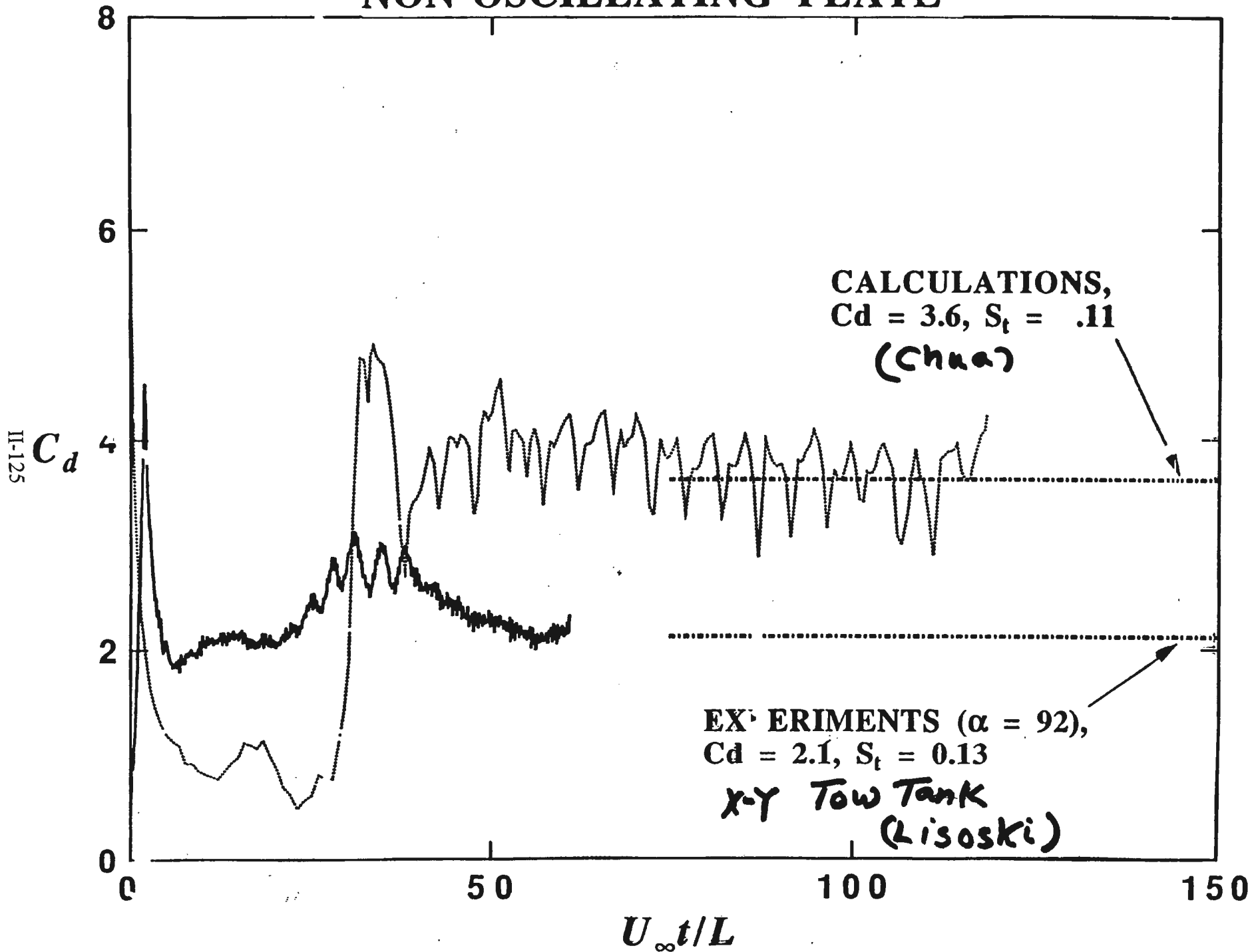


Classical Method, $O(N^2)$, $N \sim 10^3$, Fixed Separation Points

Drag history of non-oscillating plate (impulsive start)

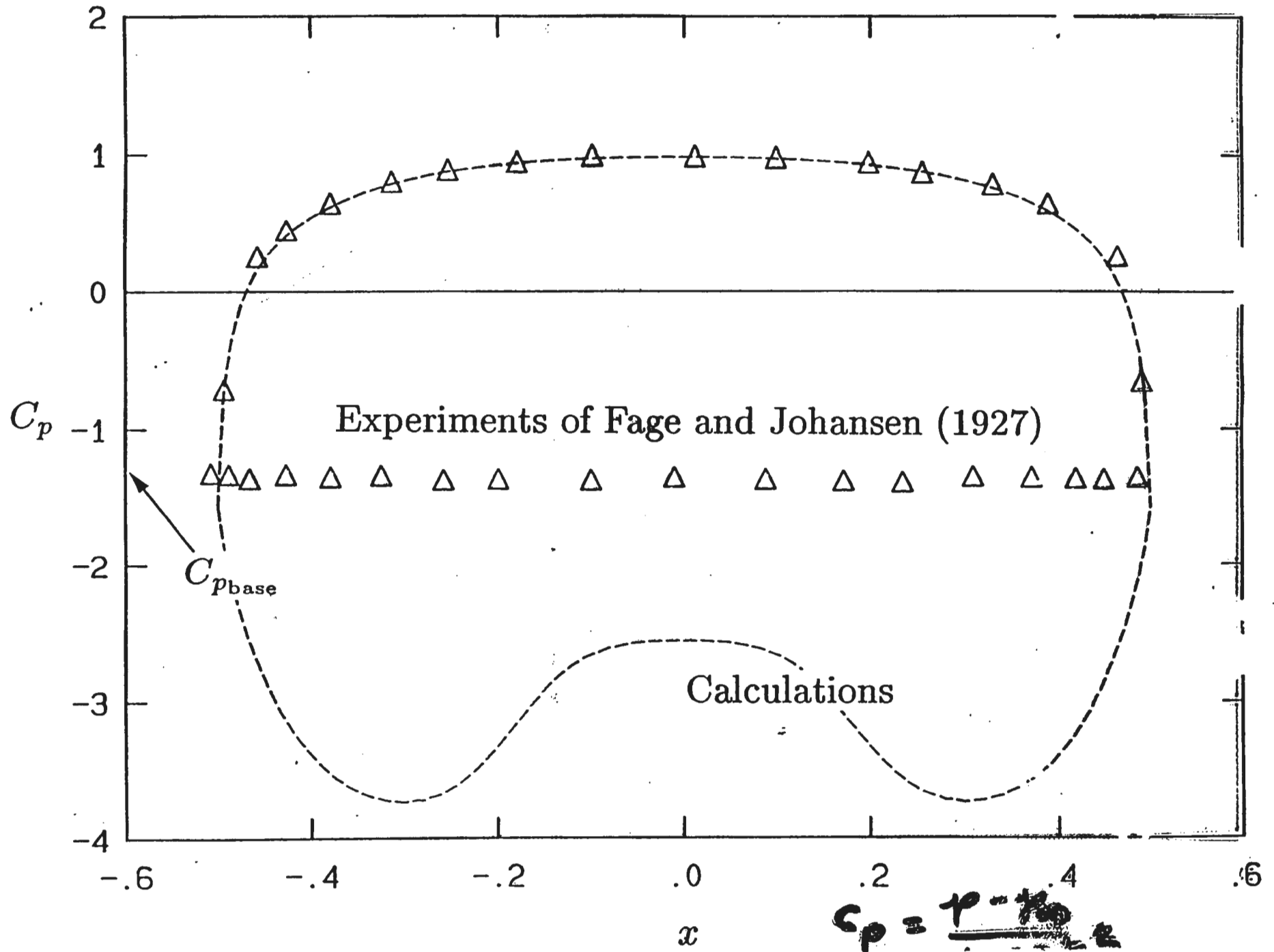


NON-OSCILLATING PLATE



Comparison of C_p to Experiments

II-126



Verification

- Starting vortices - Analytical solution

(Rott 1956, Pullin 1978)

- Recirculating bubble - Experiments

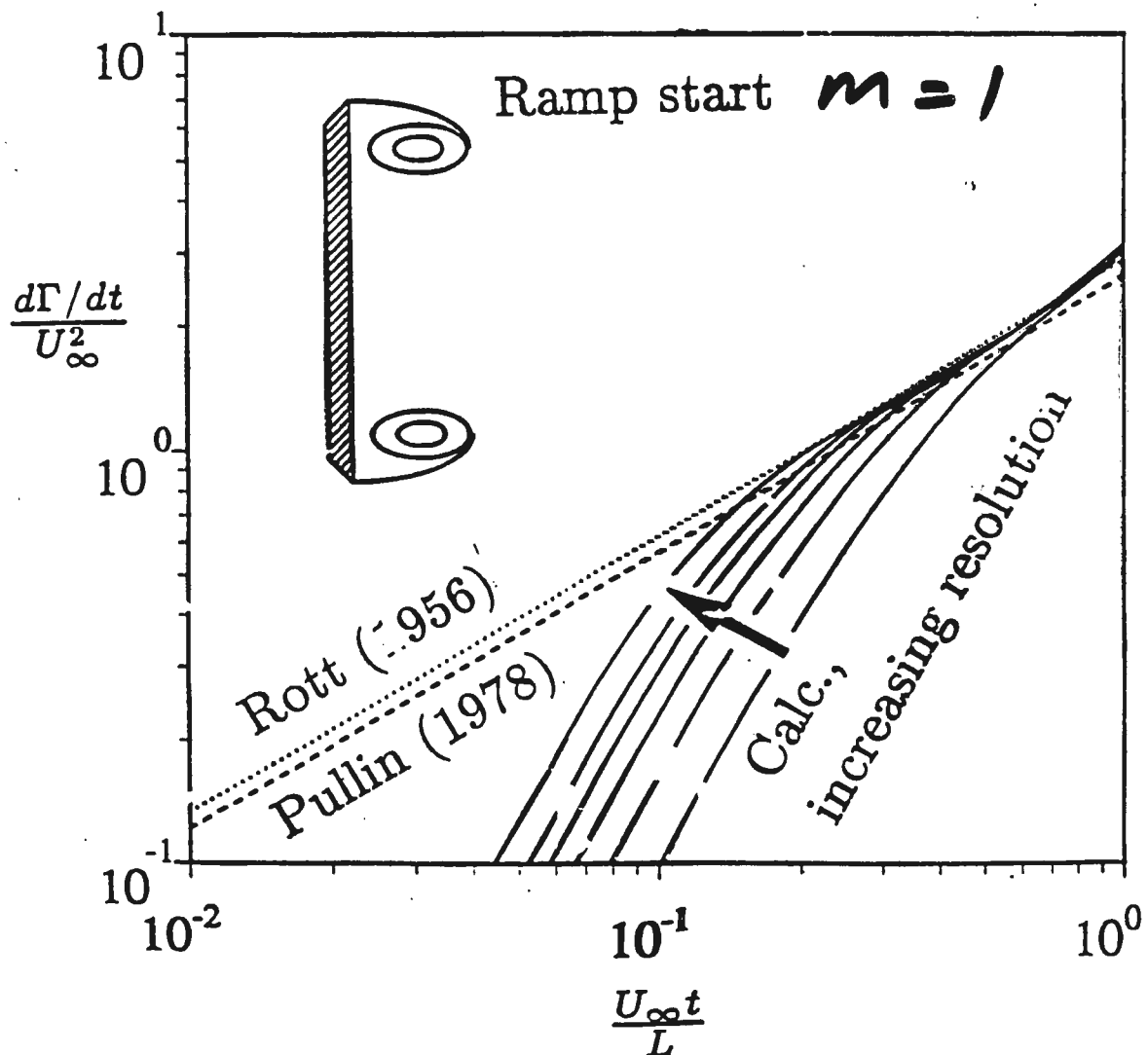
(Taneda and Honji 1971)

- Ramp-start flow - Current experiments

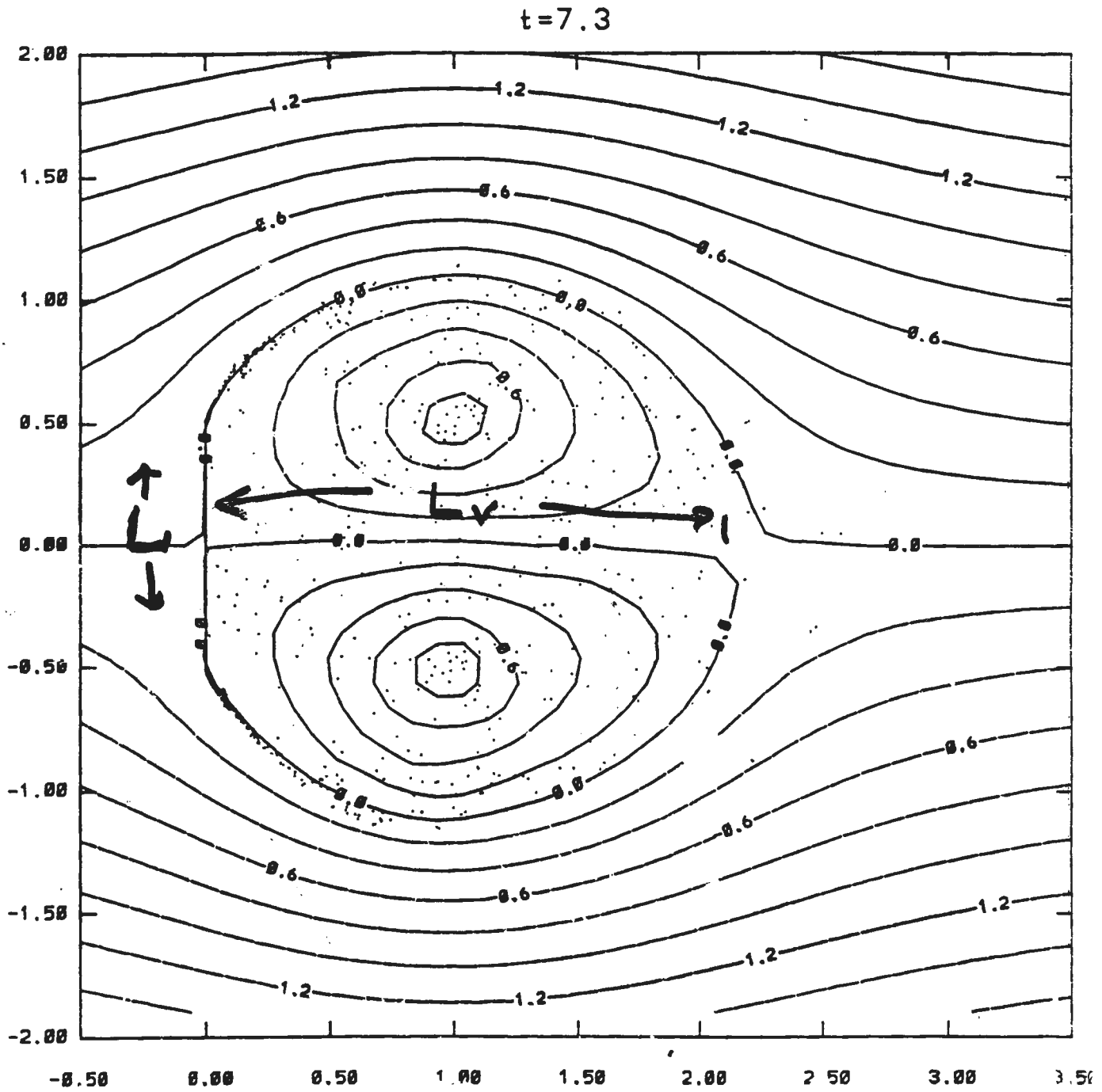
$$U(t) = U_\infty t^{1/3}$$

$$\Rightarrow \Gamma(t) = C U_\infty^{2/3} t^{4/3}$$

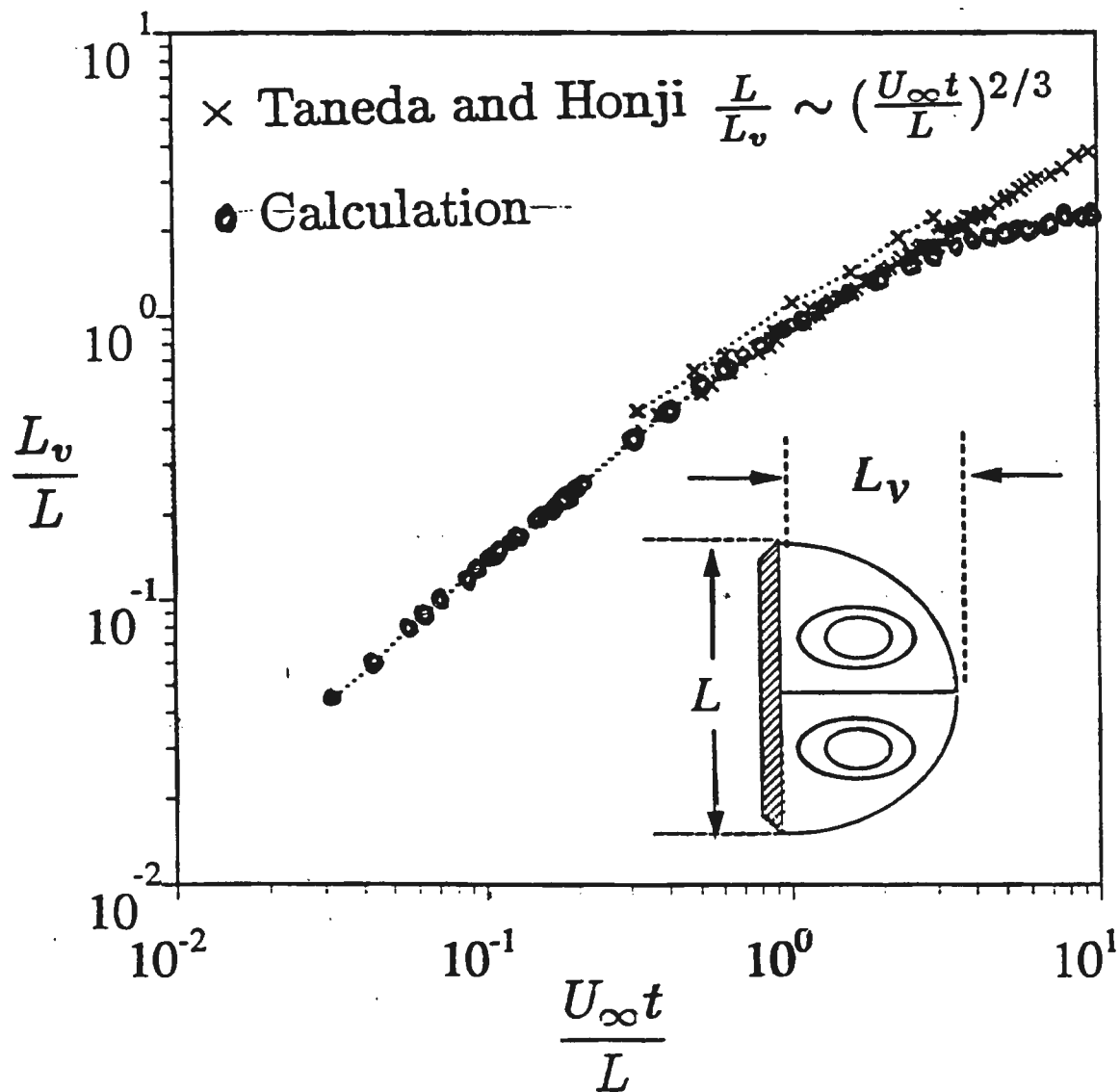
Comparison of circulation flux to analytical solution



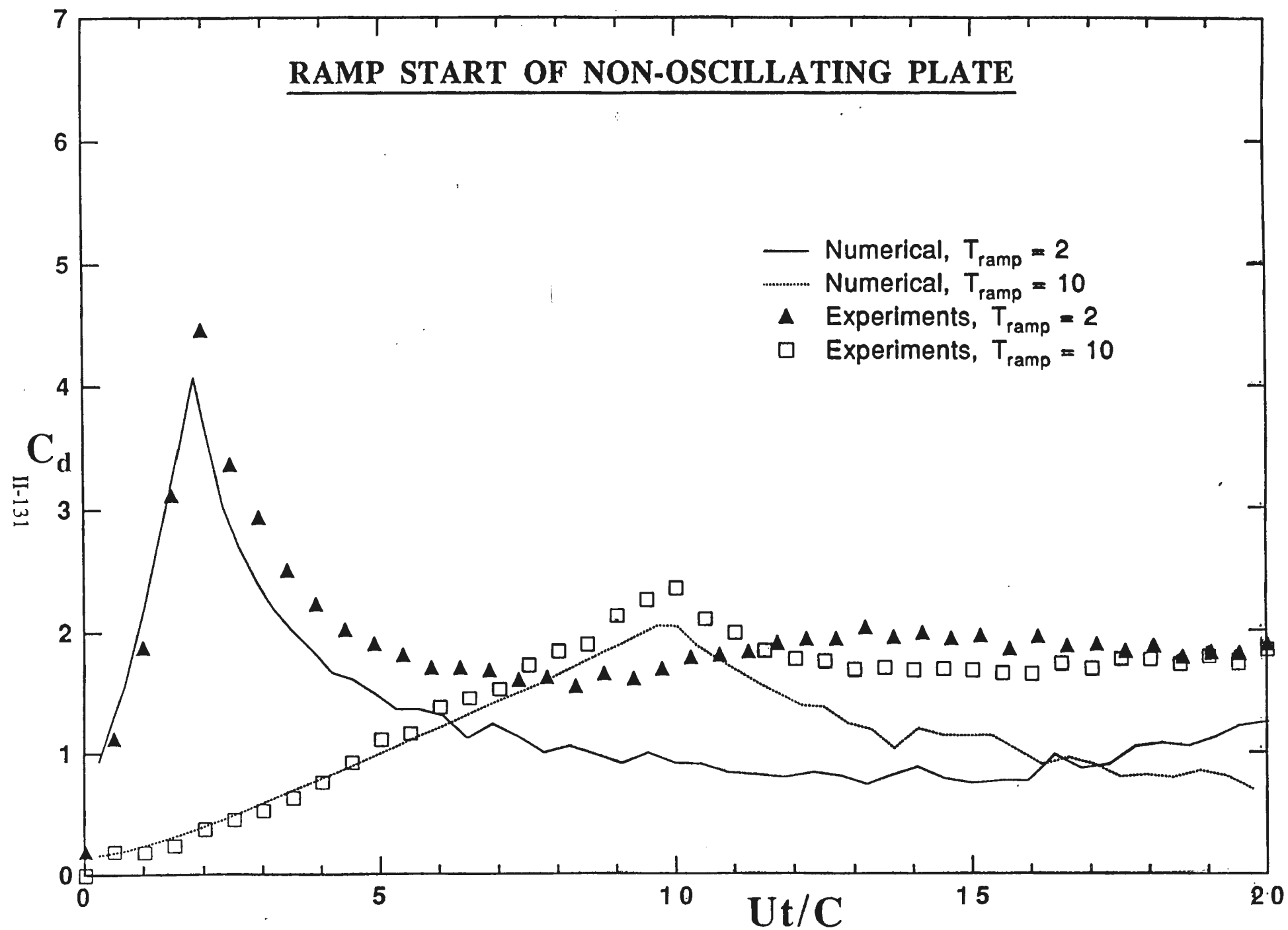
(Chua)



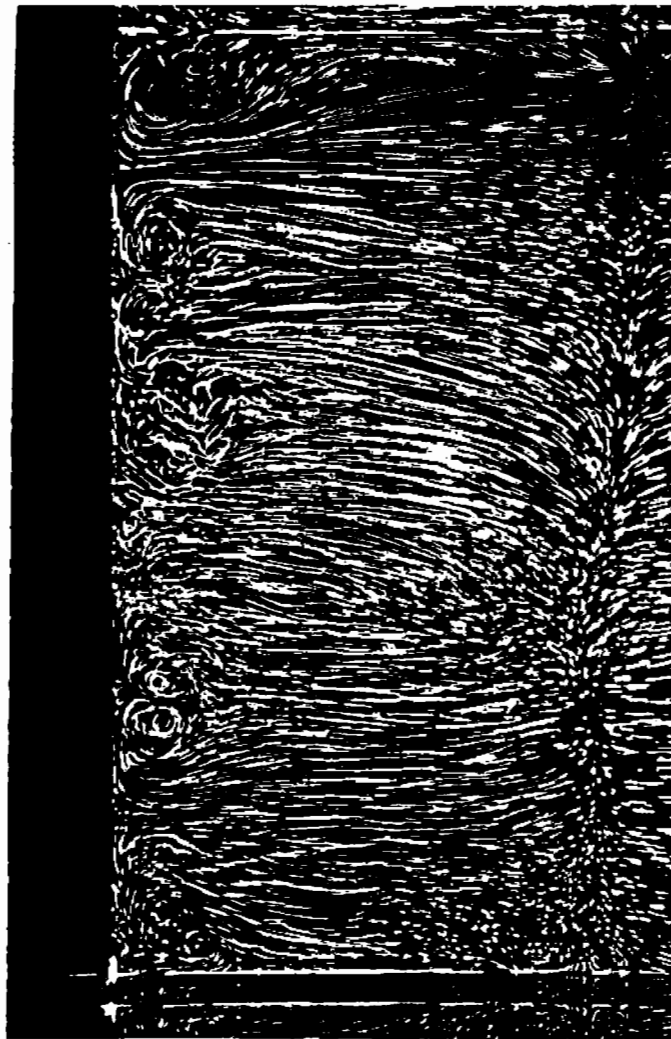
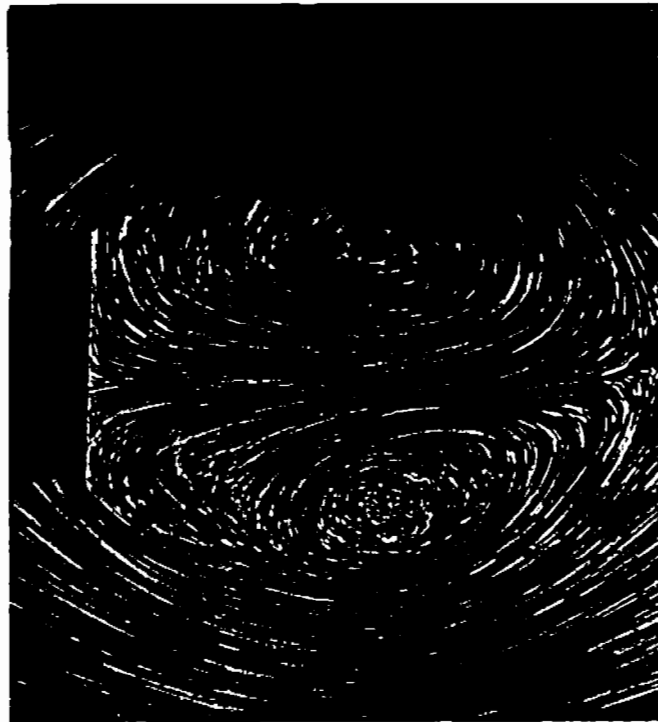
Comparison of $\frac{L_v}{L}$ to experiments



RAMP START OF NON-OSCILLATING PLATE

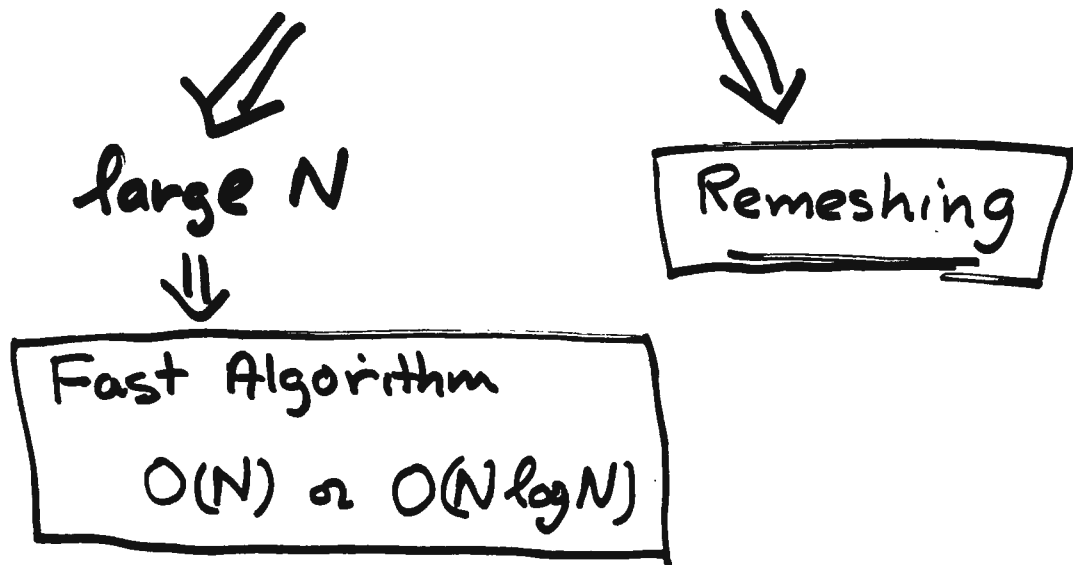


FLOW ABOUT A 2-D FLAT PLATE
(Naca & Rosinke)

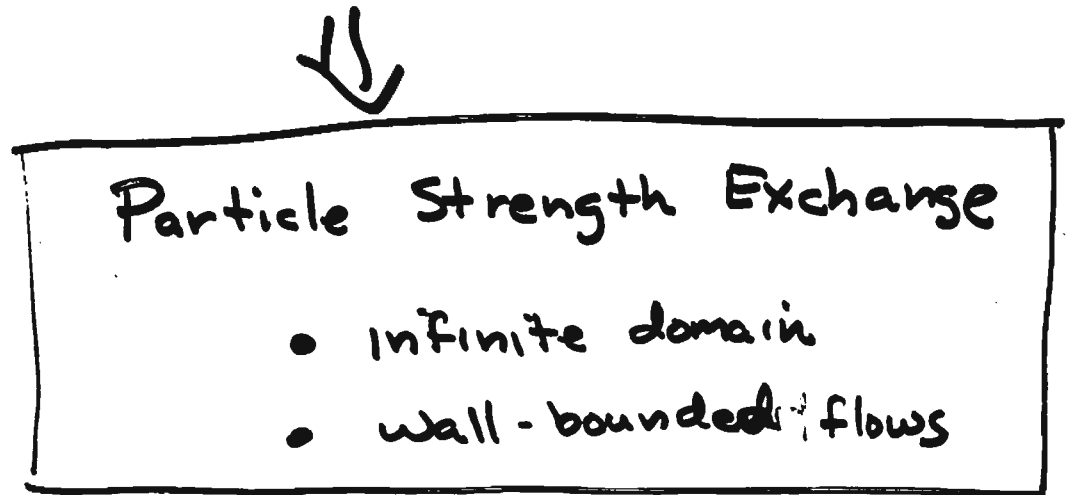


$$t^* = 7.44$$

High Resolution Solutions of Euler Eqs



Accurate Treatment of Viscous Effects



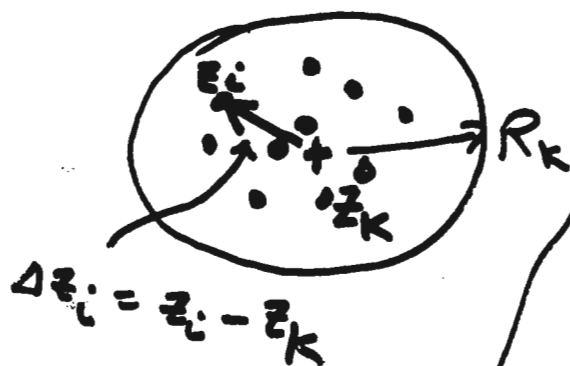
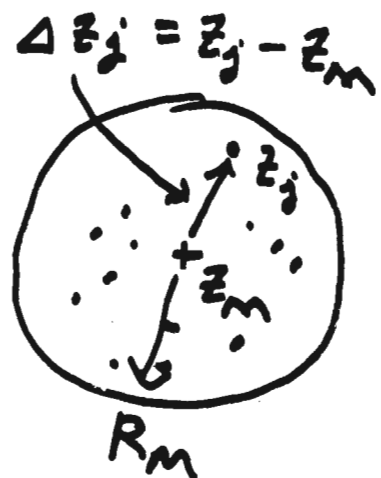
Classical Algorithm

$O(N^3)$ ops/time step.

Fast Algorithm

Complex notation

$$\frac{d\vec{z}_i^*}{dt} \sim \sum_j' \frac{\alpha_j}{z_i - z_j}$$



$$\frac{1}{z_i - z_j} = \frac{1}{z_k - z_m - (\Delta z_j - \Delta z_i)}$$

$$= \frac{1}{z_k - z_m} + \frac{\Delta z_j - \Delta z_i}{(z_k - z_m)^2} + \dots + \frac{(\Delta z_j - \Delta z_i)^{L-1}}{(z_k - z_m)^L} + \text{Error.}$$

$$\text{error} \sim \left(\frac{\max(R_k, R_m)}{|z_k - z_m|} \right)^L$$

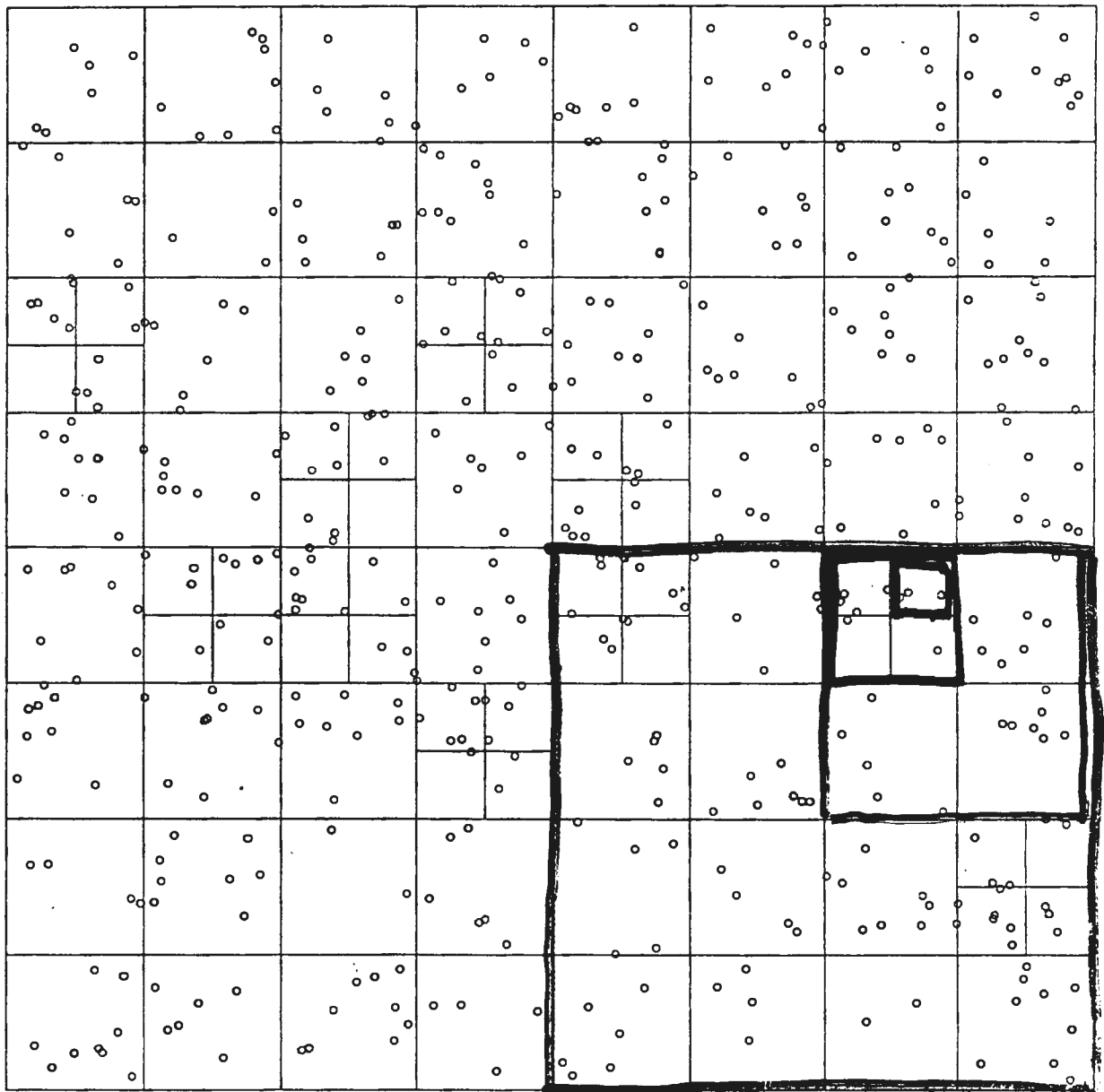
Appel (1985) $L=2$ Binary Tree Data Structure

Greengard/Rokhlin (1987) $L \approx 20$ Fixed Domains

FAST VORTEX ALGORITHM

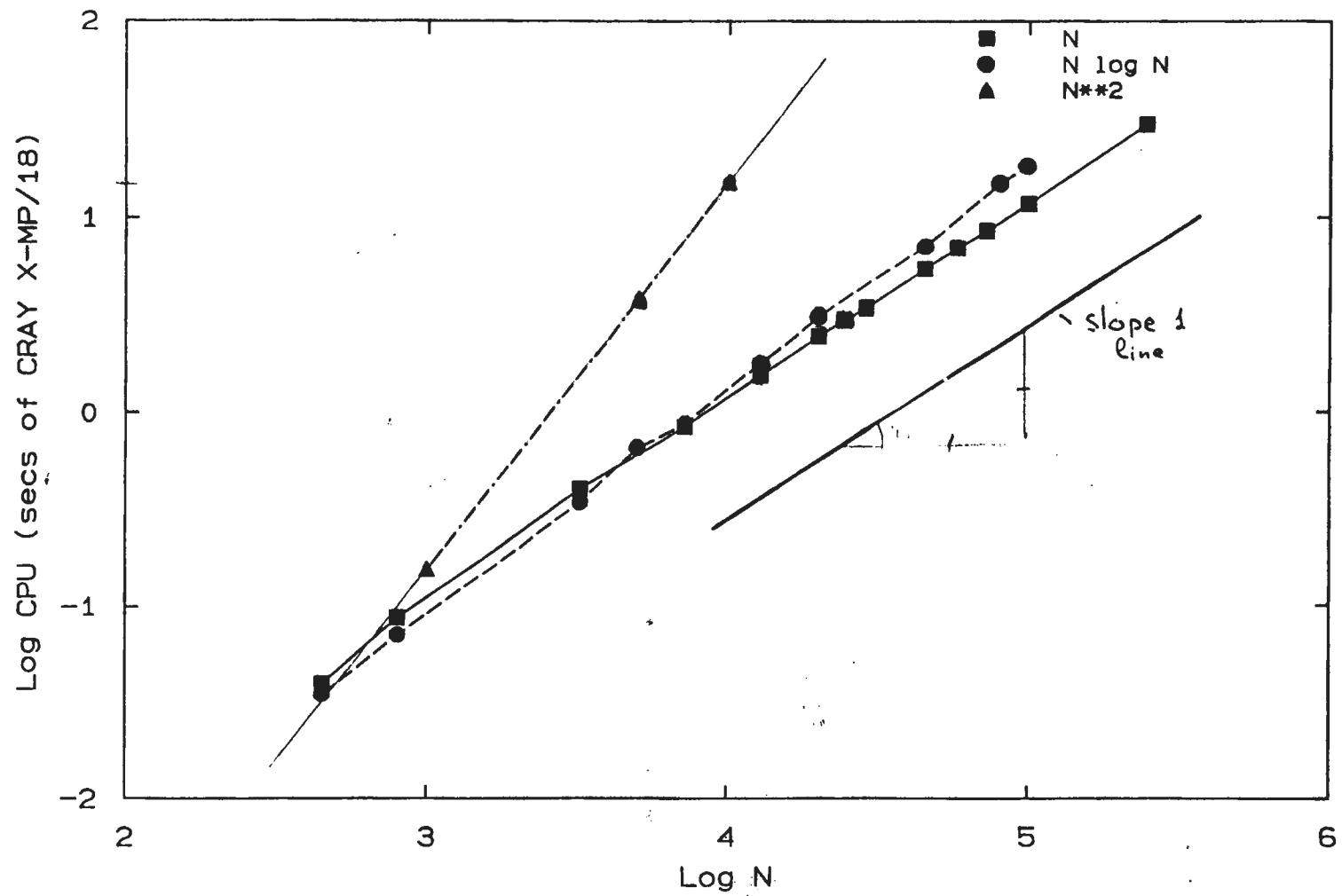
$O(N \log N)$ - Barnes & Hut

$O(N)$ - Greengard & Rokhlin

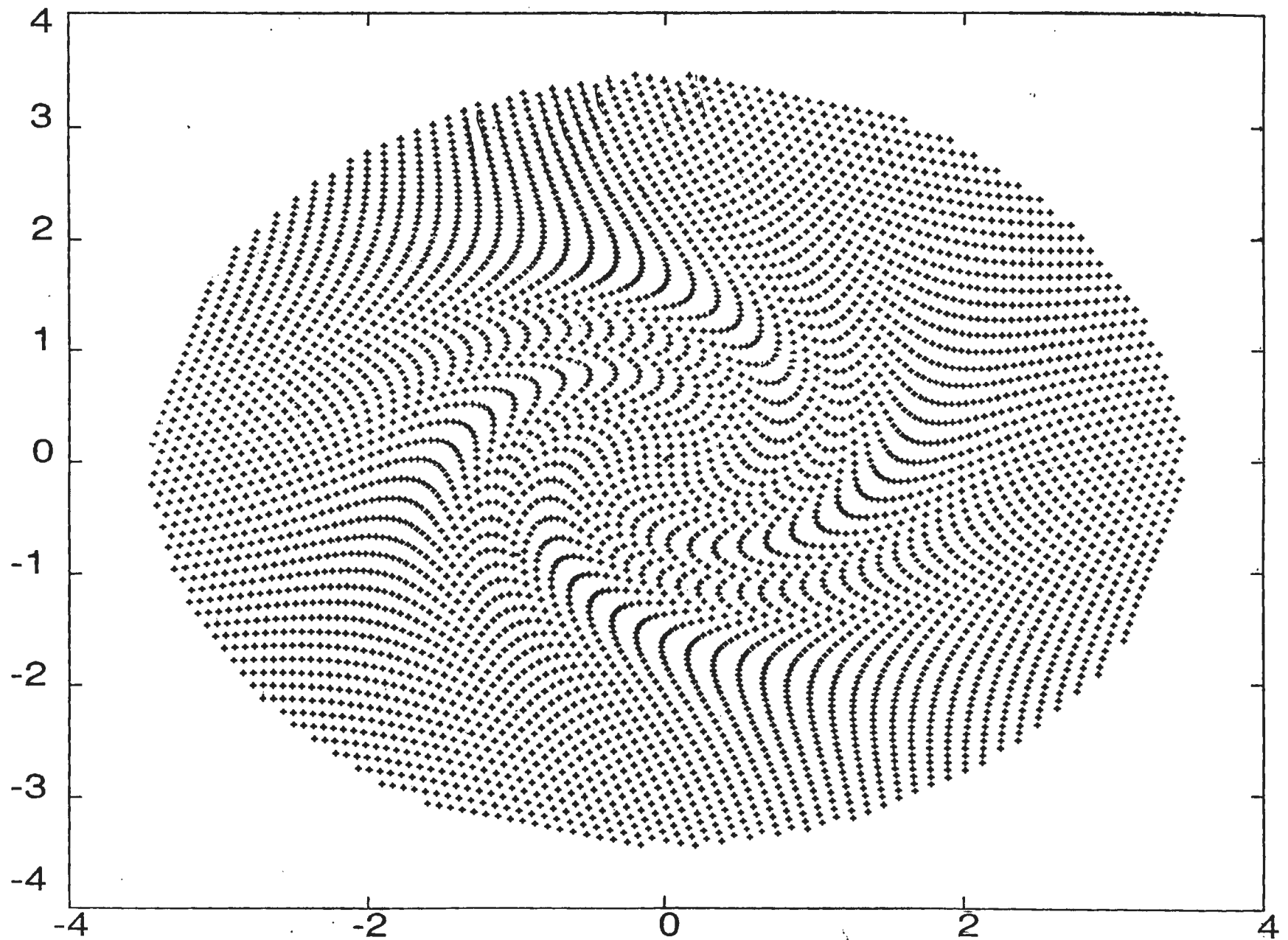


Particle-Box interactions
or

Box-Box interactions

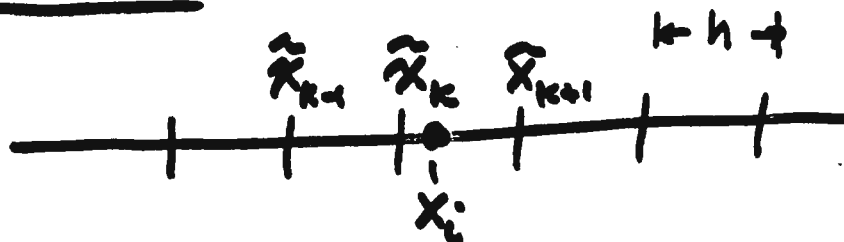


$Re = 1000 \quad t = 0.5$



Remeshing or Redistribution of Vorticity

One-dimension

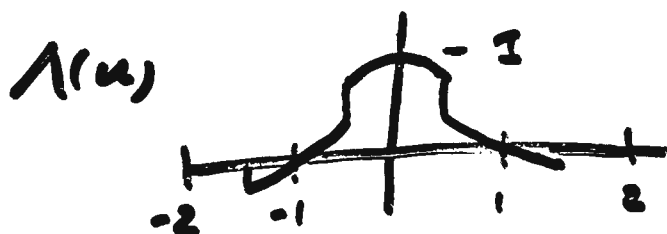


$$\eta(x - x_i) \approx \sum_j \eta(x - \hat{x}_j) \Lambda\left(\frac{\hat{x}_j - x_i}{h}\right)$$

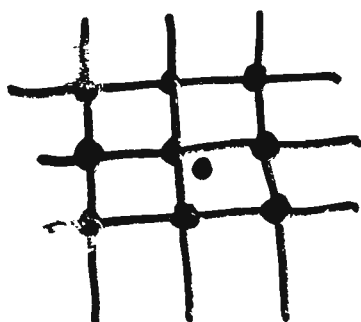
Fourier transform

$$\hat{\eta}(k) e^{ikx_i} \approx \hat{\eta}(k) \sum_j e^{ik\hat{x}_j} \Lambda\left(\frac{\hat{x}_j - x_i}{h}\right)$$

For error $O(h^3)$



Two Dimensions



$$\Delta \Pi_{j,i} = \Pi_i \Lambda\left(\frac{\hat{x}_j - x_i}{h}\right) \Lambda\left(\frac{\hat{y}_j - y_i}{h}\right)$$

Viscous effects

$$\nabla^2 \omega \approx \int G(\underline{x} - \underline{x}') [\omega(\underline{x}) - \omega(\underline{x}')] d\underline{x}'$$

$$G = \frac{1}{\sigma^2} \frac{1}{\pi \sigma^2} e^{-|\underline{x} - \underline{x}'|^2 / \sigma^2}$$

Proof - Take Fourier Trans.

$$-k^2 \hat{\omega} \approx \frac{1}{\sigma^2} (e^{-\frac{k^2 \sigma^2}{4}} - 1) \hat{\omega}$$

$$= [-k^2 + O(k^4)] \hat{\omega}$$

↑

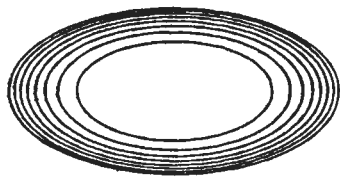
Particle Strength Exchange (infinite domain)

$$\Rightarrow \left. \frac{d\Gamma_i}{dt} \right|_{\text{vis}} = \nu \sum_j G(\underline{x}_i - \underline{x}_j) [\Gamma_i - \Gamma_j]$$

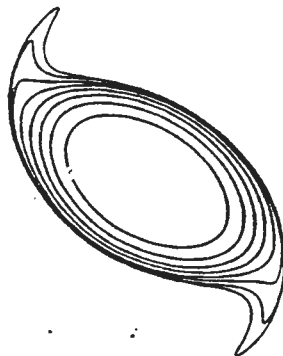
Contour Dynamics Computation

(David Dritche!)

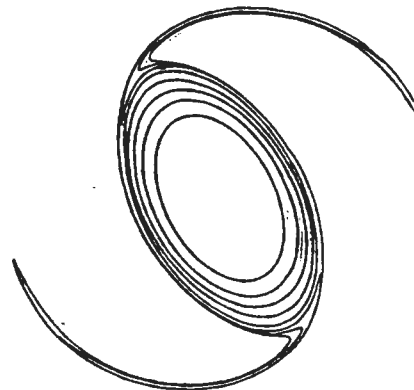
0



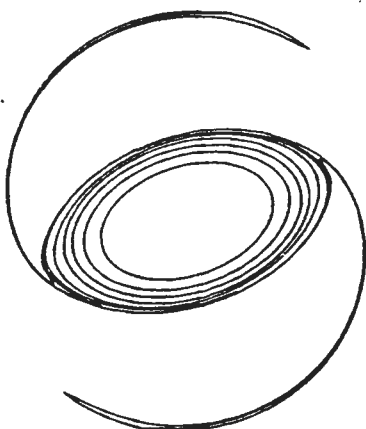
2.00



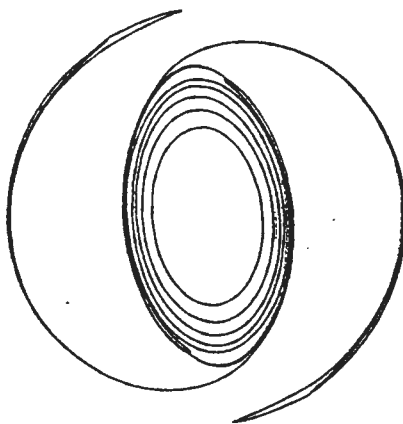
4.00



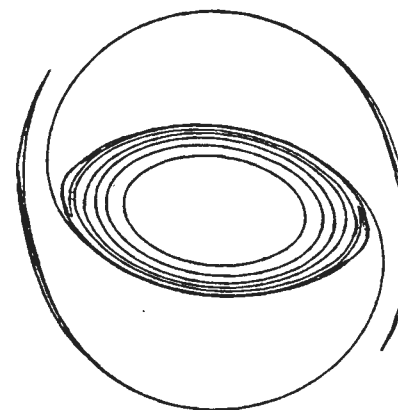
5.00



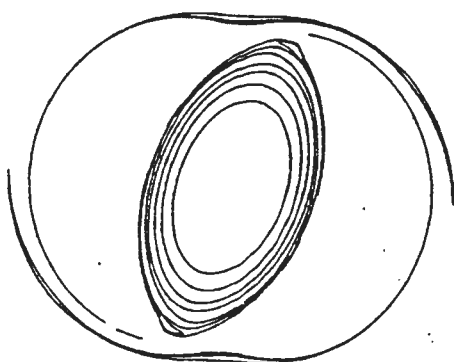
6.00



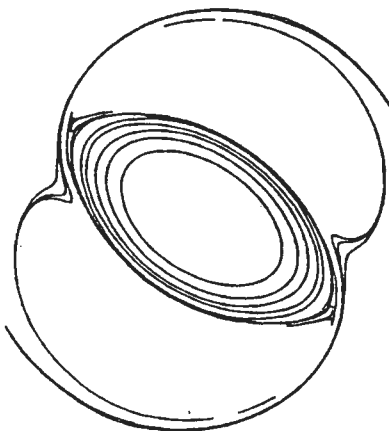
7.00



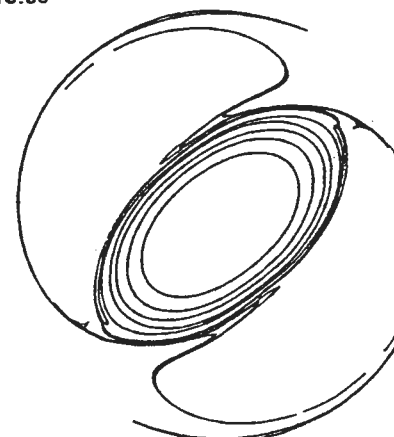
8.00



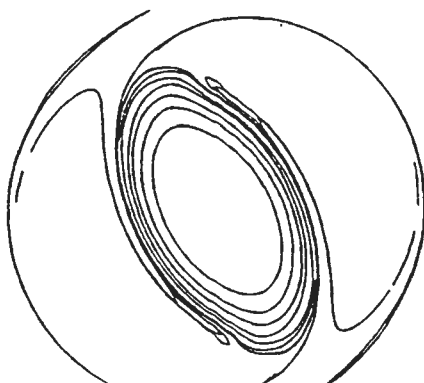
9.00



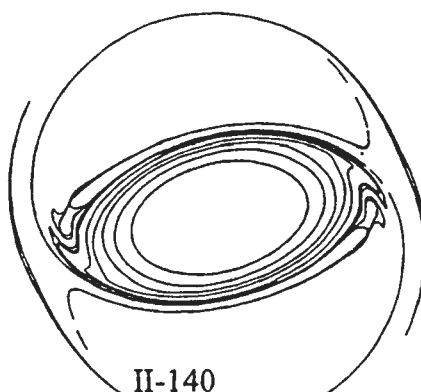
10.00



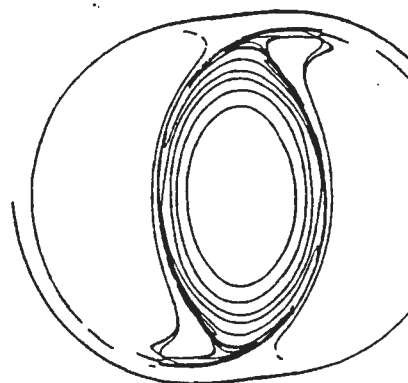
11.00



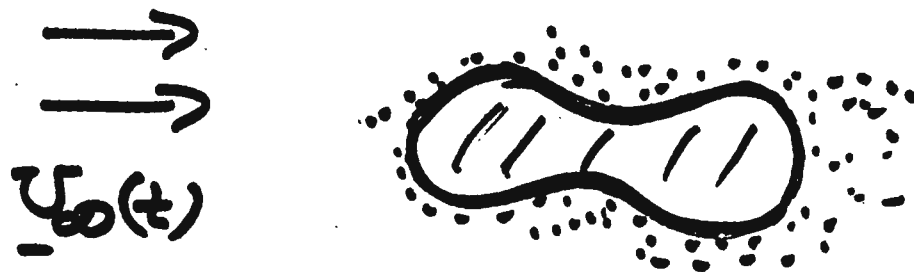
12.00



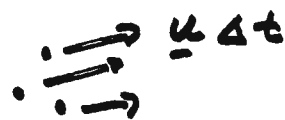
13.00



Viscous Computations / Bluff Body Flows



I. Convection Step



II. Infinite medium
Diffusion Step



III. Compute Vortex
layer at boundary

$$(\underline{U}_b \cdot \underline{t})(s) \Rightarrow \gamma(s)$$



IV Diffuse $\gamma(s)$ to
vortex elements

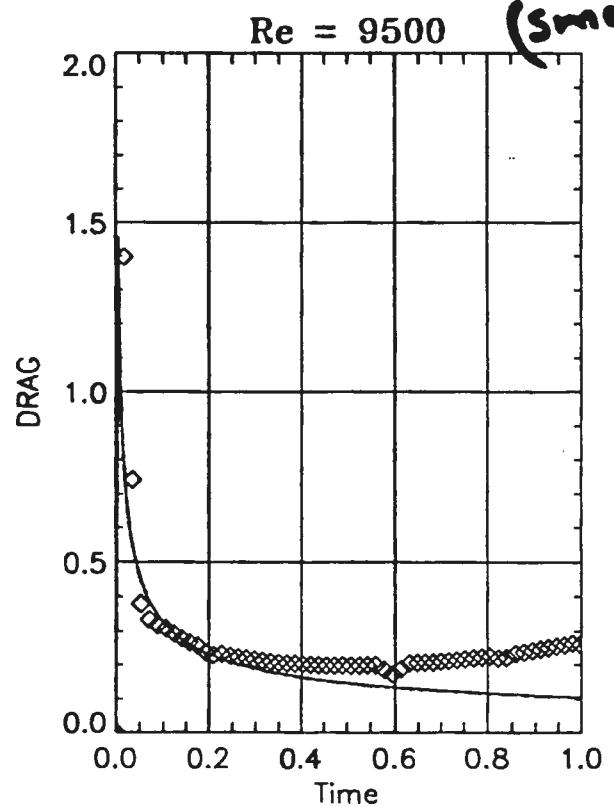
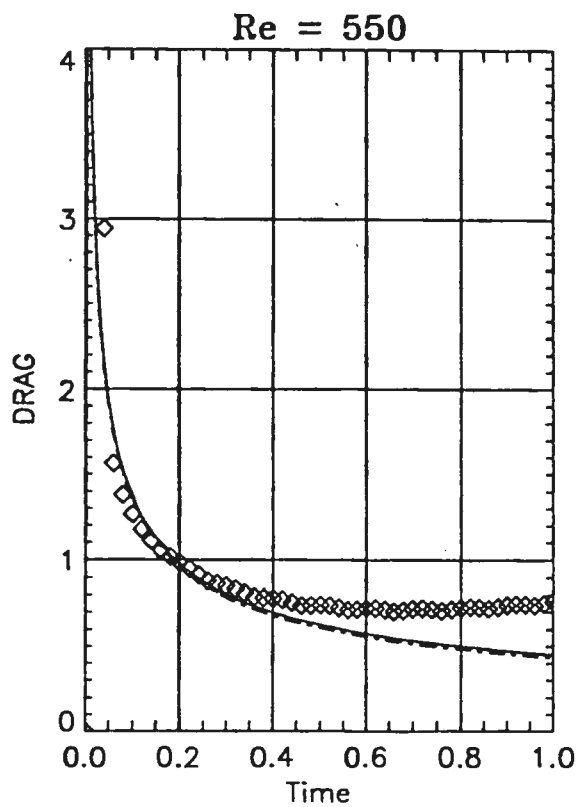
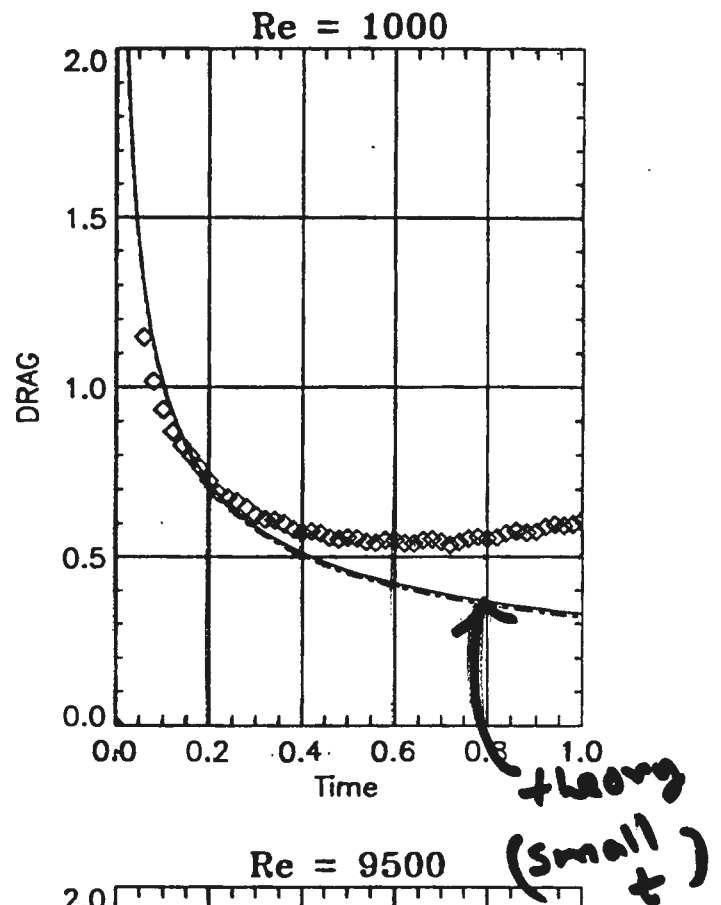
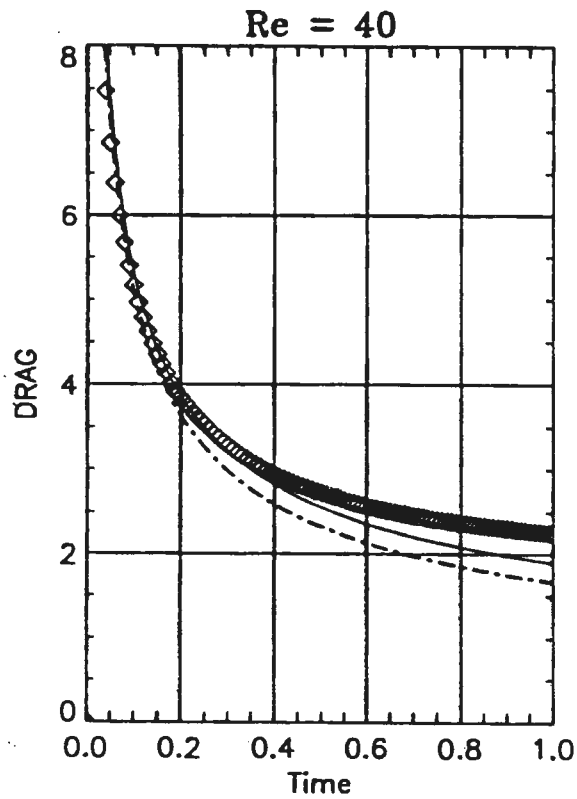


Force computation

$$\underline{F}_B = -\rho \frac{d}{dt} \int \underline{x} \times \underline{\omega} dV$$

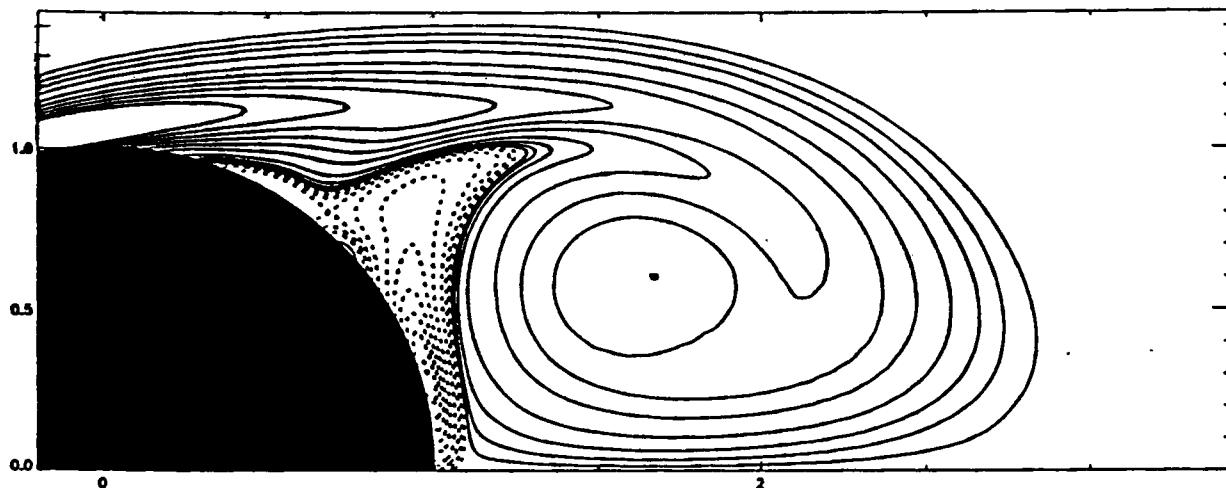
$$\nu \frac{\partial \omega}{\partial n} = \frac{\gamma(s)}{\Delta t} = -\frac{1}{\rho} \frac{\partial p}{\partial s}$$

Early histories
of the drag
**Impulsively Started
Cyl.**

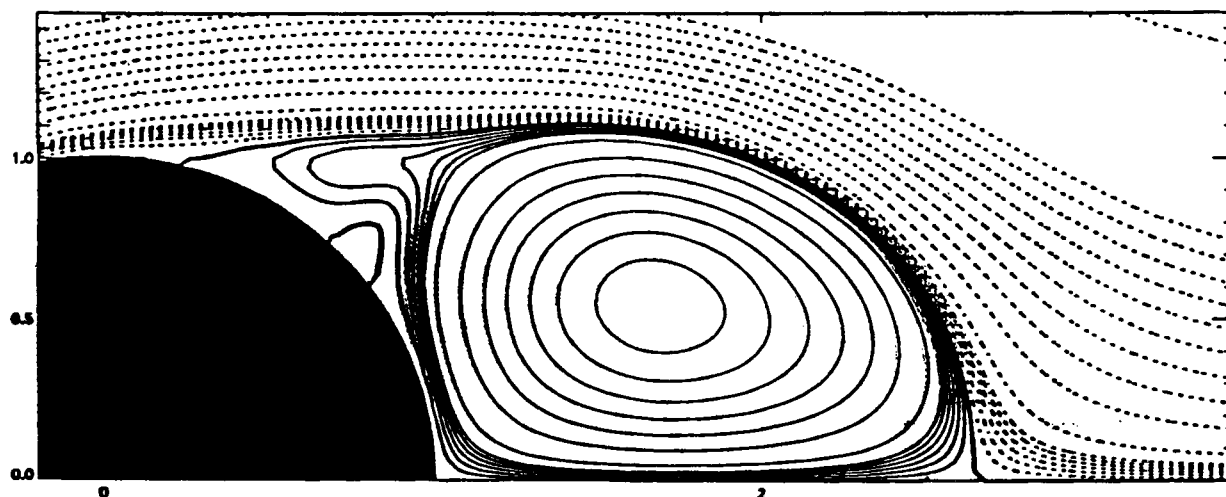


$Re = 550$

$T = 3.5$



(a) Vorticity
(Computations)



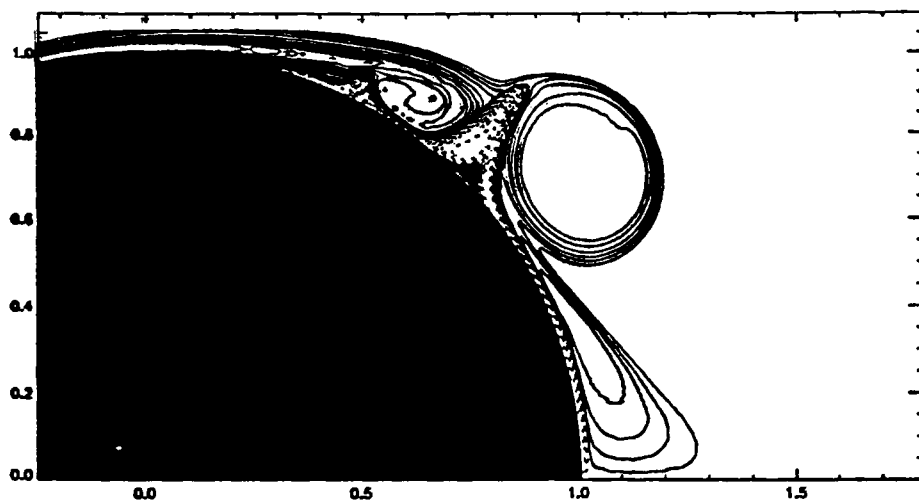
(b) Streamlines
(Computations)



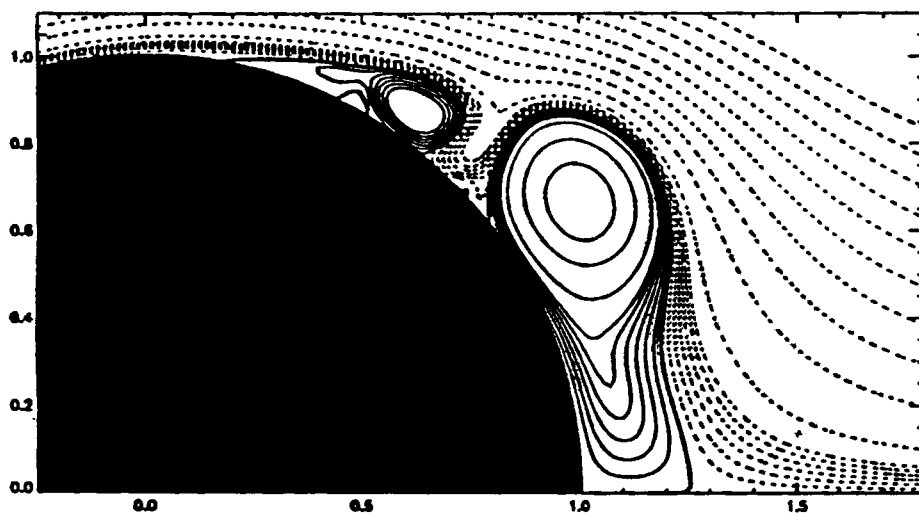
(c) Streaklines
(Experiments)

* Bonard &
Coutanceau

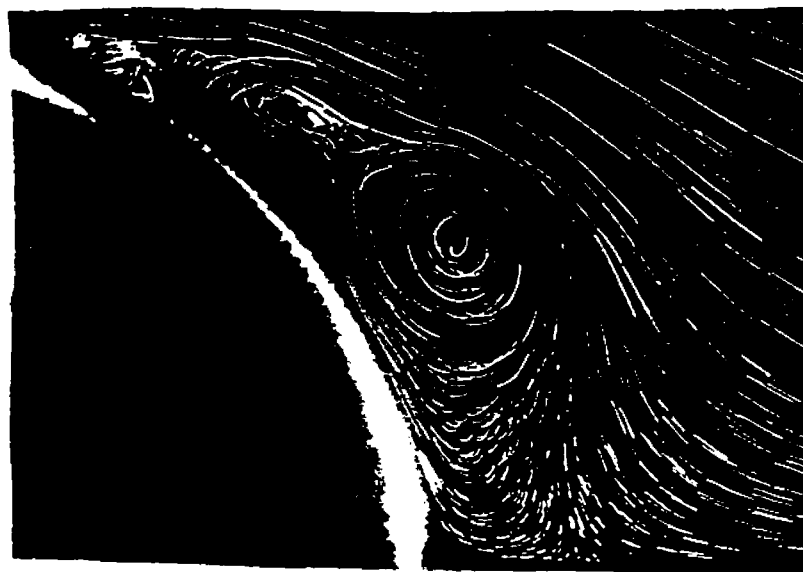
$Re = 9500$
 $T = 2.5$



(a) Vorticity
(Computations)



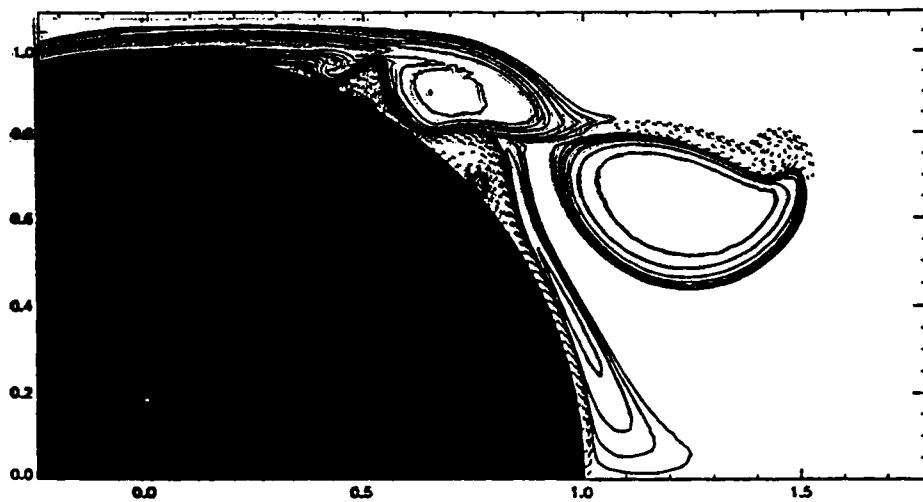
(b) Streamlines
(Computations)



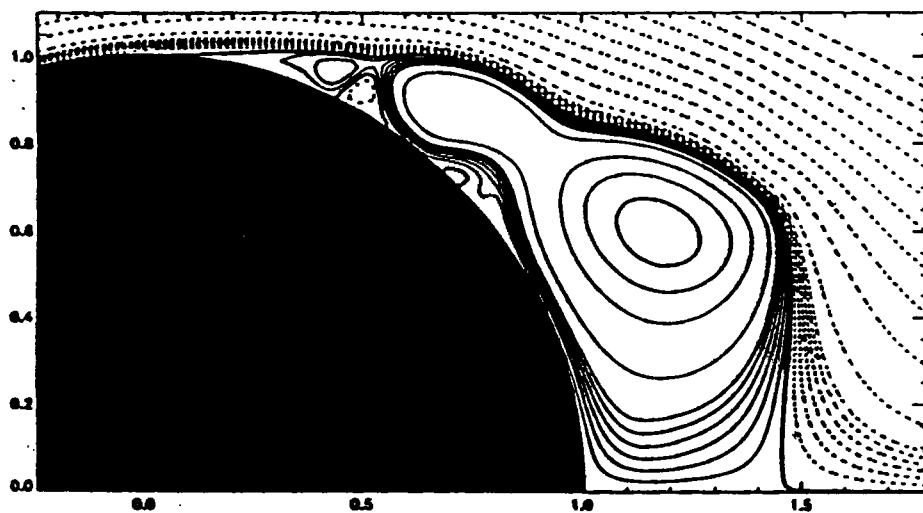
(c) Streaklines
(Experiments)

$Re = 9500$

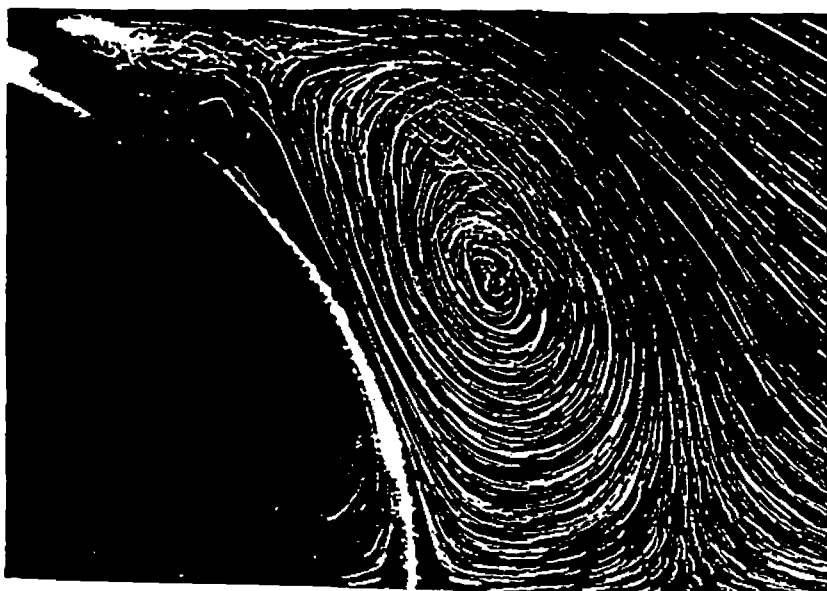
$T = 3.0$



(a) Vorticity
(Computations)

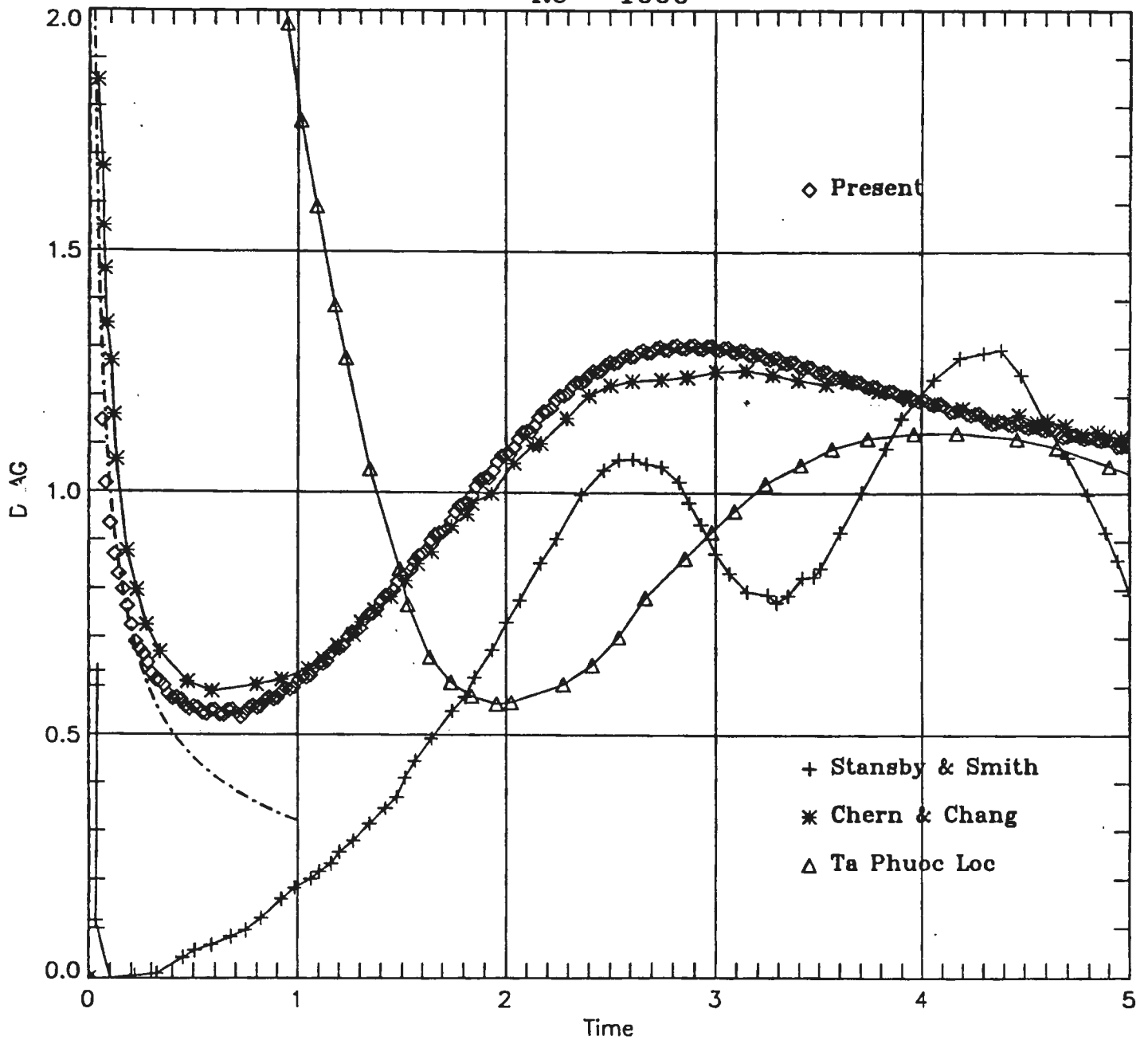


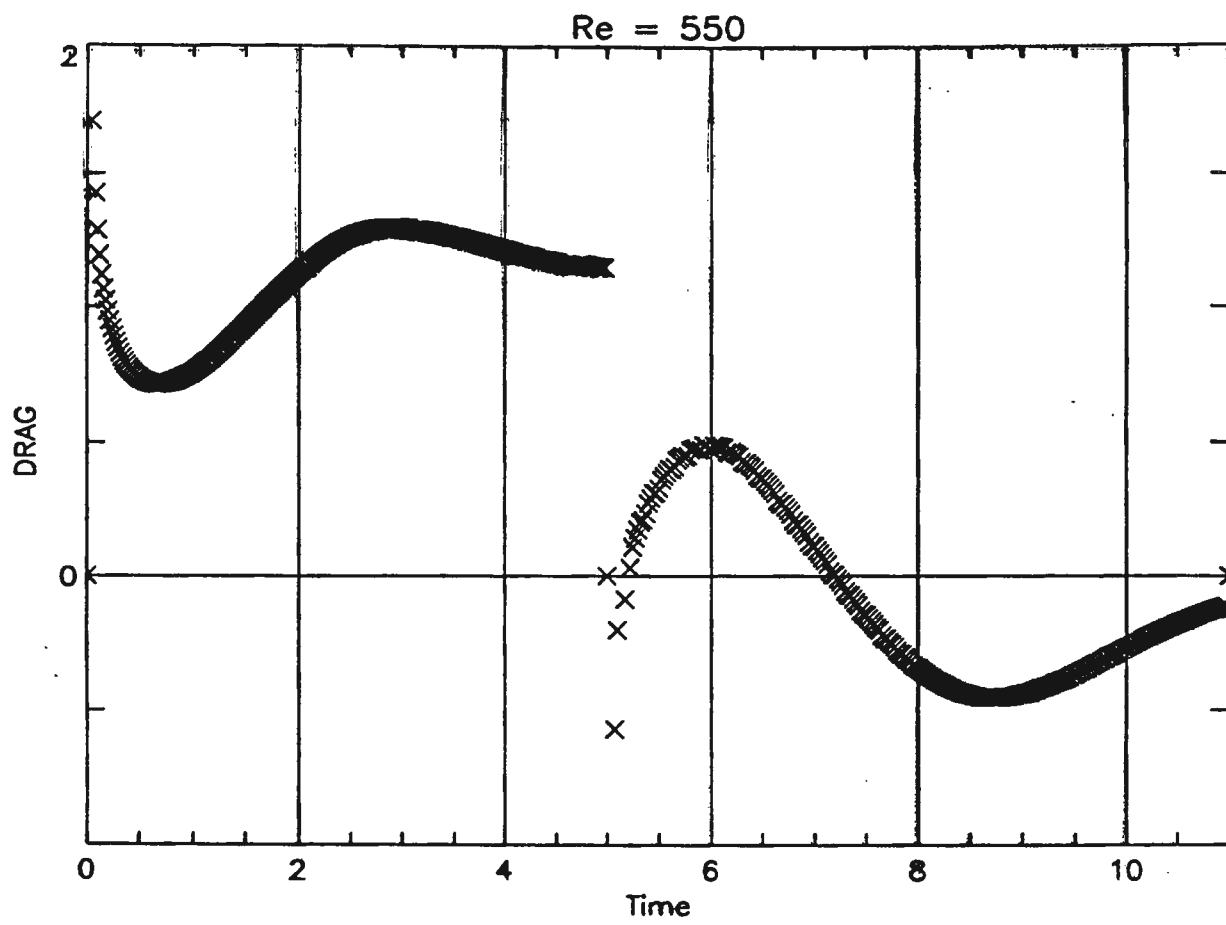
(b) Streamlines
(Computations)



(c) Streaklines
(Experiments)

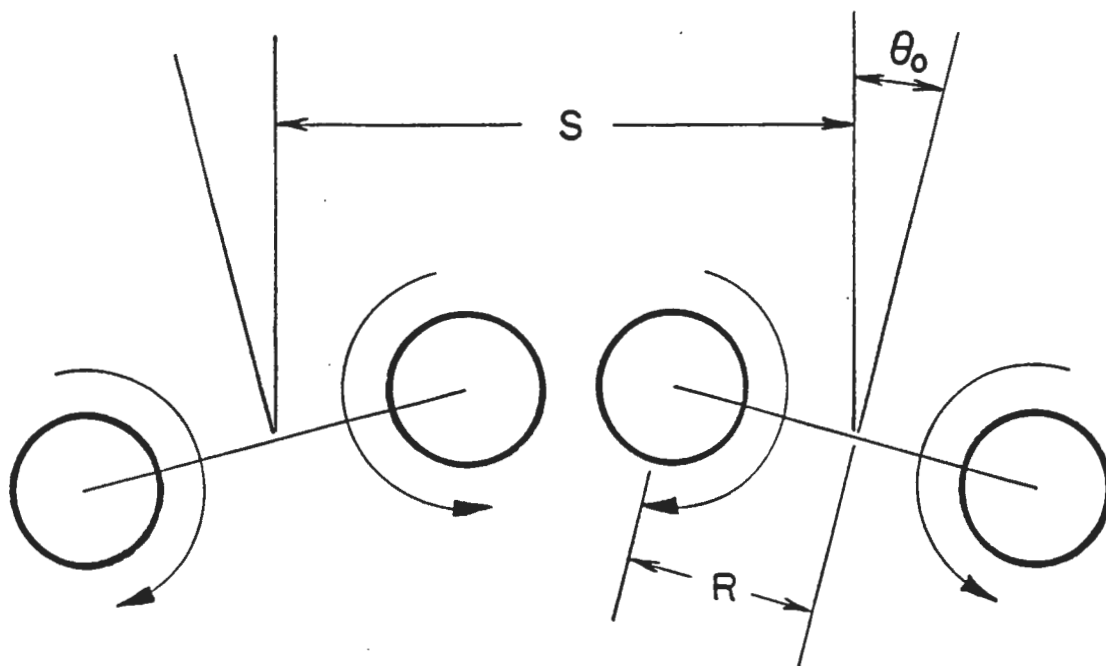
Re = 1000





Impulsively Started
& stopped
Cylinder

(G. Winckelmans)



Fusion of Vortex rings.

$$R = 1$$

$$\sigma_R = 0.1$$

$$\Gamma = \int \omega_0 ds = 1$$

$$S = 2.7$$

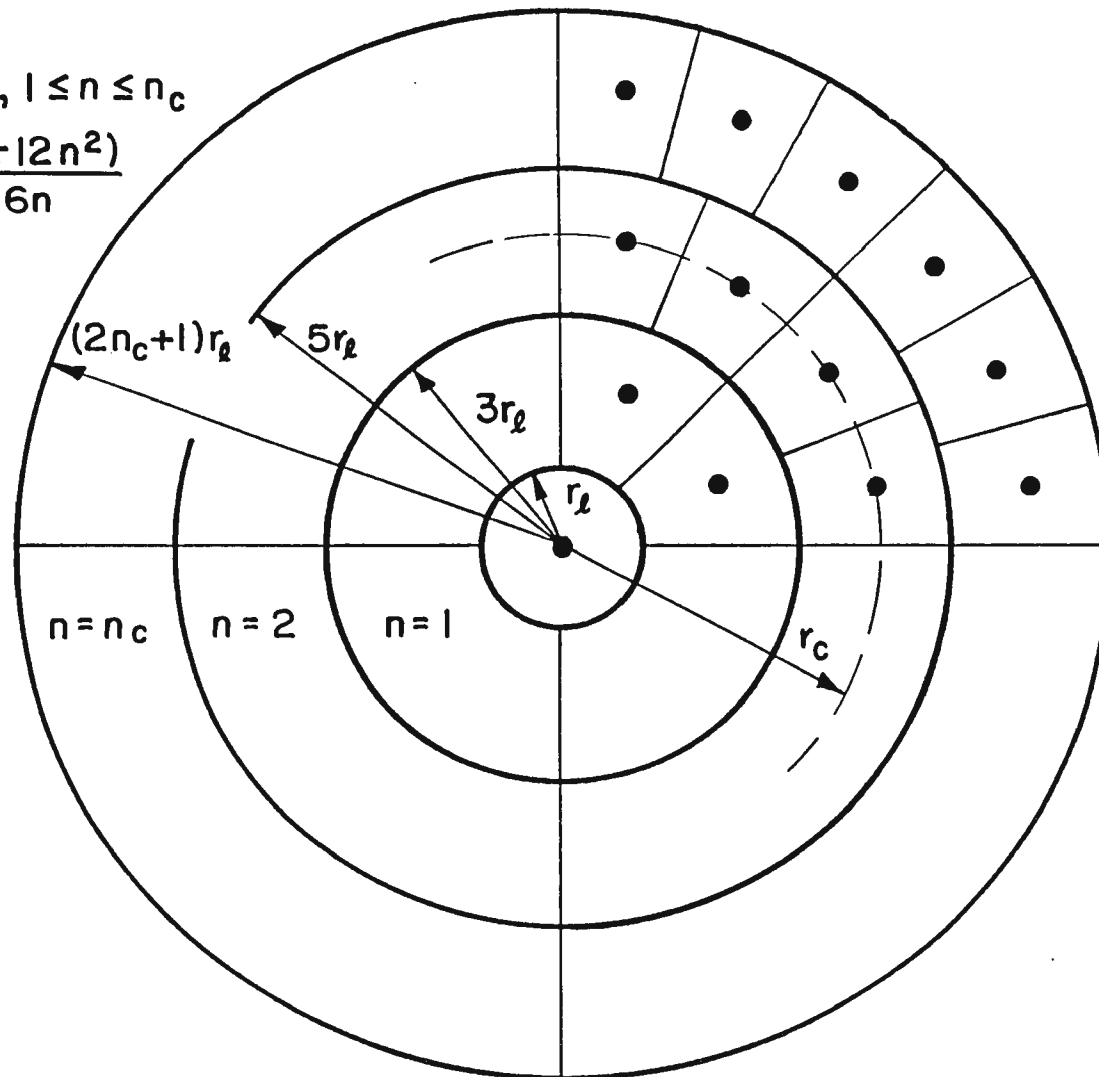
$$\theta_0 = 15^\circ$$

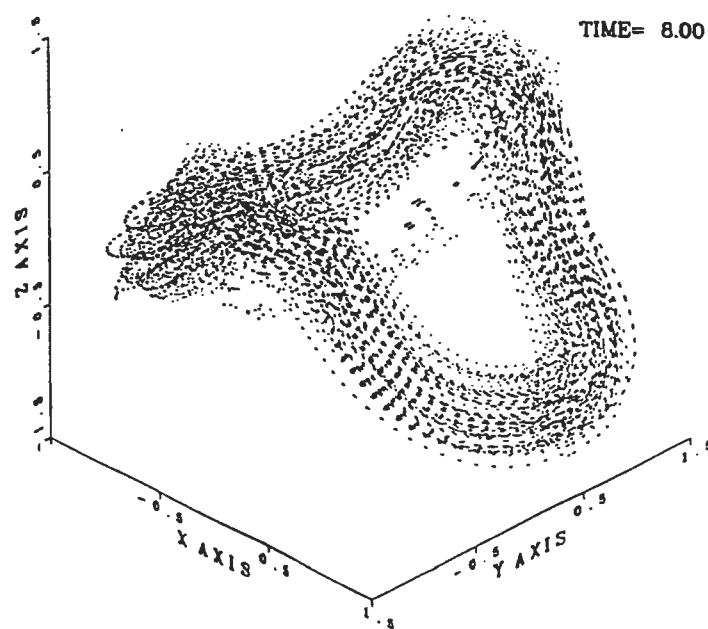
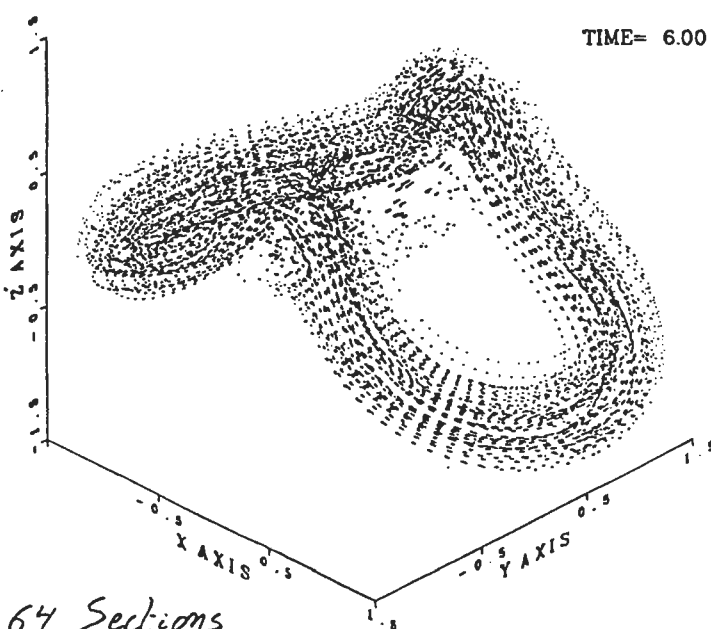
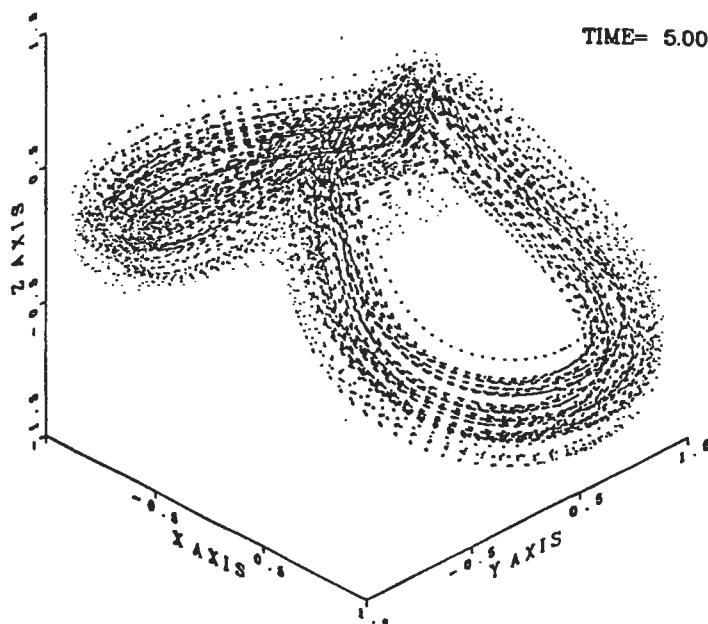
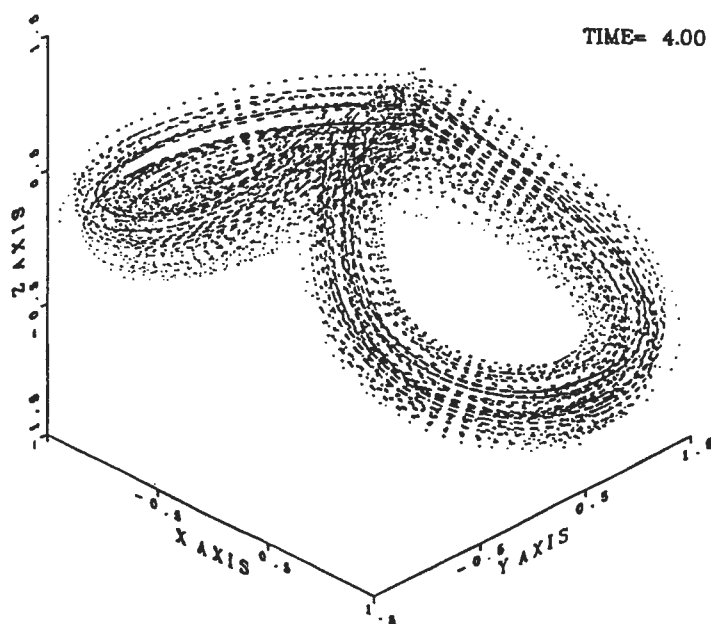
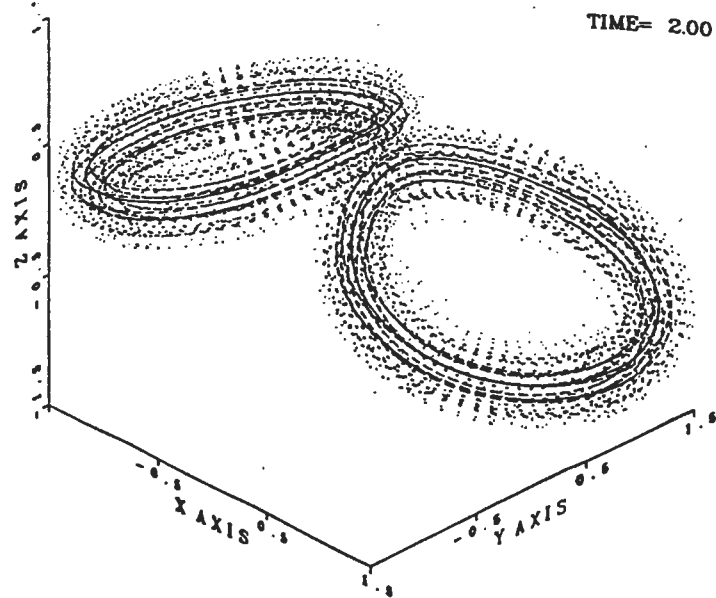
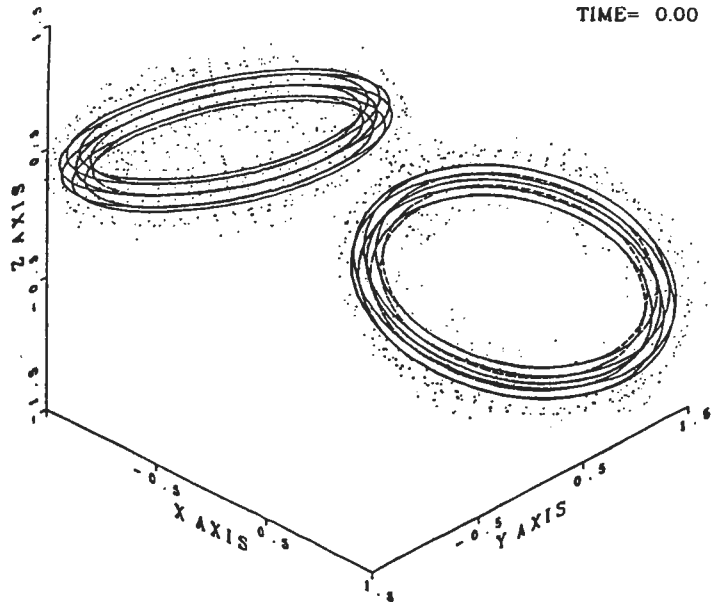
$$\omega_0 = \frac{\Gamma}{\ell \pi \sigma_R^2} \exp\left(-\frac{1}{\ell} \left(\frac{r}{\sigma_R}\right)^2\right)$$

$$\frac{r_{\max}}{\sigma_R} = 3.5$$

n_c layers, $1 \leq n \leq n_c$

$$r_c = r_\ell \frac{(1+12n^2)}{6n}$$



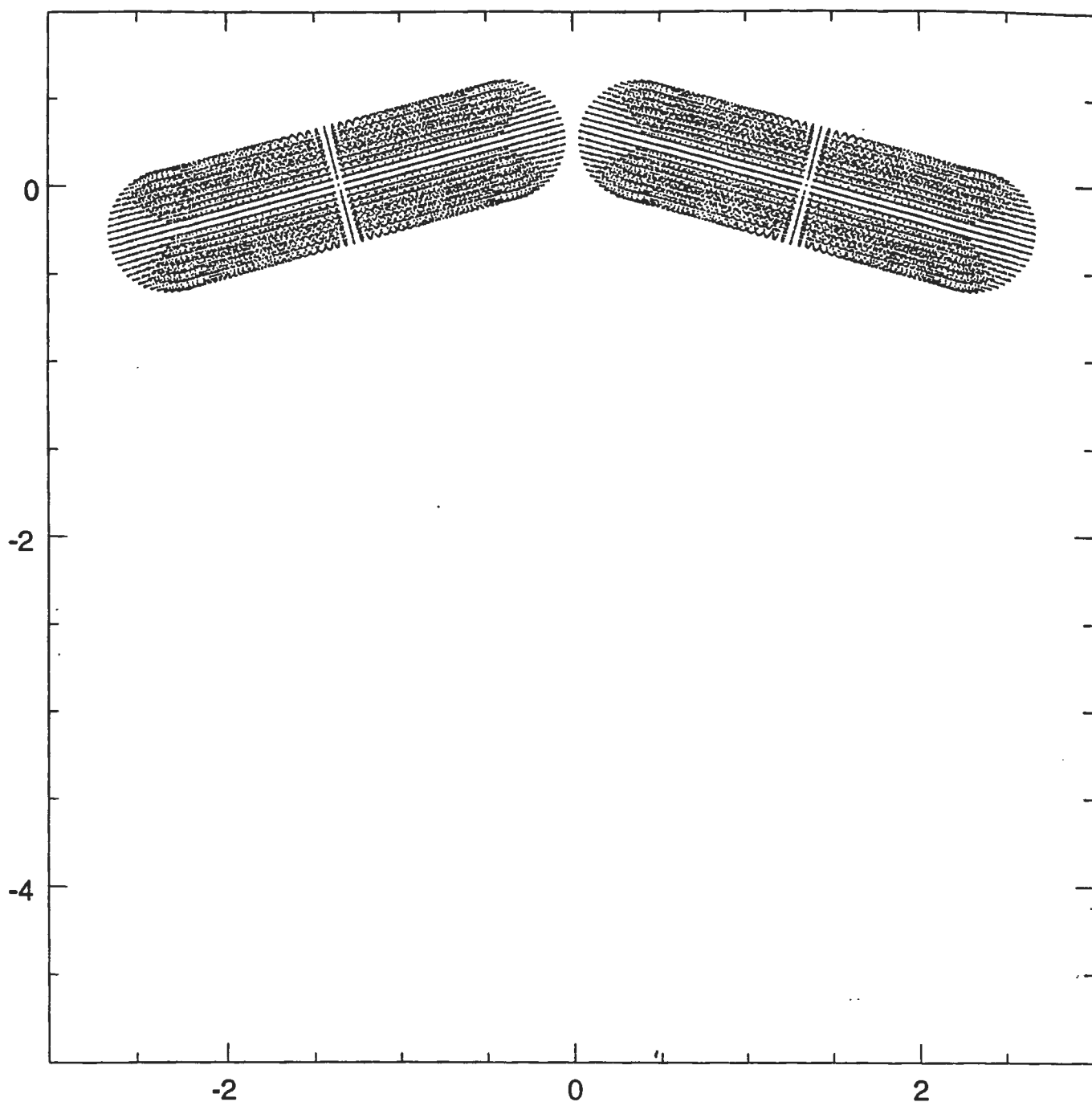


64 Sections
49 Particles/Section →

$N = 6,272$
 $h = 0.1$

$O(N^2)$ code on CRAY YMP48
(1989)

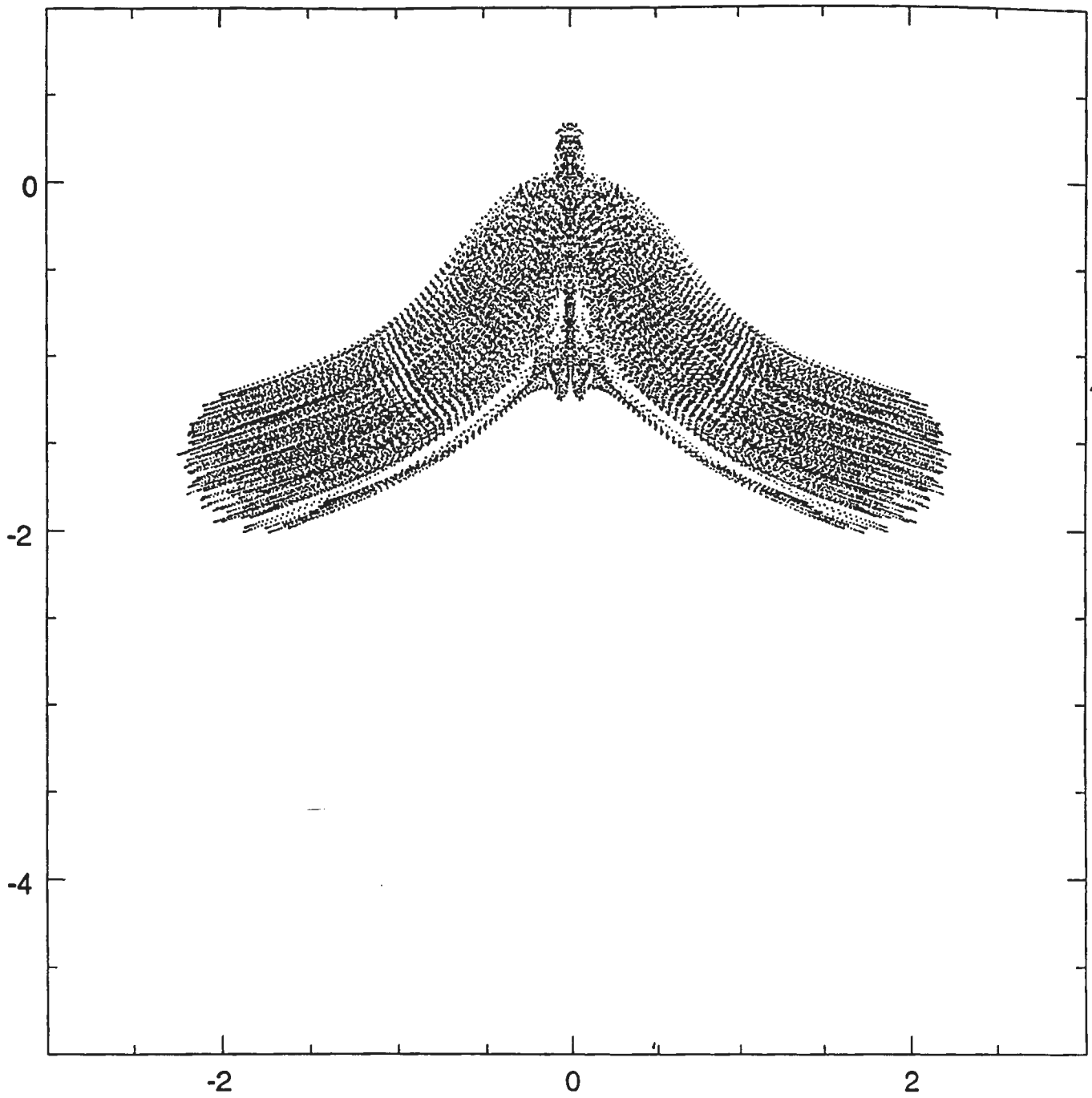
$$T = 0$$



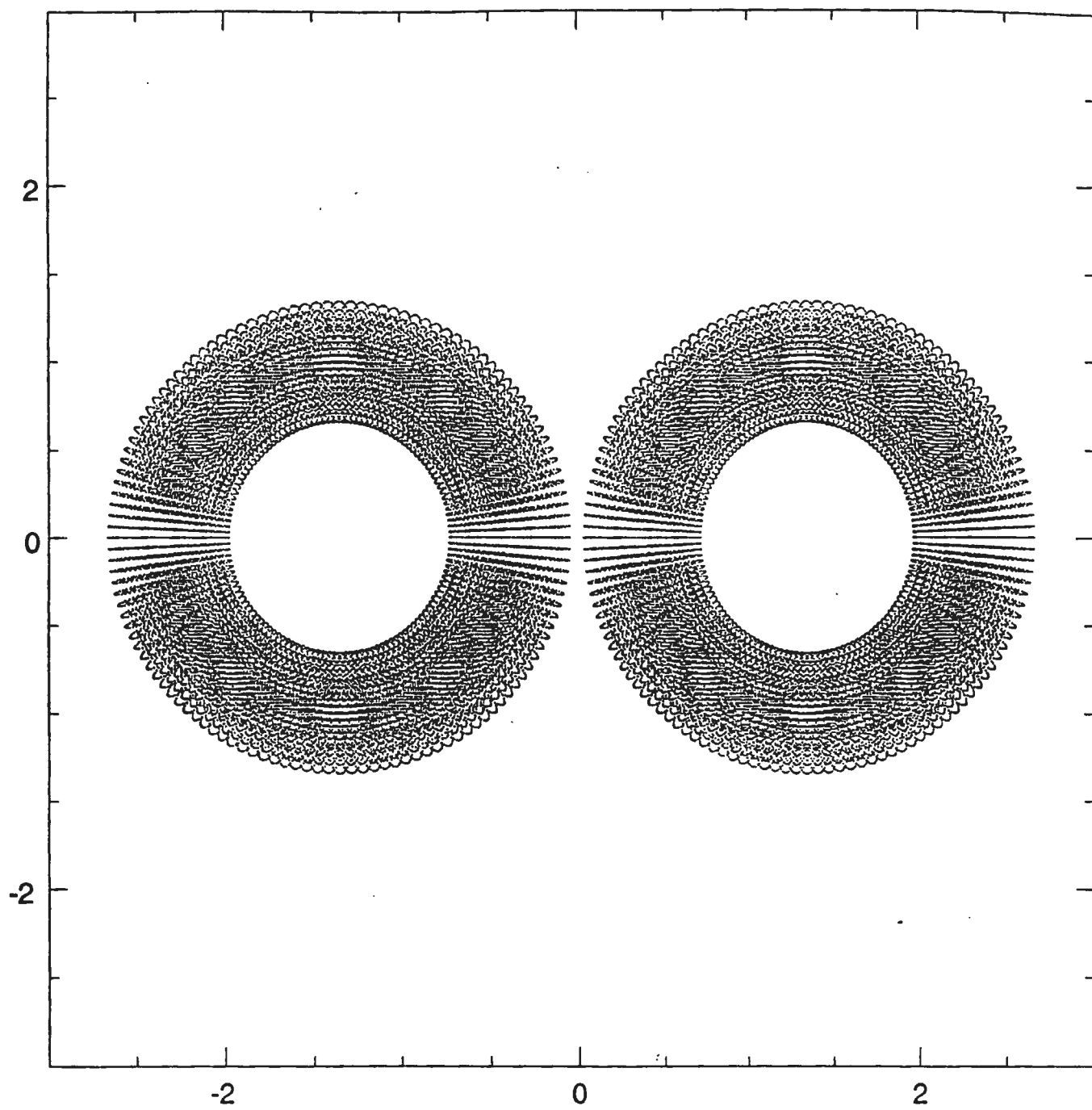
$$\left\{ \begin{array}{l} 18.8 \text{ Sections / Ring} \\ 22.5 \text{ Particles / Section (7 Layers)} \end{array} \right\} \rightarrow \left\{ \begin{array}{l} h = 0.05 \\ N = 57,600 \end{array} \right.$$

$$\left\{ \begin{array}{l} \text{Gaussian smoothing with } \sigma = 0.075 \\ e_{\parallel, \perp} \leq 10^{-3} \rightarrow 50 \text{ sec / time step on (16, 16) processors} \\ \text{Adams-Bashforth with } \delta t = 0.05 \end{array} \right.$$

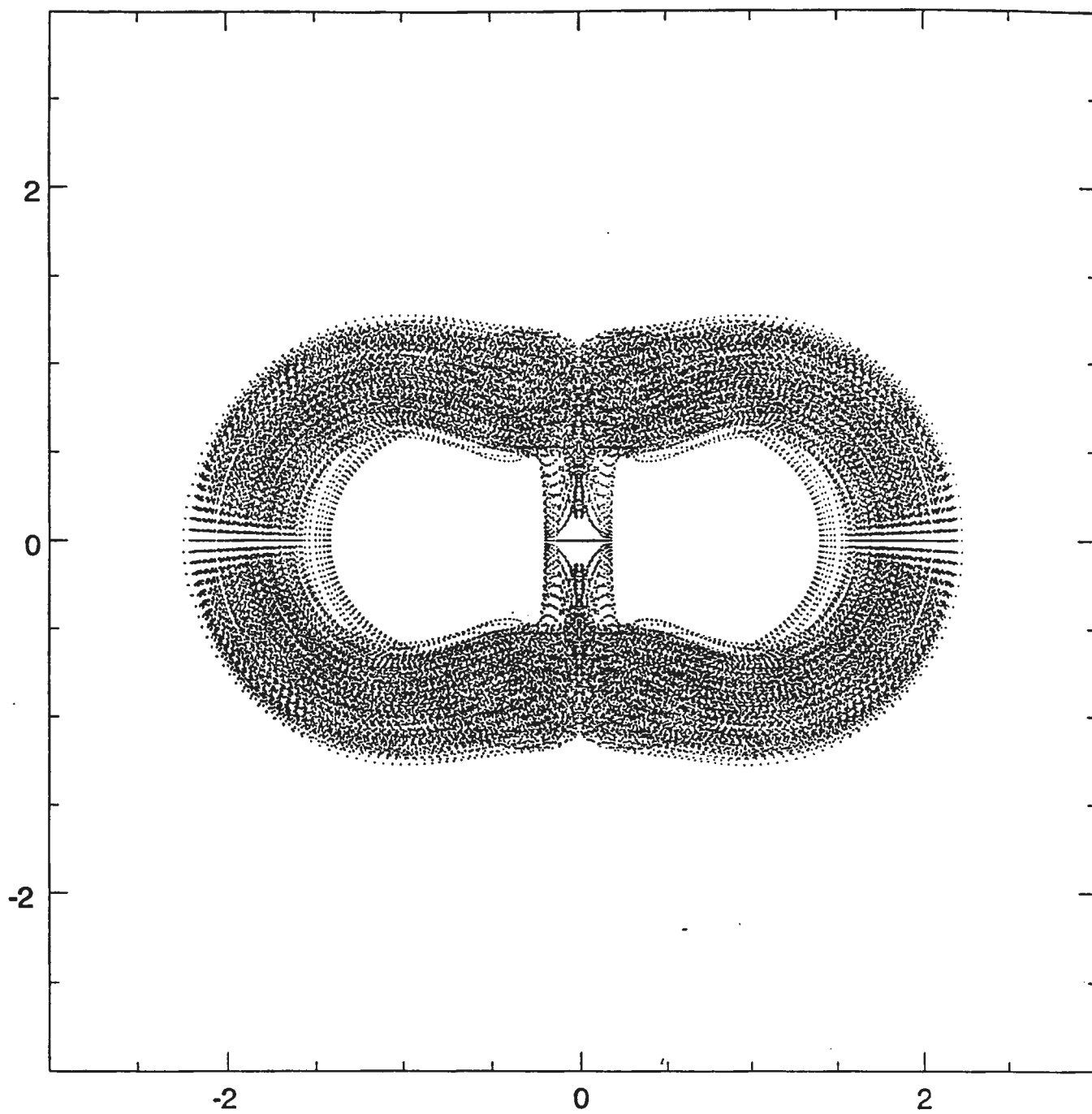
$$T = 6.0$$



$$T=0$$



$T = 6.0$



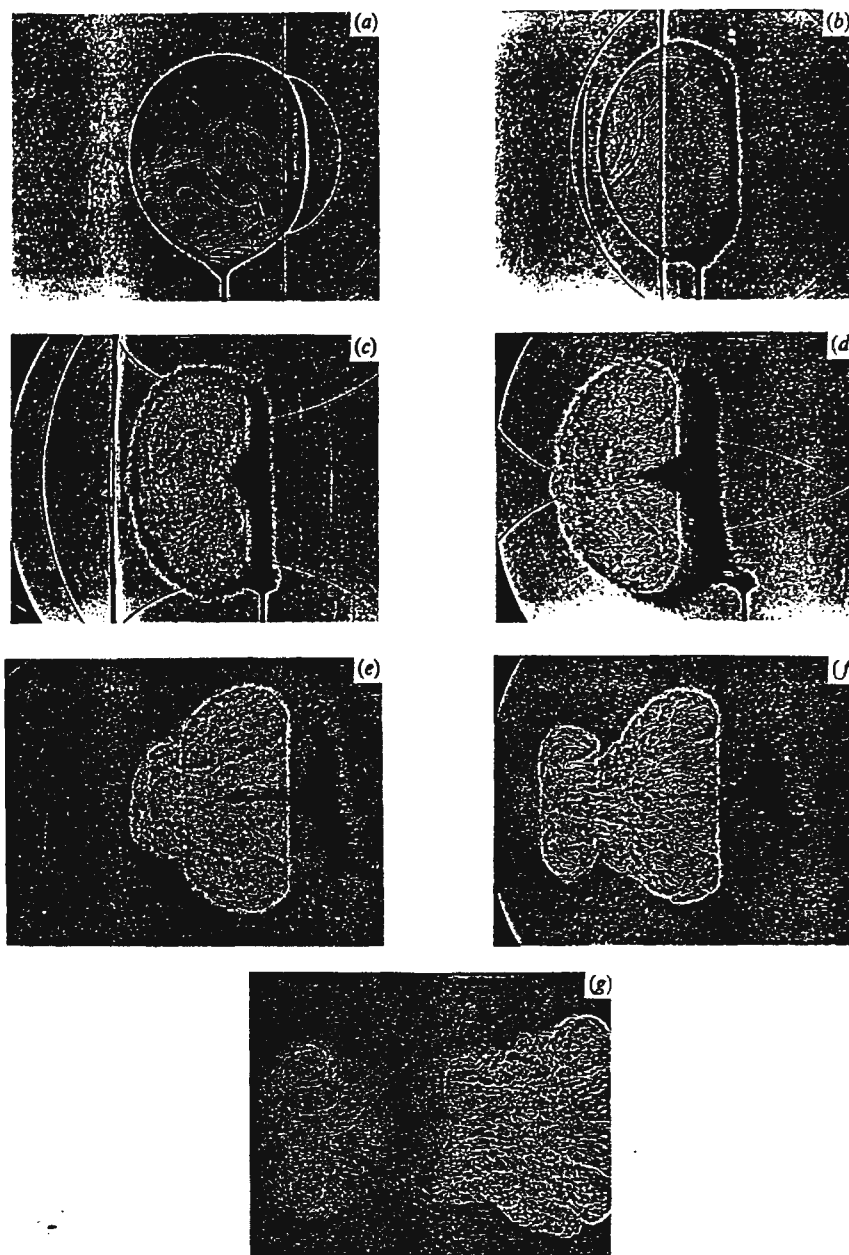


FIGURE 8. Shadow-photographs of the interaction of an $M_s = 1.25$ shock wave moving from right to left over a spherical helium volume (4.5 cm diameter). (a) $t = 20 \mu s$, (b) $82 \mu s$, (c) $145 \mu s$, (d) $223 \mu s$, (e) $350 \mu s$, (f) $600 \mu s$, (g) $1594 \mu s$.

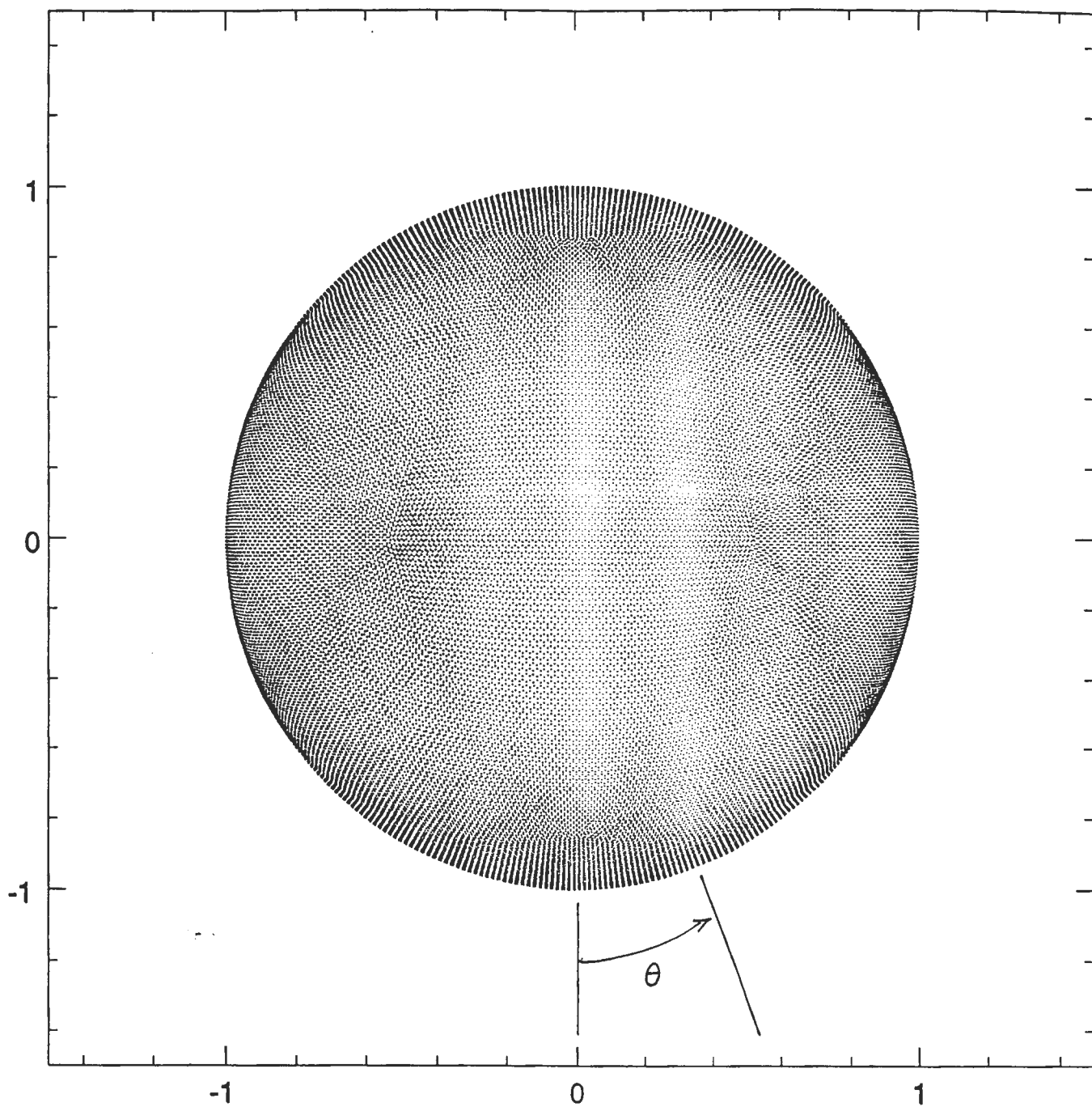
a shock-on-shock interaction, which forms a quadruple shock intersection. At $72 \mu s$ (figure 7d), the secondary transmitted waves are seen outside the volume tangentially connected to the (primary) transmitted wave and connected at the interface to the internal reflected wave, now approaching its focus. A wave reflected from the transversal beam is seen at bottom right. At $82 \mu s$ (figure 7e), the internal reflected wave has become a diverging wave, having passed through its caustic. Outside, the

J. F. Haas & B. Sturtevant

J. Fluid Mech. (1987) vol. 181, pp. 41-76

(G. Winckelmans)

Spherical Vortex Sheet: $\gamma = \frac{3}{\ell} \sin \theta \hat{e}_\varphi$



$$N = 81,920$$

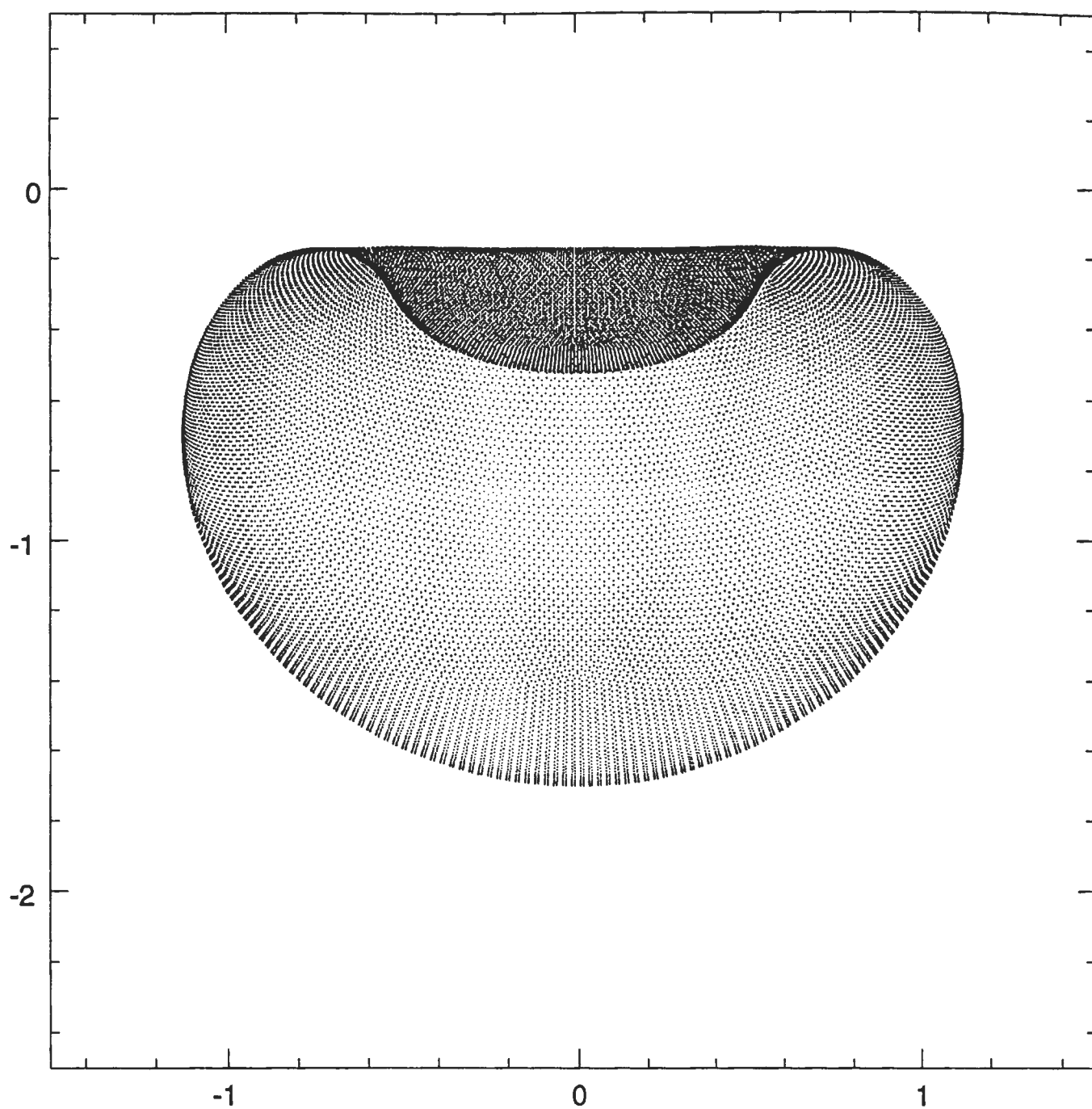
$$e_{\|V^T\|} \leq 10^{-2} \rightarrow 40 \text{ sec/time step on } (16,16) \text{ processors}$$

Gaussian smoothing with $\sigma = 0.05$

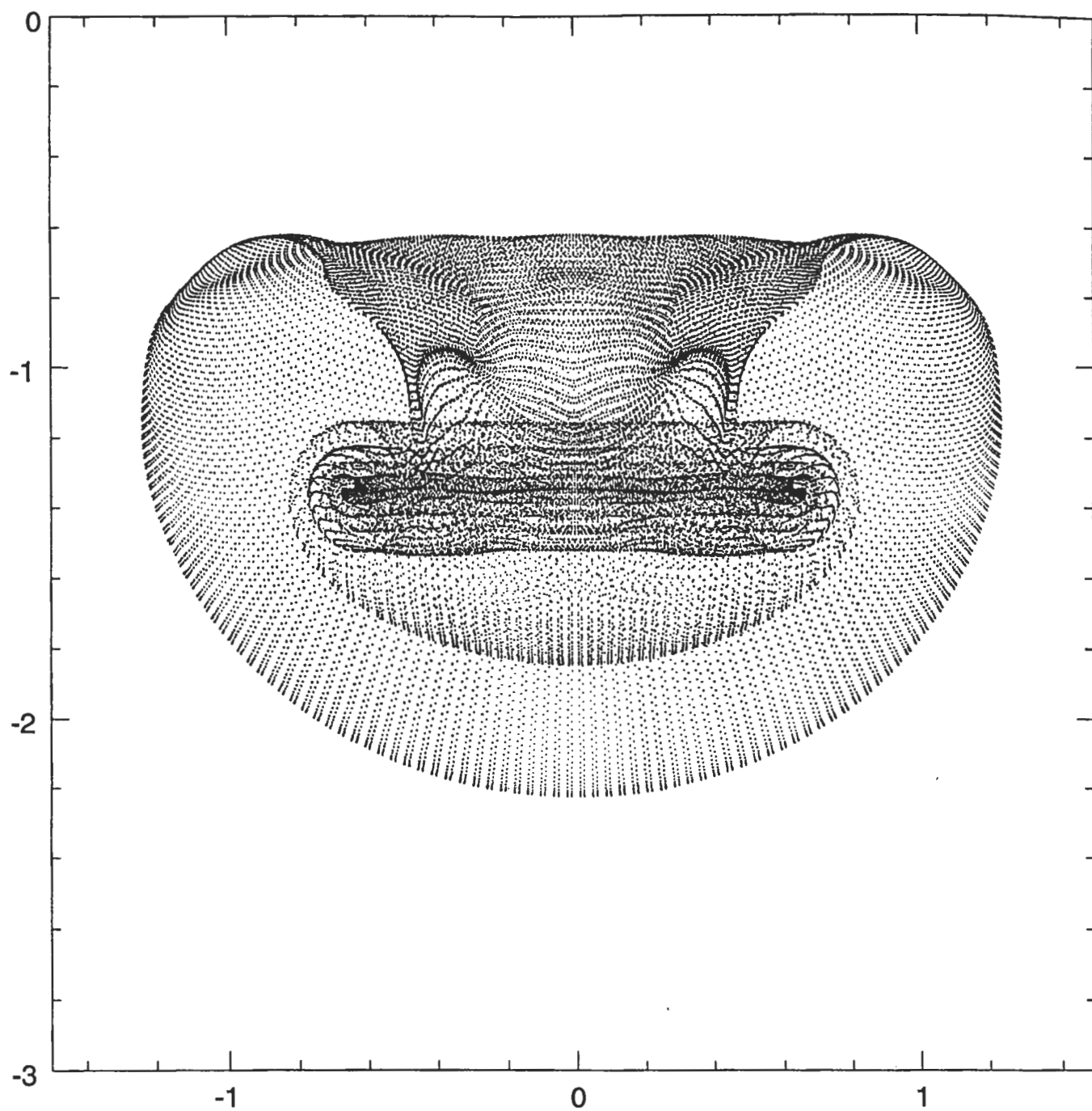
Adams-Bashforth with $St = 0.025$

Side View

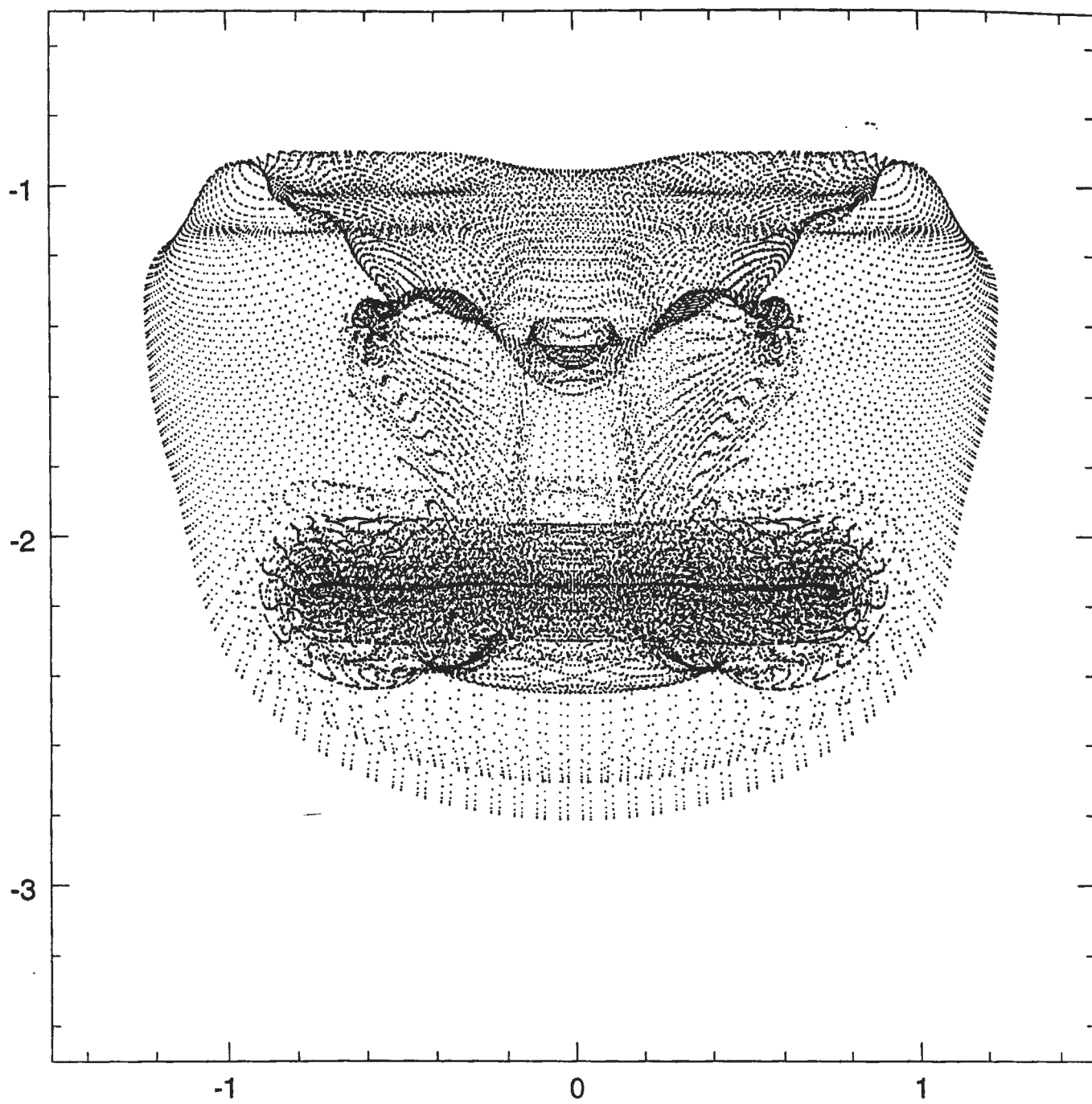
$T = 1.0$



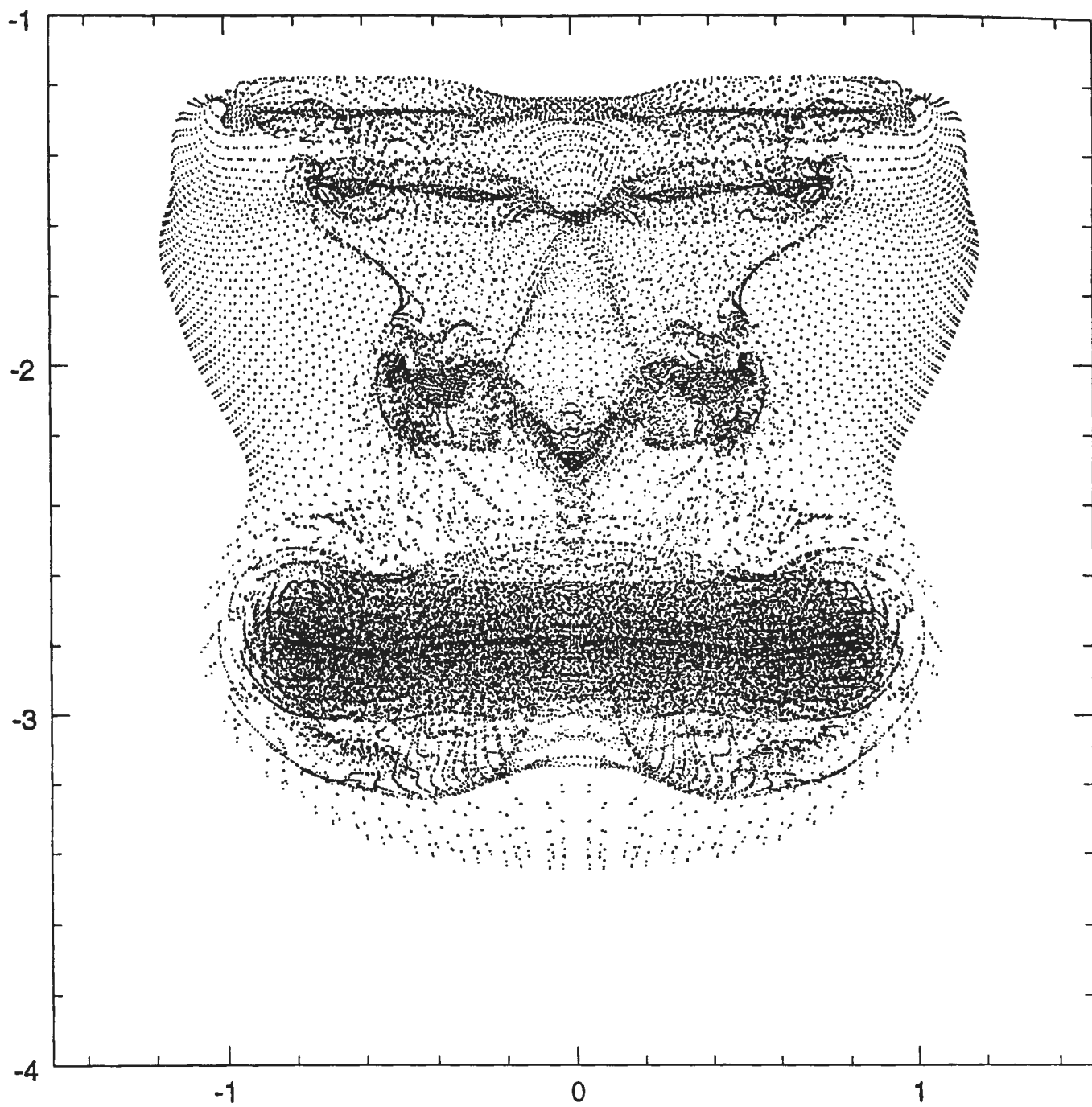
$T = 2.0$



$T=3.0$

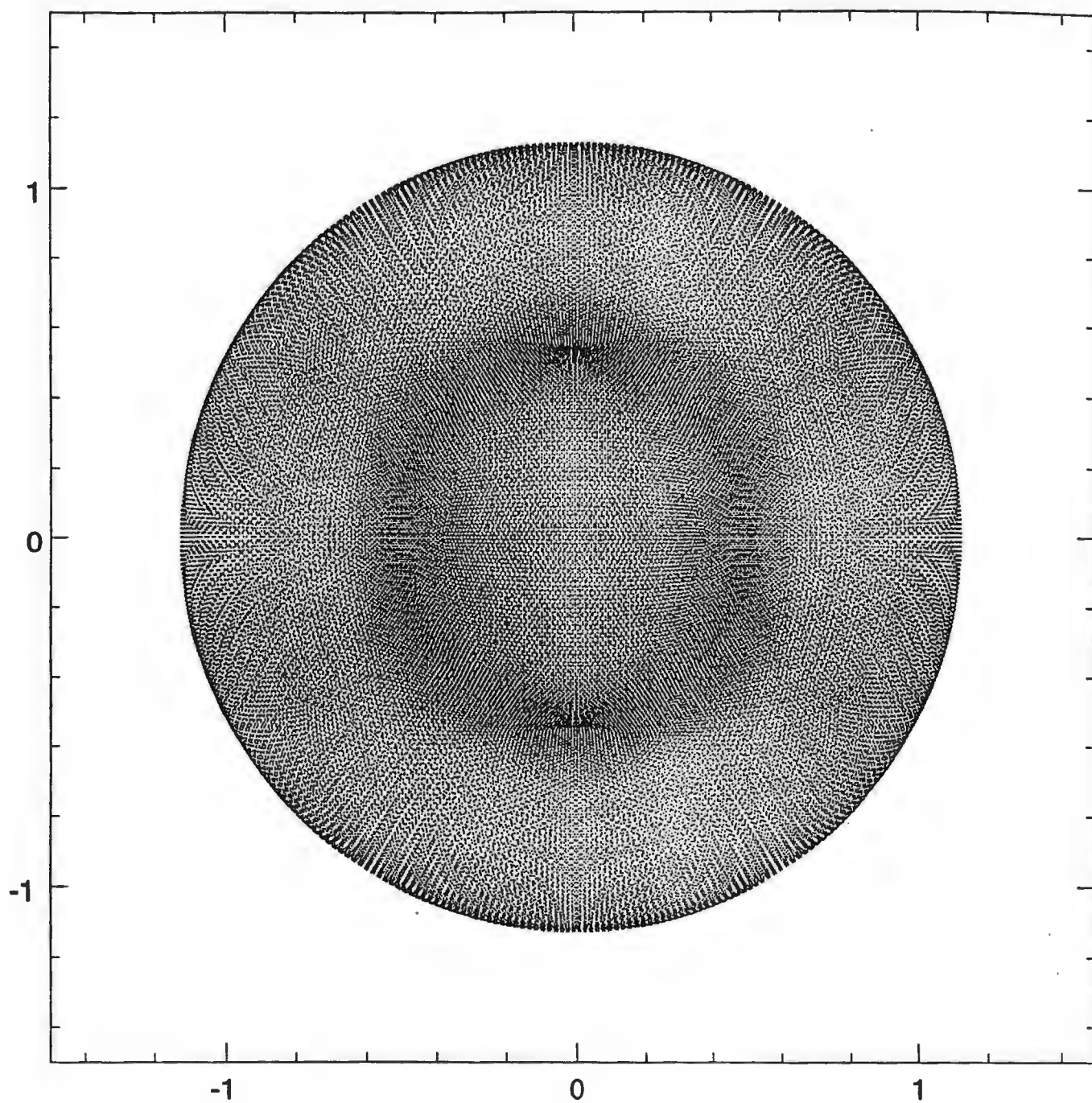


$T = 4.0$

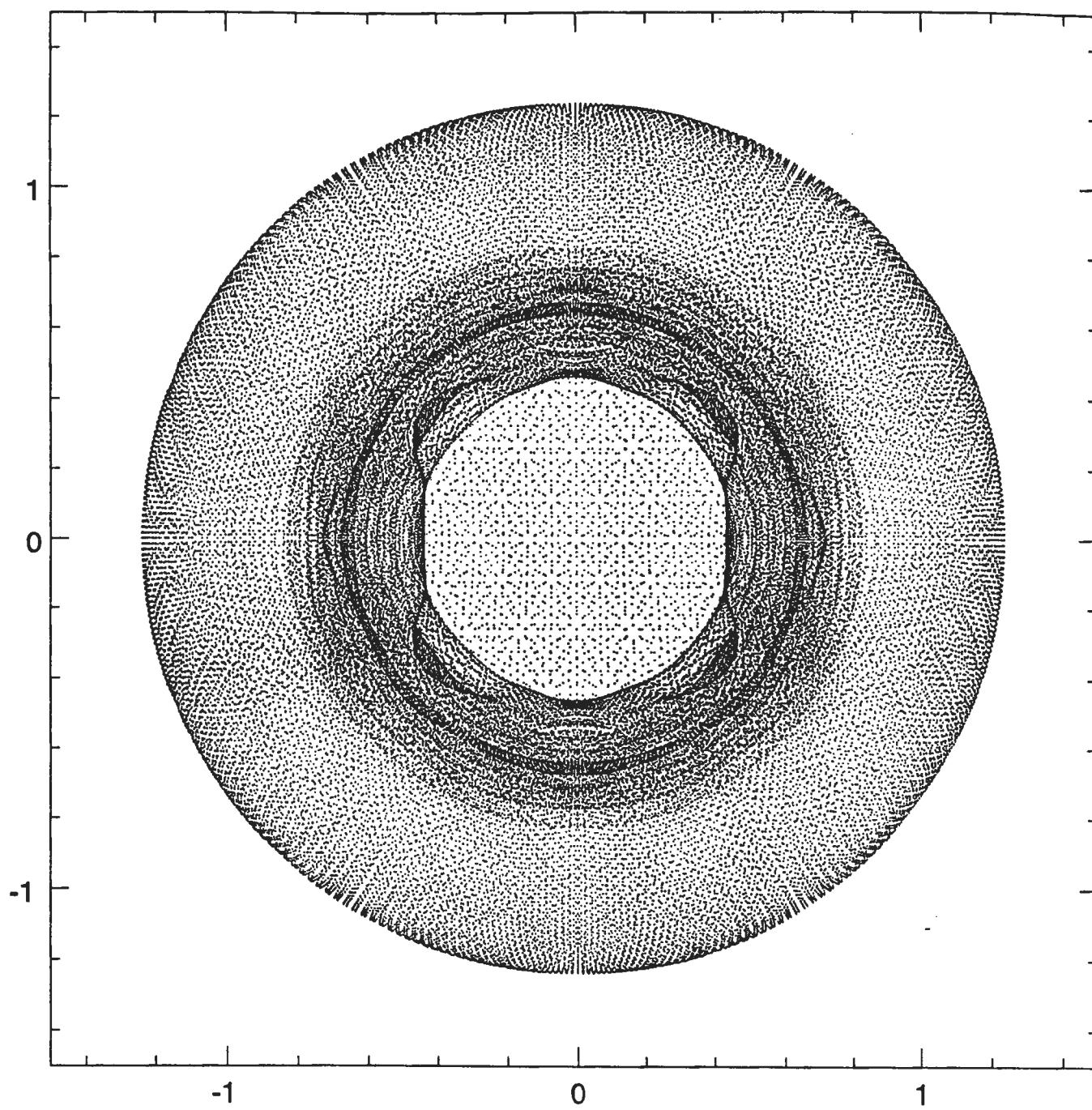


Top View

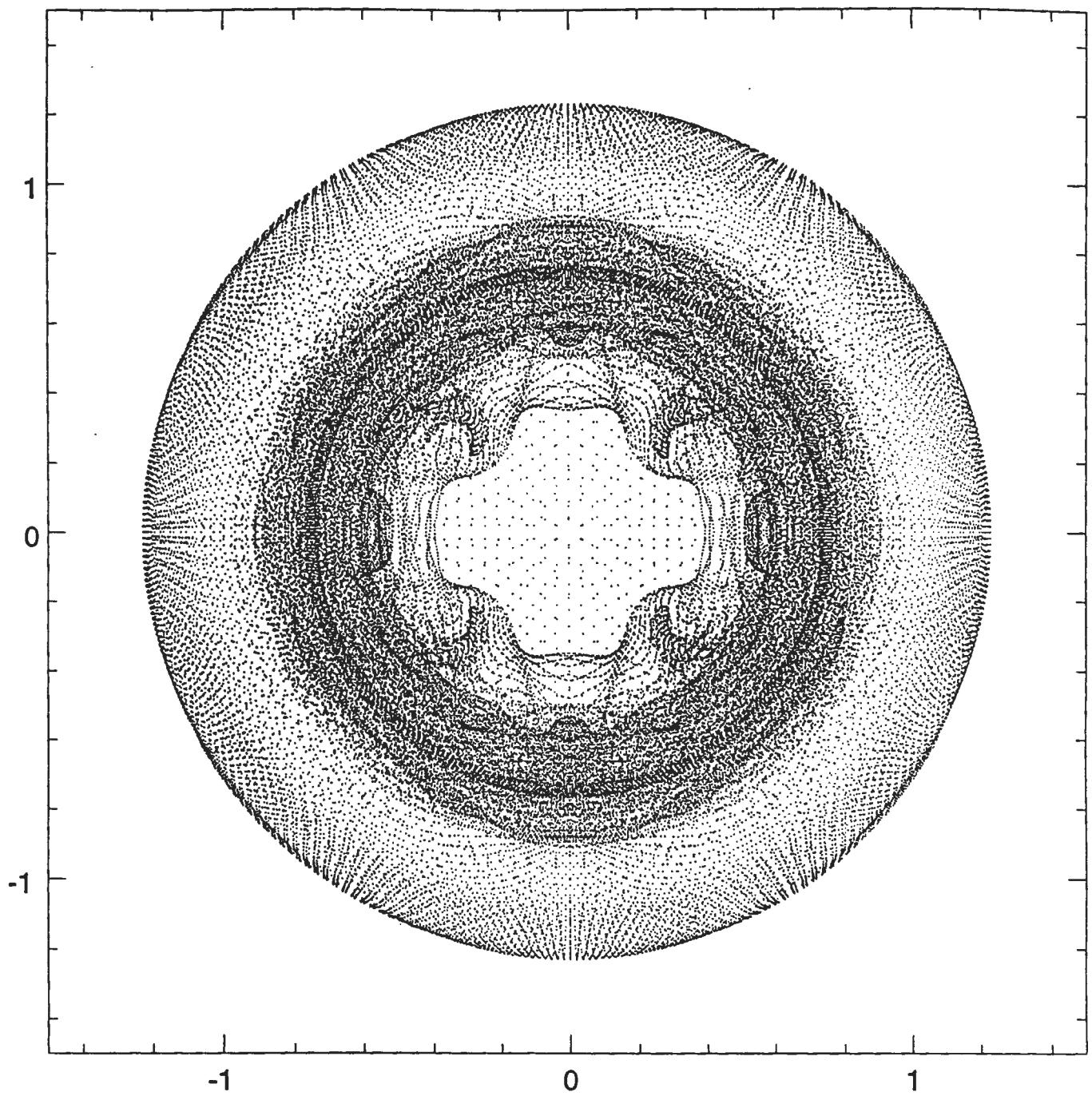
$T = 1.0$



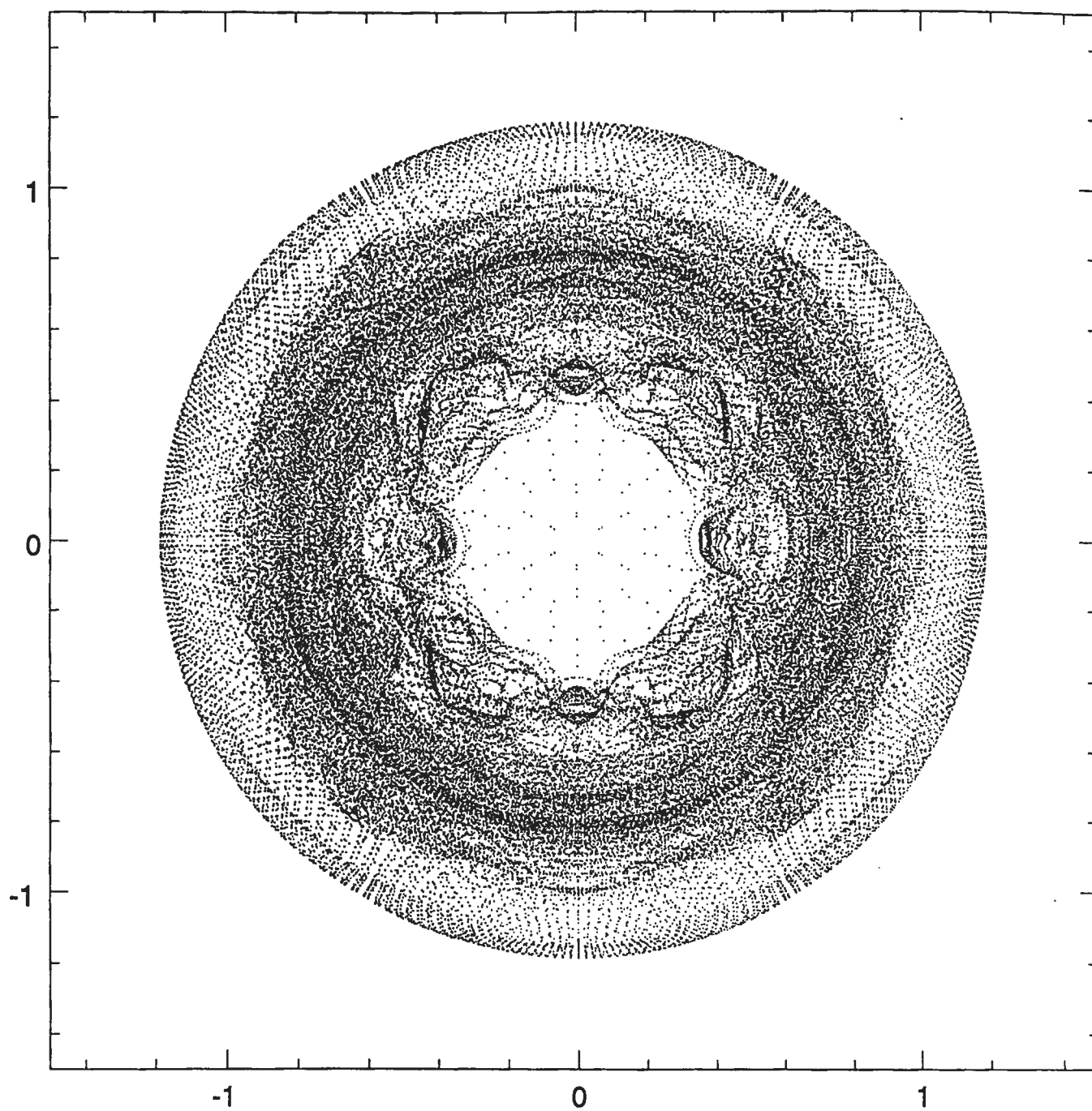
$T = 2.0$

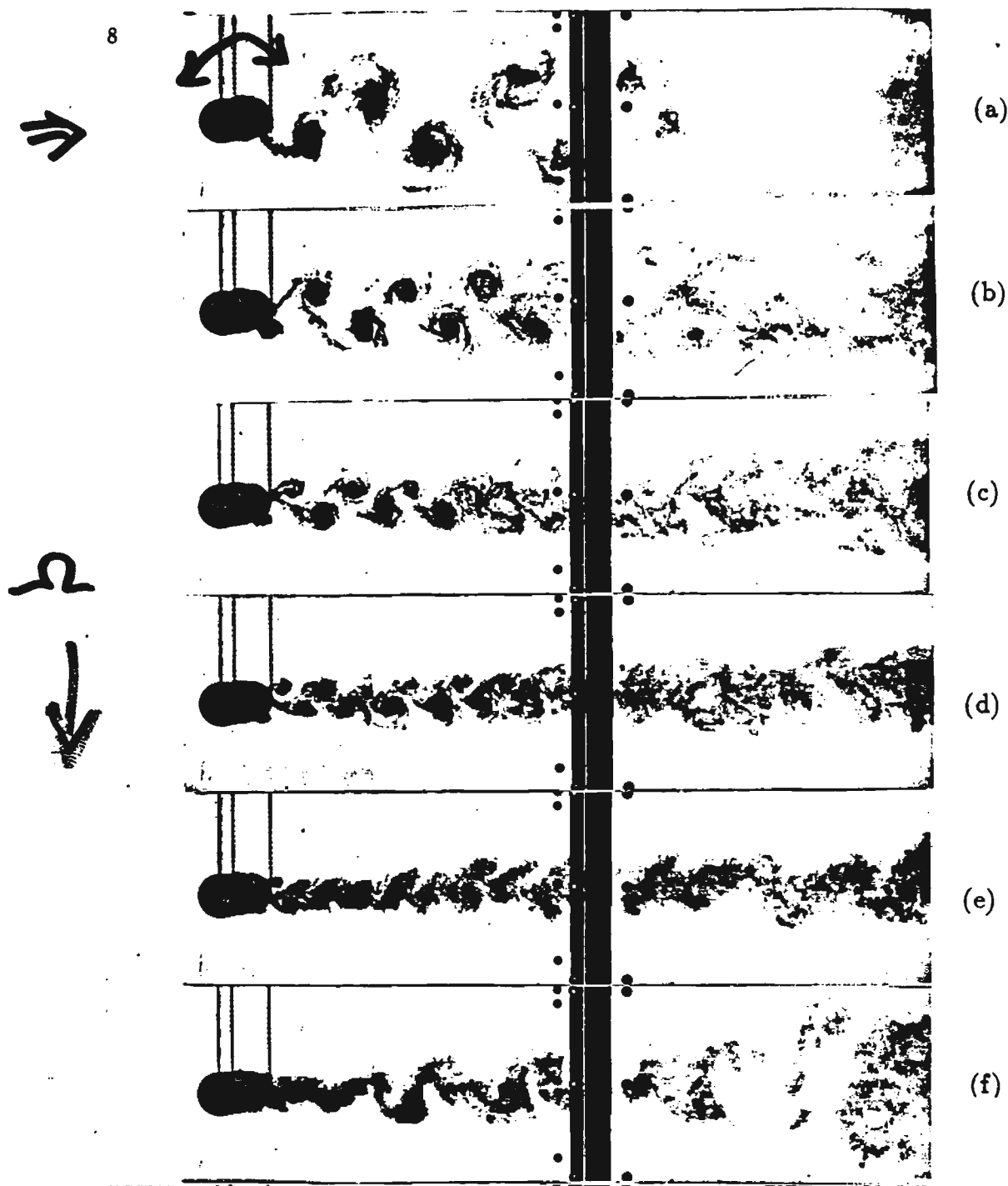


$T = 3.0$



$T = 4.0$





Cylinder Flow with Rotary Oscillations

$Re \approx 15,000$

(Tokumaru & Dimotakis, 1989)

$$\min_{\Omega} \{C_D\} \approx \frac{1}{6} C_{D_{unforced}}$$

Appendix
Biographical Information on Seminar Speakers

Kenneth S. Breuer

Department of Aeronautics and Astronautics, Room 33-214
Massachusetts Institute of Technology
Cambridge, MA 02139
(617) 253-1980
breuer@helmholtz.mit.edu

Employment

- 6/91 - Present. *Charles Stark Draper Assistant Professor of Aeronautics and Astronautics* Massachusetts Institute of Technology, Cambridge MA. Responsible for undergraduate and graduate level teaching, advising and research. Current research projects include: Active control of laminar-turbulent transition using flexible structures, active control of turbulent boundary layer structure. Design and testing of micro-machined probes for fluid mechanics, investigation of physics of ice-accretion on airfoils, effects of roughness on laminar-turbulent transition, Analysis and numerical simulation of bypass mechanisms for transition in boundary layer and pipe flows.
- 9/90 - 6/91. *Assistant Professor of Aeronautics and Astronautics* Massachusetts Institute of Technology, Cambridge MA.
- 10/88 - 8/90. *Post doctoral research associate* Center for Fluid Mechanics, Turbulence and Computation, Brown University. Research projects included: Error analysis in Chebyshev computations. Computation of generalized eigenfunctions for linear and nonlinear problems. Analysis of probability distributions in turbulent shear flows.

Education

- 6/88 PhD, Massachusetts Institute of Technology, Department of Aeronautics and Astronautics. Thesis title: "The development of a localized disturbance in a boundary layer." Thesis committee: M.T. Landahl, J.H. Haritonidis & S.E. Widnall.
- 9/84 MS, Massachusetts Institute of Technology, Department of Aeronautics and Astronautics. Thesis title: "An Experimental Investigation of Transitional Pipe Flow."
- 6/82 ScB, Brown University, Division of Engineering. Graduated Magna Cum Laude with Honors. Concentration in Fluids and Thermal Sciences.

Current research interests

Experimental, theoretical and numerical fluid mechanics, with a special interest in stability, transitional flows and coherent structures in fully turbulent flows. Active control of transitional and turbulent boundary layers; turbulent noise and drag reduction. Computational Fluid Dynamics. Experimental techniques and micro-sensor development.

Miscellaneous

- Invited researcher at NASA/Stanford Center for Turbulence Research, Royal Institute of Technology, Stockholm, NASA Langley Research Center.
- Reviewer for *Journal of Fluid Mechanics*, *Physics of Fluids*, *Sensors and Actuators*, *AIAA Journal*, *Science*
- Member of APS, AIAA.
- Citizenship: USA.

DR. MOHAMED GAD-EL-HAK
SHORT BIOGRAPHICAL SKETCH

Professor Gad-el-Hak received his B.Sc. (summa cum laude) in mechanical engineering from Ain Shams University in 1966 and his Ph.D. in fluid mechanics from the Johns Hopkins University in 1973, where he worked with Professor Stanley Corrsin. He has since taught and conducted research at the University of Virginia, University of Southern California and Institut National Polytechnique de Grenoble, and has lectured extensively at seminars in the United States and overseas. Dr. Gad-el-Hak is currently Professor of Aerospace and Mechanical Engineering at the University of Notre Dame. Prior to that, he was a Senior Research Scientist and Program Manager at Flow Research Company in Seattle, Washington, where he has managed a variety of aerodynamic and hydrodynamic research projects. Professor Gad-el-Hak has developed several novel measurement techniques for turbulent flows, and he holds two patents: one for a drag-reducing method for airplanes and underwater vehicles and the other for a lift-control device for delta wings. Dr. Gad-el-Hak has published over 170 articles in the basic and applied research areas of isotropic turbulence, boundary layer flows, stratified flows, compliant coatings, unsteady aerodynamics; biological flows, non-Newtonian fluids, and flow control. He is the editor of two volumes in Springer-Verlag's *Lecture Notes in Engineering* entitled "*Frontiers in Experimental Fluid Mechanics*," and "*Advances in Fluid Mechanics Measurements*." Professor Gad-el-Hak is a member of the American Chemical Society, an associate fellow of the American Institute of Aeronautics and Astronautics, a life member of the American Physical Society, and a member of the American Society of Mechanical Engineers. From 1988 to 1991, Dr. Gad-el-Hak served as Associate Editor for the *AIAA Journal*. He is currently serving as Associate Editor for the *Applied Mechanics Reviews* as well as a Contributing Editor for Springer-Verlag's *Lecture Notes in Engineering*. From 1988 to 1990, Dr. Gad-el-Hak served as a member of the Executive Committee of the Faculty Senate at the University of Notre Dame, Chairman of the Benefits Committee, as well as Chairman of the University Governance Committee. He served as a consultant to the U.S. Government, the Government of Egypt, the United Nations, and several industrial organizations. During the 1991/1992 academic year, Professor Gad-el-Hak was a visiting professor at the Institut de Mécanique de Grenoble, France.

RESUME

Ho, Chih-Ming

Professor Ho, Chih-Ming received his Ph.D. in Mechanics from The Johns Hopkins University and his BS in Mechanical Engineering from National Taiwan University. He is a Professor of the Mechanical, Aerospace and Nuclear Engineering Department at University of California, Los Angeles. Dr. Ho is the Director of Center for Advanced Technology of Micro Systems (C-ATOMS). He was a Professor of Aerospace Engineering at the University of Southern California. He was elected Fellow of the American Physical Society for pioneering research in controlling the evolutions of turbulent free shear layers. Dr. Ho is known for his work in the areas of turbulence, aerodynamics, aeroacoustics and bio fluid dynamics. He also specializes in sensor development and recently established the C-ATOMS at UCLA for studying micro-electro-mechanical-systems. He has published more than eighty papers in these fields and received U.S. patents in optical sensor and in nozzle design to enhance mass transfer. He has presented numerous keynote talks as well as served as chairman in international and national technical conferences. He is an Associate Editor of the ASME Journal of Fluids Engineering and was an Associate Editor of the AIAA Journal from 1985 to 1987.

Dr. Ho's research projects include microchannel flow with integrated microsensors, noise production in turbine machinery, mass transfer in turbulent wakes, instabilities in free shear layers, flow in human nasal passage, supersonic jet noise and unsteady aerodynamics.

HONORS

Fellow of the American Physical Society

Citation: For contributions in understanding the sensitivity of free shear layers under perturbations or geometrical variations in initial conditions. His pioneering works have been served as bases for controlling the evolutions of turbulent free shear layers.

Honorary Professor of Nanjing Aeronautical Institute, China

Associate Fellow of the American Institute of Aeronautics and Astronautics

Phi Beta Kappa

Tau Beta Pi

Sigma Xi

Phi Tau Phi

MEMBERSHIP IN PROFESSIONAL SOCIETIES

APS

AIAA

ASME

ADVISORY COMMITTEE

- 1980-84: Technical Committee of Aeroacoustics
American Institute of Aeronautics and Astronautics
- 1987-89: Advisor to Institute of Aeronautics and Astronautics
National Cheng-Kung University, Tainan, Taiwan
- 1992-94: Chair of Aviation Technology Advisory Committee
Center for Aviation and Space Technology
Industrial Technology Research Institute, Hsinchu, Taiwan

REFERENCES

Who's Who in Science and Engineering Who's Who in Technology Today
Who's Who in Frontier Science and Technology Who's Who in the West
Who's Who of Emerging Leaders in America

Vitae of Yu-Chong Tai

Assistant Professor of Electrical Engineering
California Institute of Technology
Pasadena, CA 91125
(818) 356-8317

Personal

[REDACTED]
[REDACTED]

PII Redacted

Education

B.S. National Taiwan University (1981).
M.S. EECS, University of California, Berkeley (1986).
Ph.D. EECS, University of California, Berkeley (1989).

Academic Experience

1983-1988 Research Assistant (EECS), U.C. Berkeley.
1986-1987 Teaching Assistant (EECS), U.C. Berkeley.
1988-1989 Graduate Instructor (EECS), U.C. Berkeley.
1989-now Assistant Professor (EE), California Institute of technology

Awards and Honors

Ross N. Tucker Award, AIME Electronics Material Award (1987).
Outstanding Student Paper Award, IEDM (1988).
IBM Fellowship (1988-1989).
David J. Sakrison Memorial Prize, U.C. Berkeley (1989).
Earnest C. Watson Lecturer, Caltech (1990).
Phi Tau Phi (1990).
Presidential Young Investigator (PYI) Award, NSF (1991-1996).
David and Lucile Packard Fellowships, David and Lucile Packard Foundation (1991-1996).

VITA

Dr. C. R. Smith
Professor of Mechanical Engineering and Mechanics
Packard Laboratory, # 19
Lehigh University
Bethlehem, PA 18015
(215) 758-4116

PII Redacted

Education

B.S. Mechanical Engineering, Stanford University, 1966
M.S. Mechanical Engineering, Stanford University, 1968
Ph.D. Mechanical Engineering, Stanford University, 1971

Professional Experience

Assistant Professor, Mechanical Engineering, Purdue Univ., 1971-76
NASA-ASEE Faculty Fellow, NASA-Ames Research Ctr., 1974
Associate Professor, Mechanical Engineering, Purdue Univ., 1976-78
Associate Professor, Mechanical Engineering, Lehigh Univ., 1978-82
Professor, Mechanical Engineering, Lehigh Univ., 1982-present
Director of Industry Liaison Program of Lehigh University
Thermo-Fluids Institute, 1980-86
Division Chairman, Thermo-Fluids Division, ME/Mech, Lehigh Univ., 1982-87

Research and Professional Activities

- Has conducted research in experimental fluid dynamics, turbulent boundary layers, turbulent flow structure, fluid mixing, flame stabilization, flow visualization, image processing, vortex-surface interactions, wake flows, unsteady separation phenomena, and "smart" material-fluid interaction.
- Has been principal investigator on contracts and grants totalling over \$3,500,000.
- Has supervised seven Ph.D. theses and seventeen M.S. theses (currently supervising three Ph.D. and two M.S. theses)
- Co-founder of Vortab, a company involved in the development and marketing of improved flow conditioners and static mixing devices
- Has consulted for over twenty firms (1973-present)
- A member of ASME, Pi Tau Sigma, Tau Beta Pi, American Physical Society, and AIAA

Biographical Sketch

Dr. Smith is a Professor of Mechanical Engineering at Lehigh University, Bethlehem, Pennsylvania, and is internationally recognized for his research in fluid mechanics, particularly the areas of turbulent flow, unsteady flow effects, flow visualization techniques, fluid dynamic image processing, flow mixing and conditioning, and fluid dynamic use of "smart" materials. He has published over seventy five archival journal and proceedings papers, and has made over one hundred conference, workshop, and invited seminar presentations.

Demetri P. Telionis

PERSONAL DATA

[REDACTED]

Telephone:

Office — (703) 231-7492

[REDACTED]

EDUCATION

PII Redacted

Cornell University (1970) Ph.D. in
Aerospace Engineering

Cornell University (1969) M.S. in
Theoretical & Applied Mechanics

National Technical University of Greece
(1964) Diploma

MILITARY SERVICE Served as Ensign in the Royal Greek Navy from 1964 to 1967.

HONORS AND RECOGNITIONS The McMullen & Glauert Fellowships at Cornell University. Invited keynote speaker at (i) CASI/AIAA Joint Aeronautical Meeting, (ii) AFOSR International Symposium on Unsteady Aerodynamics, 1975; (iii) AGARD International Symposium Unsteady Aerodynamics, 1977; (iv) AGARD-FDF-VKI Special Course Series, 1980.

The College of Engineering teaching award 1979. The SE American Association of Engineering Education Research Award for best paper in 1987. The ESM Frank E. Maher Outstanding Educator Award 1990.

MEMBERSHIP OF LEARNED SOCIETIES

AIAA (Associate Fellow), ASME, IUTAM, ASEE, Sigma Xi, Virginia Academy of Science.

EDITORIAL WORK

Associate Editor of the ASME Journal of Fluids Engineering 1987-90

Editor of the ASME Journal of Fluids Engineering 1990-95

PROFESSIONAL EXPERIENCE

GREEK NAVY SHIPYARDS, January 1965 — February 1966, Mechanical Engineer
(while serving as ensign officer)

IBM, Binghamton, NY, USA, June 1968 — October 1968, Consultant.

BMT Boatyard, Athens, Greece, May 1977 — June 1981, Consultant

FUSION SYSTEMS, INC., Washington, D.C., July 1986 — Dec. 1989, Consultant.

ITT, INC., Roanoke, VA., August 1989 — August 1990, Consultant.

TEACHING EXPERIENCE

VIRGINIA POLYTECHNIC INSTITUTE AND STATE UNIVERSITY, Blacksburg, Va

September 1970 — August 1974, Assistant Professor

September 1974 — August 1978, Associate Professor

September 1978 — Present, Professor

INVITED TALKS AND SEMINARS 18 invited seminars presented at universities or research institutes

PRESENTATIONS About 76 presentations at national and international meetings.

PUBLICATIONS

Book: Unsteady Viscous Flow, Springer Verlag, New York, Heidelberg, Berlin, Nov. 1981.

Papers: Approximately 80 referred publications in Journals and Proceedings (at least 70 of which are full papers).

FUNDED RESEARCH Directed and participated in funded research in the past 10 years for NASA, NSF, ONR, AFOSR, DOE, NAVAIR, ARO, DOT (responsible for over \$2,000,000 in total expenditures), in areas of Unsteady Boundary Layers—Numerical Analysis, Boundary—Layer Separation, Turbulent Boundary Layers and Closure Models, Homogeneous Shear Turbulent Flos, Unsteady Aerodynamics—Unsteady Stall, Flow Visualization Methods, Unsteady Waves, Aerodynamics of Ground Transportation, Laser—Doppler Velocimetry, Three—Dimensional Separation, Vortex Shedding Over Single and Multiple Bodies, Blade—Vortex Interaction.]

Anthony Leonard
Biographical Sketch

Dr. Leonard's area of interest is computational fluid dynamics and its application to a wide variety of flows including turbulence, transitional flows, and bluff-body aerodynamics. The computational tools he has been concerned with are Lagrangian vortex methods, spectral methods, and the technique of large-eddy simulation. He has also been involved, more recently, in the application of dynamical systems theory to fluid transport and mixing.

He studied mechanical engineering at the California Institute of Technology and obtained a B.S. degree in 1959. He attended graduate school at Stanford University, receiving an M.S. in Engineering Science in 1960 and a Ph.D in Mechanical Engineering in 1963. His research experience in a government/industrial setting includes three years at the RAND Corporation and twelve years at NASA's Ames Research Center in the Computational Fluid Dynamics Branch. Dr. Leonard's academic career includes seven years at Stanford as Assistant and Associate Professor of Mechanical Engineering and one year as Visiting Professor of Aeronautics at Caltech. For the past six years he has been Professor of Aeronautics at Caltech.

DISTRIBUTION LIST**Internal**

Codes	01X (Chapman)
	0251 (Conforti)
	0261
	0262 (2)
	02244
	10 (Roderick)
	102 (Lima)
	103 (Sullivan)
	106 (Dickinson)
	213 (Strawderman, Schloemer, Snarski, Tito, Payne)
	214 (Bakewell, Keith, Hurdis, Chen, Patton, Berliner, Abraham)
	22
	33A (Katz)
	2313 (Keefer)
	411 (Kalinowski, Wagner, Kieronski)
	432 (Straw)
	441 (Borgeson)
	80 (Dence)
	8141 (Galib)
	82 (White)
	821 (Nadolink)
	8211 (Aaron)
	8212 (Shonting)
	8214 (Brown, Philips, Dick, Koskie)
	8219 (Goodrich)
	823 (Meng)
	8232 (Hendricks, Temple, Hrubes, Henoch)
	8233 (Uhlman, Kirschner, Kaufman, Marshall, Kuklinski, Grant, Rice, Myers, Huyer, Krol, Koch, Varghese)
	8234 (Kemp, Jilling, Hrubes, Henoch, Lee, Doyle, Savoie, Bandyopadhyay (30))
	83 (McNally)
	8321 (Sjoblom, Barker, Parker)
	8322 (Lefebvre, Cipolla, Jordan, Schwemin)
	8323 (Bitsakis)
Total:	104